2-P

NASA CR-134547
BCAC D6-41527

727/JT8D REFAN SIDE NACELLE AIRLOADS

by R. W. Bailey
H. J. Vadset

BOEING COMMERCIAL AIRPLANE COMPANY
A DIVISION OF
THE BOEING COMPANY

Prepared for
NATIONAL AERONAUTICS AND SPACE ADMINISTRATION
NASA Lewis Research Center
Contract NAS3-17842

1. Report No.	2. Government Accession No.	3. Recipient's Catalog No.
CR-134547		

4. Title and Subtitle	5. Report Date
727/JT8D Refan Side Nacelle Airloads	March 1974
	6. Performing Organization Code

7. Author(s)	8. Performing Organization Report No.
R. W. Bailey H. J. Vadset	D6-41527
	10. Work Unit No.

9. Performing Organization Name and Address	11. Contract or Grant No.
BOEING COMMERCIAL AIRPLANE COMPANY P.O. BOX 3707 SEATTLE, WASHINGTON 98124	NAS3-17842
	13. Type of Report and Period Covered
12. Sponsoring Agency Name and Address	Contractor Report
NATIONAL AERONAUTICS AND SPACE ADMINISTRATION WASHINGTON, D.C. 20546	14. Sponsoring Agency Code

15. Supplementary Notes

PROJECT MANAGER, A.A. MEDEIROS
NASA LEWIS RESEARCH CENTER, CLEVELAND, OHIO 44135

16. Abstract

Airloads on the 727/JT8D refan side engine nacelle are presented. These consist of surface static pressure distributions from two low speed wind tunnel tests. External nacelle surface pressures are from testing of a flow-through, body mounted nacelle model, and internal inlet surface pressures are from performance testing of a forced air inlet model. The method for obtaining critical airloads on nacelle components and a representative example are discussed. These tests were conducted by the Boeing Commercial Airplane Company in support of the Phase II Program on Ground Test of Refanned JT8D Turbofan Engines and Nacelles for the 727 Airplane.

17. Key Words (Suggested by Author(s))	18. Distribution Statement
727-200 Airplane Refanned Nacelle Nacelle Airloads Wind Tunnel Surface Static Pressure Inlet Airloads	Unclassified - Unlimited

19. Security Classif. (of this report)	20. Security Classif. (of this page)	21. No. of Pages	22. Price*
Unclassified	Unclassified	261	

* For sale by the National Technical Information Service, Springfield, Virginia 22151

NASA-C-168 (Rev. 6-71)

FOREWORD

Airloads for the 727/JT8D side nacelles presented in this report were obtained from low speed nacelle and inlet wind tunnel tests by the 707/727/737 Structural Loads Staff of the Boeing Commercial Airplane Company, a division of the Boeing Company, Seattle, Washington. The work, sponsored by NASA Lewis Research Center and reported herein, was performed between October 1973 and February 1974 as part of the Phase II Program on Ground Test of Refanned JT8D Turbofan Engines and Nacelles for the 727 Airplane.

This report has been reviewed and is approved by:

J. J. Nishikawa, Group Engineer
707/727/737 Structural Loads Staff

DATE 5/23/74

J. A. Ferrell, Chief, Technology Staff
JT8D Refan Program

DATE 6/4/74

K. P. Rice
Program Manager
JT8D Refan Program

DATE 6/7/74

PRECEDING PAGE BLANK NOT FILMED

TABLE OF CONTENTS

TABLE OF CONTENTS (CONT'D)

1.0 SUMMARY

This report presents low speed nacelle airloads for the 727/JT8D refan side nacelle obtained from two low speed wind tunnel tests. External nacelle surface pressure distributions are from testing of a flow-through, body mounted nacelle model, and internal surface pressure distributions are from performance testing of a forced air inlet model. These supplement existing high speed data for the calculation of airloads on nacelle components.

Low speed airloads for the 727/JT8D refan side nacelle, based on wind tunnel test results presented in this report, are lower than preliminary estimates, due to a more detailed knowledge of the surface pressure distributions. Airloads for high speed flight conditions, based on rescaled existing standard nacelle data, give higher nacelle cowl surface pressures than low speed conditions, but lower airloads at the inlet flange and mount structure, due to more symmetrical surface pressure distributions. Estimated airloads for the standard side nacelle at the inlet attachment flange, using these low speed test results, are approximately 80% of the airloads estimated for the refan nacelle, for the same critical flight condition.

Wind tunnel testing has generally shown that low speed flaps down maneuver conditions give high wing downwash airflow at the nacelle which result in large down airloads on the nacelle. These large down airloads are a result of high wing downwash combined with high engine mass flow rates through the inlet. In general, testing has shown that more negative angles of attack and larger flap deflections produce larger downflow angles into the nacelle, and pressure distributions on the inlet are sinusoidally distributed with symmetry rotated from the vertical, due to a crossflow component of airflow into the nacelle.

2.0 INTRODUCTION

This report presents airloads for the 727/JT8D refan side nacelles from two low speed wind tunnel tests. These low speed airloads supplement existing high speed airloads available for the standard 727 airplane nacelles. These low and high speed results provide data for determining nacelle component airloads for critical flight conditions. For example, critical down airloads on the inlet attachment flange are from low speed conditions, and critical up airloads are from high speed conditions.

The refan engines, Pratt and Whitney Aircraft JT8D-109 engines, are modified JT8D-9 engines having larger diameter front fans and other modifications for quieter operation. These engines require larger diameter inlets and nacelles for mounting on the 727. Refan side nacelle design airloads are obtained for critical flight conditions from low speed airloads presented in this report and from existing high speed airloads rescaled to the enlarged refan geometry.

Side nacelle airloads presented in this report include surface static pressure distributions from two low speed wind tunnel tests, the side nacelle and the side inlet tests. External nacelle surface pressures are from testing of a flow-through, airplane body mounted nacelle model. Airflow angles into the nacelle are also from this testing. Internal inlet surface pressures are from performance testing of a forced air side inlet model. The combination of these external and internal surface pressure distributions is integrated to obtain nacelle component airloads.

Low speed wind tunnel testing of the Boeing 727-200 airplane with refan nacelles was performed at the University of Washington Aeronautical Laboratory (UWAL) low speed wind tunnel in October 1973. The right side nacelle was instrumented with pressure taps longitudinally and circumferentially to measure surface static pressure distributions. Emphasis was placed on obtaining exterior cowl pressures with enough internal inlet pressure taps for correlation with side inlet test data. Surface static

pressure distributions were obtained for various flap settings and airplane attitudes. In addition, local airflow angles into the nacelle inlet were measured by tufts mounted in front of the nacelle for 40° flap conditions.

Low speed wind tunnel testing of the 727/JT8D refan side inlet was performed by The Boeing Company, Propulsion Staff at the Boeing 9'x 9' Low Speed Wind Tunnel in December 1973. As part of this testing, surface static pressures on the upper and lower inlet surfaces were obtained for various inlet angles of attack, air speeds, and engine mass flow rates. This test is reported in reference 1.

The side nacelle pressure model and test, and the side inlet model and test are discussed in section 4.0. Test results are discussed in section 5.0 with concluding remarks in section 6.0. Figures and tables are presented in section 7.0.

3.0 NOMENCLATURE

UWAL	University of Washington Aeronautical Laboratory
psi	Pressure in pounds per square inch
psf	Pressure in pounds per square foot
N/m^2	Pressure in Newtons per square meter
C_p	Pressure coefficient, $\frac{p - p_\infty}{q_\infty}$
p	Surface static pressure
p_∞	Freestream static pressure
q_∞	Freestream dynamic pressure, $\frac{1}{2} \rho_\infty V_\infty^2$
ρ_∞	Freestream air density
V_∞	Freestream velocity
p_{T_∞}	Tunnel total pressure
M_∞	Freestream Mach number
$\frac{w\sqrt{\theta}}{\delta}$	Engine mass flow rate corrected to sea level, standard atmosphere where θ = temperature ratio, δ = static pressure ratio
γ	Specific heat ratio
δ_F	Wing flap setting, degrees
α_w	Wing pitch angle of attack, degrees - positive nose up
α_B	Body pitch angle of attack, degrees - positive nose up
ψ	Yaw angle of attack, degrees - positive nose left
θ	Nacelle circumferential position, degrees - positive clockwise from top, looking aft
ϕ_N	Downwash component of nacelle inflow relative to nacelle $\mathcal{L}$, degrees

NOMENCLATURE (Cont'd)

ϕ_B	Downwash component of nacelle inflow relative to body w.l., degrees
χ_N	Crossflow component of nacelle inflow relative to nacelle $\mathfrak{C}$, degrees
$\int_N$	Total nacelle inflow angle relative to the nacelle $\mathfrak{C}$, degrees
$\mathfrak{C}$	Centerline
w.l.	Airplane body waterline
hilite	Forward edge of inlet lip contour

4.0 MODEL AND TEST DESCRIPTION

4.1 MODEL DESCRIPTION

4.1.1 SIDE NACELLE MODEL

4.1.1.1 BASIC MODEL

The basic model configuration was a 0.075 scale model of the Boeing 727-200 airplane with model nacelles for the Pratt & Whitney JT8D-109 engine mounted in place of the standard model nacelles. The configuration, as tested in the UWAL wind tunnel, is shown in the photograph, section 7.1, figure 1, and in the sketches, figure 2.

The basic model configuration, designated TX-549-E35, had the standard 727-200 body, wings, leading edges, flaps, and tail. The horizontal stabilizer was pre-set to a nominal trim position and remained unchanged during testing. Flaps were set at 0°, 5°, 15°, 30°, and 40°, as required. Leading edge slats and Krueger flaps were set in the up position at 0° flaps and in the down position at 5°, 15°, 30°, and 40° flaps. Landing gears were down at 40° flaps.

The nacelles were modeled to simulate the refan nacelles. The right side refan nacelle was instrumented to measure surface static pressures and is more fully described in section 4.1.1.2. The left side refan nacelle was an aerodynamic flow-through model without the pressure taps. The refan center engine inlet was simulated with an aerodynamic bulb.

4.1.1.2 NACELLE PRESSURE MODEL

The right side nacelle was a flow-through type pressure model instrumented with pressure taps to measure surface static pressure distributions. The nacelle was mounted to the airplane body on the standard strut design. The inlet had 0° cant relative to the nacelle centerline and the internal design was symmetrical. Nozzle exit diameter on the model was enlarged from that of the actual nacelles to better simulate engine mass flow rates. Nacelle geometry, as tested, is shown in figure 3.

Surface pressures were measured by pressure taps located longitudinally on the nacelle top, bottom, and sides, with circumferential bands on the interior and exterior inlet lip. Tap locations are as indicated in figure 3. There were 70 pressure taps total.

4.1.2 SIDE INLET MODEL

The side inlet model was a 0.30 scale forced air model with symmetrical internal and external cowls. Data presented in this report is for the inlet model with a splitter ring and center body installed (refan configuration 2). The model was instrumented, in part, with pressure taps longitudinally on the top and bottom, internal and external cowls to measure surface static pressure. Details of the side inlet model are reported in reference 1.

4.2 TEST FACILITIES AND MODEL INSTALLATIONS

4.2.1 SIDE NACELLE TEST

Side nacelle testing was performed in the 8 x 12 foot (2.44 x 3.66 meter) low speed wind tunnel at the University of Washington Aeronautical Laboratory. The tunnel is a closed, double return type with viewing windows located on the top and sides of the test section.

The airplane model was balance mounted on a strut from the floor. Remote capability was available to vary pitch and yaw angles. Tunnel entry could easity be made to change flap and leading edge configurations.

Instrumentation consisted of the usual tunnel measurements with the additional capability of measuring nacelle surface static pressures. Pressures were transmitted by tubing lines from the pressure taps on the nacelle surface to four scanivalves mounted inside the airplane model aft body. By remotely phasing these scanivalves, tap pressures were tranmitted through lines to the tunnel instrumentation and data system outside the test section. In addition, a rod with three tufts could be attached to the airplane model body in front of the right nacelle so that airflow

angles into the nacelle could be measured. The rod was removed when nacelle pressure data was taken. The rod was mounted as indicated in figure 2, approximately one and a half inlet diameters in front of the inlet hilite, with the tufts centered in the stream tube entering the nacelle inlet.

4.2.2 SIDE INLET TEST

Side inlet testing was performed in the Boeing 9 x 9 foot Low Speed Wind Tunnel, Seattle, Washington. The tunnel is an open, non-return type. The inlet model was mounted on an air duct through the test section floor to a jet engine which provided forced air for engine mass flow rate simulation. Details of the inlet test facility and model installation are reported in reference 1.

4.3 TEST PROCEDURE

4.3.1 SIDE NACELLE TEST

The configurations and conditions tested are indicated in Table 1. Surface static pressure data were taken for 0°, 5°, 15°, 30°, and 40° flap angles at wing pitch angles at attack from -11° to 23°. The most severe nacelle airloads were expected for high flap angles, but lower flap angles were tested for completeness and correlation with existing high speed airload data. Dynamic pressures were nominally 50 psf or 30 psf (2390 and 1440 N/m^2). At several high angles of attack drag force limits of the balance mount were met, forcing lower dynamic pressure testing. Tufts were installed with the 40° flap condition to check the airflow into the nacelle from wing downwash. In doing so, crossflow angles were noted. Subsequently, pressure data and tuft photographs were taken at yaw angles of $+10^{\circ}$ and -10° to further investigate this flow.

4.3.2 SIDE INLET TEST

Inlet performance for various inlet angles of attack, engine mass flow rates, and airspeeds was tested. Details of the inlet test procedure are reported in reference 1.

5.0 DISCUSSION OF TEST RESULTS

5.1 SIDE NACELLE TEST

5.1.1 NACELLE SURFACE PRESSURE DISTRIBUTIONS

Refan side nacelle surface static pressure distributions are presented in section 7.2.1, figures 8 through 183. Test data are presented as indicated in the figure number index at the beginning of the section. Longitudinal and circumferential surface pressure distributions are presented for each band of pressure taps. For clarity, each run has been divided and shown in two angle of attack groups. To better define longitudinal pressure coefficients on the nacelle inlet, these are shown with an expanded scale on additional figures. The inlet hilite location is indicated on each figure, with the internal pressures plotted forward of the inlet hilite on a reverse scale for clarity. Tunnel corrections have been made to all data in these figures. Pressure data are presented as pressure coefficients, Cp, which is the relationship:

$$Cp = \frac{\Delta p}{q_\infty} = \frac{p - p_\infty}{\frac{1}{2} \rho_\infty V_\infty^2}$$

where p = surface static pressure

p_∞ = free stream static pressure

ρ_∞ = free stream density

q_∞ = free stream dynamic pressure

V_∞ = free stream velocity

The surface pressure data show that pressures vary with airplane attitude and flap setting. More severe pressure distributions are indicated for flight conditions with more negative pitch angle of attack and larger flap settings, conditions producing downwash airflow from the wing. Highest pressures are forward on the inlet. Circumferential pressure coefficient distributions on the inlet lip, in general, are sinusoidal with symmetry rotated from the vertical. There are only small differences in pressure coefficients between runs with dynamic pressures of 30 and 50 psf (1460 and 2390 N/m^2) for the same test configuration. Pressure

coefficients may be considered independent of dynamic pressure for this dynamic pressure range.

Nacelle surface static pressures appear to have been successfully measured. The use of surface pressure data for the aft portion of the nacelle should consider the influence of exhaust airflow and the enlarged model exit diameter. Nacelle pressures are found to correlate reasonably well with existing high speed wind tunnel data.

5.1.2 NACELLE INFLOW ANGLES

Photographs were taken from the test section top and side of tufts mounted in front of the nacelle. These indicate downwash and crossflow components of airflow into the nacelle. These photographs are for the 40° flap condition, where large downwash angles were expected, and are presented in section 7.2.2, figures 184 through 188.

Downwash and crossflow components of airflow into the nacelle have been measured from these photographs and are tabulated in table 2, section 7.1. Total inflow angles have been calculated and are also shown in table 2. Figures 4 and 5 show downwash and total inflow angles for the center tuft plotted versus wing angle of attack. The measured inflow angles vary with angle of attack. Downwash angles are larger at higher negative angles of attack. Crossflow angles show an influence of the aircraft fuselage at negative angles of attack and yaw conditions. It should be noted, however, that inflow angles at extreme negative angles of attack seem to be influenced by the center engine inlet aerodynamic bulb.

5.2 SIDE INLET TEST

Side refan inlet surface static pressure distributions from inlet performance testing are presented in section 7.2.3, figures 189 through 236. Test data are presented as indicated in the figure number index at the beginning of the section. The inlet hilite location is indicated on each figure, with the external pressures plotted forward of the inlet hilite on a reverse scale for clarity. Pressure data are presented as a surface static pressure ratio, which is the relationship:

$$\frac{p}{p_{T\infty}}$$

where p = surface static pressure

$p_{T\infty}$ = tunnel total pressure

The pressure ratios are applicable to flight conditions with the same Mach Number, M_∞, and the same corrected engine mass flow rates, $\frac{w\sqrt{\theta}}{\delta}$. Velocities indicated have been corrected to sea level, standard atmosphere. Pressures follow the isentropic flow relationship:

$$\frac{p_\infty}{p_{T\infty}} = \left[1 + \frac{\gamma - 1}{2} M^2_\infty\right]^{-\gamma/\gamma-1}$$

where γ = specific heat ratio

The inlet surface pressure data show that the location of the stagnation point is dependent on the local inflow angle, engine mass flow rate, and freestream velocity. The inlet surface pressures internal from the stagnation point are dependent on engine mass flow rate. The inlet pressure distributions external from the stagnation point are dependent on freestream velocity. Zero degree inlet angle of attack conditions show inlet symmetry. For increasing inlet angle of attack, pressure distributions on the upper and lower surface of the inlet become increasingly asymmetrical. Inlet pressures are found to correlate reasonably well with side nacelle pressures.

5.3 SIDE NACELLE AIRLOADS

Low speed airloads on refan side nacelle components are obtained from the test results presented in this report. They are a combination of external nacelle pressures from side nacelle testing and internal pressures from side inlet testing. The determination of design component airloads involves the following factors:

1) The selection of critical aircraft attitudes and airspeeds which depend on gross weight, allowable load factor, flap setting, and allowable airspeed.
2) The external nacelle surface pressure distribution for critical aircraft attitudes and airspeeds.

3) The airflow angle into the nacelle for critical aircraft attitudes and airspeeds.
4) The internal inlet surface pressure distribution at the nacelle inflow angle and engine mass flow rate for critical aircraft flight conditions.
5) The integration of internal and external surface pressure distributions for critical aircraft flight conditions to obtain component airloads.

Airloads on the inlet attachment flange may be considered a representative example of airloads on nacelle components. Pressure distributions which give critical down airloads at the inlet flange and, as a result, large airloads on the mounting structure, are shown in figures 6 and 7. These are for a flaps down approach condition for an aircraft with 40° flaps, low gross weight, a large negative pitch angle of attack, and requiring high engine thrust. This condition results in high downwash airflow aft of the wing, giving a large airflow angle relative to the nacelle centerline. Surface pressures are found to be distributed sinusoidally on the inlet circumference with symmetry 30° from the top, due to a crossflow component of airflow. It may be noted that internal inlet airloads at the inlet flange are nearly 75% of the total airloads for this condition. These low speed down airloads at the inlet flange are approximately four times higher than the up airloads for high speed flight conditions, due to a more assymmetrical pressure distribution. They are, however, lower than preliminary refan estimates. High speed airloads on the nacelle cowl surface are greater than low speed airloads, but a lower angle of inflow to the nacelle gives a more symmetrical pressure distribution. Estimated standard side nacelle airloads at the inlet flange for this condition, using results presented in this report, are approximately 80% of the refan nacelle airloads.

6.0 CONCLUSIONS

Low speed airloads for the 727/JT8D refan side nacelle, based on wind tunnel test results presented in this report, are lower than preliminary estimates, due to a more detailed knowledge of the surface pressure distributions. Airloads for high speed flight conditions, based on rescaled existing standard nacelle data, give higher nacelle cowl surface pressures than low speed conditions, but lower airloads at the inlet flange and mount structure, due to more symmetrical pressure distributions. Estimated airloads for the standard side nacelle at the inlet attachment flange, using these low speed test results, are approximately 80% of the airloads estimated for the refan nacelle, for the same critical flight condition.

The following general conclusions from low speed wind tunnel testing can be made:

1. High wing downwash airflow at the nacelle exists for flaps down conditions and gives high inflow angles to the nacelle.
2. Downflow angles of airflow into the nacelle are larger at more negative pitch angles of attack.
3. Internal inlet airloads are predominant for low speed flight conditions requiring high engine mass flow rates.
4. The combination of large flap deflections, large negative pitch angle of attack, and high engine mass flow rates gives large airloads at the inlet attachment flange.
5. Surface pressure distributions on the inlet circumference are in general, sinusoidally distributed with symmetry rotated from the vertical, due to a crossflow component of airflow into the nacelle.

7.0 FIGURES AND TABLES

7.1 GENERAL FIGURES AND TABLES

Presented in this section are general figures and tables discussed in the report text. These are presented as listed below.

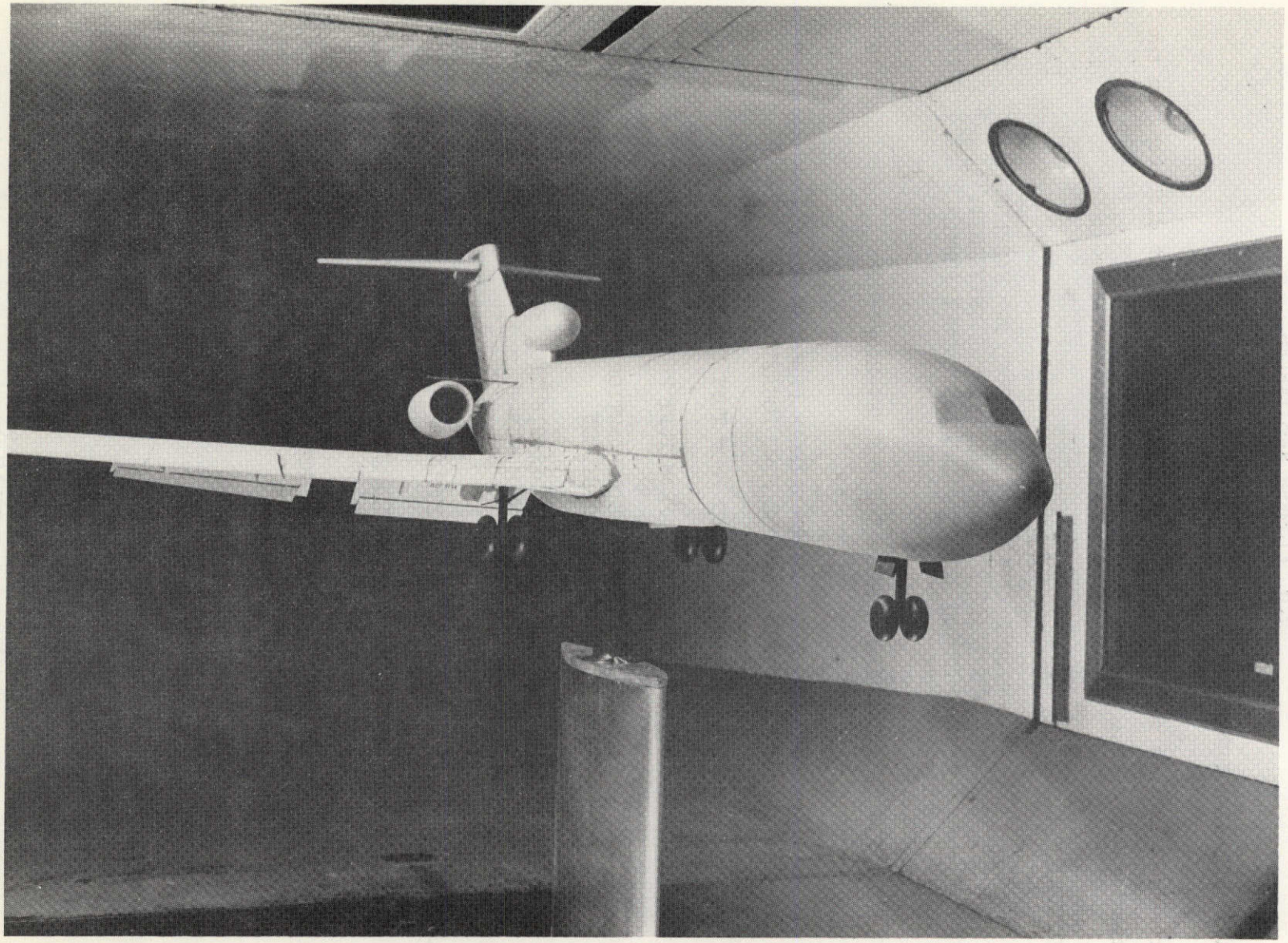

FIGURE 1. - 727-200/JT8D REFAN AIRPLANE MODEL FOR NACELLE PRESSURE LOADS AS INSTALLED IN THE UNIVERSITY OF WASHINGTON AERONAUTICAL LABORATORY (UWAL) WIND TUNNEL (40° FLAP CONDITION)

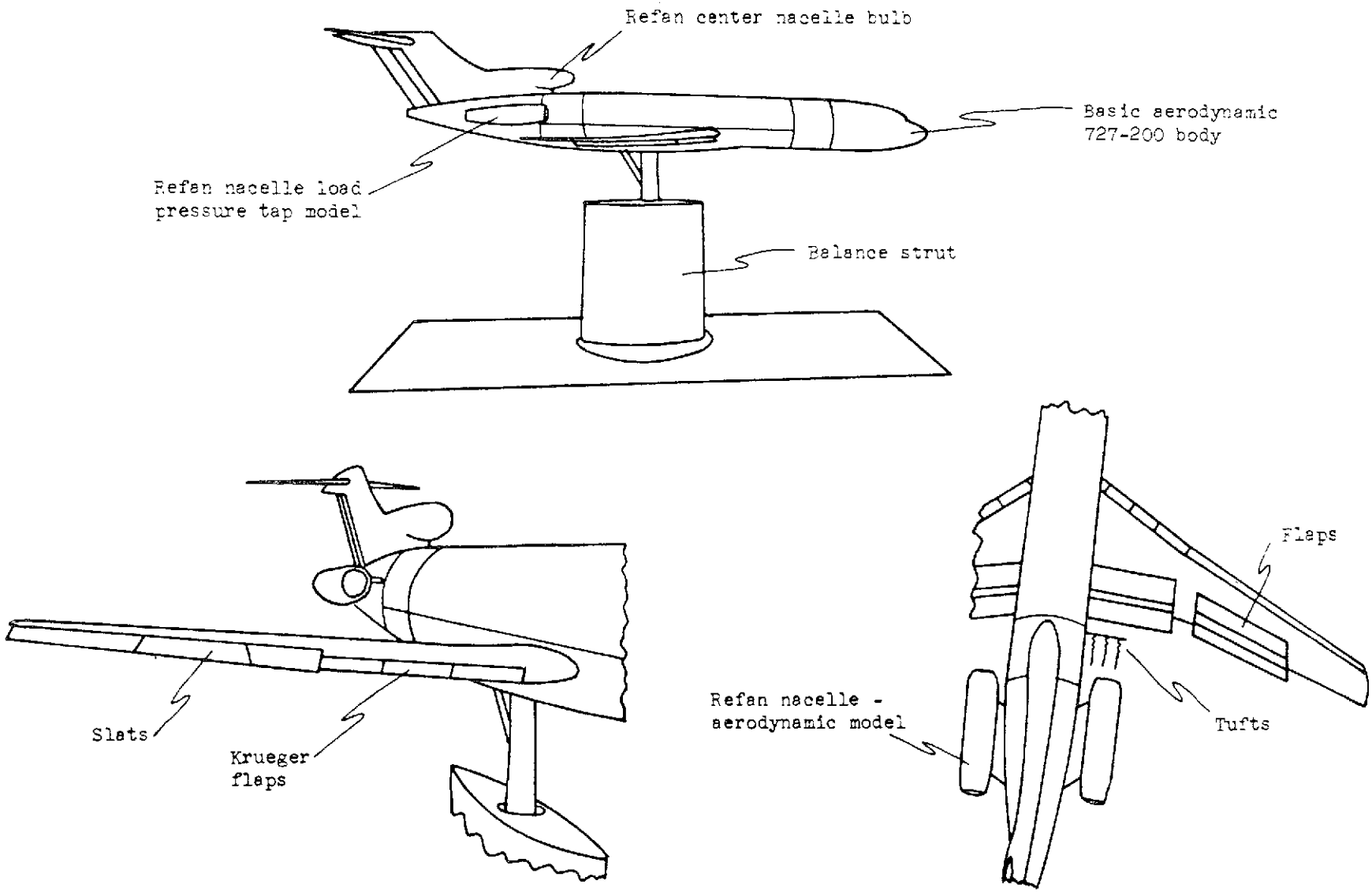

FIGURE 2.4 - TEST CONFIGURATION FOR THE 727-200/JT8D REFAN NACELLE MODEL

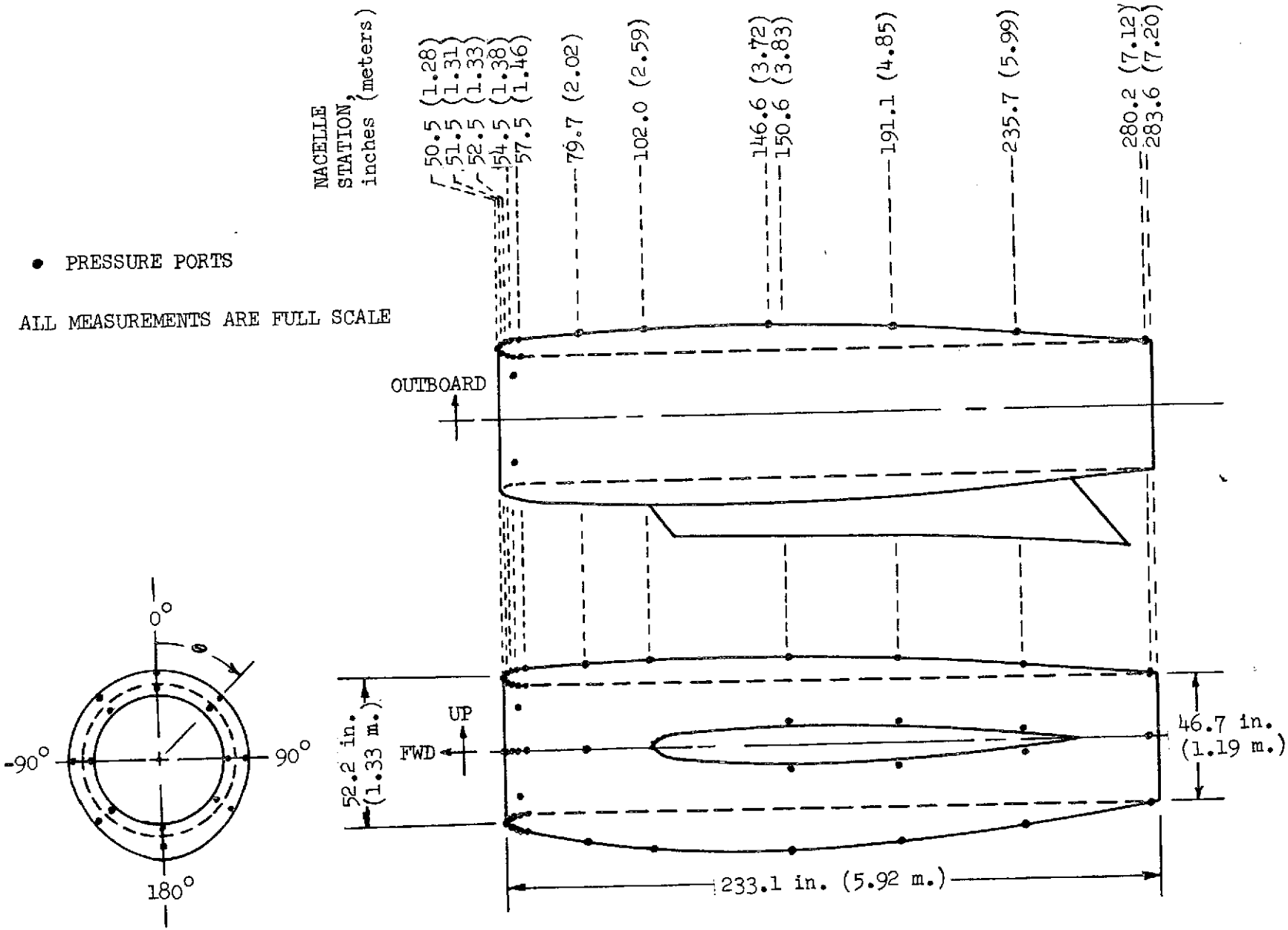

FIGURE 3.- 727/JT8D RIGHT REFAN NACELLE PRESSURE MODEL - GEOMETRY AND PRESSURE PORT LOCATION

TABLE 1. - TEST CONDITIONS FOR 727/JT8D REFAN NACELLE LOADS PRESSURE MODEL

Run No.	Dynamic pressure, q_∞, psf(N/m^2)	Flap setting, δ_F	Wing angle of attack, α_w (a)	Yaw angle, ψ (d)	Type of Run	
					Surface Pressures	Tufts W/Photos
1	50 (2394)	15°	-5° to 23°	0°	X	
2	b 50 (2394)	40°	-11°, -9°to23°	0°	X	
3	30 (1436)	40°	-11°,-9°to 23°	0°	X	
4	30 (1436)	40°	-11°,-5°,12°	0°		X
5	50 (2394)	40°	-11°,-5°,12°	0°		X
6	30 (1436)	40°	-11°,-9°to 23°	+10°	X	
7	c 50 (2394)	30°	-5° to 23°	0°	X	
8	50 (2394)	5°	-5° to 23°	0°	X	
9	30 (1436)	40°	-11°,-9°to 23°	-10°	X	
10	30 (1436)	40°	-11°,-5°,12°	-10°		X
11	30 (1436)	40°	-11°,-5°,12°	+10°		X
12	50 (2394)	0°	-5° to 23°	0°	X	

a By 4° Increments; α Wing = α Body + 2°

b q = 45 psf (2155 N/m^2) at α_w = 19°, drag limited
q = 40 psf (1915 N/m^2) at α_w = 23°, drag limited

c q = 40 psf (1915 N/m^2) at α_w = 23°, drag limited

d + yaw, nose left; -yaw, nose right

TABLE 2. - NACELLE INLET FLOW ANGLE FROM TUFT PHOTOGRAPHS[a]

Yaw Angle, ψ	Wing Pitch Angle of Attack, α Wing	Crossflow angle, χ_N, deg. Tuft Number[e] 1	2	3	Downwash angle, ϕ_N, deg. Tuft Number 1	2	3	Total inflow angle, ζ_N, deg.[b] Tuft Number 1	2	3
-10° (nose right)	-11°	21	14	8	27	24	24	[c] 32	[c] 27	[c] 25
	(d) -5°	18	16	8	21	18	18	[c] 27	24	20
	12°	8	9	3	13	13	13	15	16	13
0°	(d) -11°	8	4	1	23	23	23	24	23	23
	(d) -5°	8	4	1	19	19	19	20	19	19
	(d) 12°	5	3	-4	3	3	3	6	4	4
$+10^\circ$ (nose left)	-11°	3	-2	-9	18	18	18	18	18	20
	(d) -5°	2	-5	-12	17	17	17	17	18	21
	12°	-7	-6	-15	-1	-1	-1	7	6	15

a Flaps are set at 40° for all conditions and χ_N, ϕ_N, ζ_N are all relative to the nacelle $\mathcal{L}$

b Calculated from $\frac{1}{\cos^2 \zeta_N} = \frac{1}{\cos^2 \chi_N} + \frac{1}{\cos^2 \phi_N} - 1$

c Possible influence of center engine bulb

d Photographs shown in Figures 184. through 188.

e tufts numbered as below:

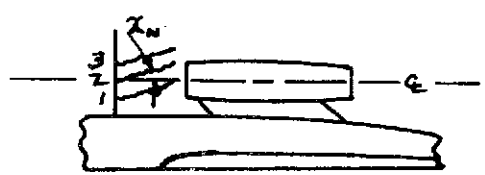

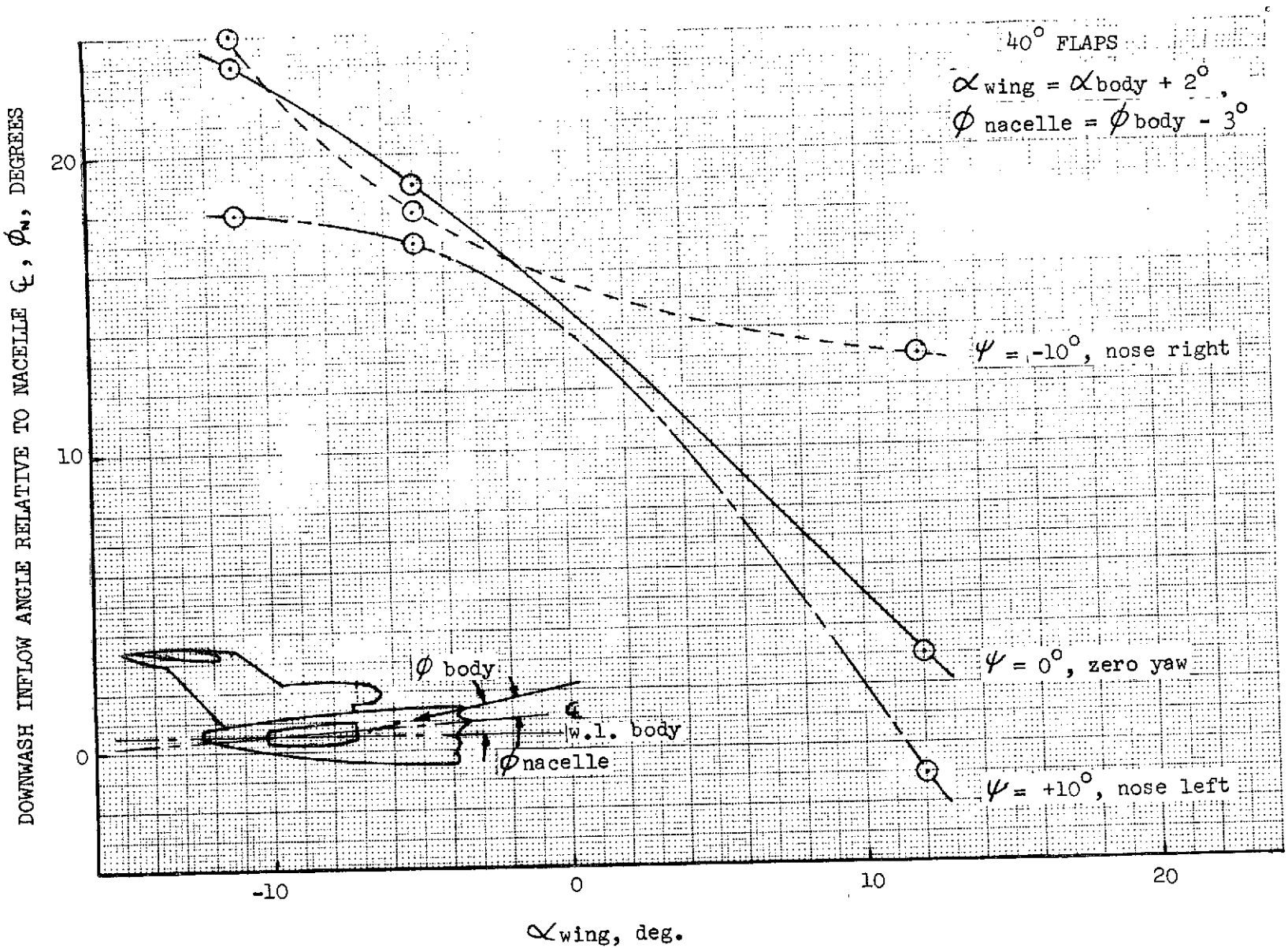

FIGURE 4. - INLET DOWNWASH ANGLES FROM TUFT PHOTOGRAPHS

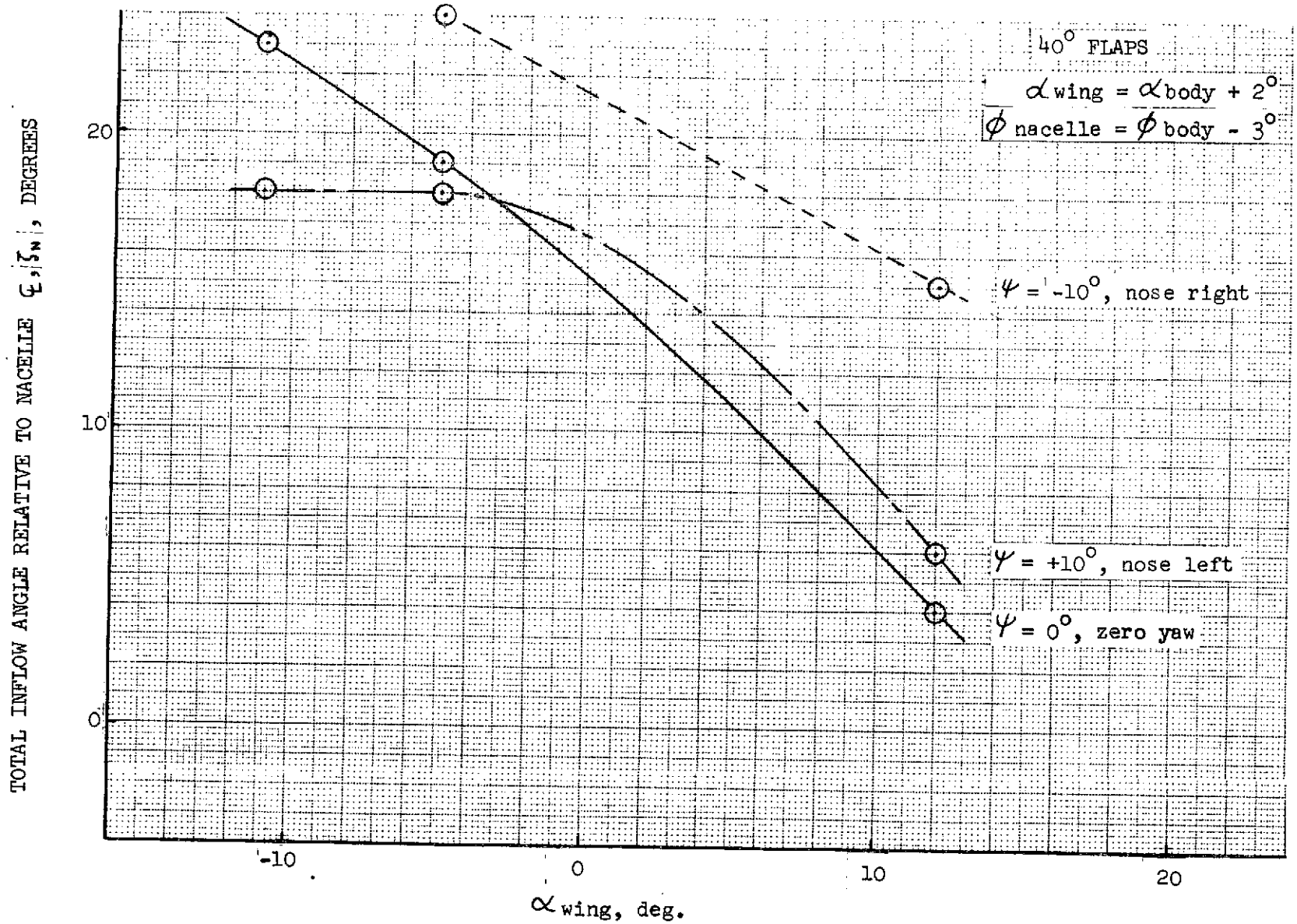

FIGURE 5. - TOTAL INFLOW ANGLES FROM TUFT PHOTOGRAPHS

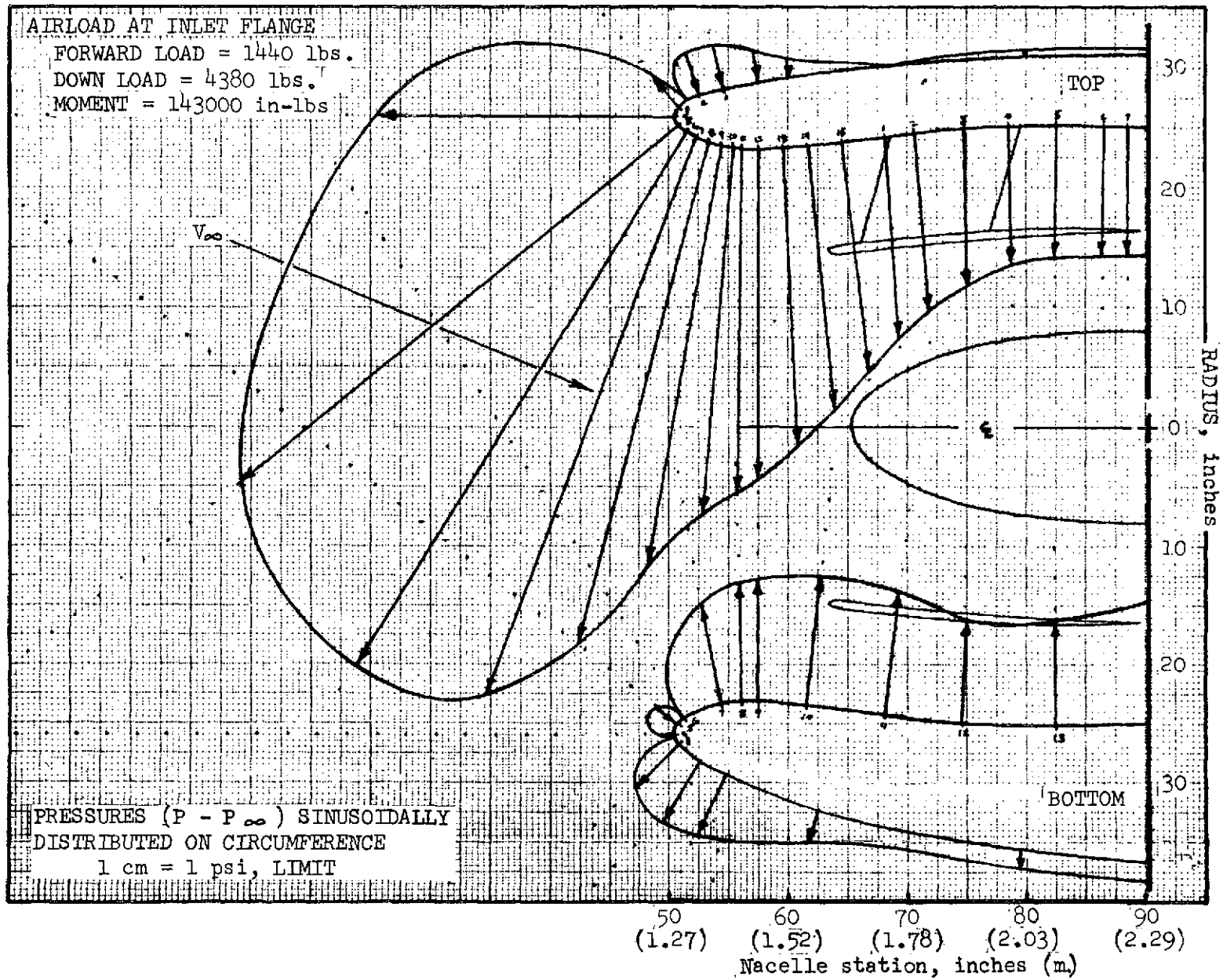

FIGURE 6.- SIDE INLET PRESSURE DISTRIBUTION FOR THE EXAMPLE FLAPS DOWN CONDITION

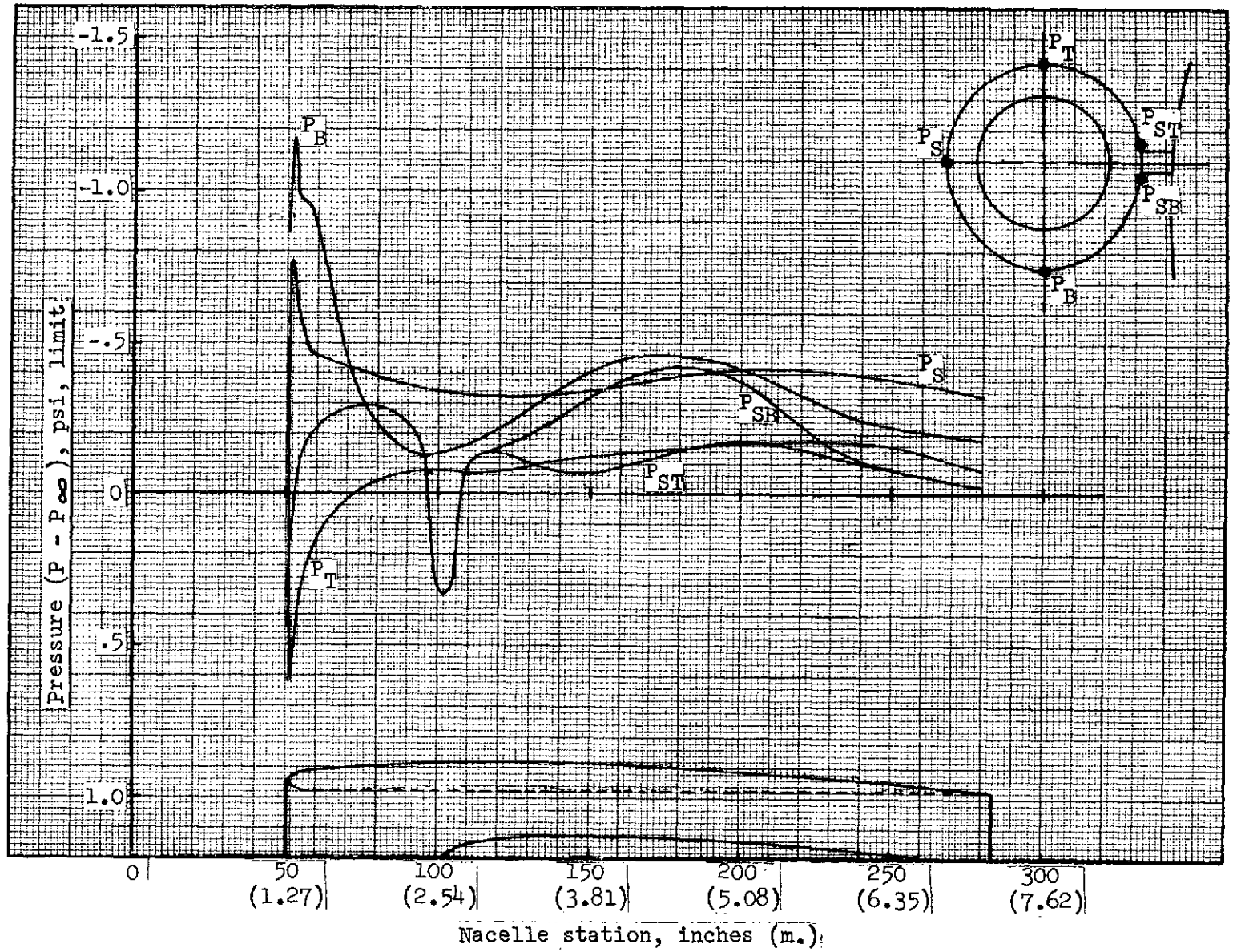

FIGURE 7.- SIDE NACELLE PRESSURE DISTRIBUTION FOR THE EXAMPLE FLAPS DOWN CONDITION

7.2 WIND TUNNEL DATA RESULTS

7.2.1 NACELLE PRESSURE COEFFICIENT DISTRIBUTIONS

Presented in this section are nacelle surface static pressure coefficient distributions obtained from the wind tunnel test discussed in Section 4.0. Data are presented on pages 28 through 203 as shown in the figure number index below.

FIGURE NUMBER INDEX FOR NACELLE
PRESSURE COEFFICIENT DISTRIBUTIONS

TEST CONDITION				TOP		INBOARD ABOVE STRUT		INBOARD BELOW STRUT		BOTTOM		OUTBOARD		EXTERNAL CIRCUM.	INTERNAL CIRCUM.
FLAPS	YAW (c)	q, psf (a)	RUN	INLET	NACELLE	INLET	NACELLE	INLET	NACELLE	INLET	NACELLE	INLET	NACELLE	AT STA. 54.5 IN (b)	AT STA. 54.5 IN.
0°	0°	50	12	8 10	9 11	12 14	13 15	X	16 17	18 20	19 21	22 24	23 25	26 27	28 29
5°	0°	50	8	30 32	31 33	34 36	35 37	X	38 39	40 42	41 43	44 46	45 47	48 49	50 51
15°	0°	50	1	52 54	53 55	56 58	57 59	X	60 61	62 64	63 65	66 68	67 69	70 71	72 73
30°	0°	50	7	74 76	75 77	78 80	79 81	X	82 83	84 86	85 87	88 90	89 91	92 93	94 95
40°	0°	50	2	96 98	97 99	100 102	101 103	X	104 105	106 108	107 109	110 112	111 113	114 115	116 117
40°	0°	30	3	118 120	119 121	122 124	123 125	X	126 127	128 130	129 131	132 134	133 135	136 137	138 139
40°	-10°	30	9	140 142	141 143	144 146	145 147	X	148 149	150 152	151 153	154 156	155 157	158 159	160 161
40°	+10°	30	6	162 164	163 165	166 168	167 169	X	170 171	172 174	173 175	176 178	177 179	180 181	182 183

(a) 50 psf = 2394 N/m^2, 30 psf = 1436 N/m^2.

(b) 54.5 in. = 1.38 m.

(c) + yaw, nose left; -yaw, nose right

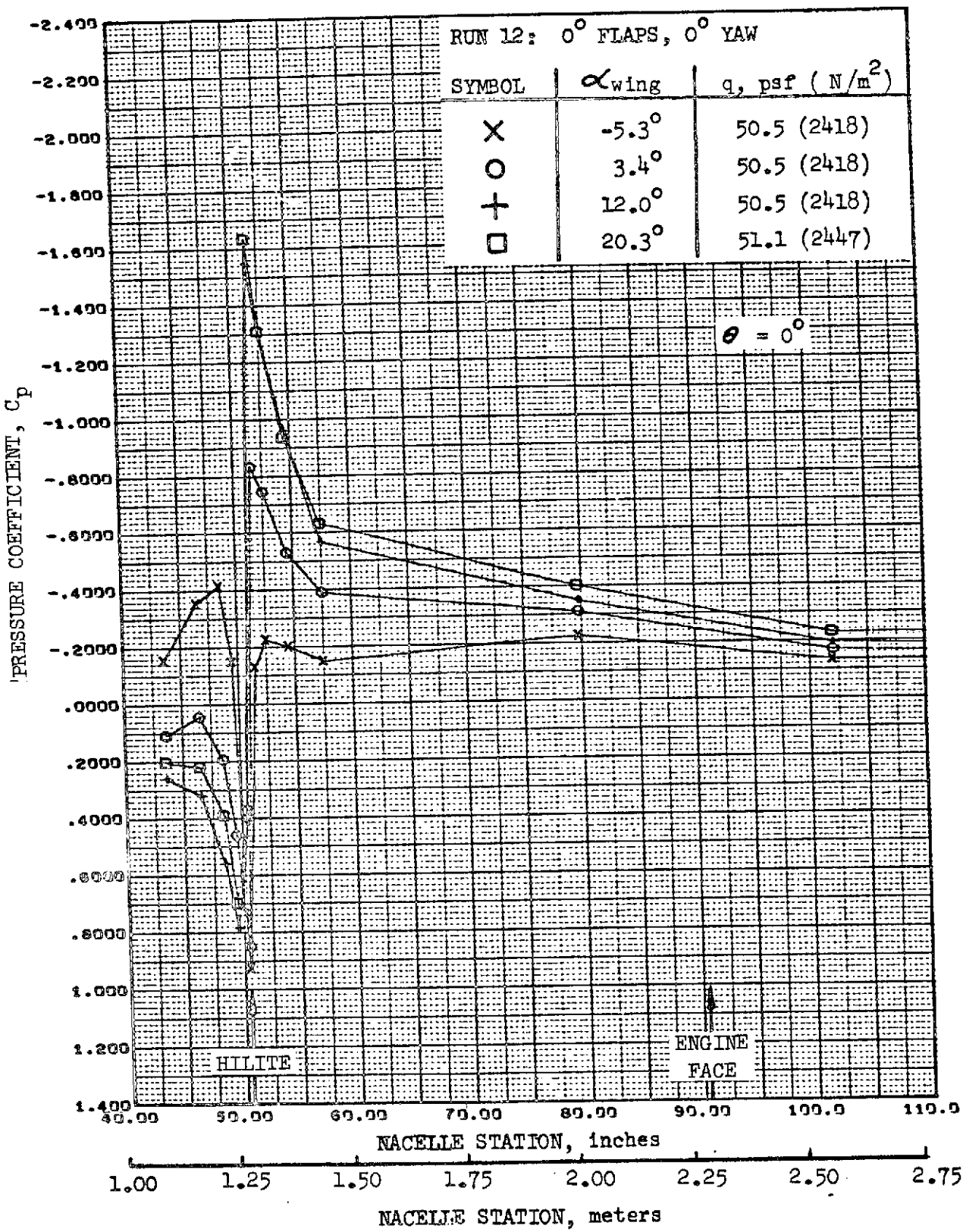

FIGURE 8. -REFAN NACELLE INLET COWL PRESSURE COEFFICIENT DISTRIBUTION, TOP LONGITUDINAL

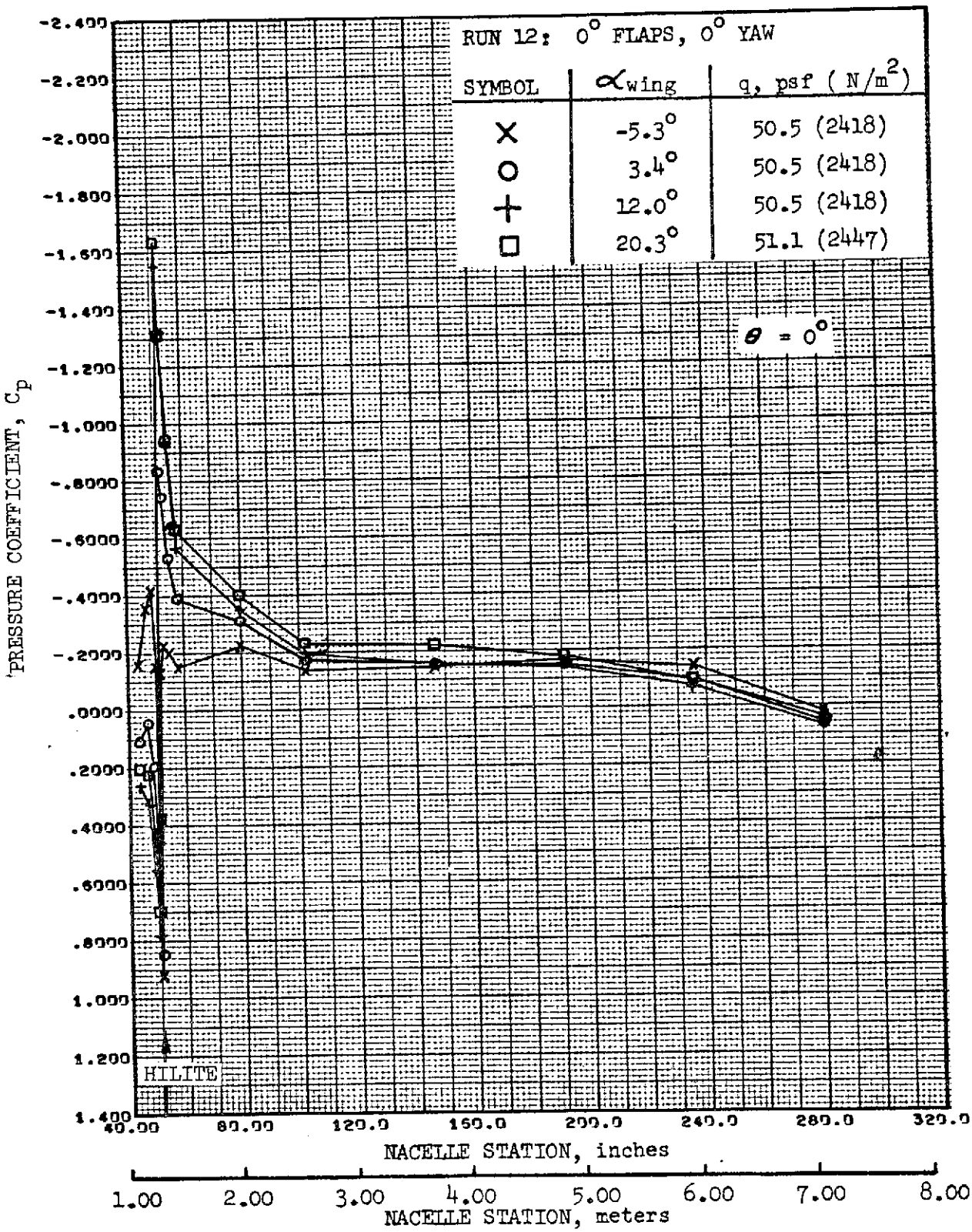

FIGURE 9. -REFAN NACELLE PRESSURE COEFFICIENT DISTRIBUTION, TOP LONGITUDINAL

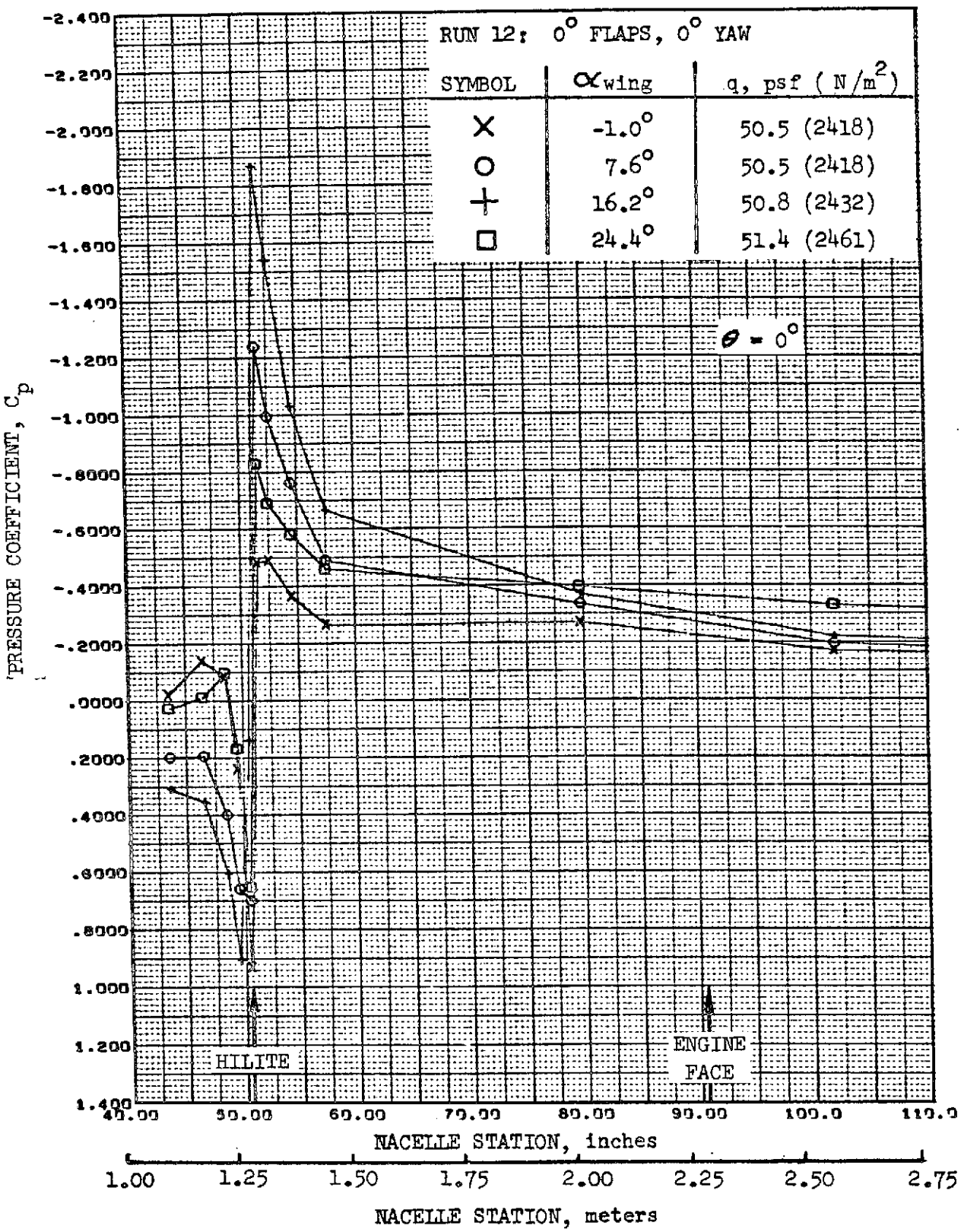

FIGURE 10. -REFAN NACELLE INLET COWL PRESSURE COEFFICIENT DISTRIBUTION, TOP LONGITUDINAL

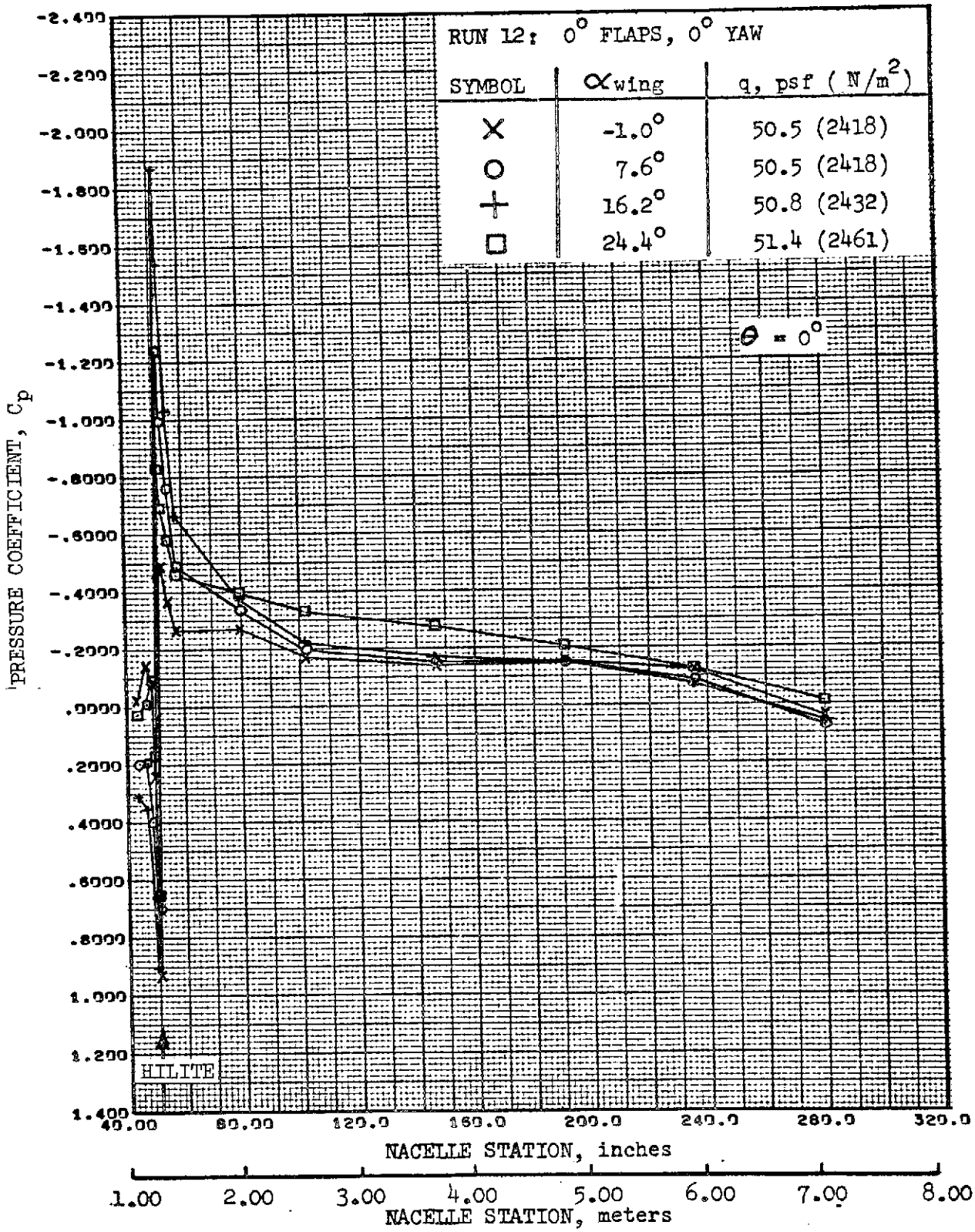

FIGURE 11. -REFAN NACELLE PRESSURE COEFFICIENT DISTRIBUTION, TOP LONGITUDINAL

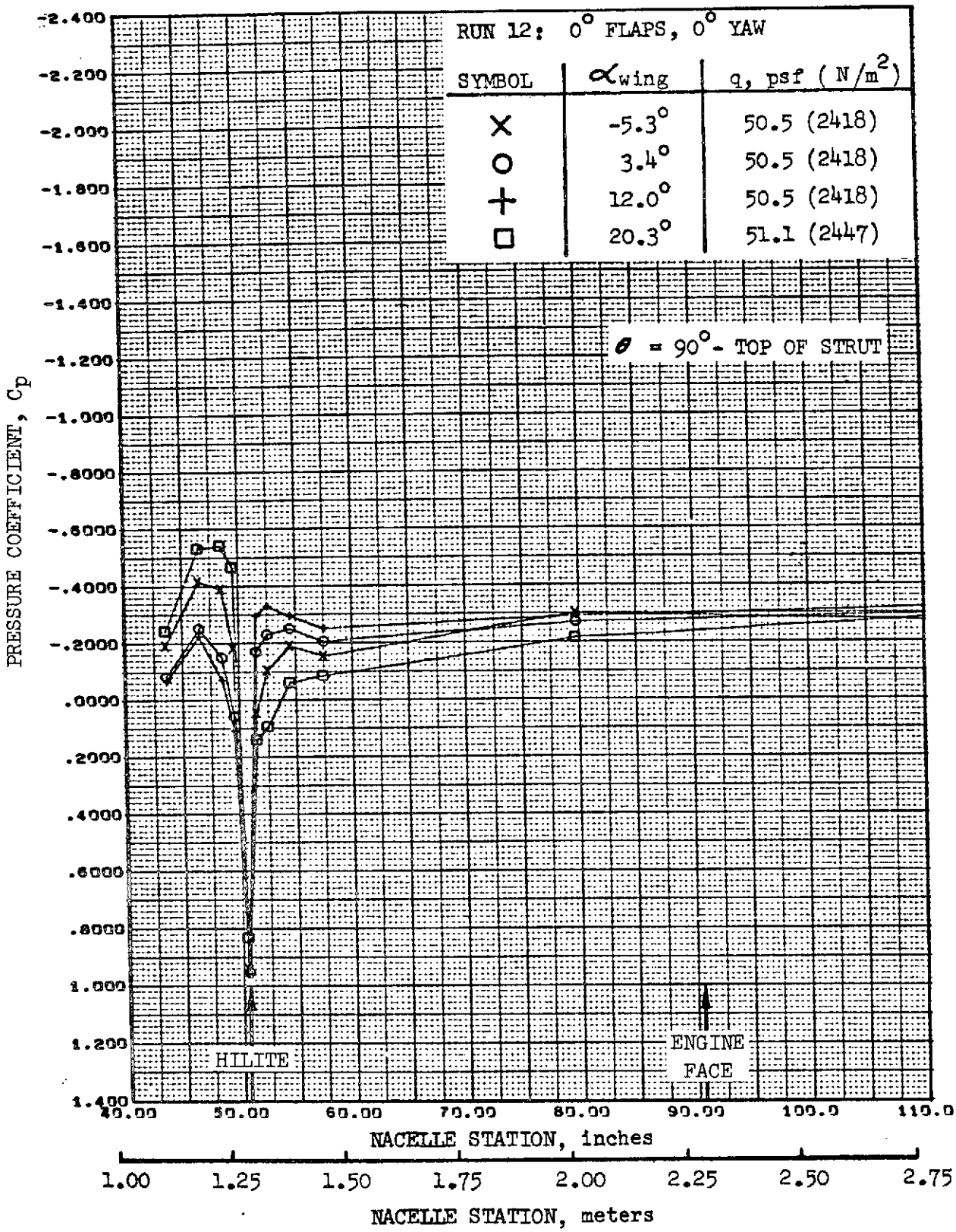

FIGURE 12. -REFAN NACELLE INLET COWL PRESSURE COEFFICIENT DISTRIBUTION, INBOARD SIDE-ABOVE STRUT

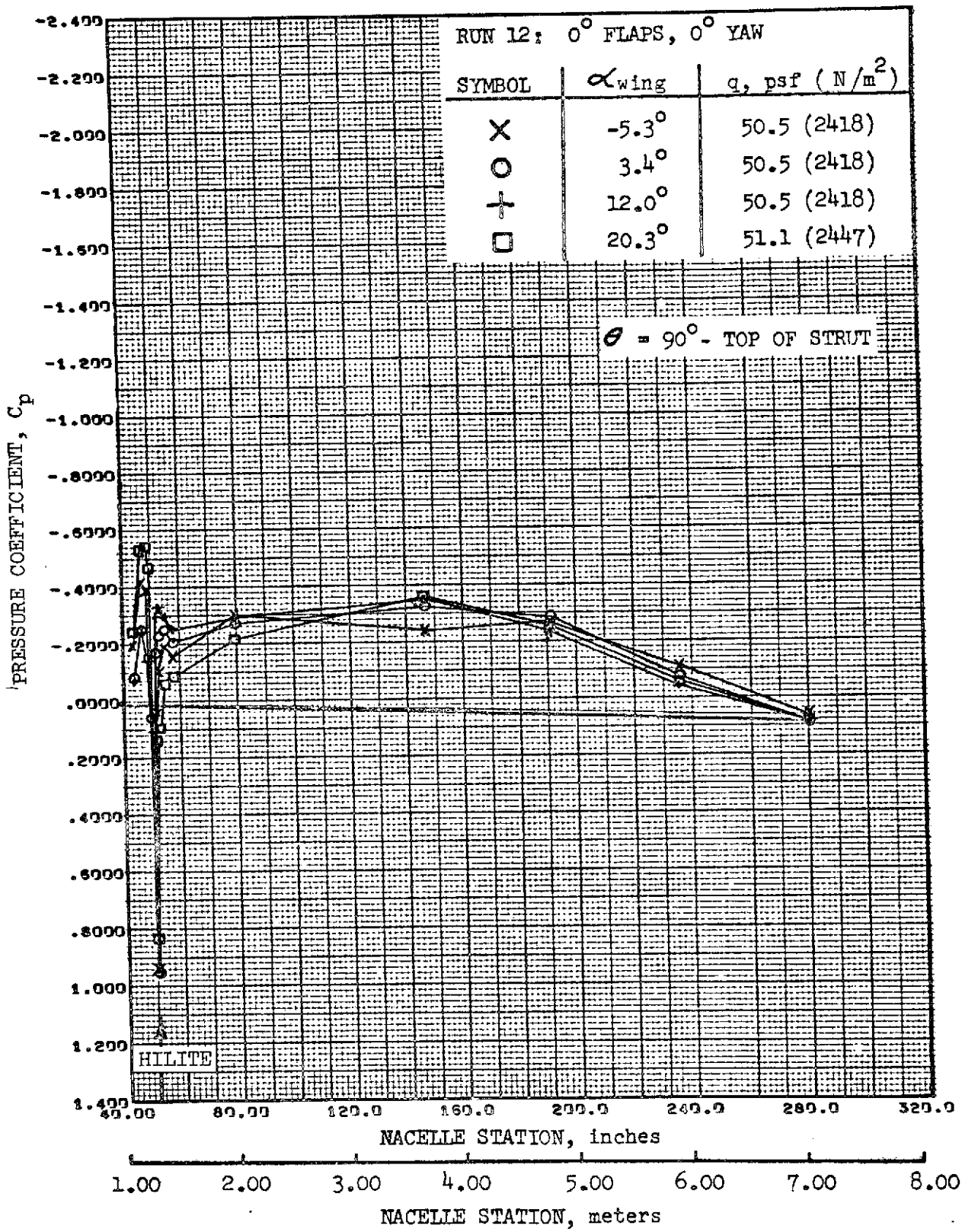

FIGURE 13. -REFAN NACELLE PRESSURE COEFFICIENT DISTRIBUTION, INBOARD SIDE-ABOVE STRUT

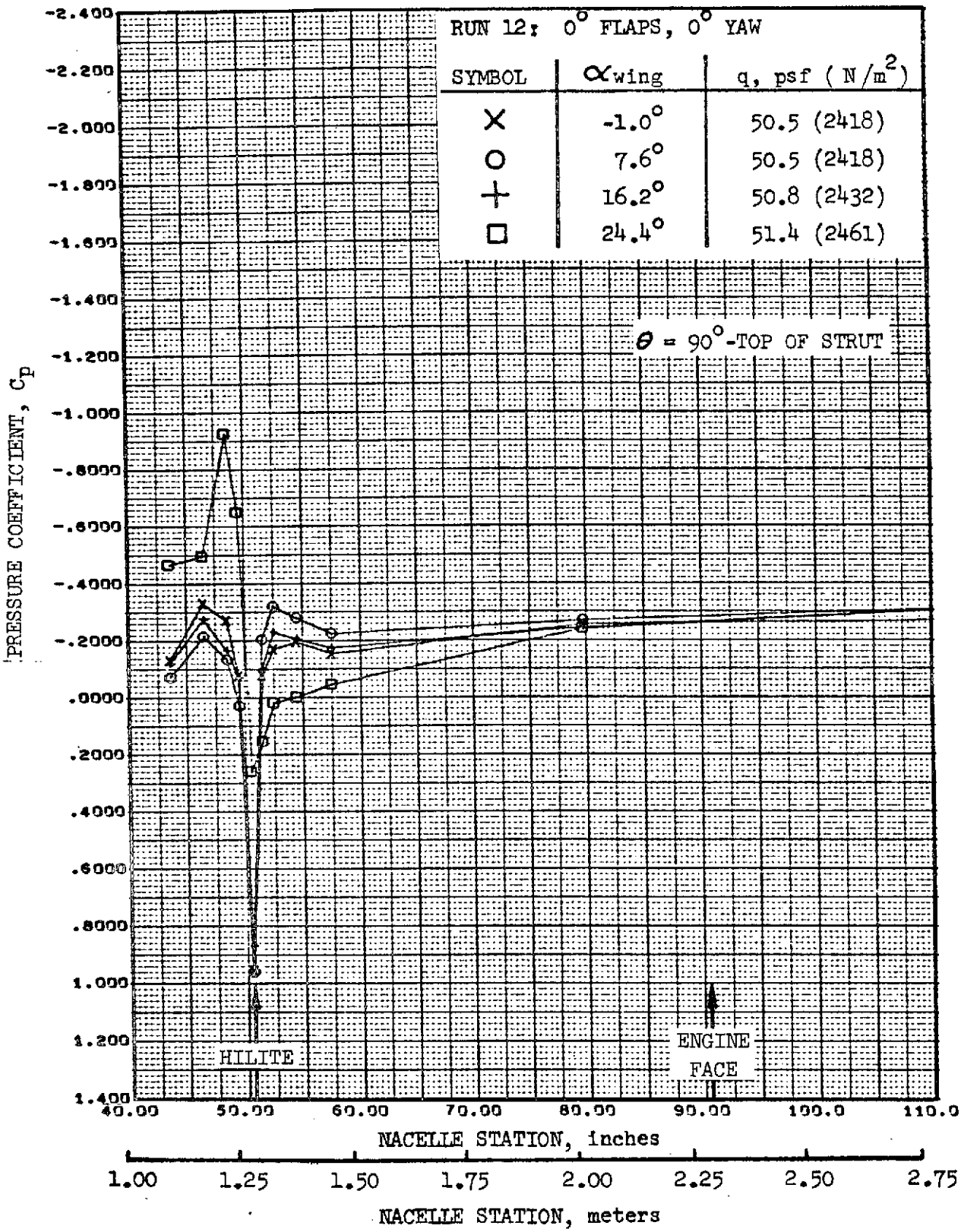

FIGURE 14. -REFAN NACELLE INLET COWL PRESSURE COEFFICIENT DISTRIBUTION, INBOARD SIDE-ABOVE STRUT

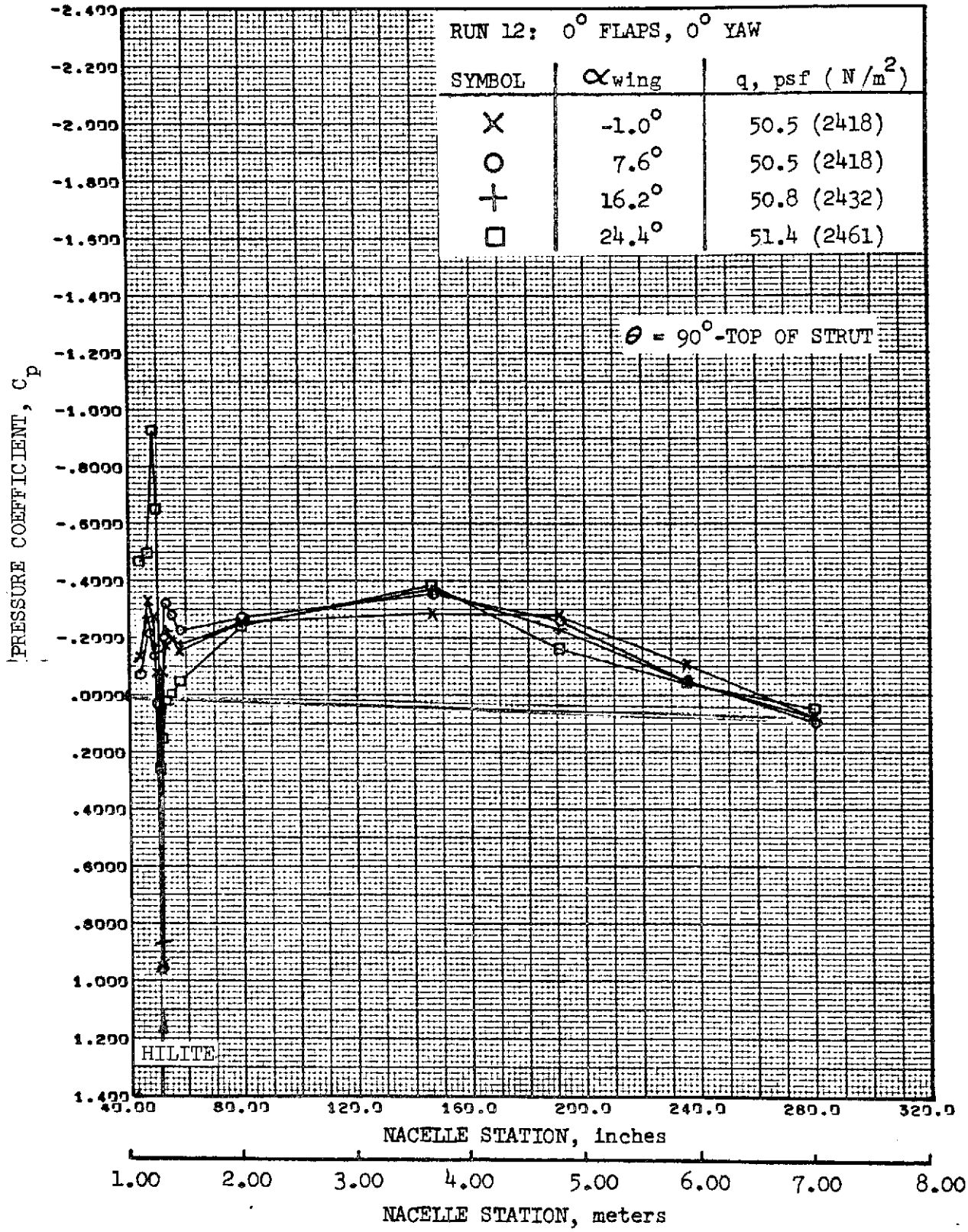

FIGURE 15. -REFAN NACELLE PRESSURE COEFFICIENT DISTRIBUTION, INBOARD SIDE-ABOVE STRUT

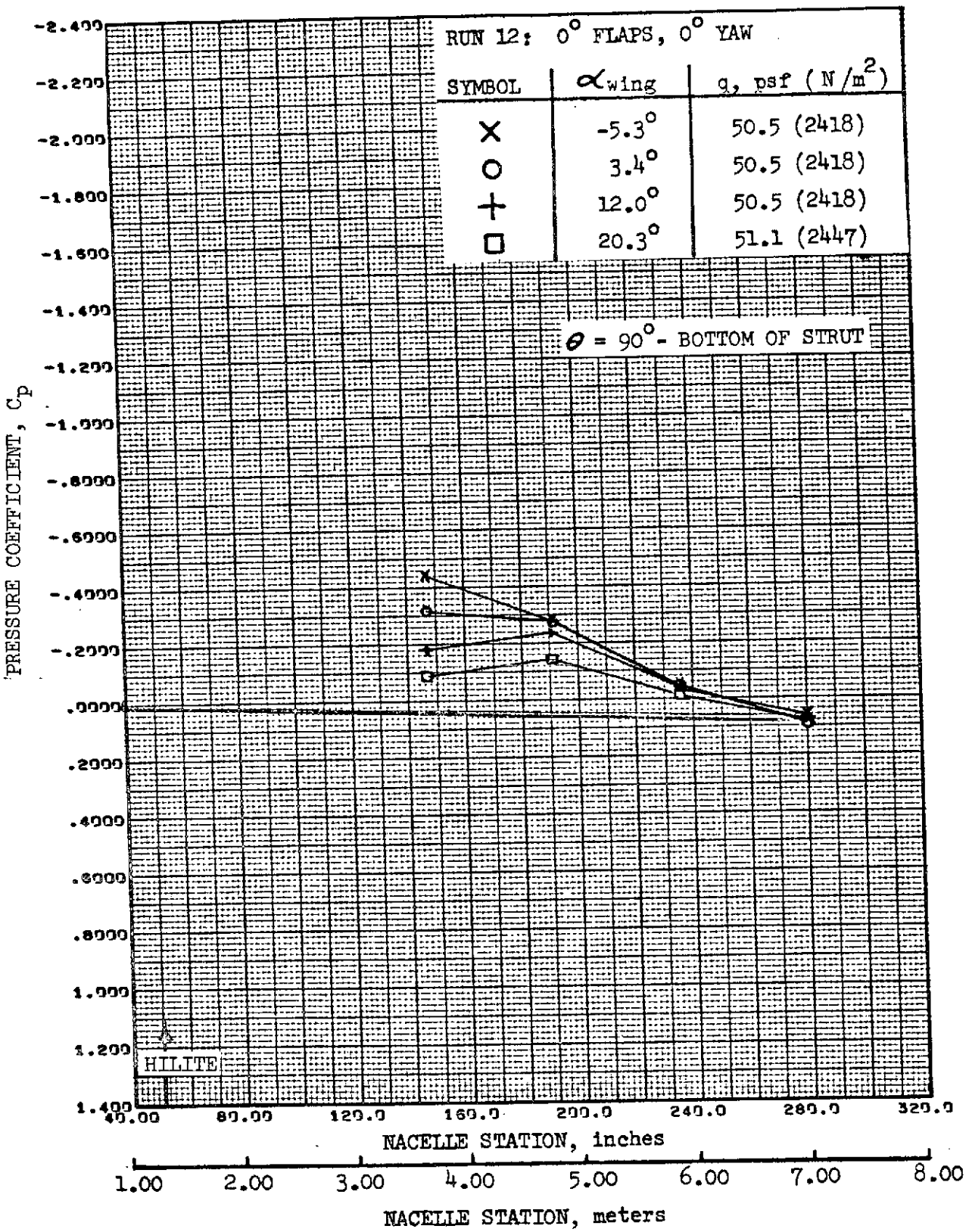

FIGURE 16. -REFAN NACELLE PRESSURE COEFFICIENT DISTRIBUTION, INBOARD SIDE-BELOW STRUT

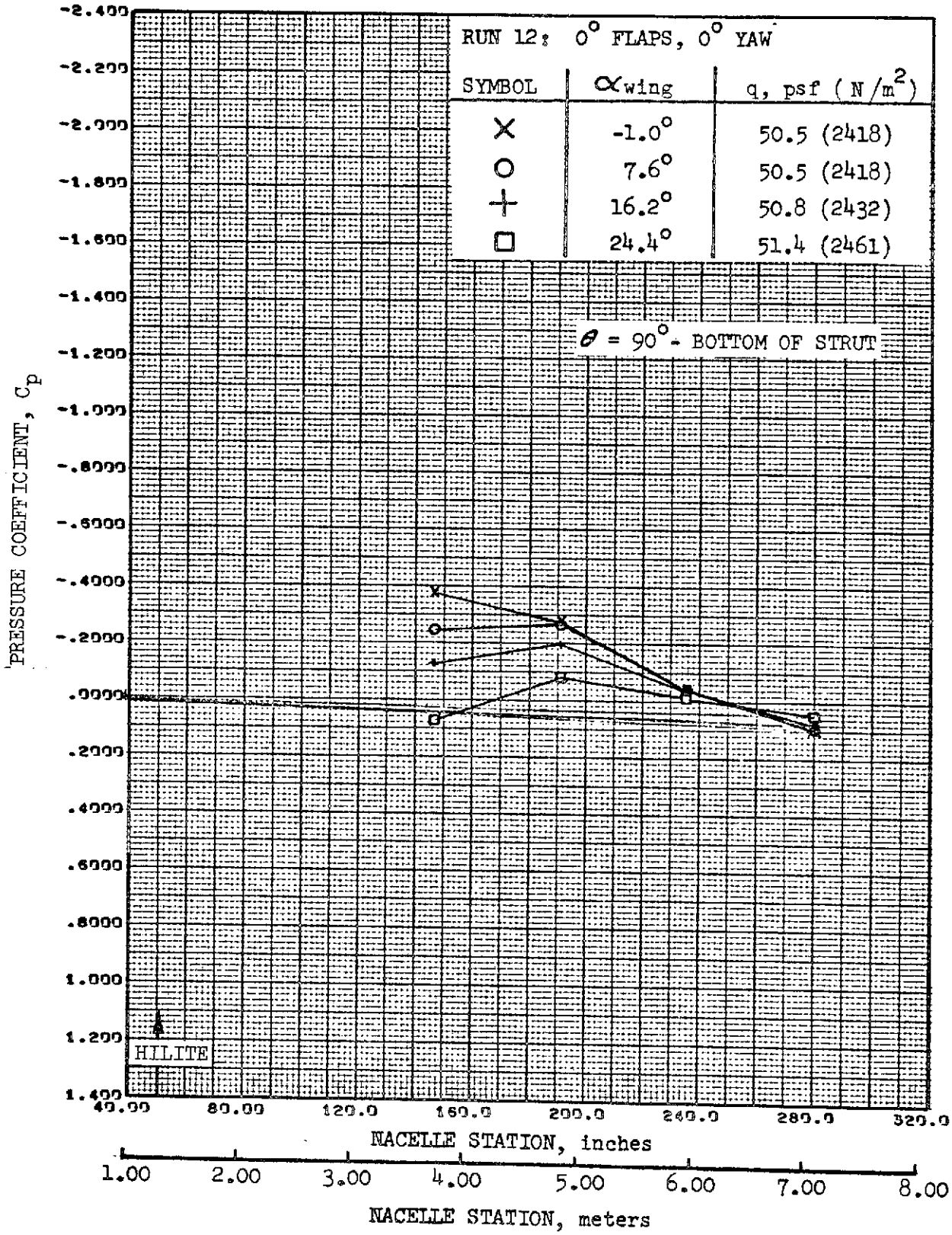

FIGURE 17. -REFAN NACELLE PRESSURE COEFFICIENT DISTRIBUTION, INBOARD SIDE-BELOW STRUT

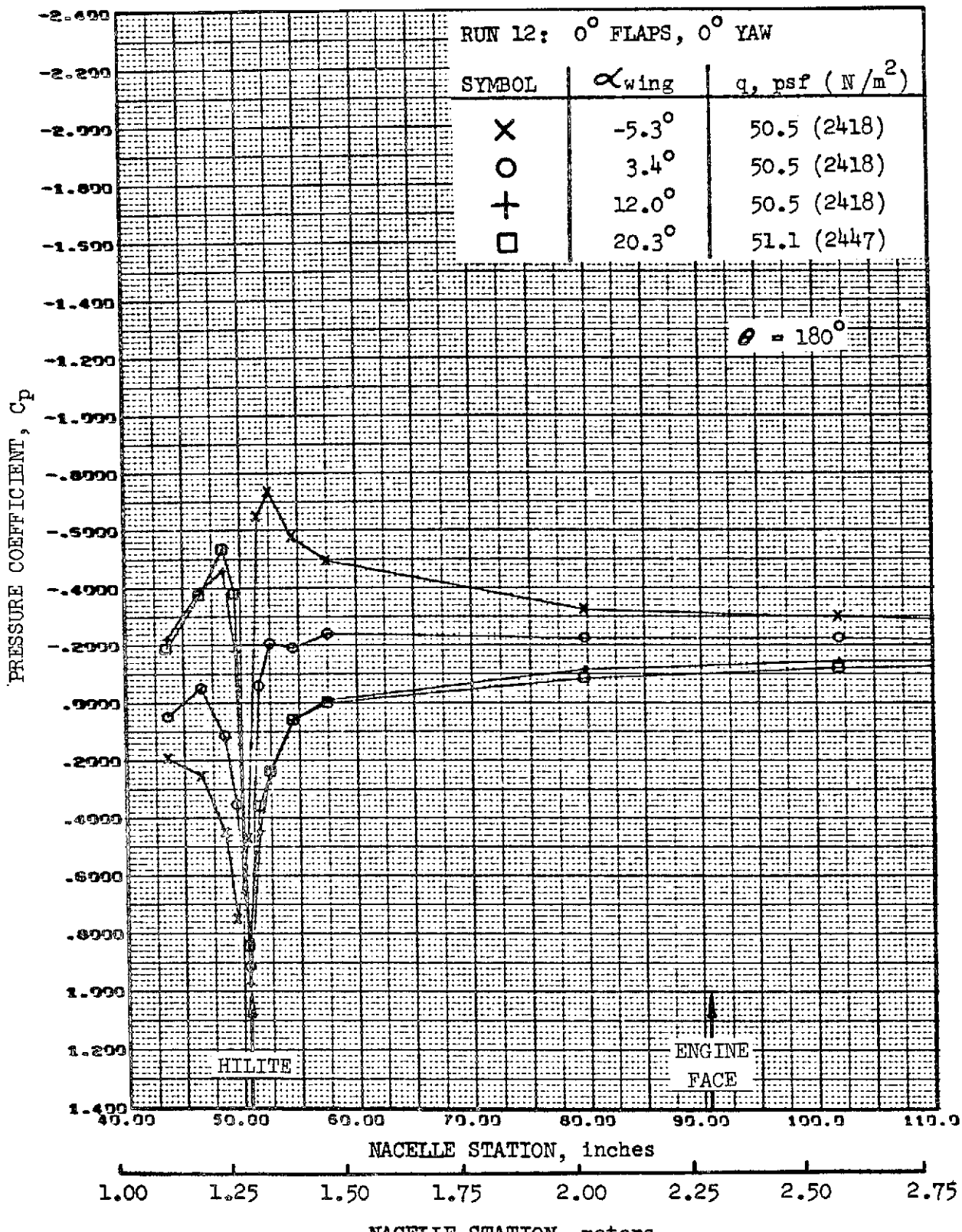

FIGURE 18. -REFAN NACELLE INLET COWL PRESSURE COEFFICIENT DISTRIBUTION, BOTTOM LONGITUDINAL

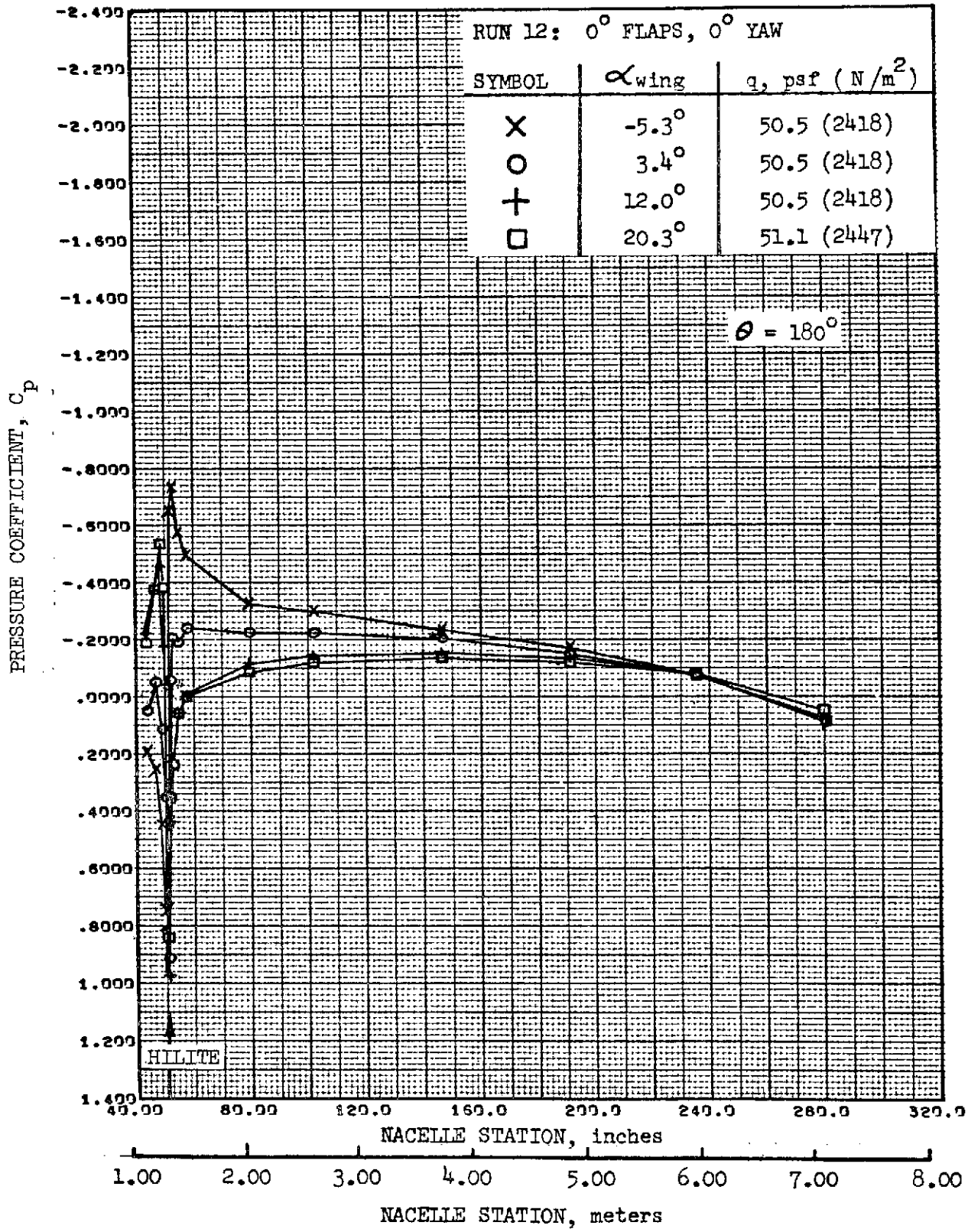

FIGURE 19. -REFAN NACELLE PRESSURE COEFFICIENT DISTRIBUTION, BOTTOM LONGITUDINAL

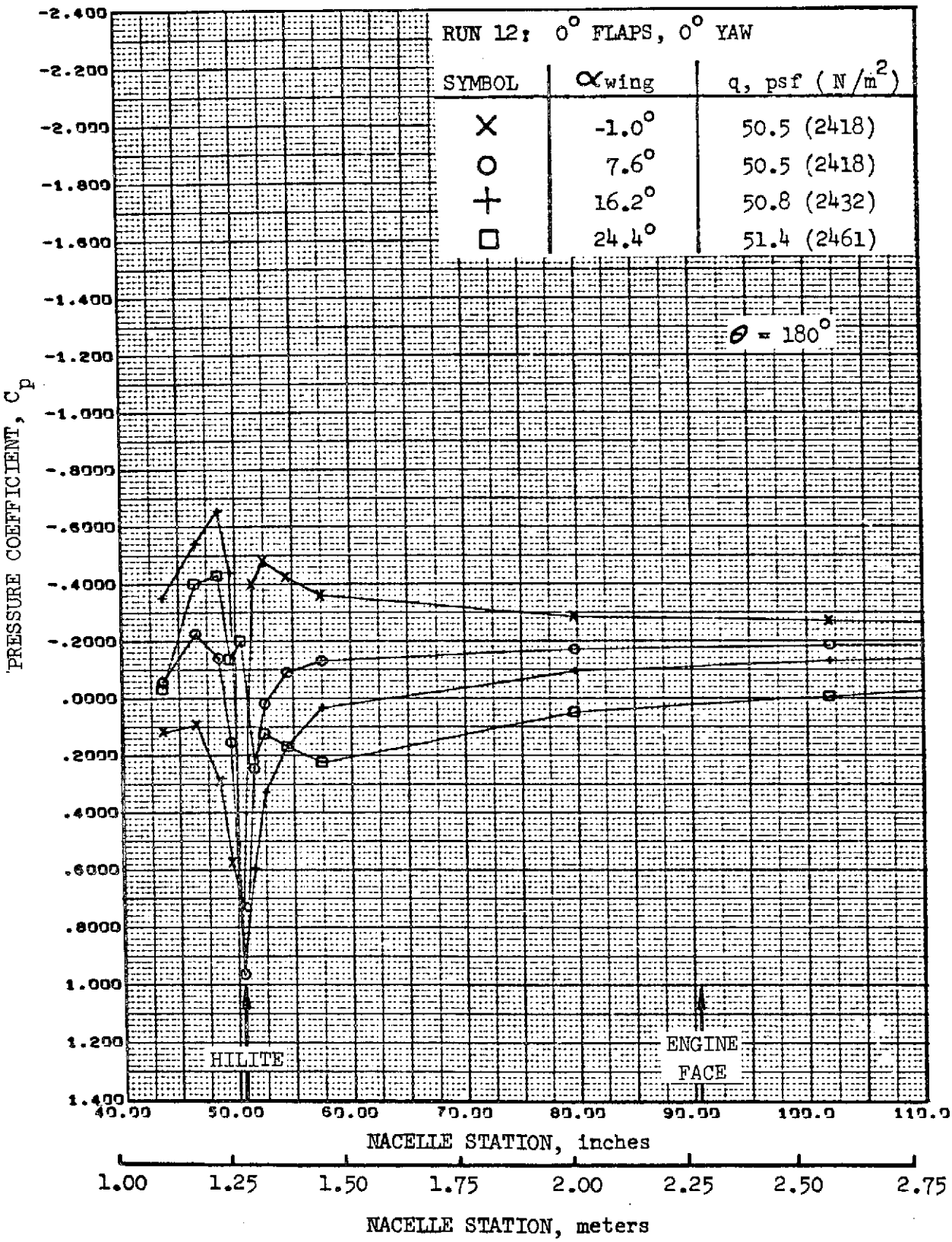

FIGURE 20. -REFAN NACELLE INLET COWL PRESSURE COEFFICIENT DISTRIBUTION, BOTTOM LONGITUDINAL

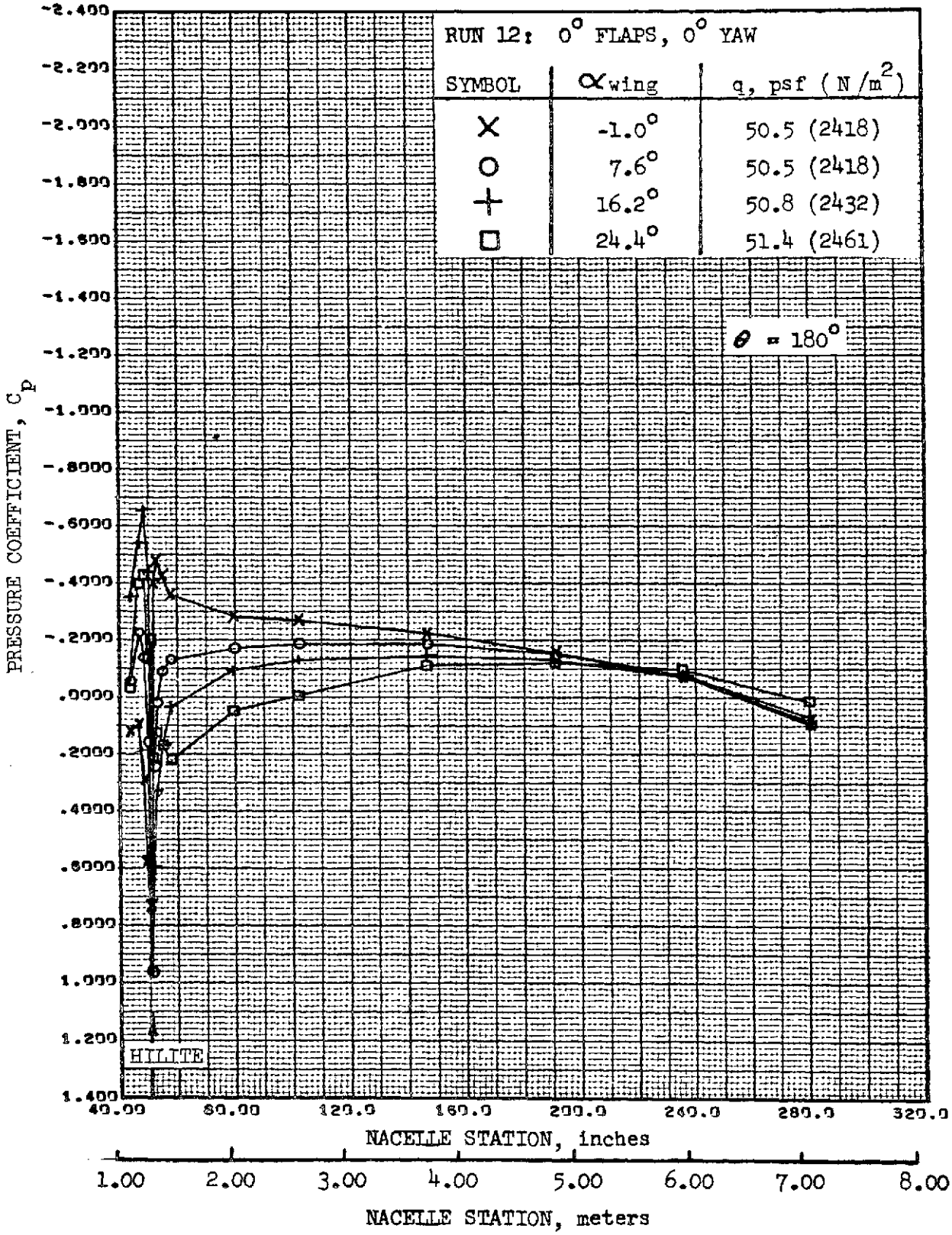

FIGURE 21. -REFAN NACELLE PRESSURE COEFFICIENT DISTRIBUTION, BOTTOM LONGITUDINAL

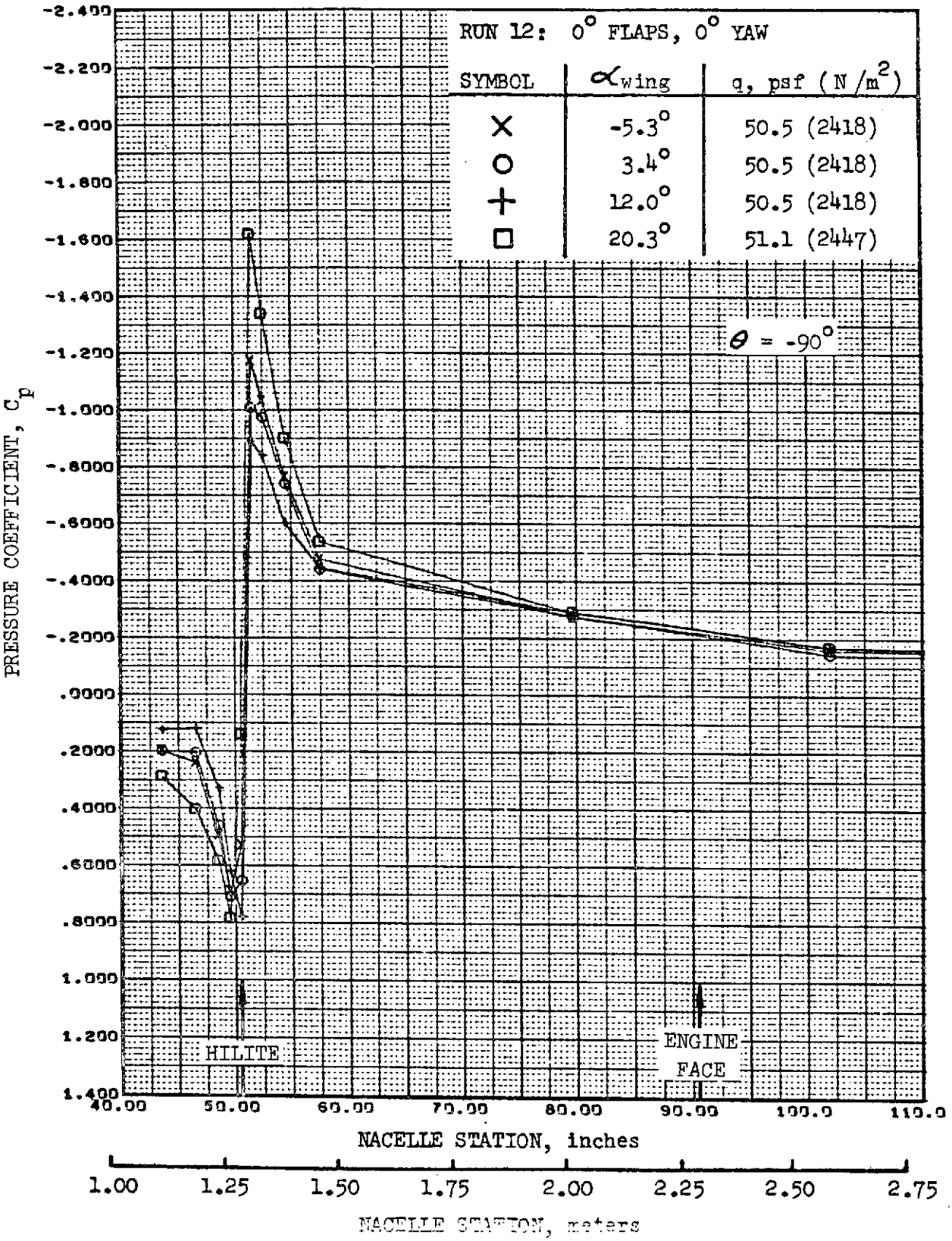

FIGURE 22. -REFAN NACELLE INLET COWL PRESSURE COEFFICIENT DISTRIBUTION, OUTBOARD SIDE

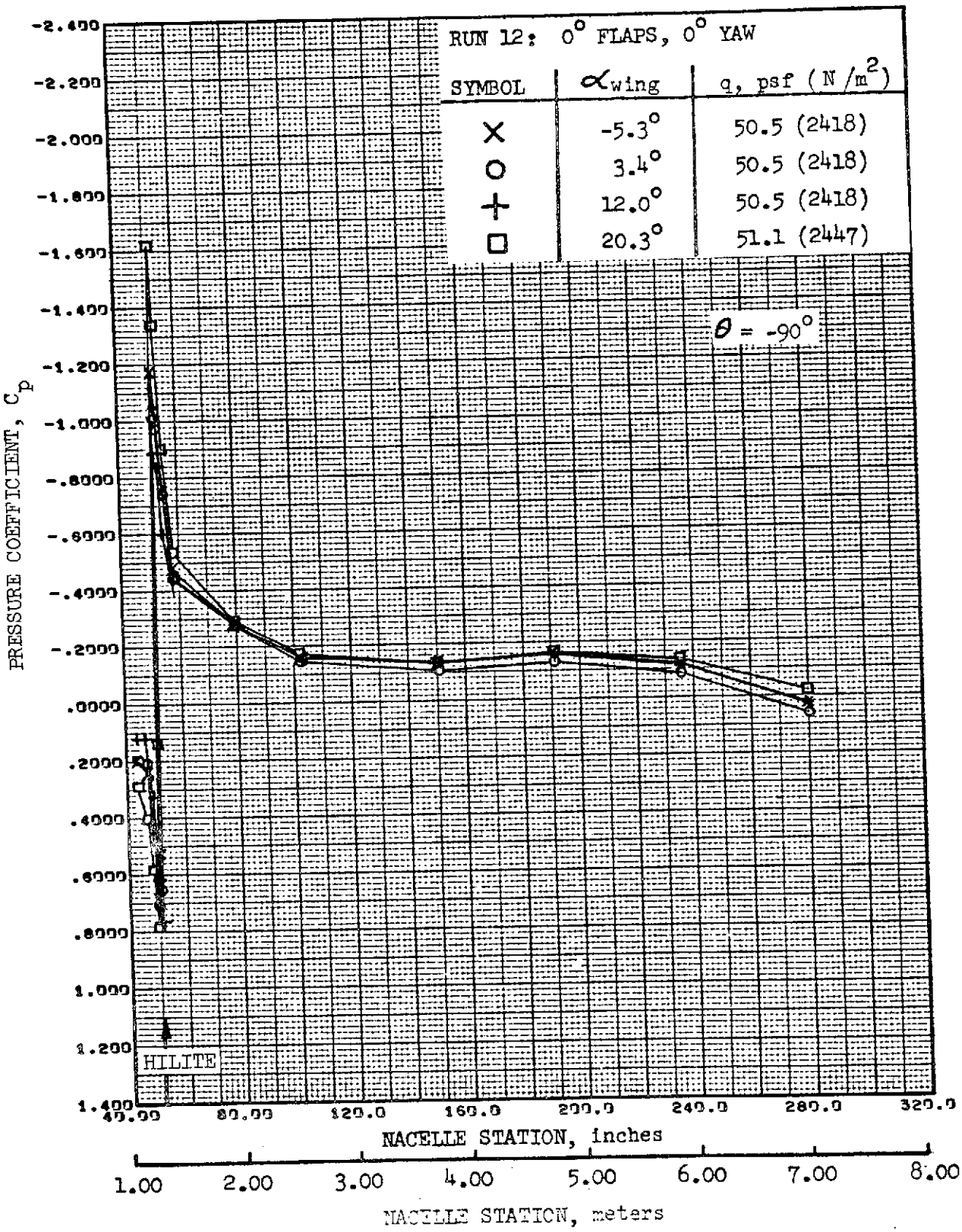

FIGURE 23. -REFAN NACELLE PRESSURE COEFFICIENT DISTRIBUTION, OUTBOARD SIDE

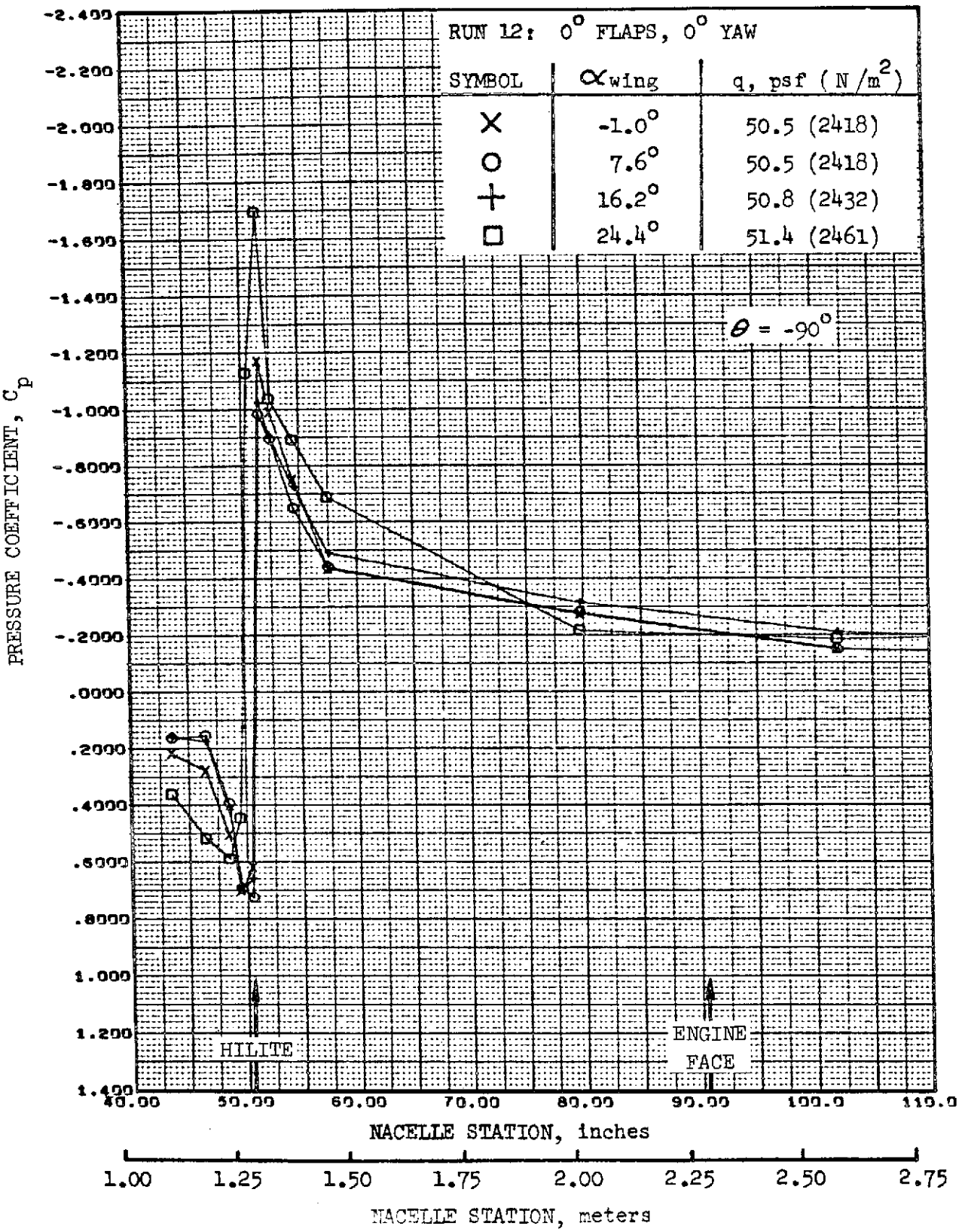

FIGURE 24. -REFAN NACELLE INLET COWL PRESSURE COEFFICIENT DISTRIBUTION, OUTBOARD SIDE

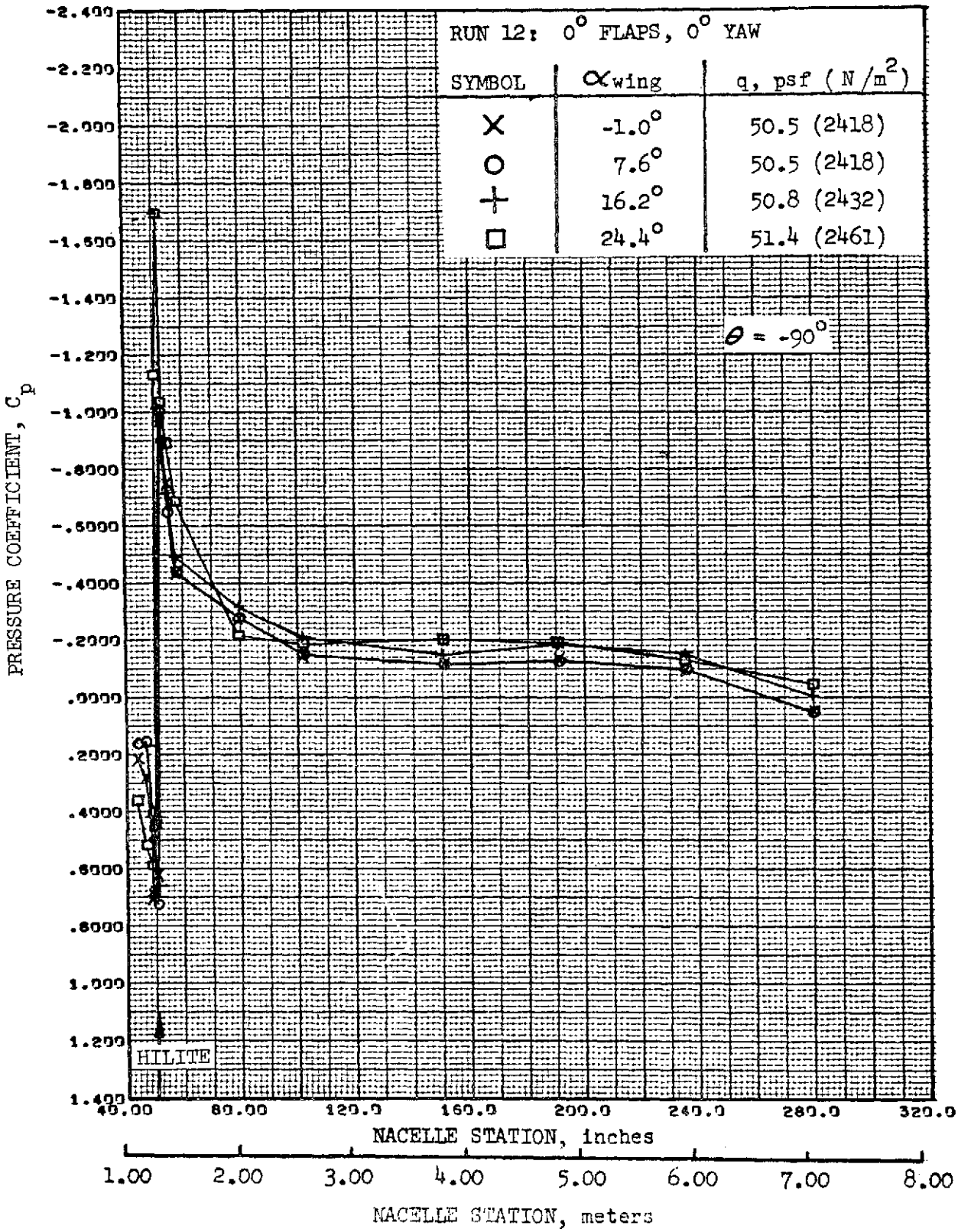

FIGURE 25. -REFAN NACELLE PRESSURE COEFFICIENT DISTRIBUTION, OUTBOARD SIDE

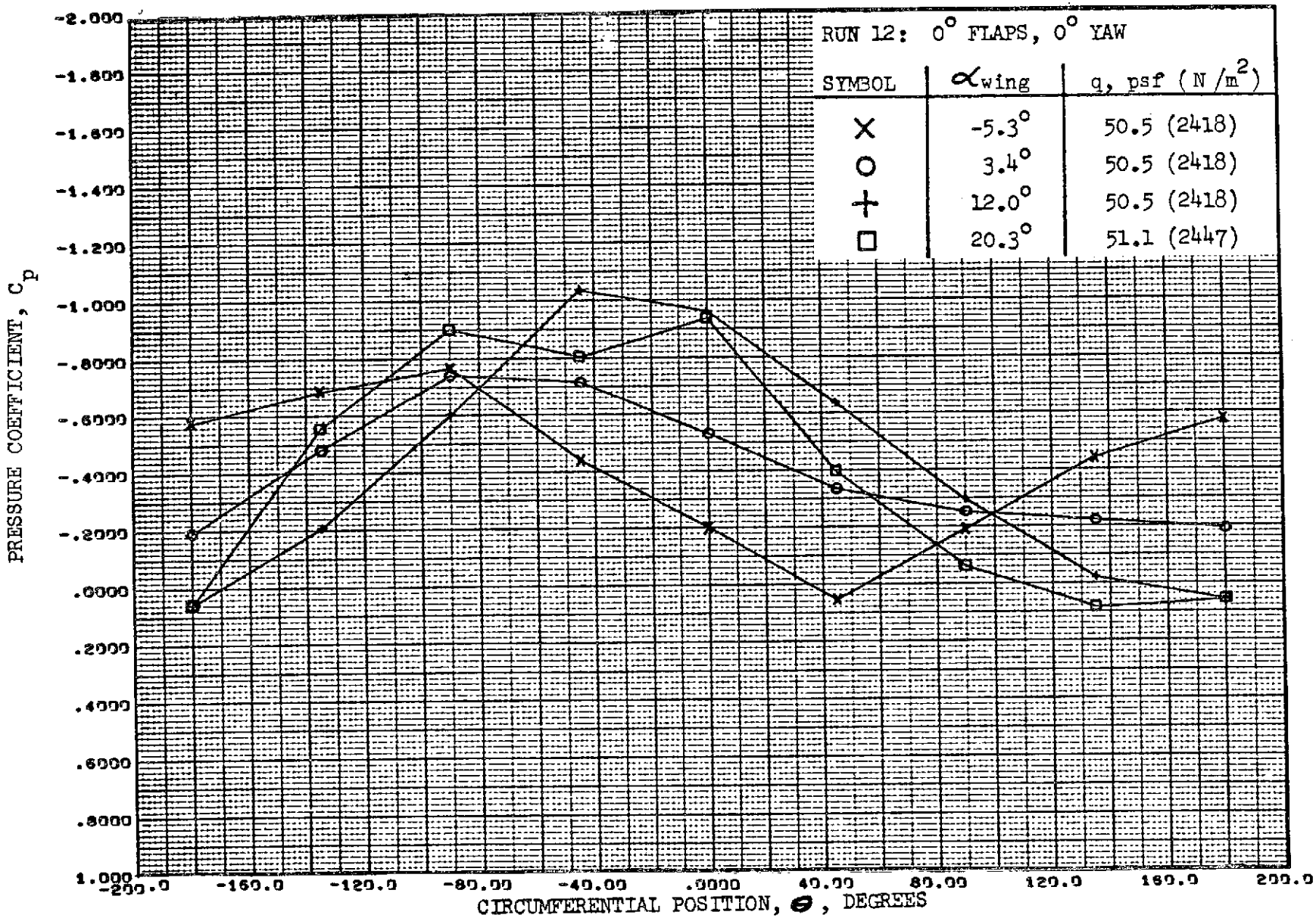

FIGURE 26. - REFAN NACELLE PRESSURE COEFFICIENT DISTRIBUTION, EXTERNAL CIRCUMFERENTIAL AT STATION 54.5 INCHES (1.38 METERS)

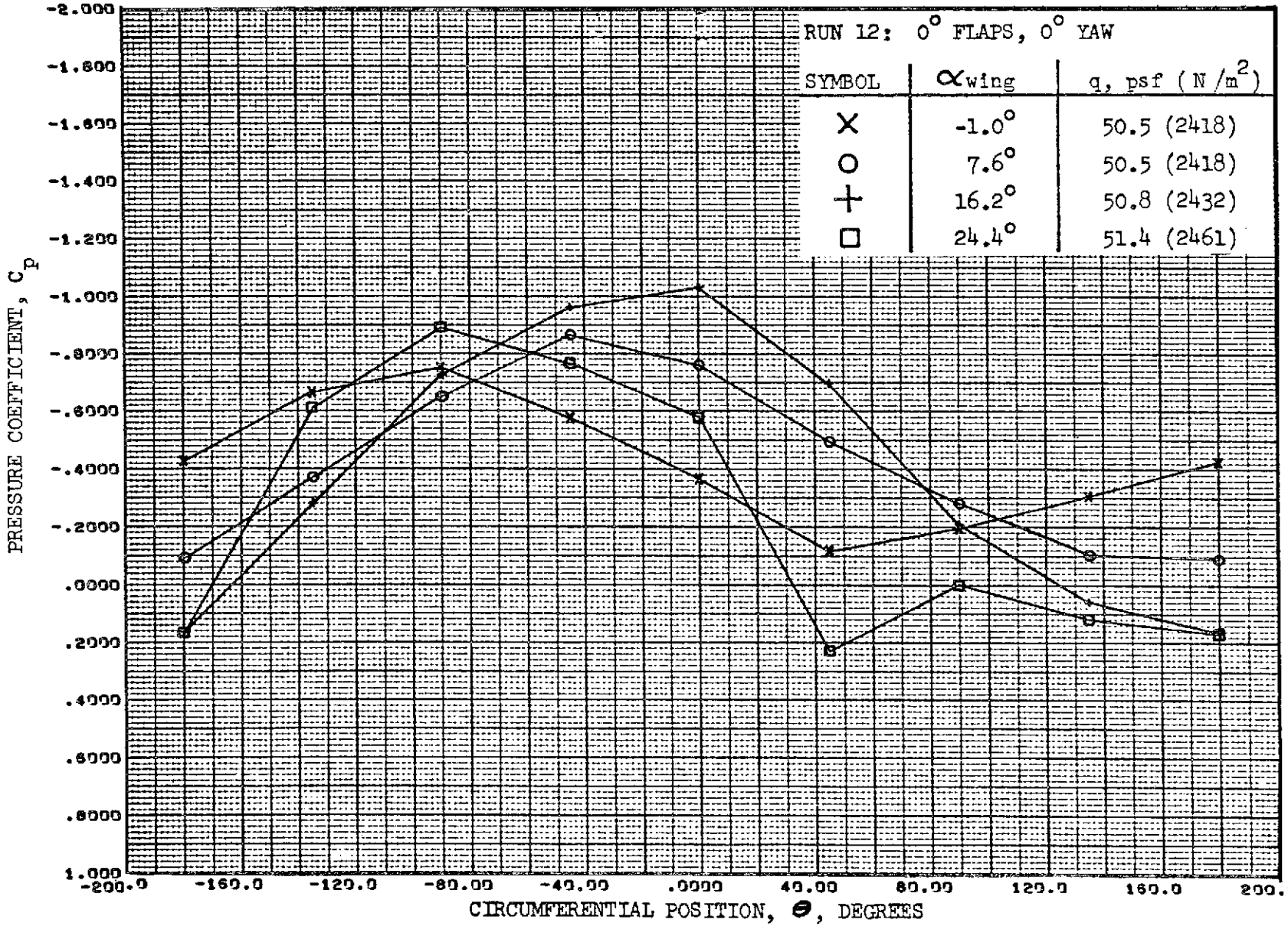

FIGURE 27. - REFAN NACELLE PRESSURE COEFFICIENT DISTRIBUTION, EXTERNAL CIRCUMFERENTIAL AT STATION 54.5 INCHES (1.38 METERS)

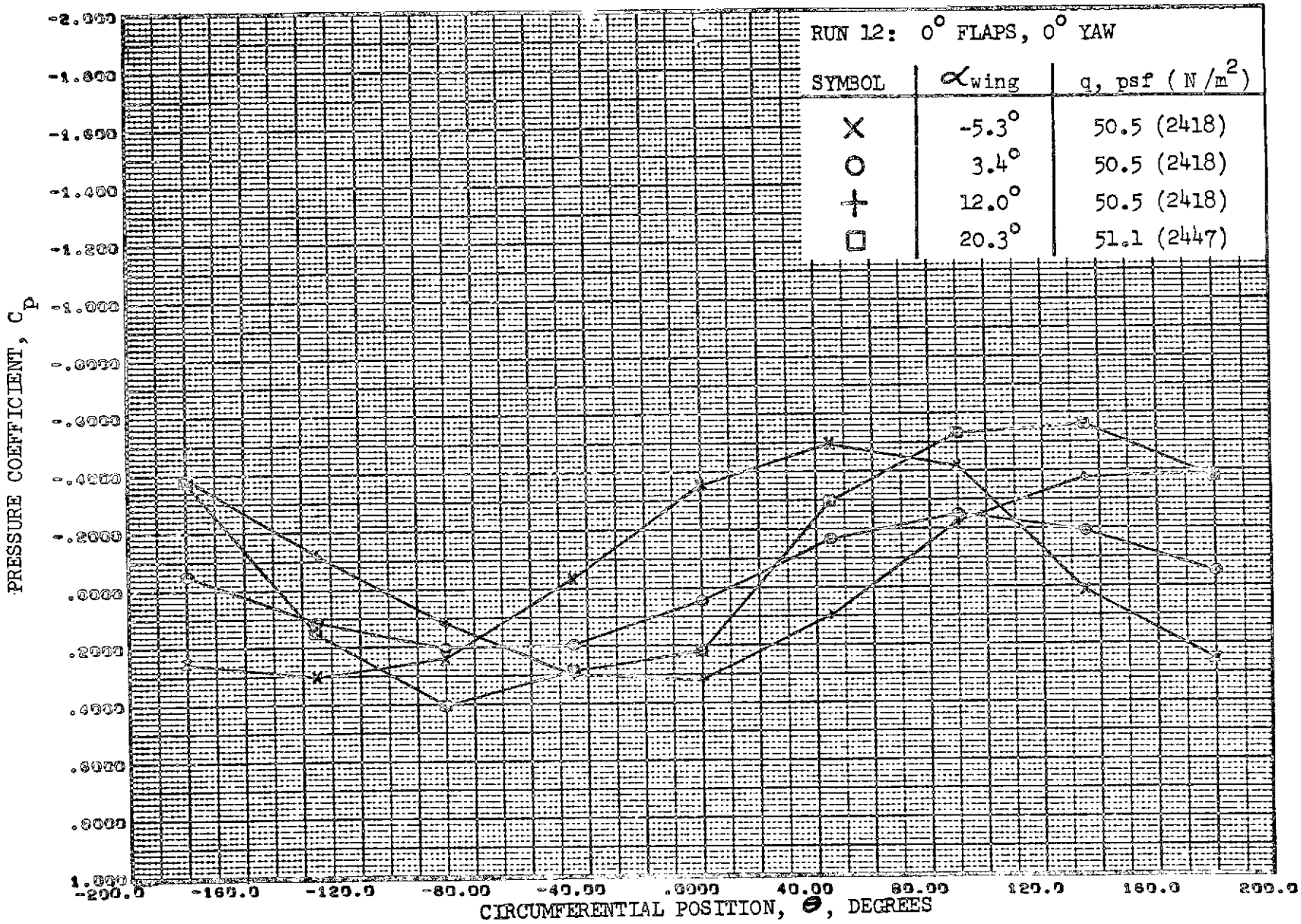

FIGURE 28. - REFAN NACELLE PRESSURE COEFFICIENT DISTRIBUTION, INTERNAL CIRCUMFERENTIAL AT STATION 54.5 INCHES (1.38 METERS)

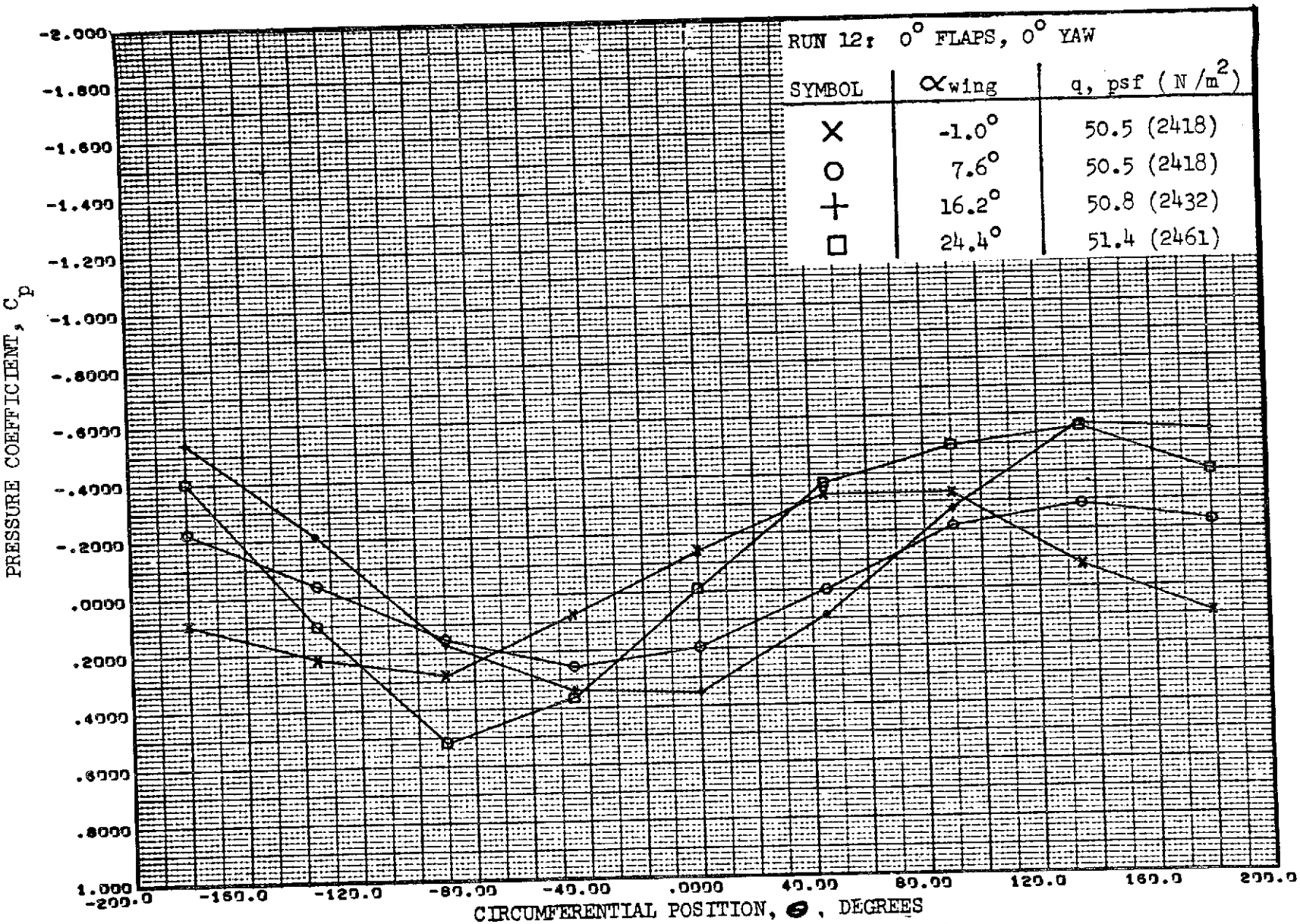

FIGURE 29. - REFAN NACELLE PRESSURE COEFFICIENT DISTRIBUTION, INTERNAL CIRCUMFERENTIAL AT STATION 54.5 INCHES (1.38 METERS)

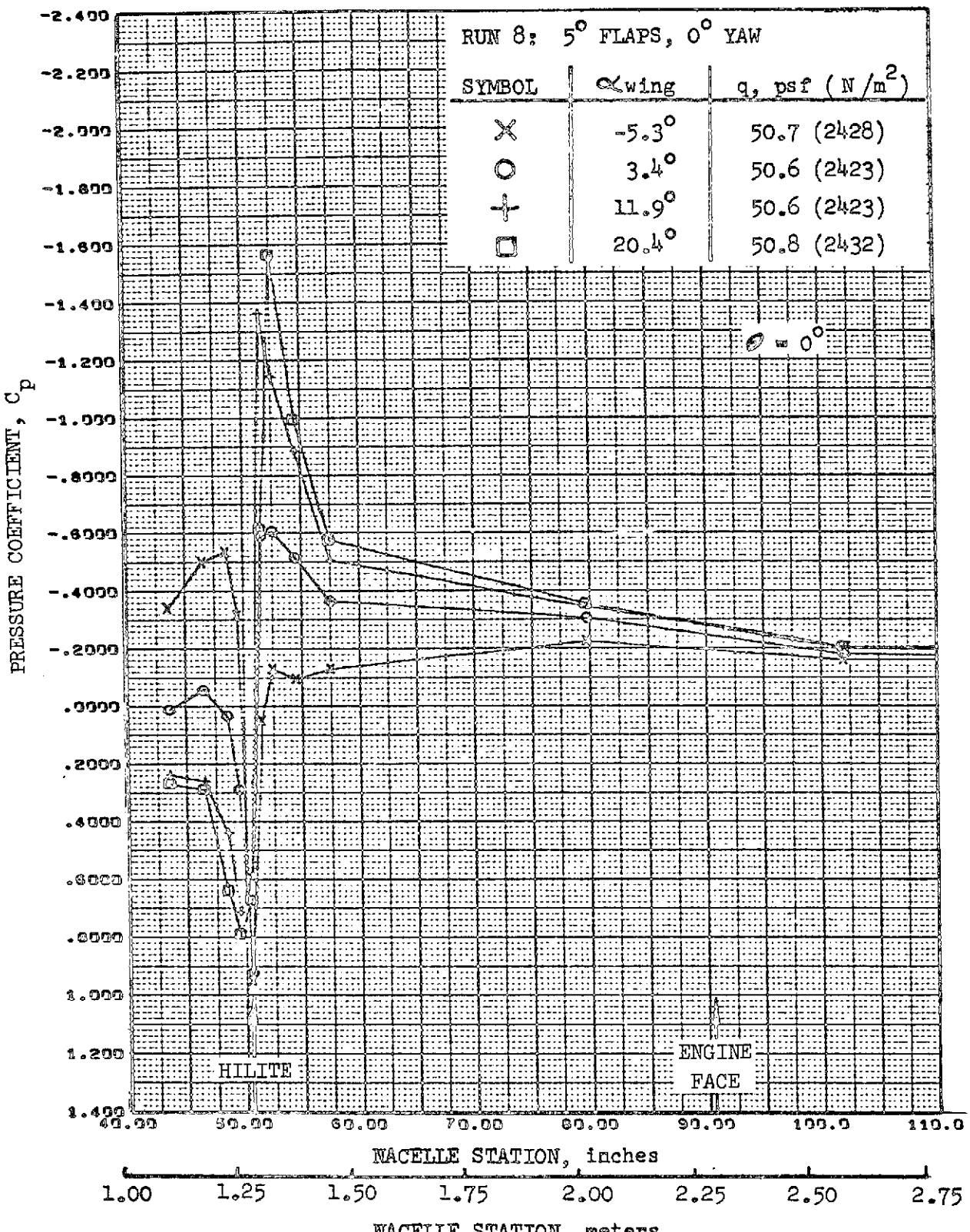

FIGURE 30. -REFAN NACELLE INLET COWL PRESSURE COEFFICIENT DISTRIBUTION, TOP LONGITUDINAL

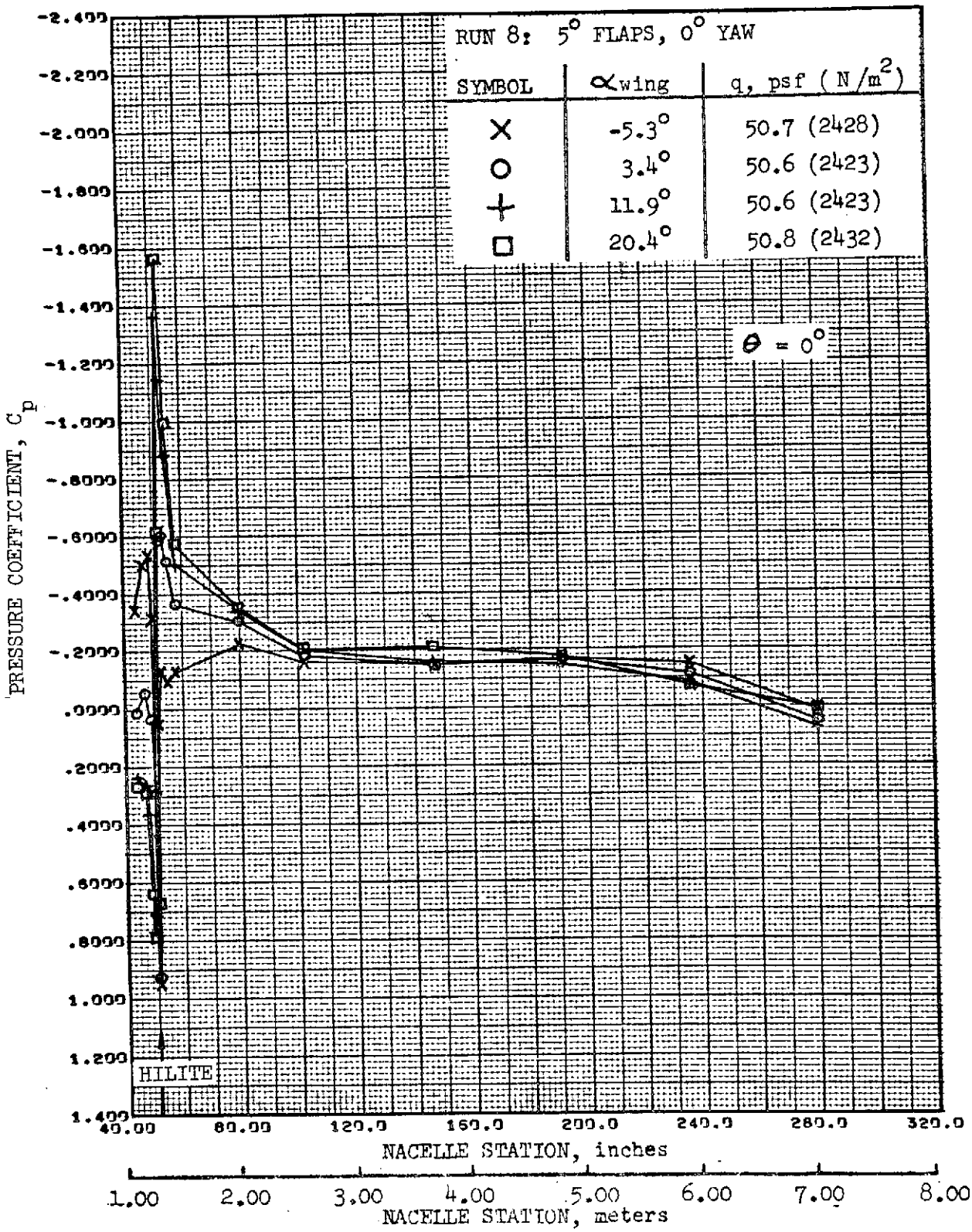

FIGURE 31. -REFAN NACELLE PRESSURE COEFFICIENT DISTRIBUTION, TOP LONGITUDINAL

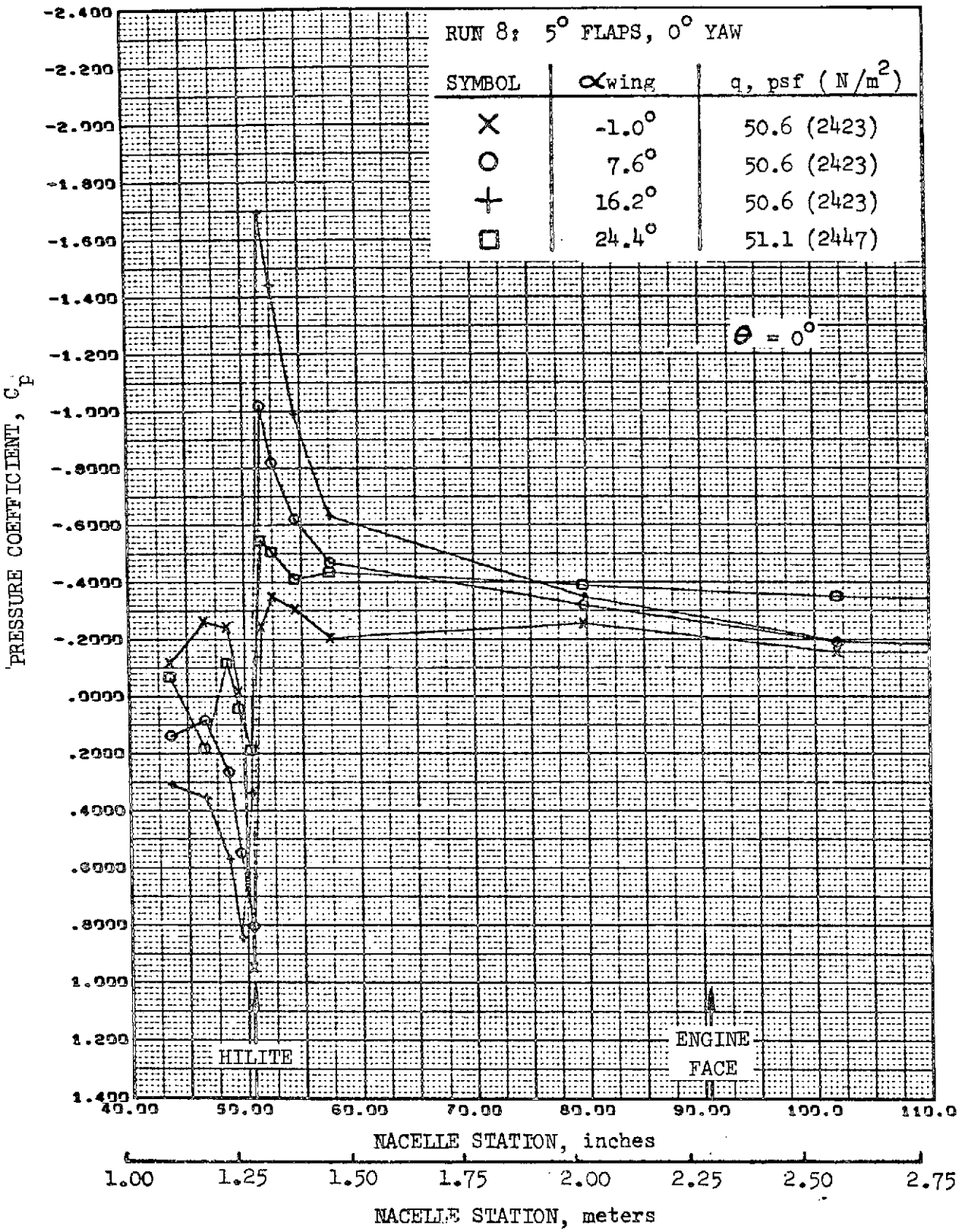

FIGURE 32. -REFAN NACELLE INLET COWL PRESSURE COEFFICIENT DISTRIBUTION, TOP LONGITUDINAL

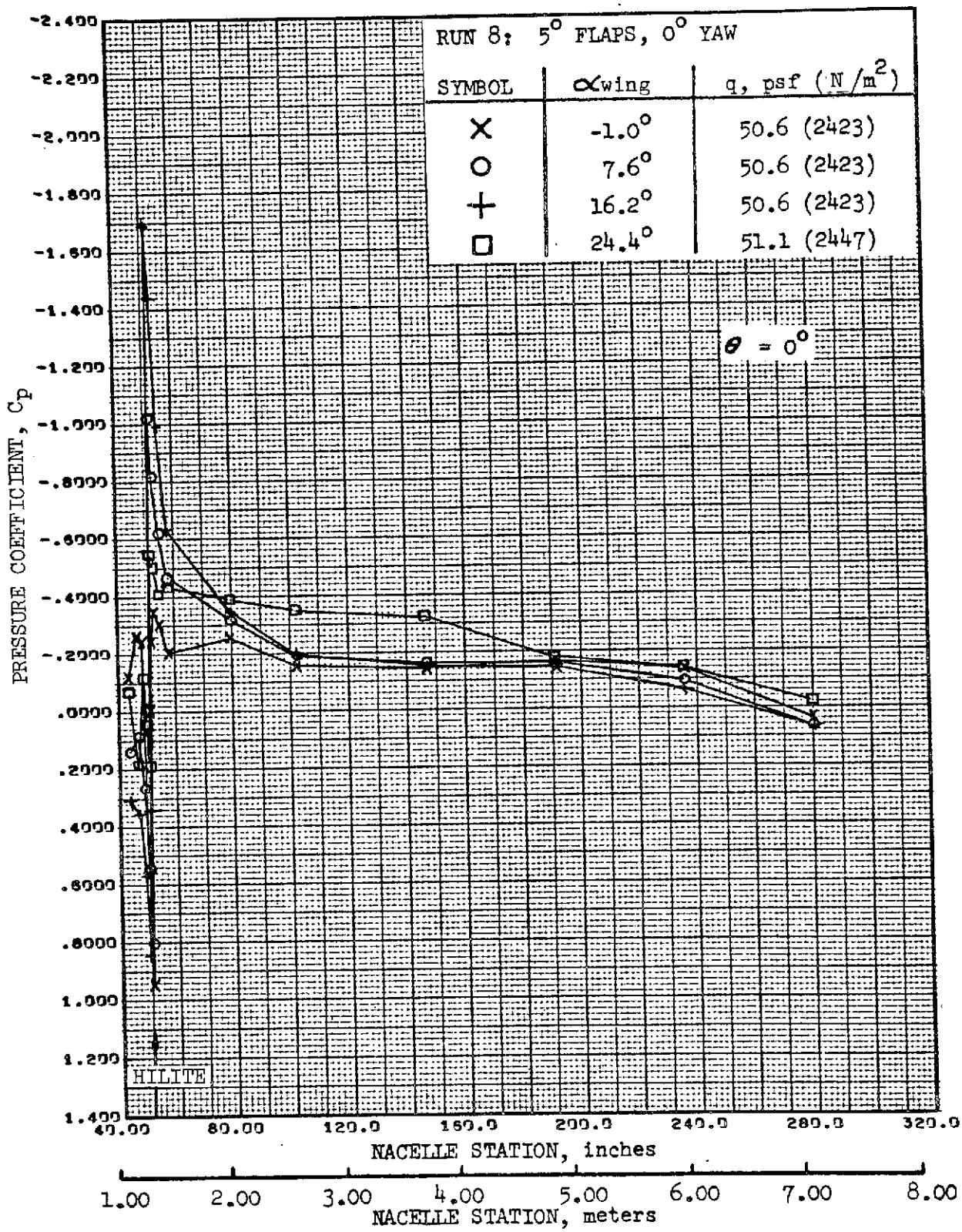

FIGURE 33. -REFAN NACELLE PRESSURE COEFFICIENT DISTRIBUTION, TOP LONGITUDINAL

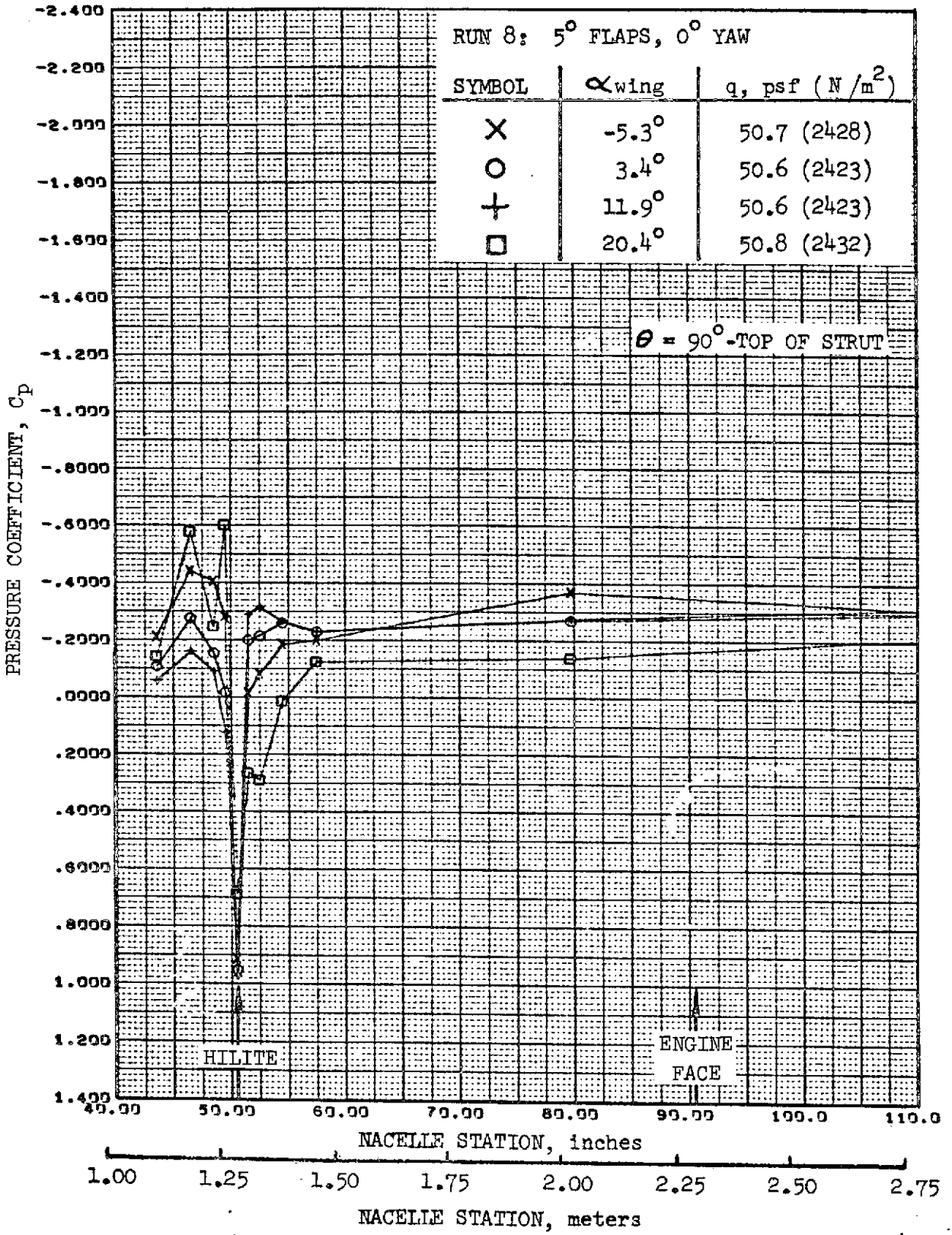

FIGURE 34. -REFAN NACELLE INLET COWL PRESSURE COEFFICIENT DISTRIBUTION, INBOARD SIDE-ABOVE STRUT

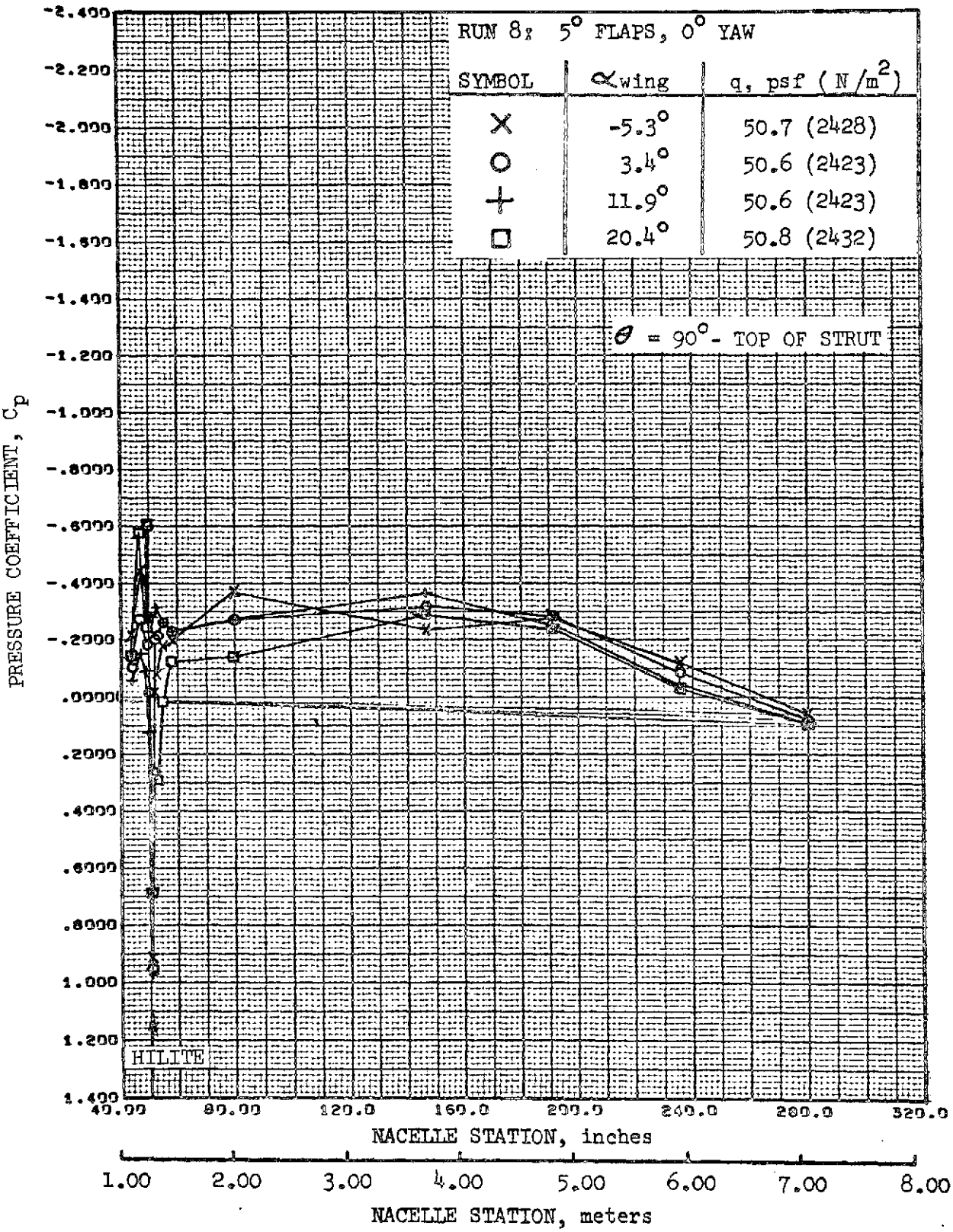

FIGURE 35. -REFAN NACELLE PRESSURE COEFFICIENT DISTRIBUTION, INBOARD SIDE-ABOVE STRUT

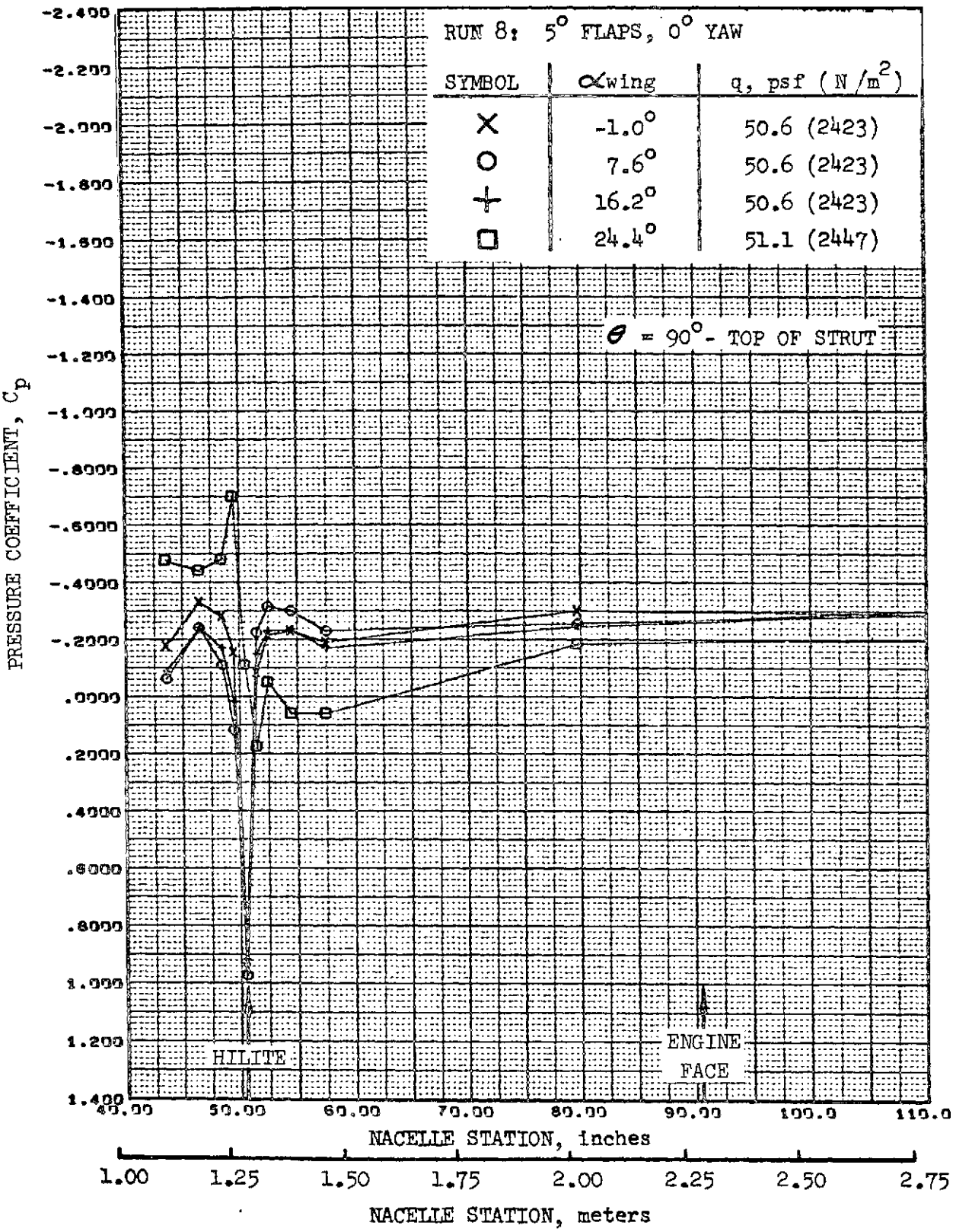

FIGURE 36. -REFAN NACELLE INLET COWL PRESSURE COEFFICIENT DISTRIBUTION, INBOARD SIDE-ABOVE STRUT

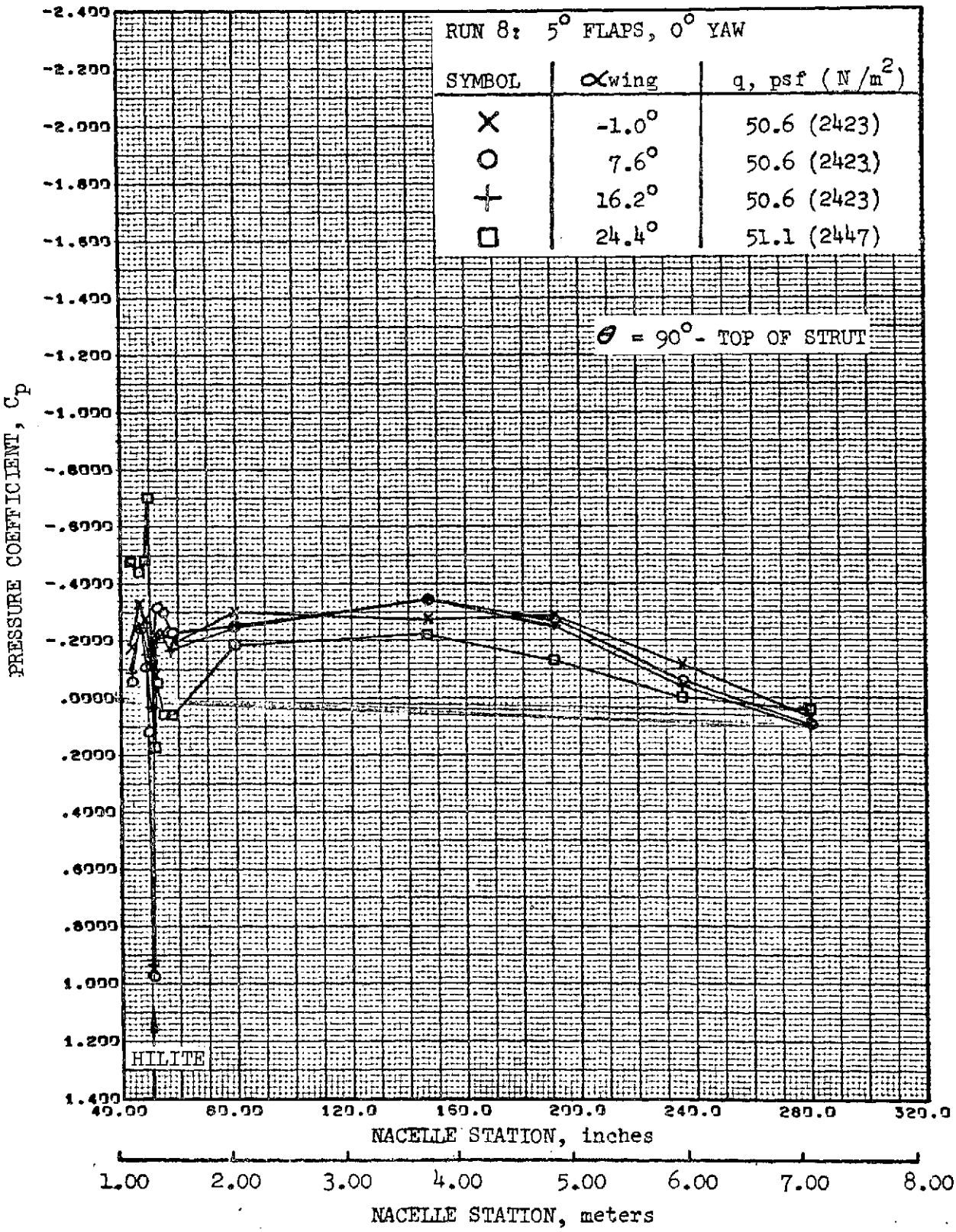

FIGURE 37. -REFAN NACELLE PRESSURE COEFFICIENT DISTRIBUTION, INBOARD SIDE-ABOVE STRUT

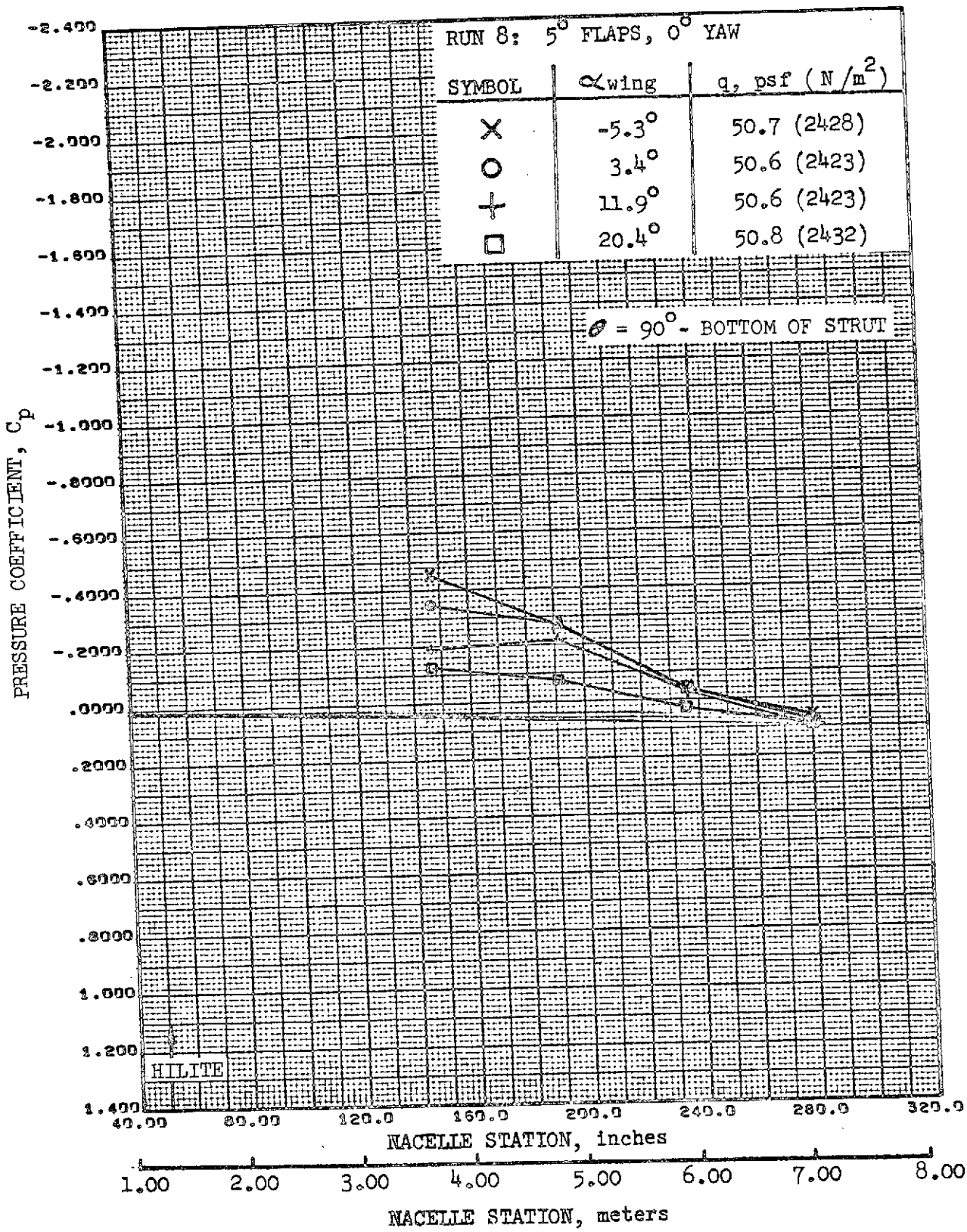

FIGURE 38. -REFAN NACELLE PRESSURE COEFFICIENT DISTRIBUTION, INBOARD SIDE-BELOW STRUT

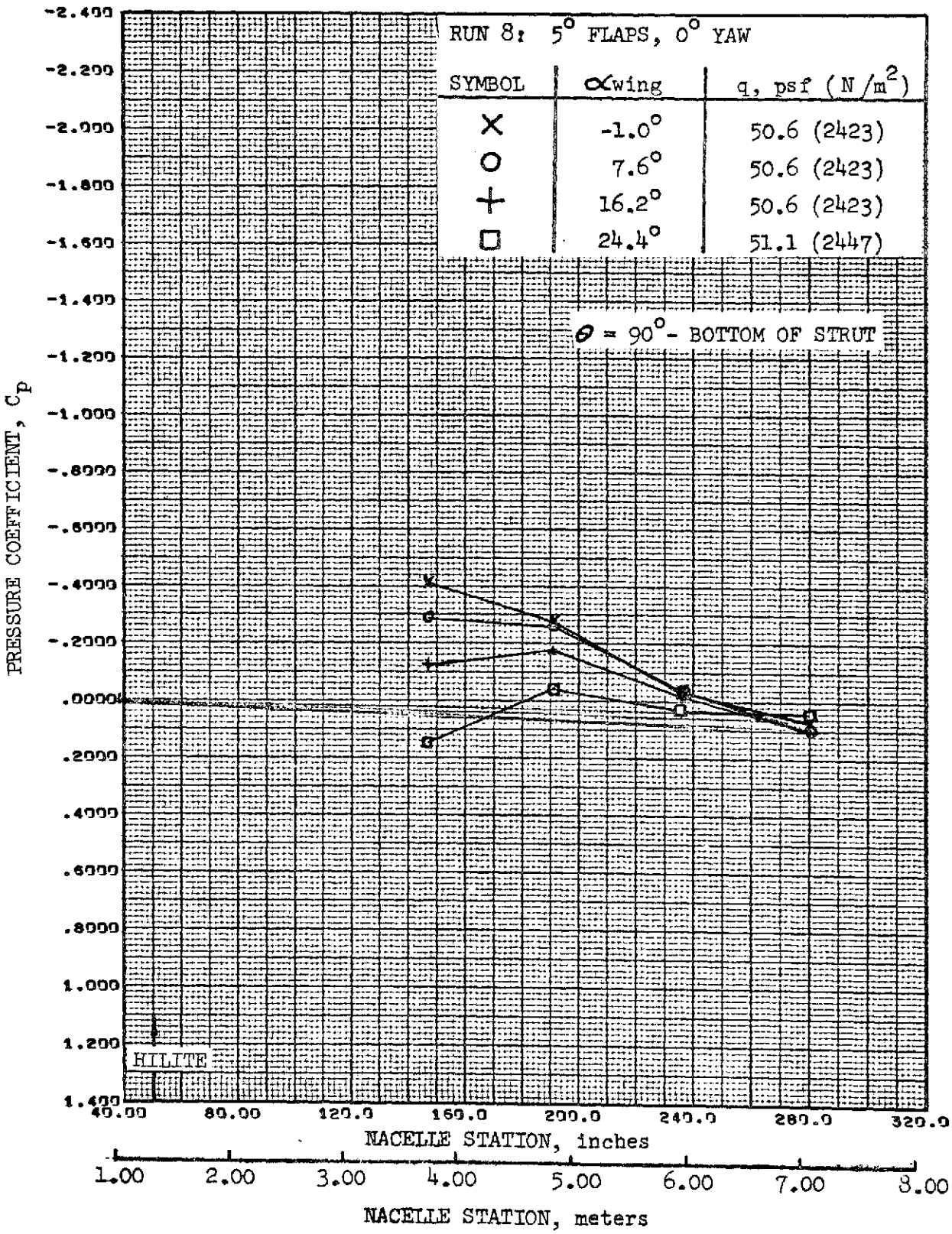

FIGURE 39. -REFAN NACELLE PRESSURE COEFFICIENT DISTRIBUTION, INBOARD SIDE-BELOW STRUT

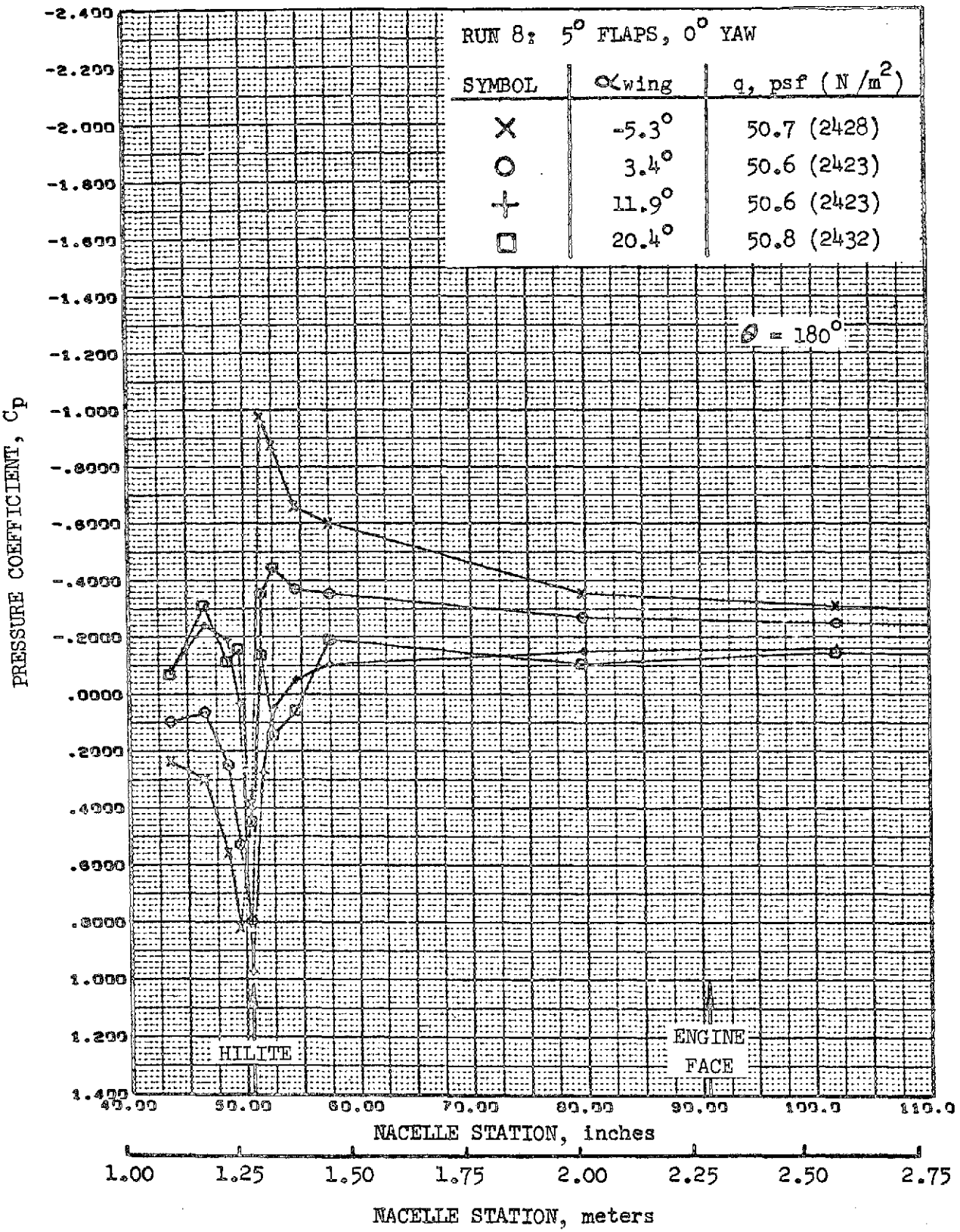

FIGURE 40. -REFAN NACELLE INLET COWL PRESSURE COEFFICIENT DISTRIBUTION, BOTTOM LONGITUDINAL

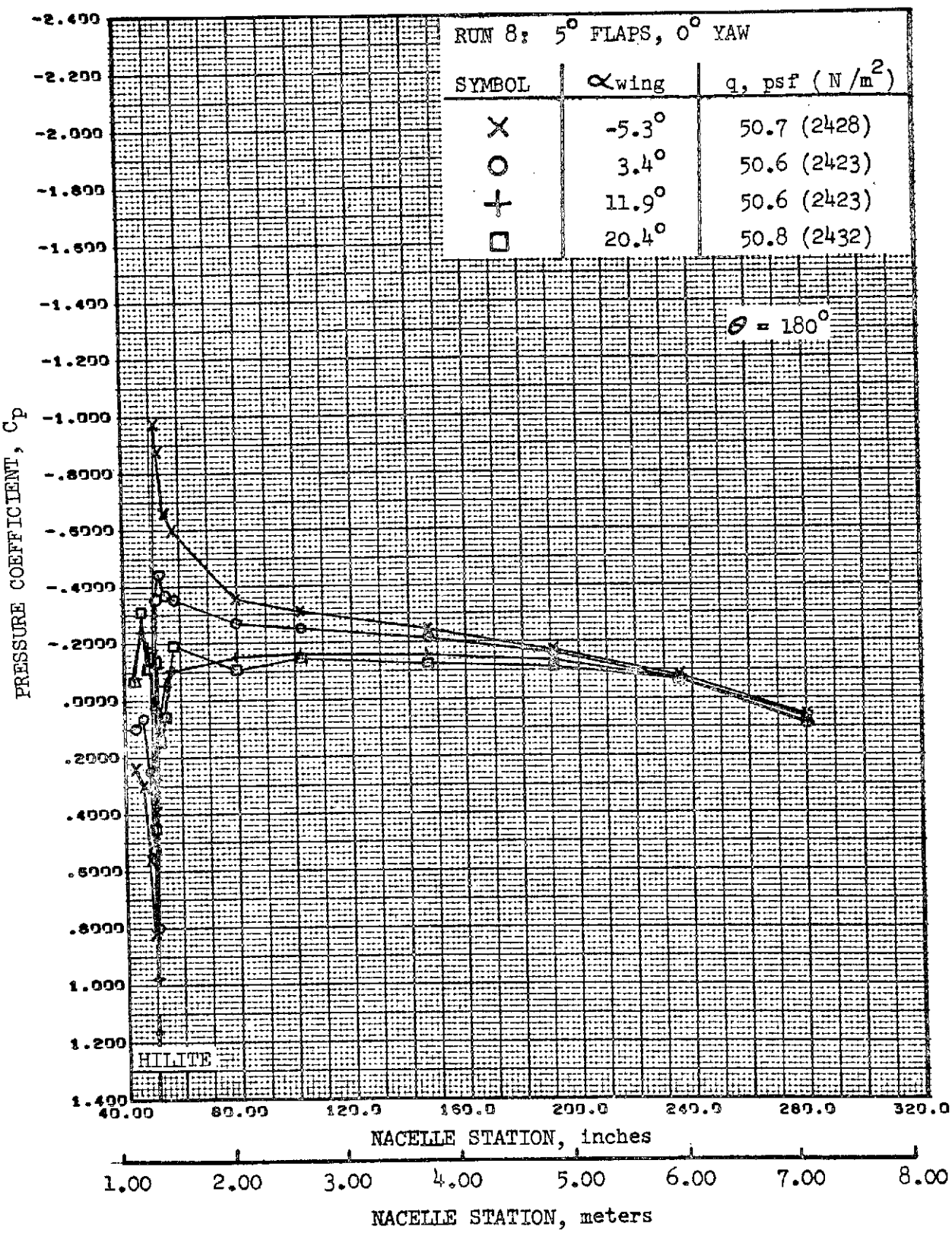

FIGURE 41. -REFAN NACELLE PRESSURE COEFFICIENT DISTRIBUTION, BOTTOM LONGITUDINAL

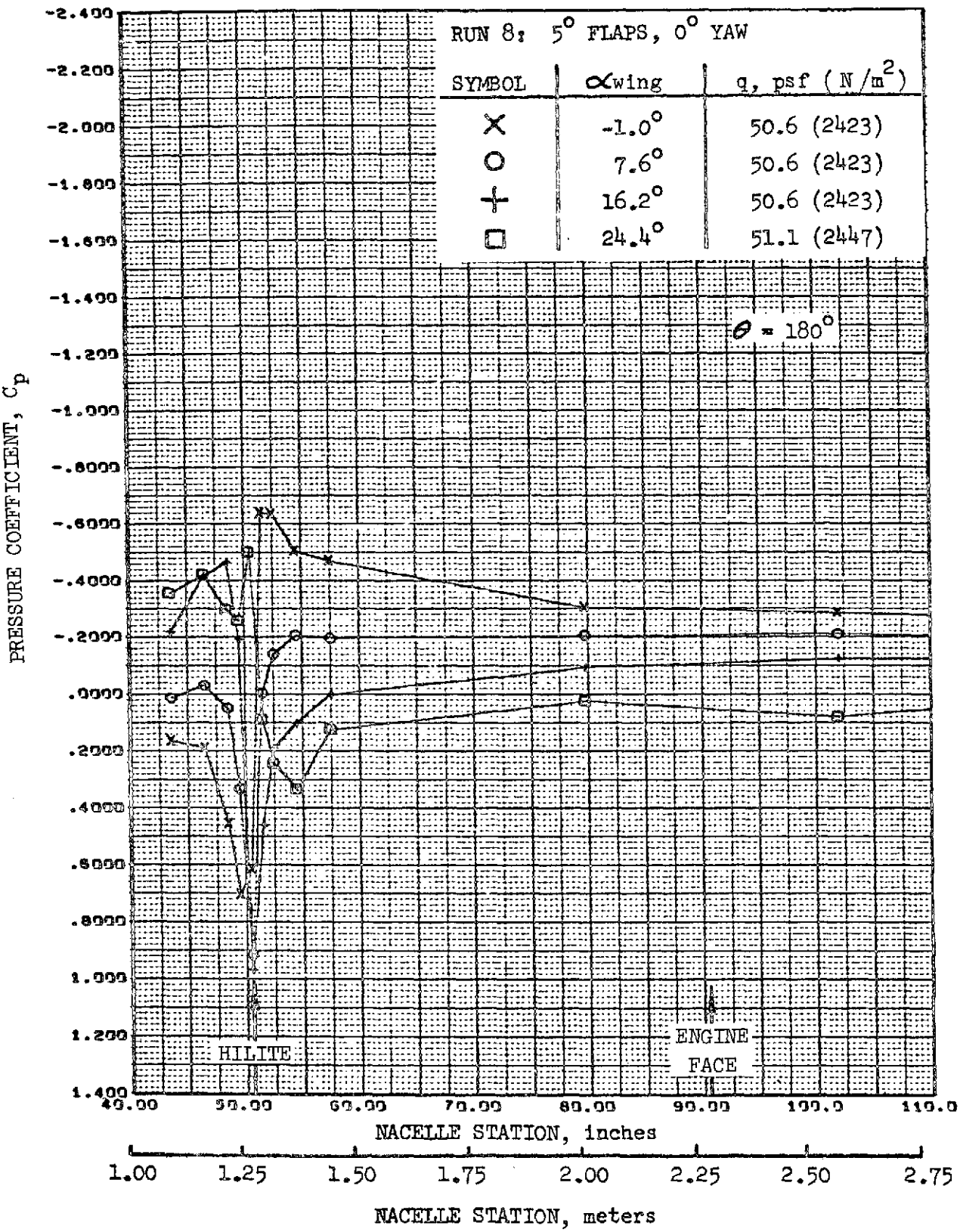

FIGURE 42. -REFAN NACELLE INLET COWL PRESSURE COEFFICIENT DISTRIBUTION, BOTTOM LONGITUDINAL

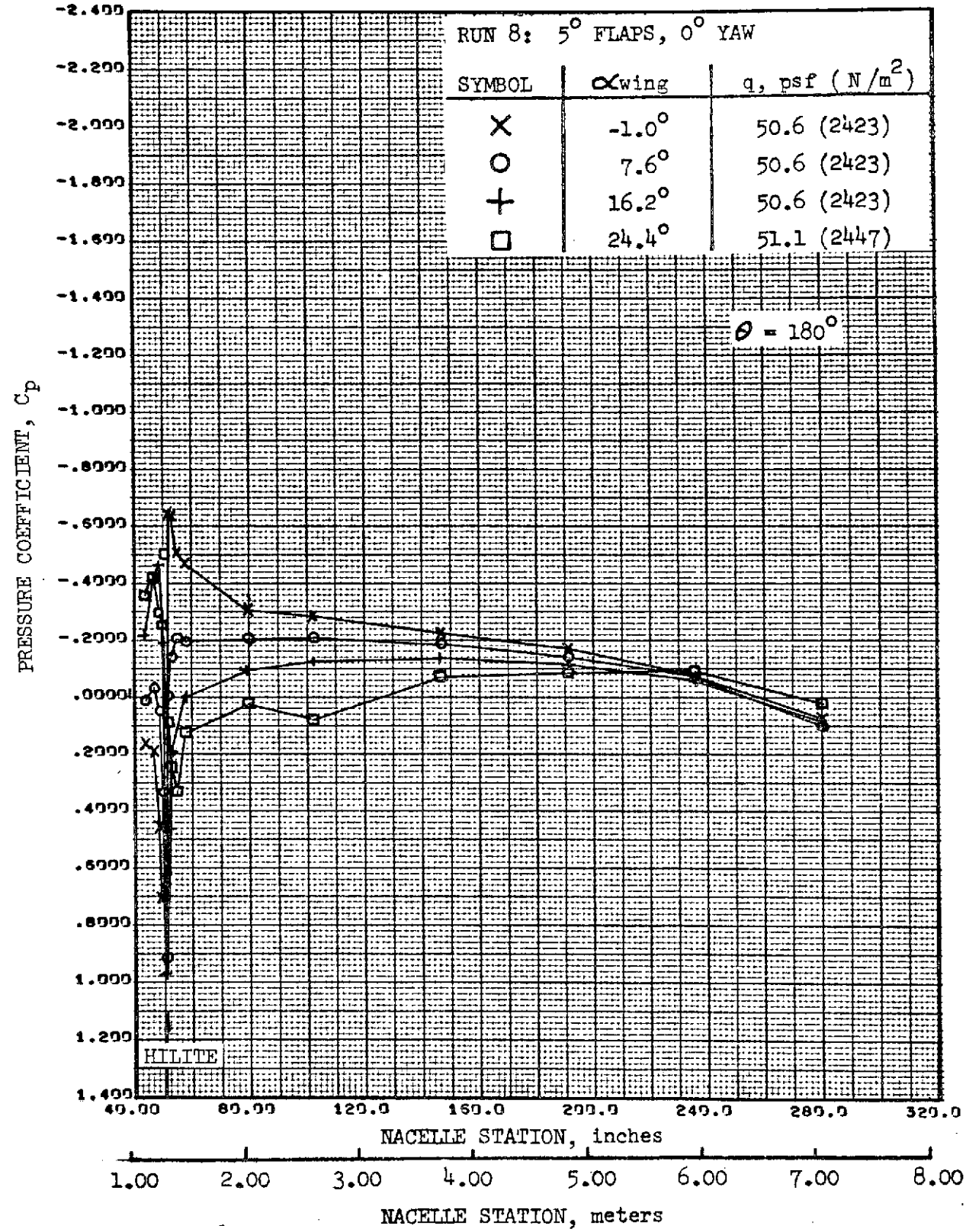

FIGURE 43. -REFAN NACELLE PRESSURE COEFFICIENT DISTRIBUTION, BOTTOM LONGITUDINAL

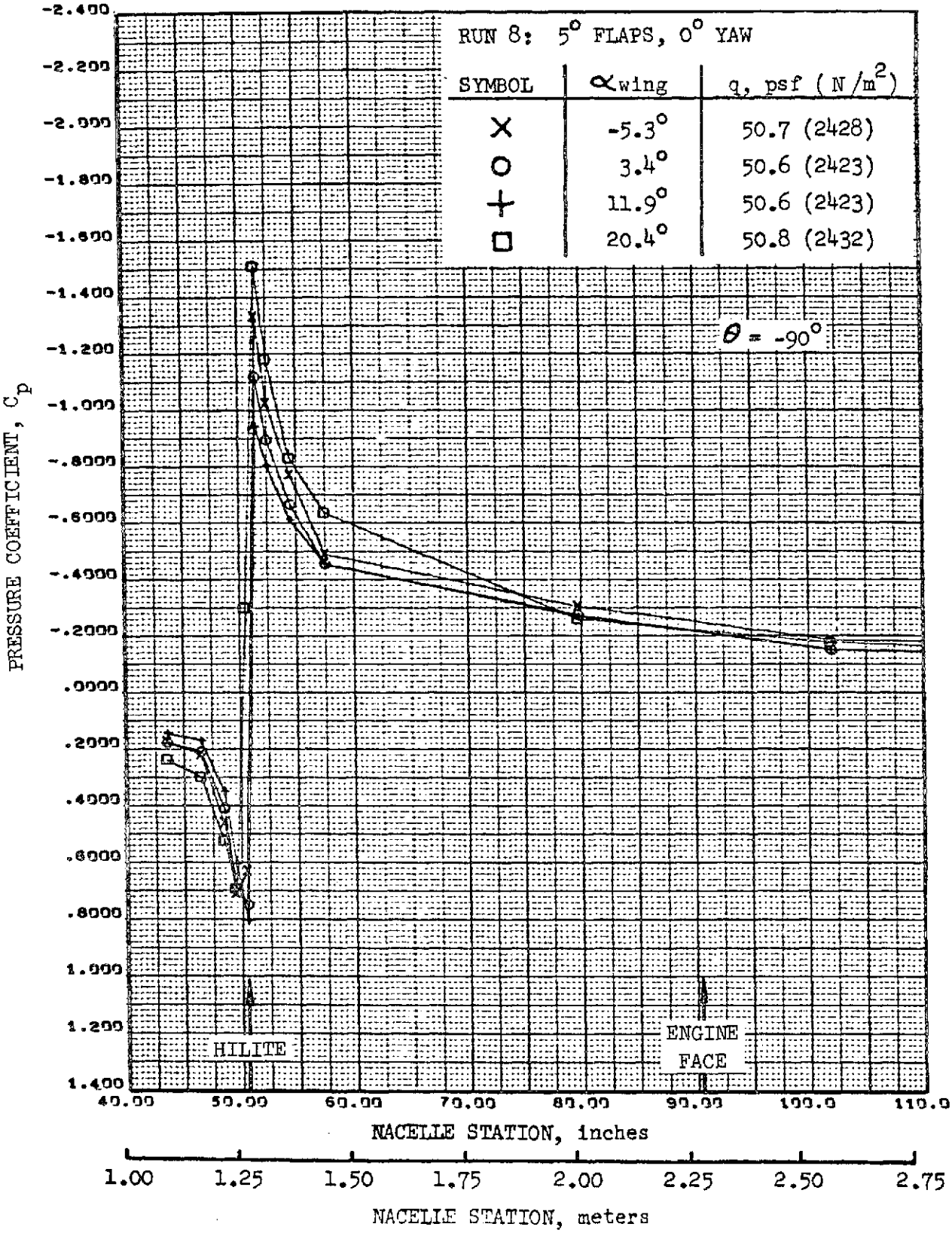

FIGURE 44. -REFAN NACELLE INLET COWL PRESSURE COEFFICIENT DISTRIBUTION, OUTBOARD SIDE

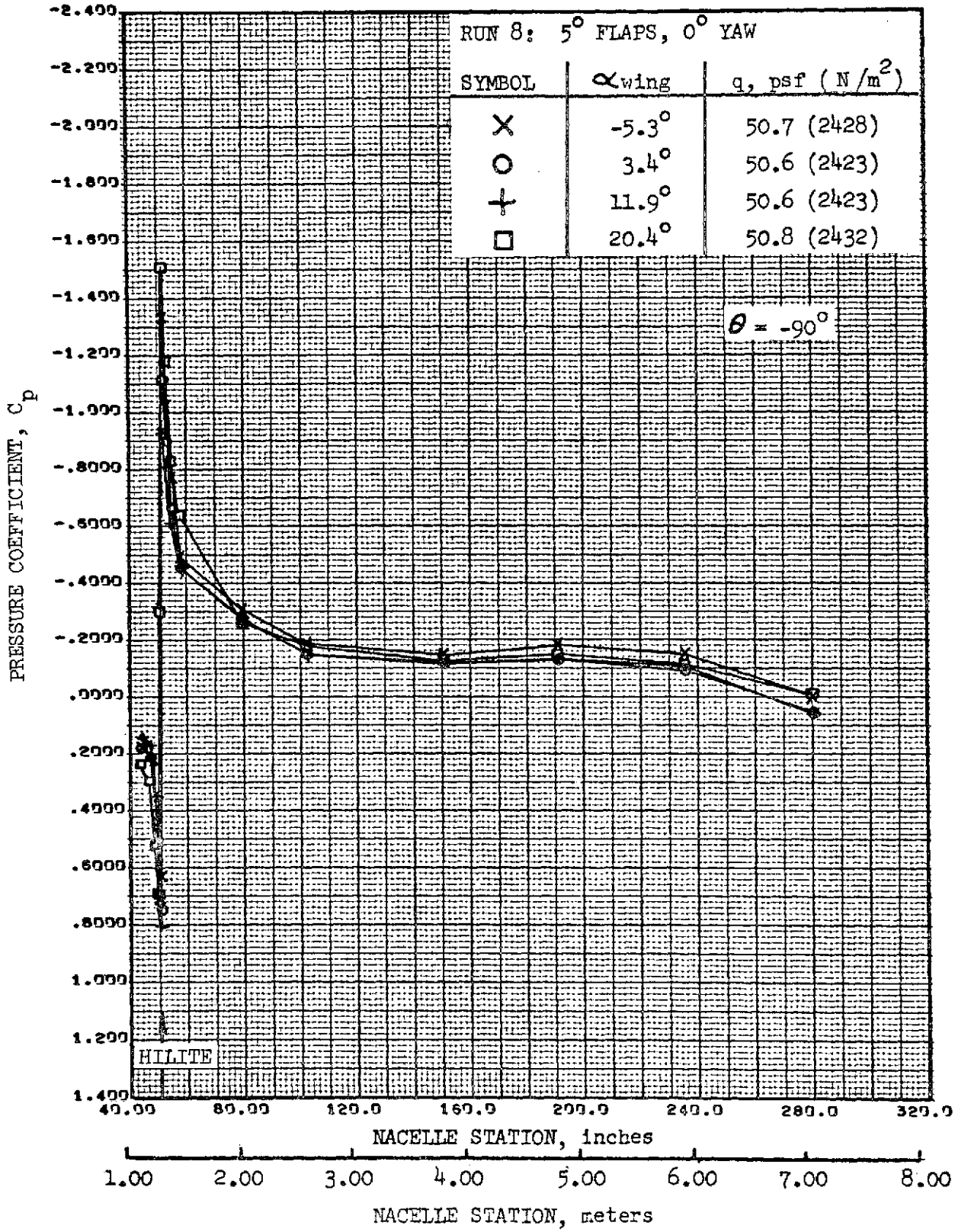

FIGURE 45. -REFAN NACELLE PRESSURE COEFFICIENT DISTRIBUTION, OUTBOARD SIDE

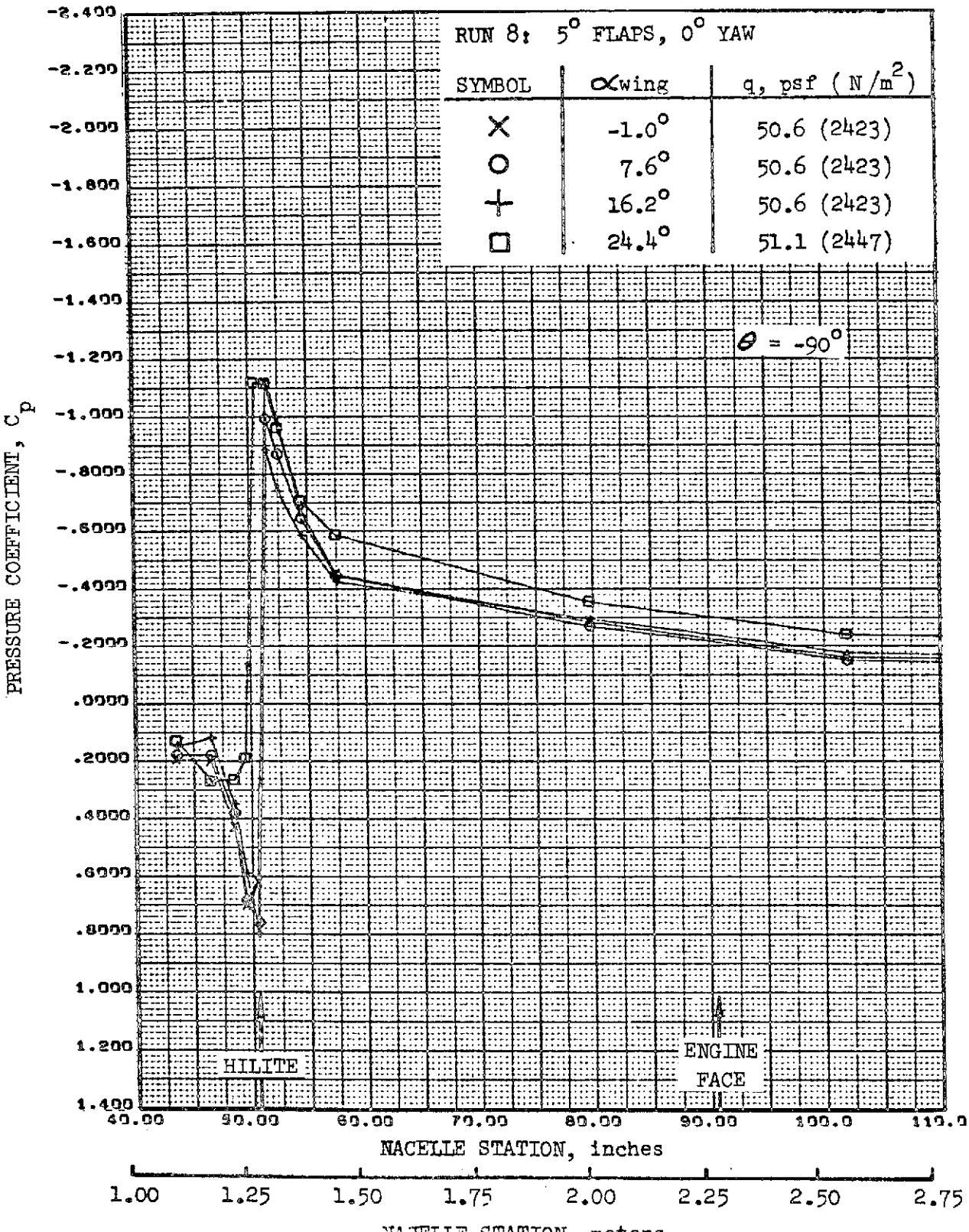

FIGURE 46. -REFAN NACELLE INLET COWL PRESSURE COEFFICIENT DISTRIBUTION, OUTBOARD SIDE

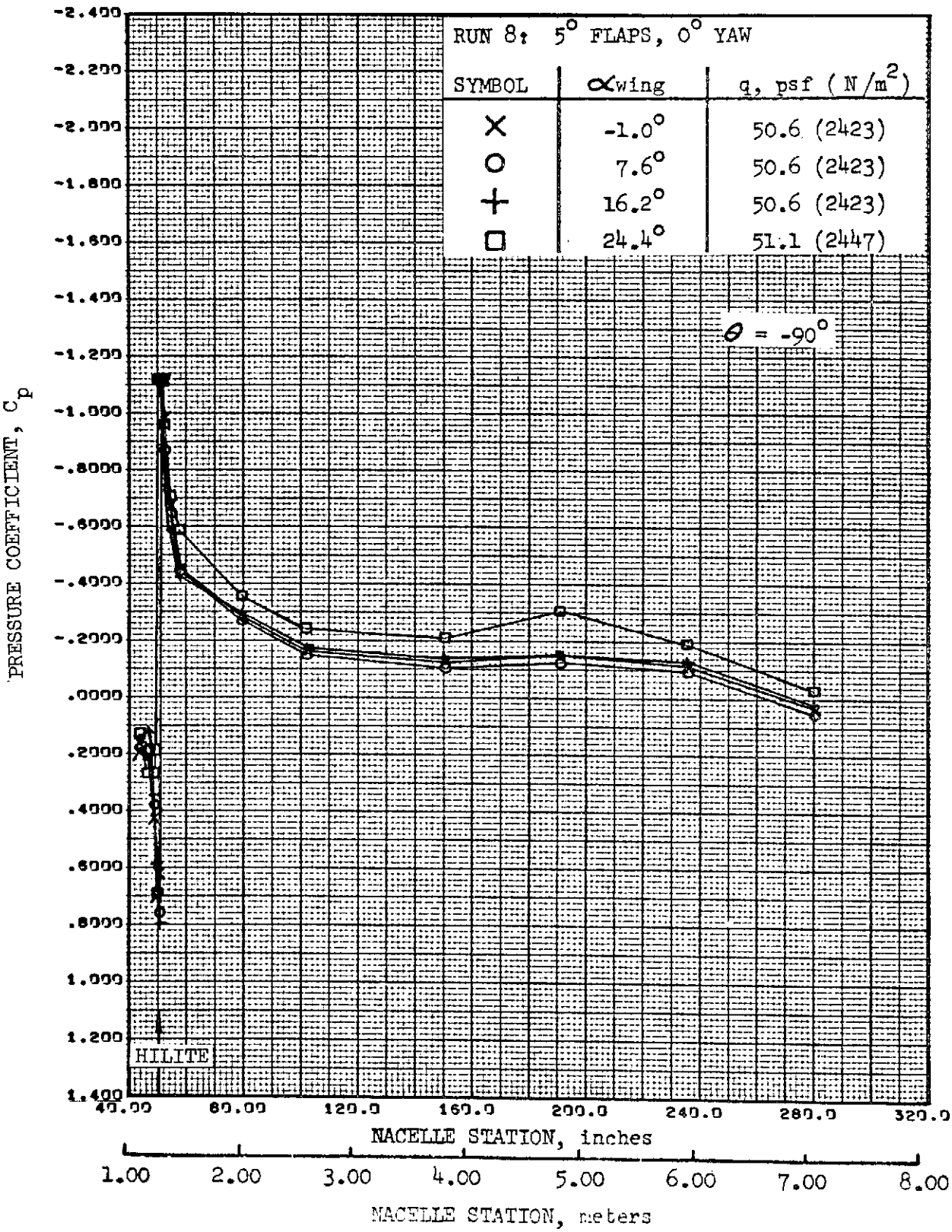

FIGURE 47. -REFAN NACELLE PRESSURE COEFFICIENT DISTRIBUTION, OUTBOARD SIDE

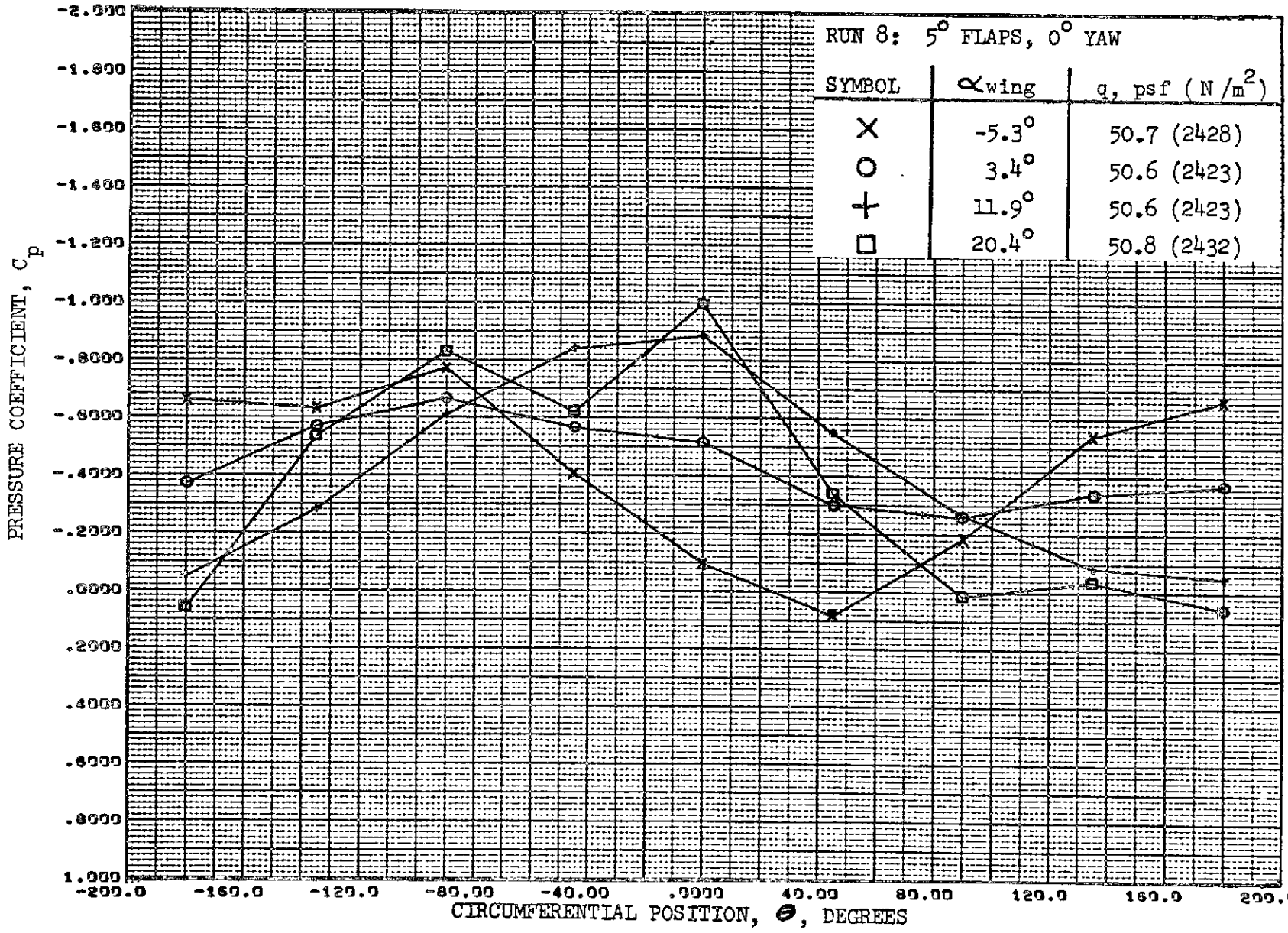

FIGURE 48. - REFAN NACELLE PRESSURE COEFFICIENT DISTRIBUTION, EXTERNAL CIRCUMFERENTIAL AT STATION 54.5 INCHES (1.38 METERS)

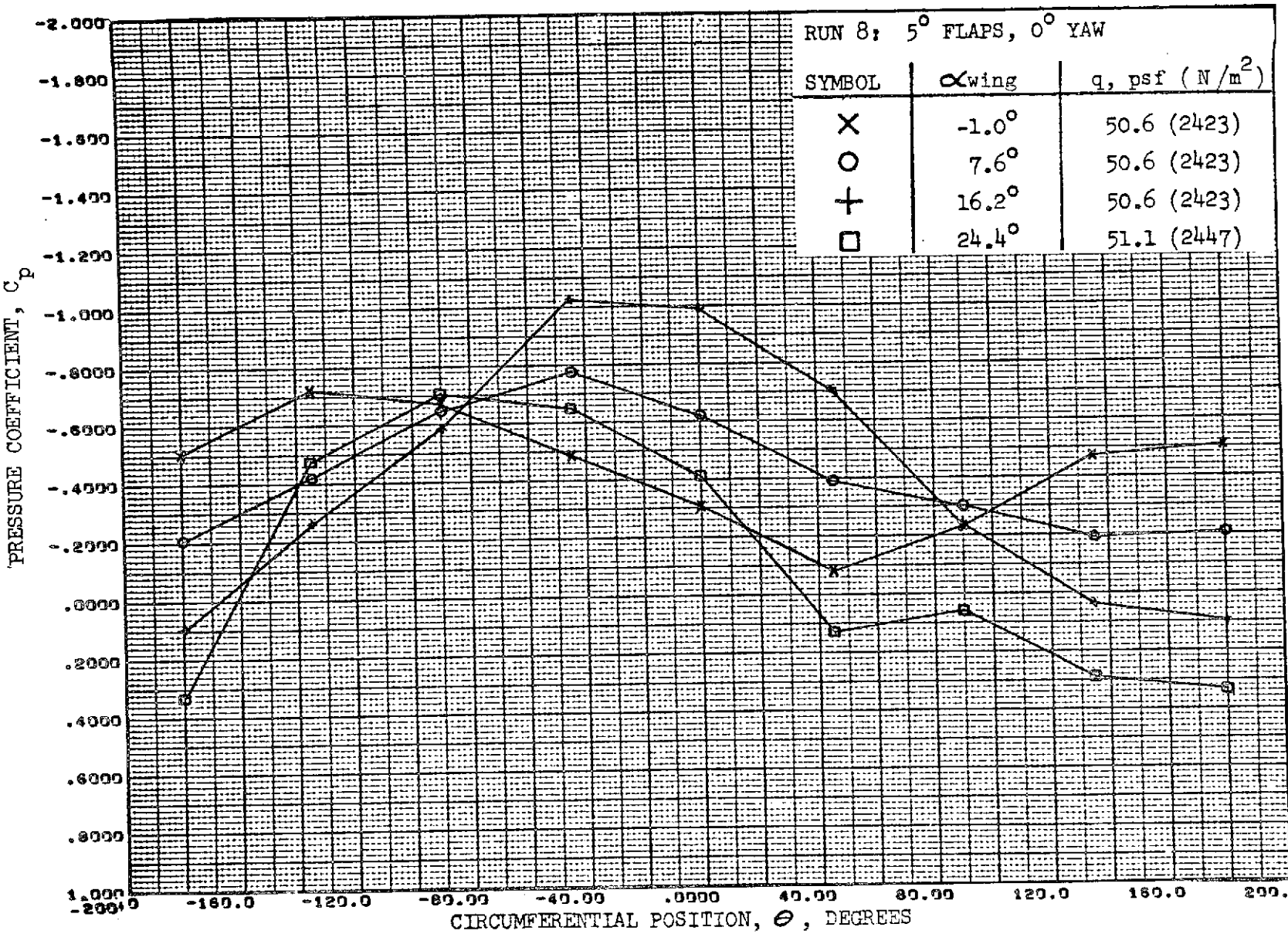

FIGURE 49. - REFAN NACELLE PRESSURE COEFFICIENT DISTRIBUTION, EXTERNAL CIRCUMFERENTIAL AT STATION 54.5 INCHES (1.38 METERS)

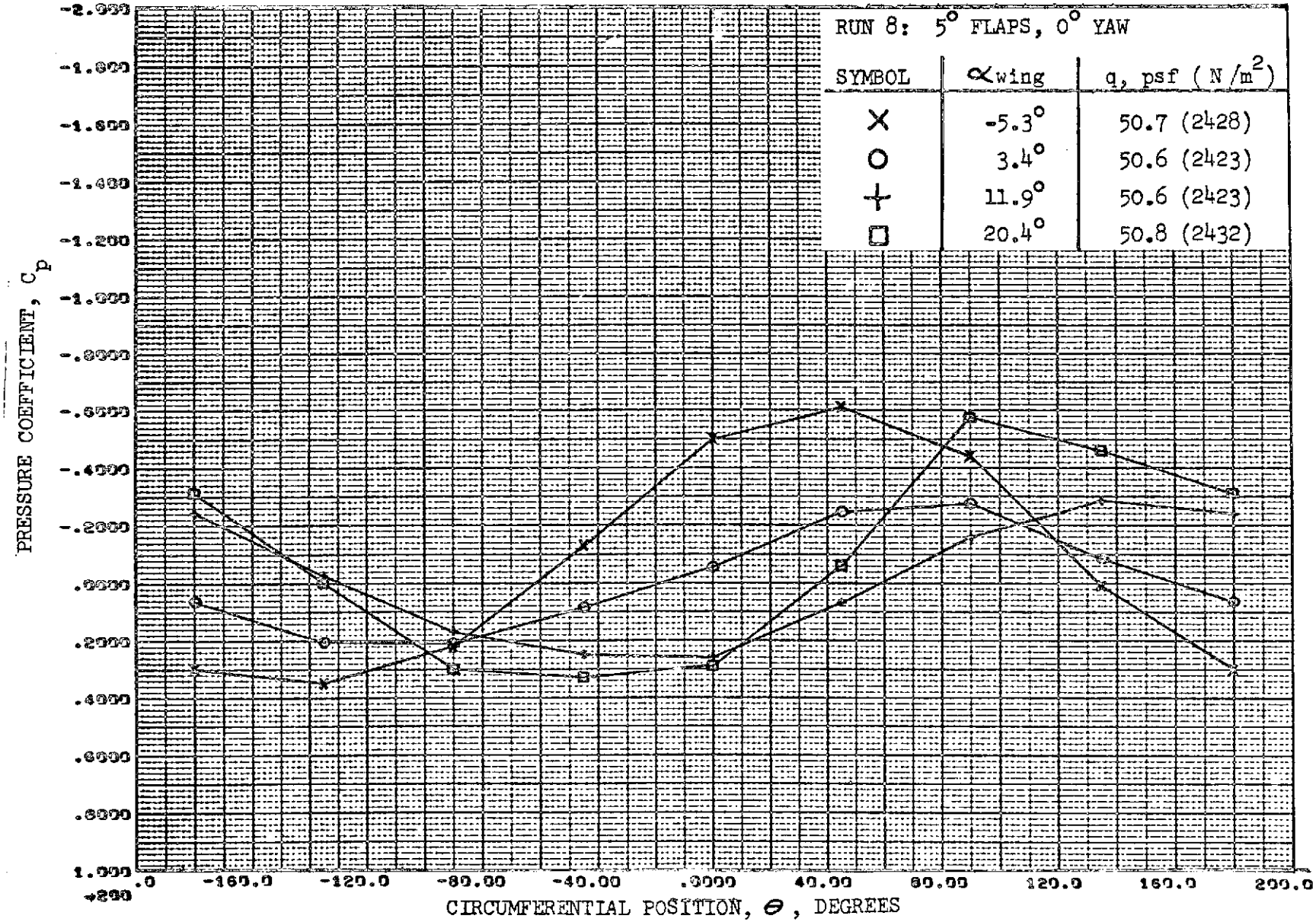

FIGURE 50. - REFAN NACELLE PRESSURE COEFFICIENT DISTRIBUTION, INTERNAL CIRCUMFERENTIAL AT STATION 54.5 INCHES (1.38 METERS)

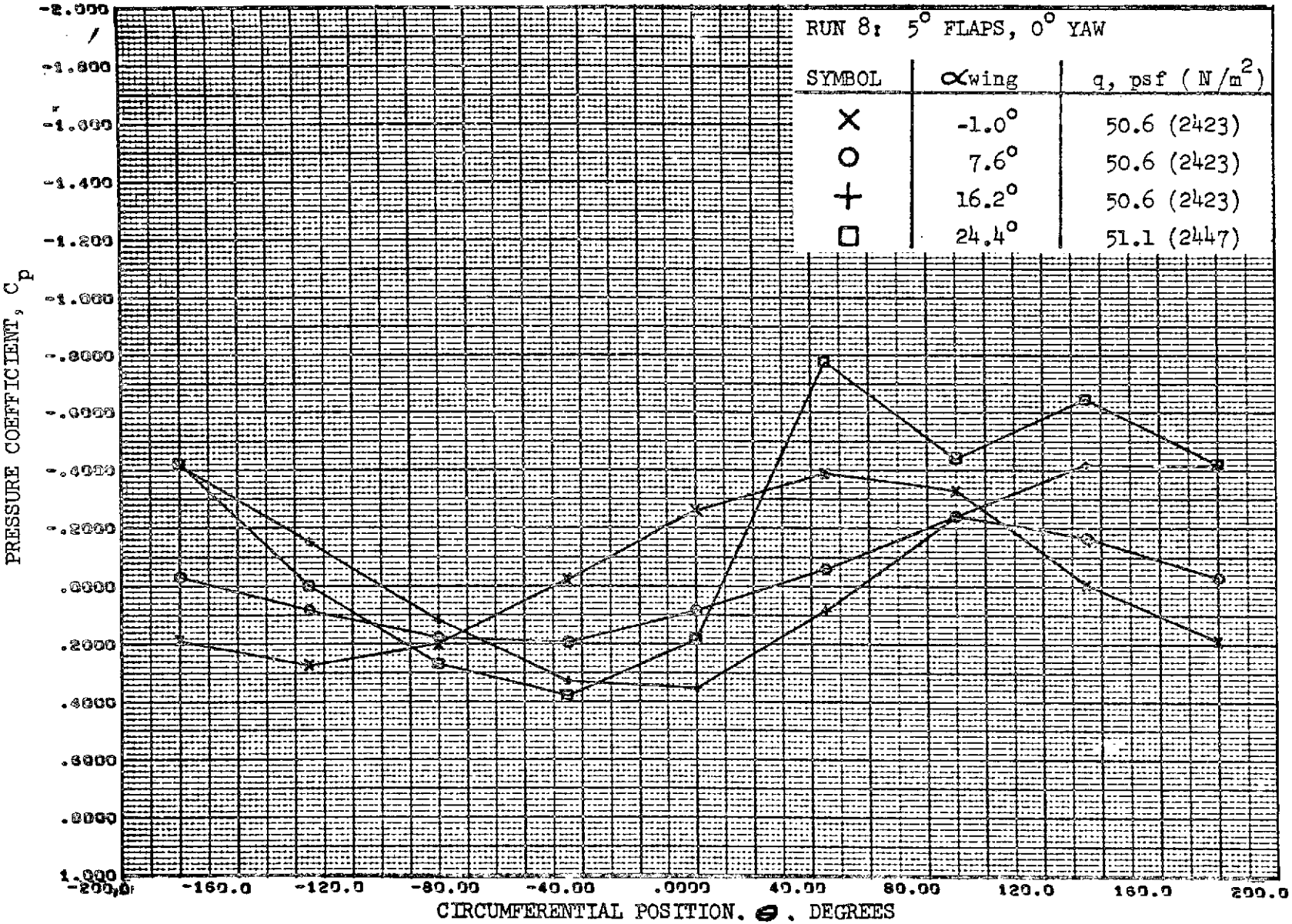

FIGURE 51. - REFAN NACELLE PRESSURE COEFFICIENT DISTRIBUTION, INTERNAL CIRCUMFERENTIAL AT STATION 54.5 INCHES (1.38 METERS)

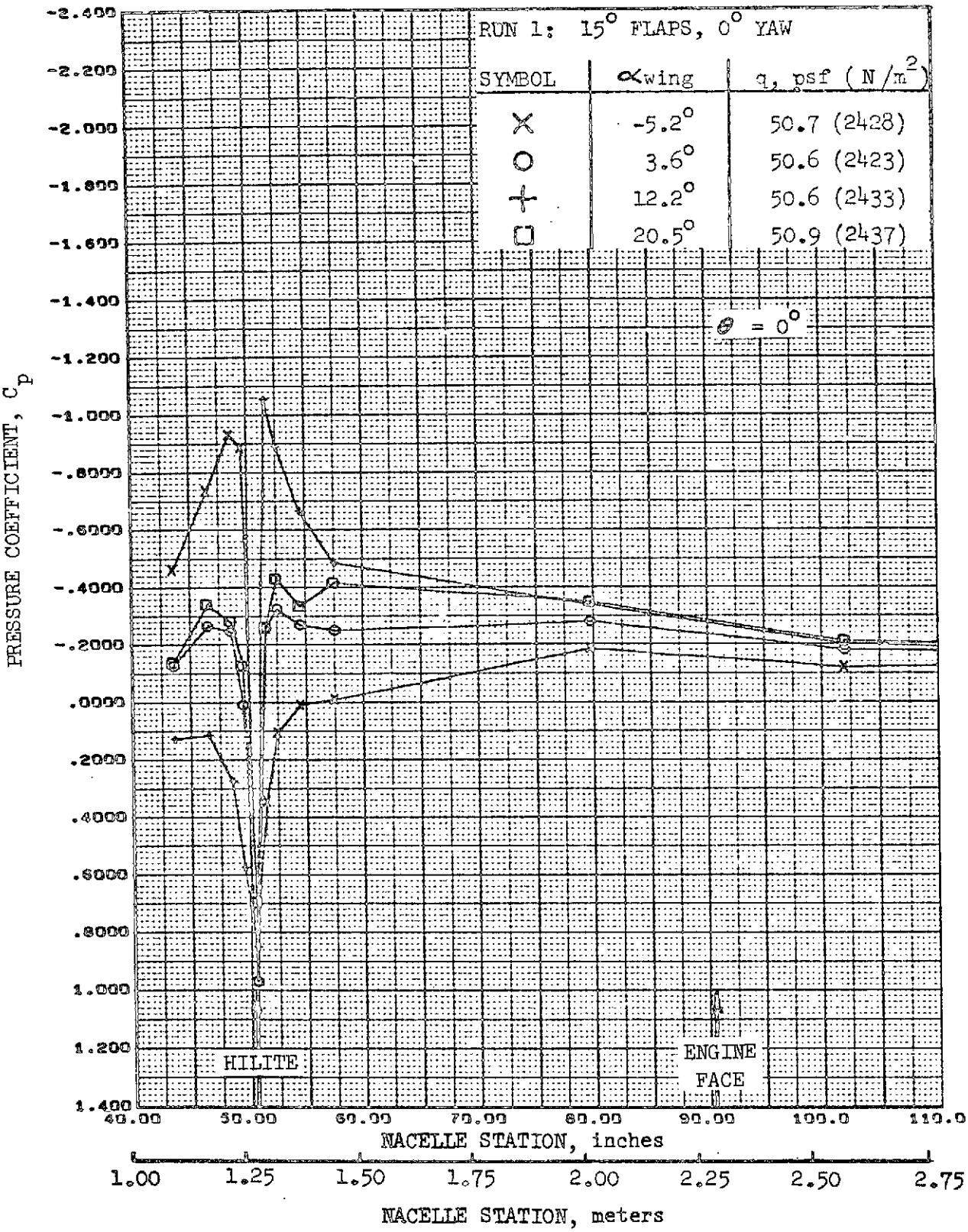

FIGURE 52. -REFAN NACELLE INLET COWL PRESSURE COEFFICIENT DISTRIBUTION, TOP LONGITUDINAL

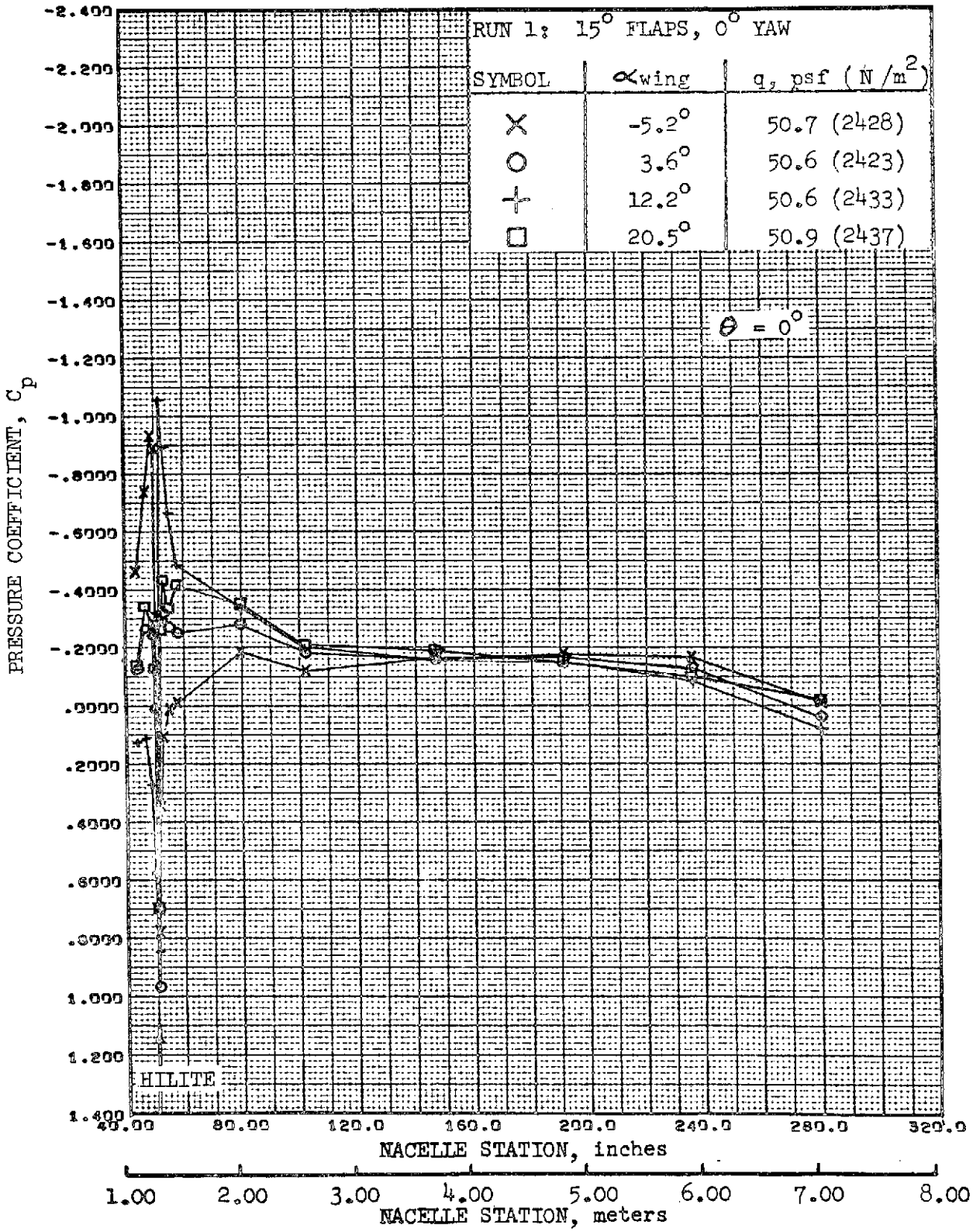

FIGURE 53. -REFAN NACELLE PRESSURE COEFFICIENT DISTRIBUTION, TOP LONGITUDINAL

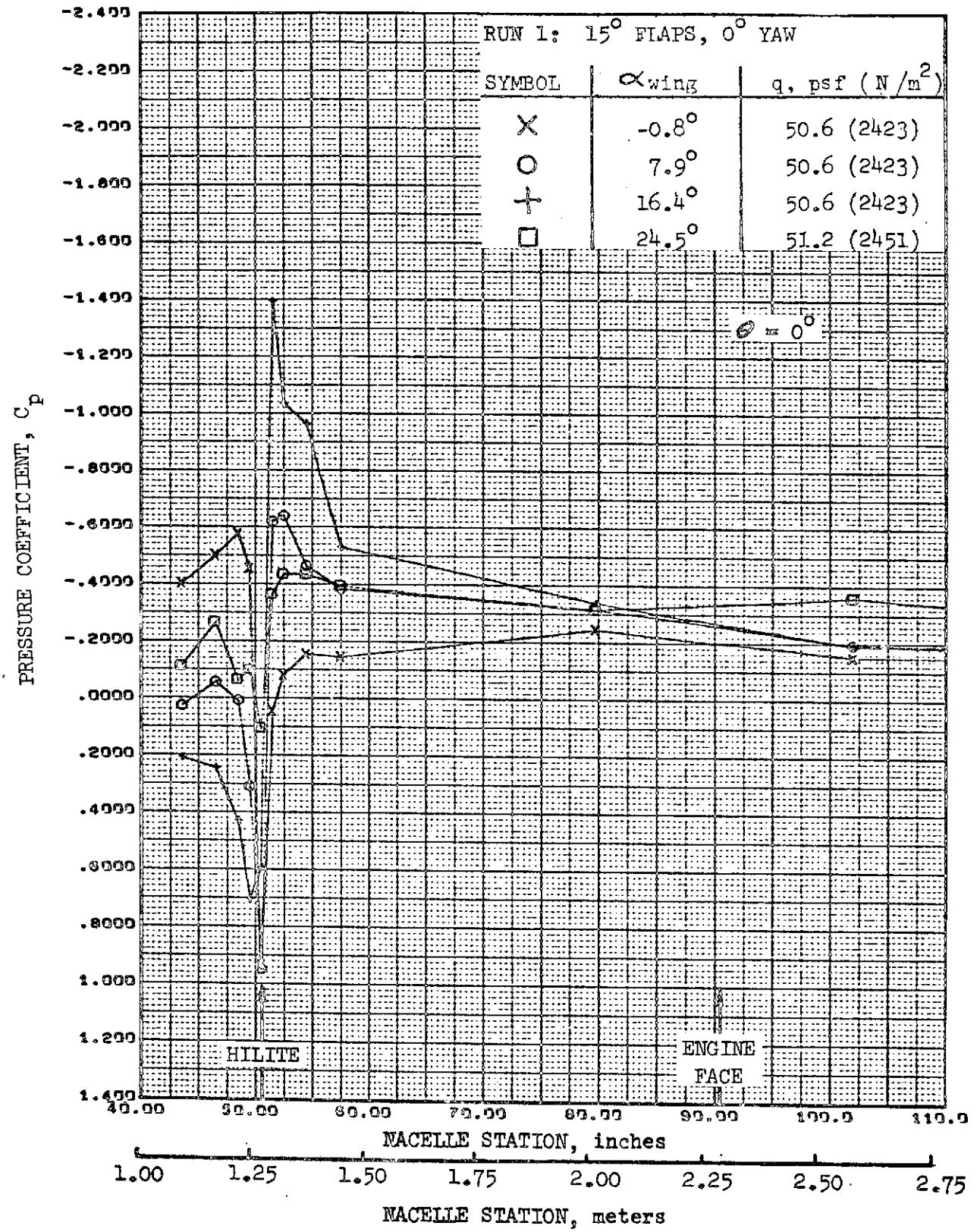

FIGURE 54. -REFAN NACELLE INLET COWL PRESSURE COEFFICIENT DISTRIBUTION, TOP LONGITUDINAL

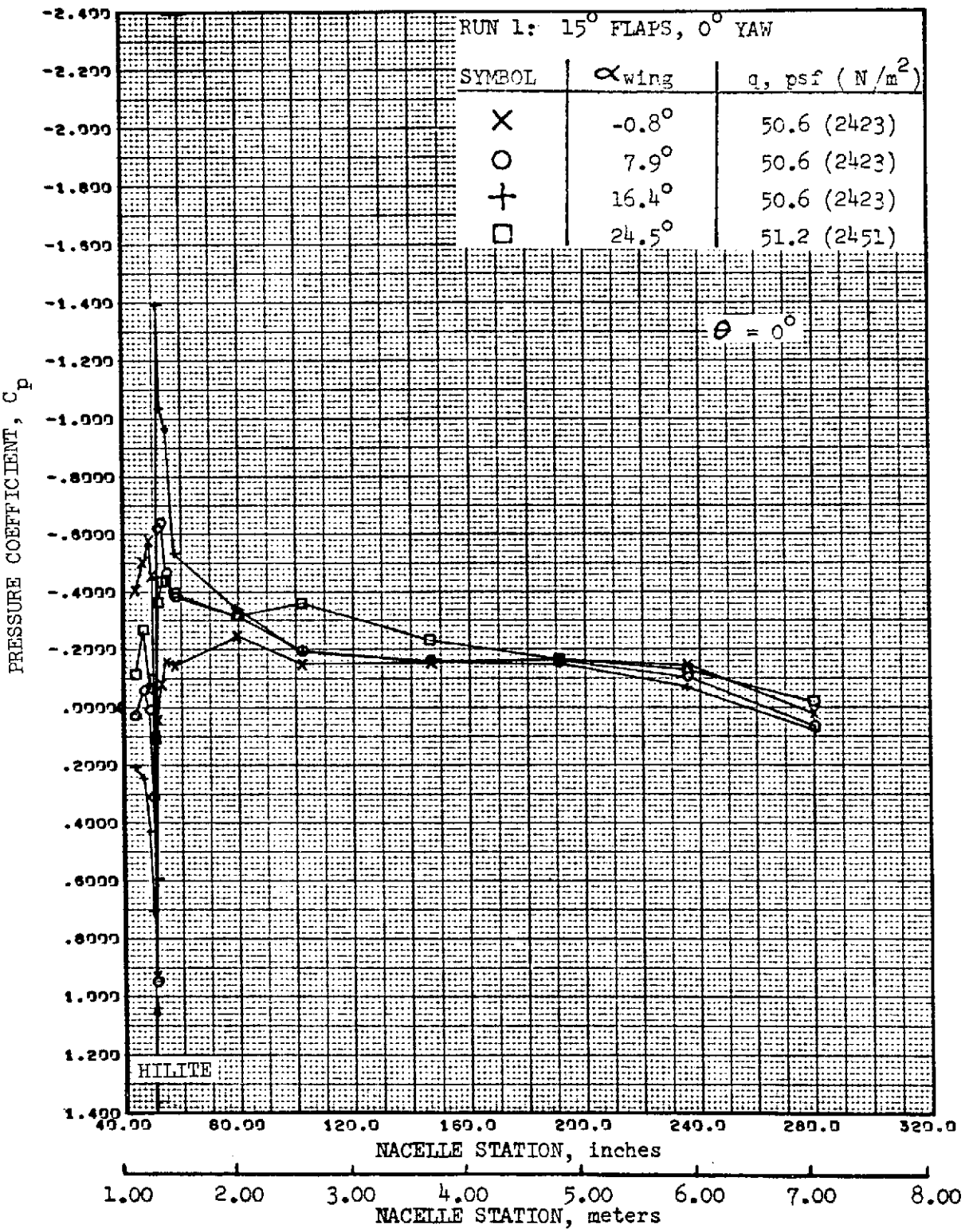

FIGURE 55. -REFAN NACELLE PRESSURE COEFFICIENT DISTRIBUTION, TOP LONGITUDINAL

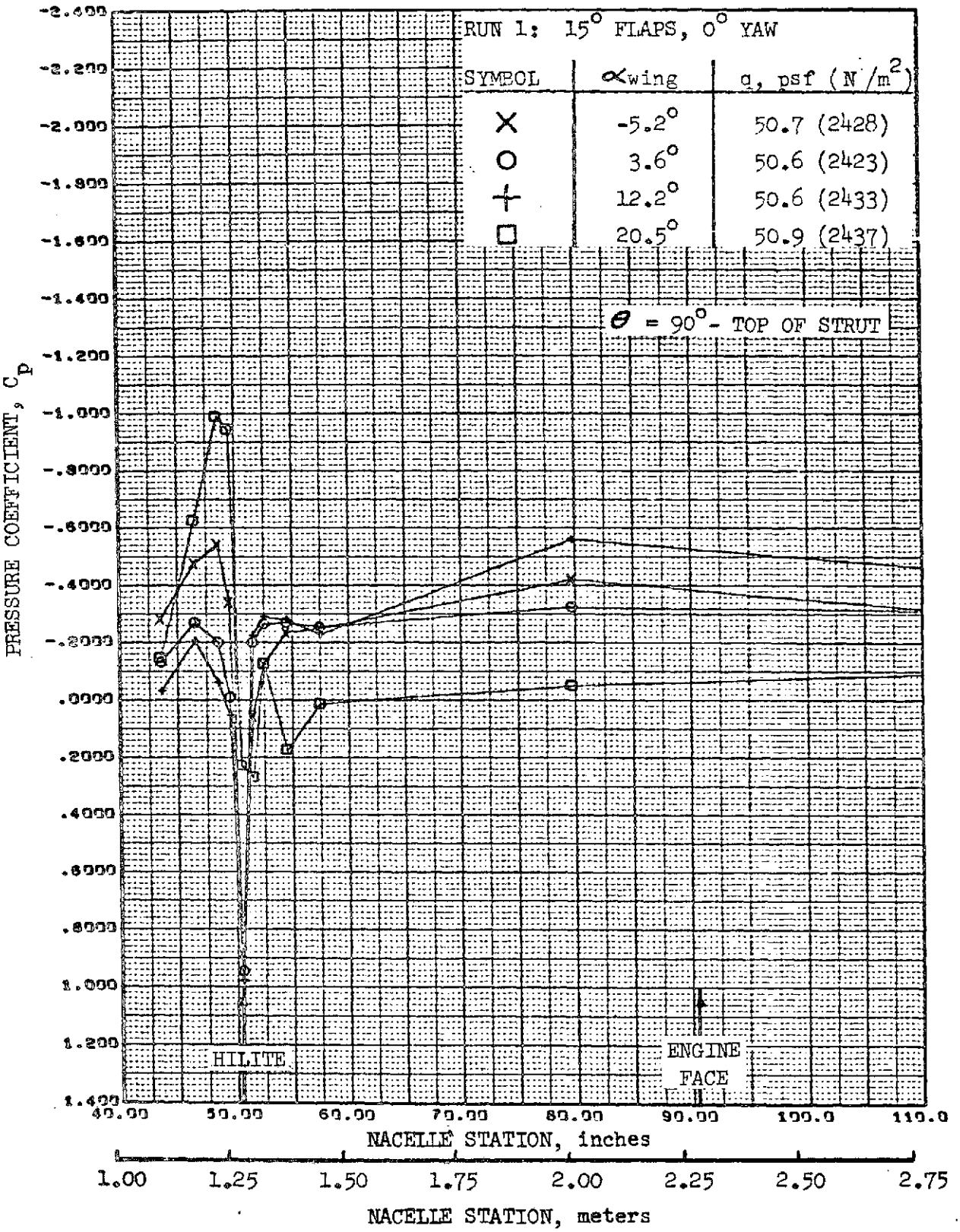

FIGURE 56. -REFAN NACELLE INLET COWL PRESSURE COEFFICIENT DISTRIBUTION, INBOARD SIDE-ABOVE STRUT

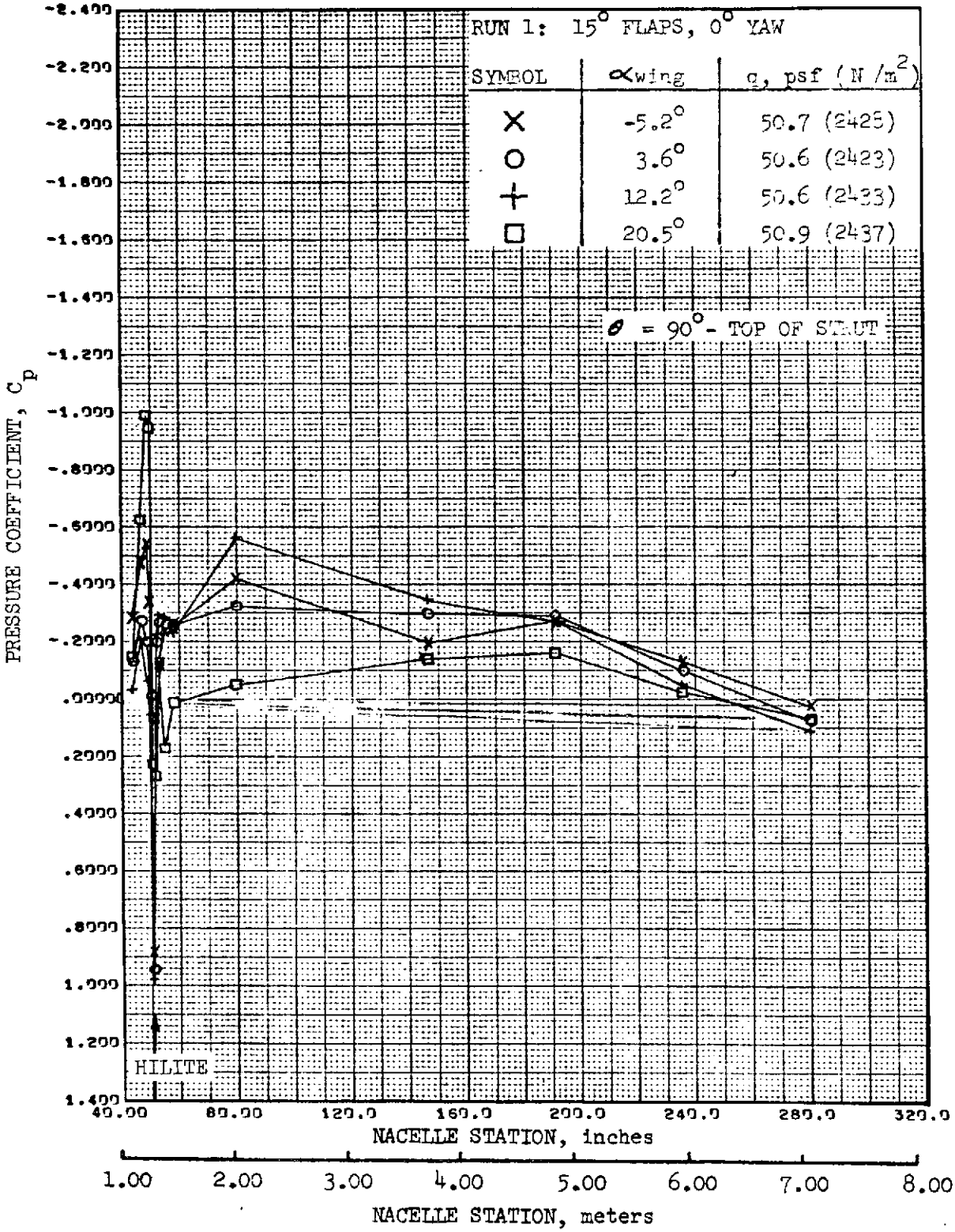

FIGURE 57. -REFAN NACELLE PRESSURE COEFFICIENT DISTRIBUTION, INBOARD SIDE-ABOVE STRUT

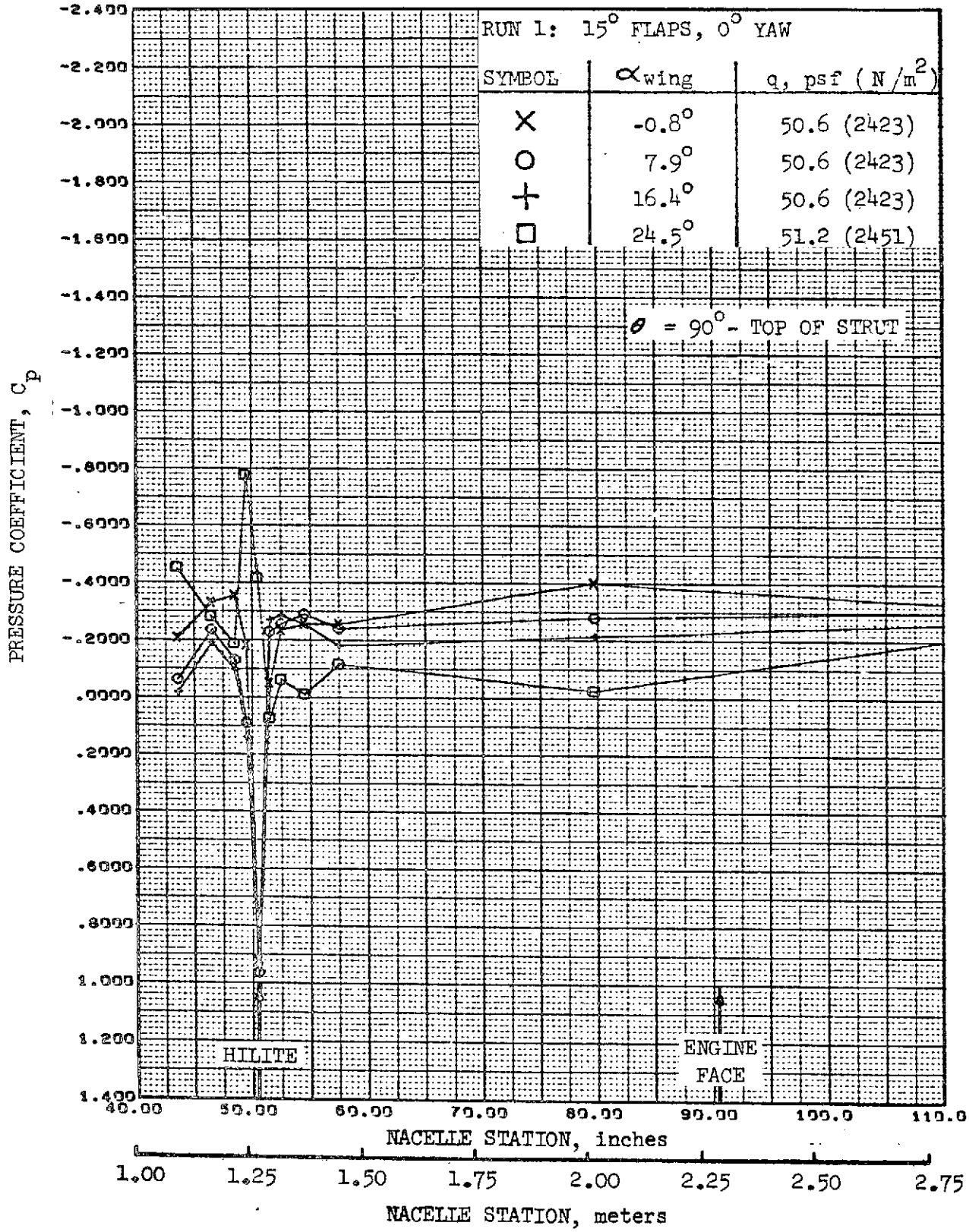

FIGURE 58. -REFAN NACELLE INLET COWL PRESSURE COEFFICIENT DISTRIBUTION, INBOARD SIDE-ABOVE STRUT

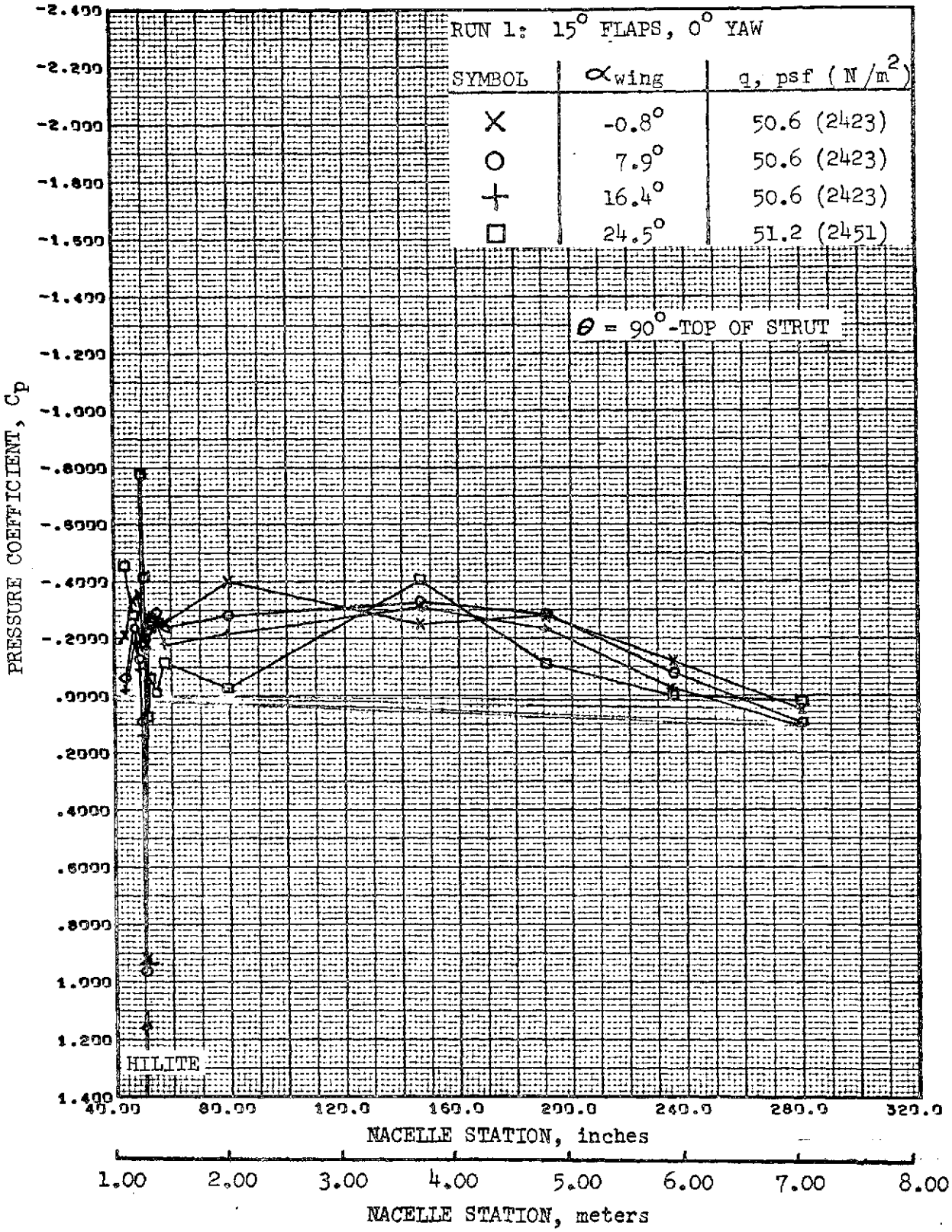

FIGURE 59. -REFAN NACELLE PRESSURE COEFFICIENT DISTRIBUTION, INBOARD SIDE-ABOVE STRUT

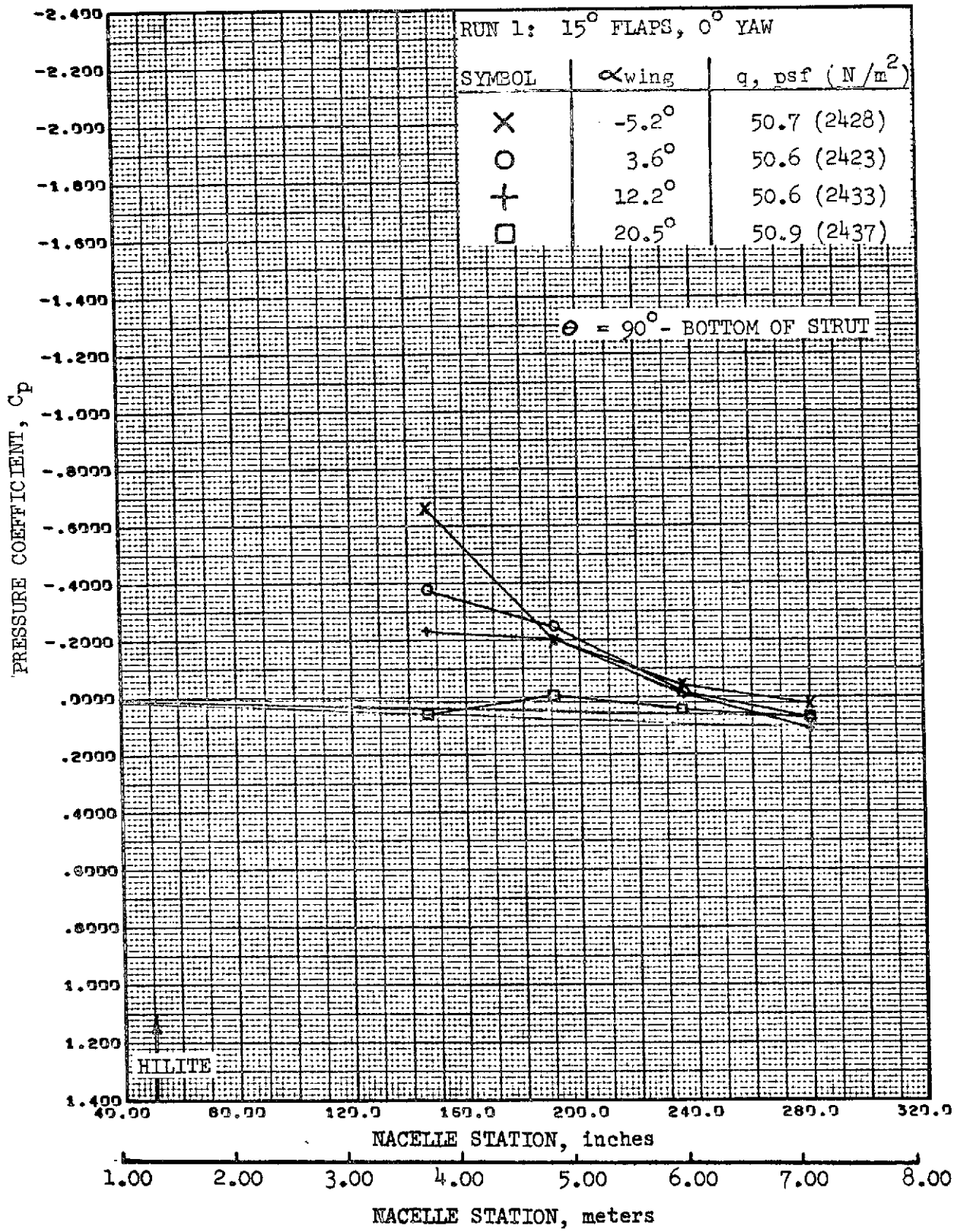

FIGURE 60. -REFAN NACELLE PRESSURE COEFFICIENT DISTRIBUTION, INBOARD SIDE-BELOW STRUT

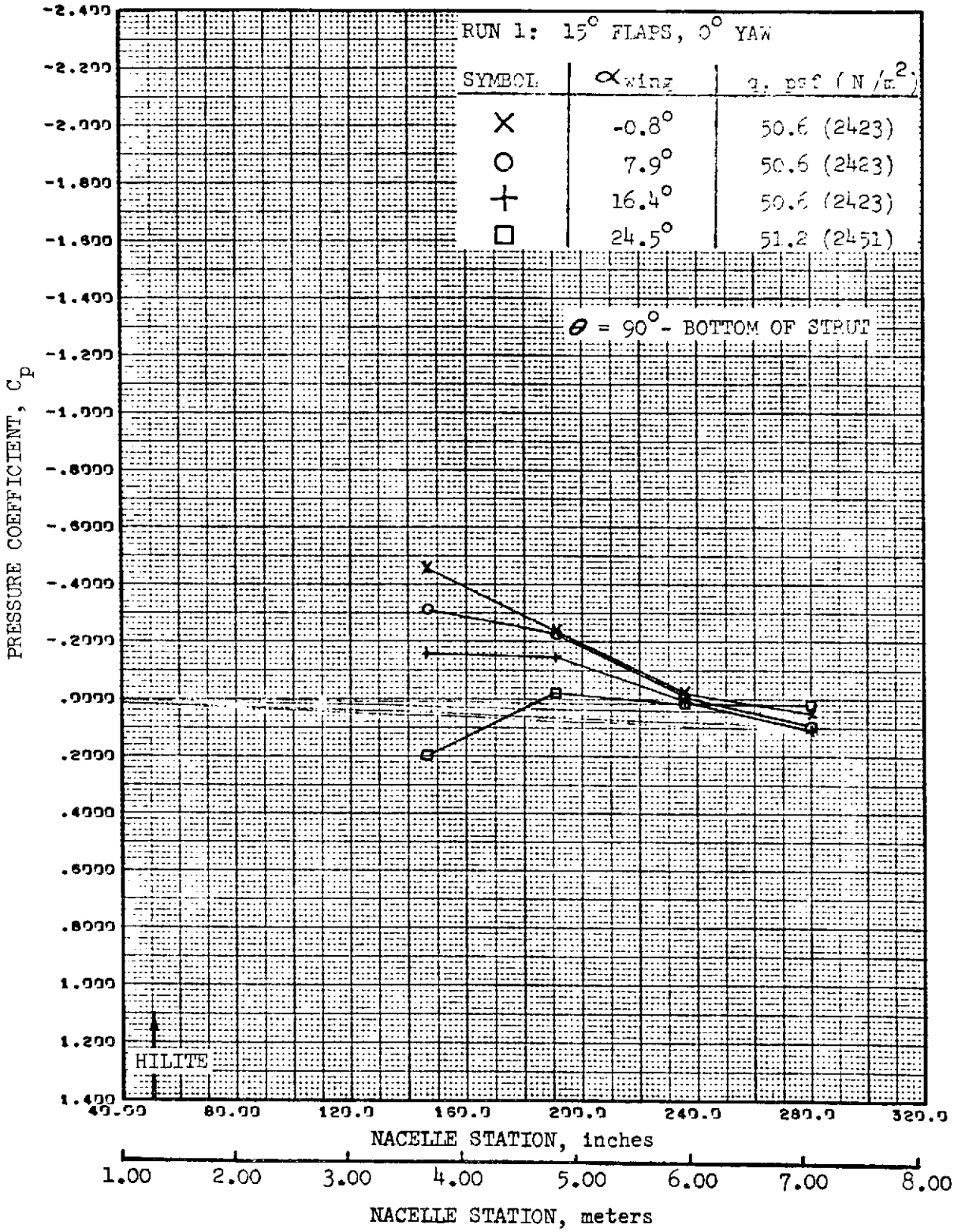

FIGURE 61. -REFAN NACELLE PRESSURE COEFFICIENT DISTRIBUTION, INBOARD SIDE-BELOW STRUT

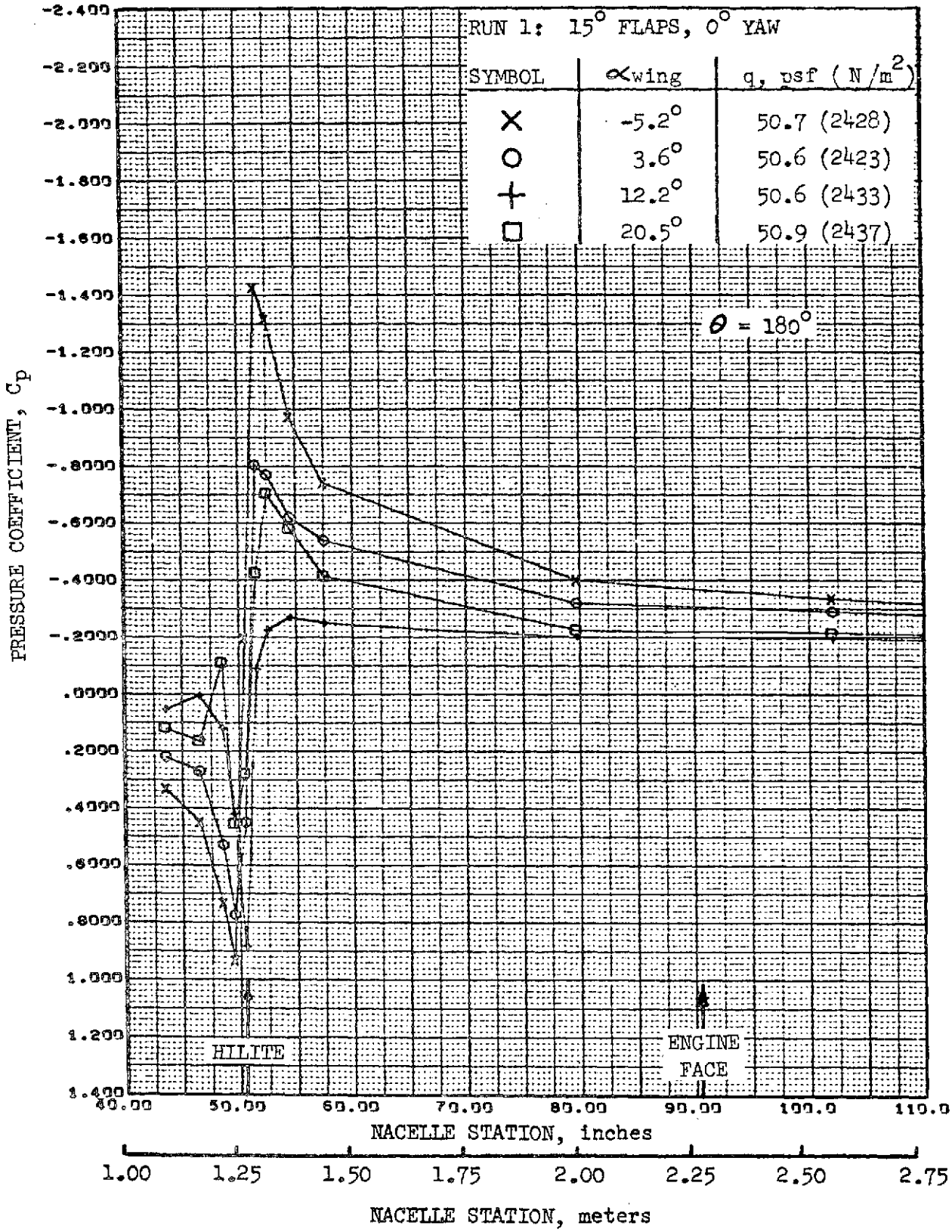

FIGURE 62. -REFAN NACELLE INLET COWL PRESSURE COEFFICIENT DISTRIBUTION, BOTTOM LONGITUDINAL

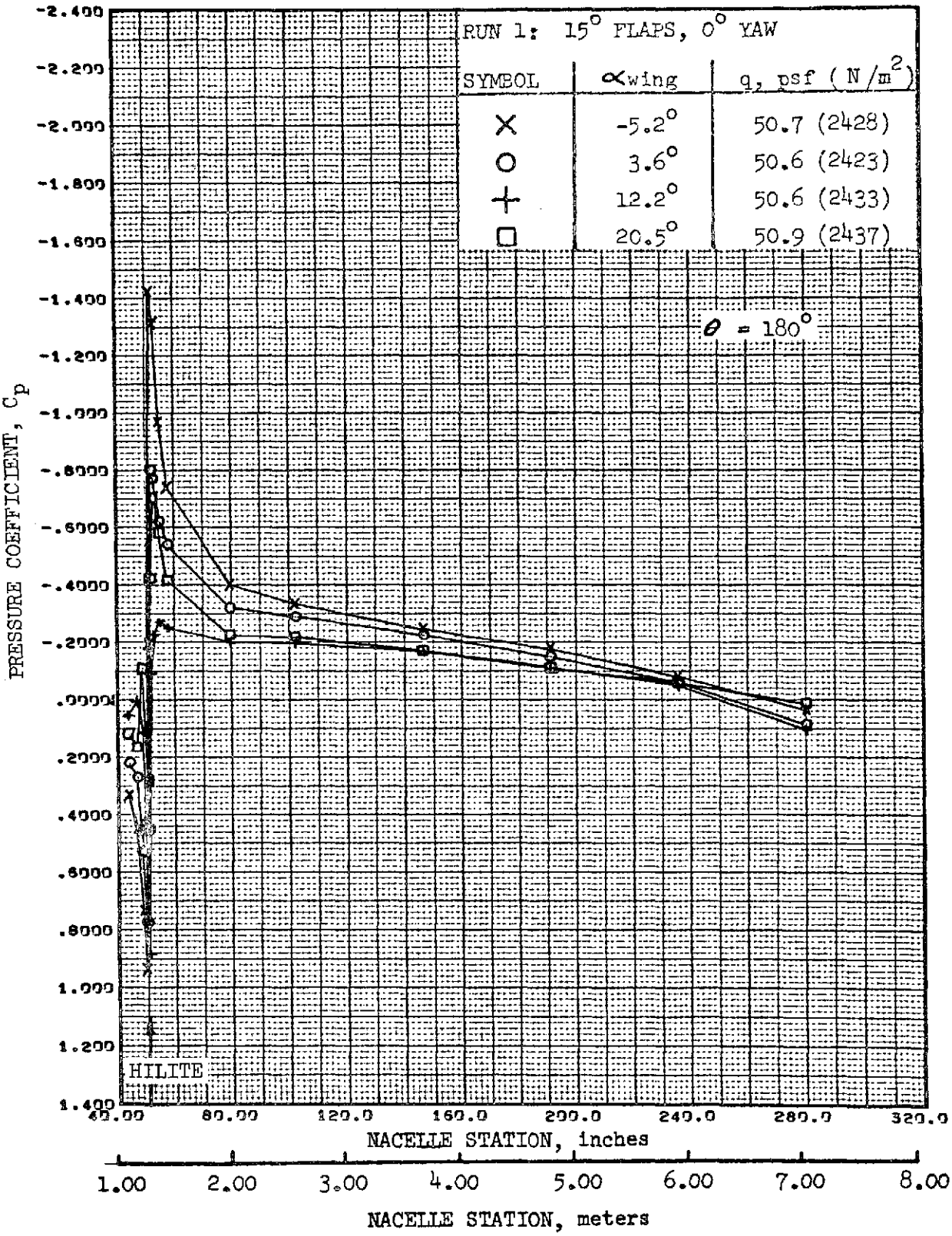

FIGURE 63. -REFAN NACELLE PRESSURE COEFFICIENT DISTRIBUTION, BOTTOM LONGITUDINAL

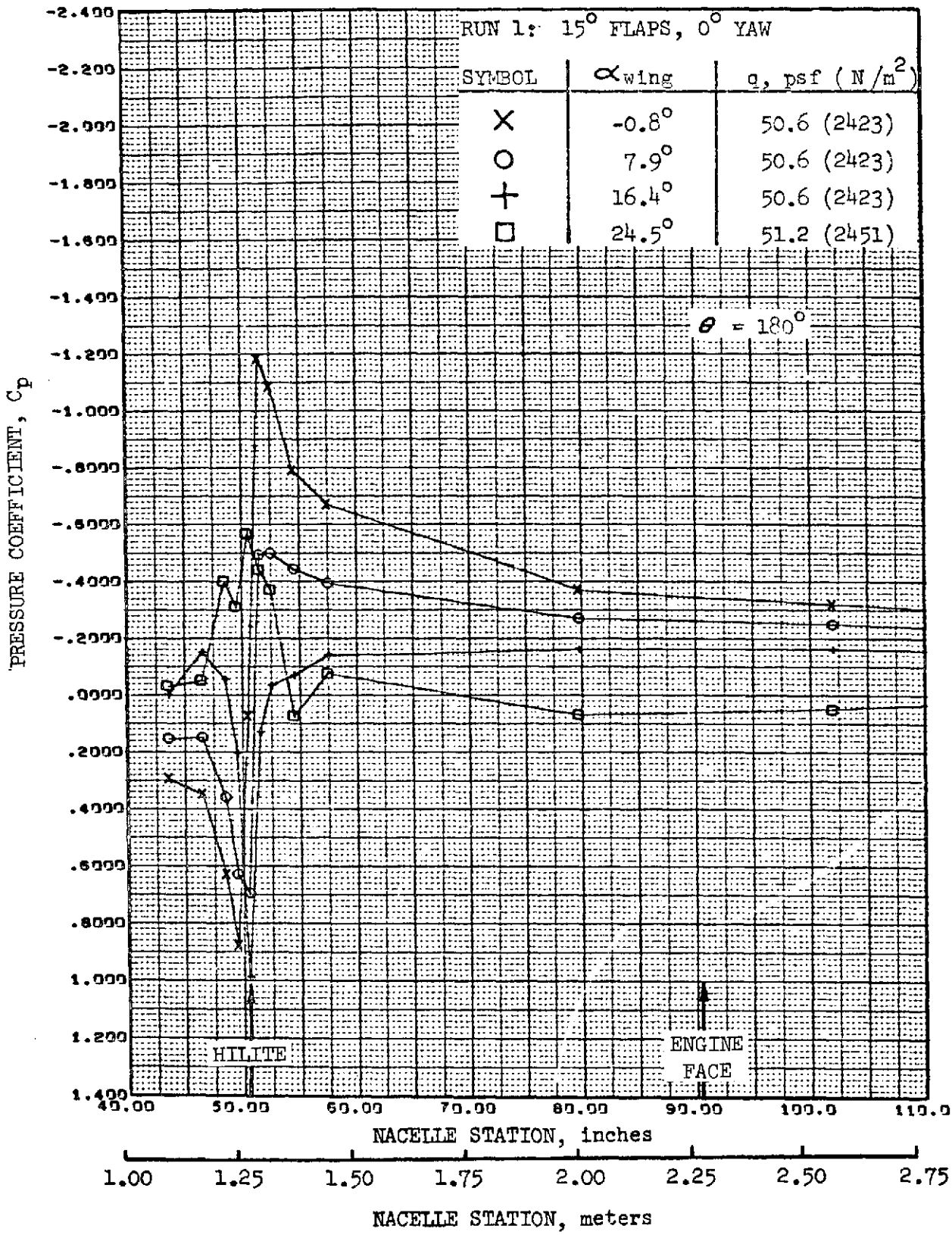

FIGURE 64. -REFAN NACELLE INLET COWL PRESSURE COEFFICIENT DISTRIBUTION, BOTTOM LONGITUDINAL

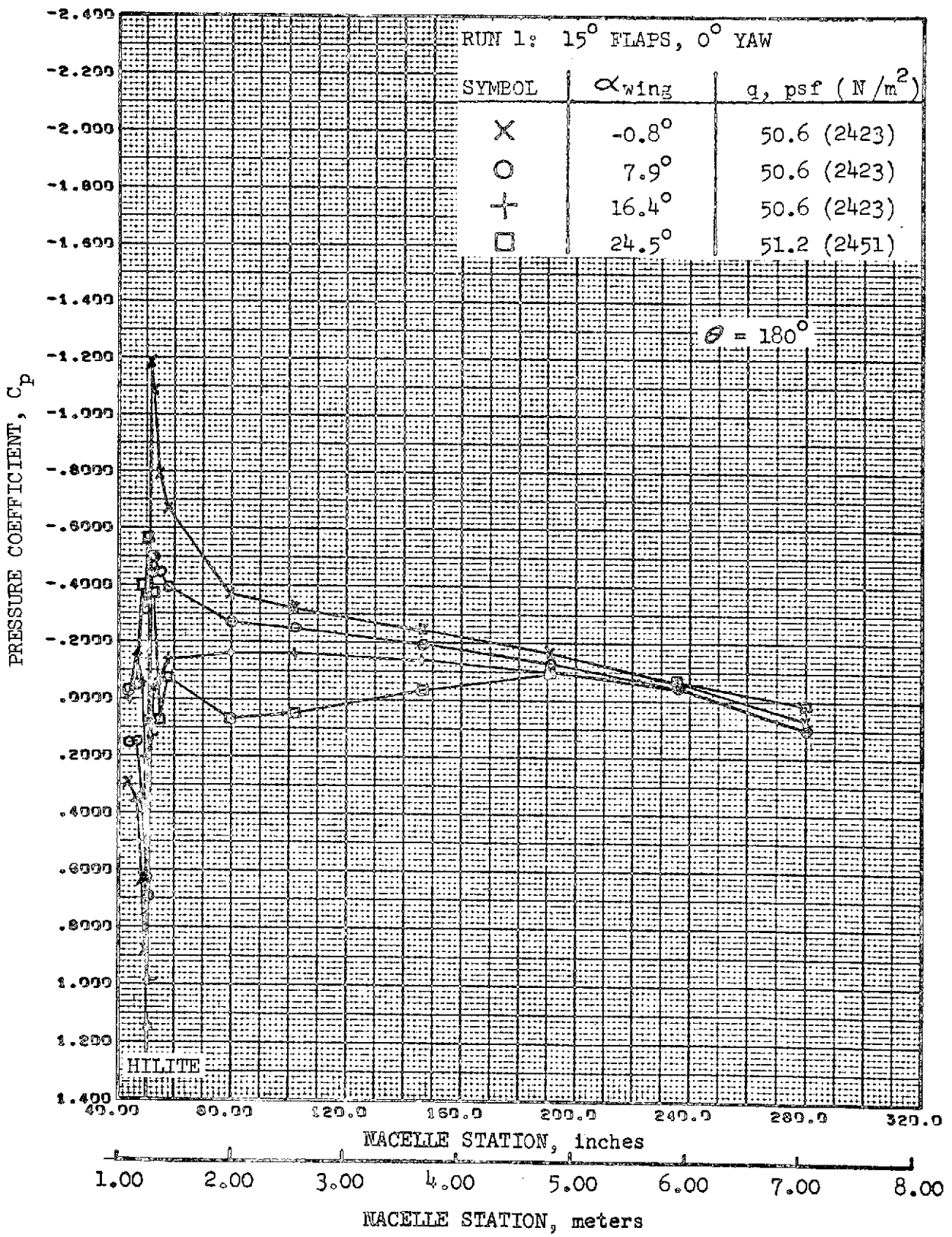

FIGURE 65. -REFAN NACELLE PRESSURE COEFFICIENT DISTRIBUTION, BOTTOM LONGITUDINAL

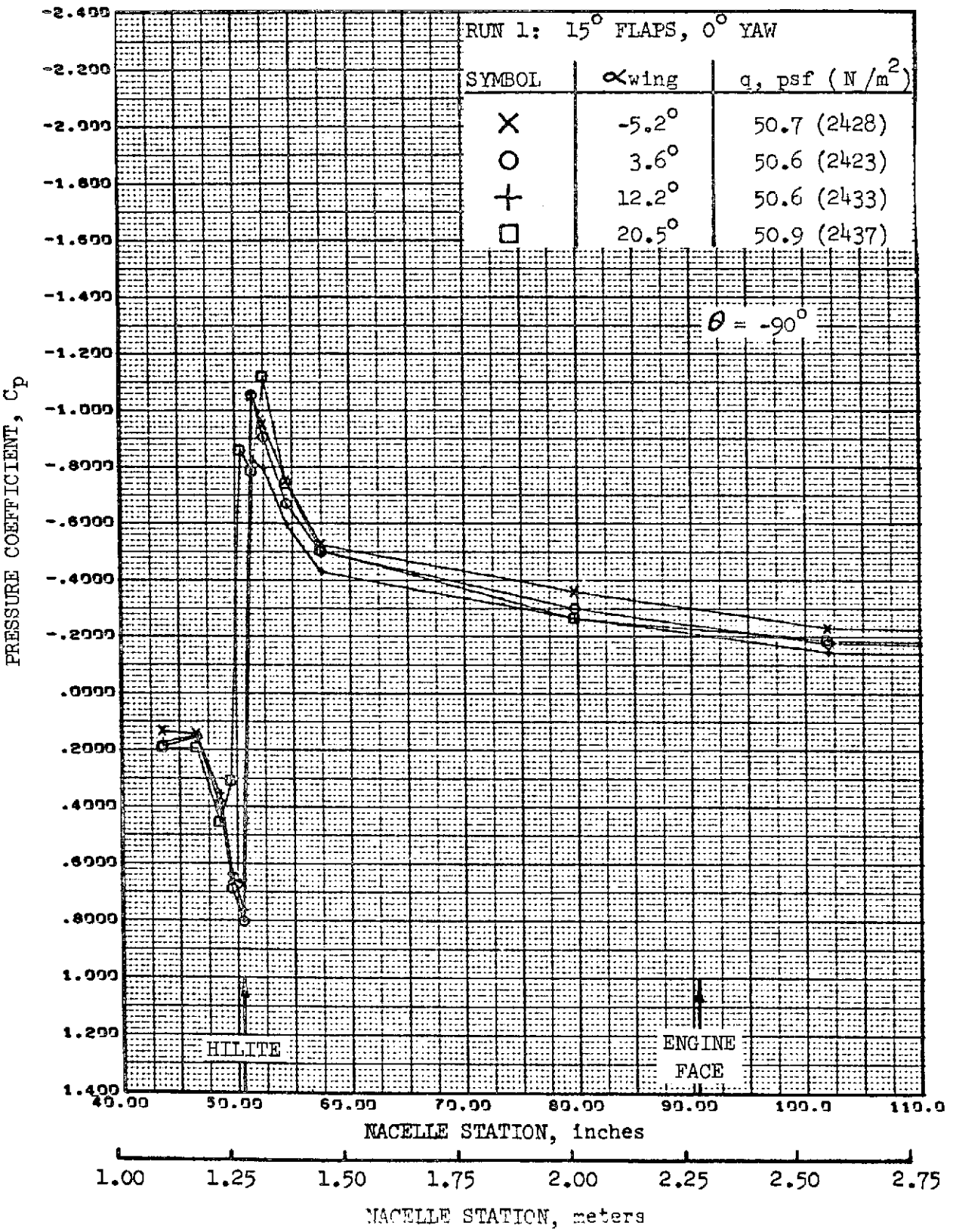

FIGURE 66. -REFAN NACELLE INLET COWL PRESSURE COEFFICIENT DISTRIBUTION, OUTBOARD SIDE

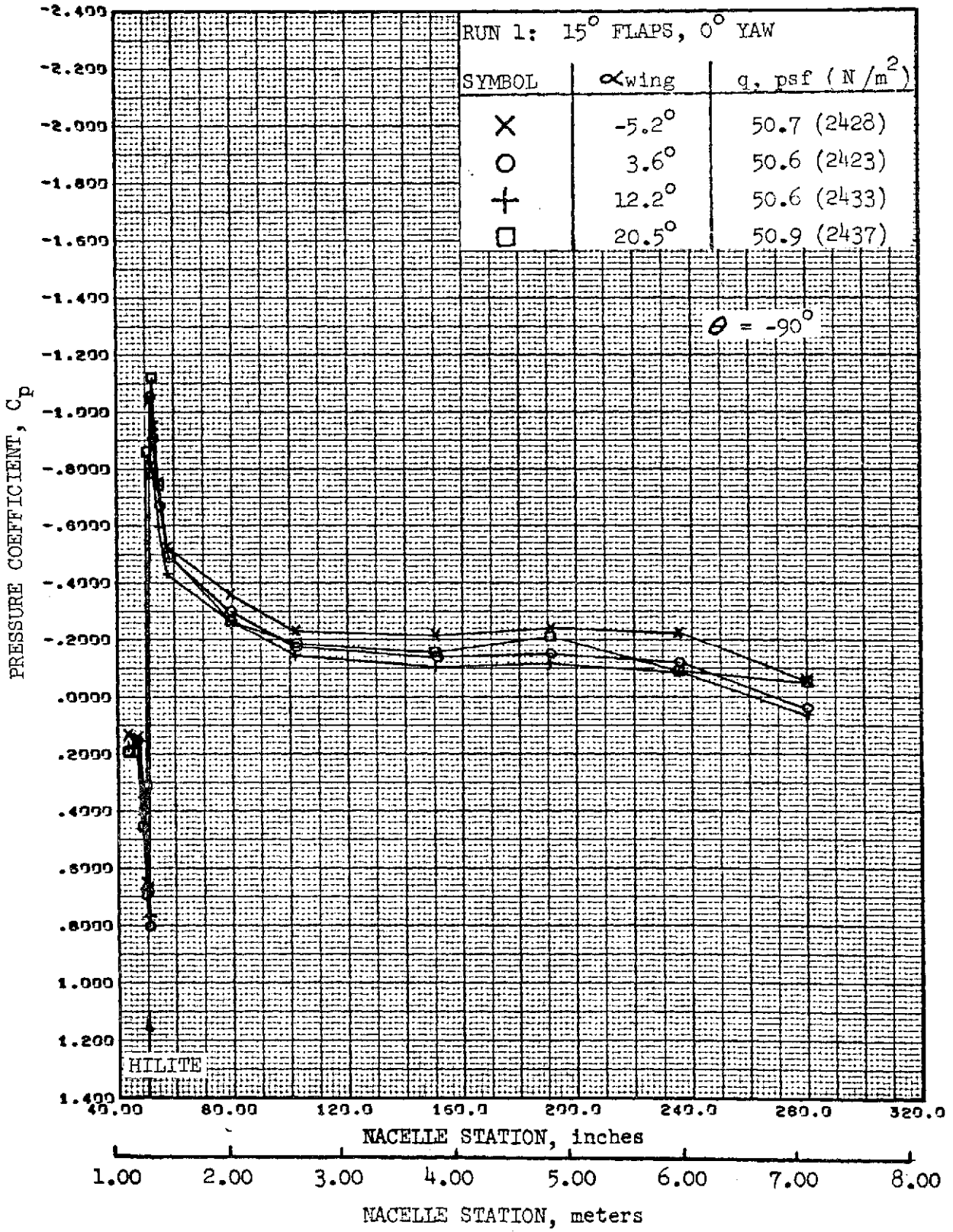

FIGURE 67. -REFAN NACELLE PRESSURE COEFFICIENT DISTRIBUTION, OUTBOARD SIDE

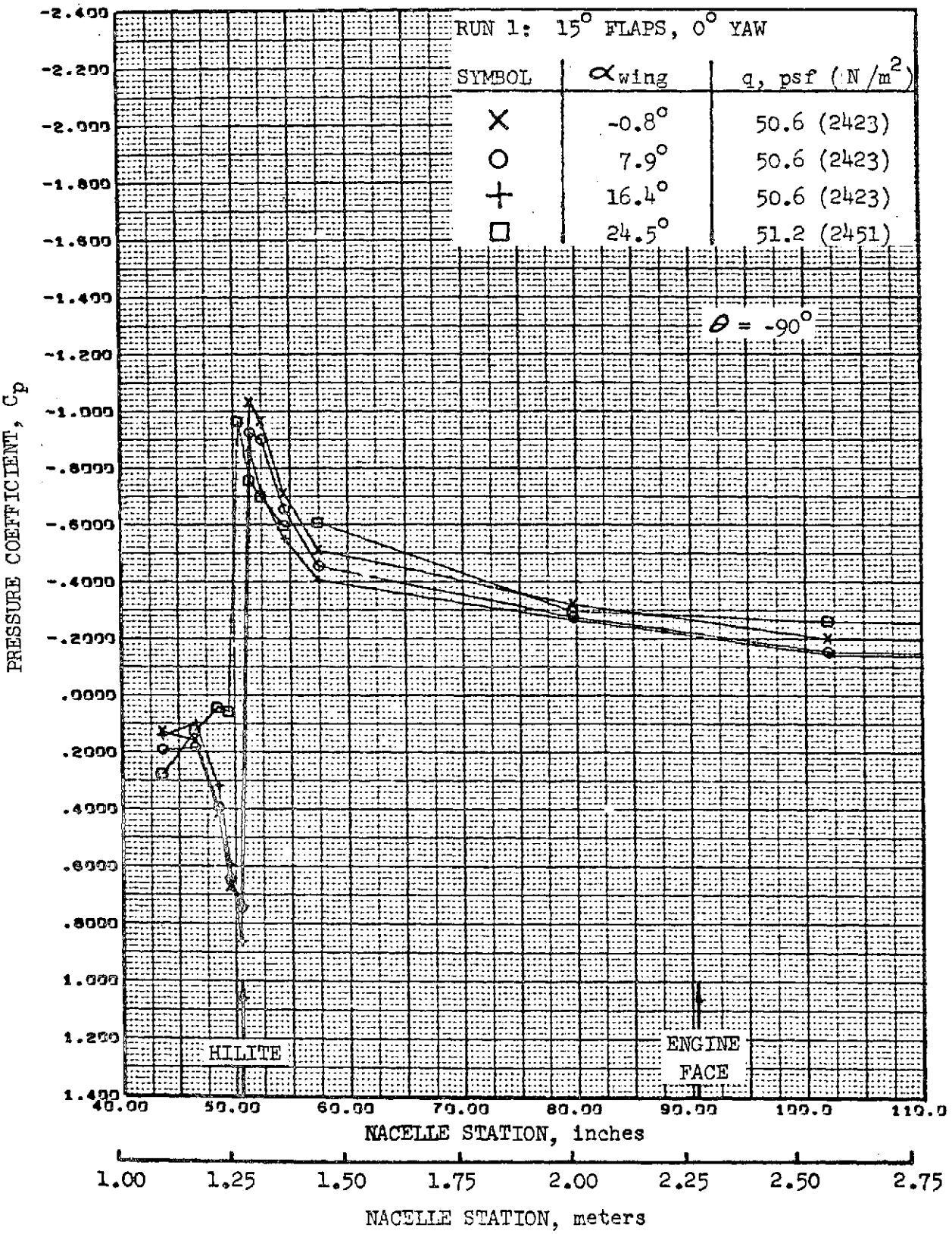

FIGURE 68. -REFAN NACELLE INLET COWL PRESSURE COEFFICIENT DISTRIBUTION, OUTBOARD SIDE

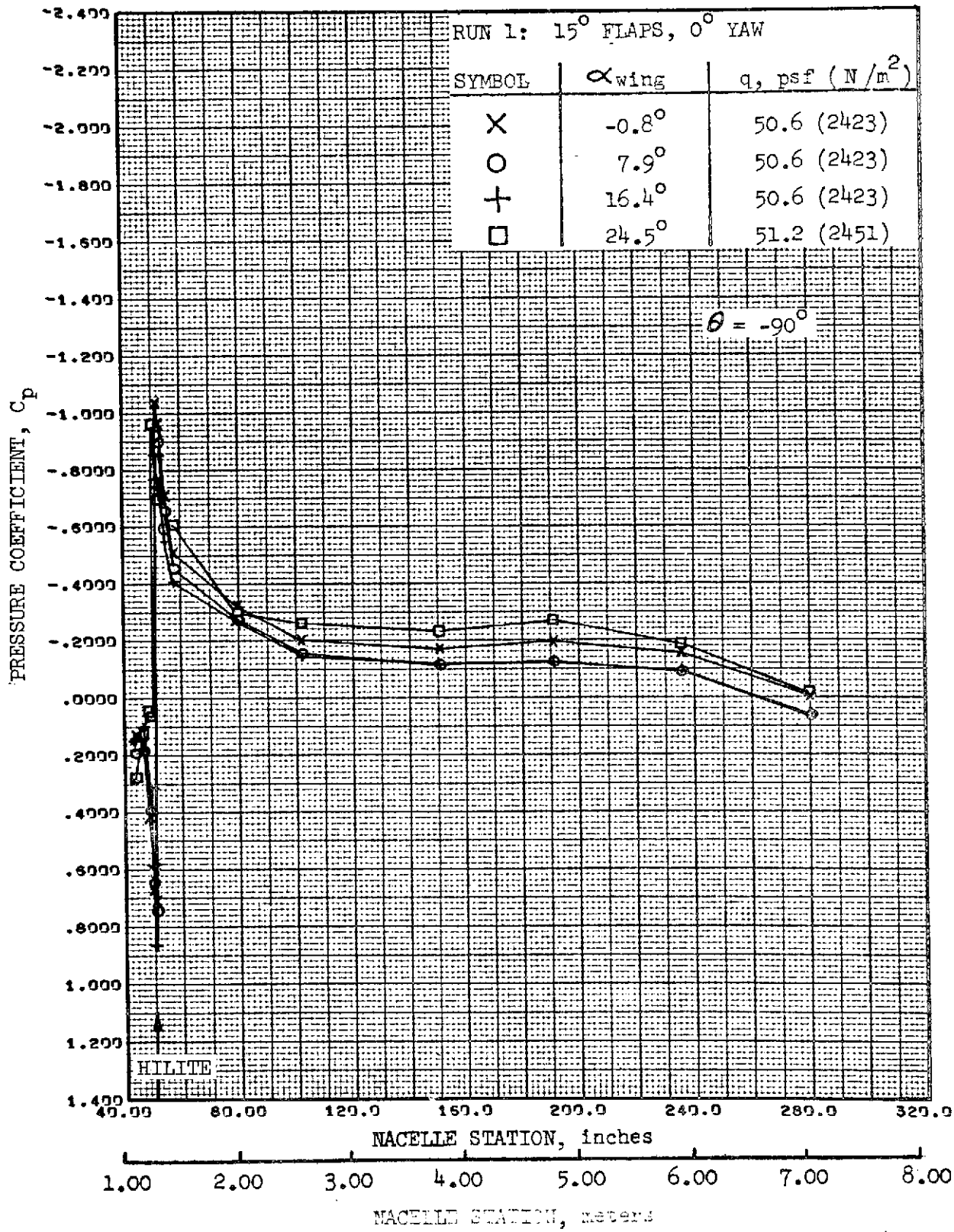

FIGURE 69. -REFAN NACELLE PRESSURE COEFFICIENT DISTRIBUTION, OUTBOARD SIDE

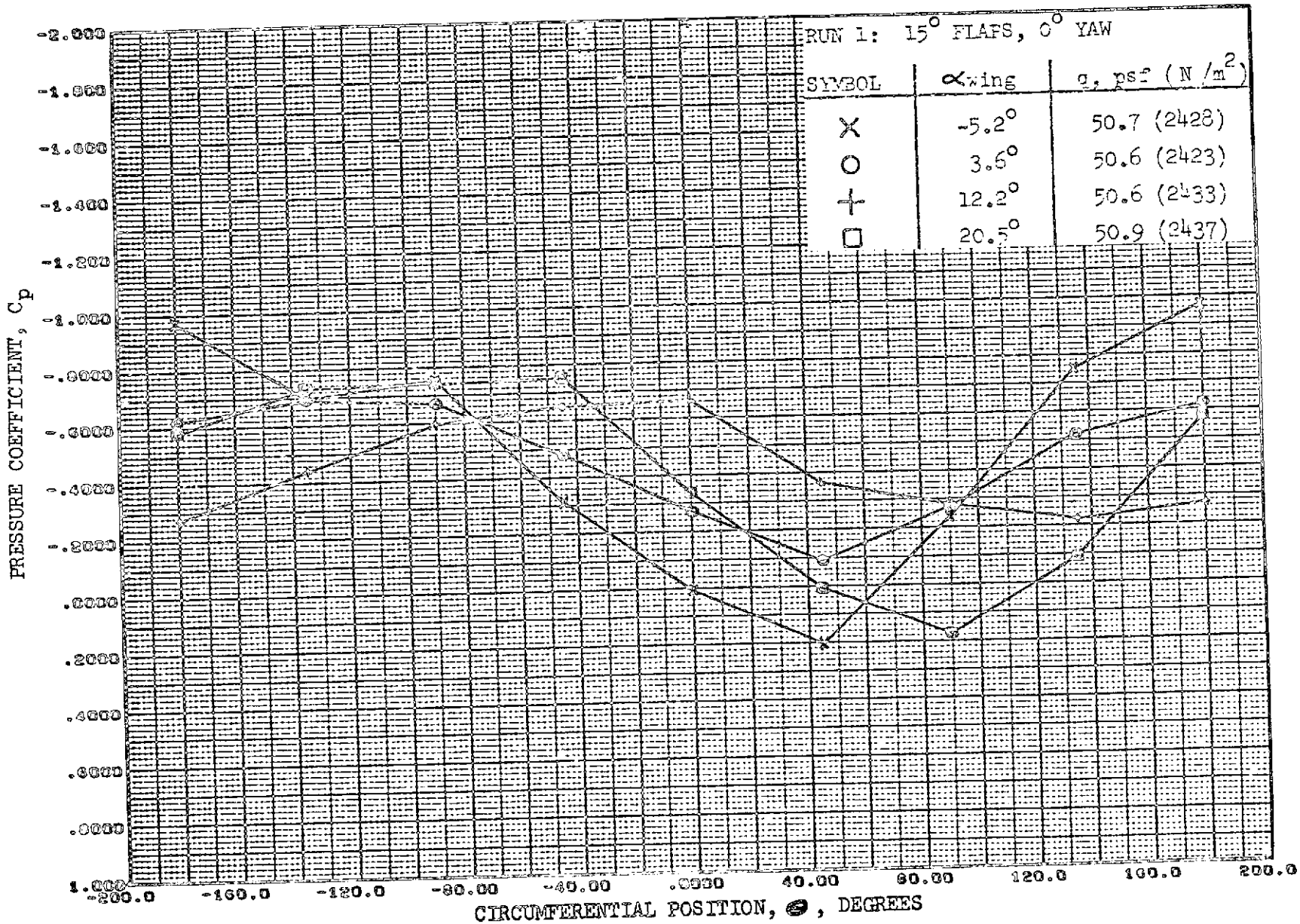

FIGURE 70. - REFAN NACELLE PRESSURE COEFFICIENT DISTRIBUTION, EXTERNAL CIRCUMFERENTIAL AT STATION 54.5 INCHES (1.38 METERS)

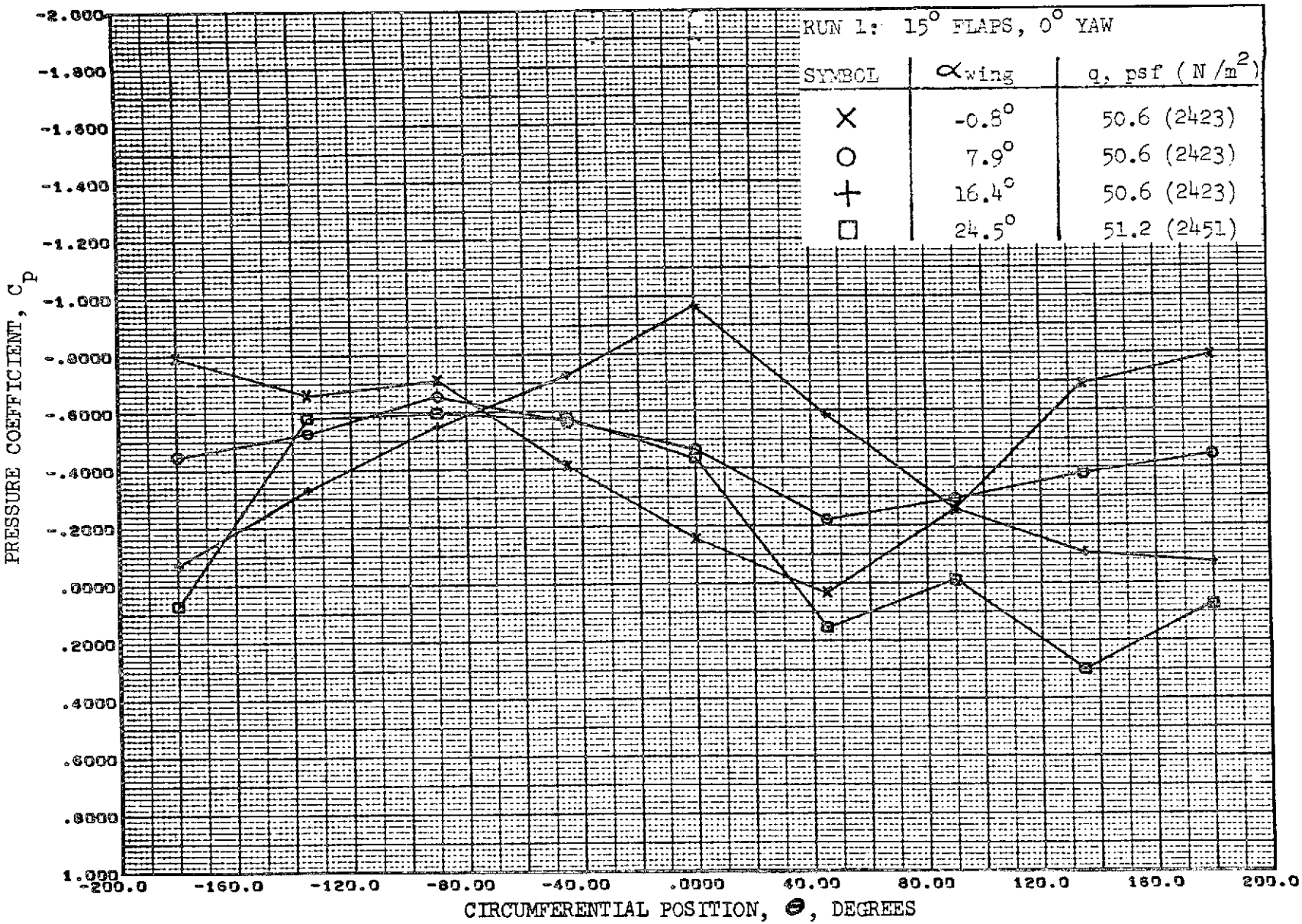

FIGURE 71. - REFAN NACELLE PRESSURE COEFFICIENT DISTRIBUTION, EXTERNAL CIRCUMFERENTIAL AT STATION 54.5 INCHES (1.38 METERS)

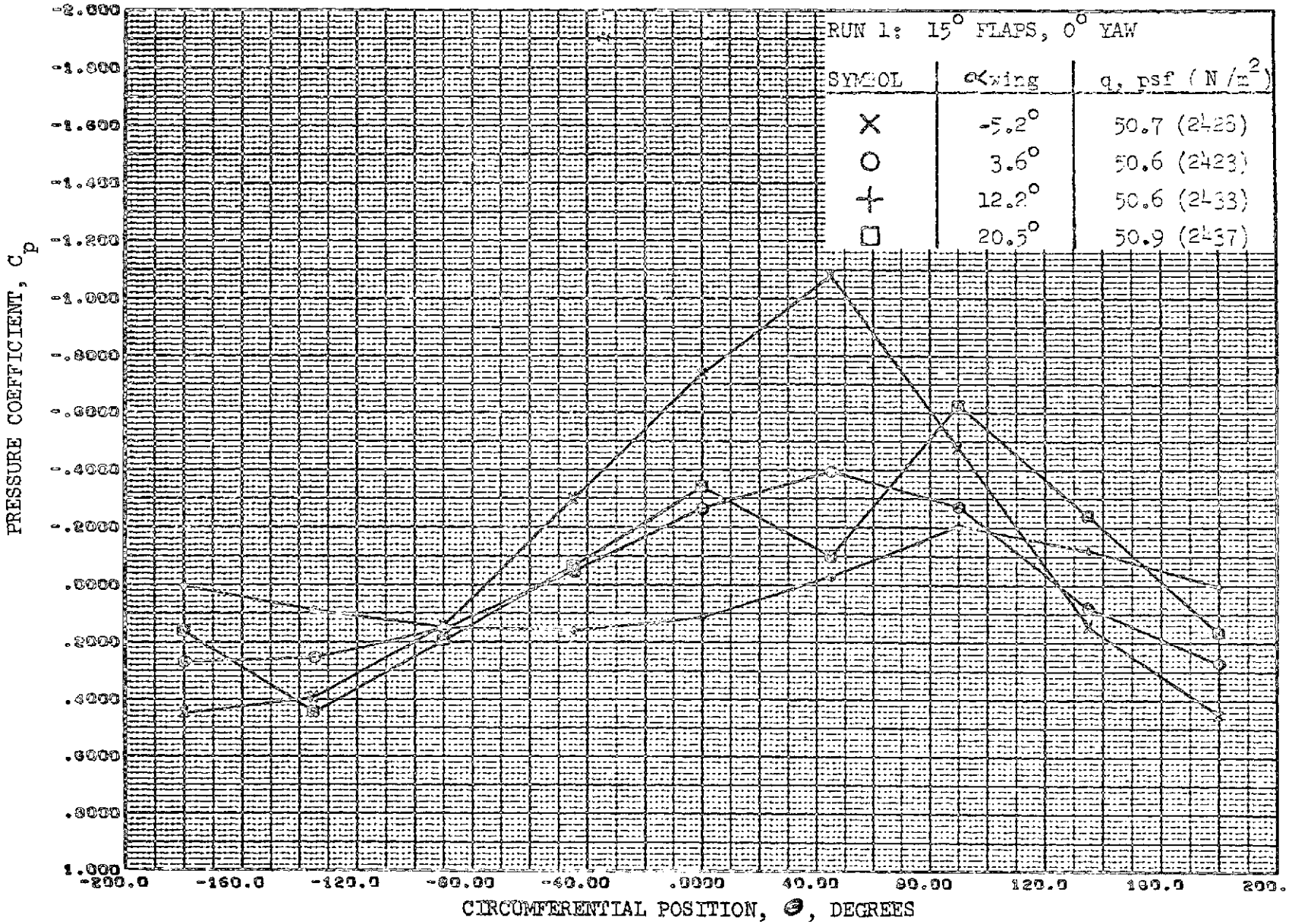

FIGURE 72. - REFAN NACELLE PRESSURE COEFFICIENT DISTRIBUTION, INTERNAL CIRCUMFERENTIAL AT STATION 54.5 INCHES (1.38 METERS)

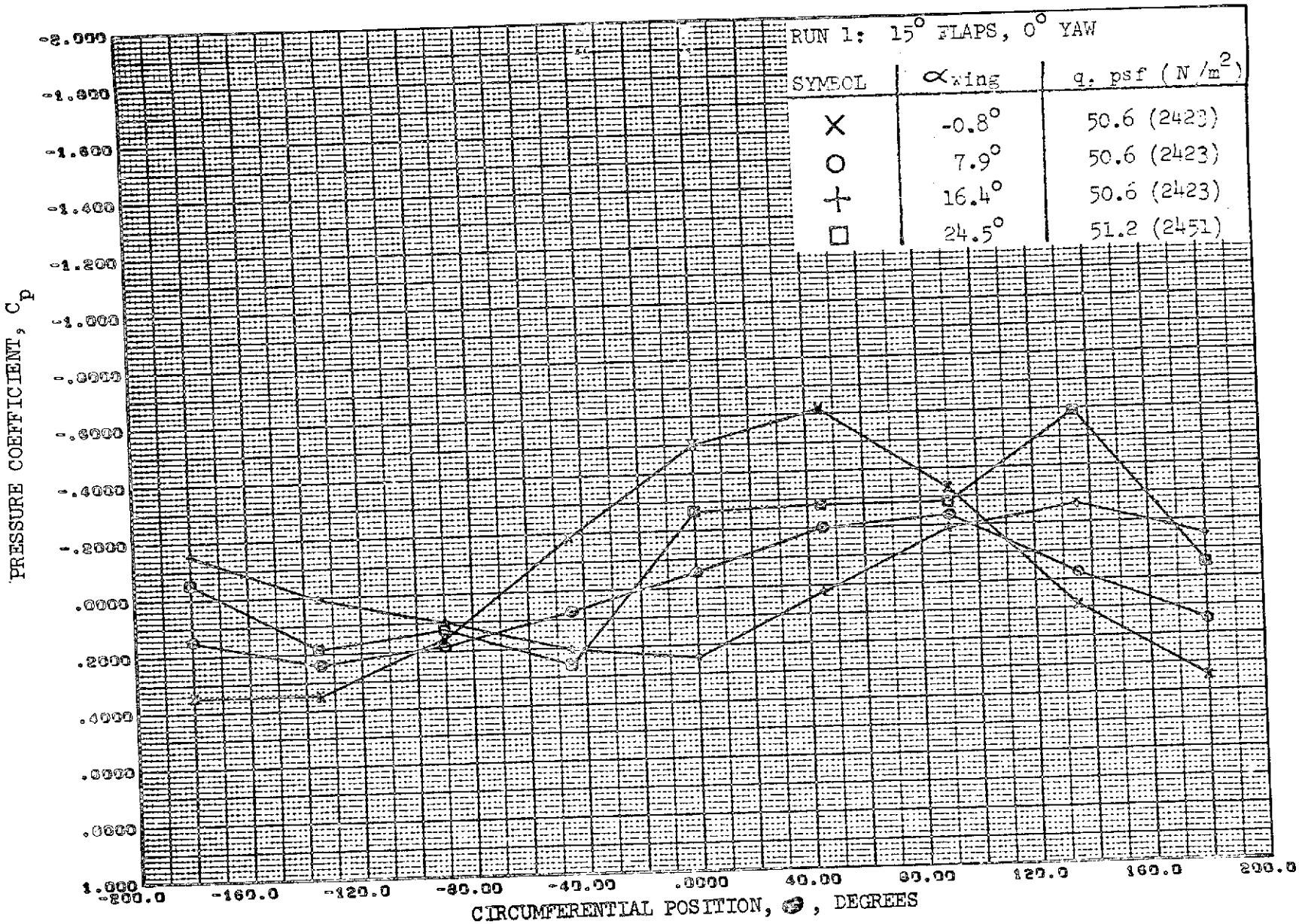

FIGURE 73. - REFAN NACELLE PRESSURE COEFFICIENT DISTRIBUTION, INTERNAL CIRCUMFERENTIAL AT STATION 54.5 INCHES (1.38 METERS)

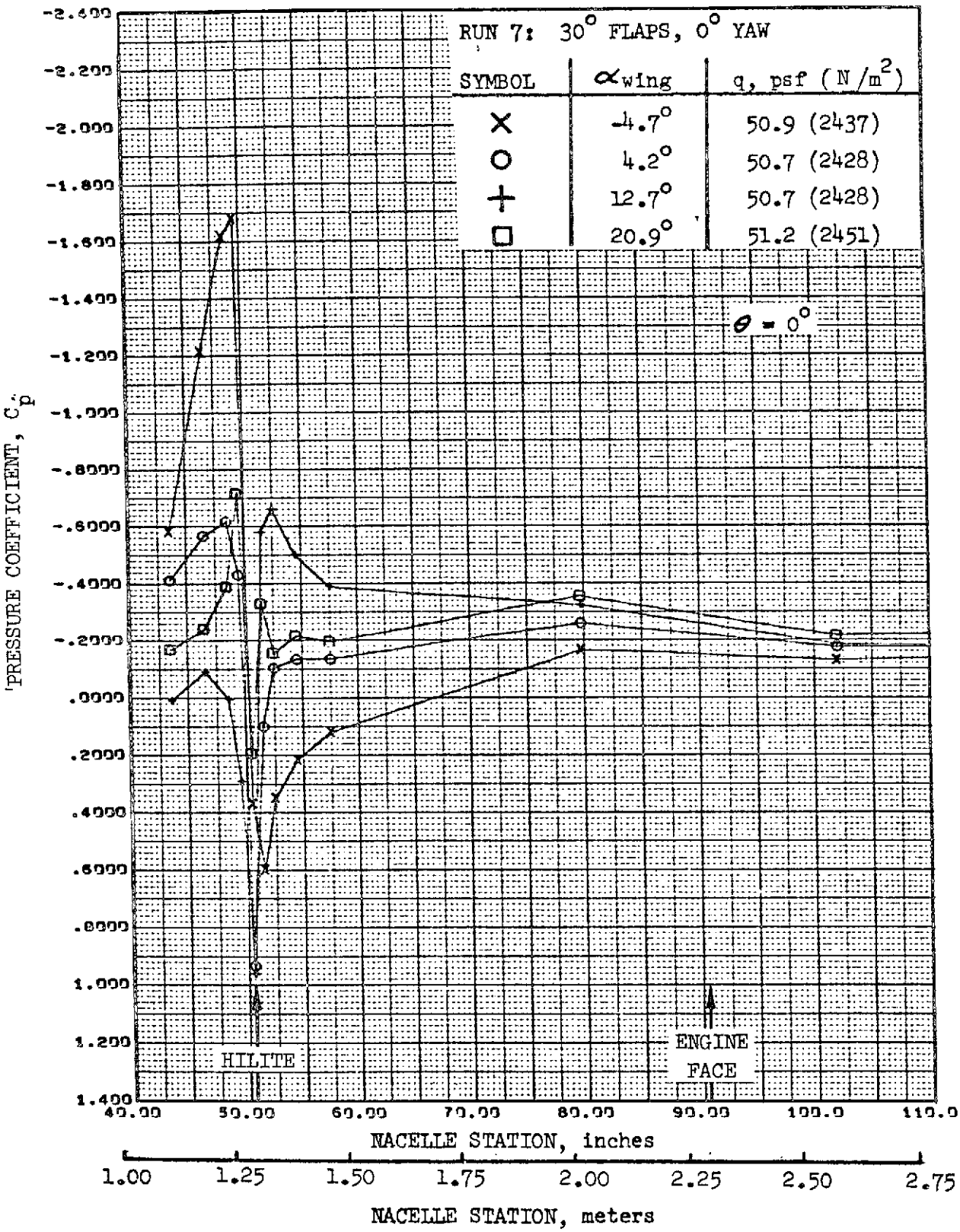

FIGURE 74. -REFAN NACELLE INLET COWL PRESSURE COEFFICIENT DISTRIBUTION, TOP LONGITUDINAL

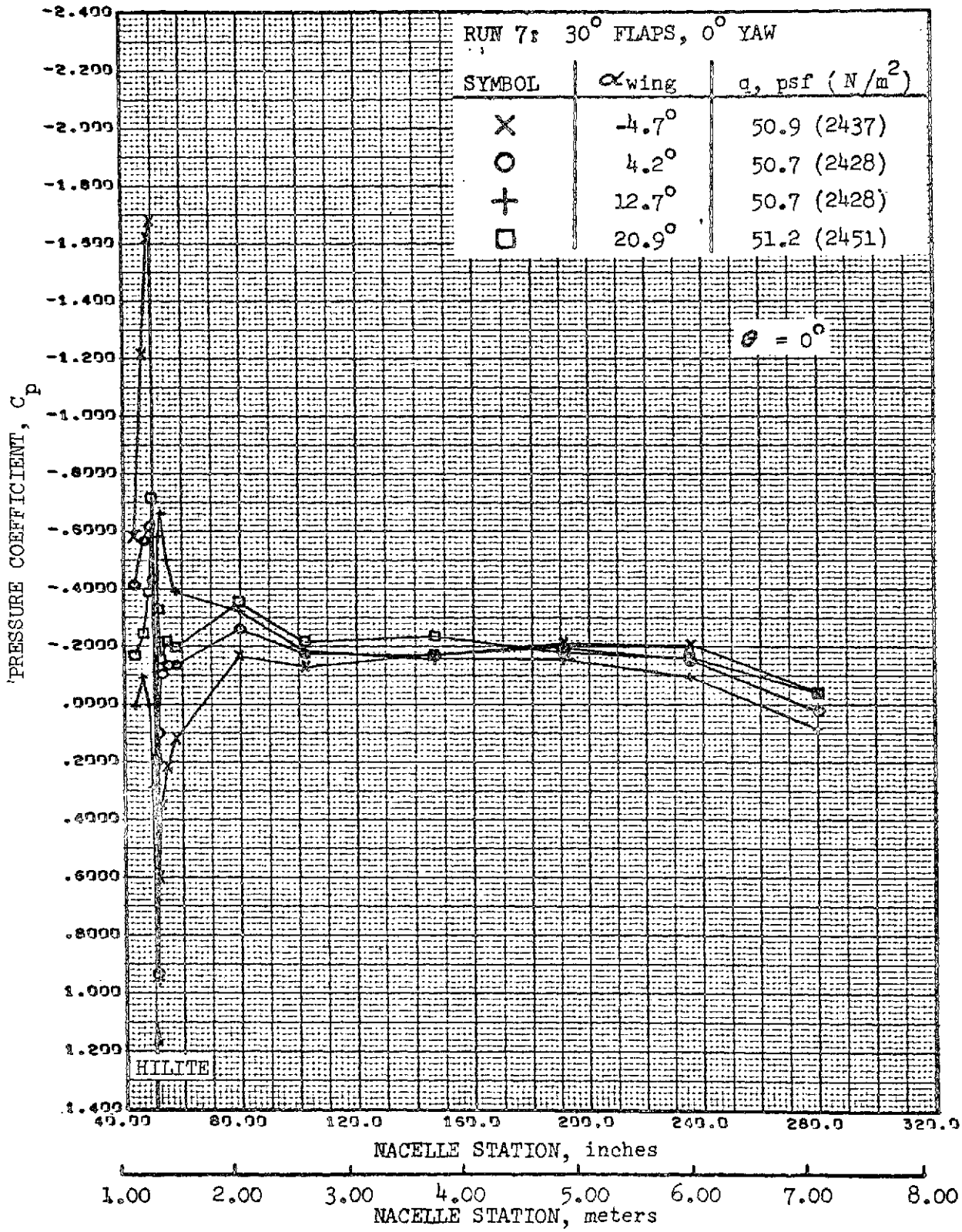

FIGURE 75. -REFAN NACELLE PRESSURE COEFFICIENT DISTRIBUTION, TOP LONGITUDINAL

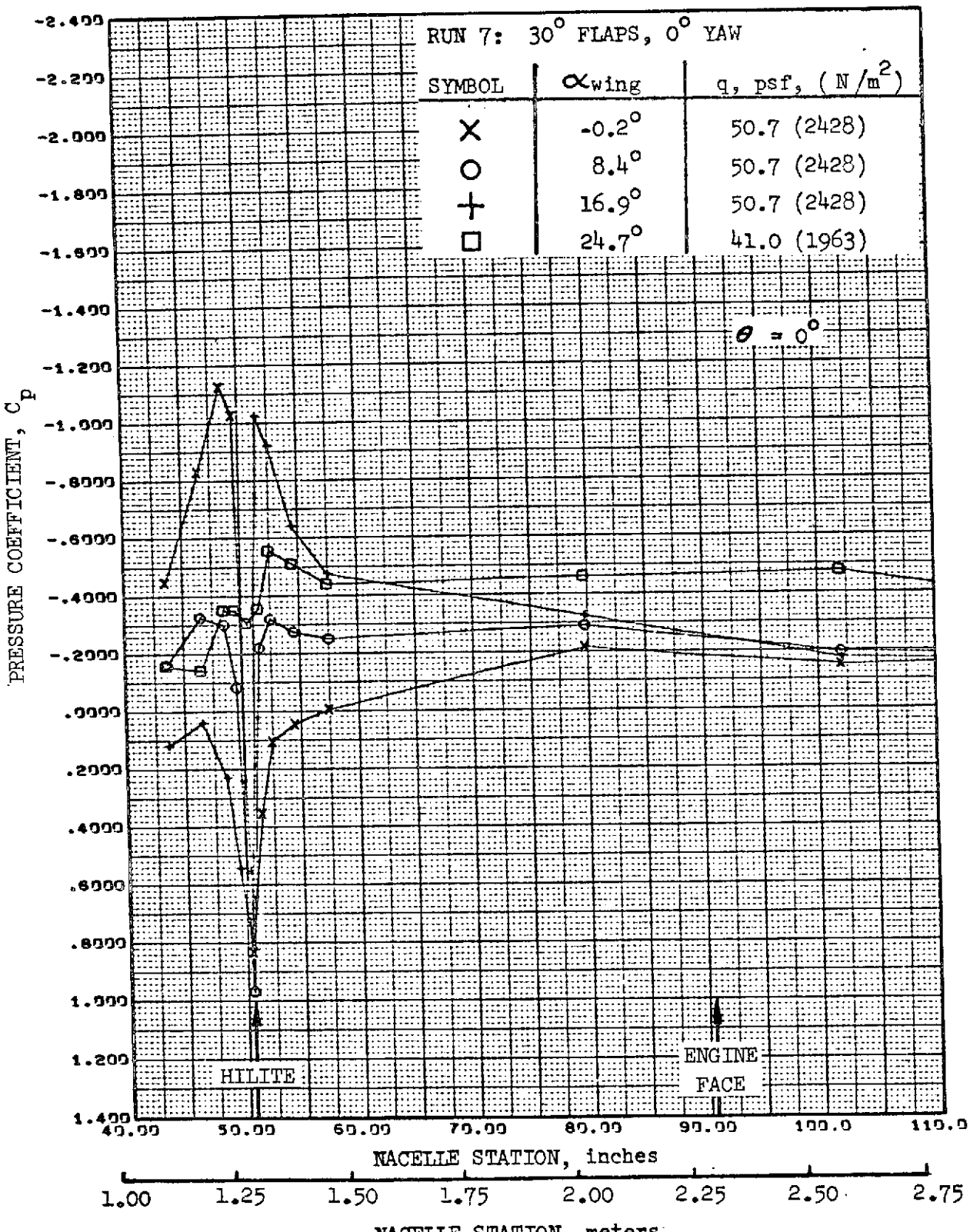

FIGURE 76. -REFAN NACELLE INLET COWL PRESSURE COEFFICIENT DISTRIBUTION, TOP LONGITUDINAL

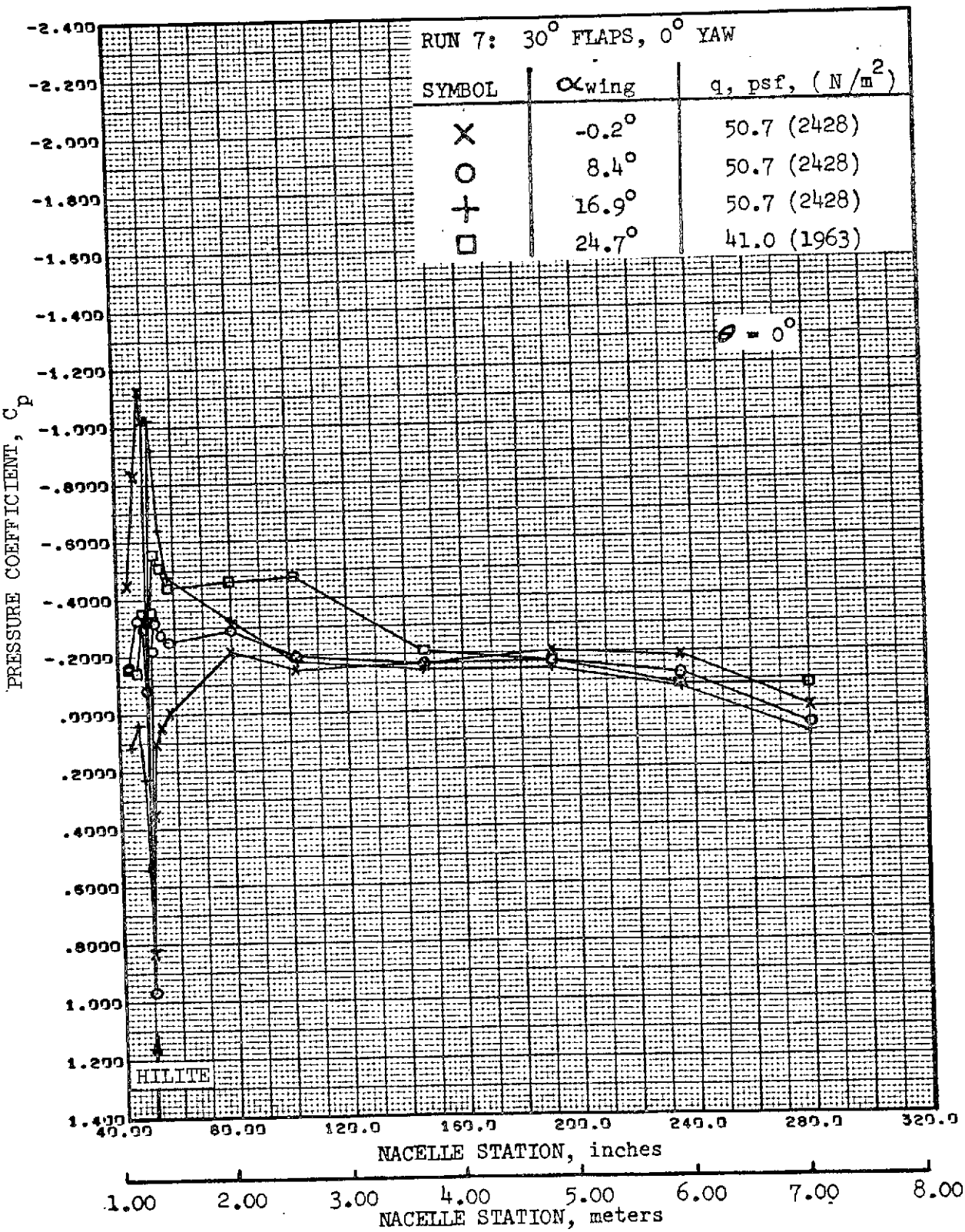

FIGURE 77. -REFAN NACELLE PRESSURE COEFFICIENT DISTRIBUTION, TOP LONGITUDINAL

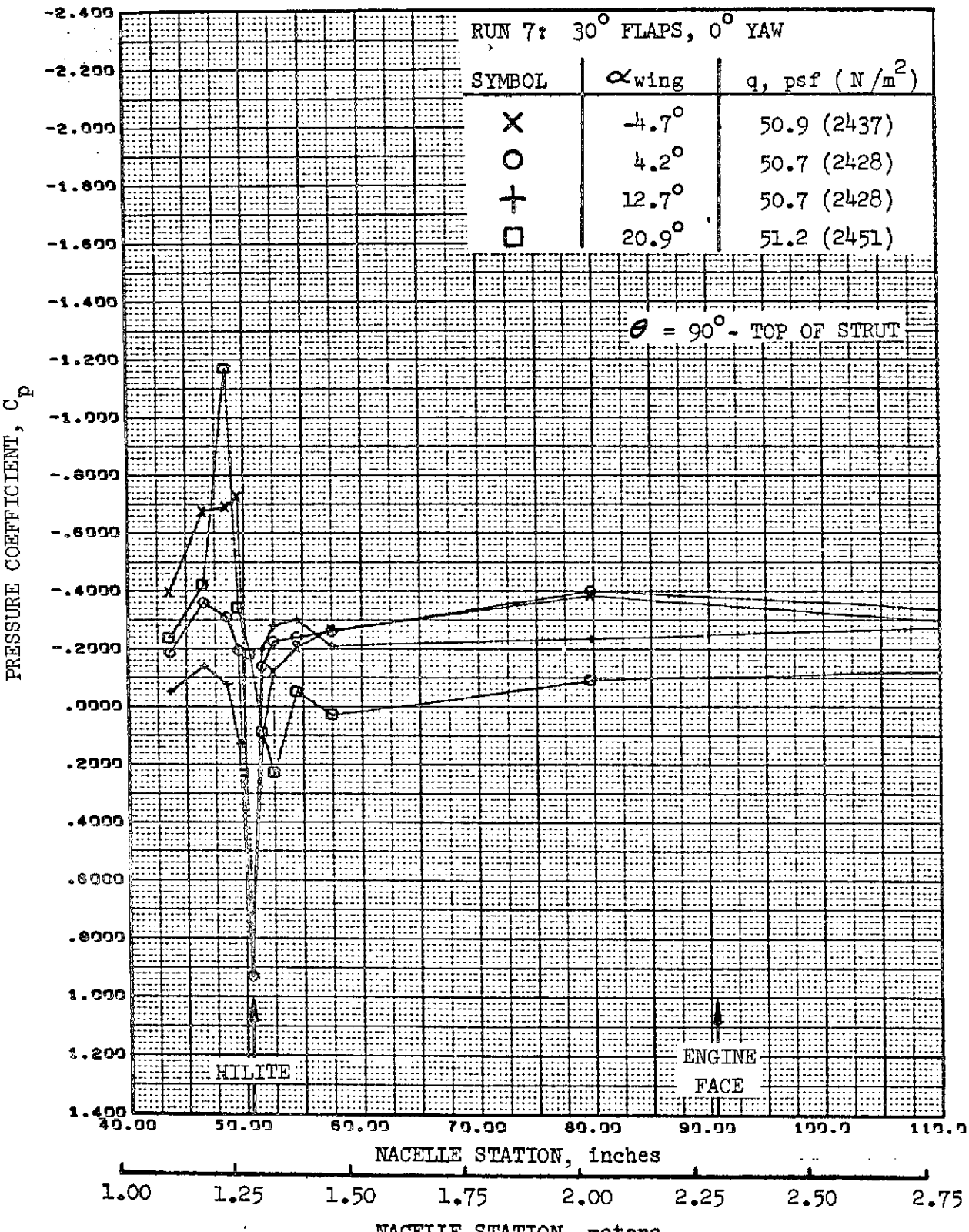

FIGURE 78. -REFAN NACELLE INLET COWL PRESSURE COEFFICIENT DISTRIBUTION, INBOARD SIDE-ABOVE STRUT

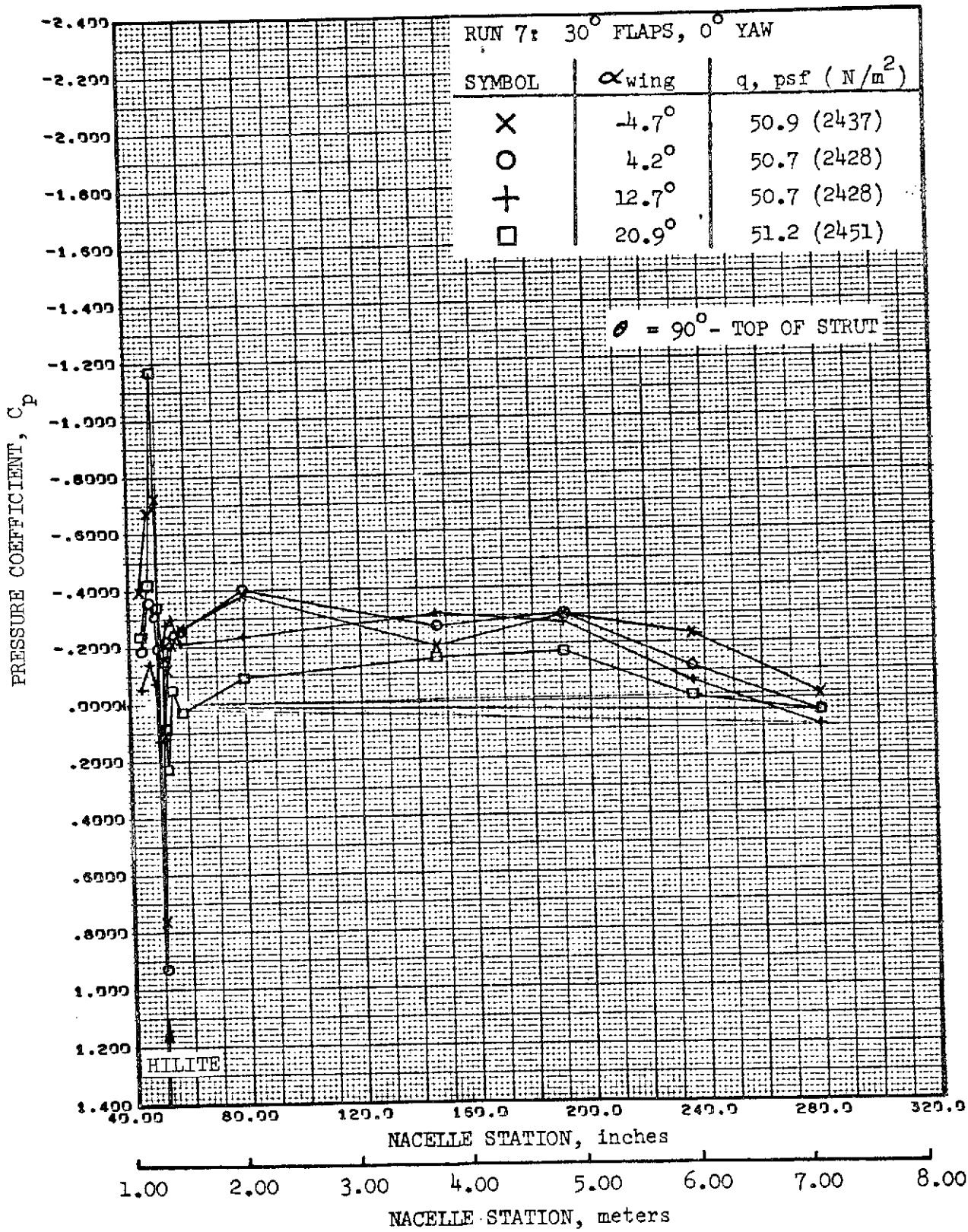

FIGURE 79. -REFAN NACELLE PRESSURE COEFFICIENT DISTRIBUTION, INBOARD SIDE-ABOVE STRUT

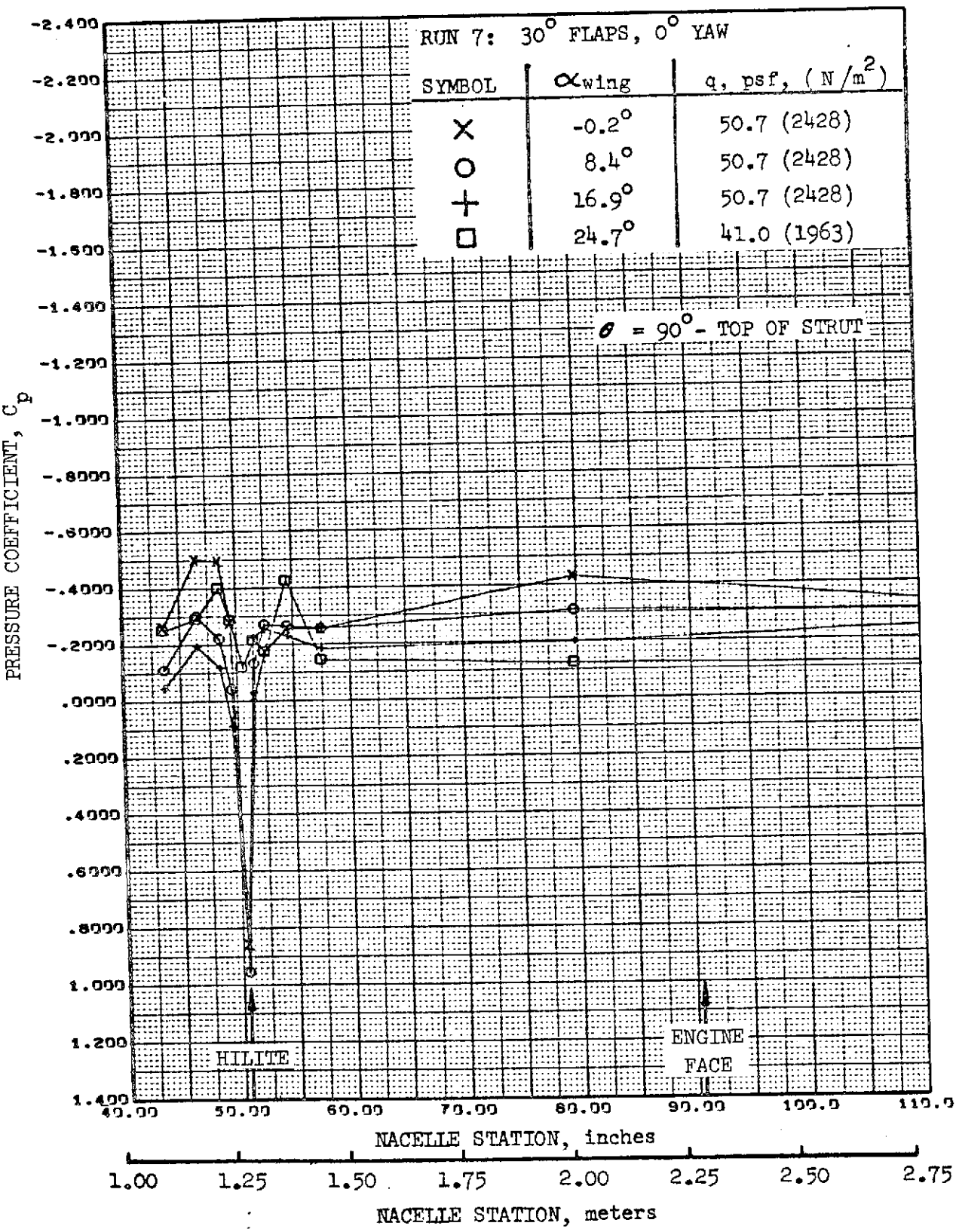

FIGURE 80. REFAN NACELLE INLET COWL PRESSURE COEFFICIENT DISTRIBUTION, INBOARD SIDE-ABOVE STRUT

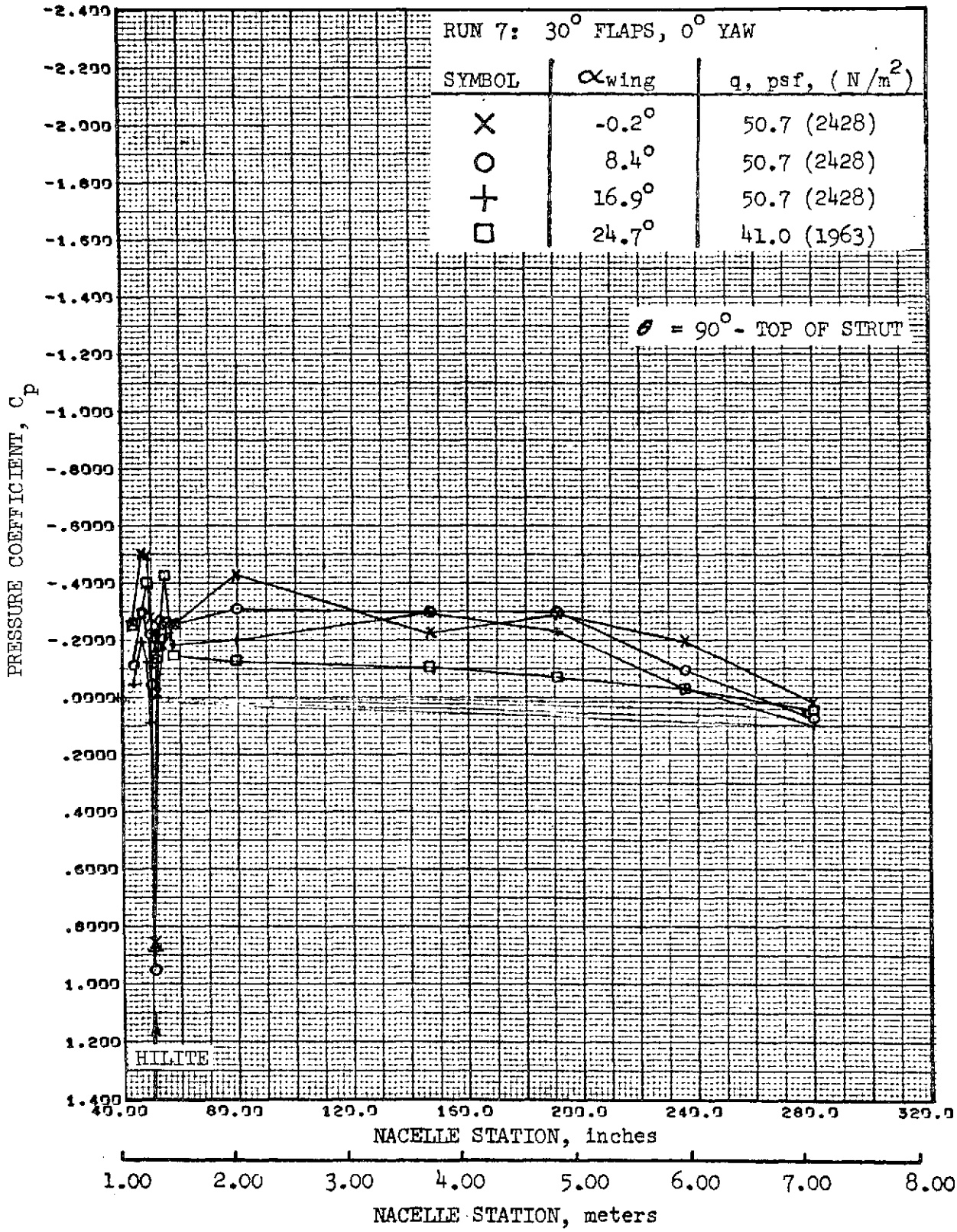

FIGURE 81. -REFAN NACELLE PRESSURE COEFFICIENT DISTRIBUTION, INBOARD SIDE-ABOVE STRUT

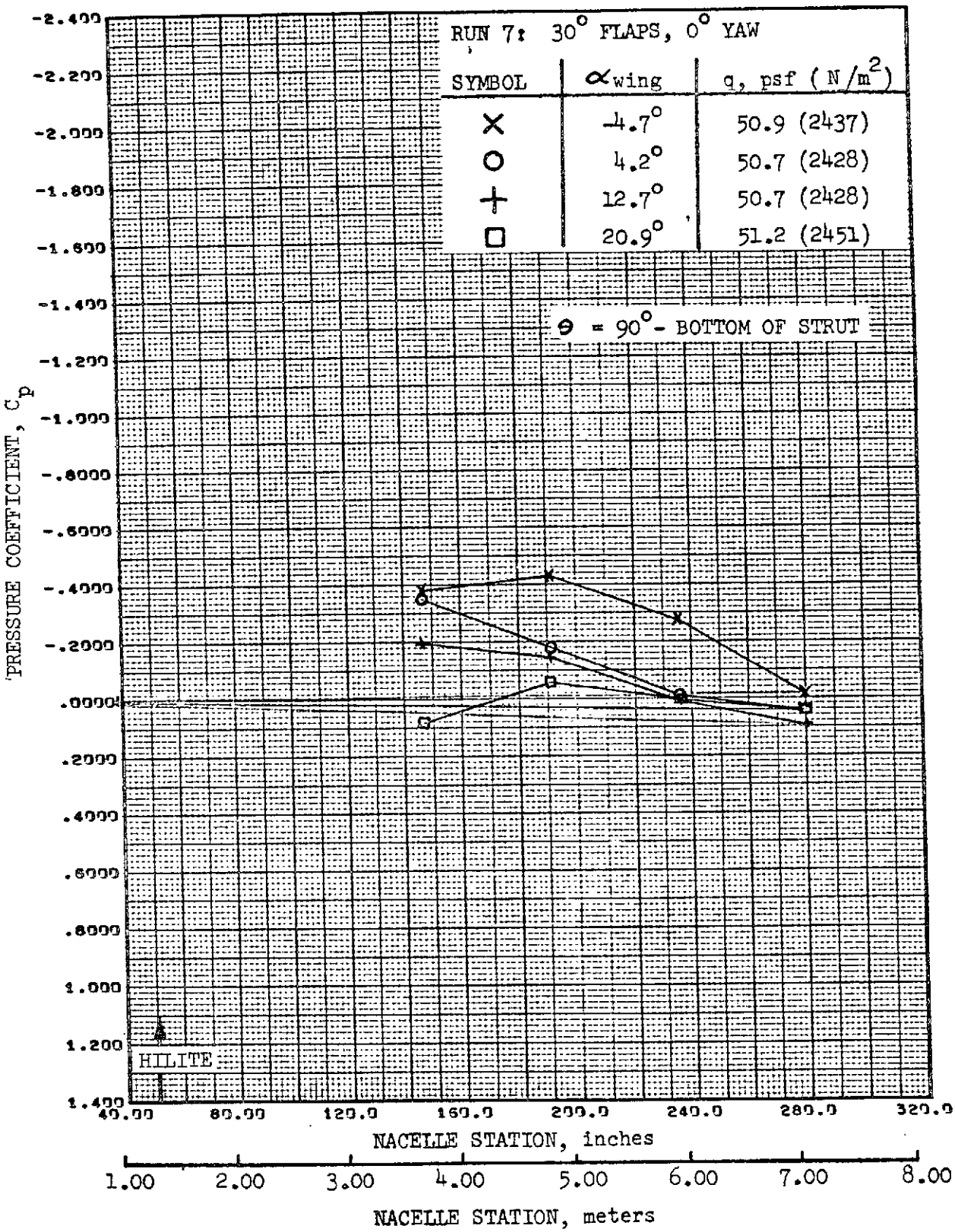

FIGURE 82. -REFAN NACELLE PRESSURE COEFFICIENT DISTRIBUTION, INBOARD SIDE-BELOW STRUT

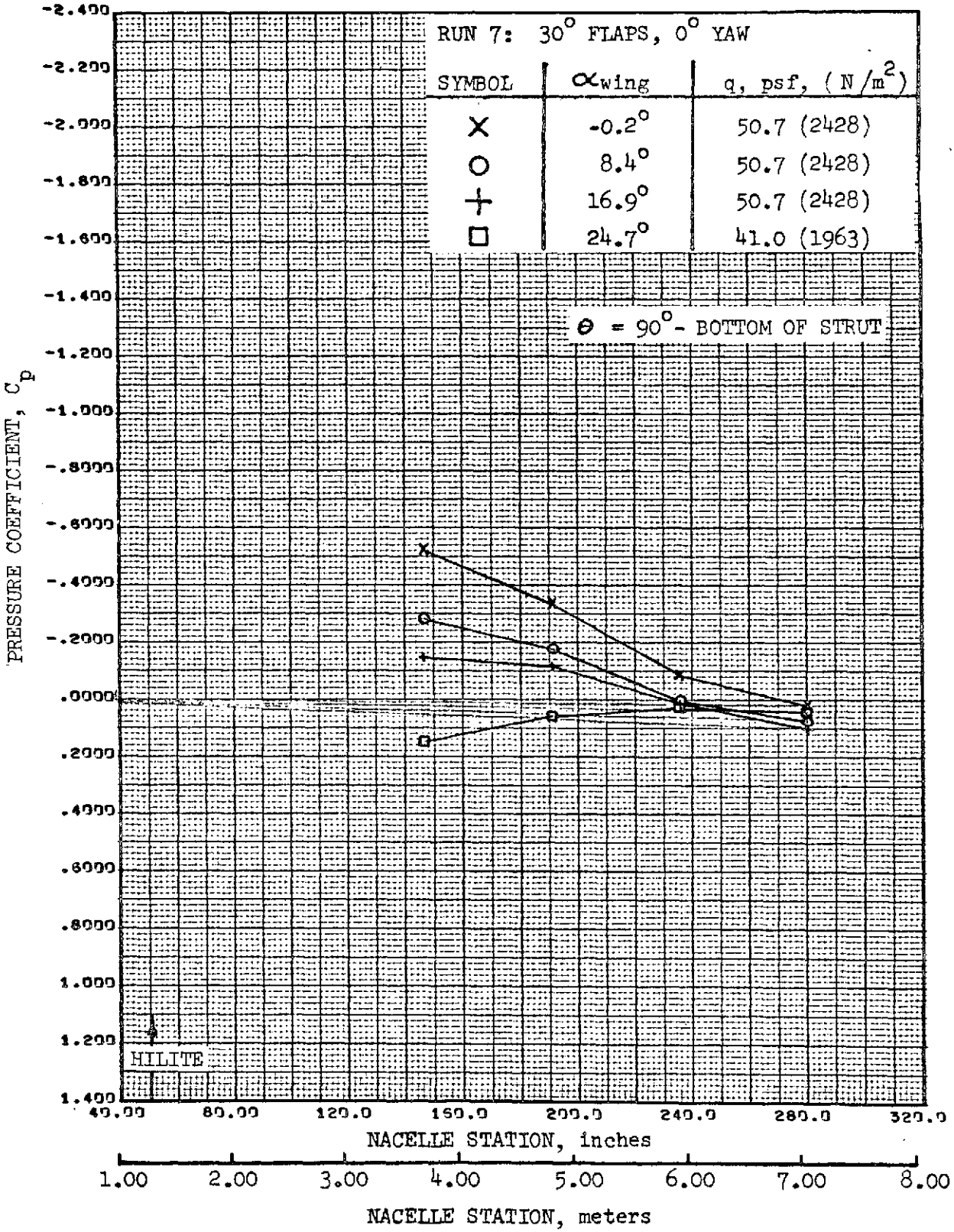

FIGURE 83. -REFAN NACELLE PRESSURE COEFFICIENT DISTRIBUTION, INBOARD SIDE-BELOW STRUT

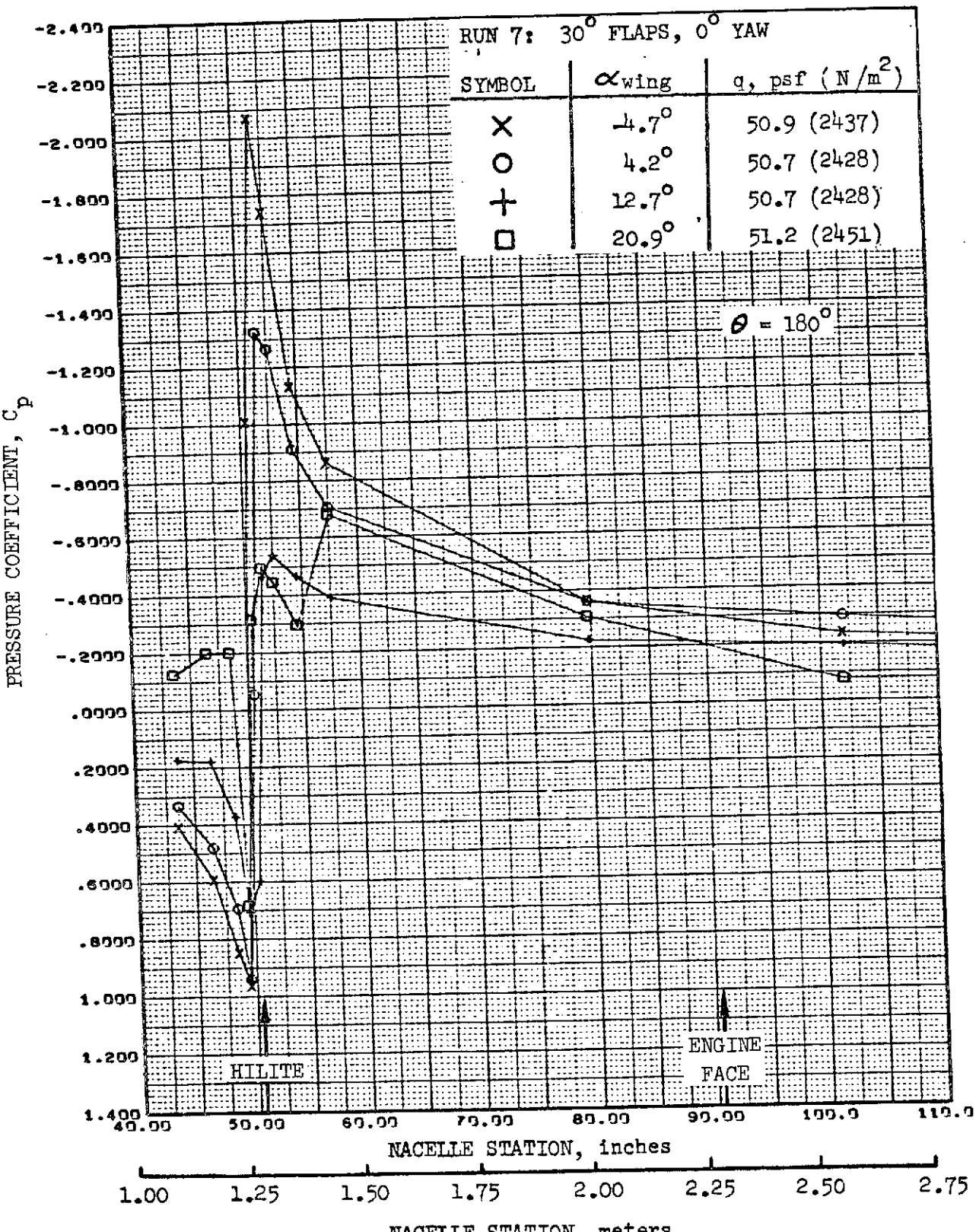

FIGURE 84. -REFAN NACELLE INLET COWL PRESSURE COEFFICIENT DISTRIBUTION BOTTOM LONGITUDINAL

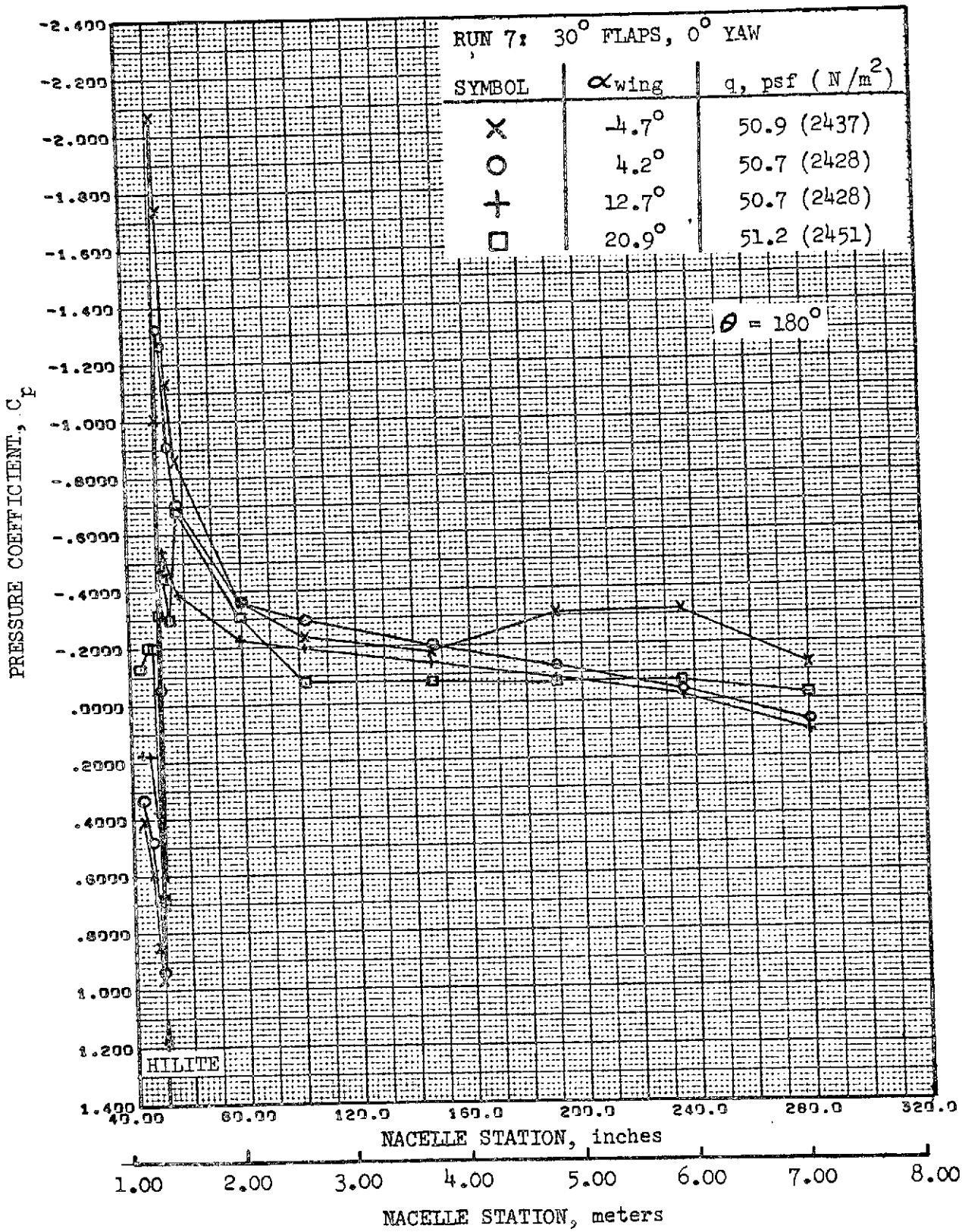

FIGURE 85.-REFAN NACELLE PRESSURE COEFFICIENT DISTRIBUTION, BOTTOM LONGITUDINAL

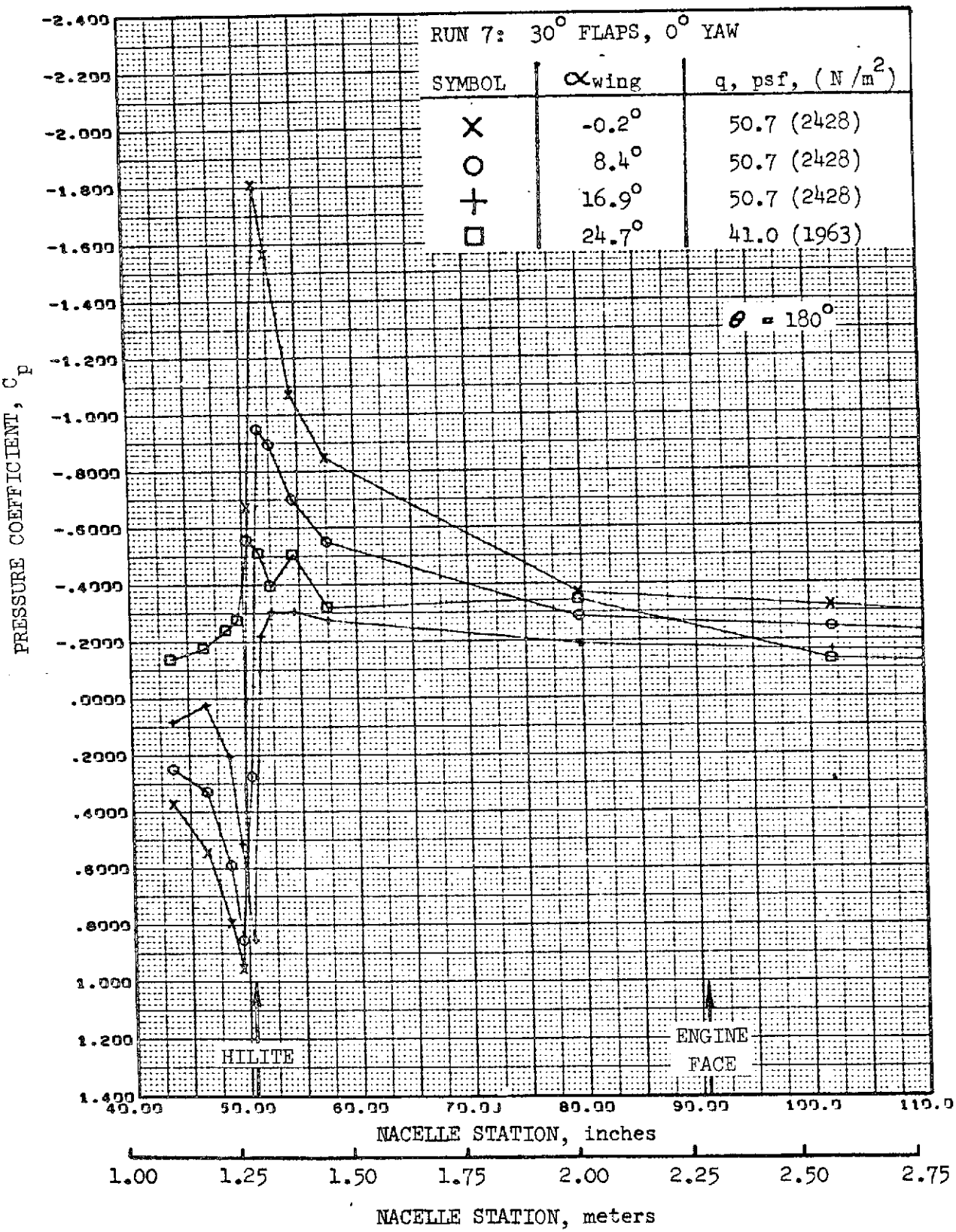

FIGURE 86. -REFAN NACELLE INLET COWL PRESSURE COEFFICIENT DISTRIBUTION, BOTTOM LONGITUDINAL

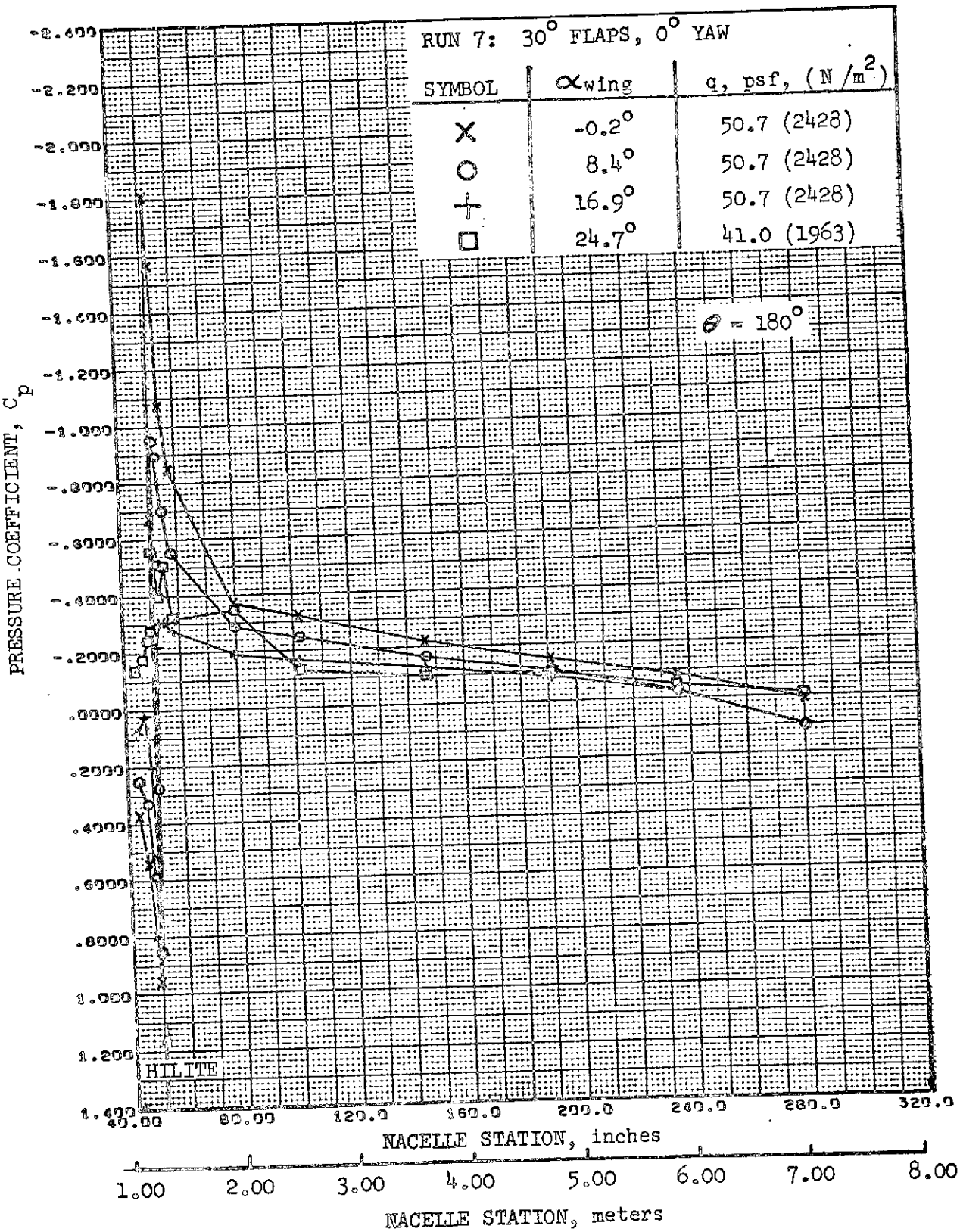

FIGURE 87. -REFAN NACELLE PRESSURE COEFFICIENT DISTRIBUTION, BOTTOM LONGITUDINAL

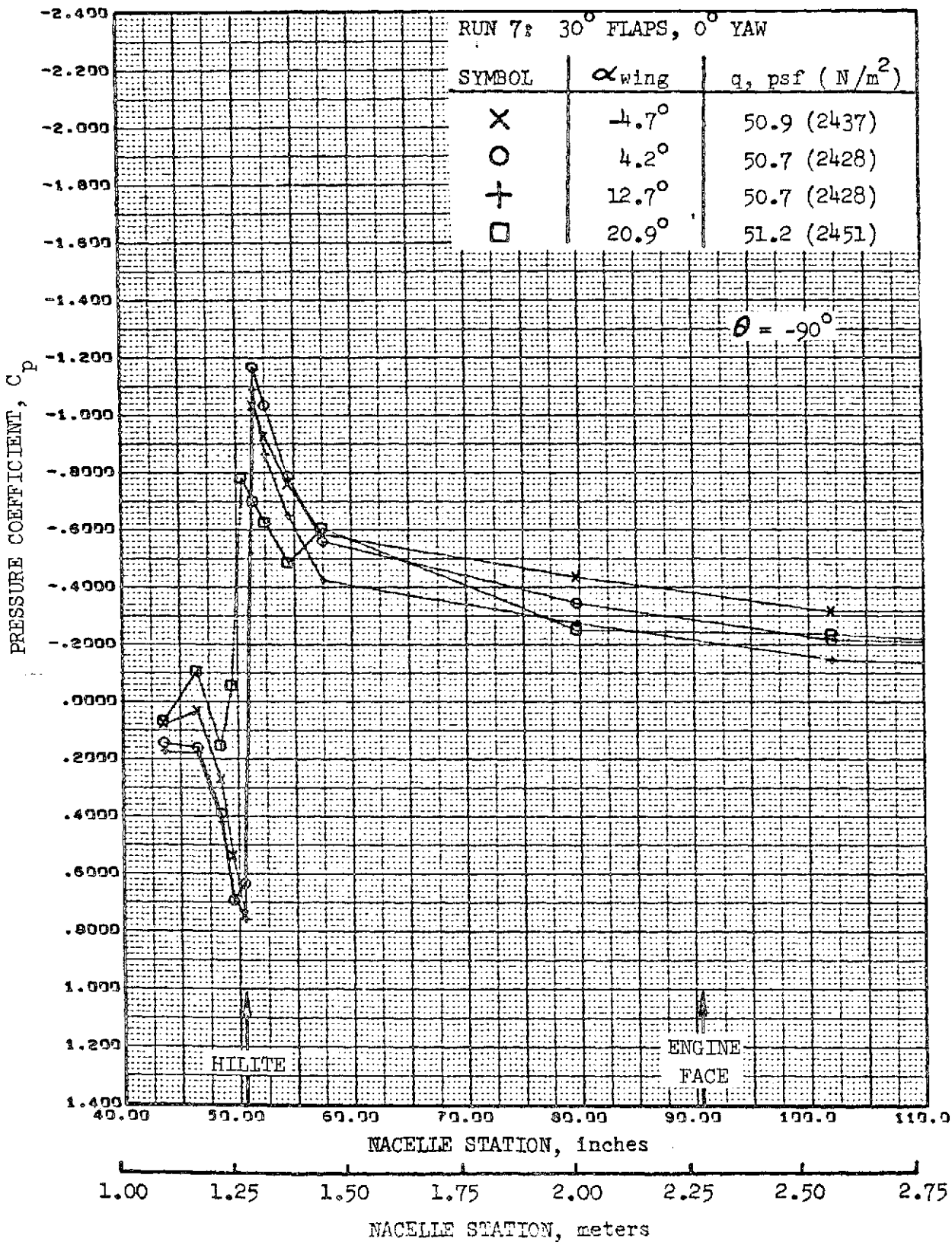

FIGURE 88. -REFAN NACELLE INLET COWL PRESSURE COEFFICIENT DISTRIBUTION, OUTBOARD SIDE

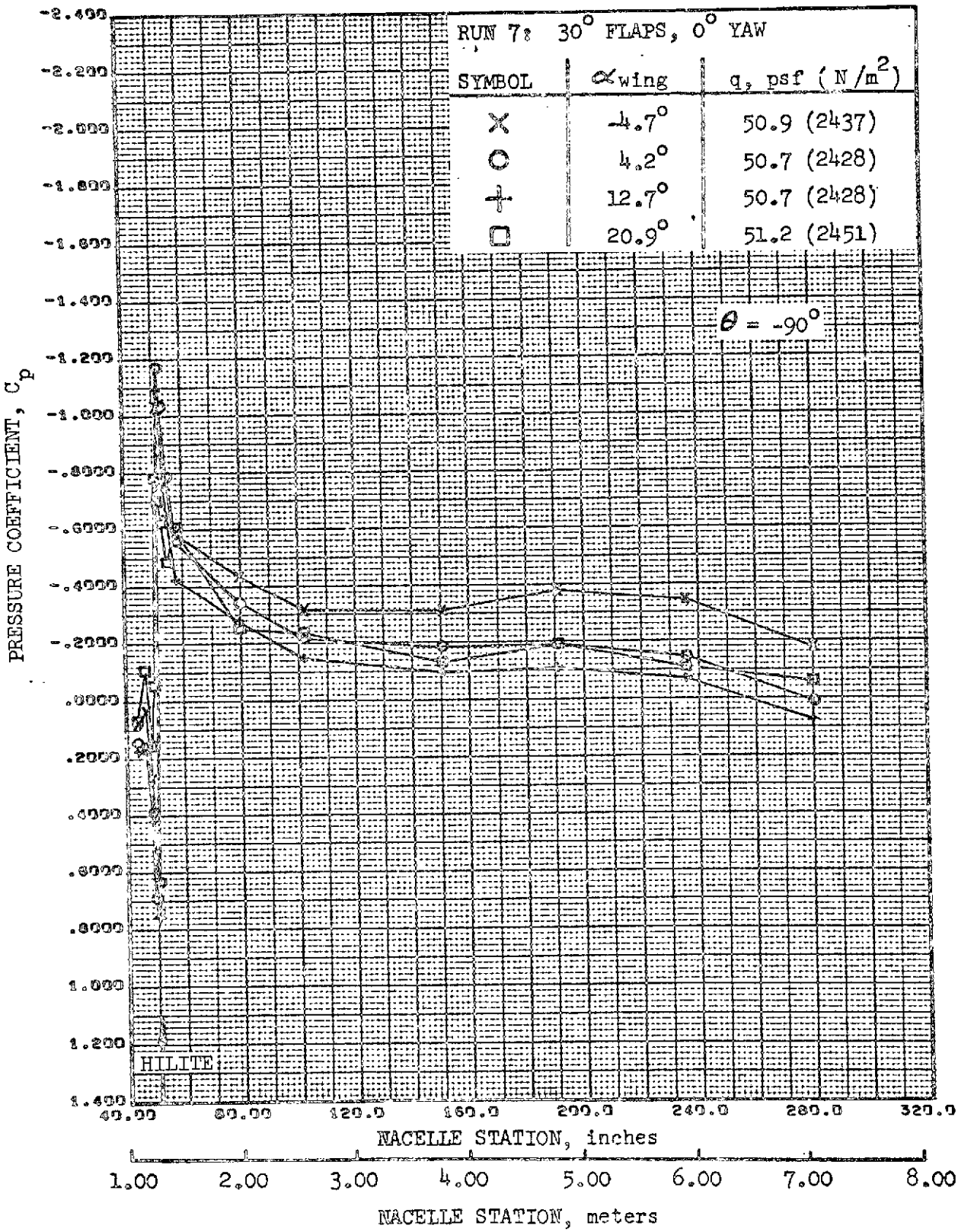

FIGURE 89.-REFAN NACELLE PRESSURE COEFFICIENT DISTRIBUTION, OUTBOARD SIDE

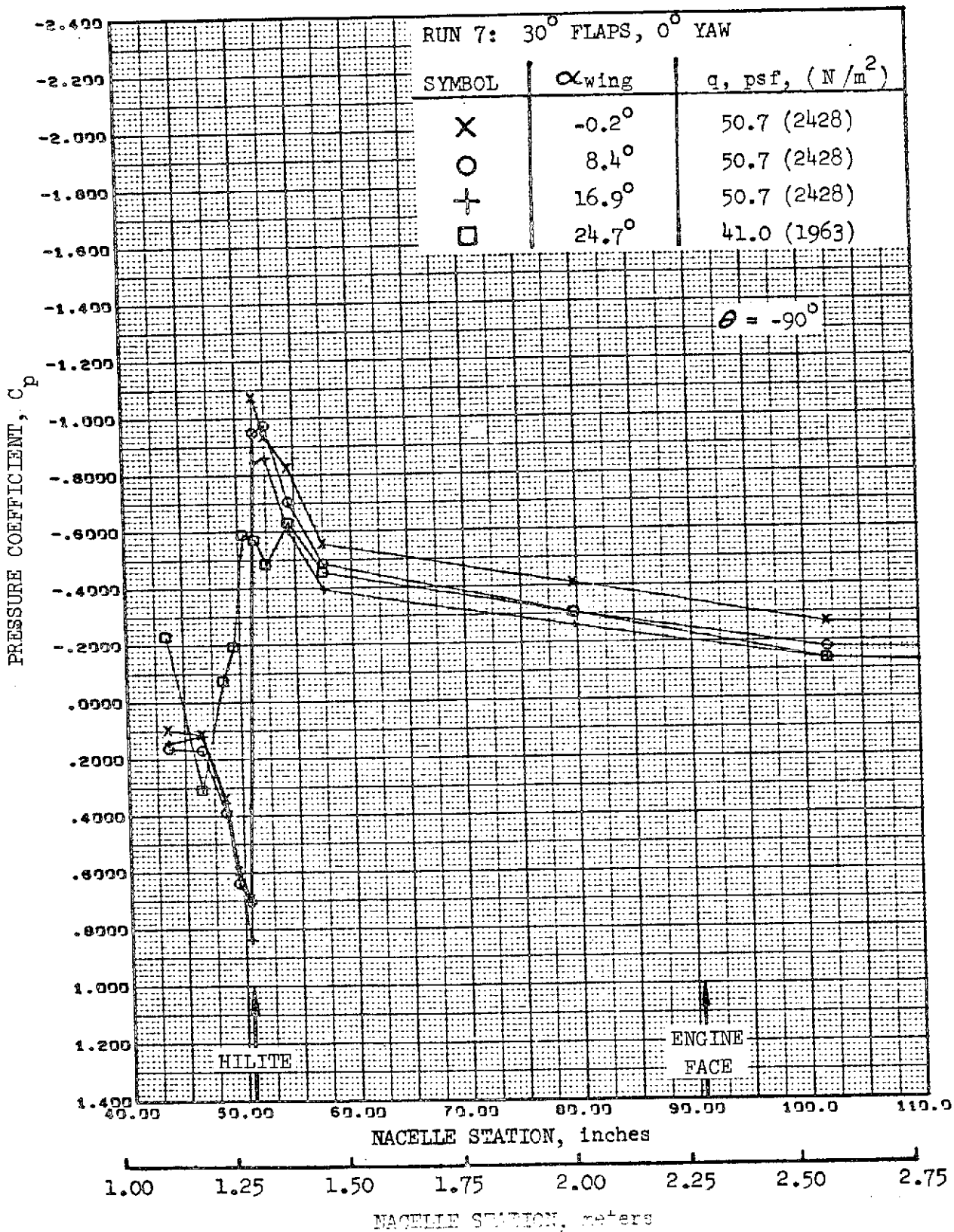

FIGURE 90. -REFAN NACELLE INLET COWL PRESSURE COEFFICIENT DISTRIBUTION, OUTBOARD SIDE

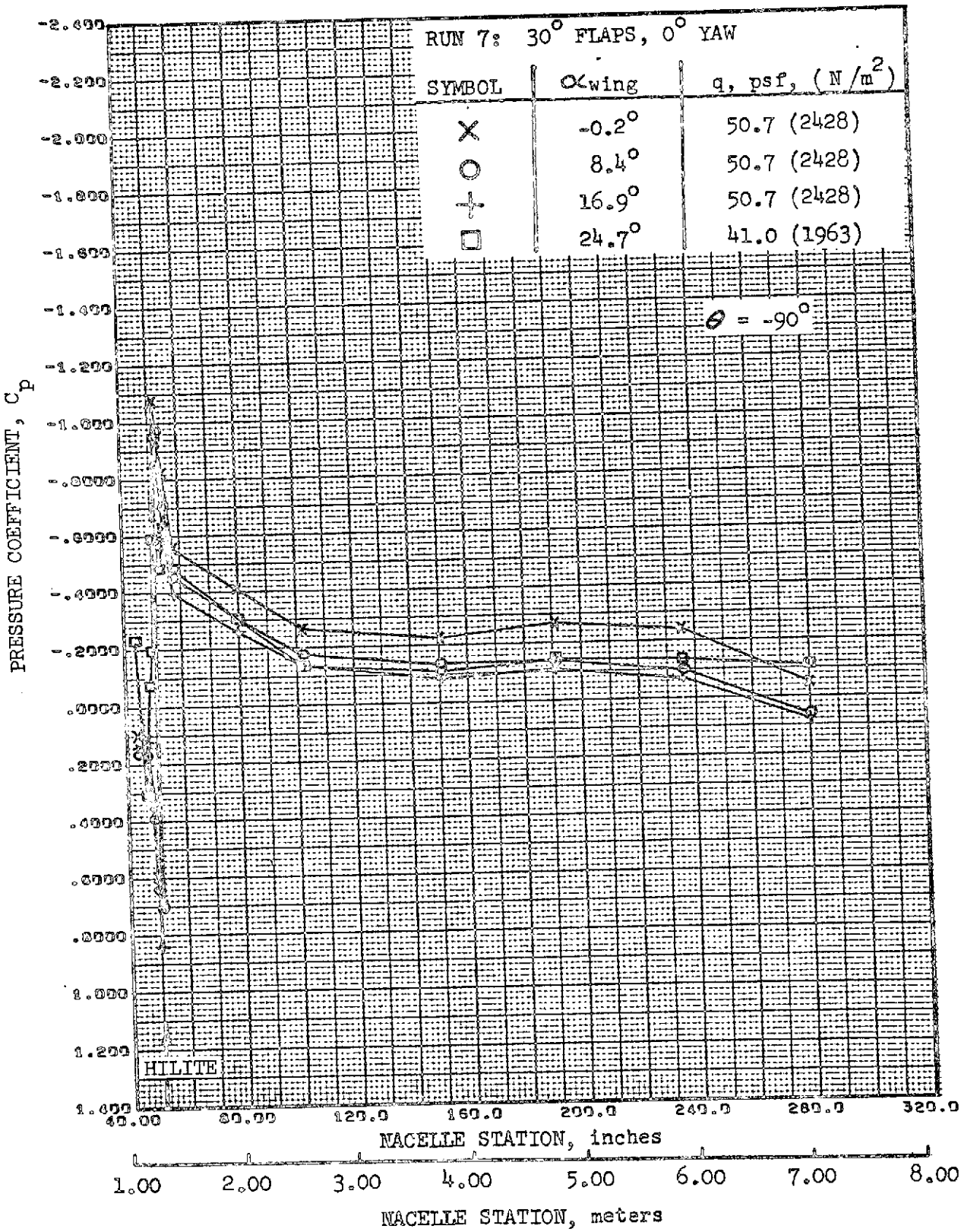

FIGURE 91. -REFAN NACELLE PRESSURE COEFFICIENT DISTRIBUTION, OUTBOARD SIDE

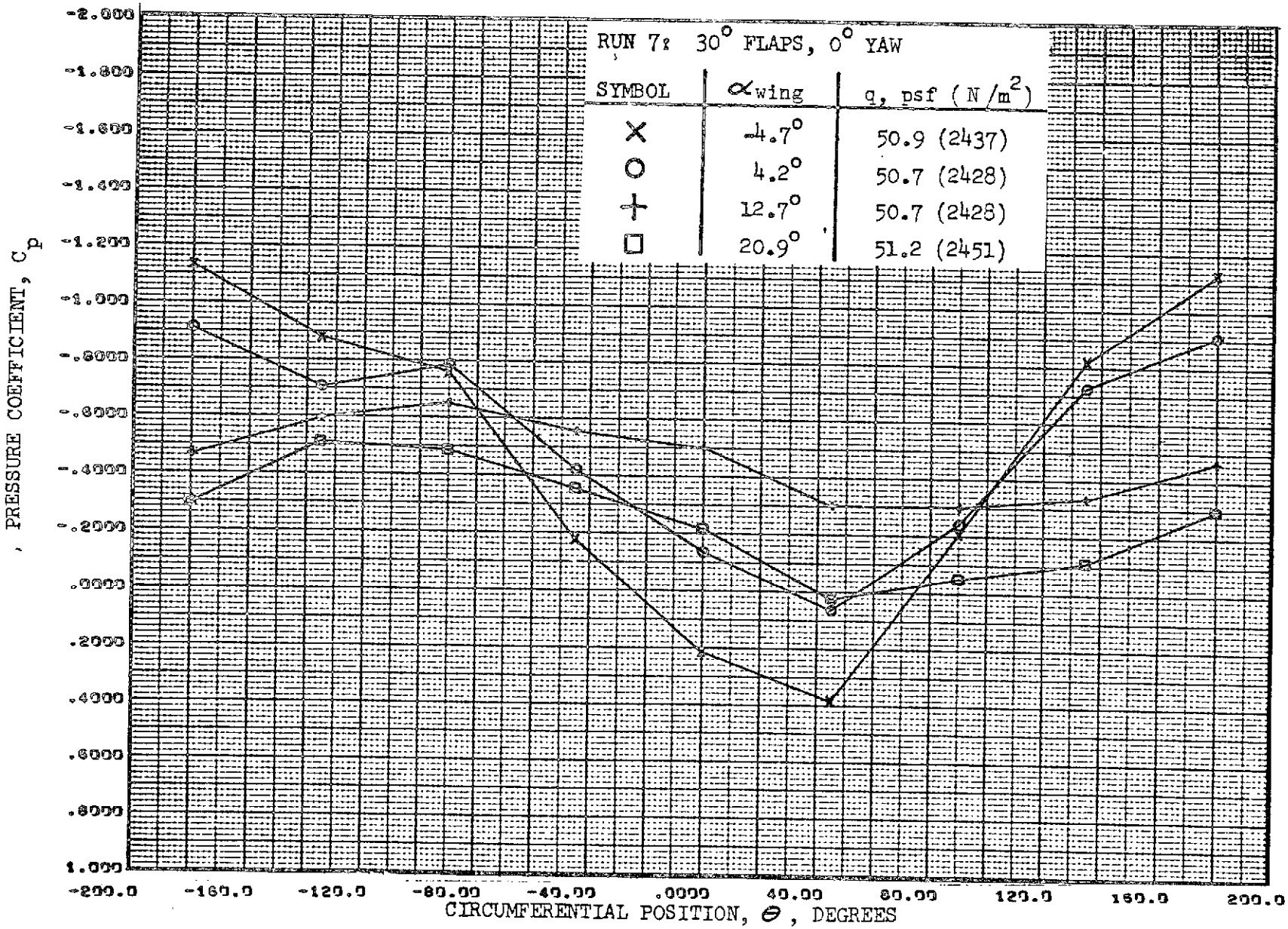

FIGURE 92. - REFAN NACELLE PRESSURE COEFFICIENT DISTRIBUTION, EXTERNAL CIRCUMFERENTIAL AT STATION 54.5 INCHES (1.38 METERS)

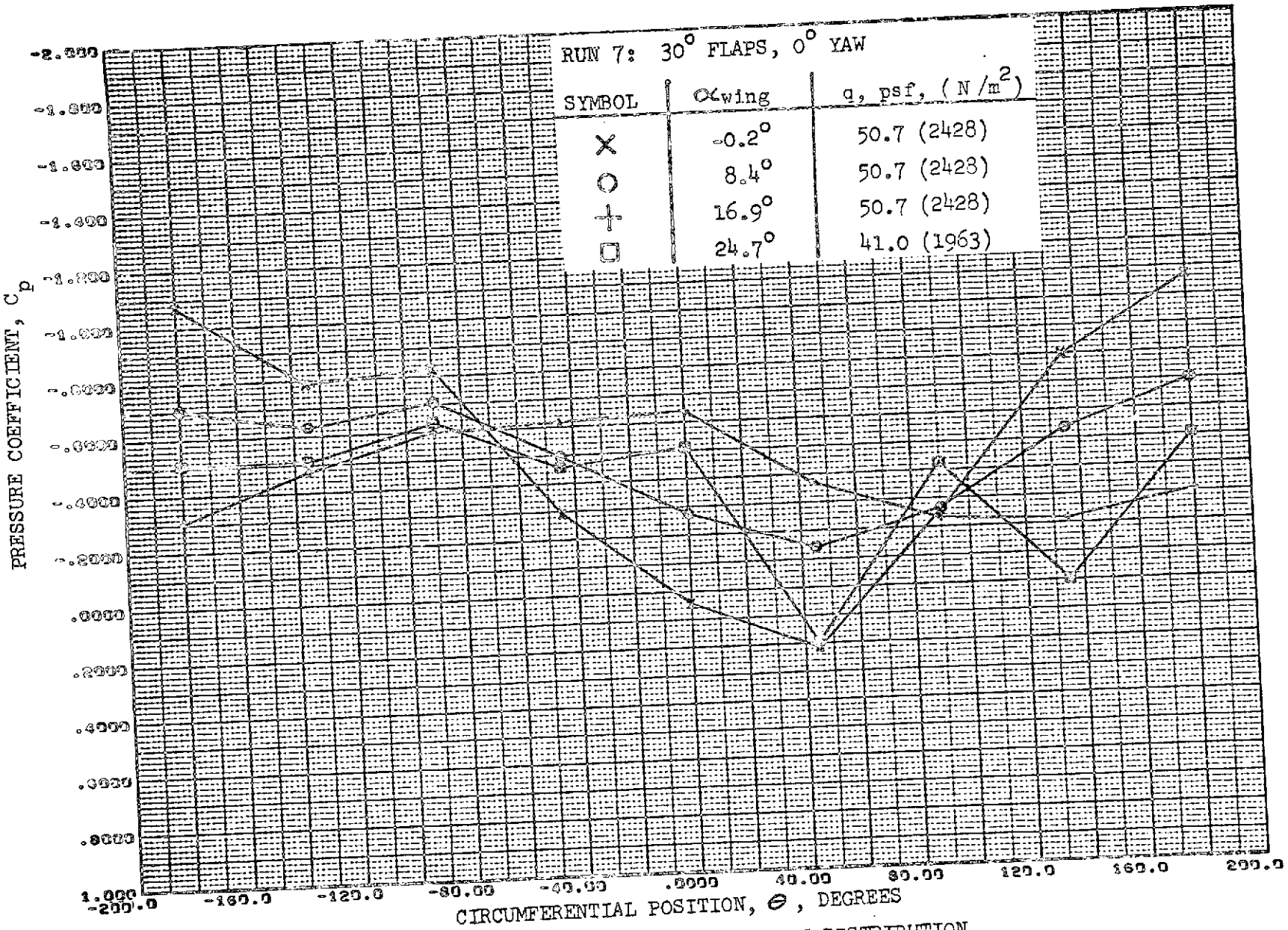

FIGURE 93. - REFAN NACELLE PRESSURE COEFFICIENT DISTRIBUTION, EXTERNAL CIRCUMFERENTIAL AT STATION 54.5 INCHES (1.38 METERS)

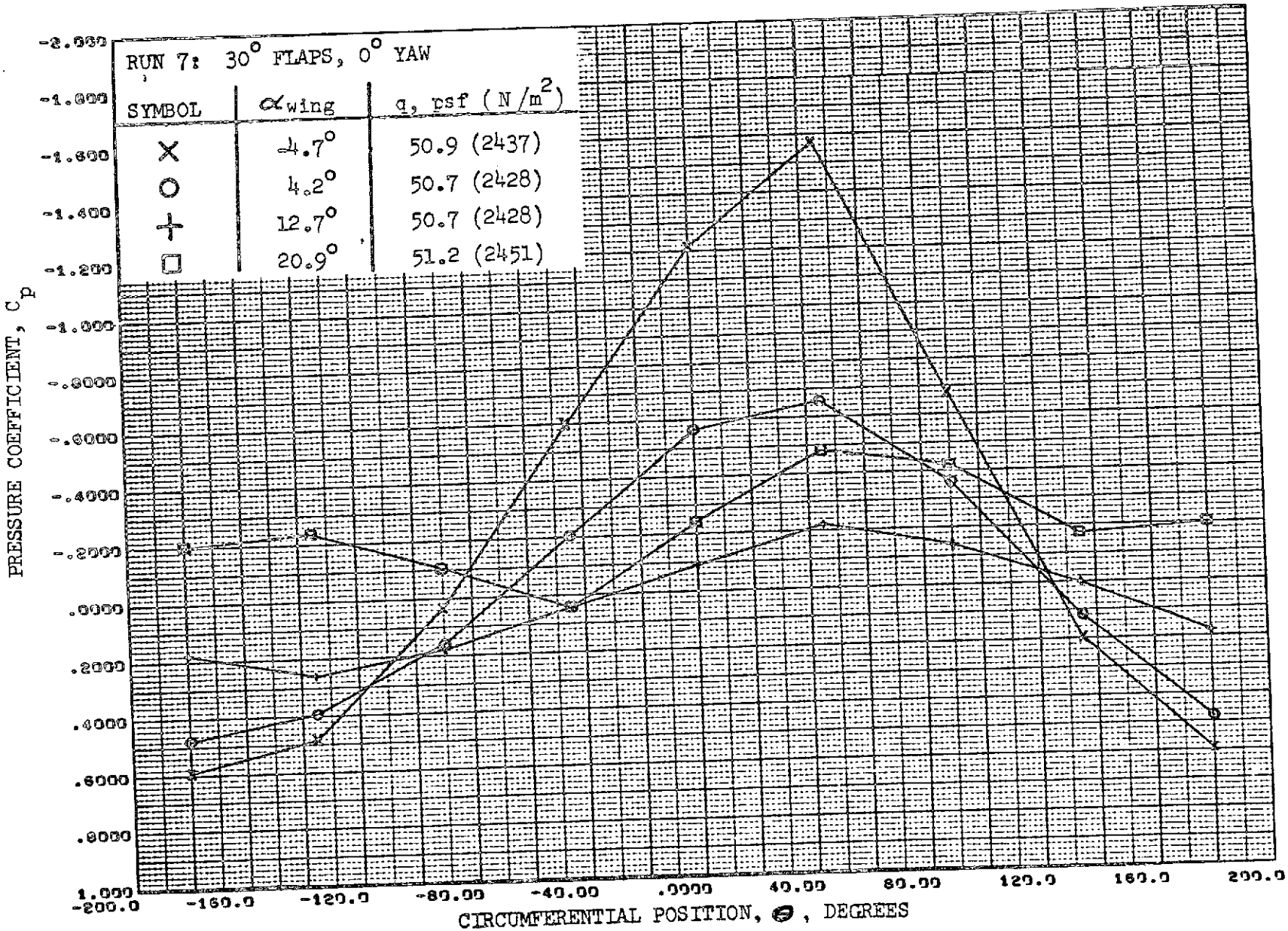

FIGURE 94. - REFAN NACELLE PRESSURE COEFFICIENT DISTRIBUTION, INTERNAL CIRCUMFERENTIAL AT STATION 54.5 INCHES (1.38 METERS)

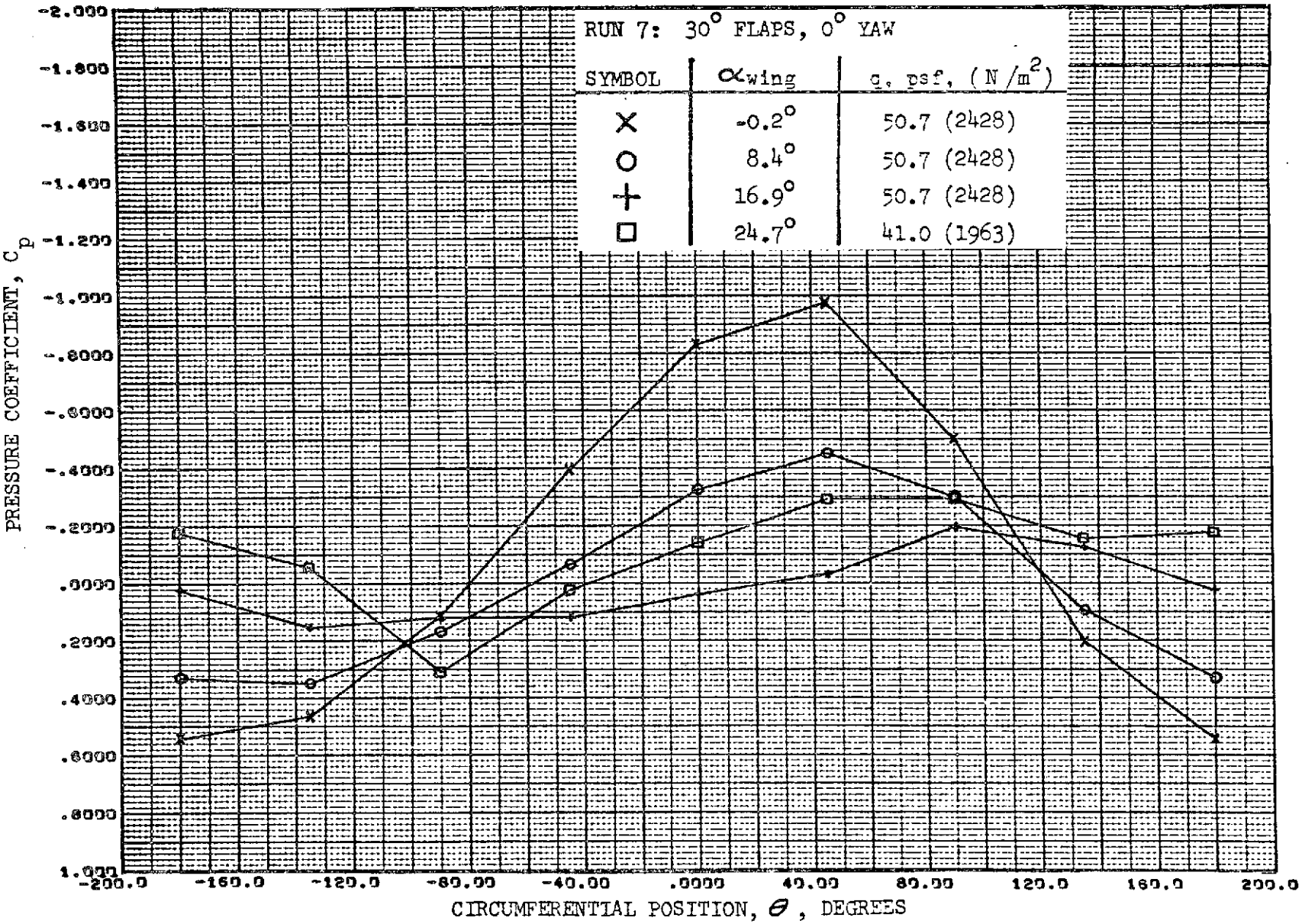

FIGURE 95. - REFAN NACELLE PRESSURE COEFFICIENT DISTRIBUTION, INTERNAL CIRCUMFERENTIAL AT STATION 54.5 INCHES (1.38 METERS)

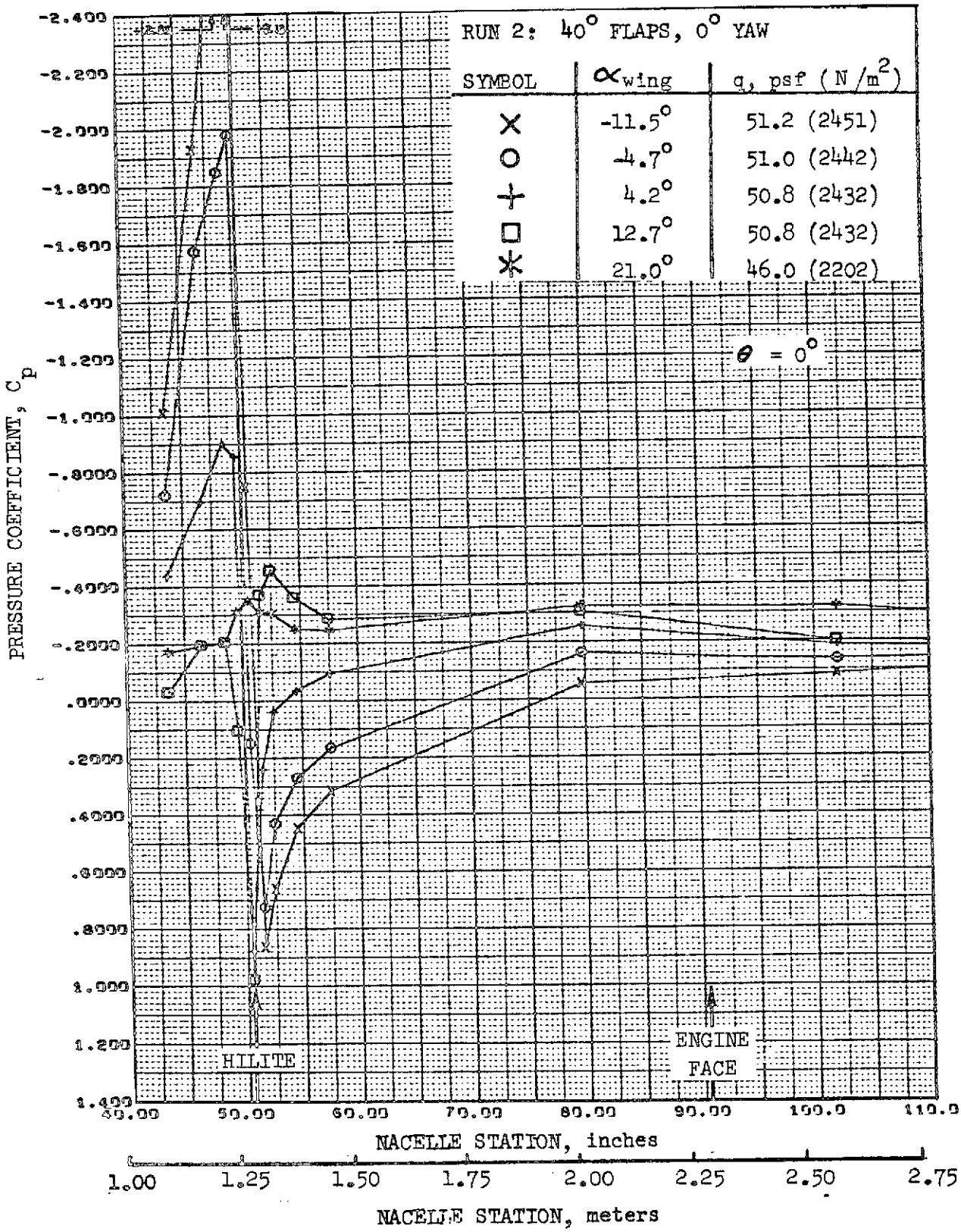

FIGURE 96. -REFAN NACELLE INLET COWL PRESSURE COEFFICIENT DISTRIBUTION, TOP LONGITUDINAL

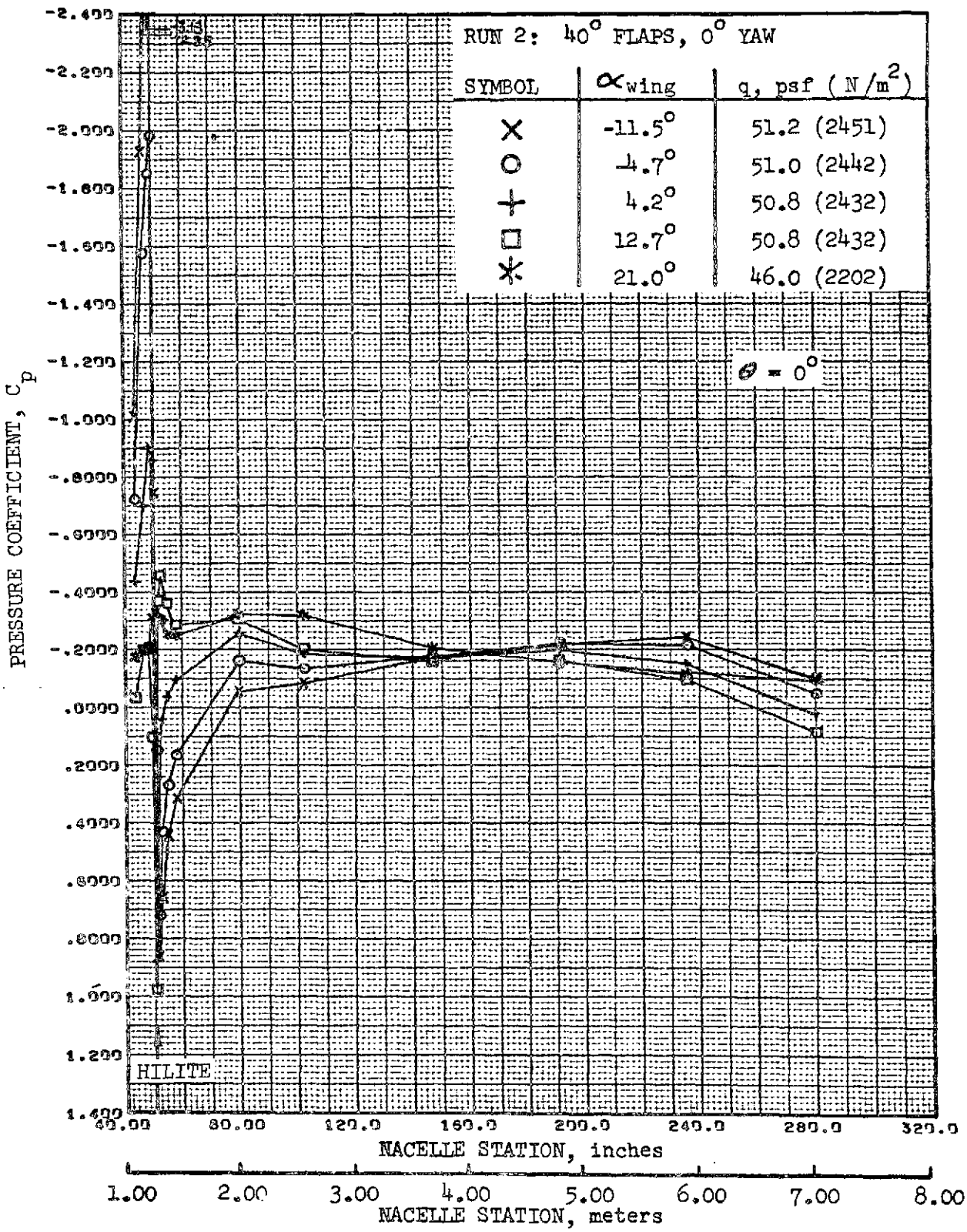

FIGURE 97. -REFAN NACELLE PRESSURE COEFFICIENT DISTRIBUTION, TOP LONGITUDINAL

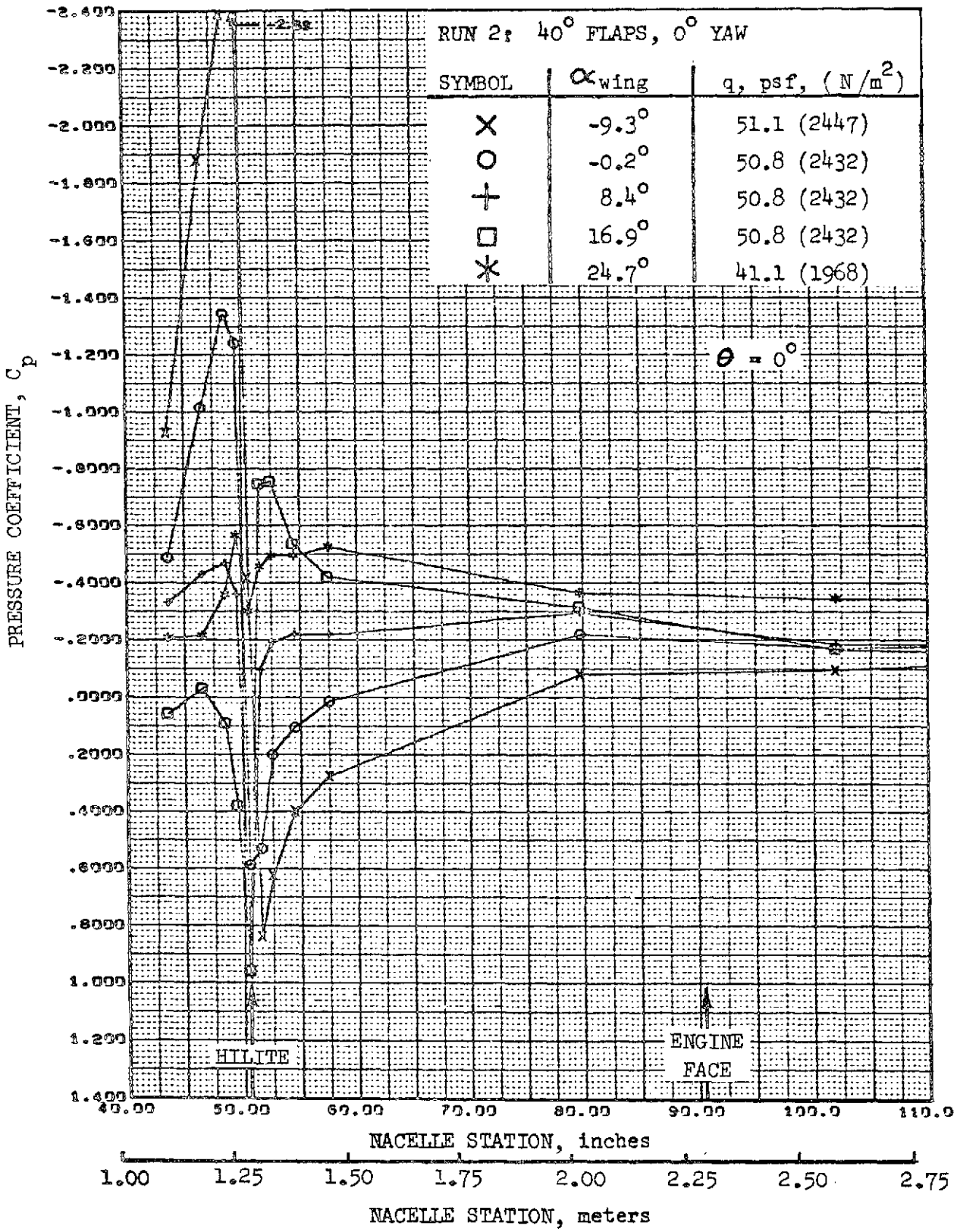

FIGURE 98.-REFAN NACELLE INLET COWL PRESSURE COEFFICIENT DISTRIBUTION, TOP LONGITUDINAL

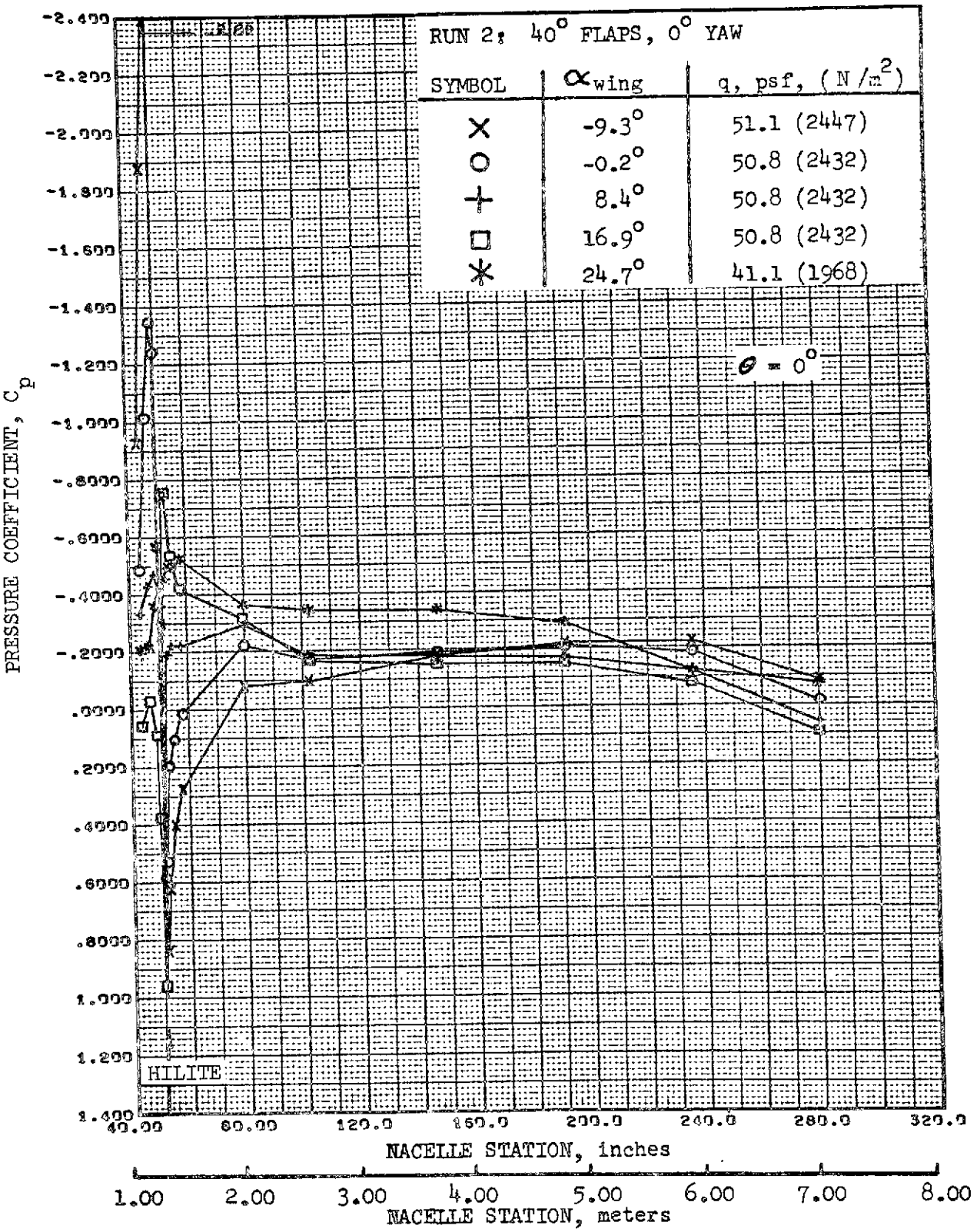

FIGURE 99. REFAN NACELLE PRESSURE COEFFICIENT DISTRIBUTION, TOP LONGITUDINAL

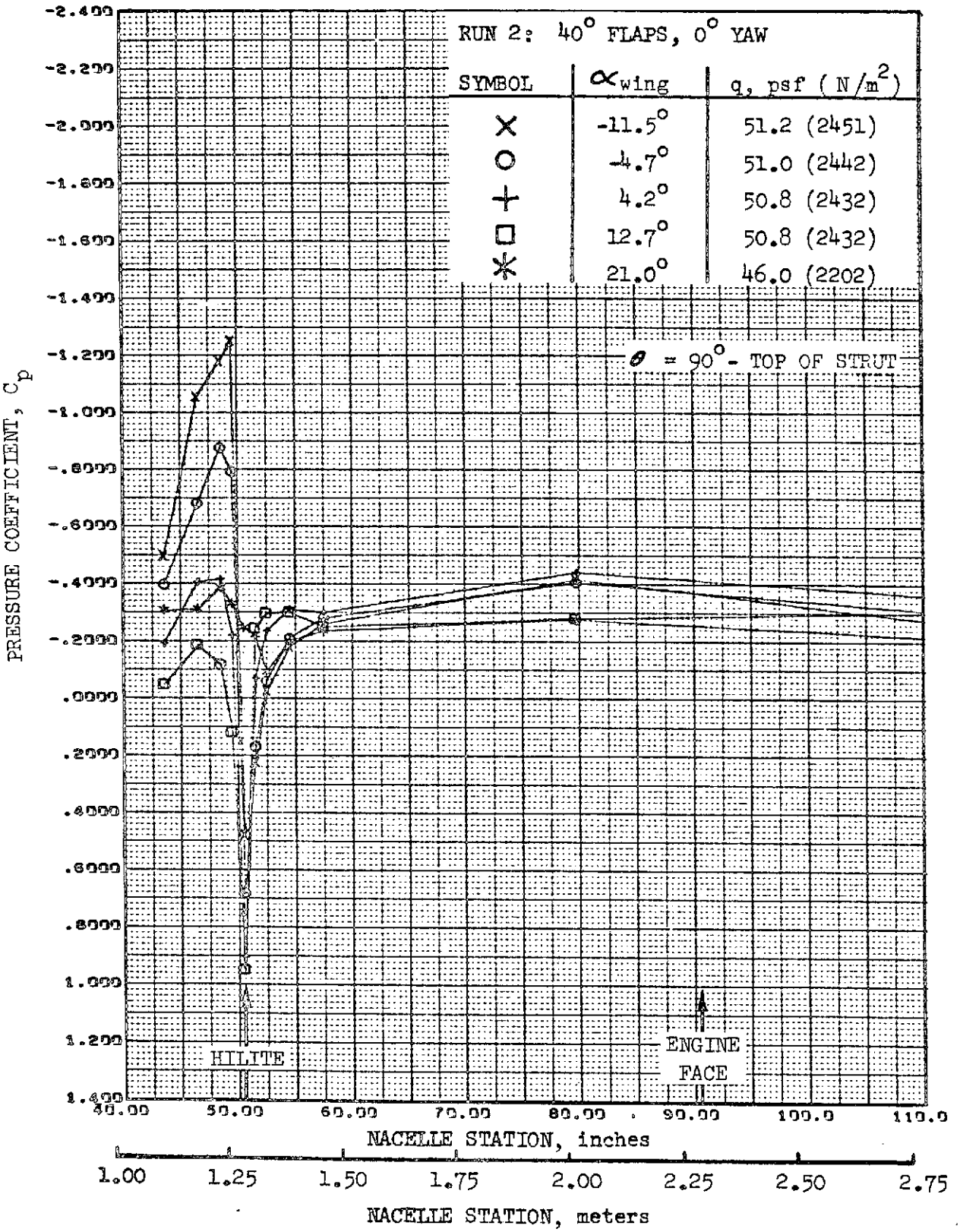

FIGURE 100.-REFAN NACELLE INLET COWL PRESSURE COEFFICIENT DISTRIBUTION, INBOARD SIDE-ABOVE STRUT

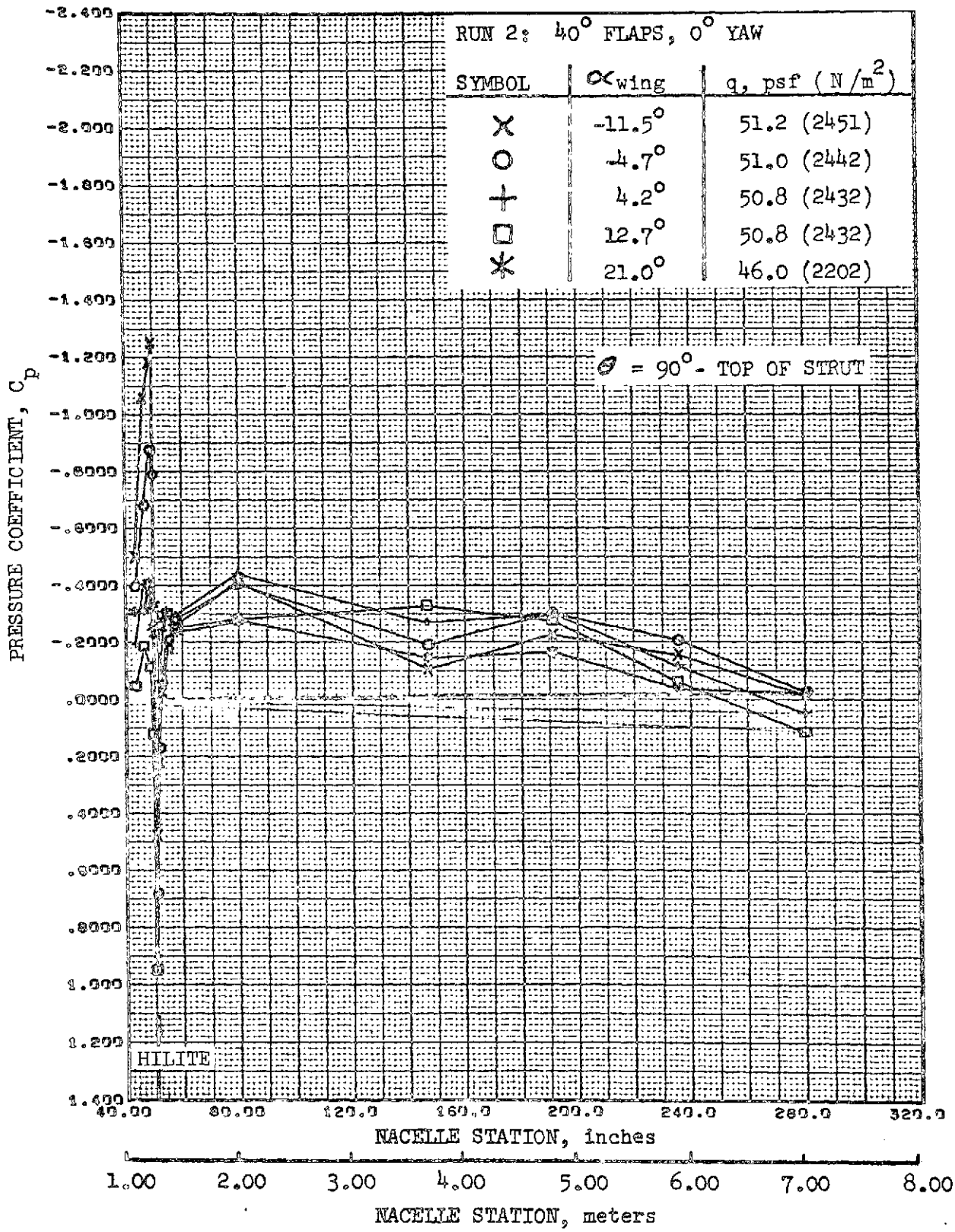

FIGURE 101.-REFAN NACELLE PRESSURE COEFFICIENT DISTRIBUTION, INBOARD SIDE-ABOVE STRUT

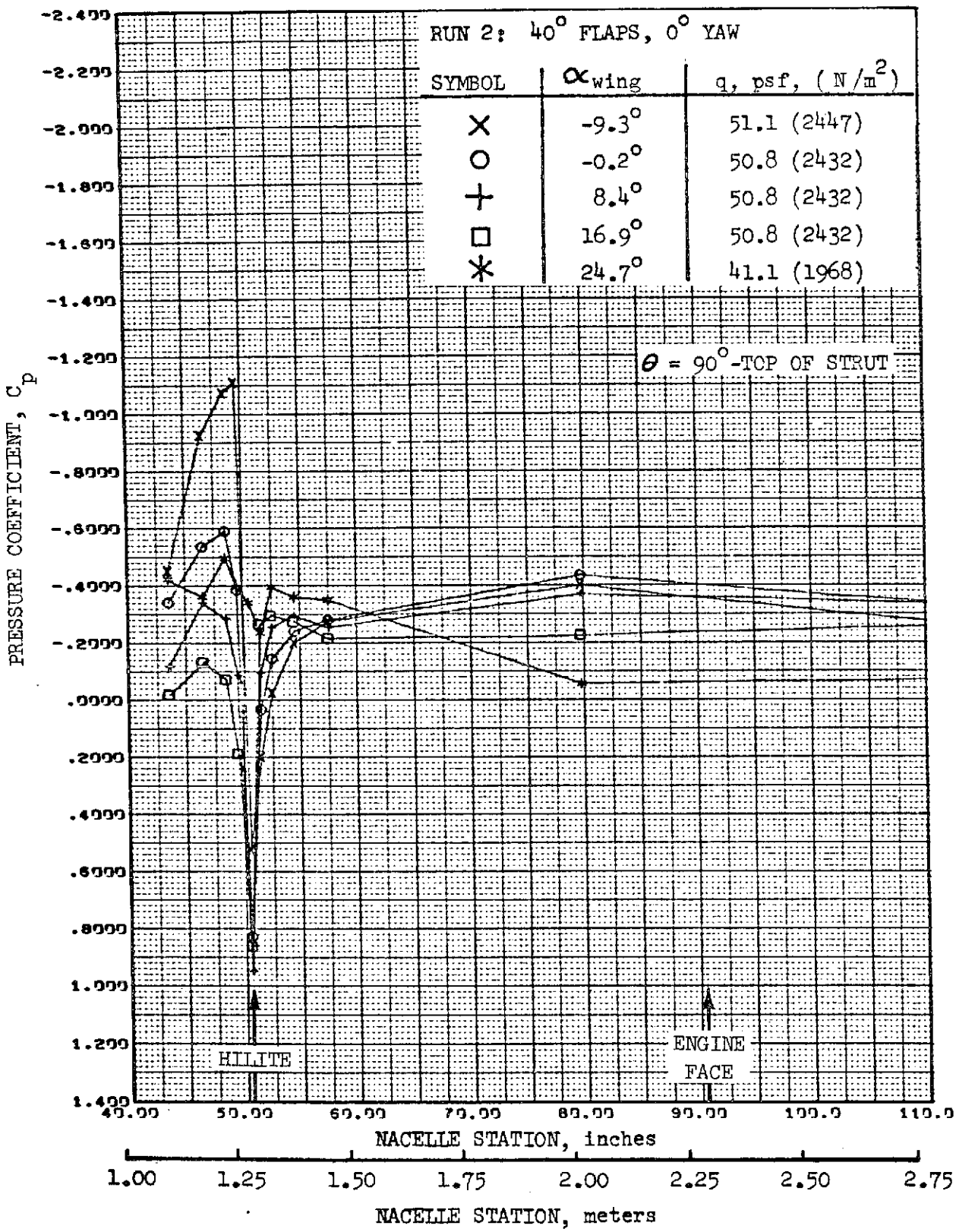

FIGURE 102.-REFAN NACELLE INLET COWL PRESSURE COEFFICIENT DISTRIBUTION, INBOARD SIDE-ABOVE STRUT

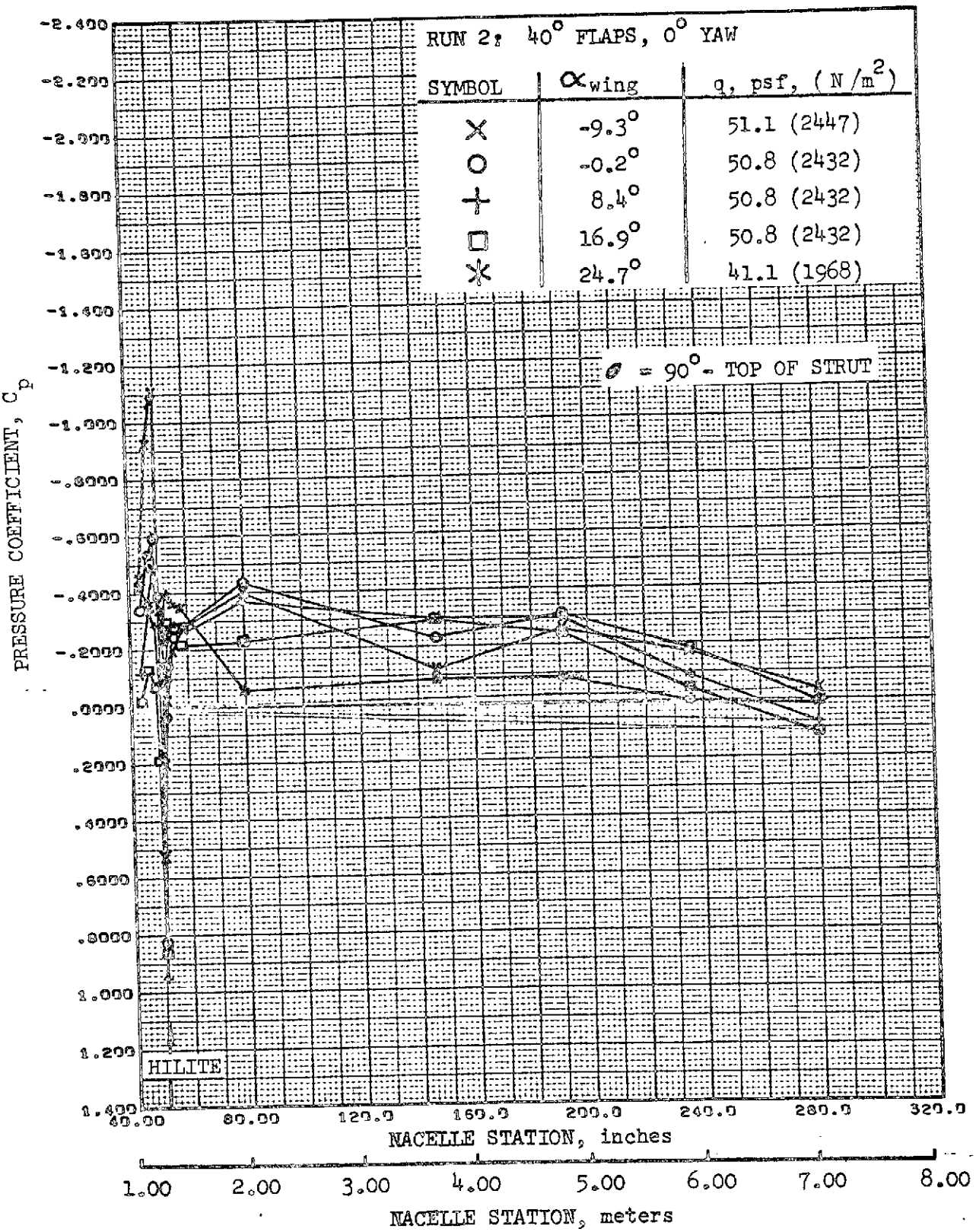

FIGURE 103. REFAN NACELLE PRESSURE COEFFICIENT DISTRIBUTION, INBOARD SIDE-ABOVE STRUT

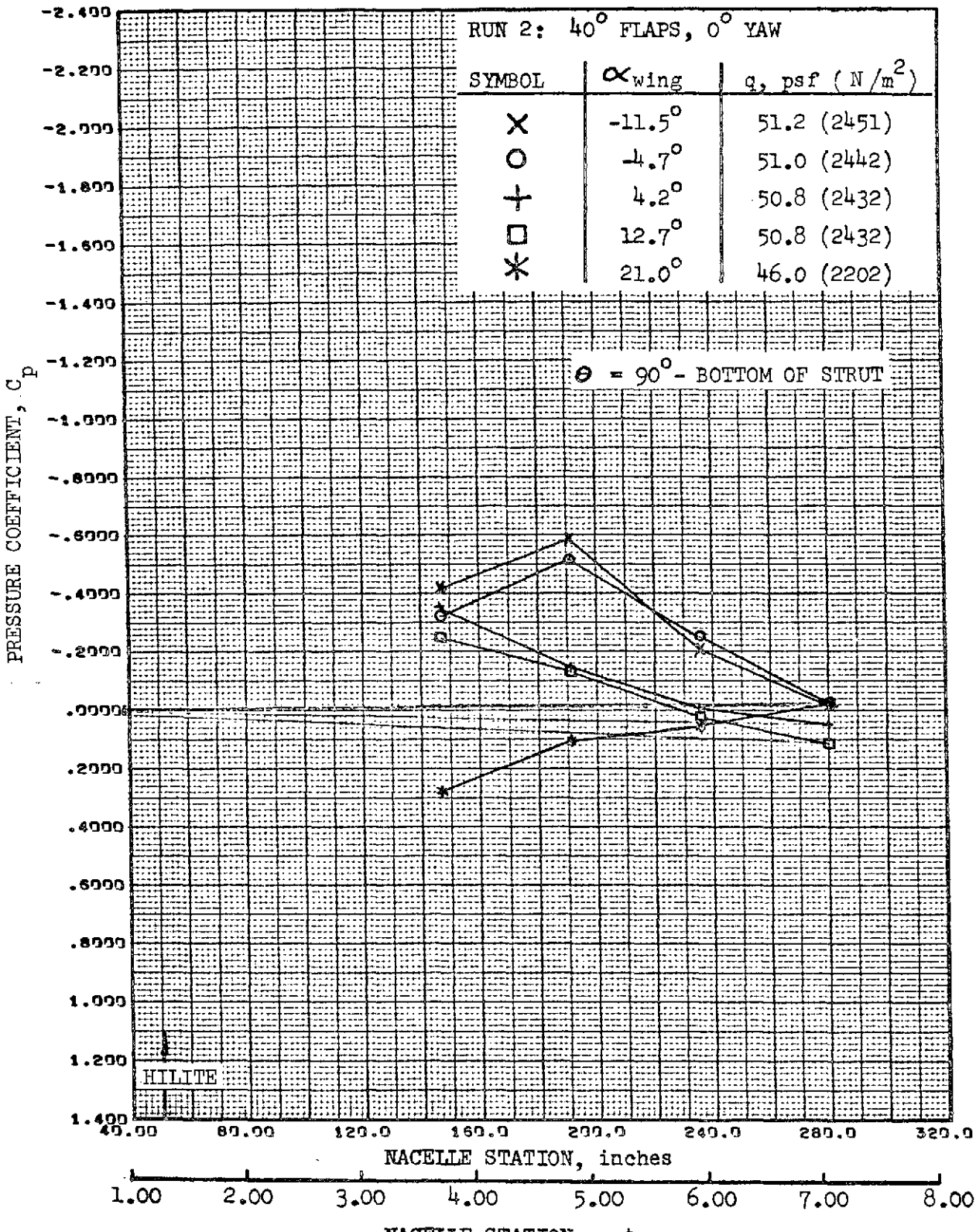

FIGURE 104.-REFAN NACELLE PRESSURE COEFFICIENT DISTRIBUTION, INBOARD SIDE-BELOW STRUT

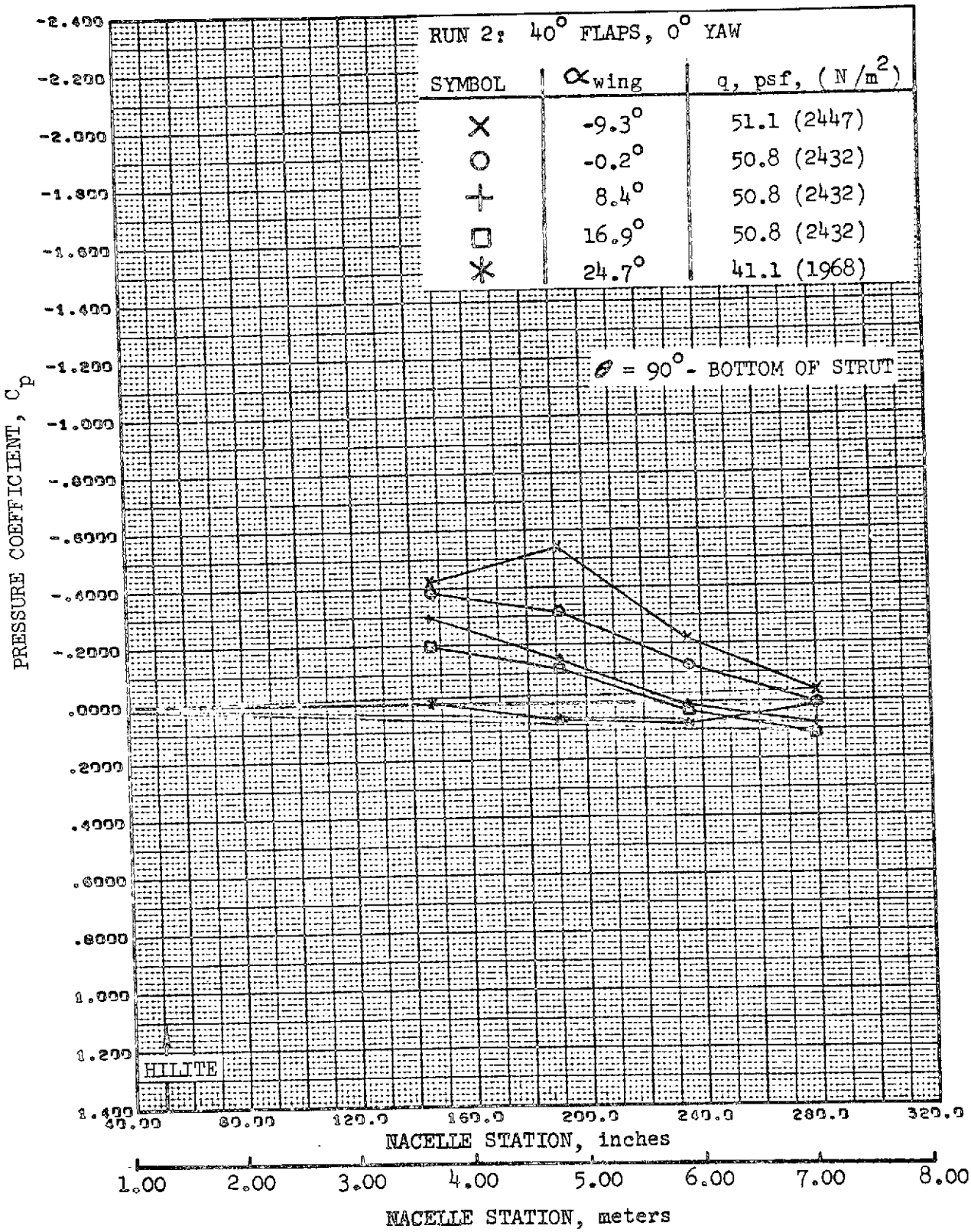

FIGURE 105.-REFAN NACELLE PRESSURE COEFFICIENT DISTRIBUTION, INBOARD SIDE-BELOW STRUT

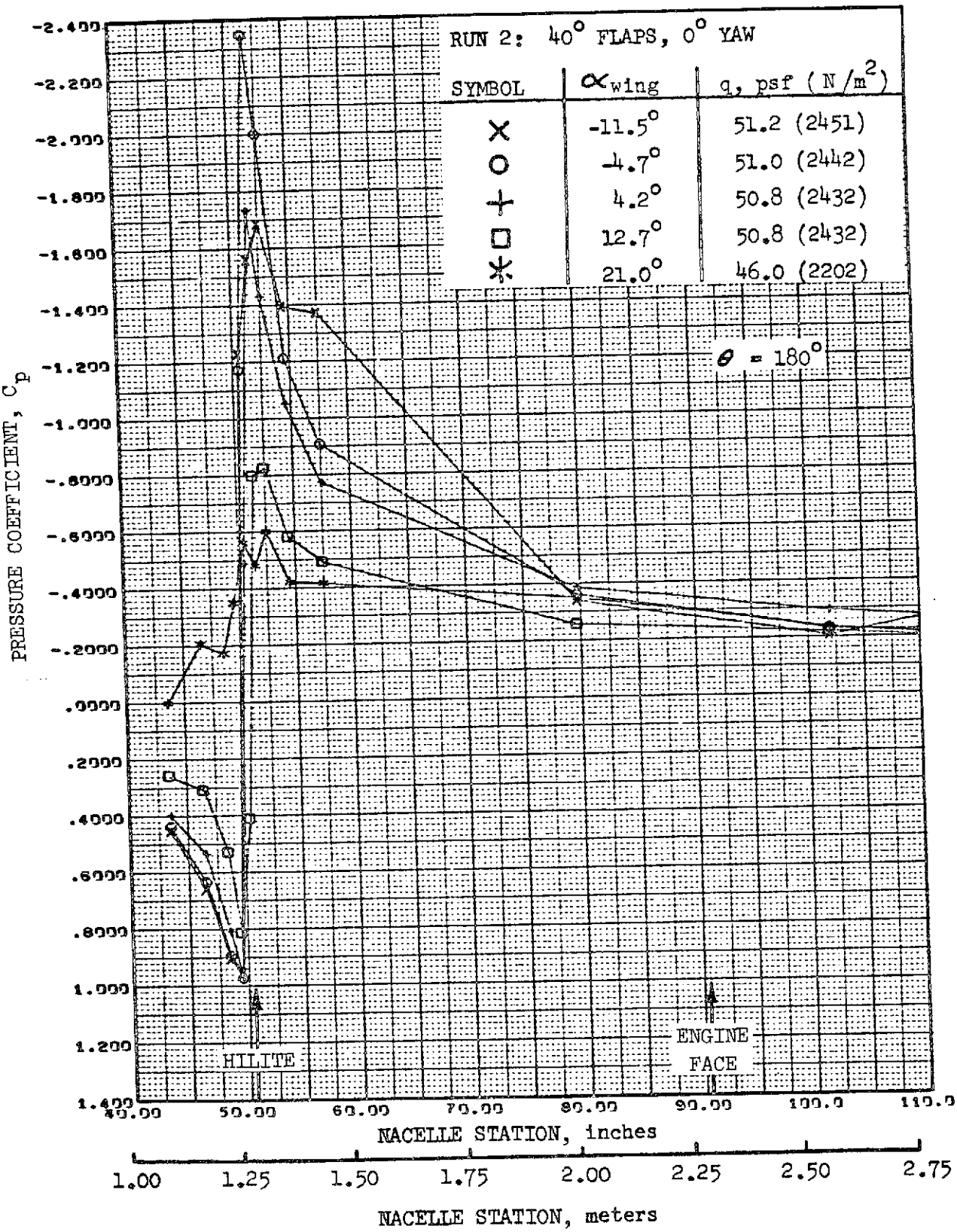

FIGURE 106.-REFAN NACELLE INLET COWL PRESSURE COEFFICIENT DISTRIBUTION, BOTTOM LONGITUDINAL

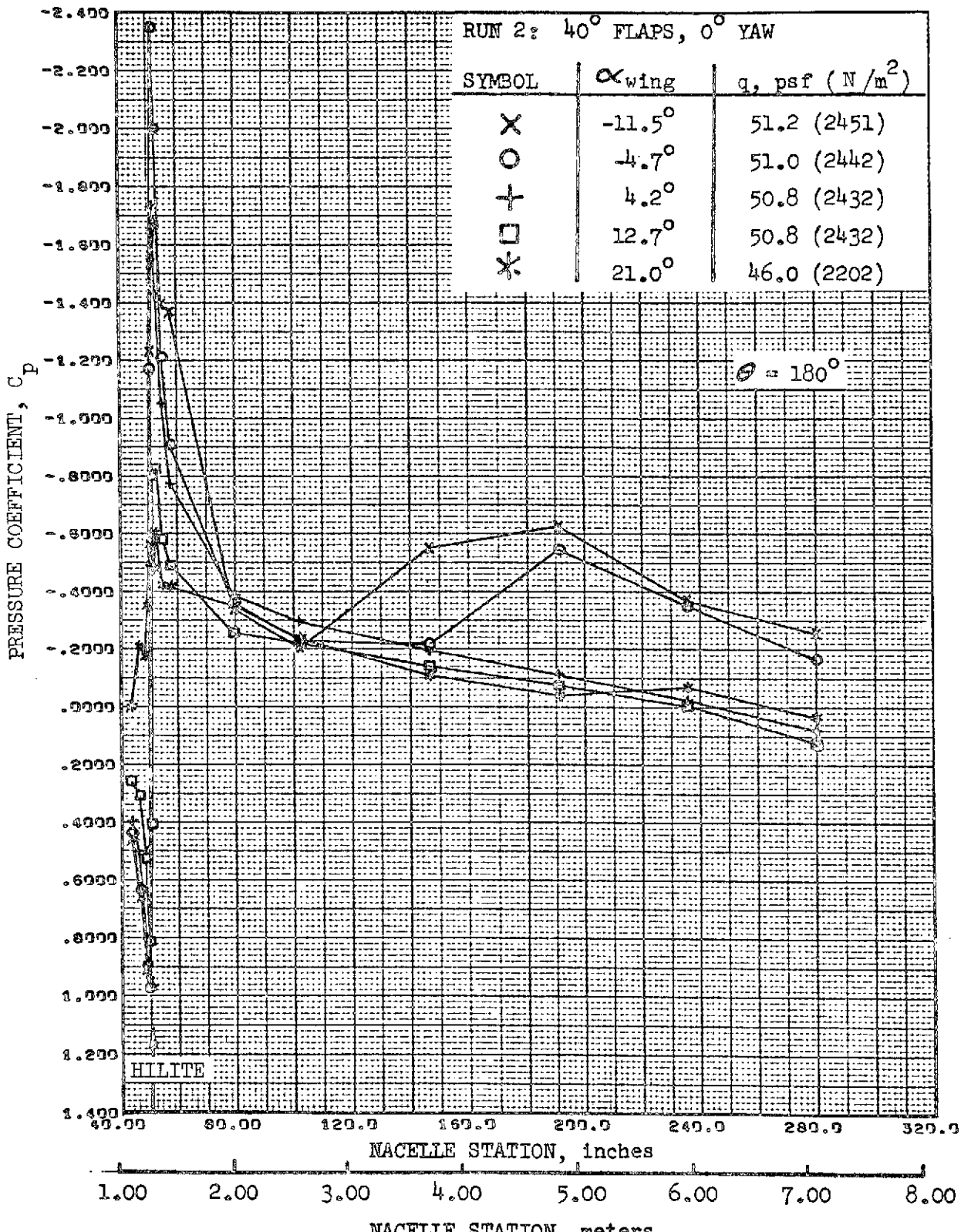

FIGURE 107.-REFAN NACELLE PRESSURE COEFFICIENT DISTRIBUTION, BOTTOM LONGITUDINAL

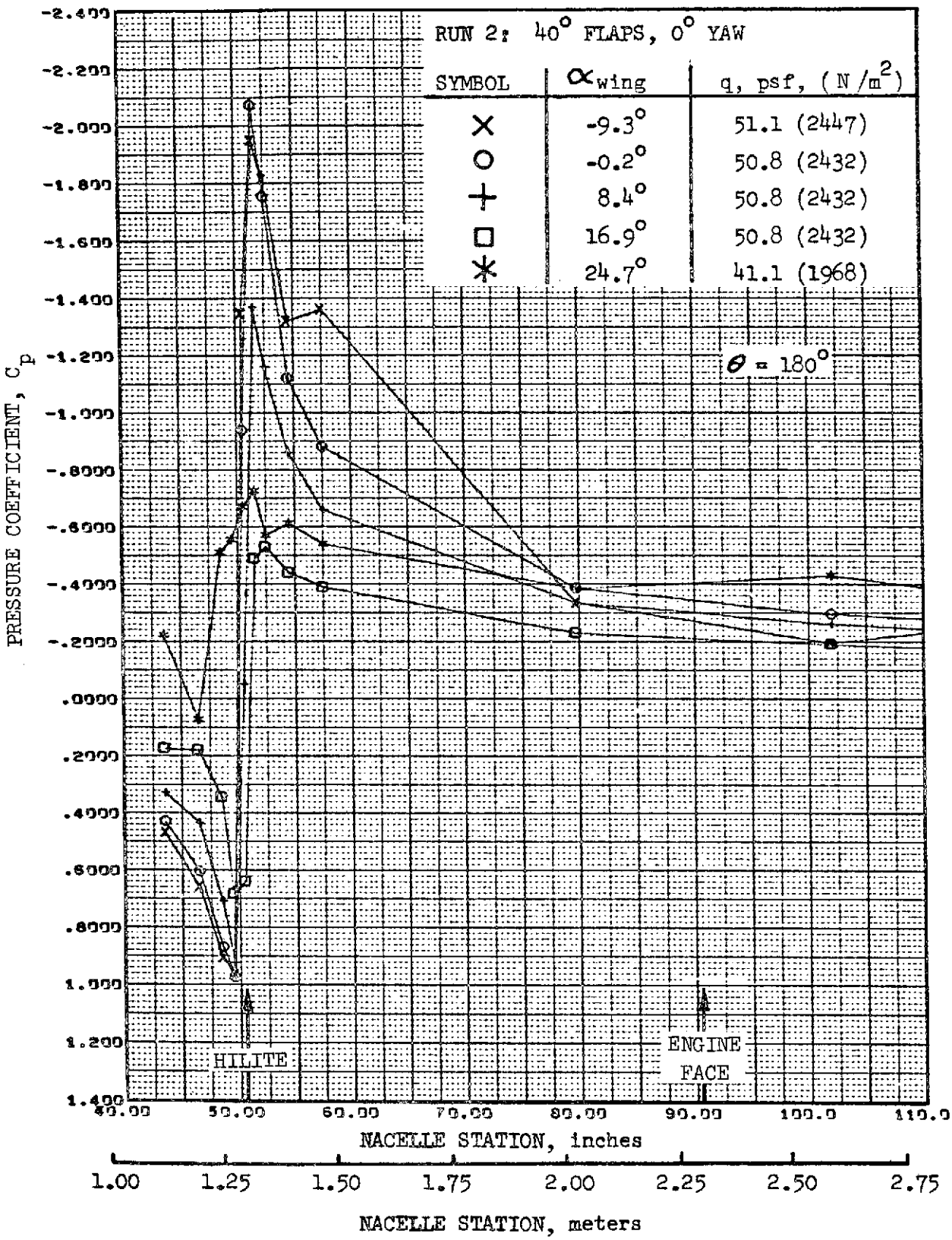

FIGURE 108.-REFAN NACELLE INLET COWL PRESSURE COEFFICIENT DISTRIBUTION, BOTTOM LONGITUDINAL

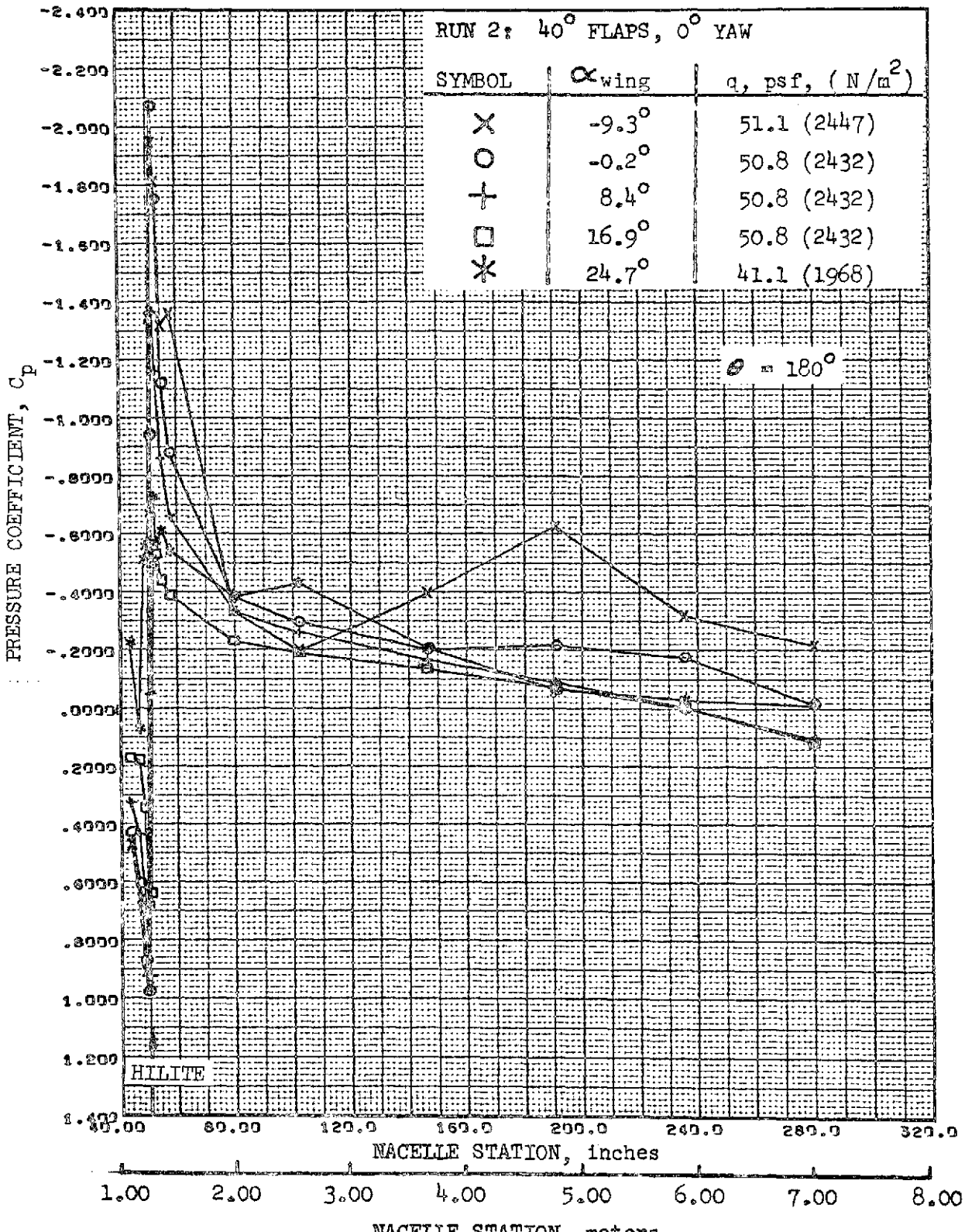

FIGURE 109.-REFAN NACELLE PRESSURE COEFFICIENT DISTRIBUTION, BOTTOM LONGITUDINAL

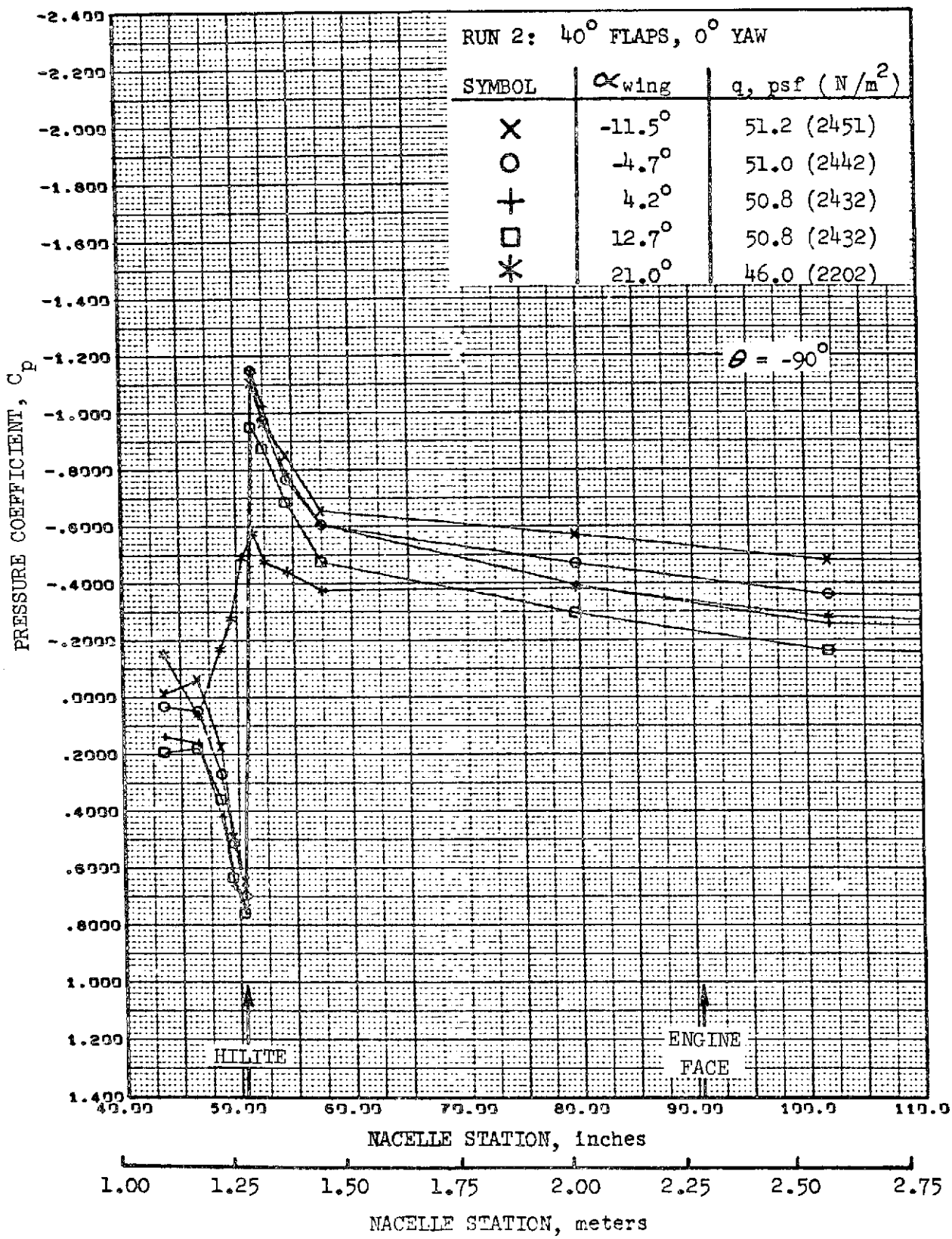

FIGURE 110.-REFAN NACELLE INLET COWL PRESSURE COEFFICIENT DISTRIBUTION, OUTBOARD SIDE

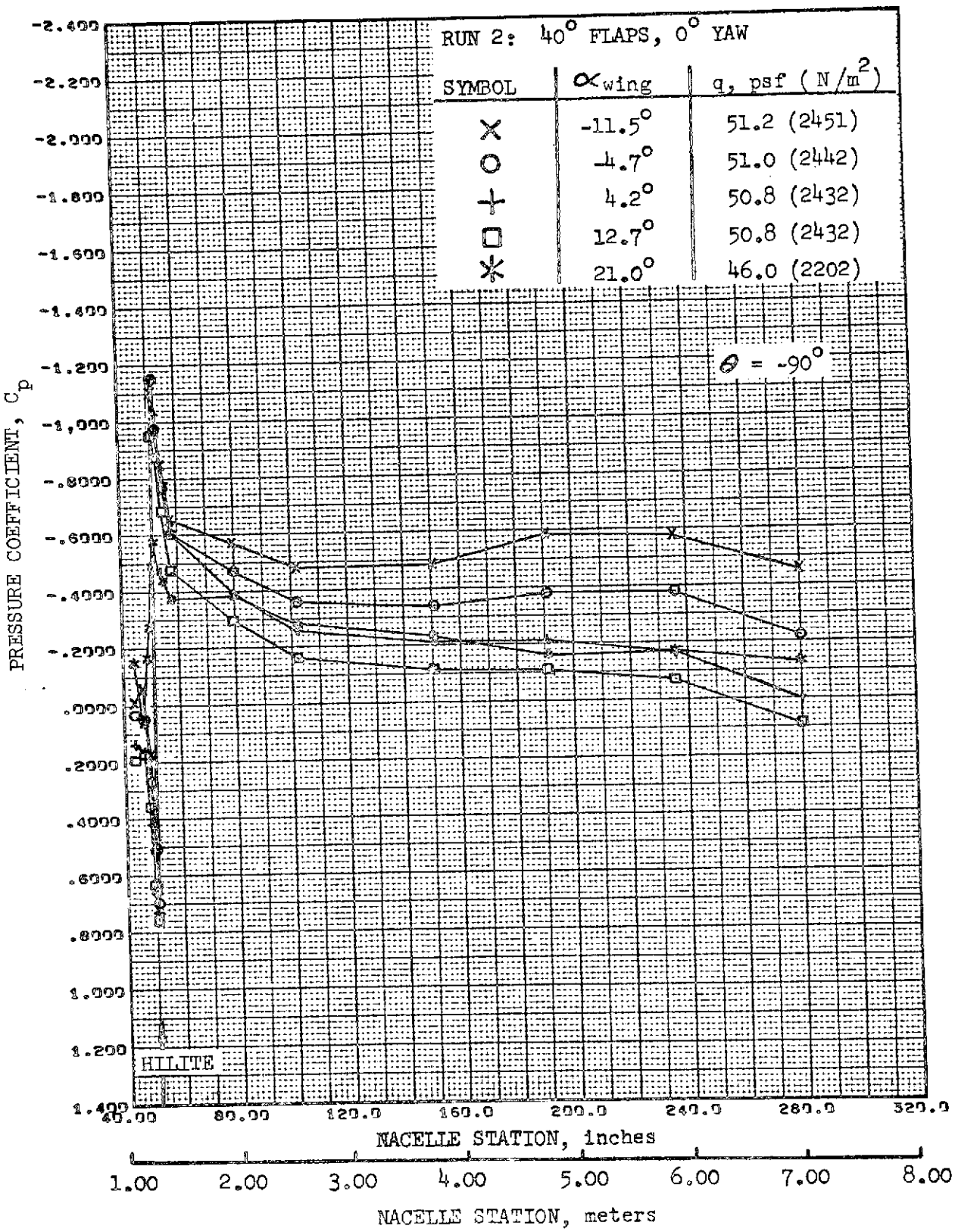

FIGURE 111.-REFAN NACELLE PRESSURE COEFFICIENT DISTRIBUTION, OUTBOARD SIDE

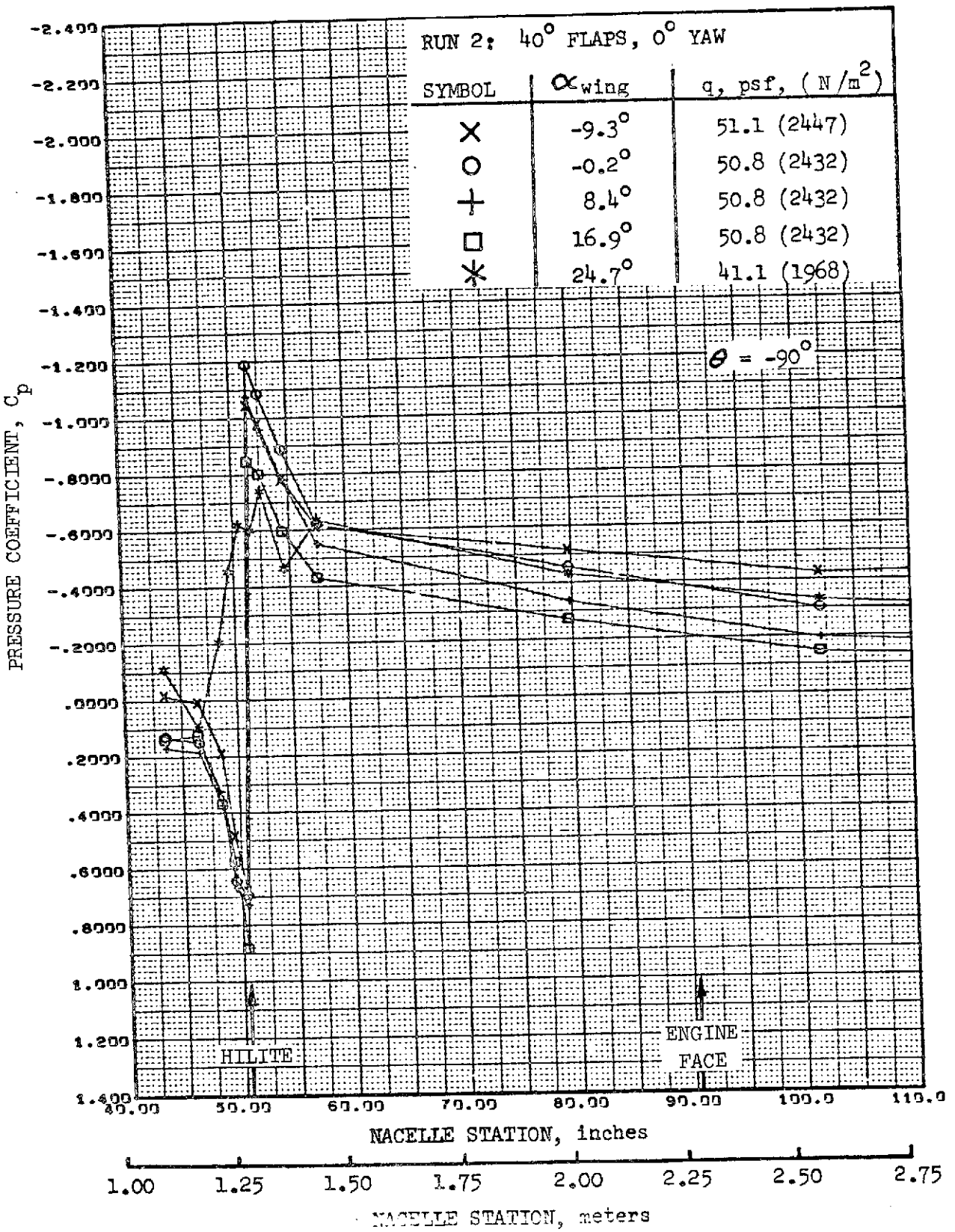

FIGURE 112.-REFAN NACELLE INLET COWL PRESSURE COEFFICIENT DISTRIBUTION, OUTBOARD SIDE

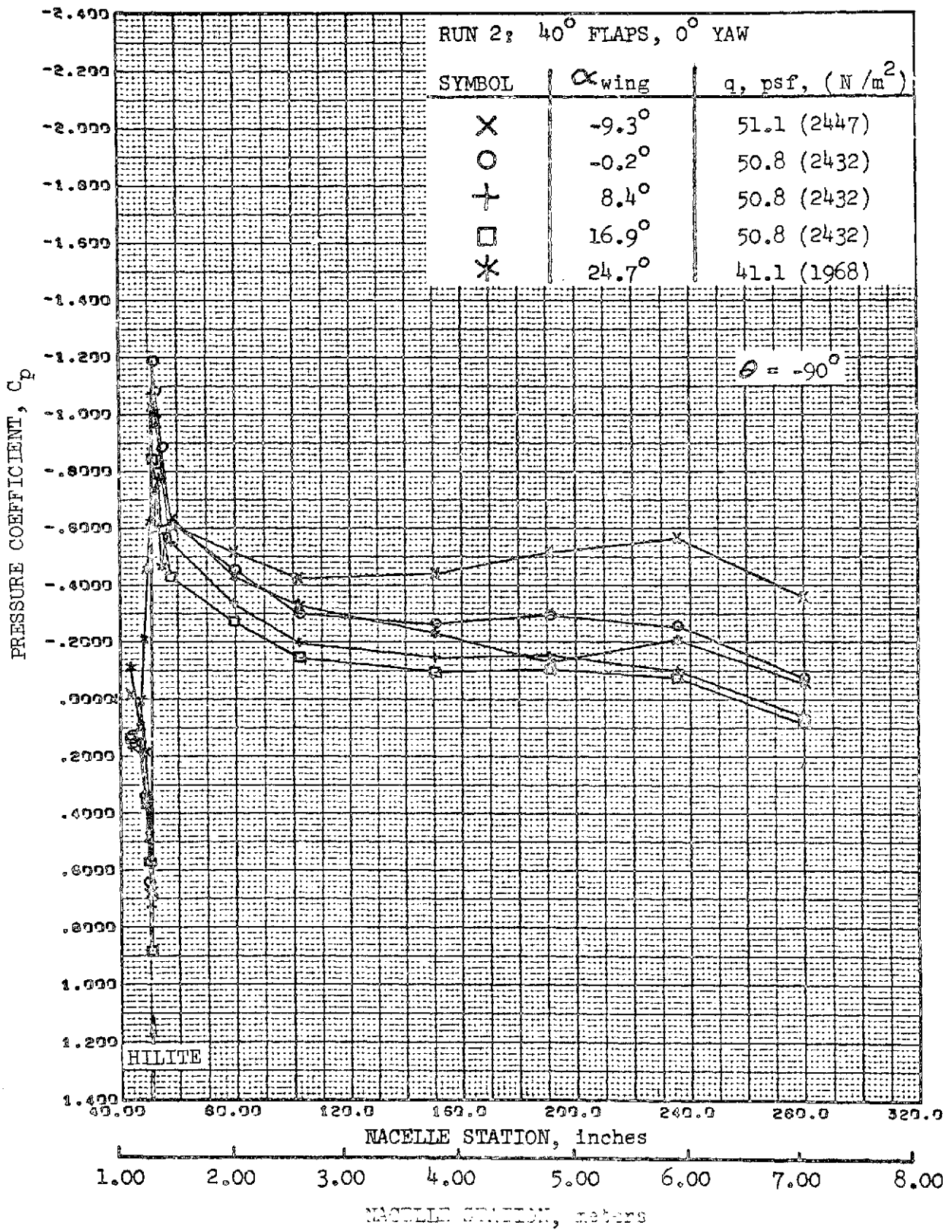

FIGURE 113.-REFAN NACELLE PRESSURE COEFFICIENT DISTRIBUTION, OUTBOARD SIDE

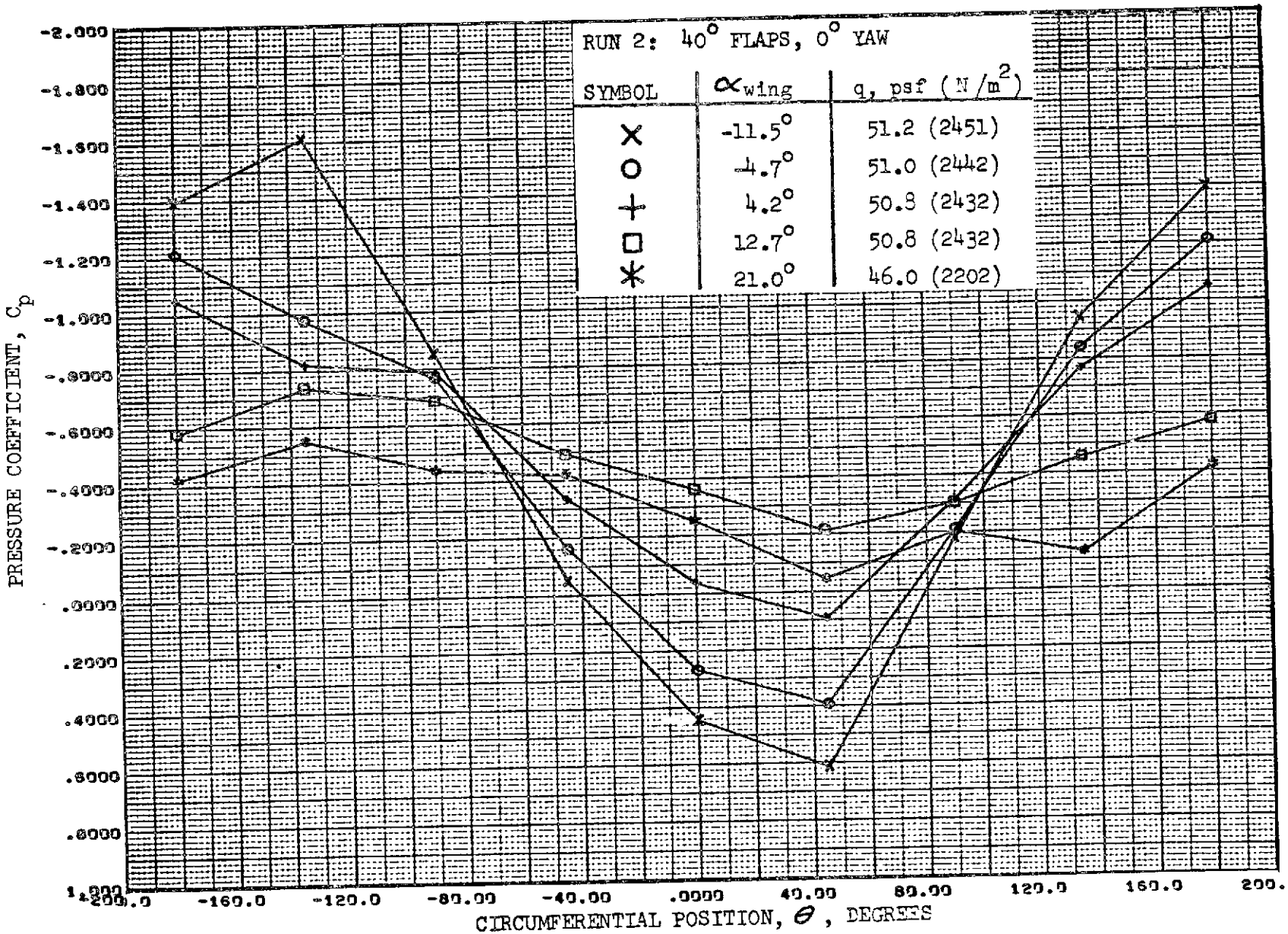

FIGURE 114. - REFAN NACELLE PRESSURE COEFFICIENT DISTRIBUTION, EXTERNAL CIRCUMFERENTIAL AT STATION 54.5 INCHES (1.38 METERS)

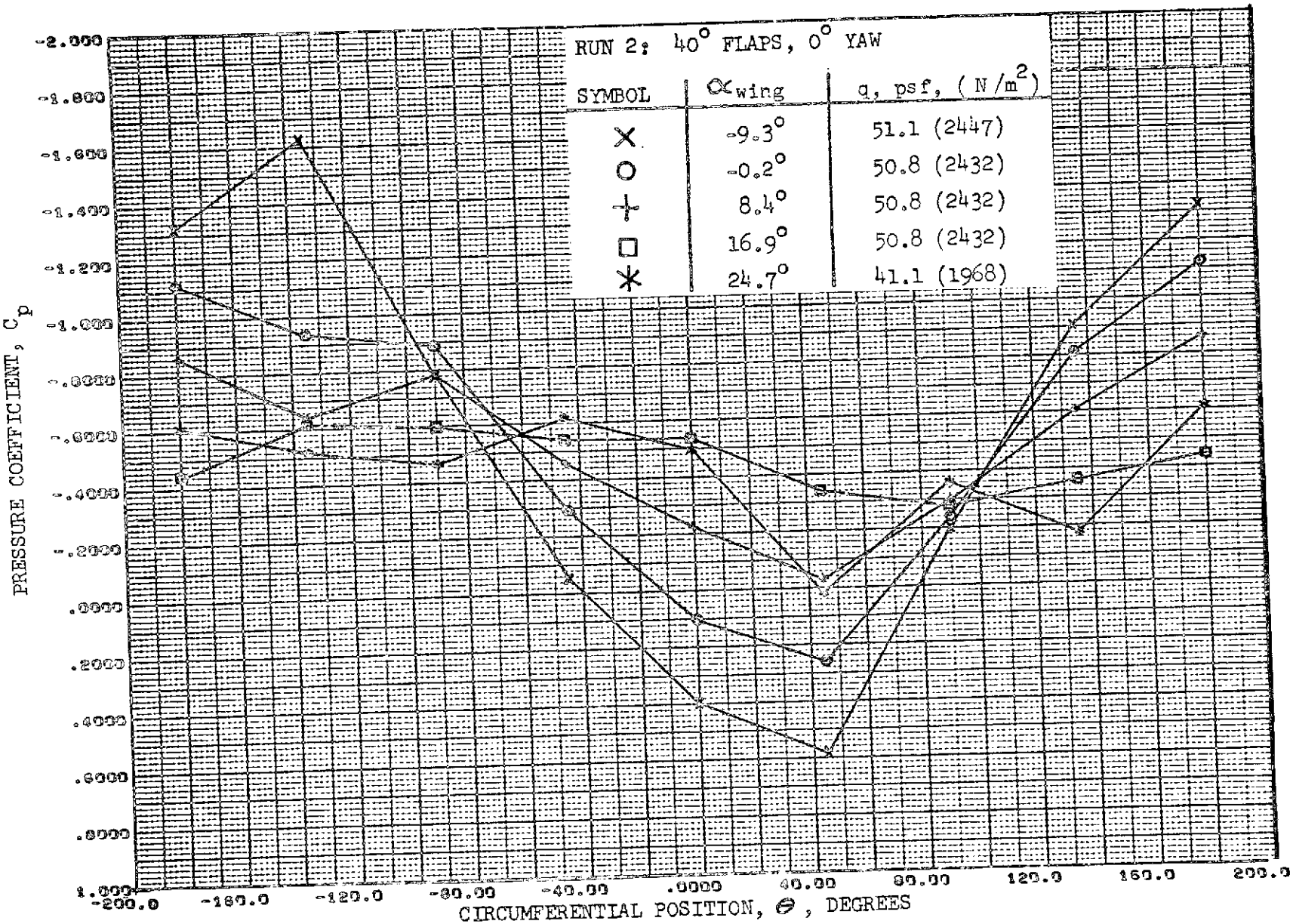

FIGURE 115. - REFAN NACELLE PRESSURE COEFFICIENT DISTRIBUTION, EXTERNAL CIRCUMFERENTIAL AT STATION 54.5 INCHES (1.38 METERS)

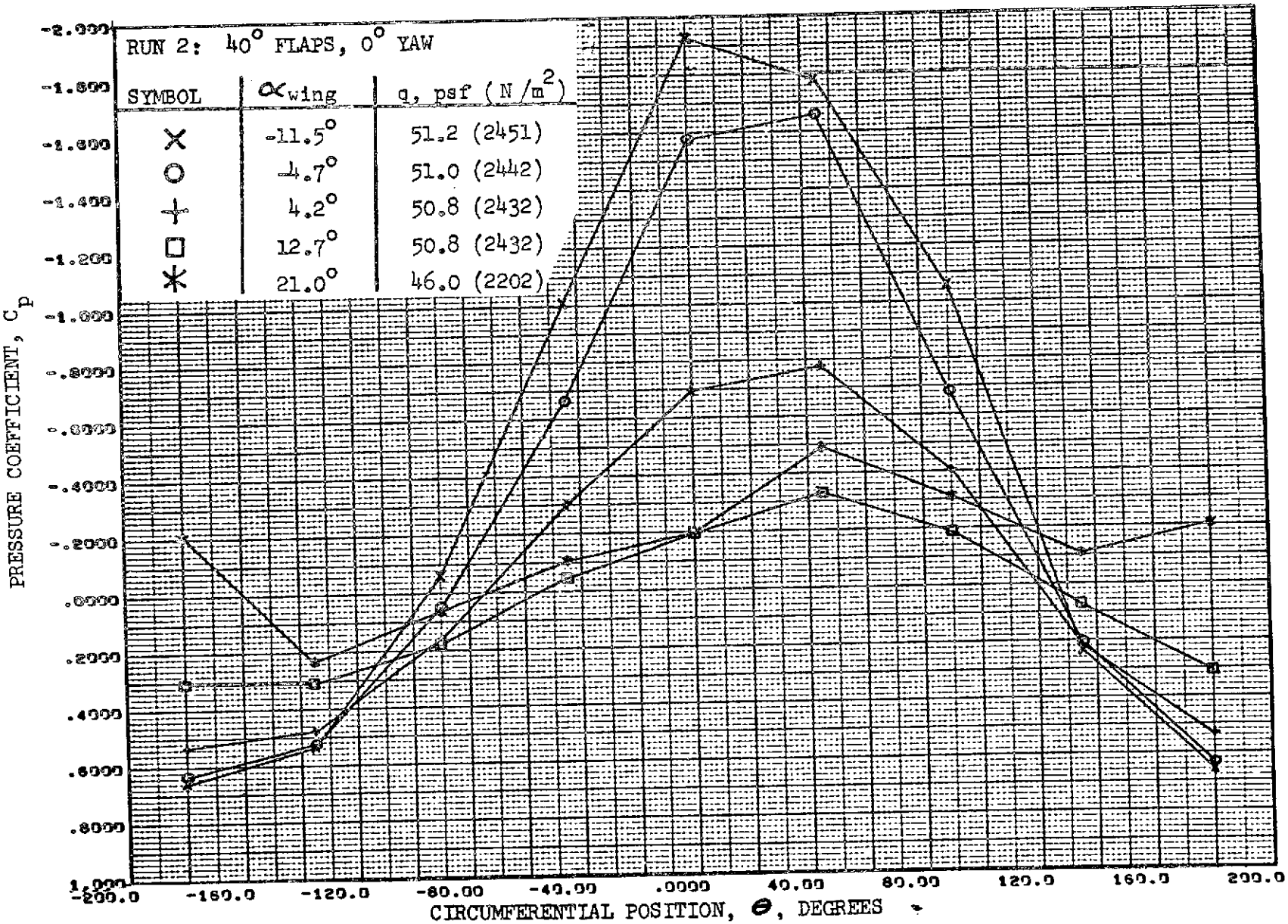

FIGURE 116. - REFAN NACELLE PRESSURE COEFFICIENT DISTRIBUTION, INTERNAL CIRCUMFERENTIAL AT STATION 54.5 INCHES (1.38 METERS)

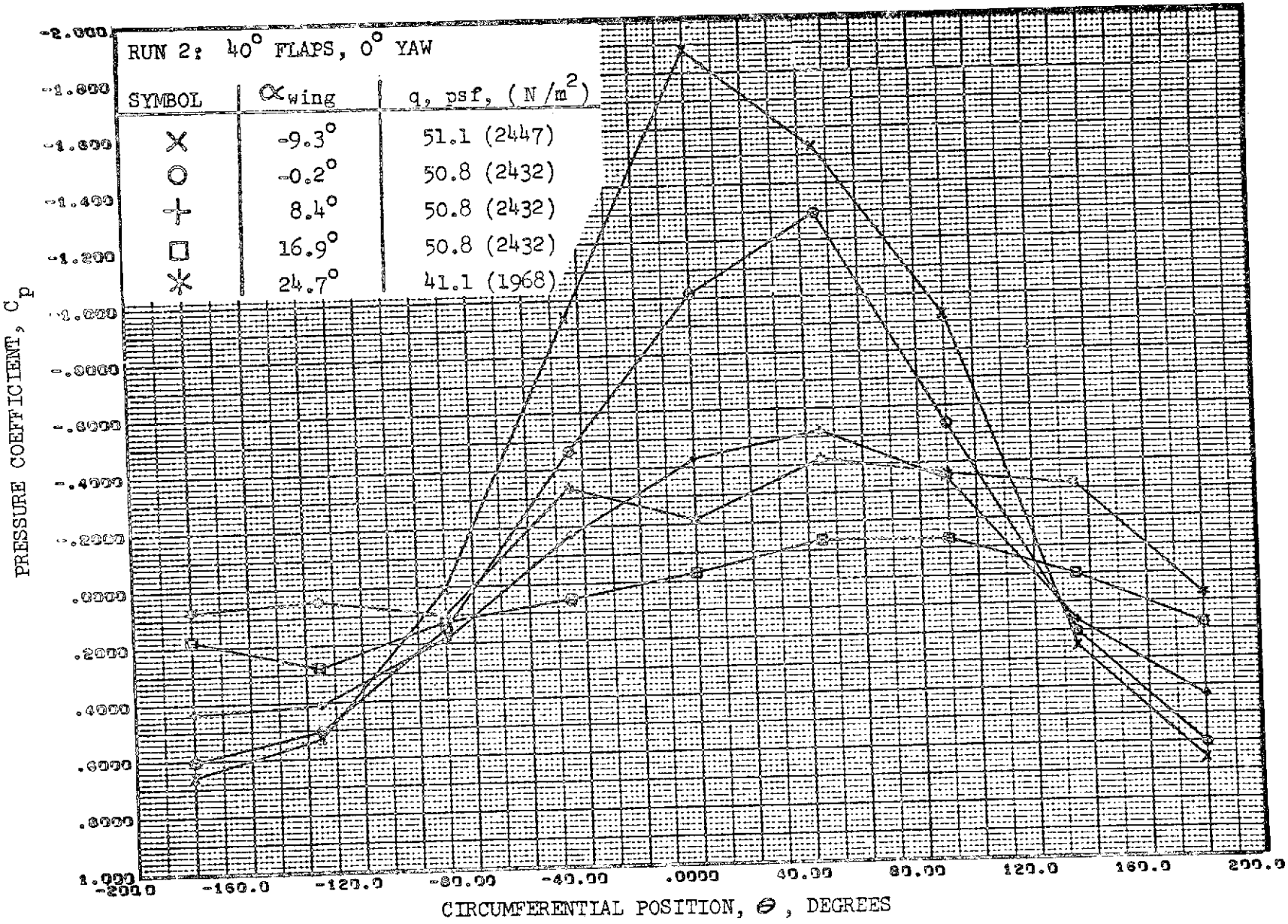

FIGURE 117. - REFAN NACELLE PRESSURE COEFFICIENT DISTRIBUTION, INTERNAL CIRCUMFERENTIAL AT STATION 54.5 INCHES (1.38 METERS)

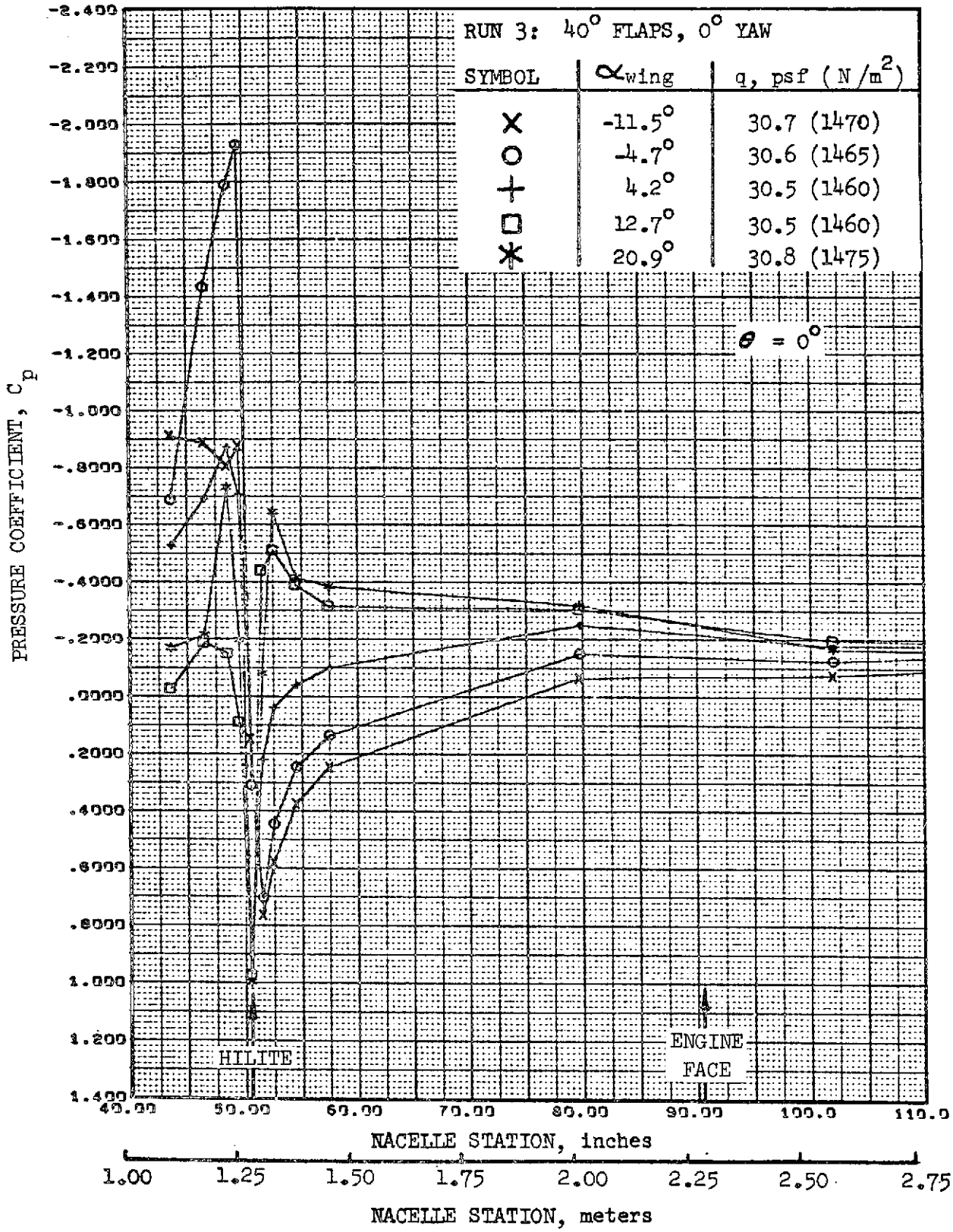

FIGURE 118.-REFAN NACELLE INLET COWL PRESSURE COEFFICIENT DISTRIBUTION, TOP LONGITUDINAL

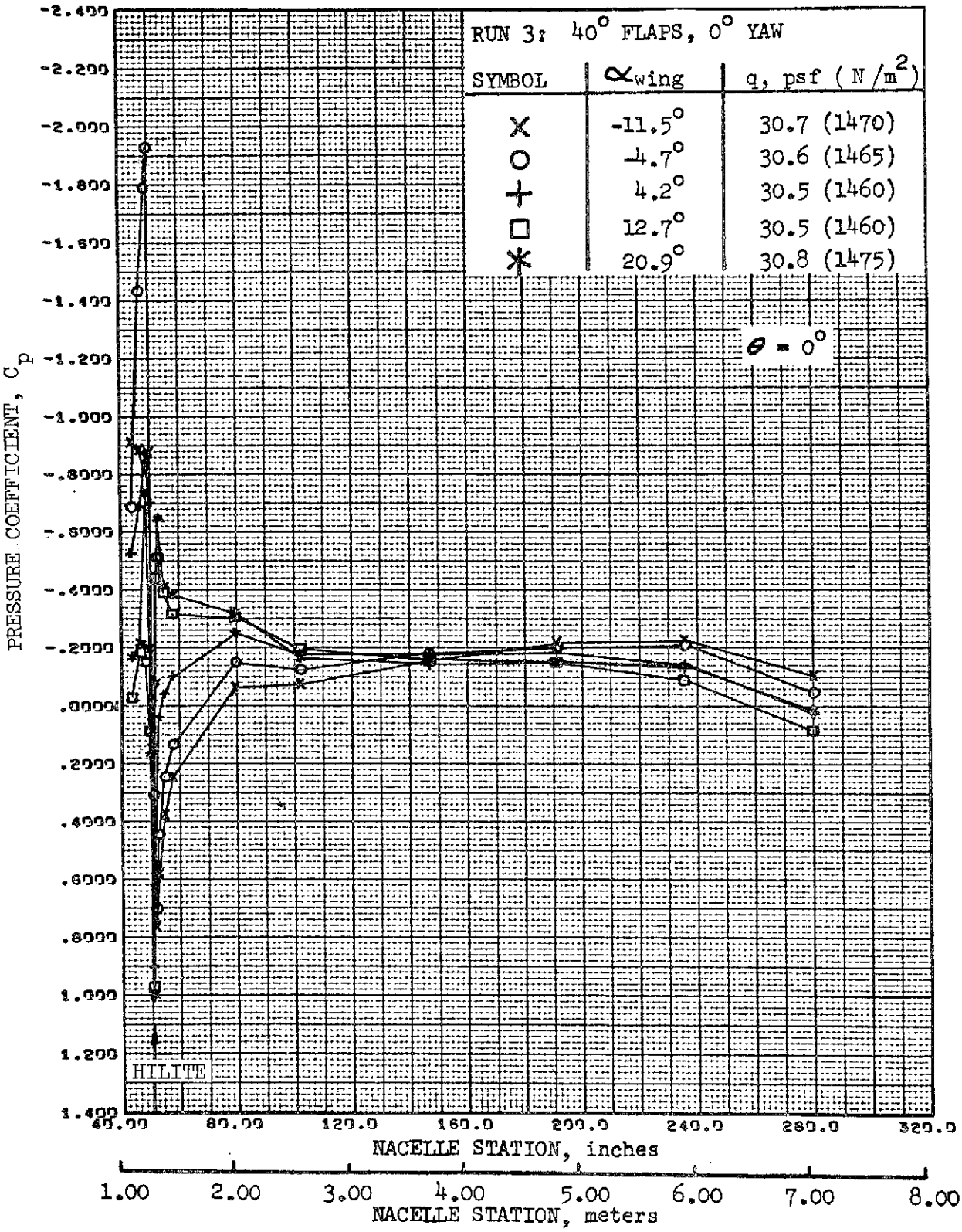

FIGURE 119.-REFAN NACELLE PRESSURE COEFFICIENT DISTRIBUTION, TOP LONGITUDINAL

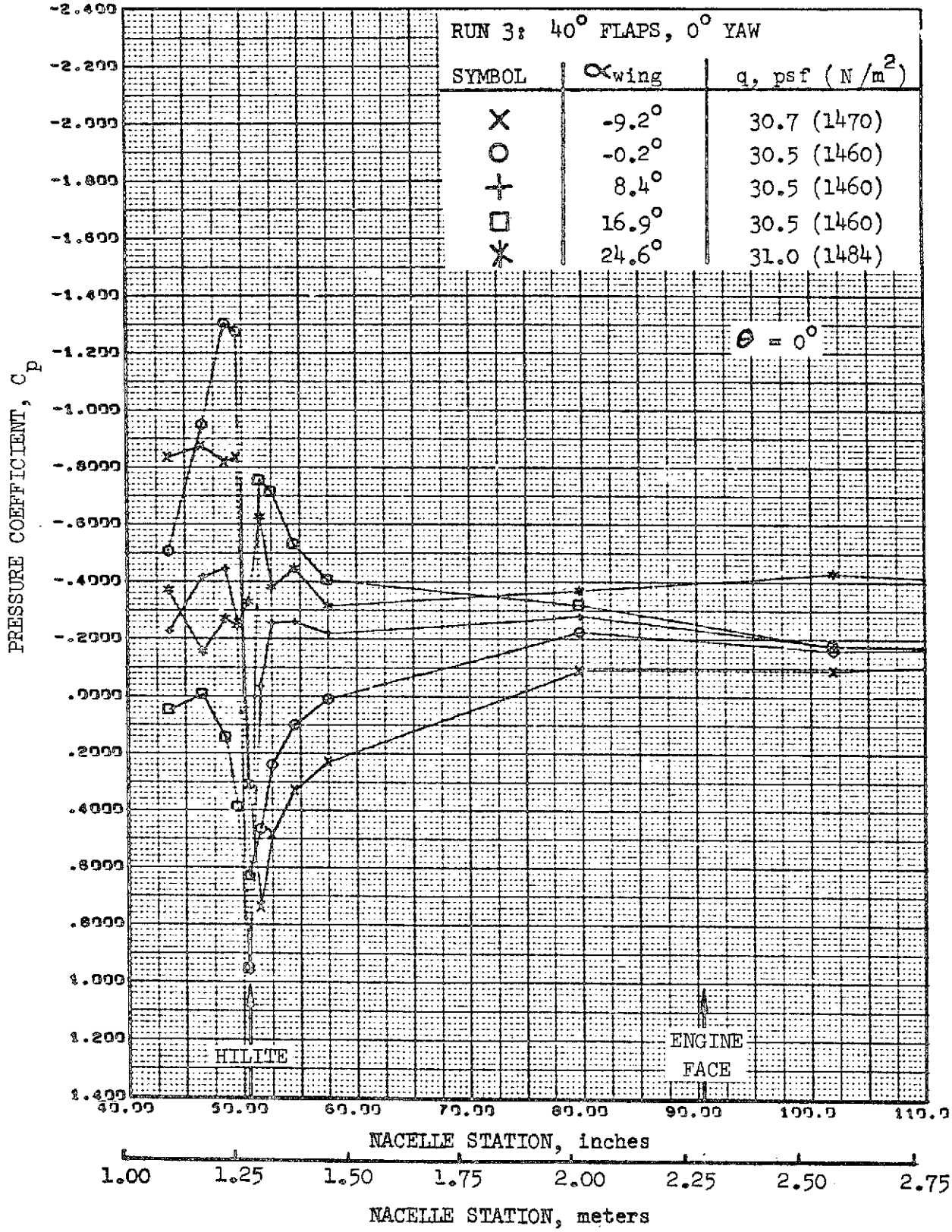

FIGURE 120.-REFAN NACELLE INLET COWL PRESSURE COEFFICIENT DISTRIBUTION, TOP LONGITUDINAL

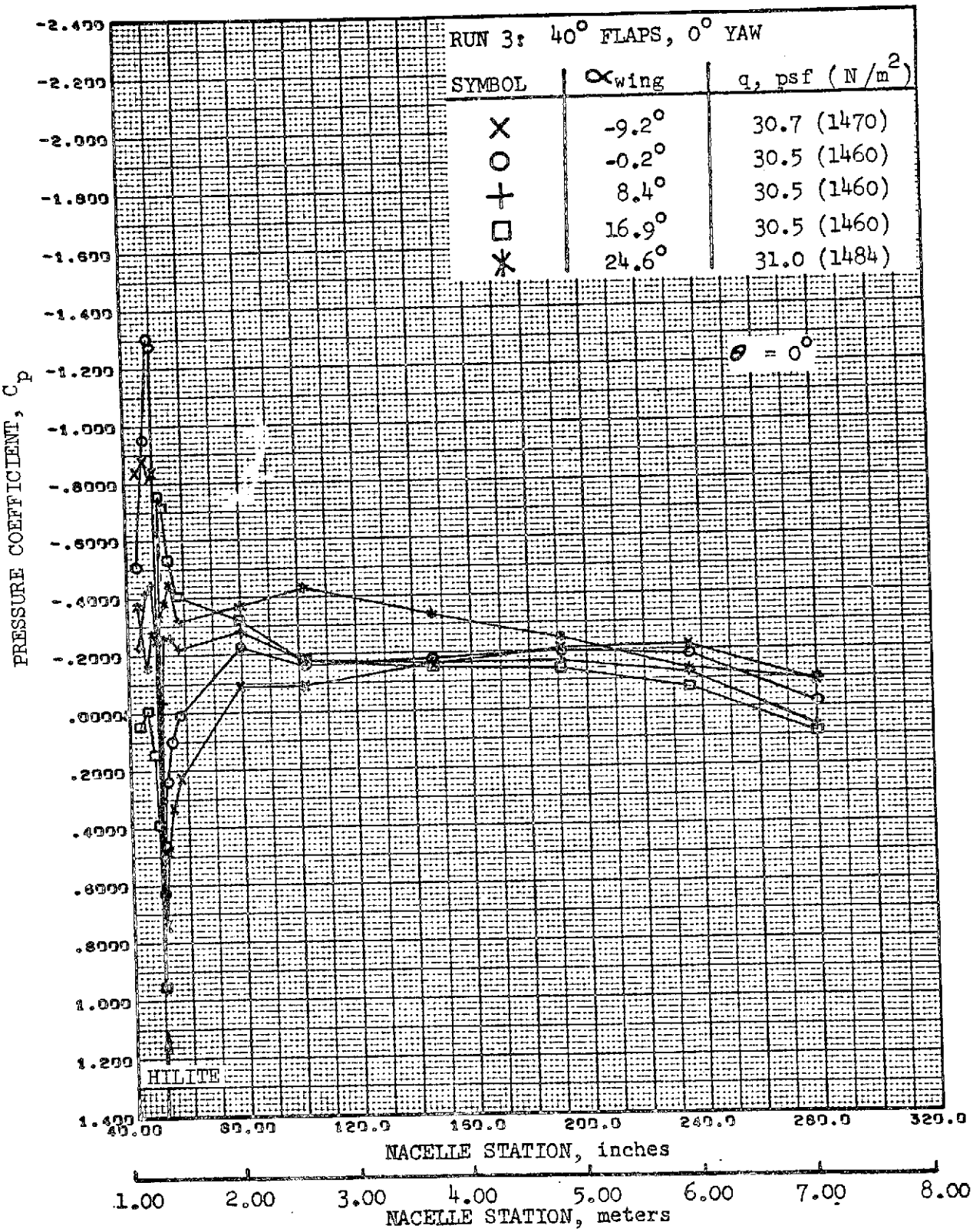

FIGURE 121. REFAN NACELLE PRESSURE COEFFICIENT DISTRIBUTION, TOP LONGITUDINAL

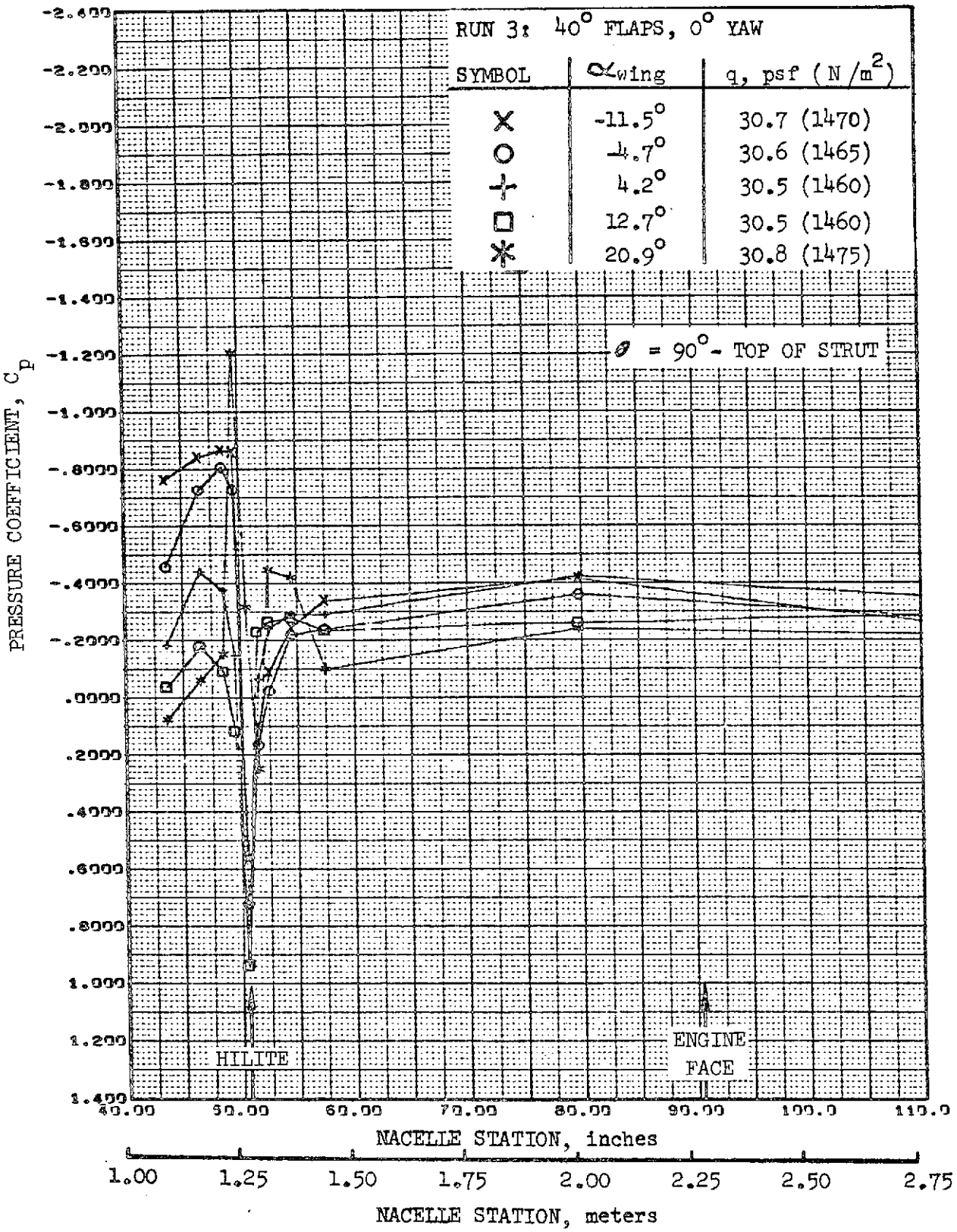

FIGURE 122.-REFAN NACELLE INLET COWL PRESSURE COEFFICIENT DISTRIBUTION, INBOARD SIDE-ABOVE STRUT

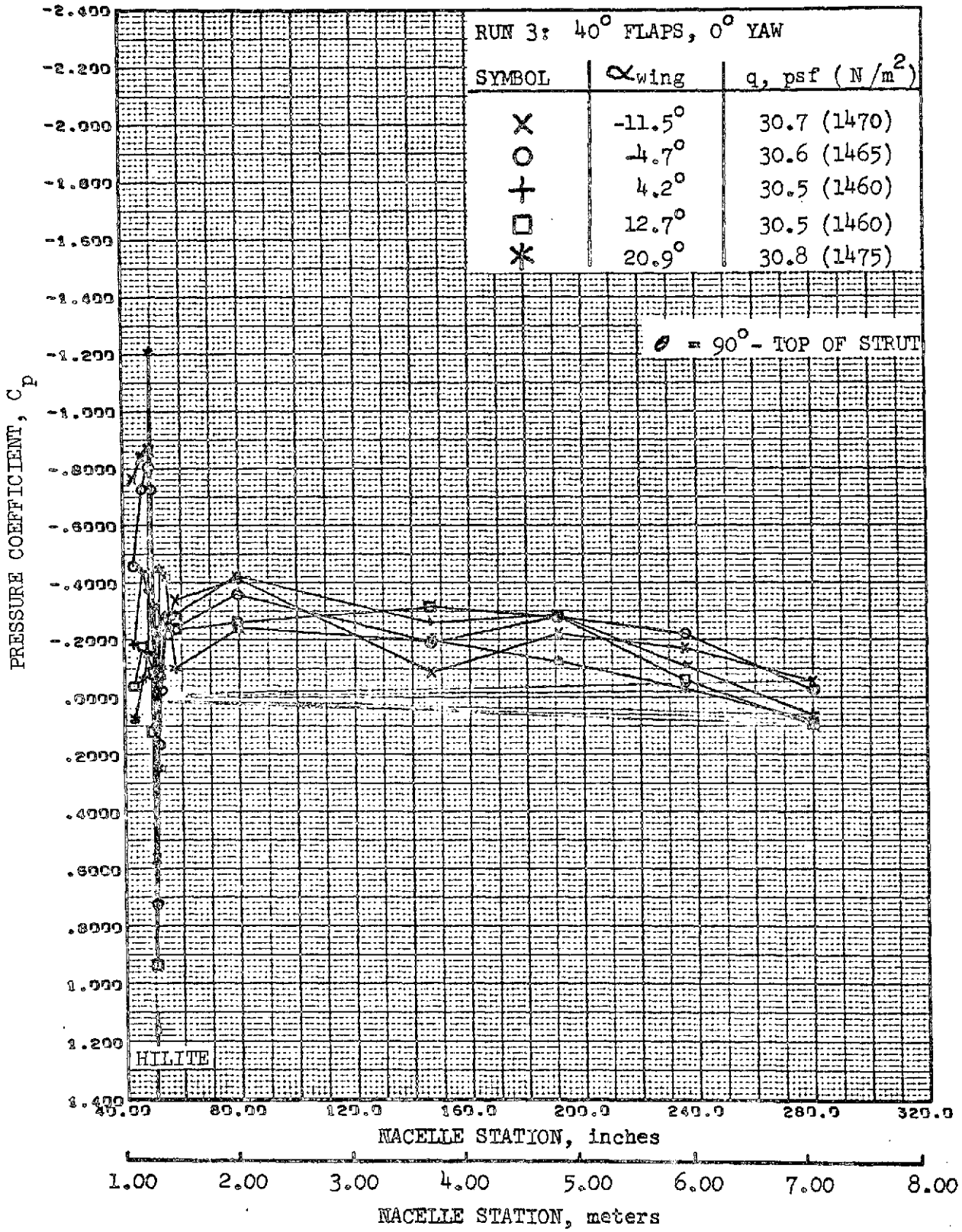

FIGURE 123.-REFAN NACELLE PRESSURE COEFFICIENT DISTRIBUTION, INBOARD SIDE-ABOVE STRUT

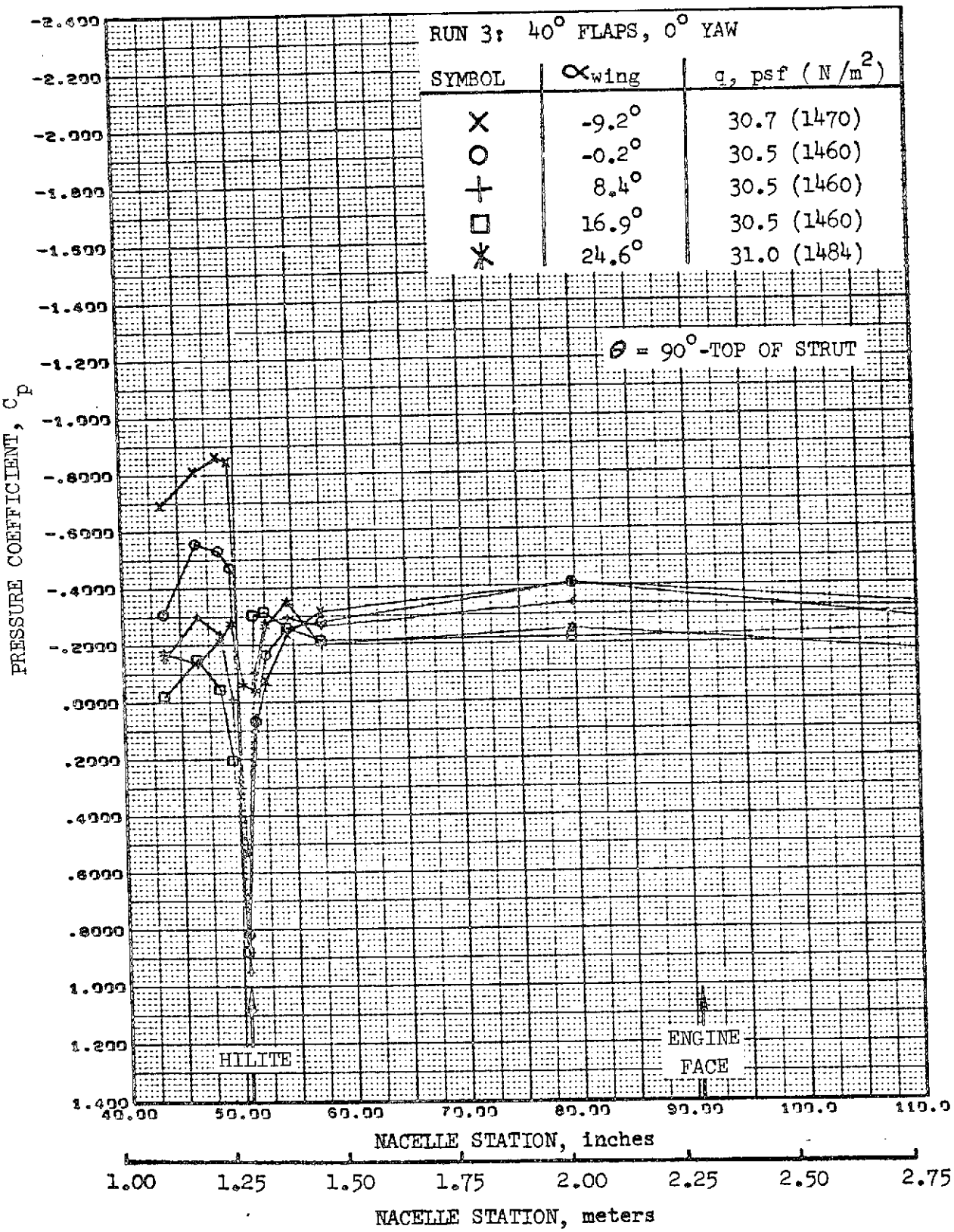

FIGURE 124.-REFAN NACELLE INLET COWL PRESSURE COEFFICIENT DISTRIBUTION, INBOARD SIDE-ABOVE STRUT

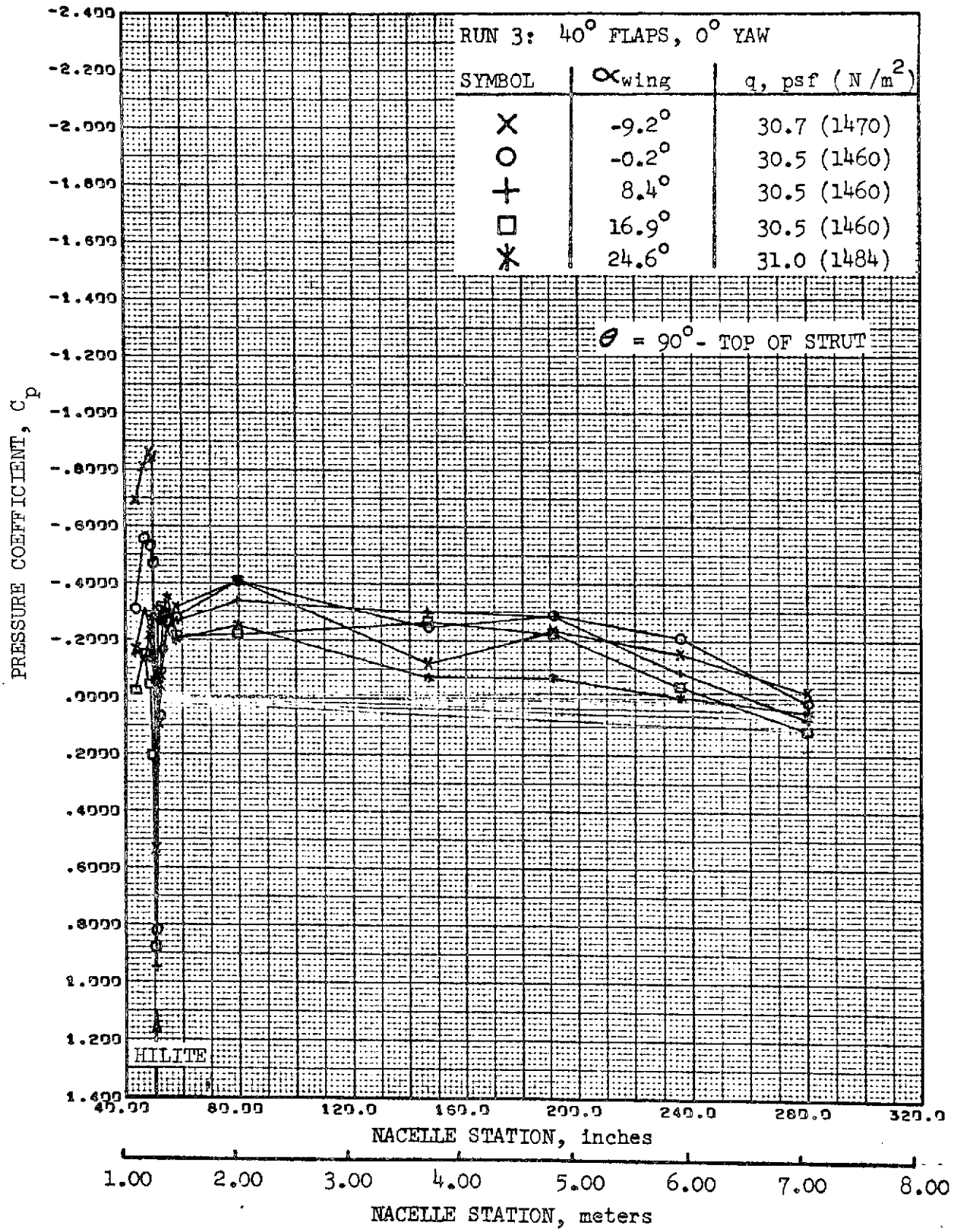

FIGURE 125.-REFAN NACELLE PRESSURE COEFFICIENT DISTRIBUTION, INBOARD SIDE-ABOVE STRUT

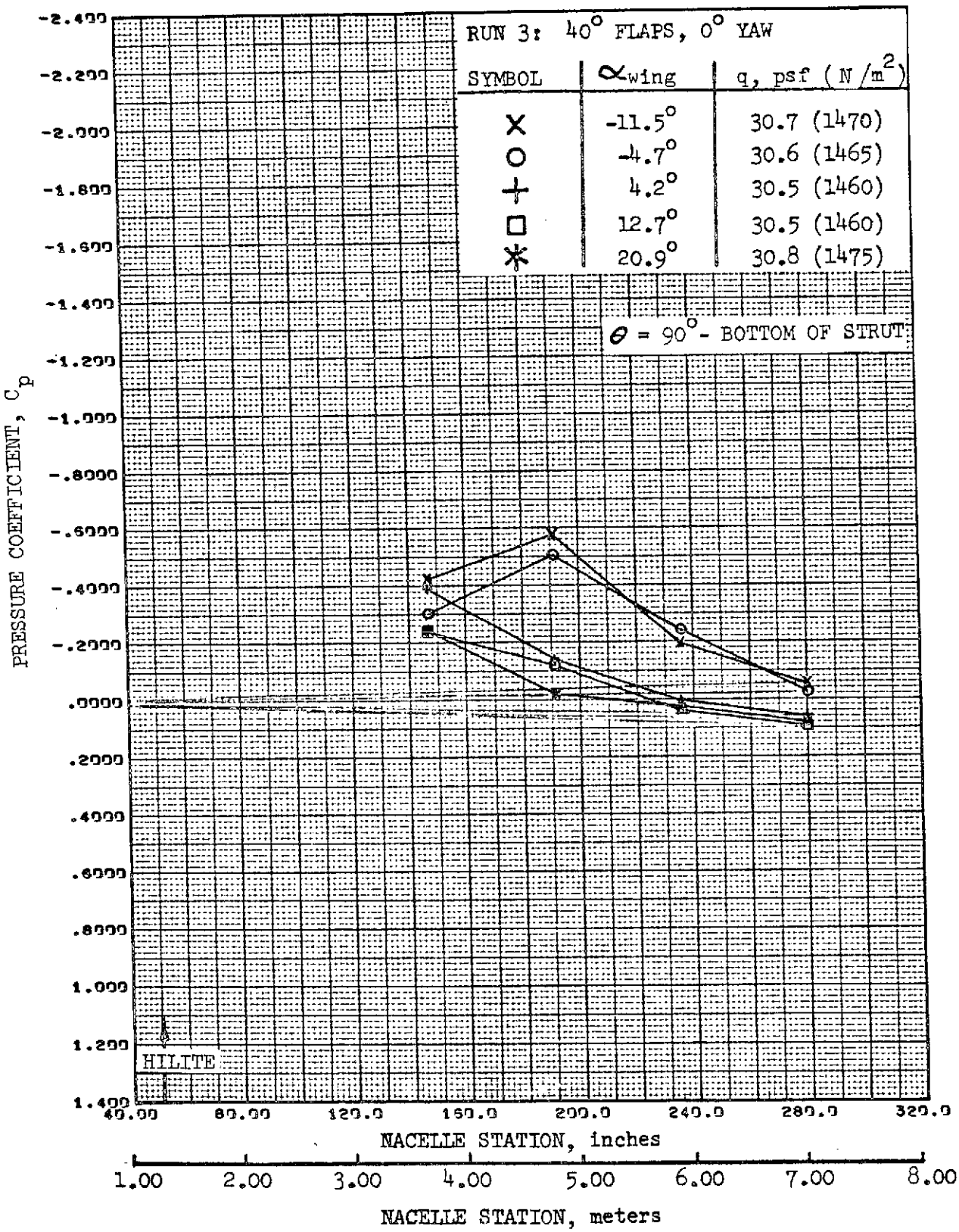

FIGURE 126.-REFAN NACELLE PRESSURE COEFFICIENT DISTRIBUTION, INBOARD SIDE-BELOW STRUT

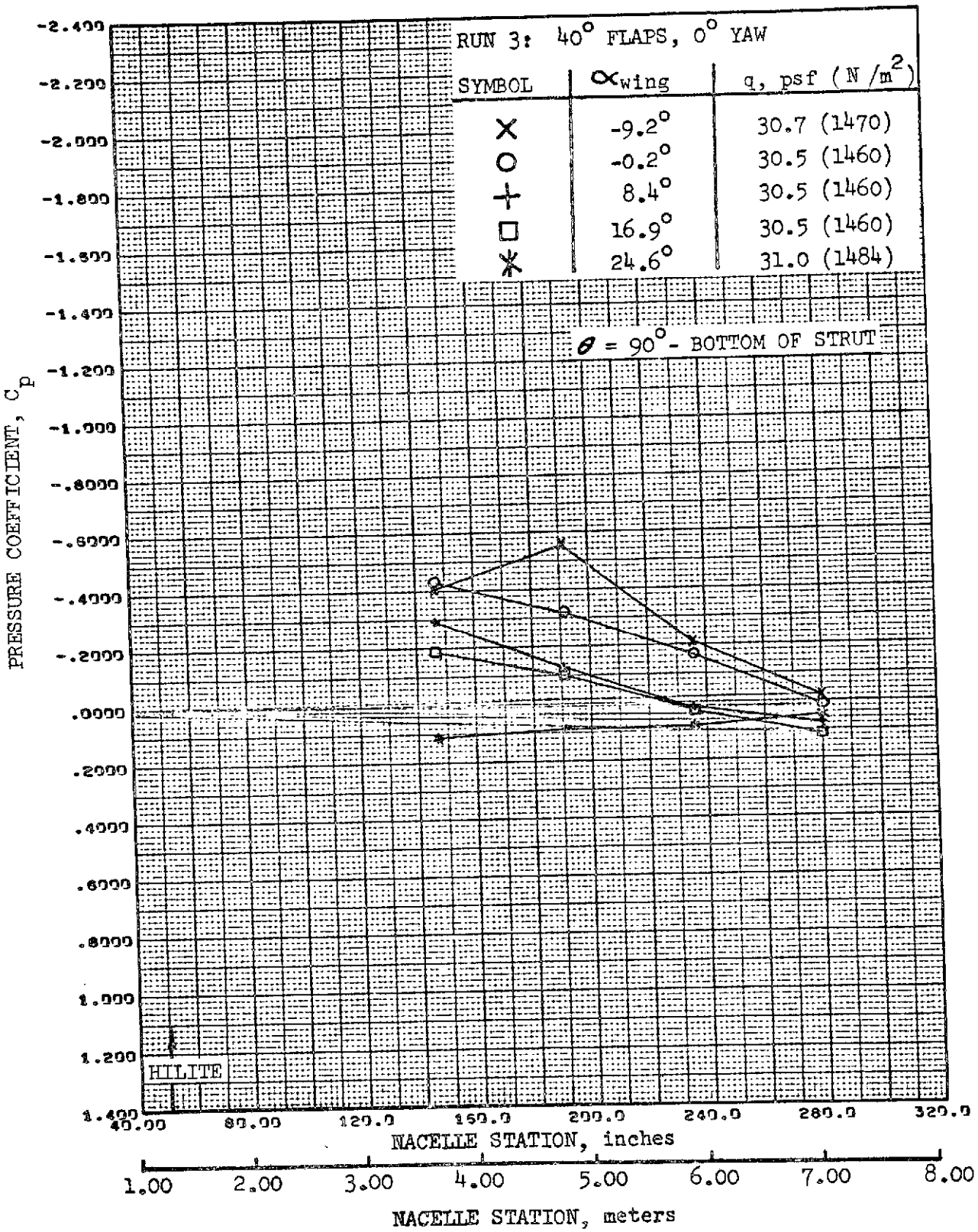

FIGURE 127.-REFAN NACELLE PRESSURE COEFFICIENT DISTRIBUTION, INBOARD SIDE-BELOW STRUT

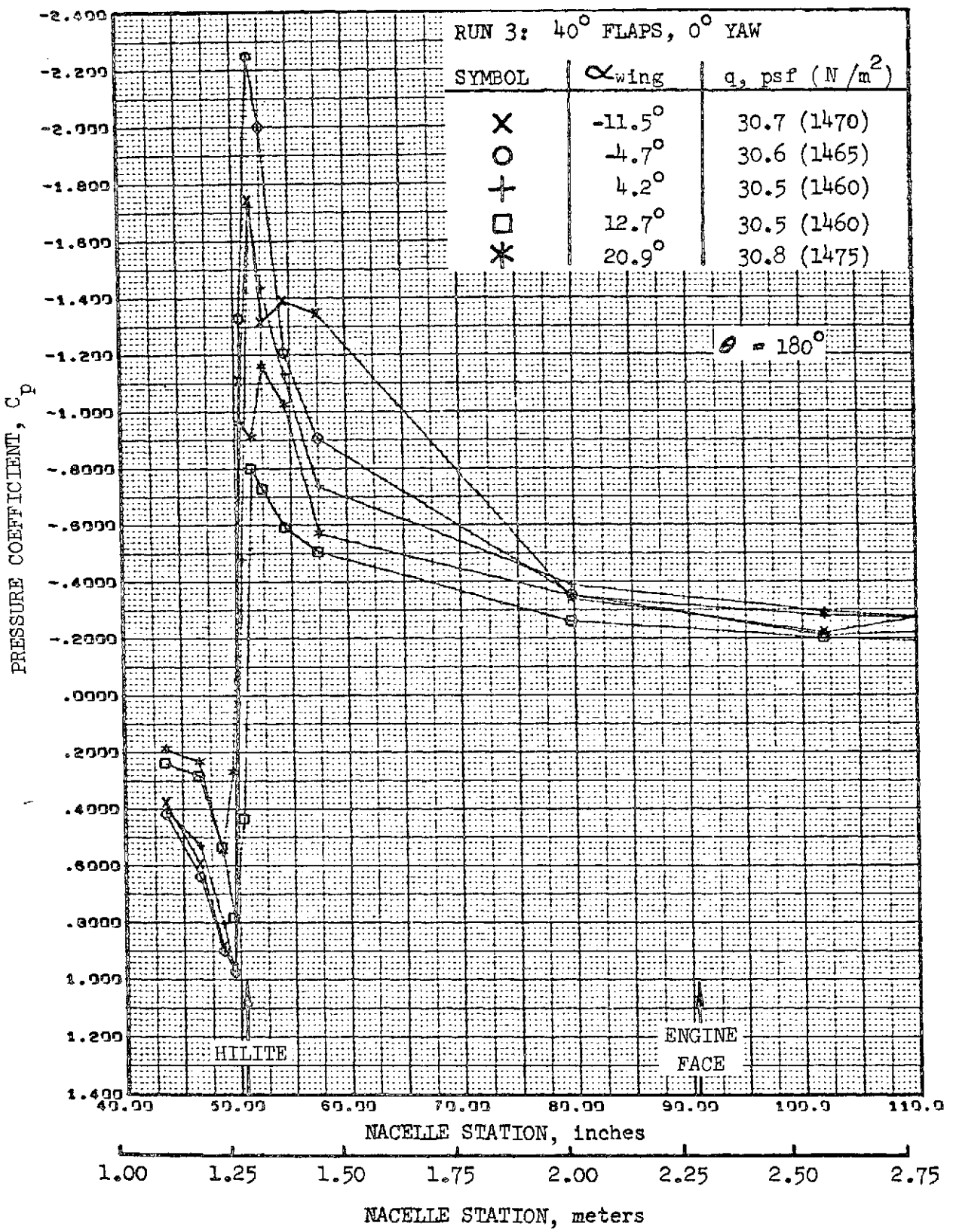

FIGURE 128.-REFAN NACELLE INLET COWL PRESSURE COEFFICIENT DISTRIBUTION, BOTTOM LONGITUDINAL

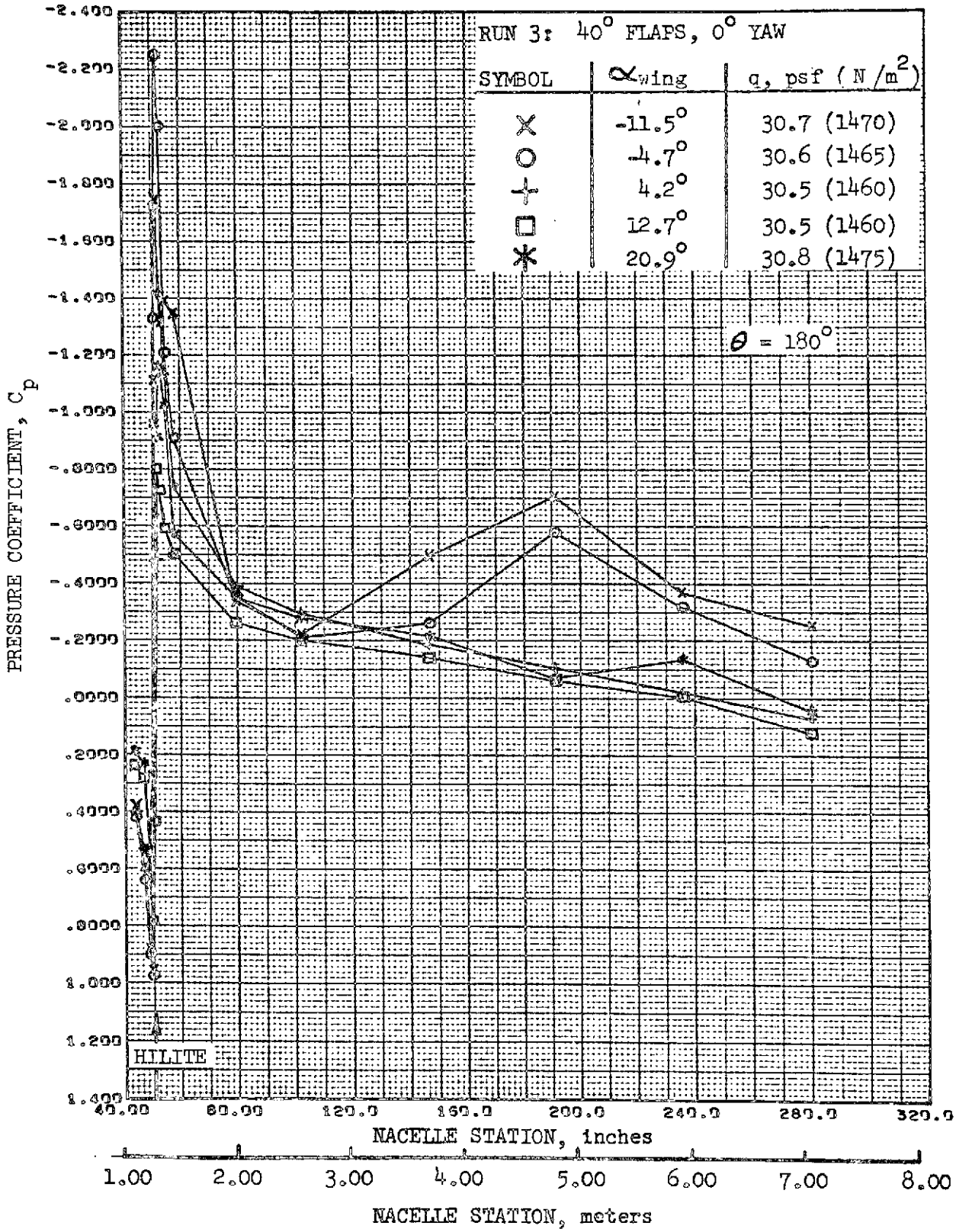

FIGURE 129.-REFAN NACELLE PRESSURE COEFFICIENT DISTRIBUTION, BOTTOM LONGITUDINAL

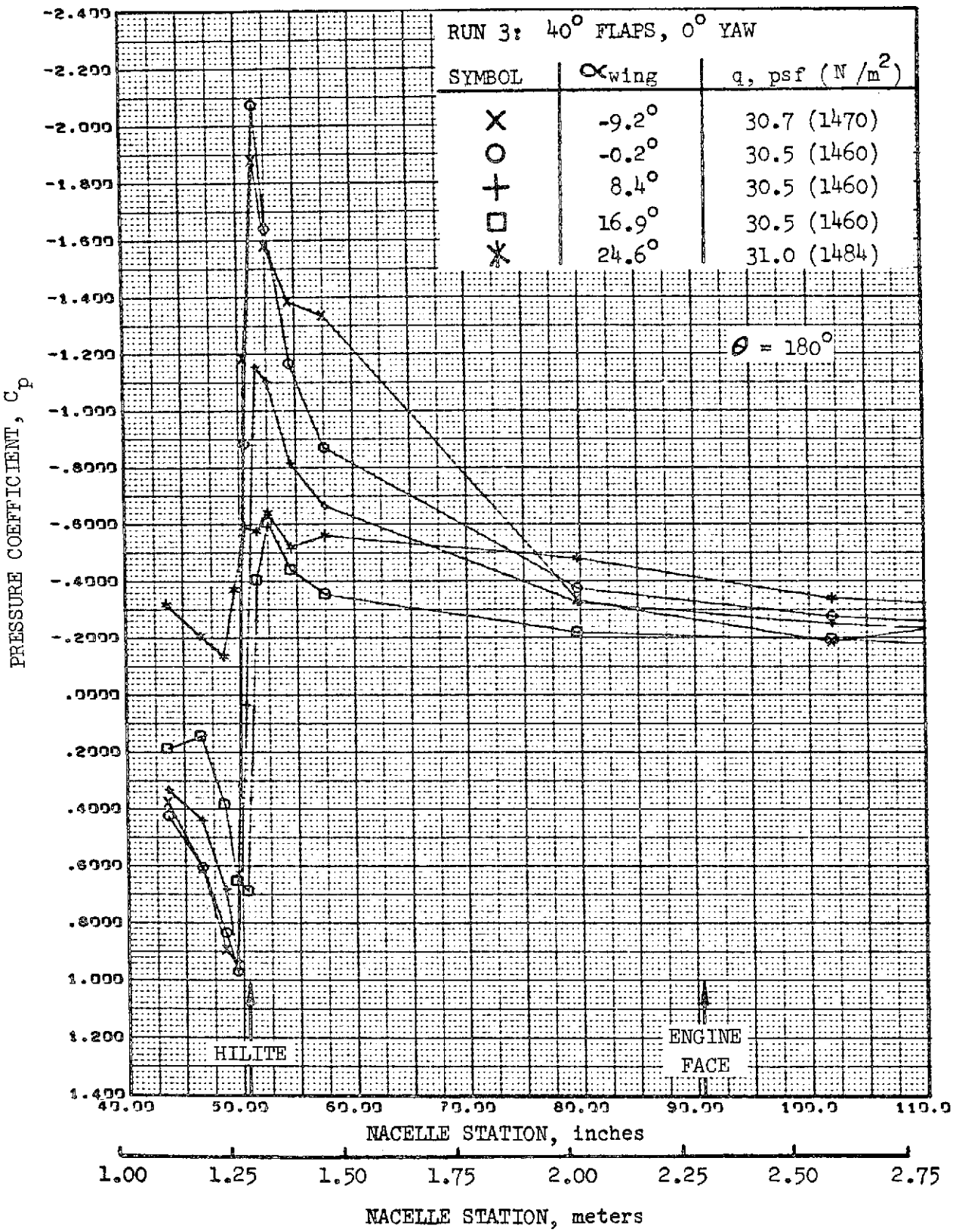

FIGURE 130.-REFAN NACELLE INLET COWL PRESSURE COEFFICIENT DISTRIBUTION, BOTTOM LONGITUDINAL

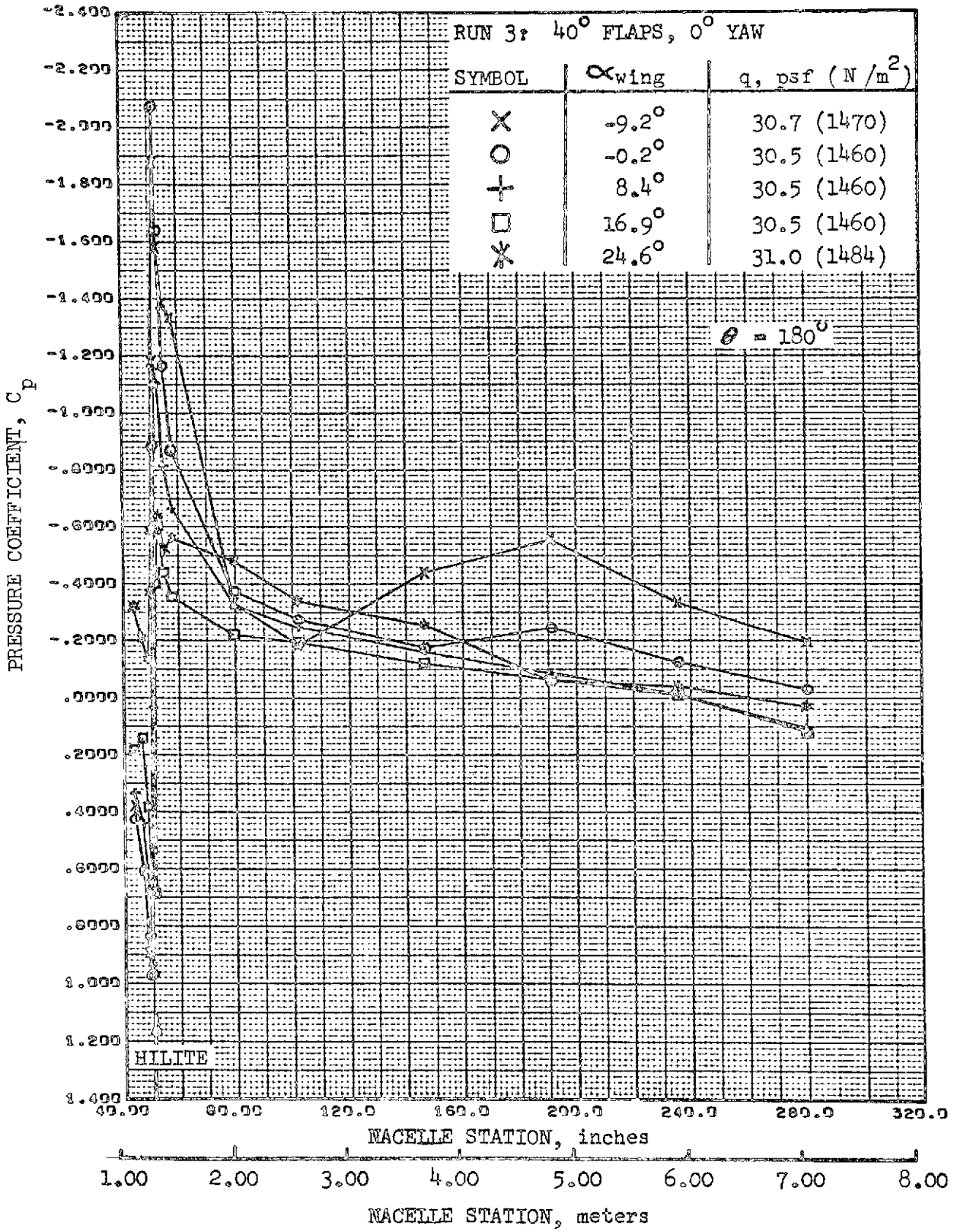

FIGURE 131.-REFAN NACELLE PRESSURE COEFFICIENT DISTRIBUTION, BOTTOM LONGITUDINAL

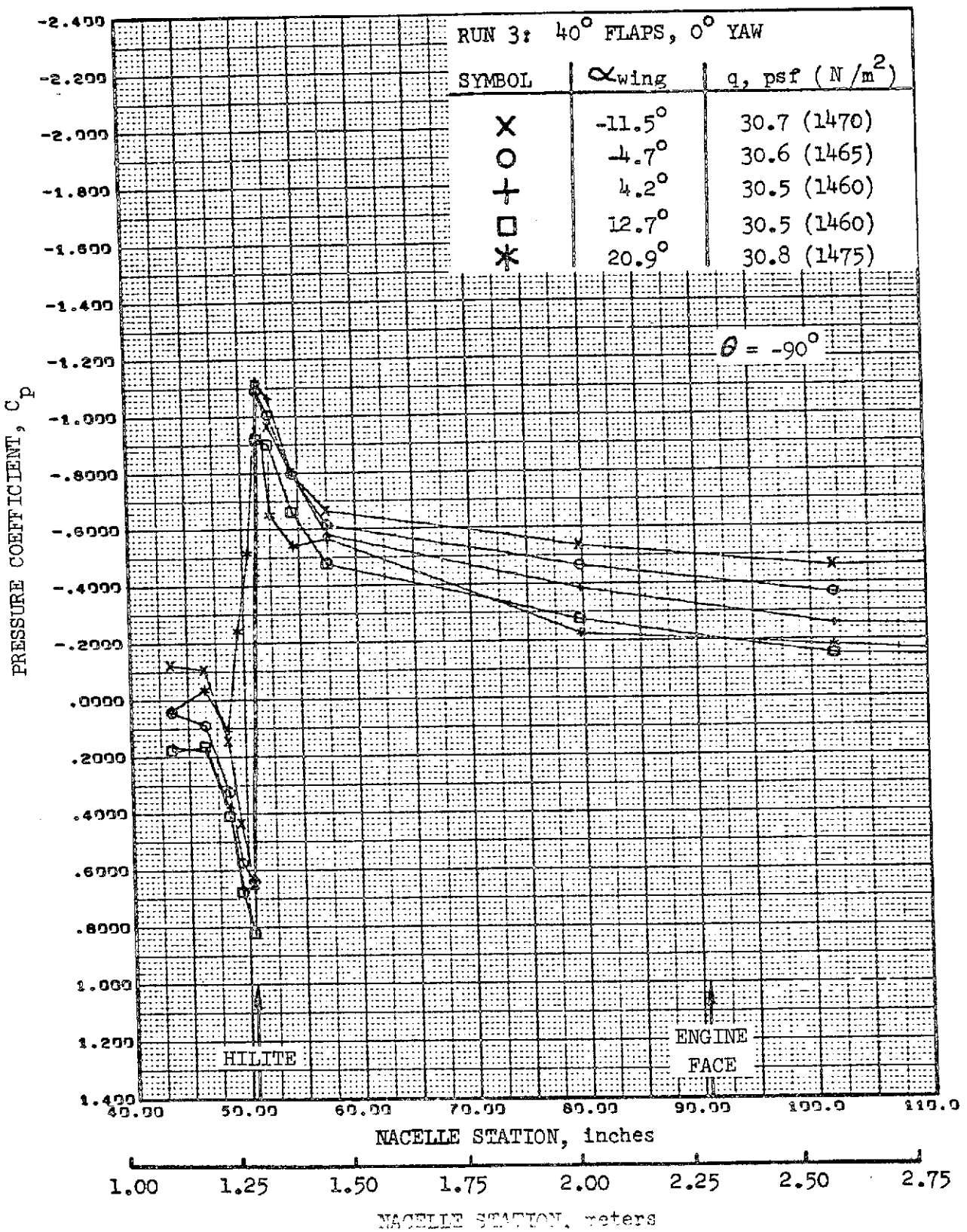

FIGURE 132.-REFAN NACELLE INLET COWL PRESSURE COEFFICIENT DISTRIBUTION, OUTBOARD SIDE

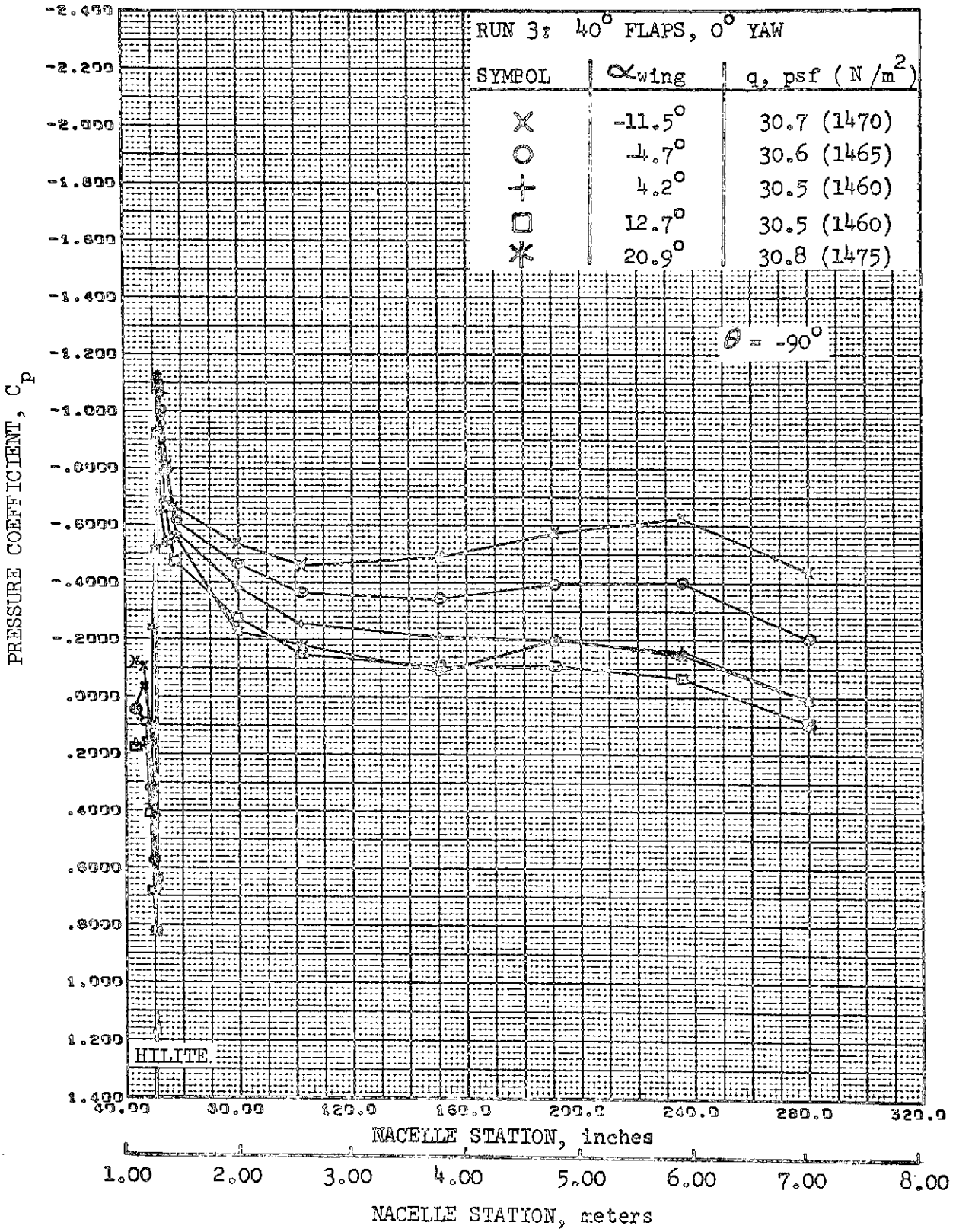

FIGURE 133. REFAN NACELLE PRESSURE COEFFICIENT DISTRIBUTION, OUTBOARD SIDE

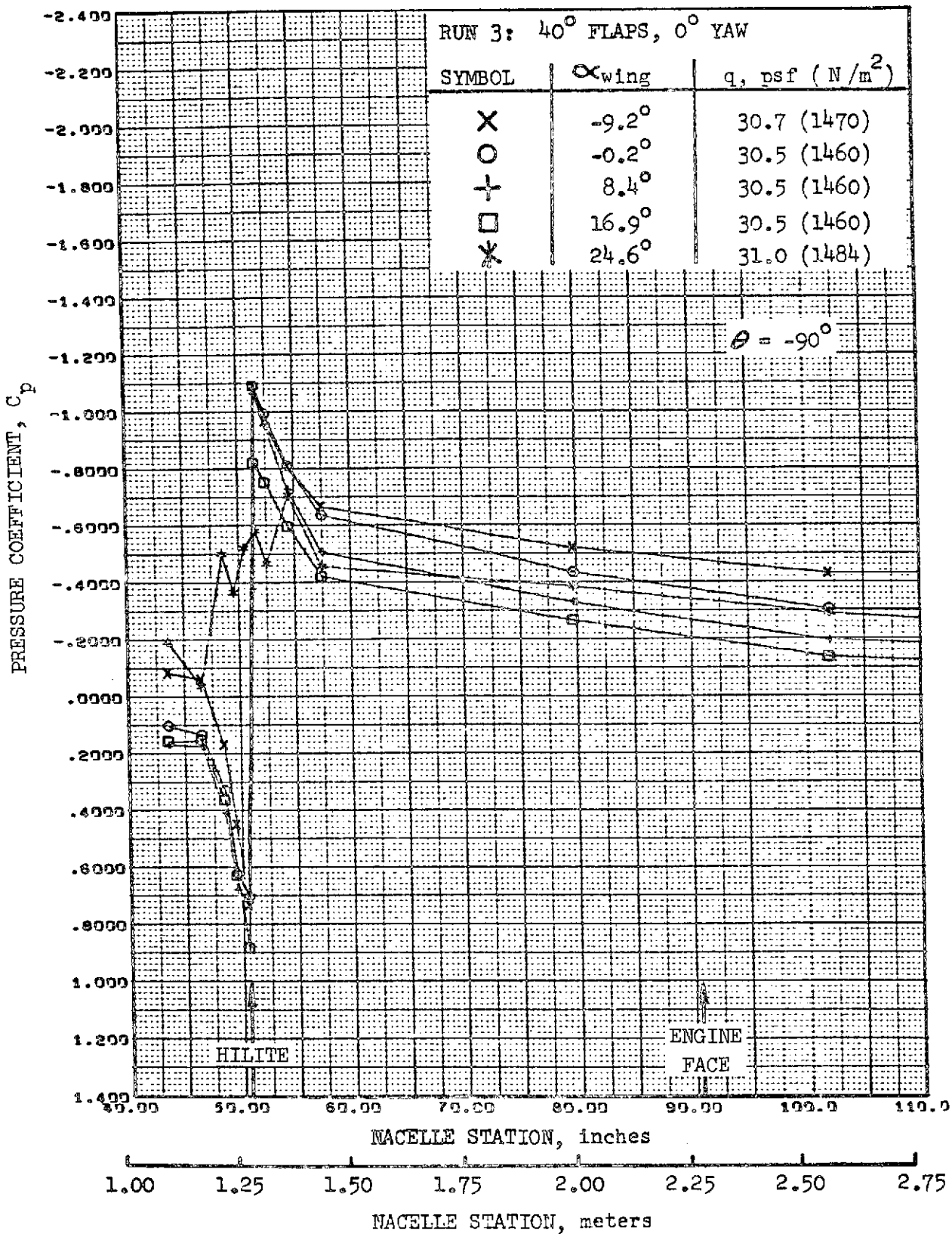

FIGURE 134. -REFAN NACELLE INLET COWL PRESSURE COEFFICIENT DISTRIBUTION, OUTBOARD SIDE

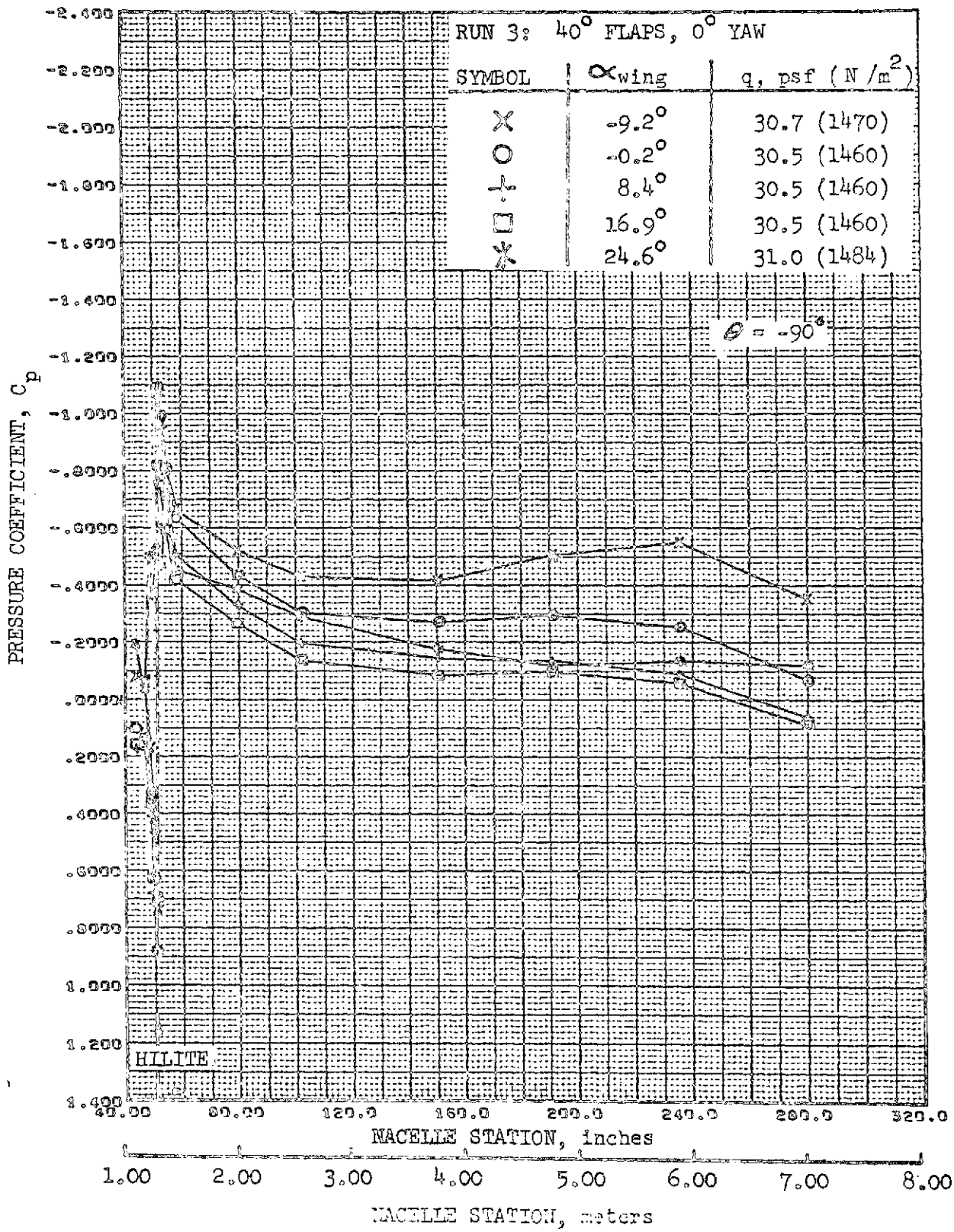

FIGURE 135.-REFAN NACELLE PRESSURE COEFFICIENT DISTRIBUTION, OUTBOARD SIDE

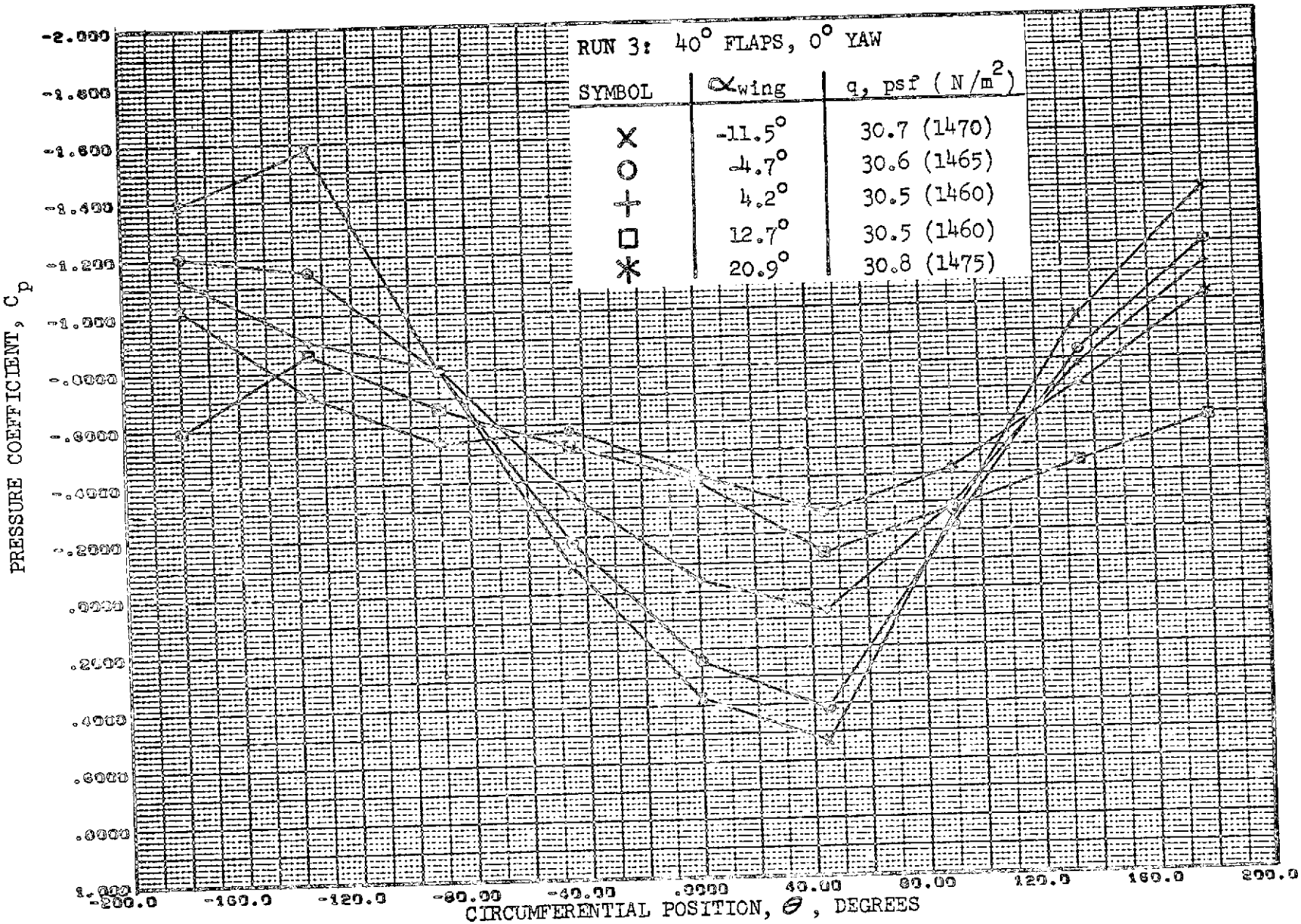

FIGURE 136. - REFAN NACELLE PRESSURE COEFFICIENT DISTRIBUTION, EXTERNAL CIRCUMFERENTIAL AT STATION 54.5 INCHES (1.38 METERS)

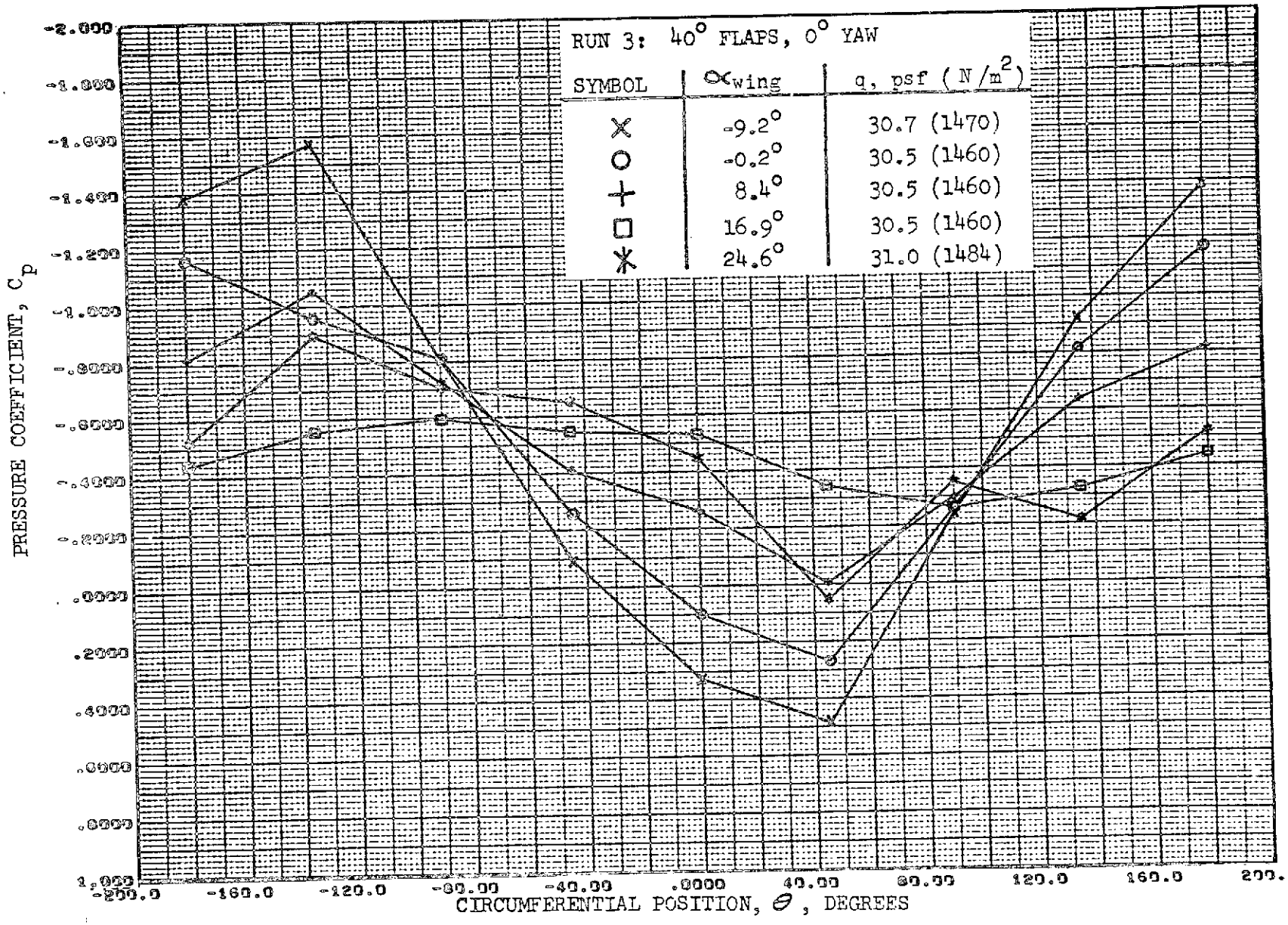

FIGURE 137. - REFAN NACELLE PRESSURE COEFFICIENT DISTRIBUTION, EXTERNAL CIRCUMFERENTIAL AT STATION 54.5 INCHES (1.38 METERS)

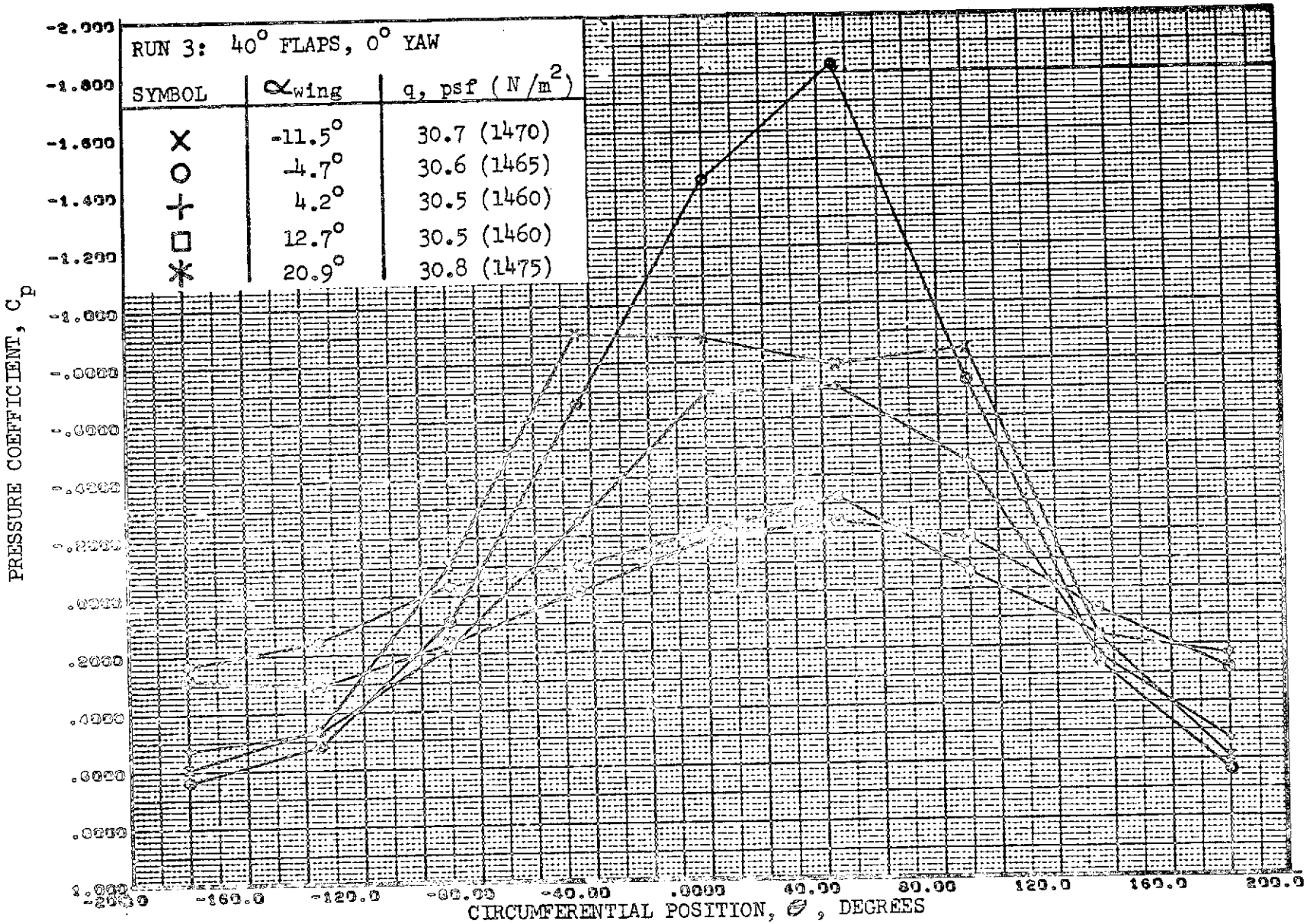

FIGURE 138. - REFAN NACELLE PRESSURE COEFFYCIENT DISTRIBUTION, INTERNAL CIRCUMFERENTIAL AT STATION 54.5 INCHES (1.38 METERS)

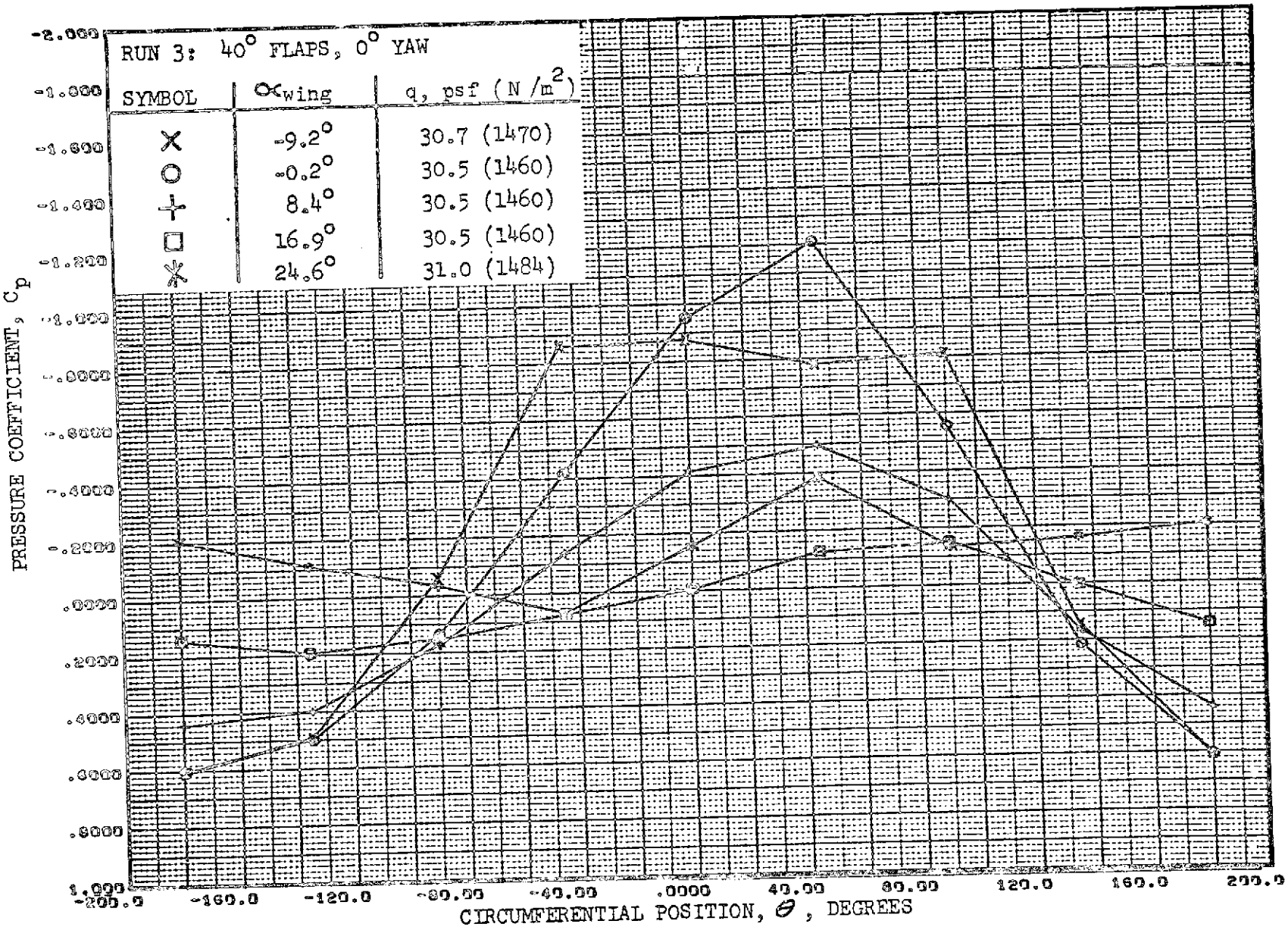

FIGURE 139. - REFAN NACELLE PRESSURE COEFFICIENT DISTRIBUTION, INTERNAL CIRCUMFERENTIAL AT STATION 54.5 INCHES (1.38 METERS)

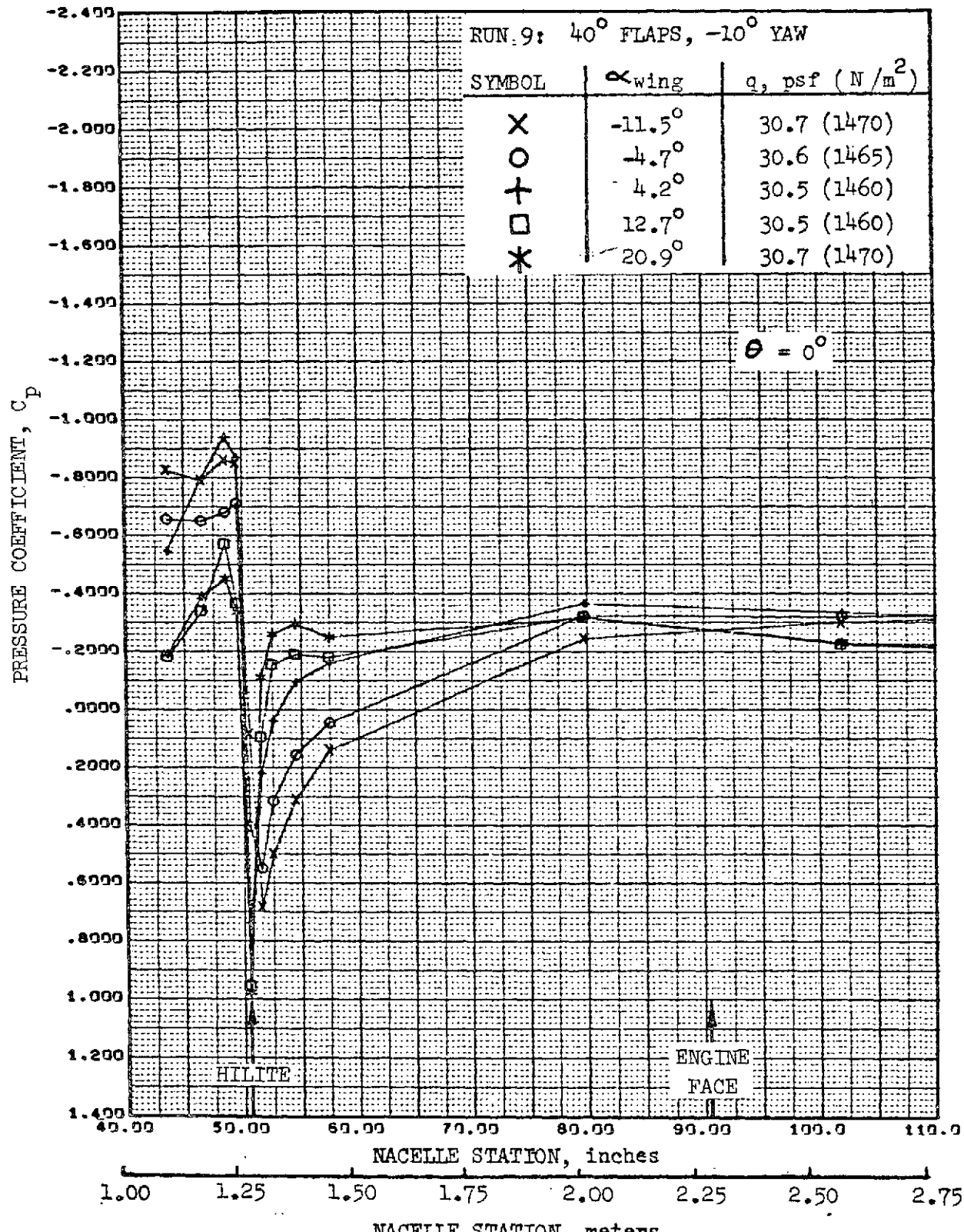

FIGURE 140.-REFAN NACELLE INLET COWL PRESSURE COEFFICIENT DISTRIBUTION, TOP LONGITUDINAL

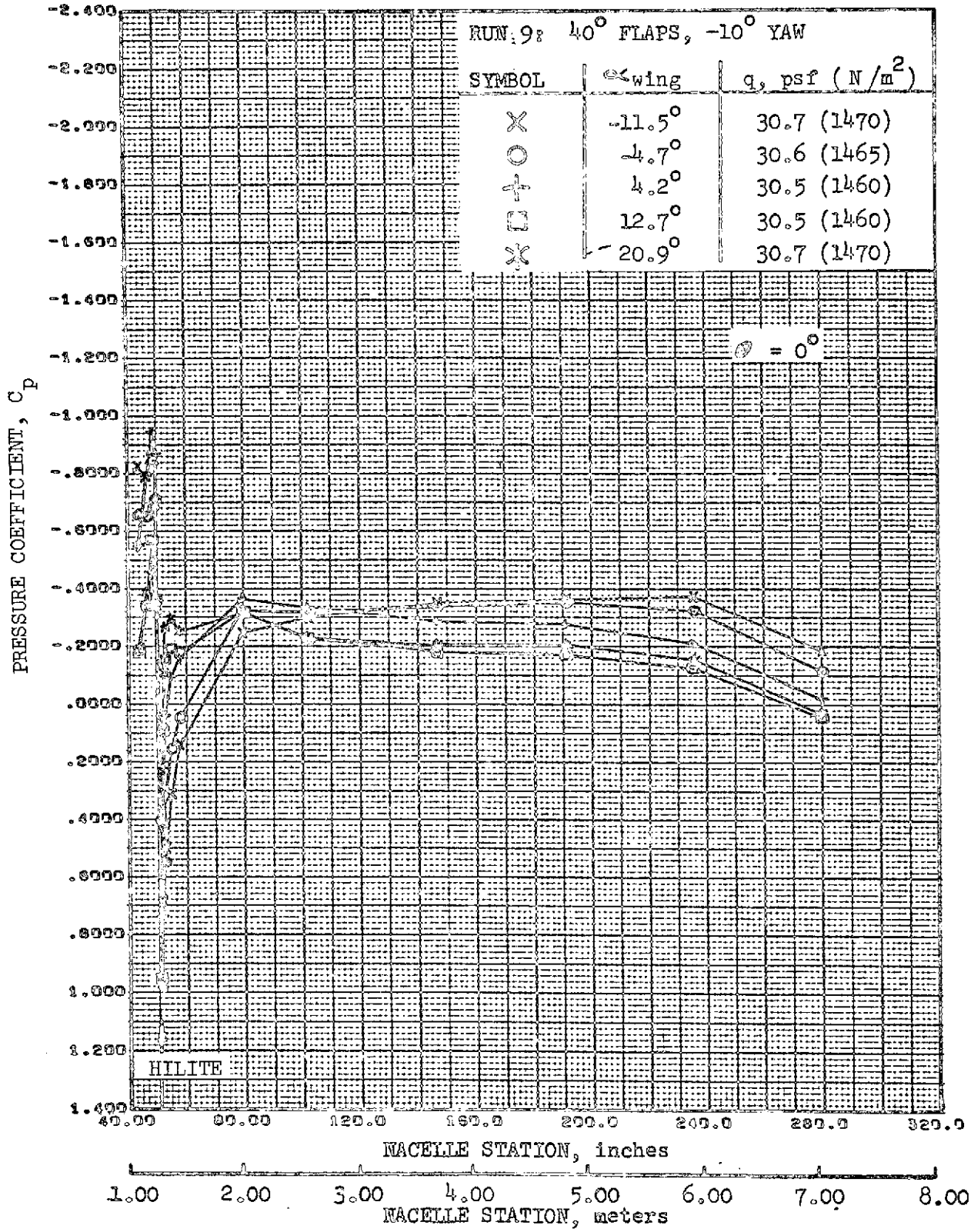

FIGURE 141. REFAN NACELLE PRESSURE COEFFICIENT DISTRIBUTION, TOP LONGITUDINAL

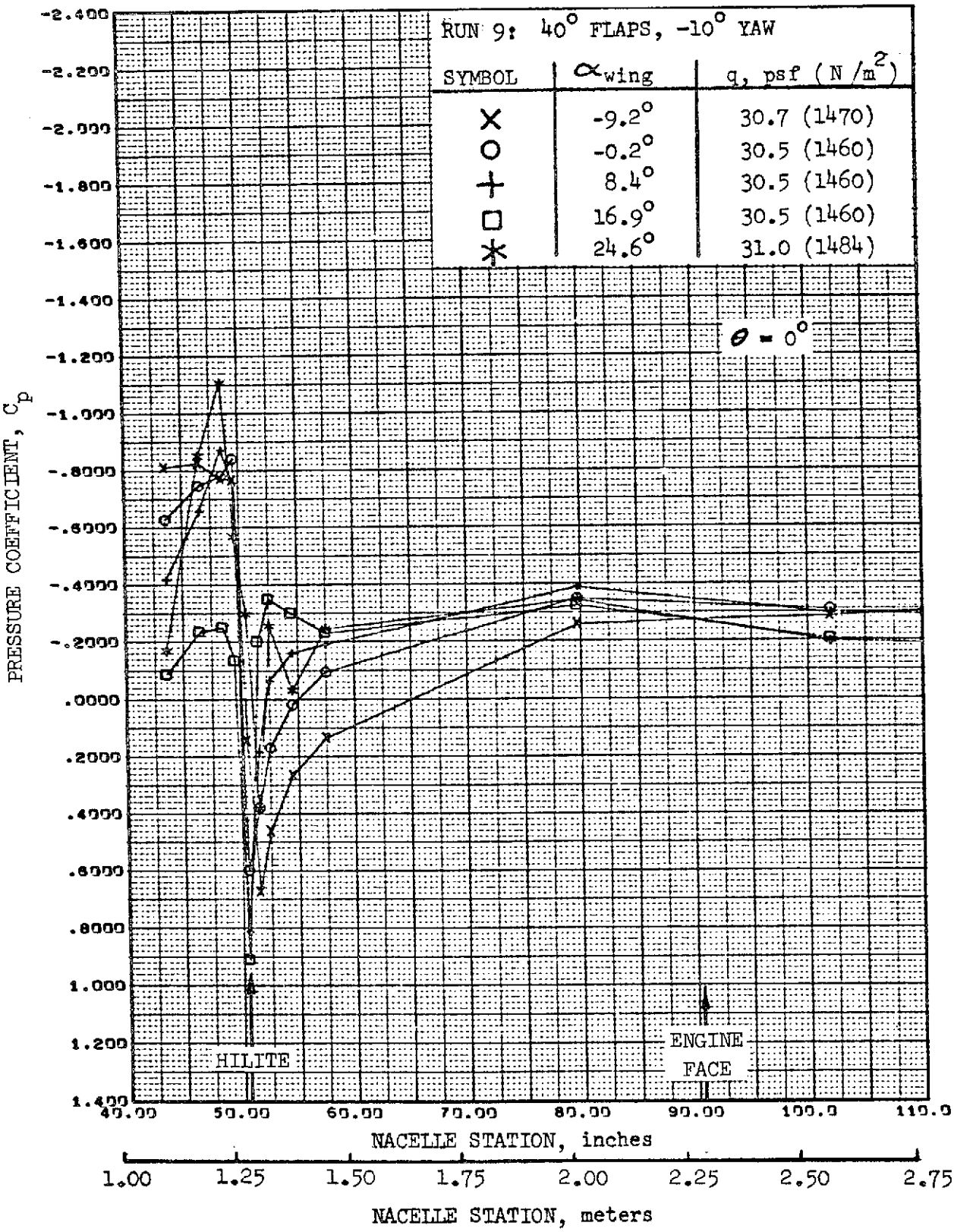

FIGURE 142.-REFAN NACELLE INLET COWL PRESSURE COEFFICIENT DISTRIBUTION, TOP LONGITUDINAL

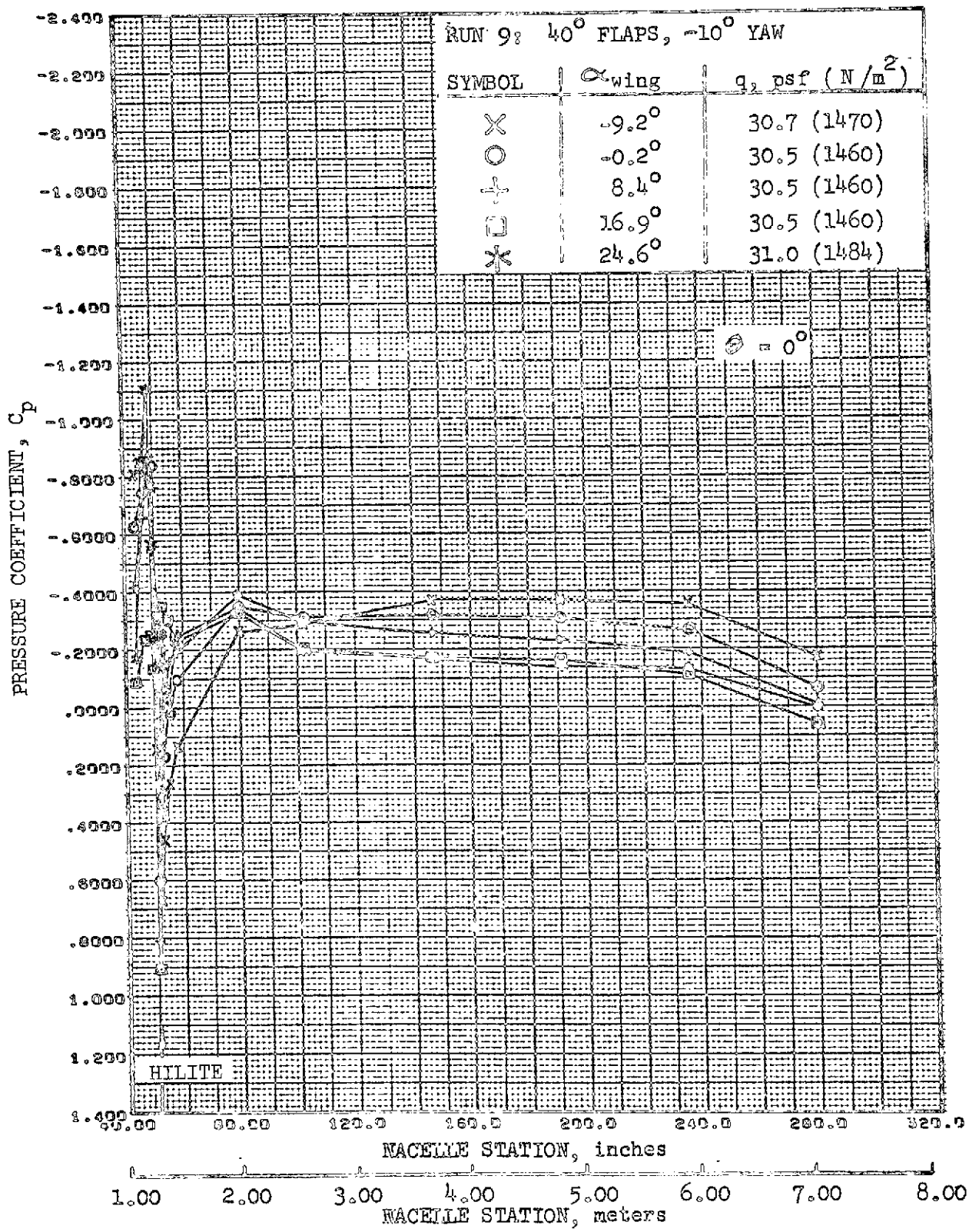

FIGURE 143. REFAN NACELLE PRESSURE COEFFICIENT DISTRIBUTION, TOP LONGITUDINAL

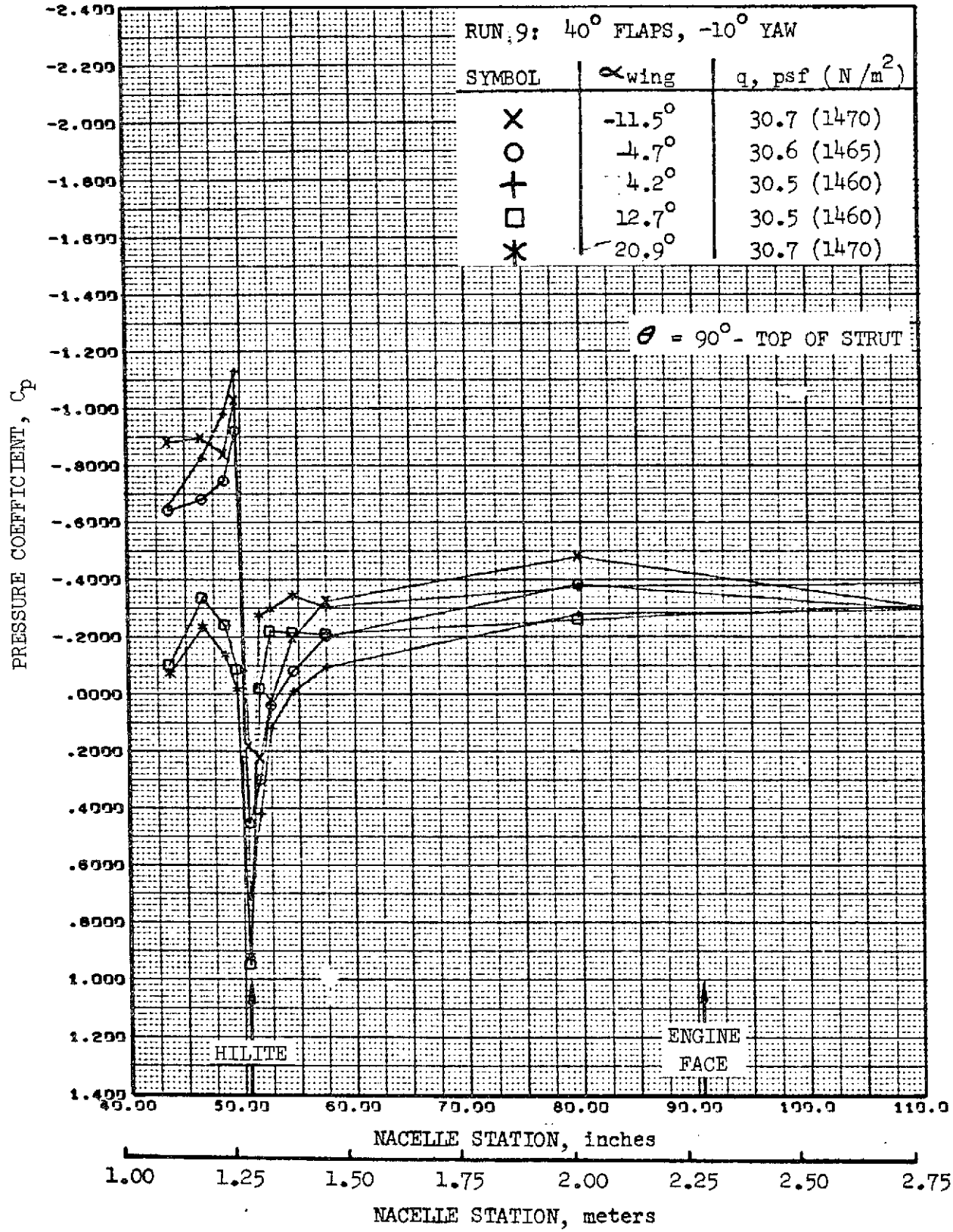

FIGURE 144.-REFAN NACELLE INLET COWL PRESSURE COEFFICIENT DISTRIBUTION, INBOARD SIDE-ABOVE STRUT

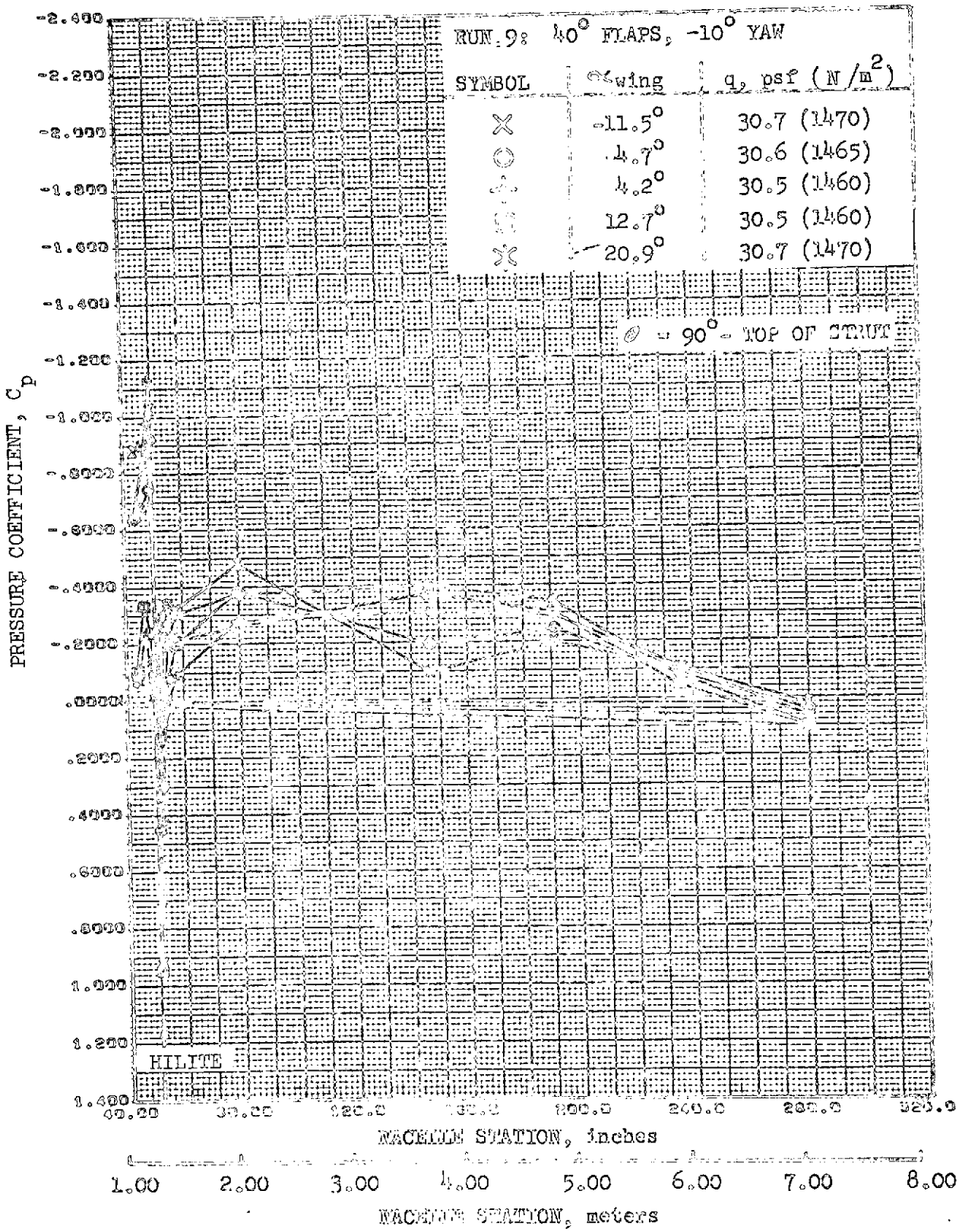

FIGURE 145. REFAN NACELLE PRESSURE COEFFICIENT DISTRIBUTION, INBOARD SIDE ABOVE STRUT

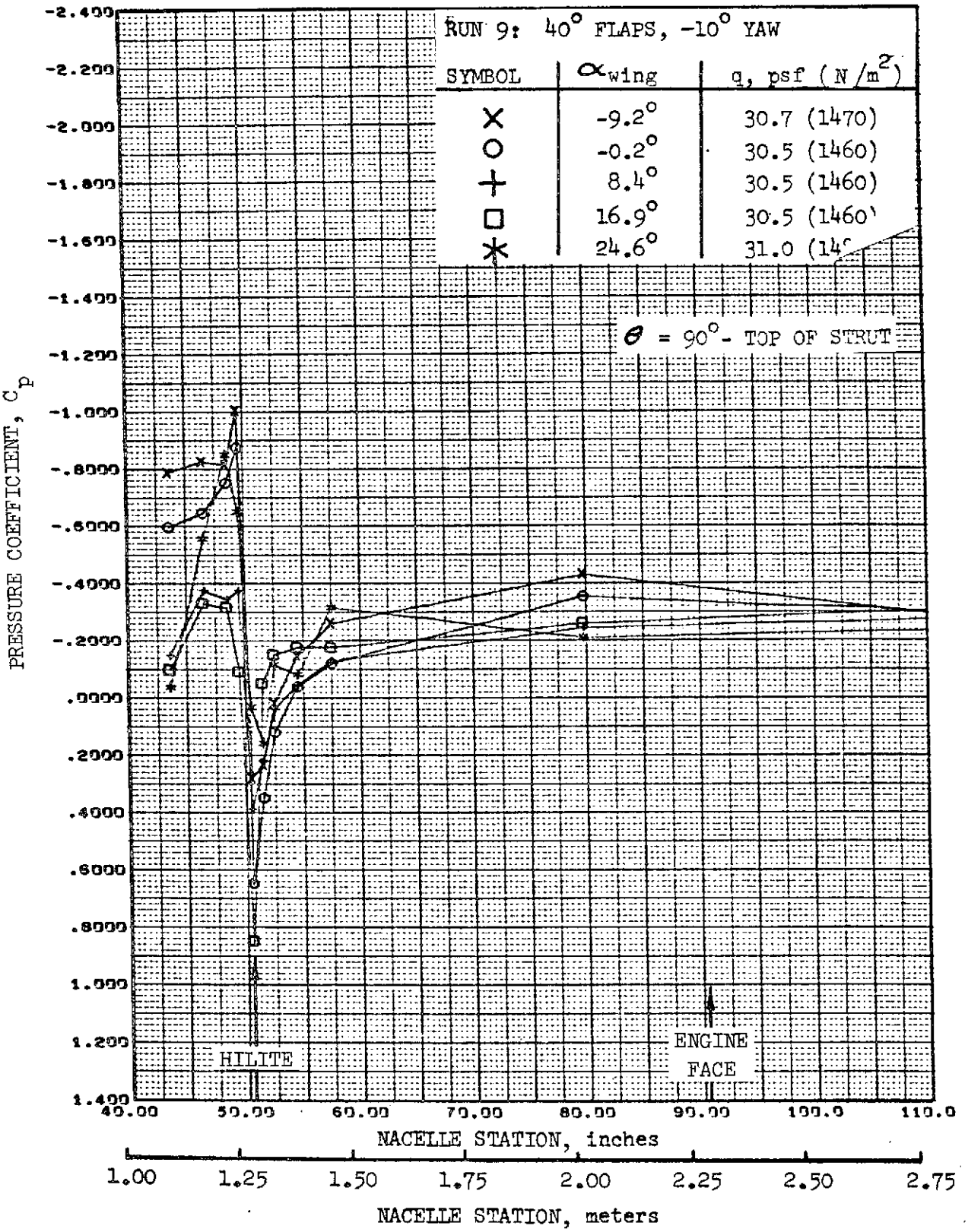

FIGURE 146. -REFAN NACELLE INLET COWL PRESSURE COEFFICIENT DISTRIBUTION, INBOARD SIDE-ABOVE STRUT

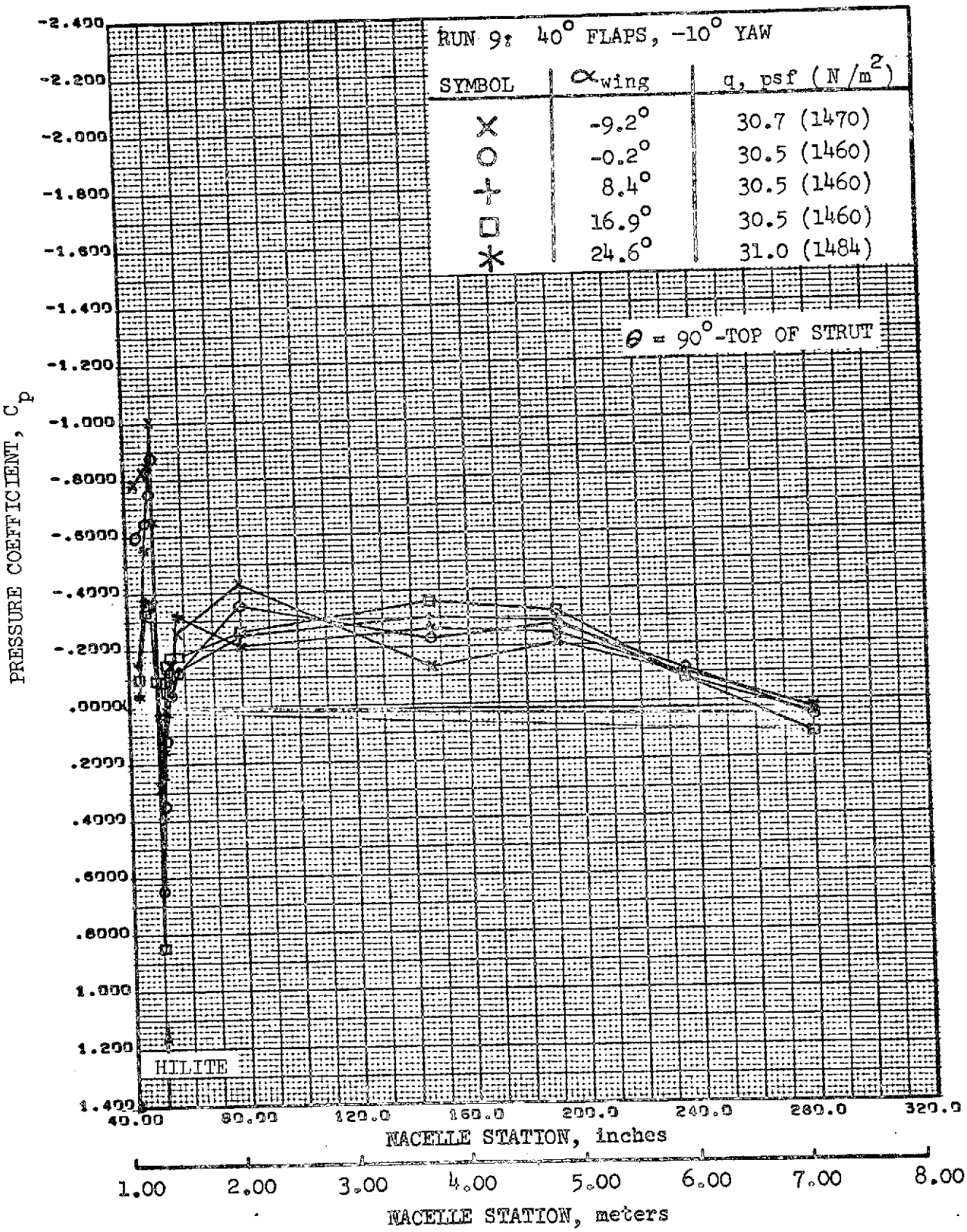

FIGURE 147.-REFAN NACELLE PRESSURE COEFFICIENT DISTRIBUTION, INBOARD SIDE-ABOVE STRUT

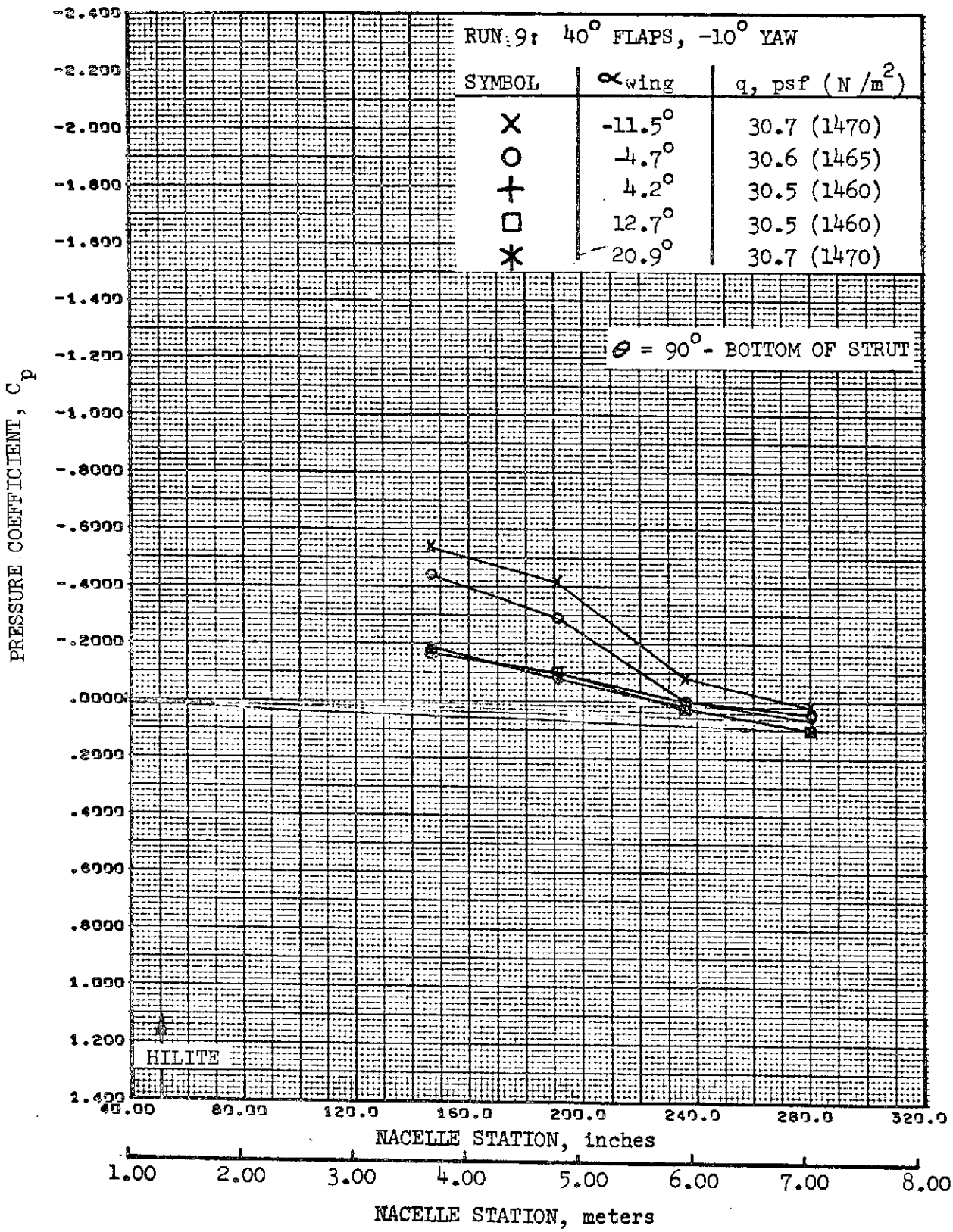

FIGURE 148.-REFAN NACELLE PRESSURE COEFFICIENT DISTRIBUTION, INBOARD SIDE-BELOW STRUT

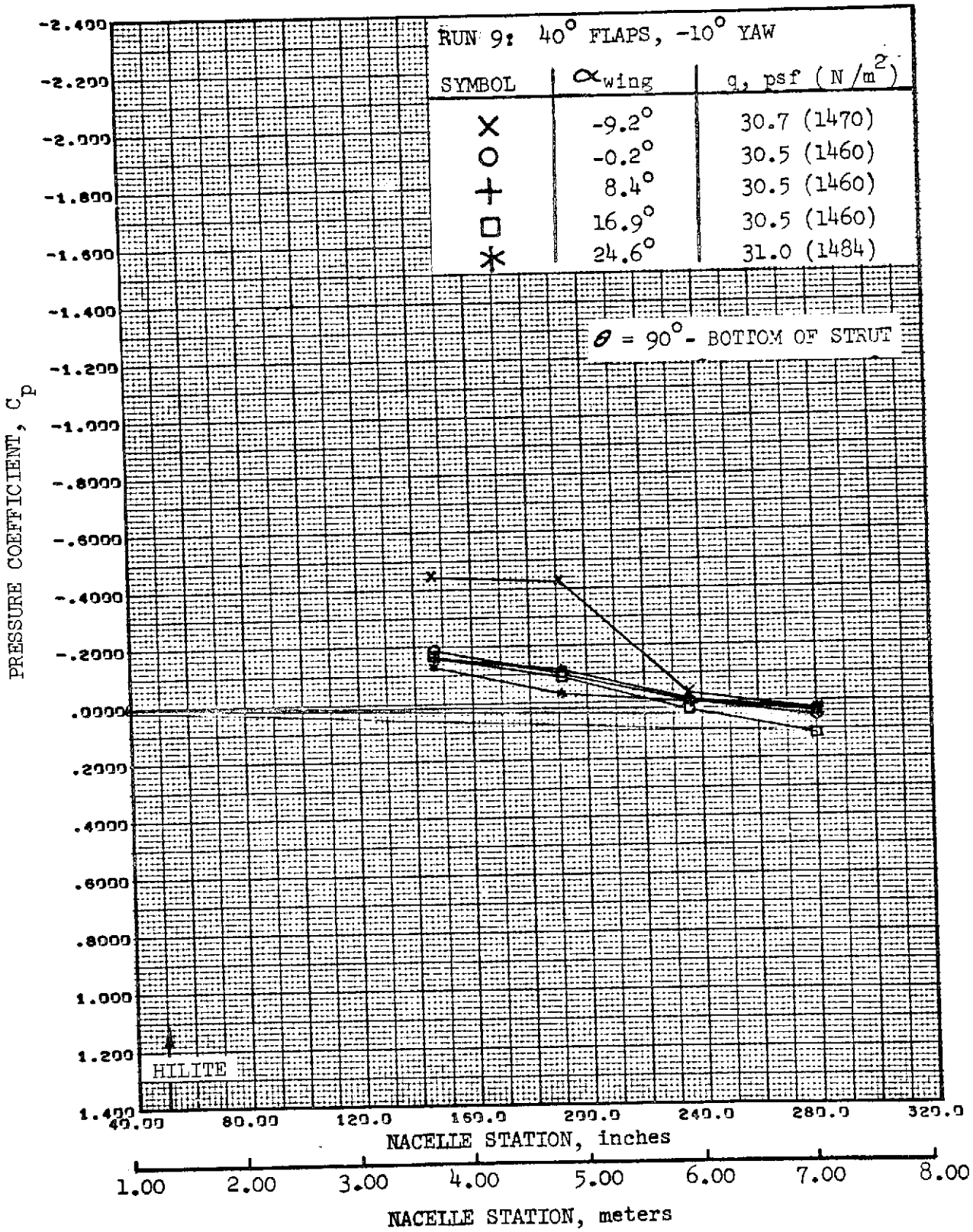

FIGURE 149.-REFAN NACELLE PRESSURE COEFFICIENT DISTRIBUTION, INBOARD SIDE-BELOW STRUT

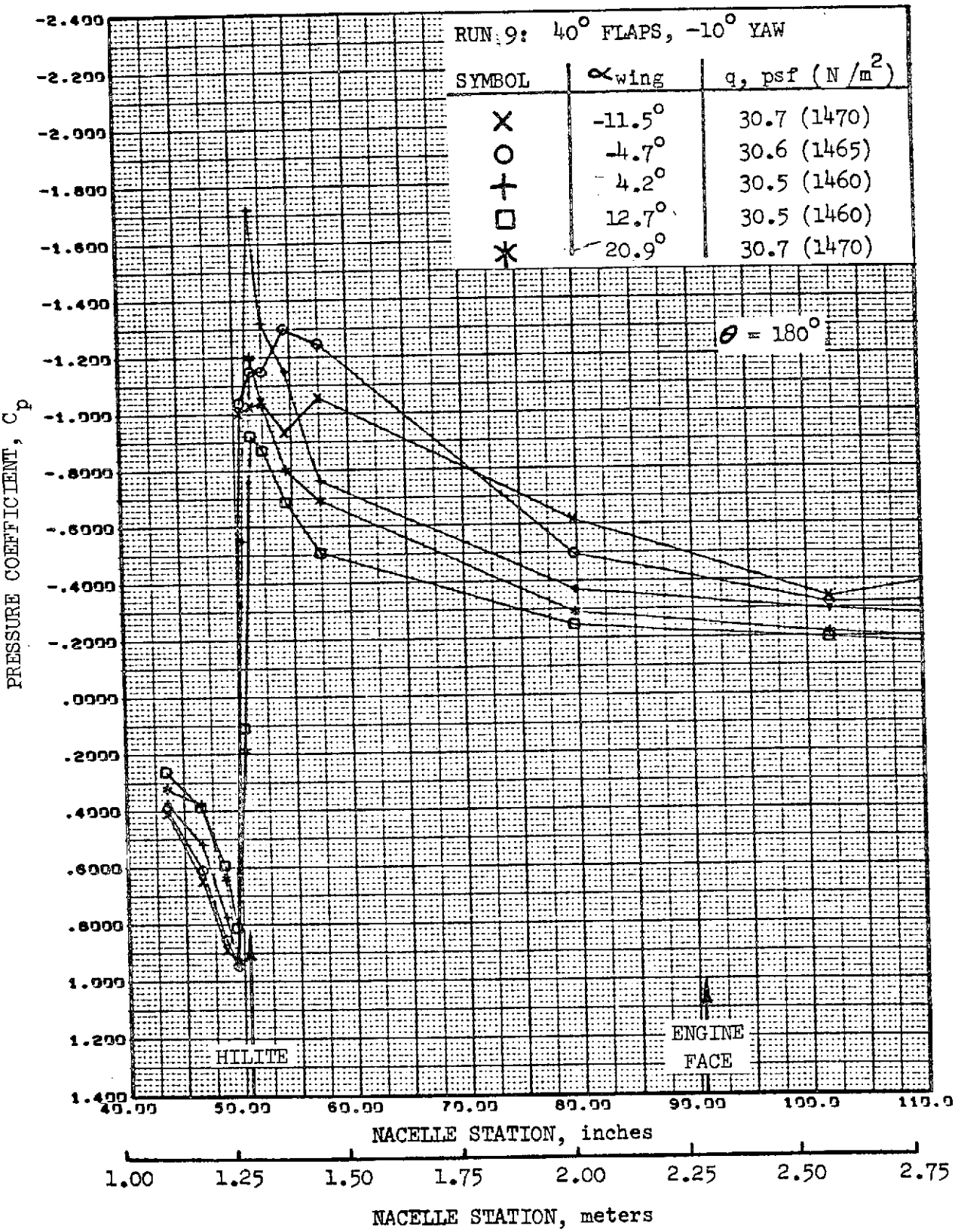

FIGURE 150.-REFAN NACELLE INLET COWL PRESSURE COEFFICIENT DISTRIBUTION, BOTTOM LONGITUDINAL

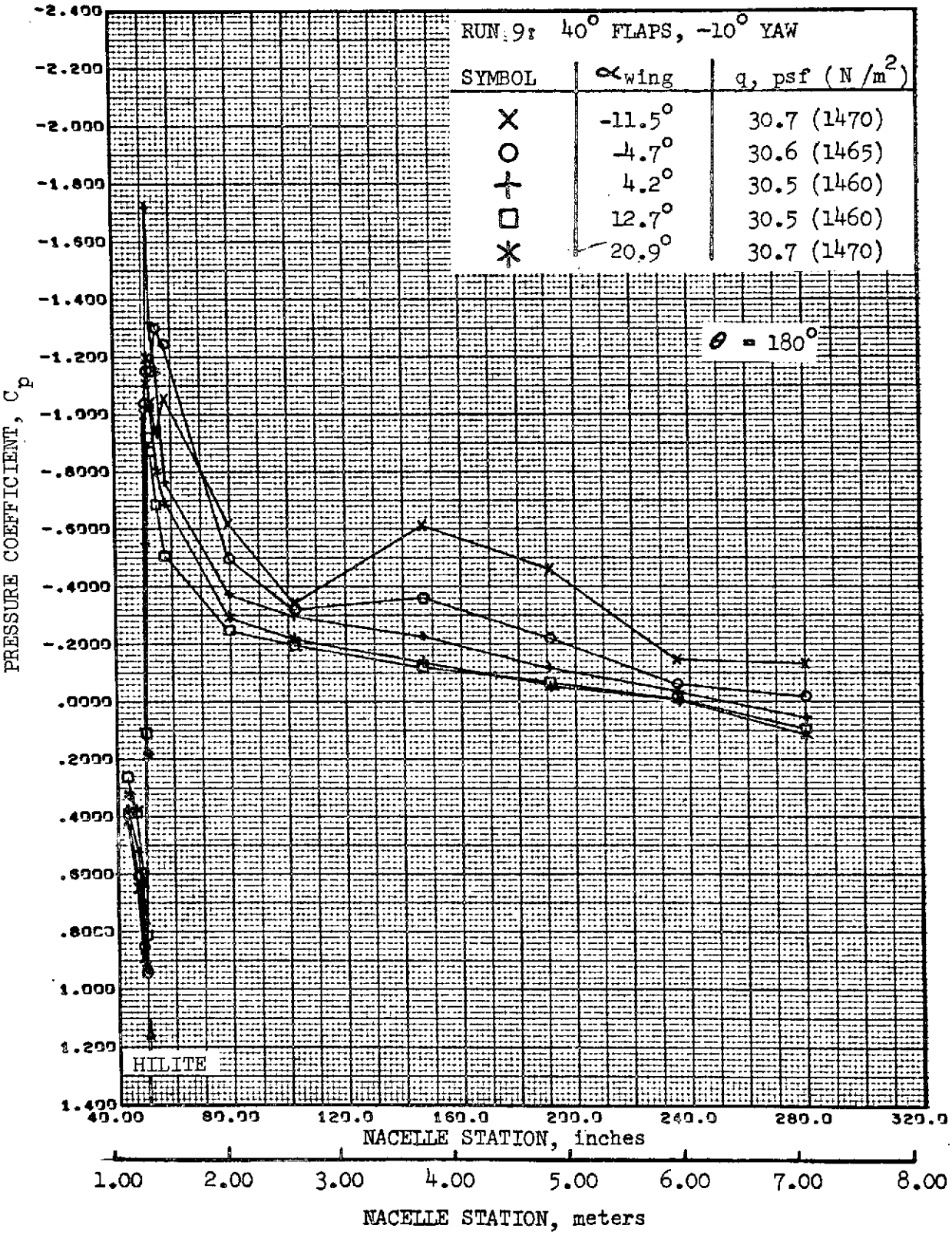

FIGURE 151.-REFAN NACELLE PRESSURE COEFFICIENT DISTRIBUTION, BOTTOM LONGITUDINAL

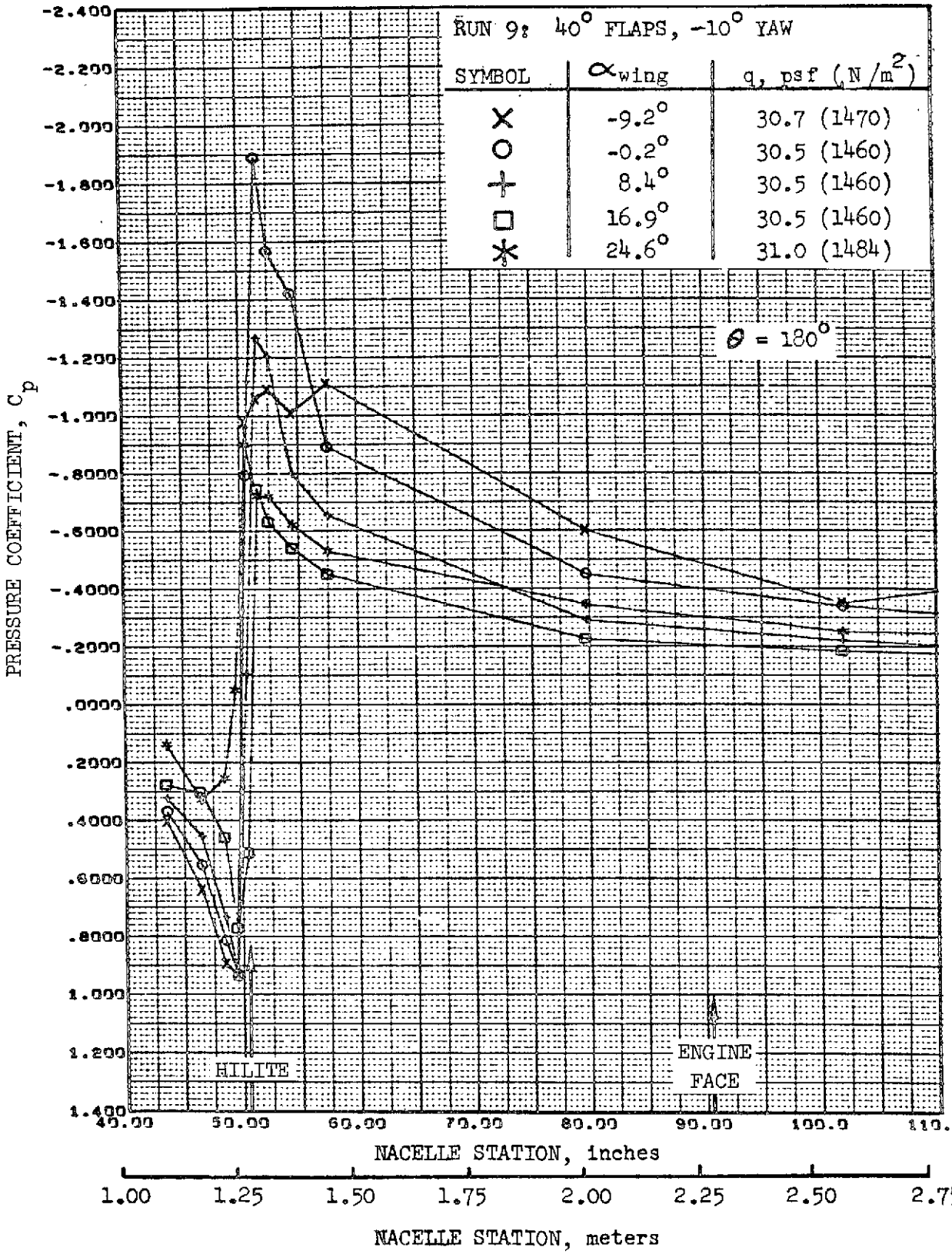

FIGURE 152.-REFAN NACELLE INLET COWL PRESSURE COEFFICIENT DISTRIBUTION, BOTTOM LONGITUDINAL

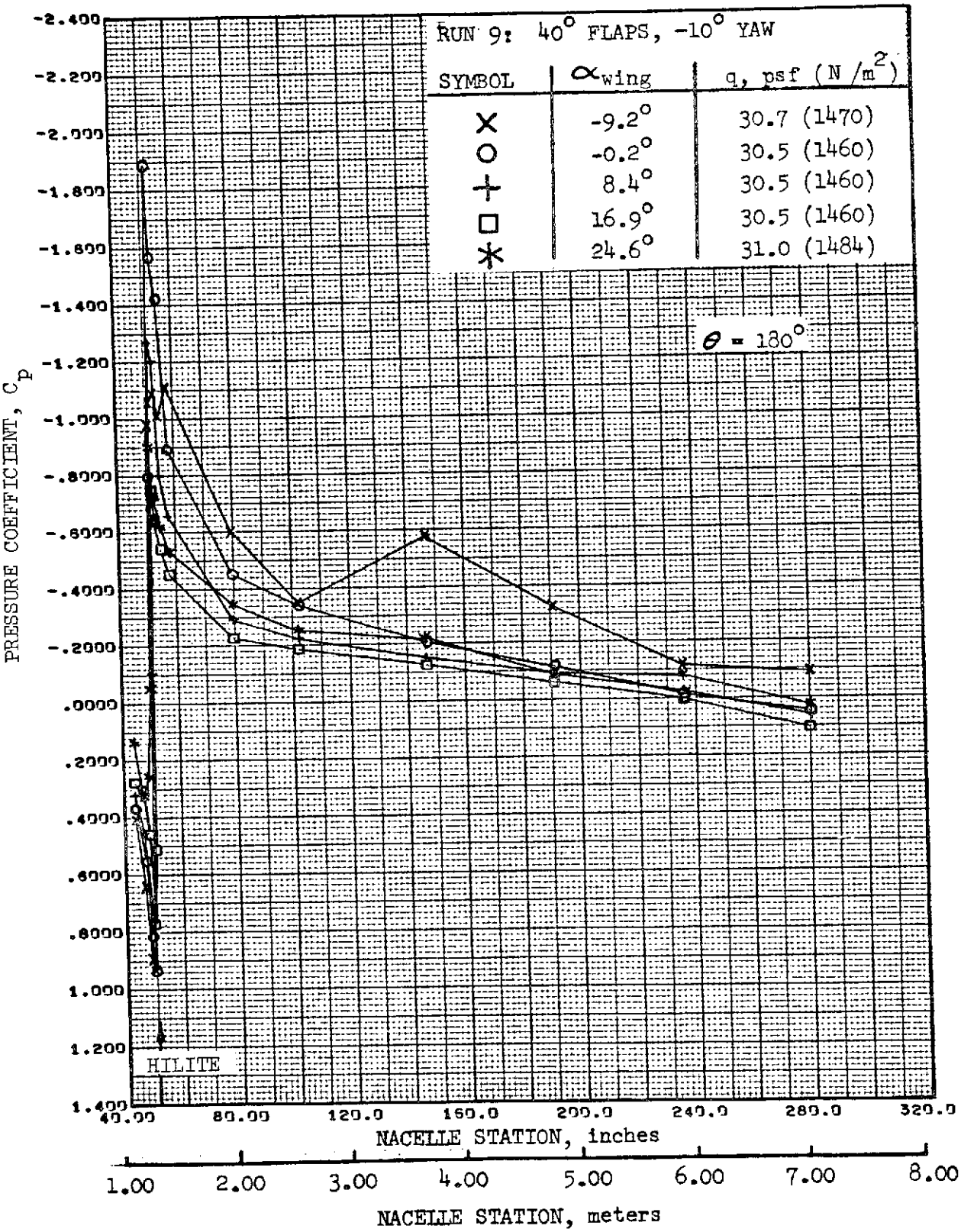

FIGURE 153.-REFAN NACELLE PRESSURE COEFFICIENT DISTRIBUTION, BOTTOM LONGITUDINAL

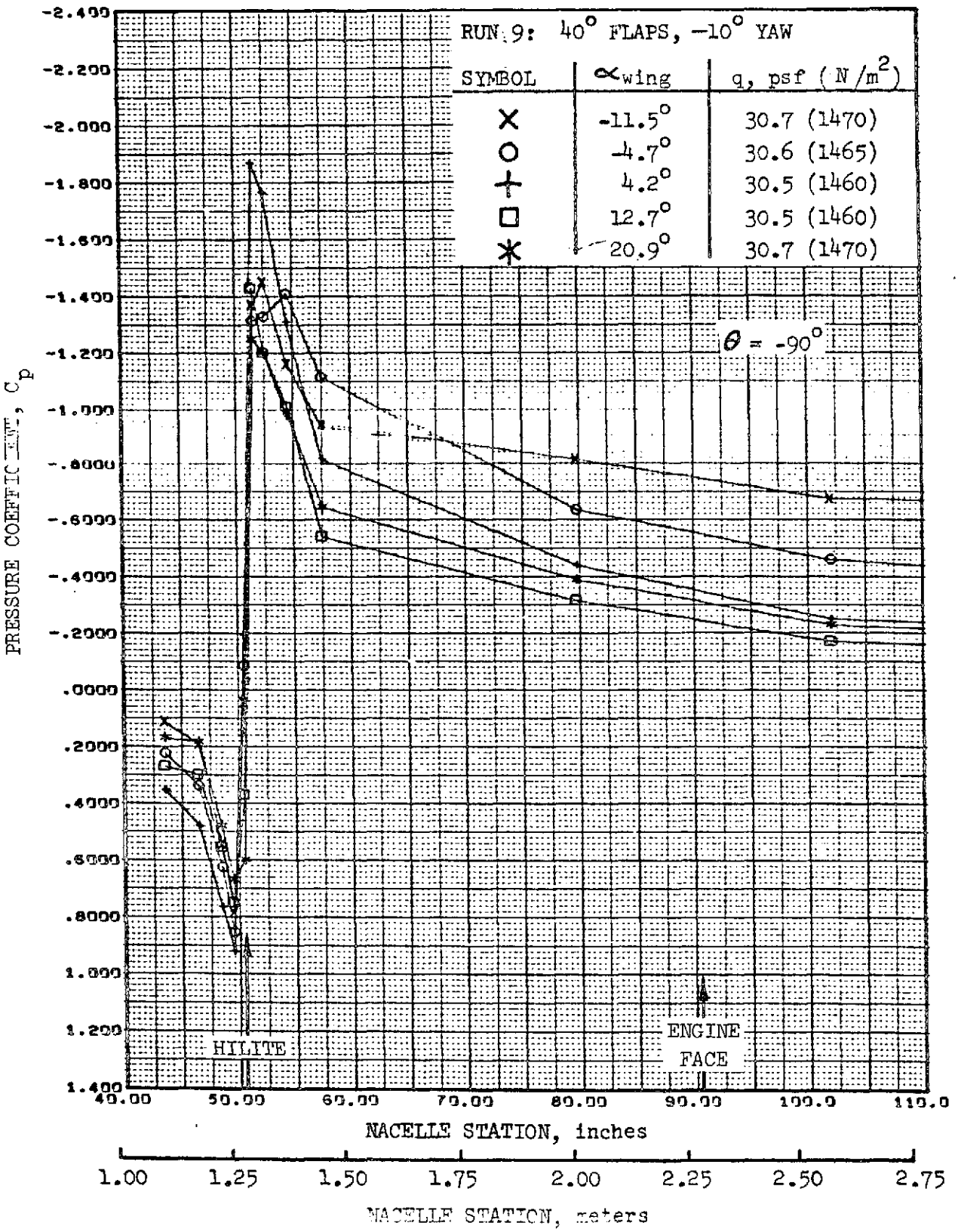

FIGURE 154.-REFAN NACELLE INLET COWL PRESSURE COEFFICIENT DISTRIBUTION, OUTBOARD SIDE

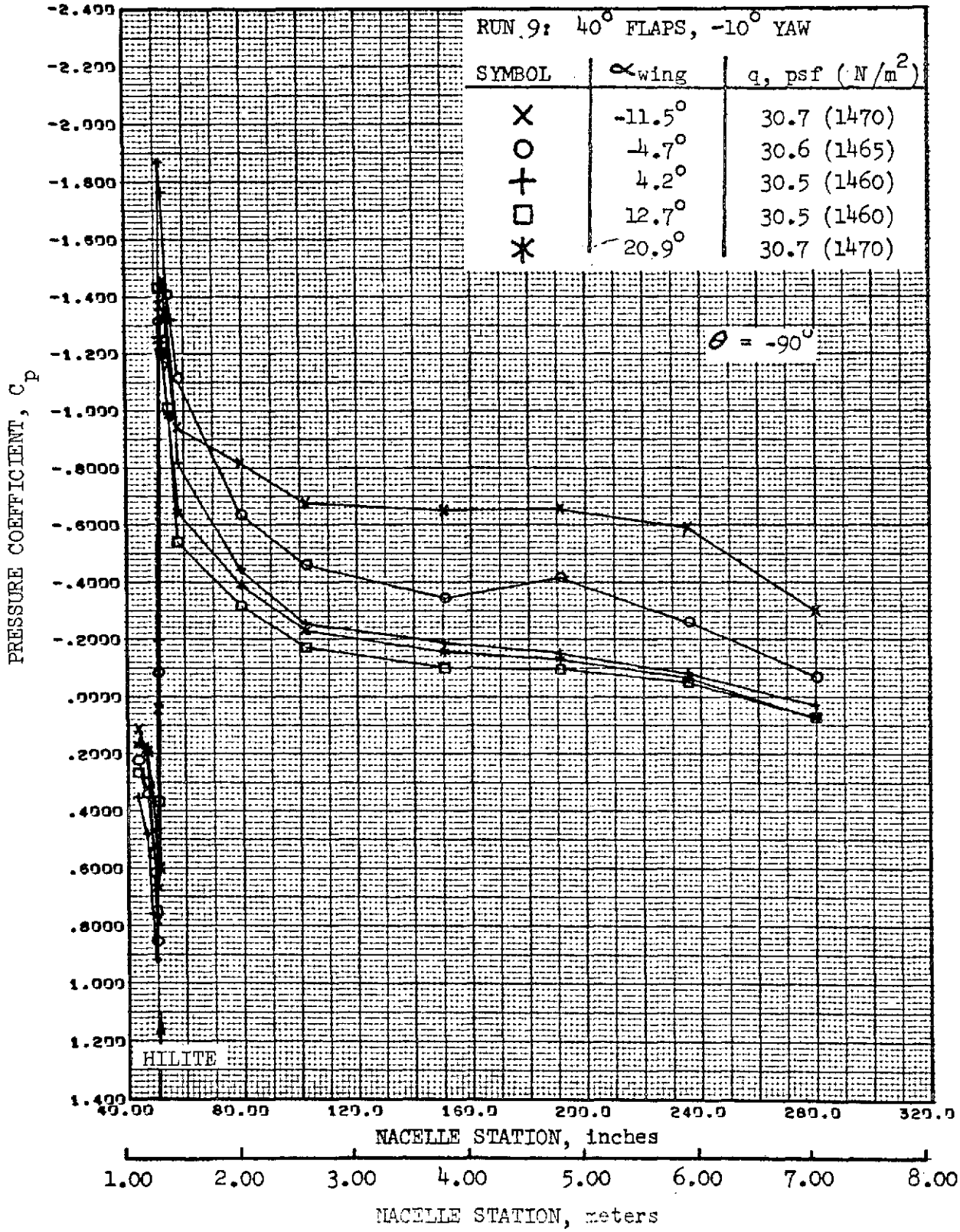

FIGURE 155.-REFAN NACELLE PRESSURE COEFFICIENT DISTRIBUTION, OUTBOARD SIDE

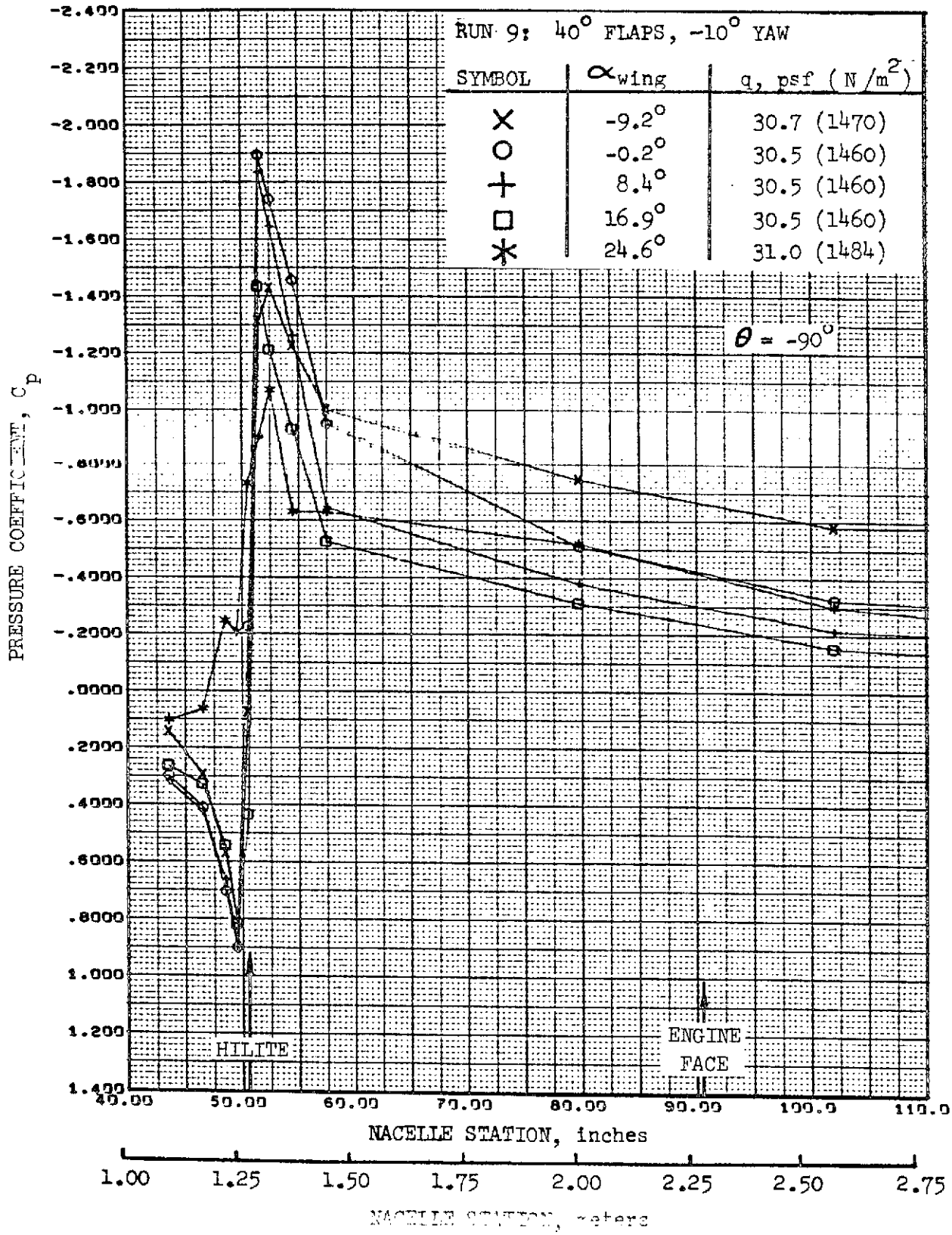

FIGURE 156.-REFAN NACELLE INLET COWL PRESSURE COEFFICIENT DISTRIBUTION, OUTBOARD SIDE

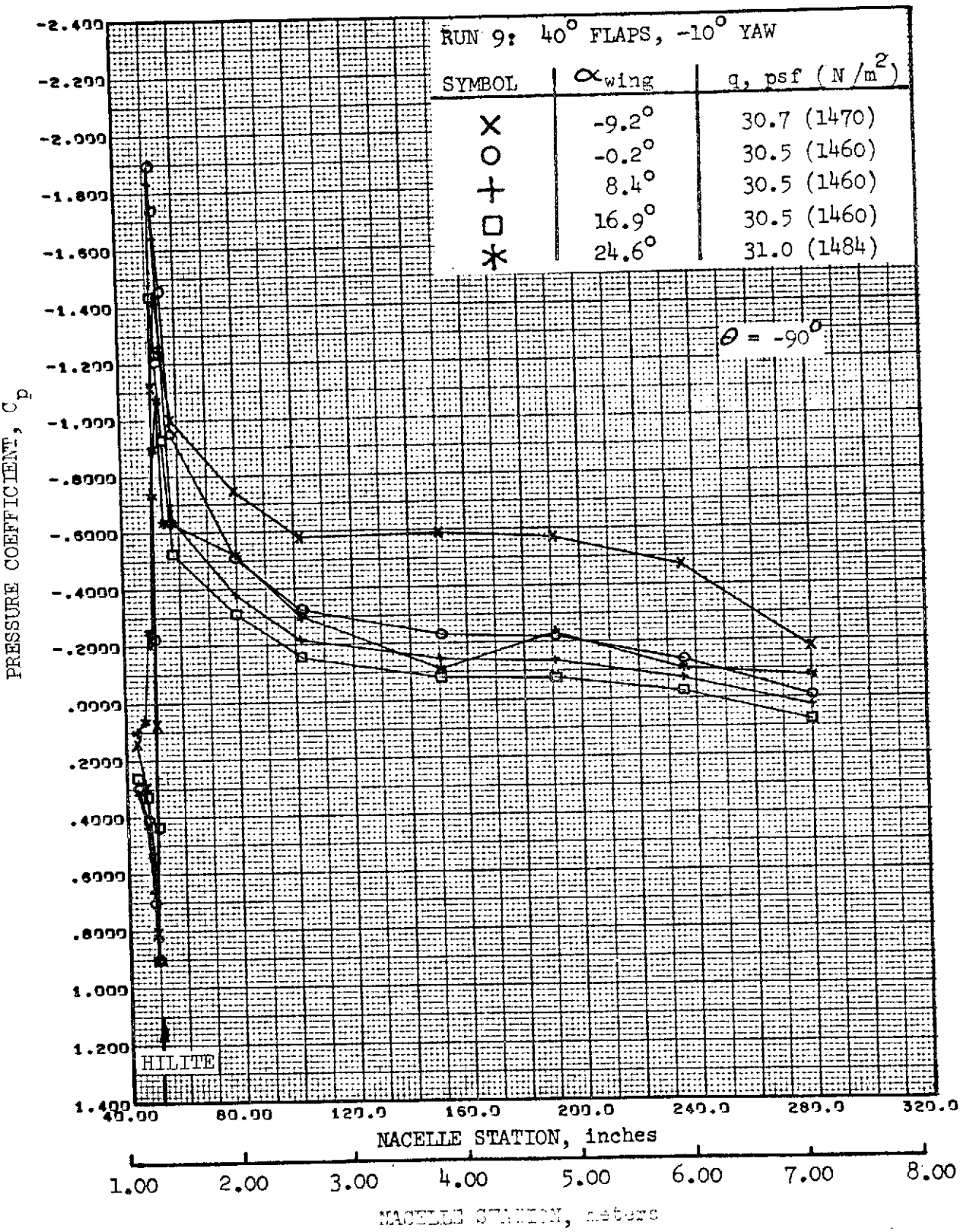

FIGURE 157.-REFAN NACELLE PRESSURE COEFFICIENT DISTRIBUTION, OUTBOARD SIDE

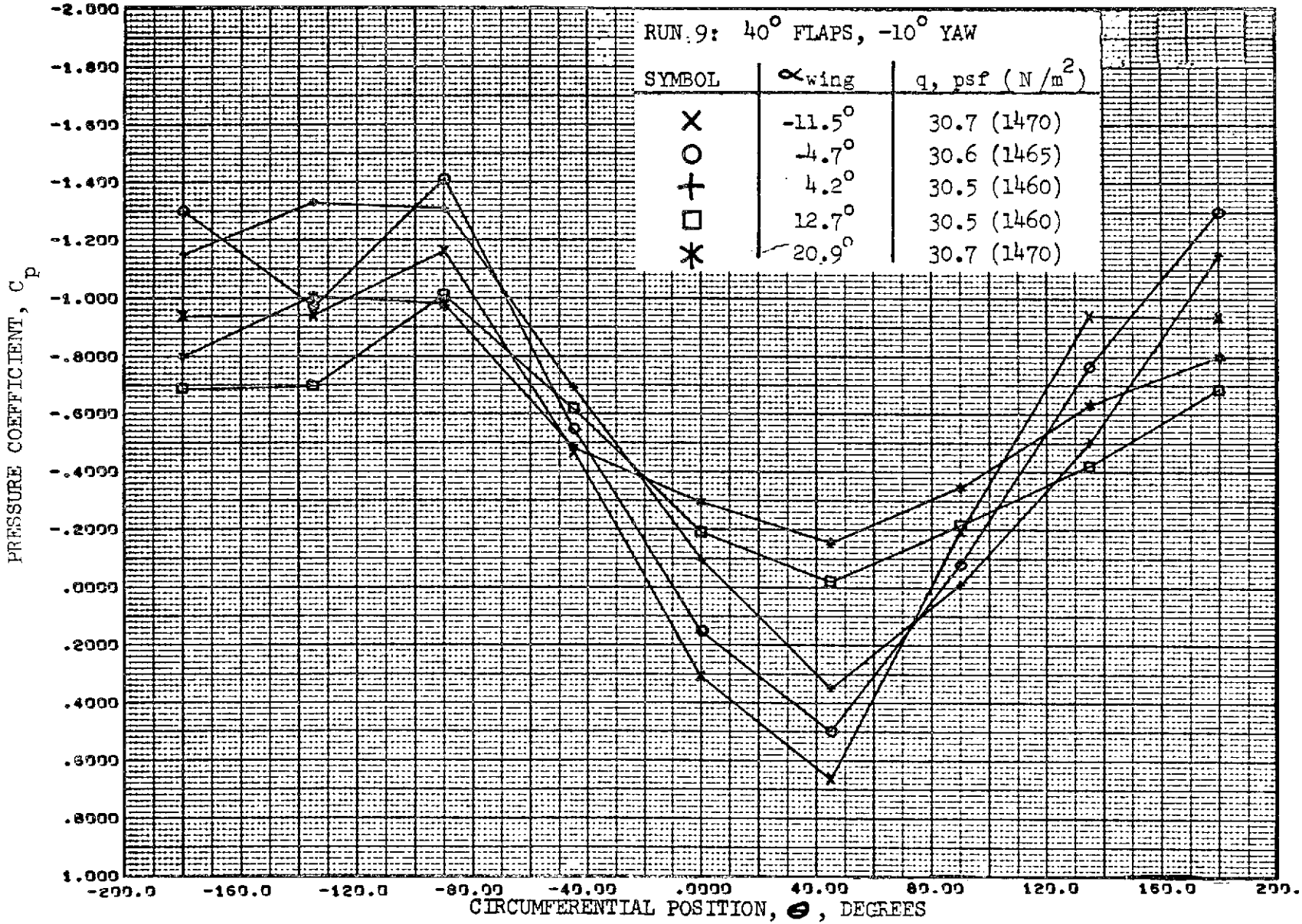

FIGURE 158. - REFAN NACELLE PRESSURE COEFFICIENT DISTRIBUTION, EXTERNAL CIRCUMFERENTIAL AT STATION 54.5 INCHES (1.38 METERS)

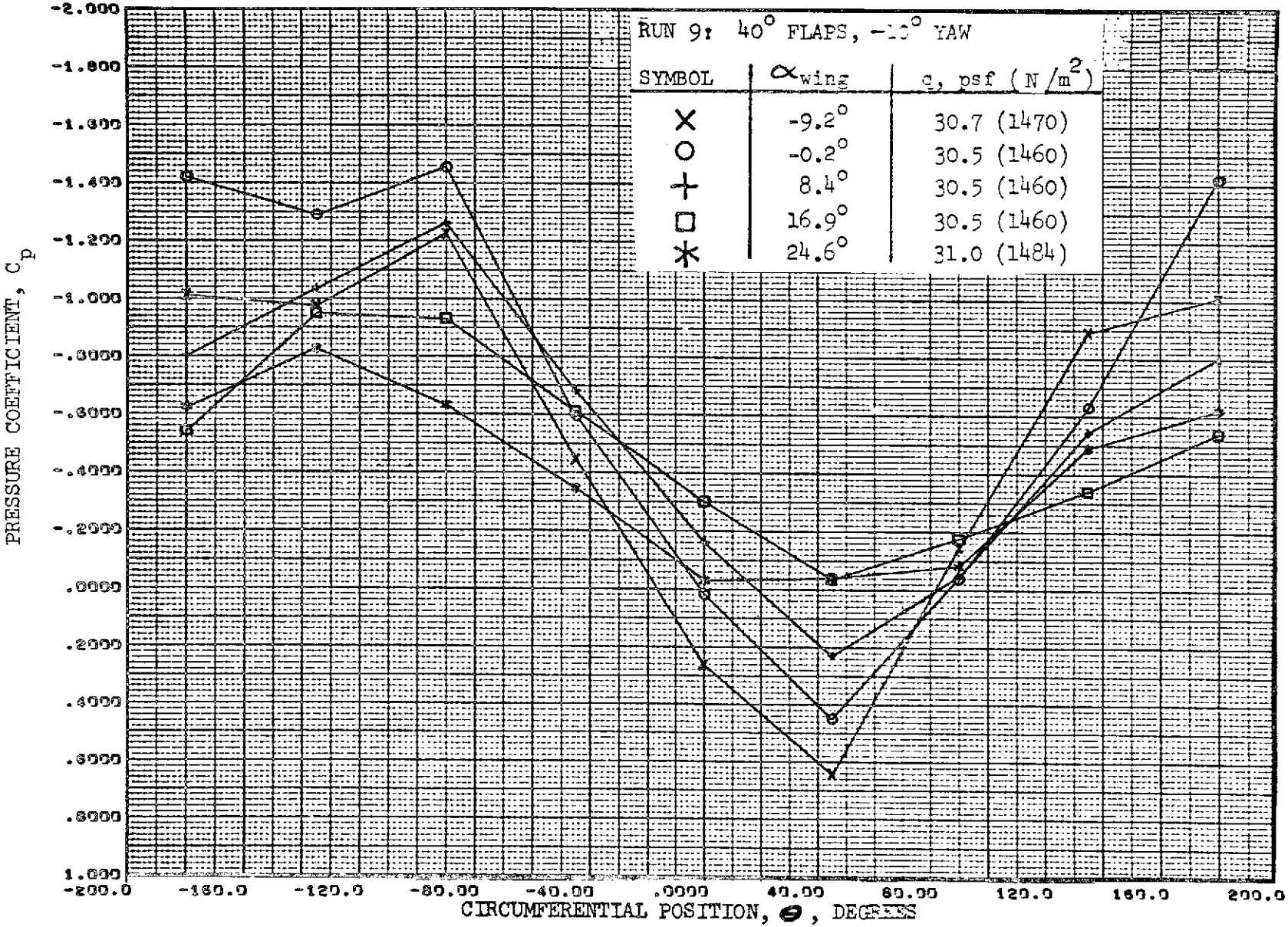

FIGURE 159. - REFAN NACELLE PRESSURE COEFFICIENT DISTRIBUTION, EXTERNAL CIRCUMFERENTIAL AT STATION 54.5 INCHES (1.38 METERS)

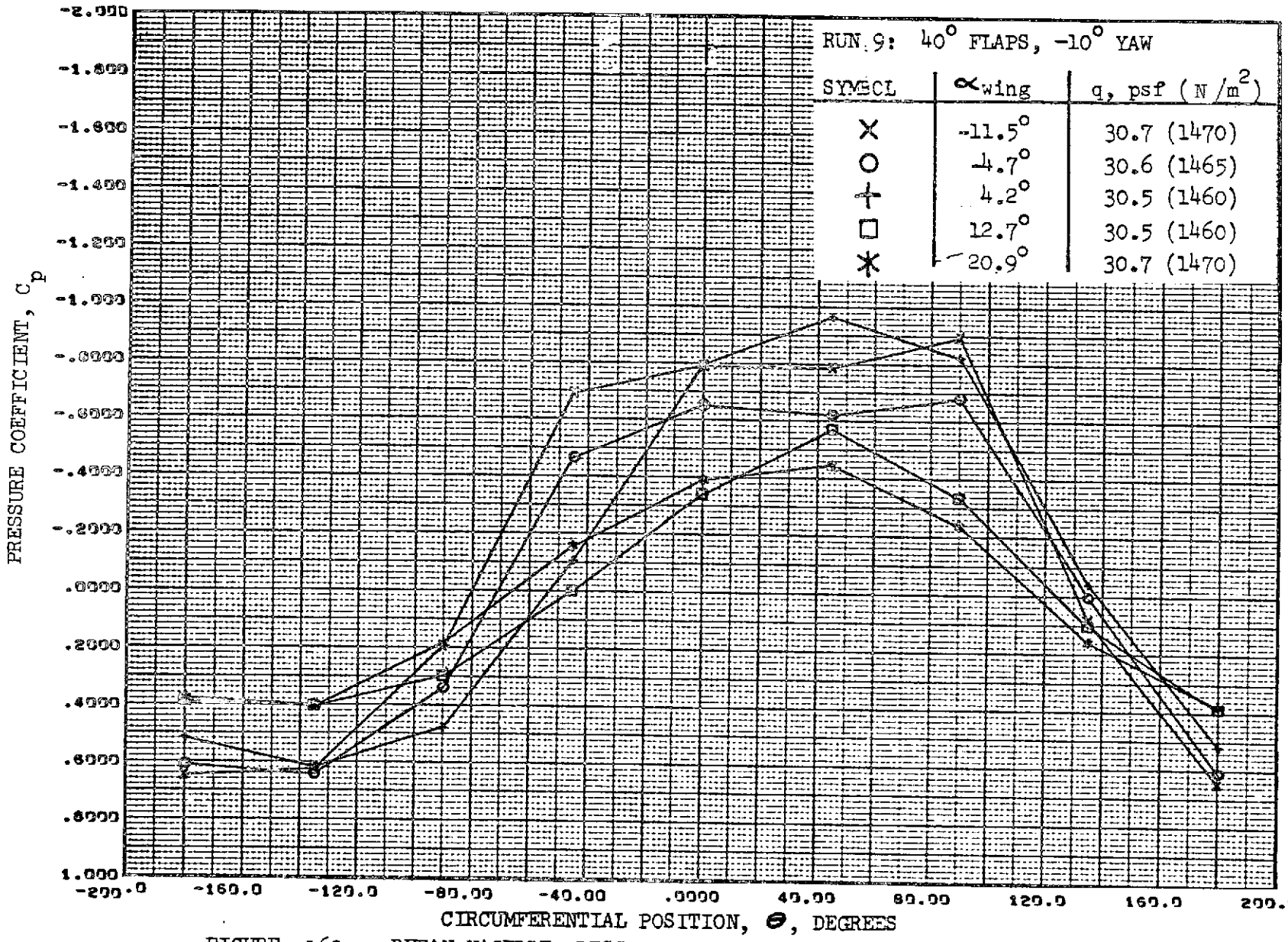

FIGURE 160. - REFAN NACELLE PRESSURE COEFFICIENT DISTRIBUTION, INTERNAL CIRCUMFERENTIAL AT STATION 54.5 INCHES (1.38 METERS)

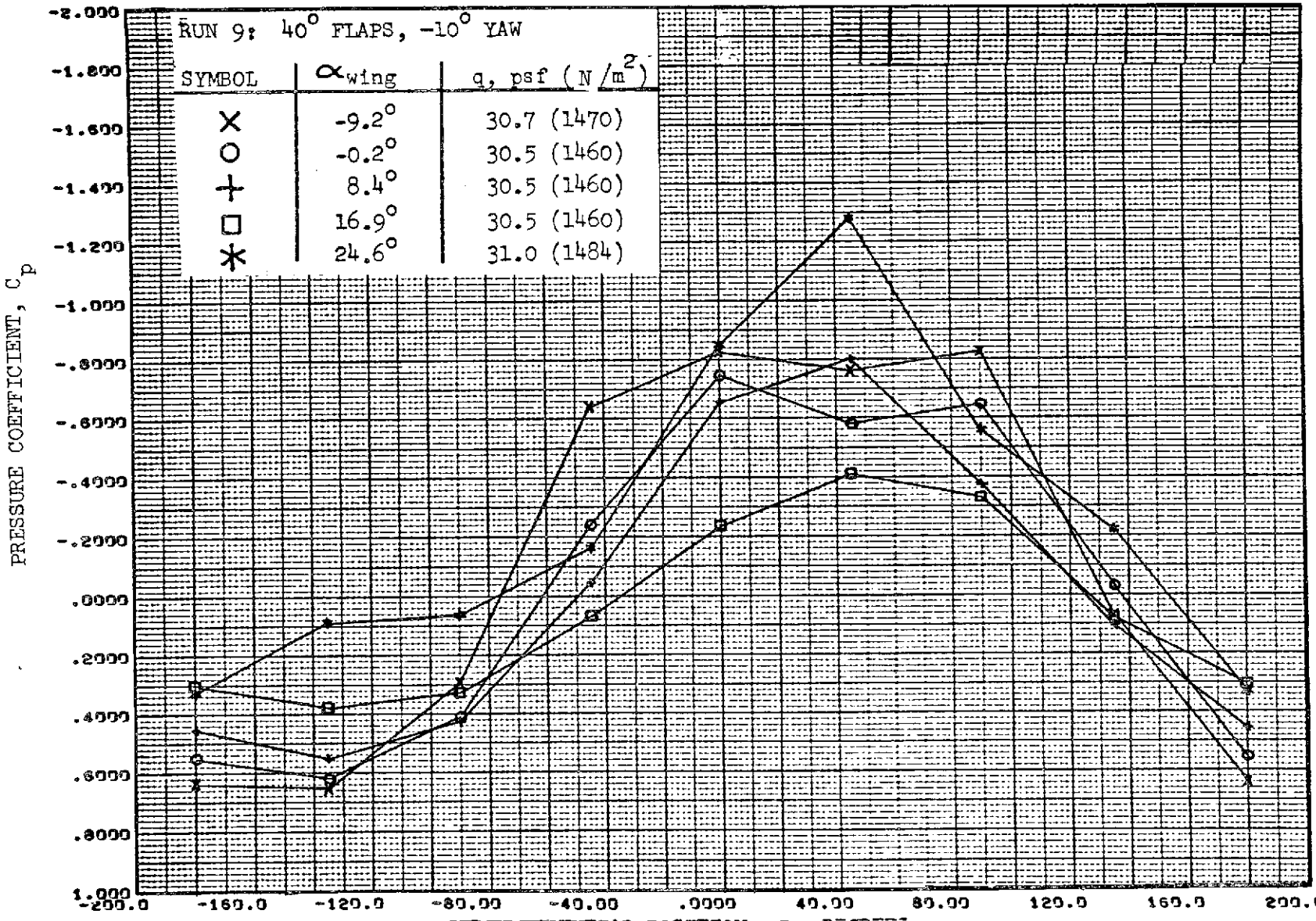

FIGURE 161. - REFAN NACELLE PRESSURE COEFFICIENT DISTRIBUTION, INTERNAL CIRCUMFERENTIAL AT STATION 54.5 INCHES (1.38 METERS)

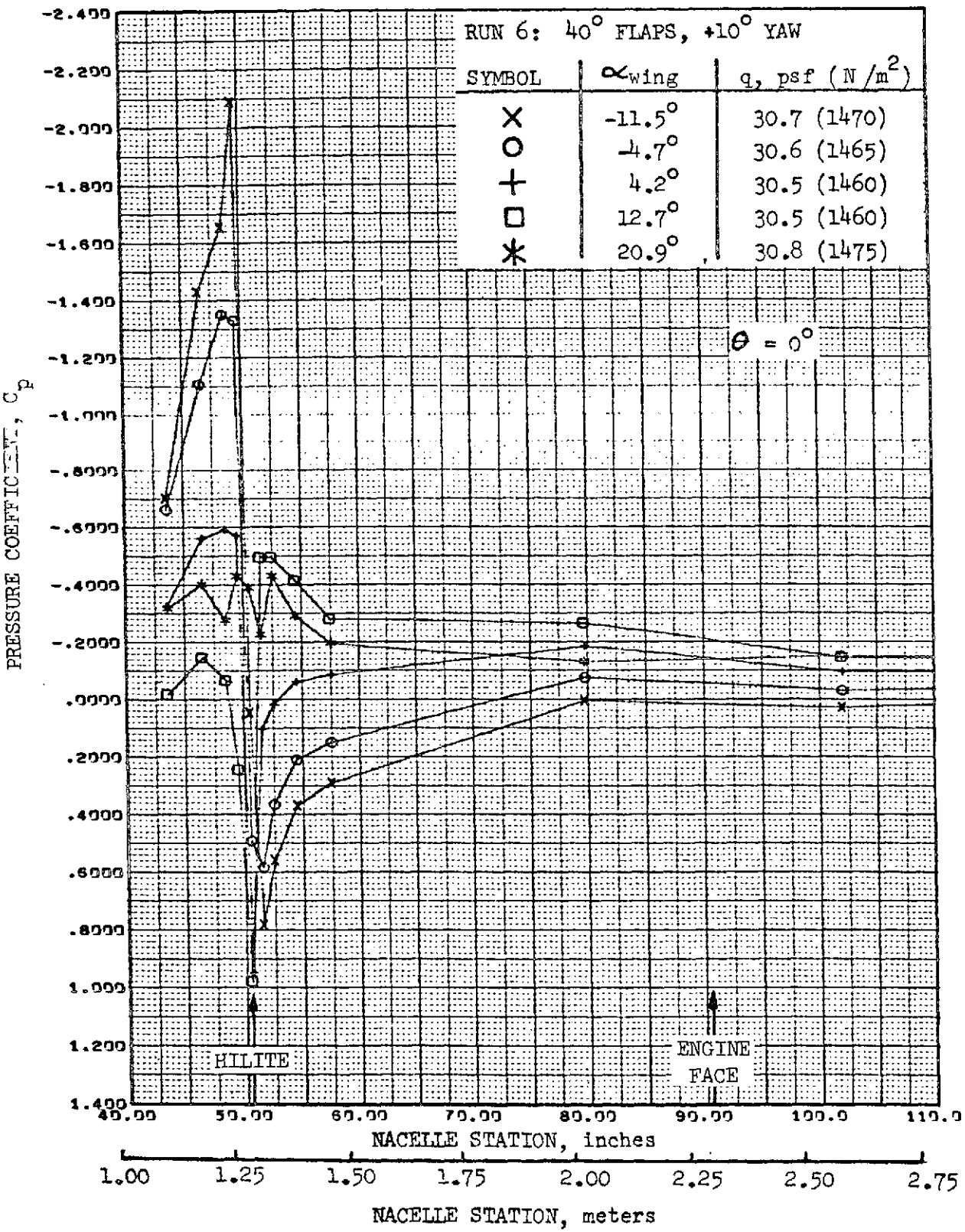

FIGURE 162.-REFAN NACELLE INLET COWL PRESSURE COEFFICIENT DISTRIBUTION, TOP LONGITUDINAL

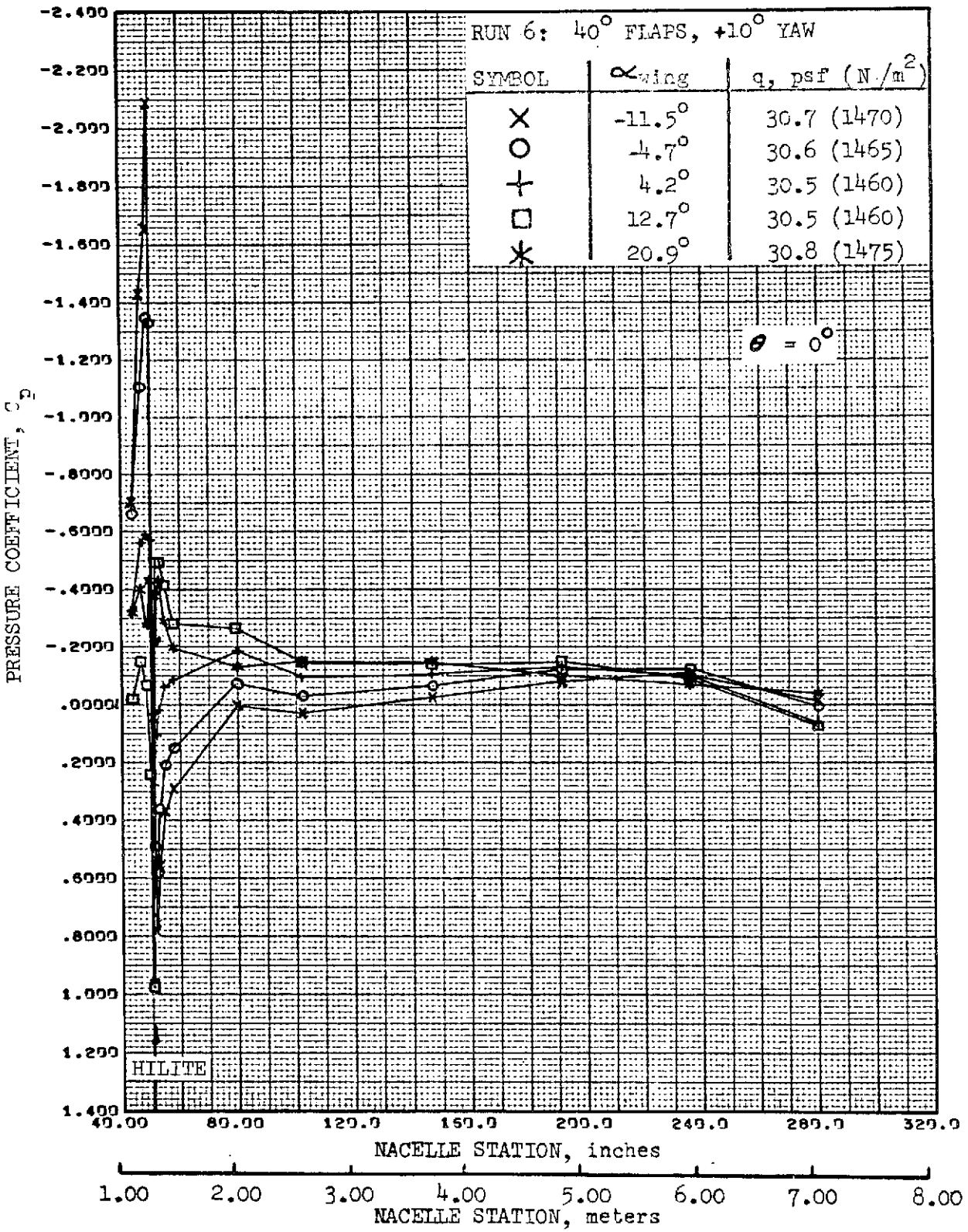

FIGURE 163.-REFAN NACELLE PRESSURE COEFFICIENT DISTRIBUTION, TOP LONGITUDINAL

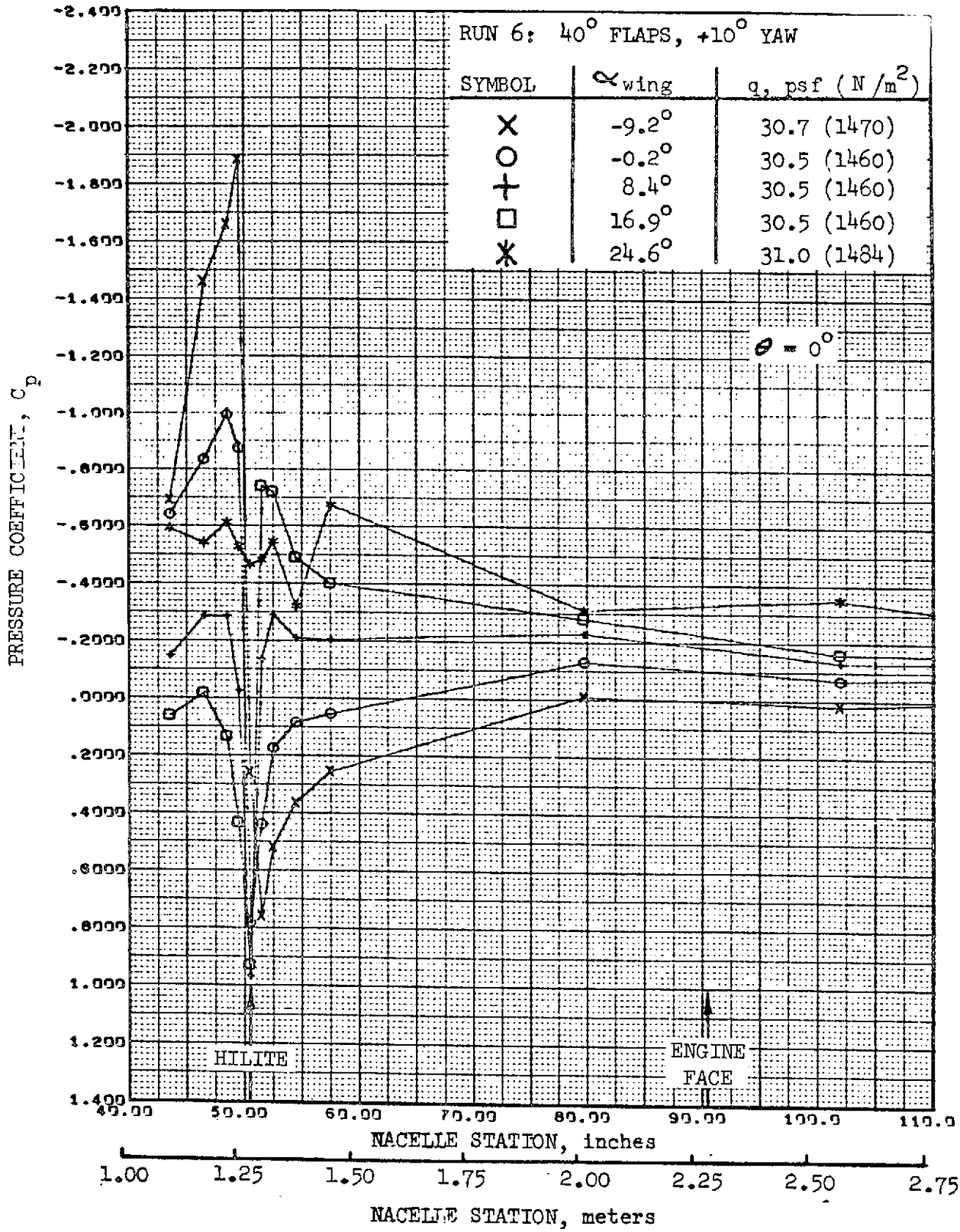

FIGURE 164.-REFAN NACELLE INLET COWL PRESSURE COEFFICIENT DISTRIBUTION, TOP LONGITUDINAL

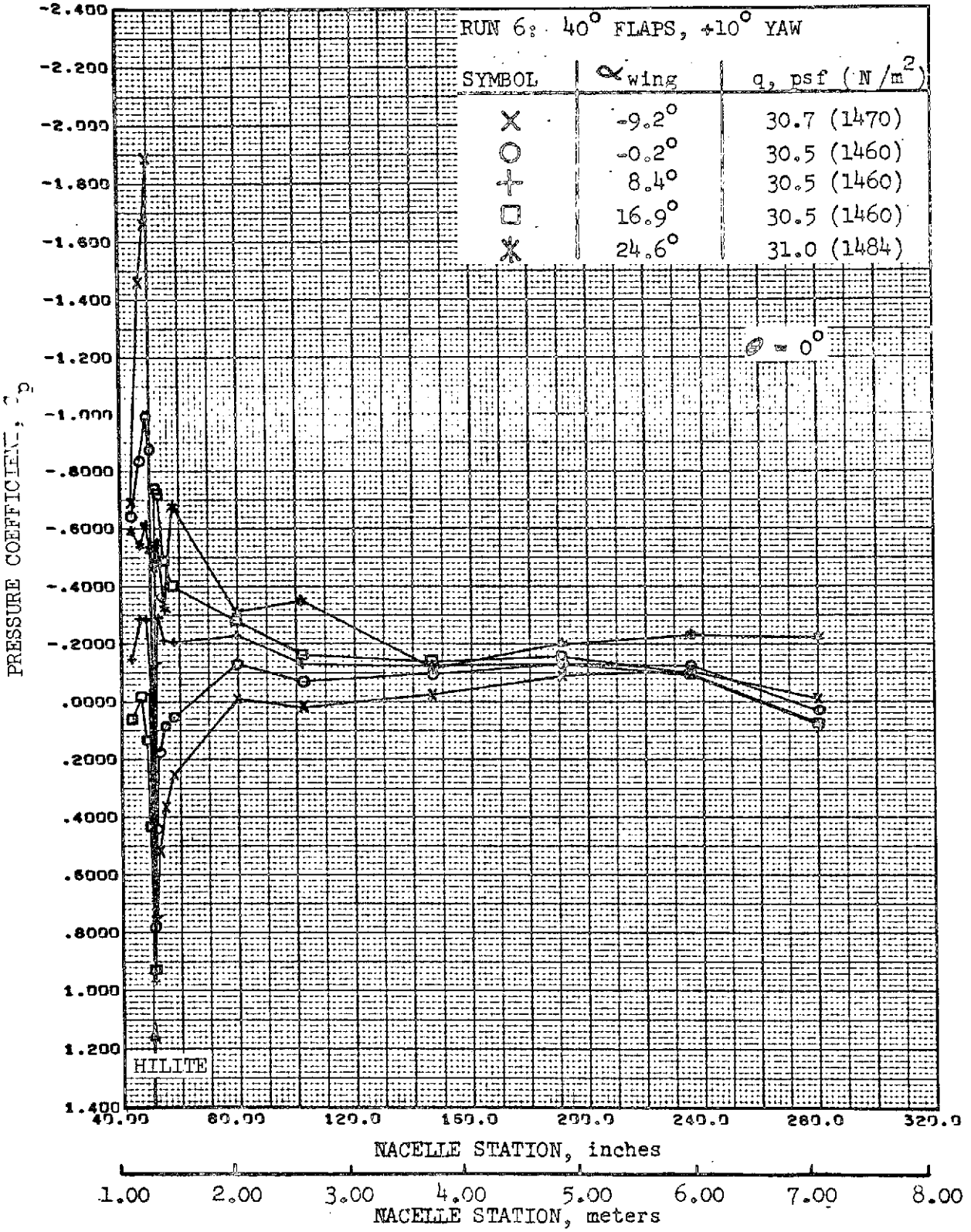

FIGURE 165. -REFAN NACELLE PRESSURE COEFFICIENT DISTRIBUTION, TOP LONGITUDINAL

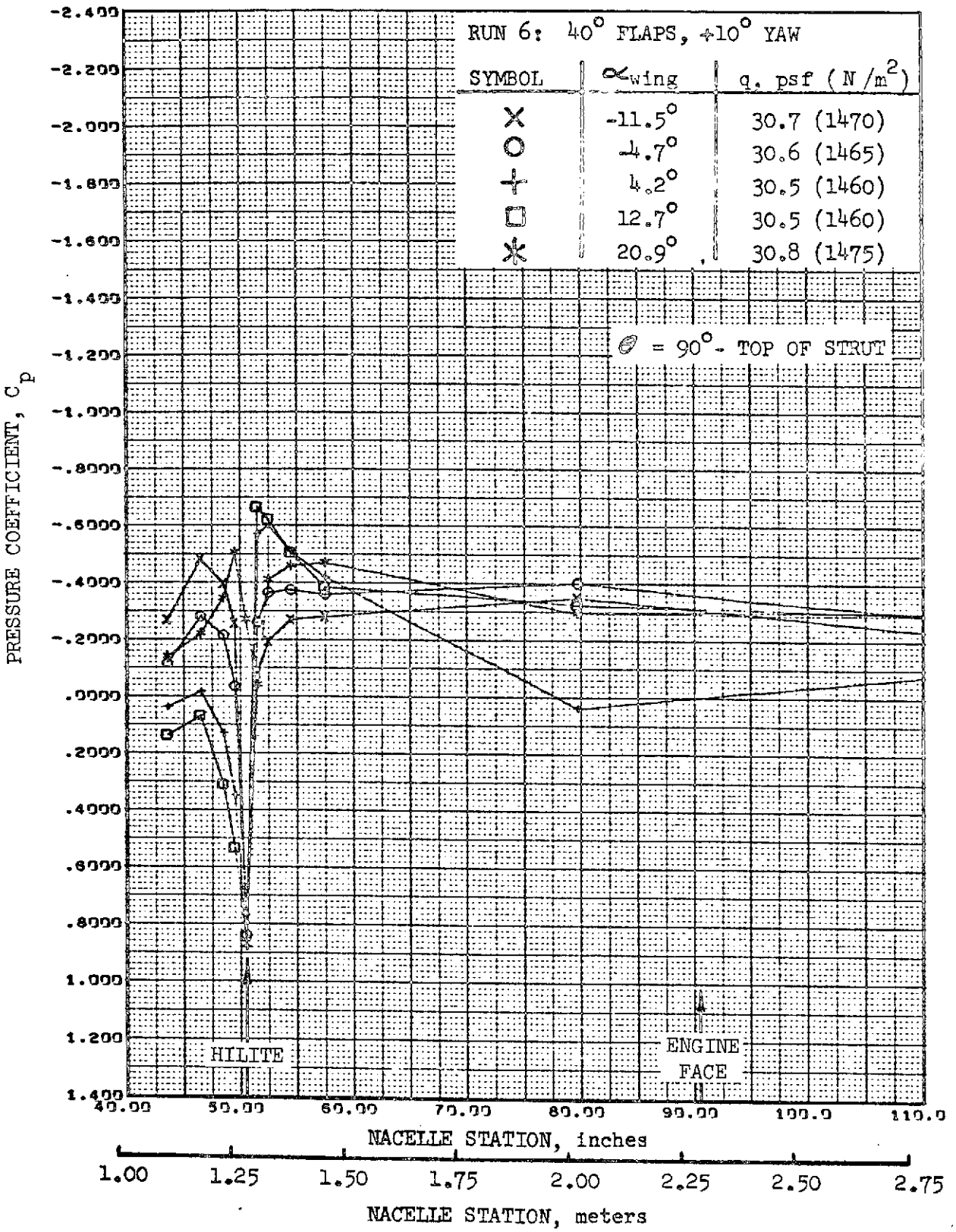

FIGURE 166.-REFAN NACELLE INLET COWL PRESSURE COEFFICIENT DISTRIBUTION, INBOARD SIDE-ABOVE STRUT

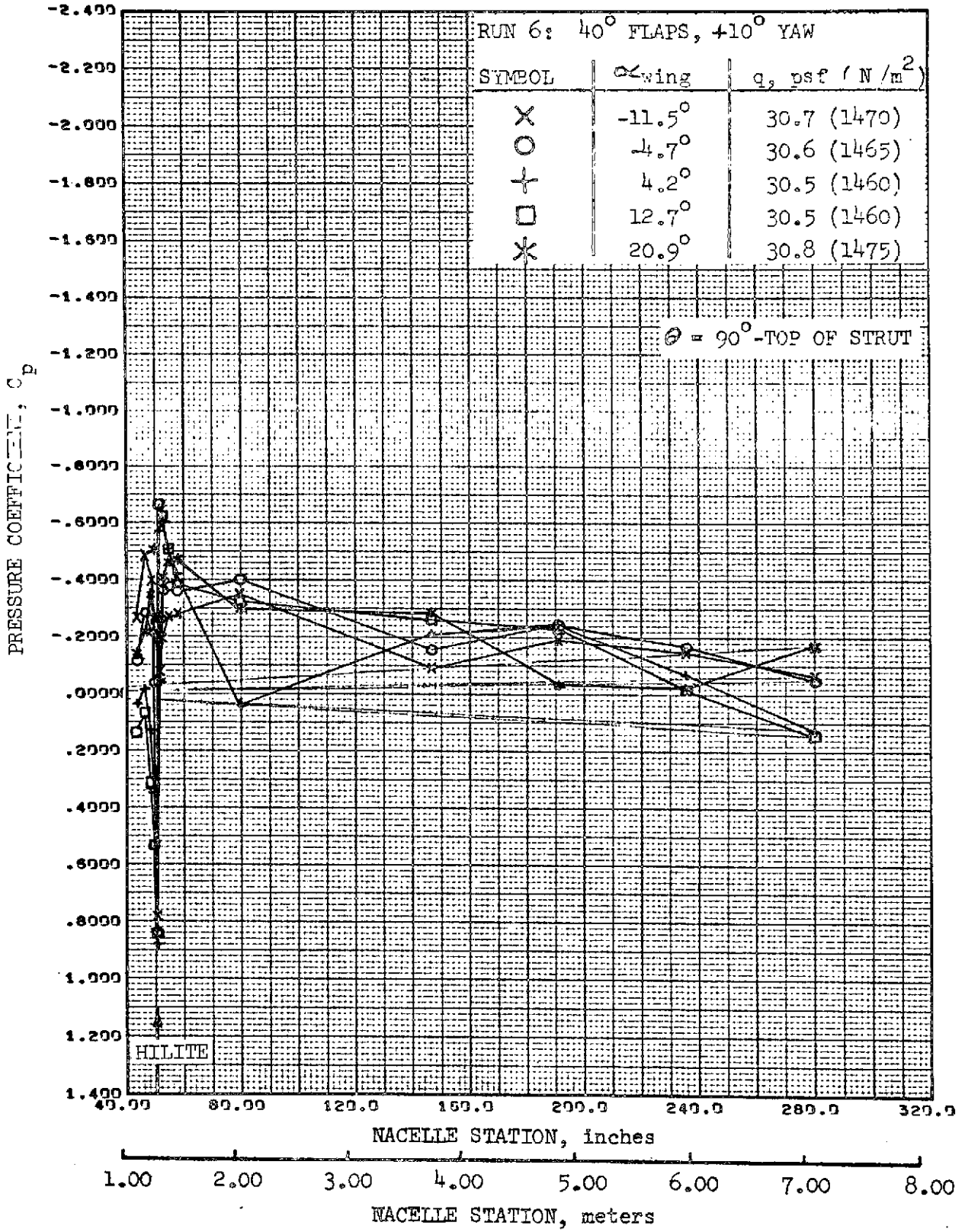

FIGURE 167.-REFAN NACELLE PRESSURE COEFFICIENT DISTRIBUTION, INBOARD SIDE-ABOVE STRUT

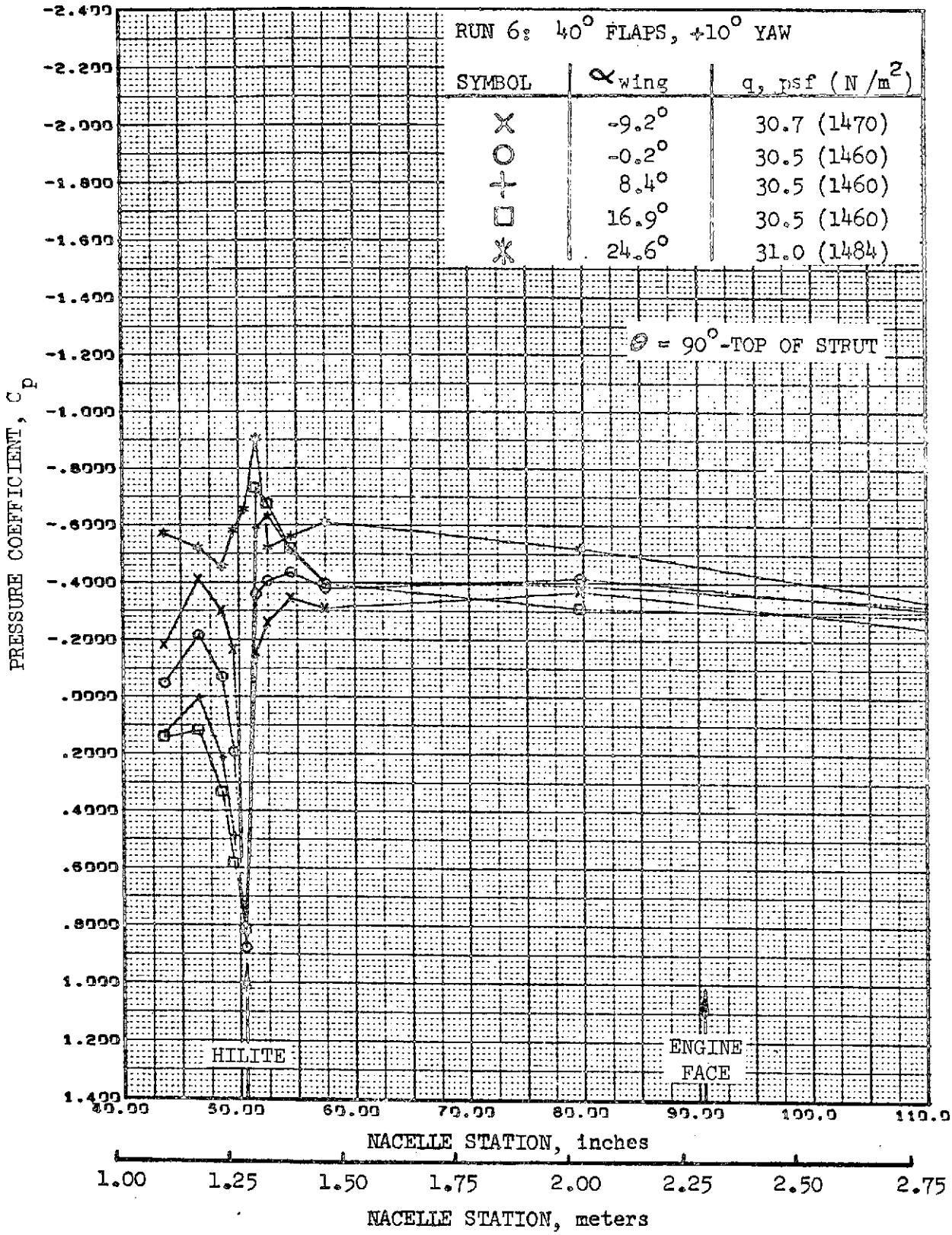

FIGURE 168.-REFAN NACELLE INLET COWL PRESSURE COEFFICIENT DISTRIBUTION, INBOARD SIDE-ABOVE STRUT

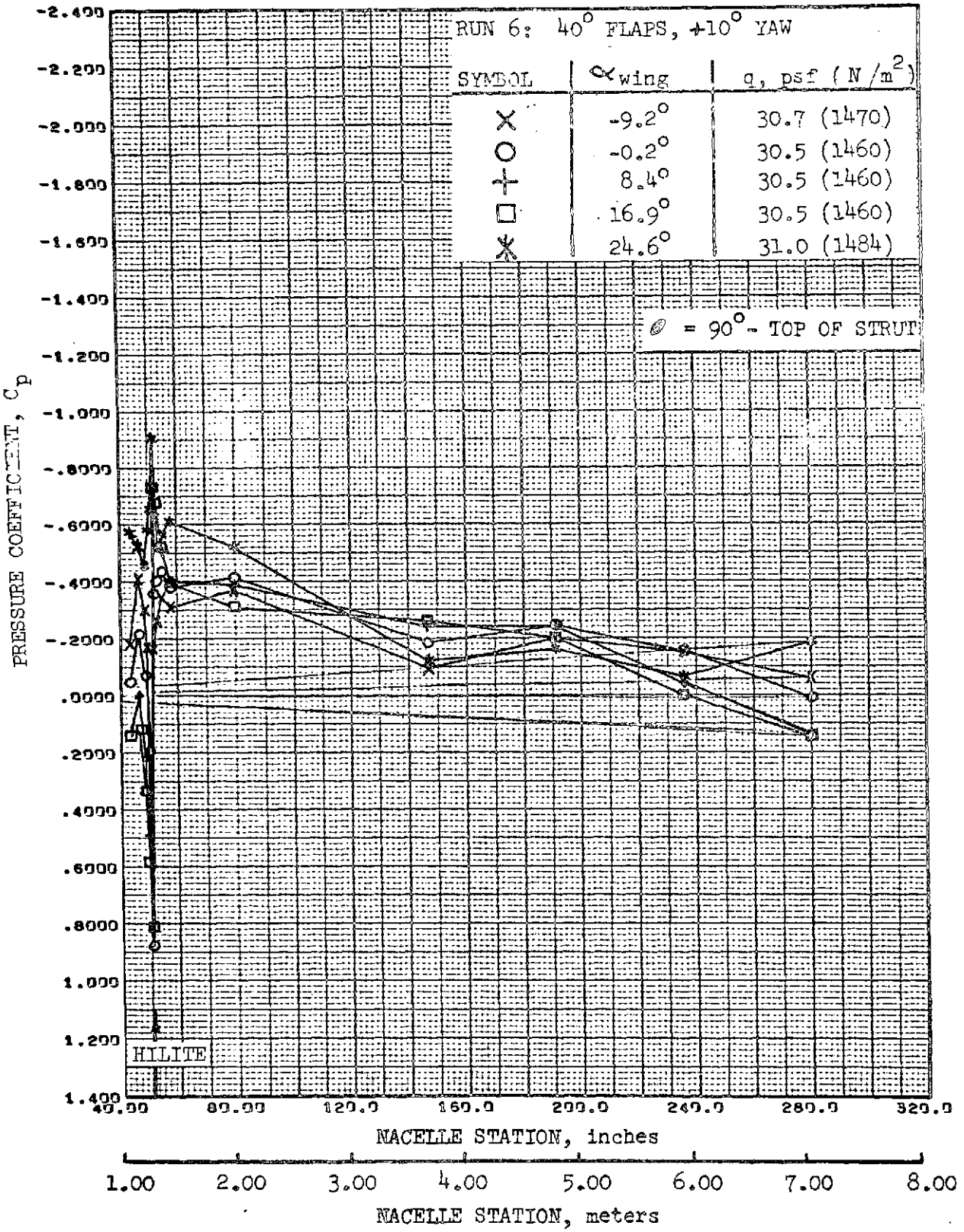

FIGURE 169.-REFAN NACELLE PRESSURE COEFFICIENT DISTRIBUTION, INBOARD SIDE-ABOVE STRUT

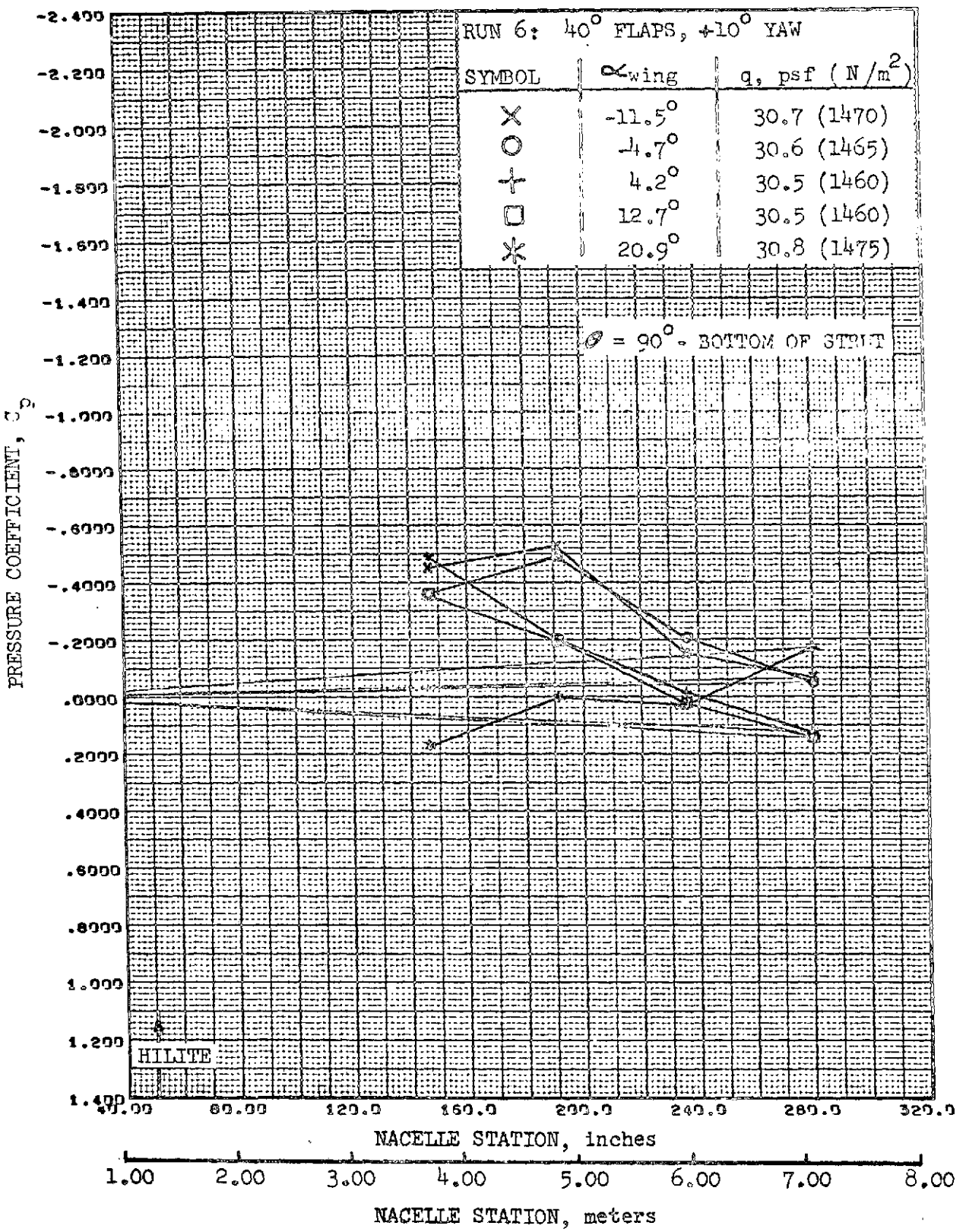

FIGURE 170.-REFAN NACELLE PRESSURE COEFFICIENT DISTRIBUTION, INBOARD SIDE-BELOW STRUT

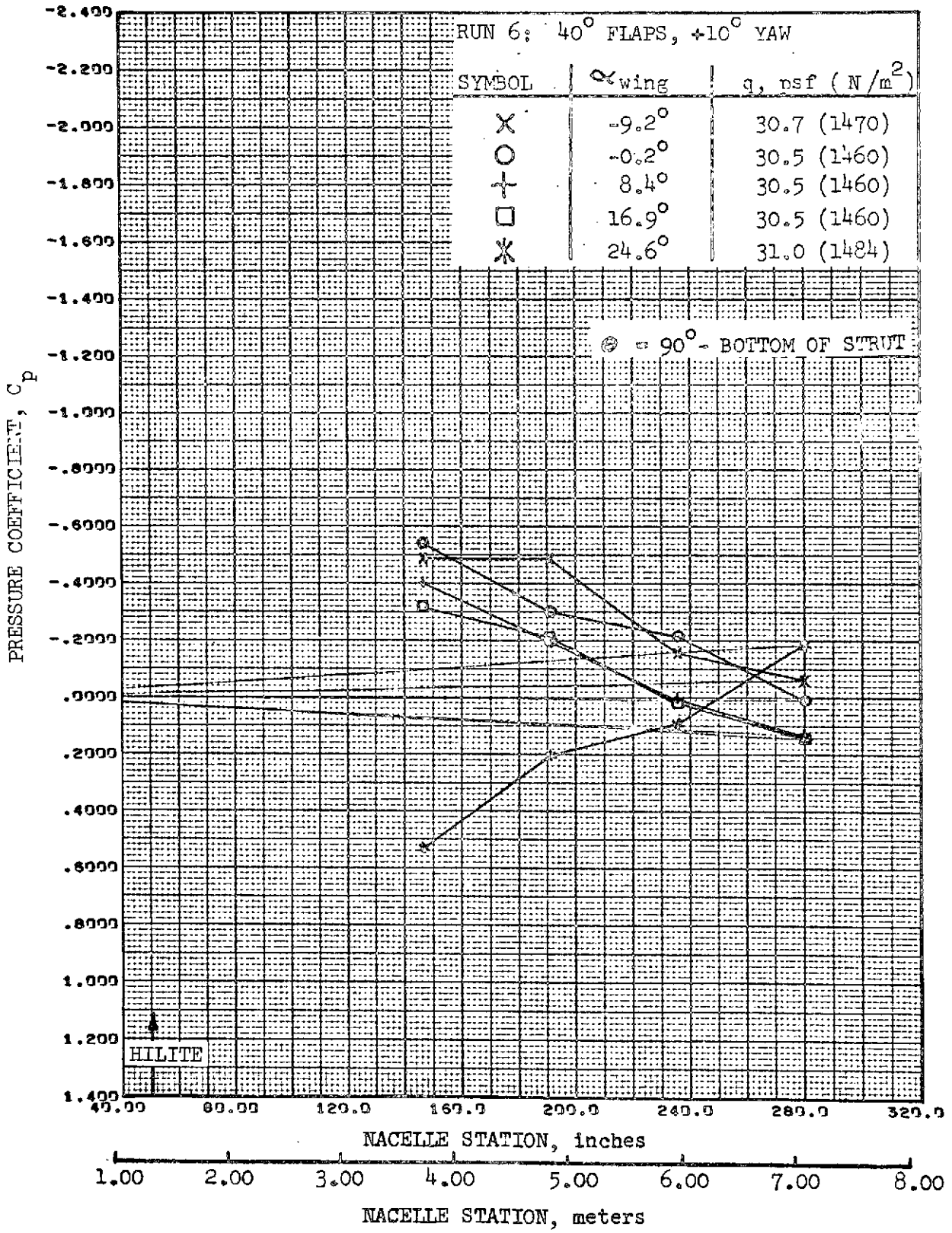

FIGURE 171.-REFAN NACELLE PRESSURE COEFFICIENT DISTRIBUTION, INBOARD SIDE-BELOW STRUT

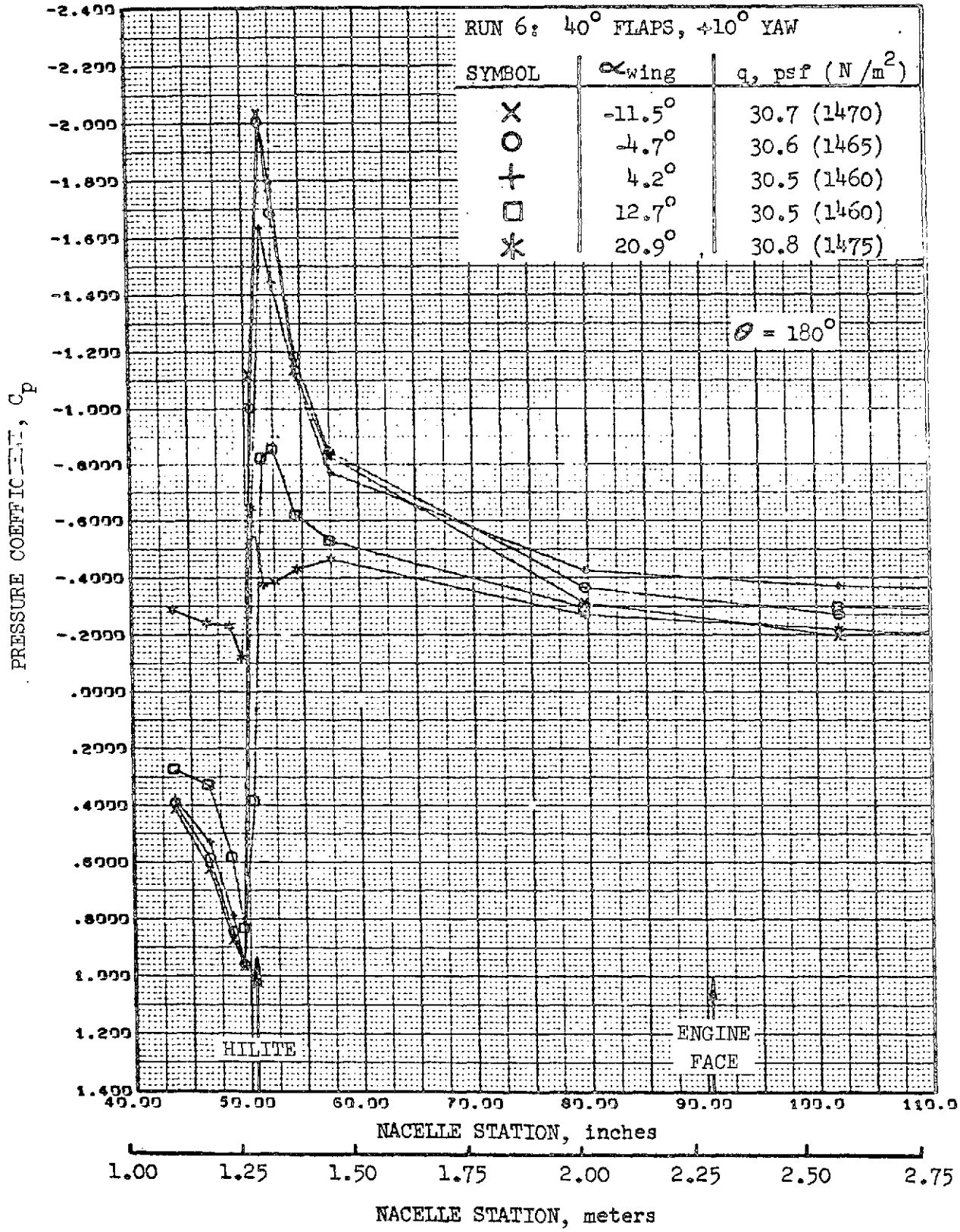

FIGURE 172.-REFAN NACELLE INLET COWL PRESSURE COEFFICIENT DISTRIBUTION, BOTTOM LONGITUDINAL

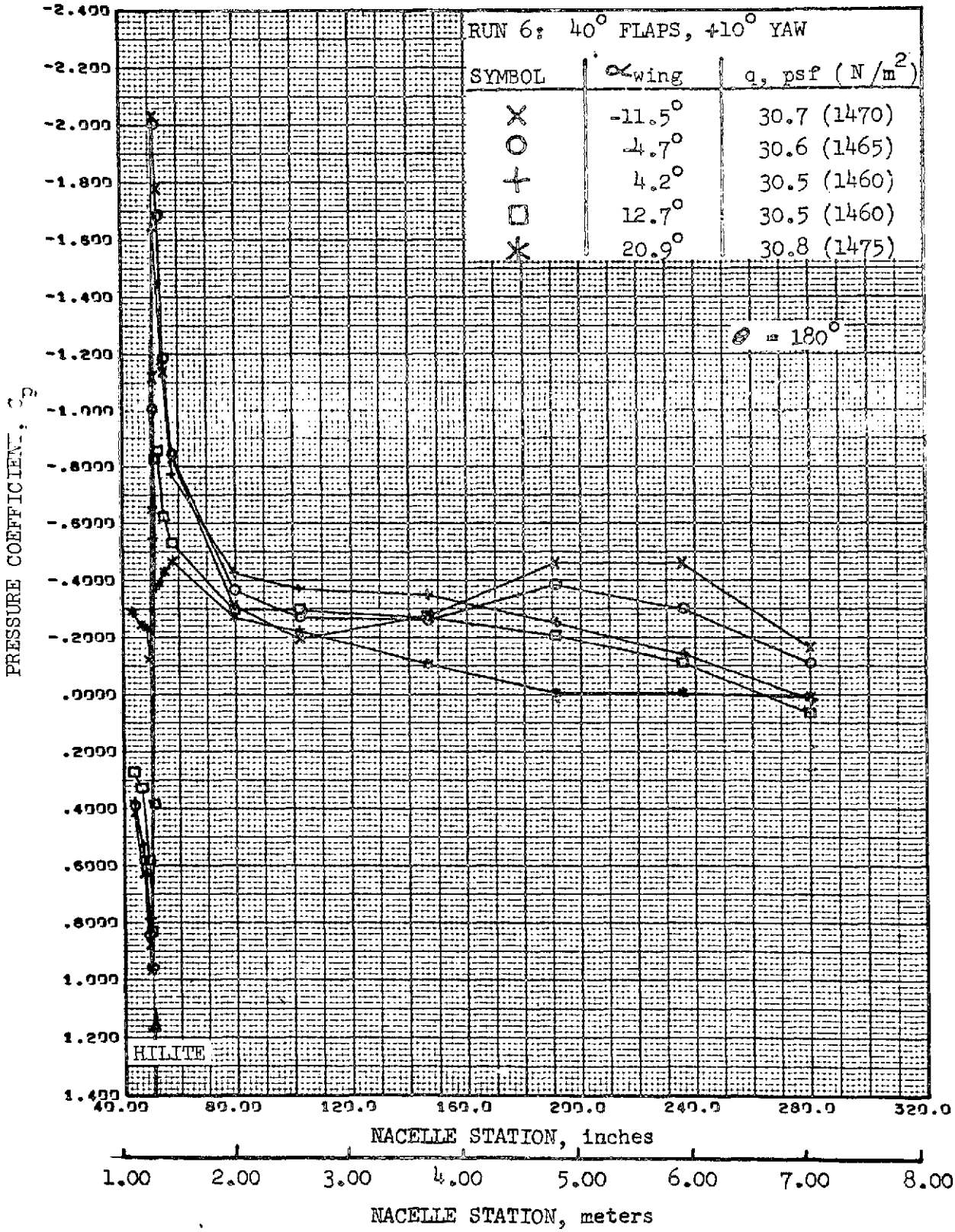

FIGURE 173.-REFAN NACELLE PRESSURE COEFFICIENT DISTRIBUTION, BOTTOM LONGITUDINAL

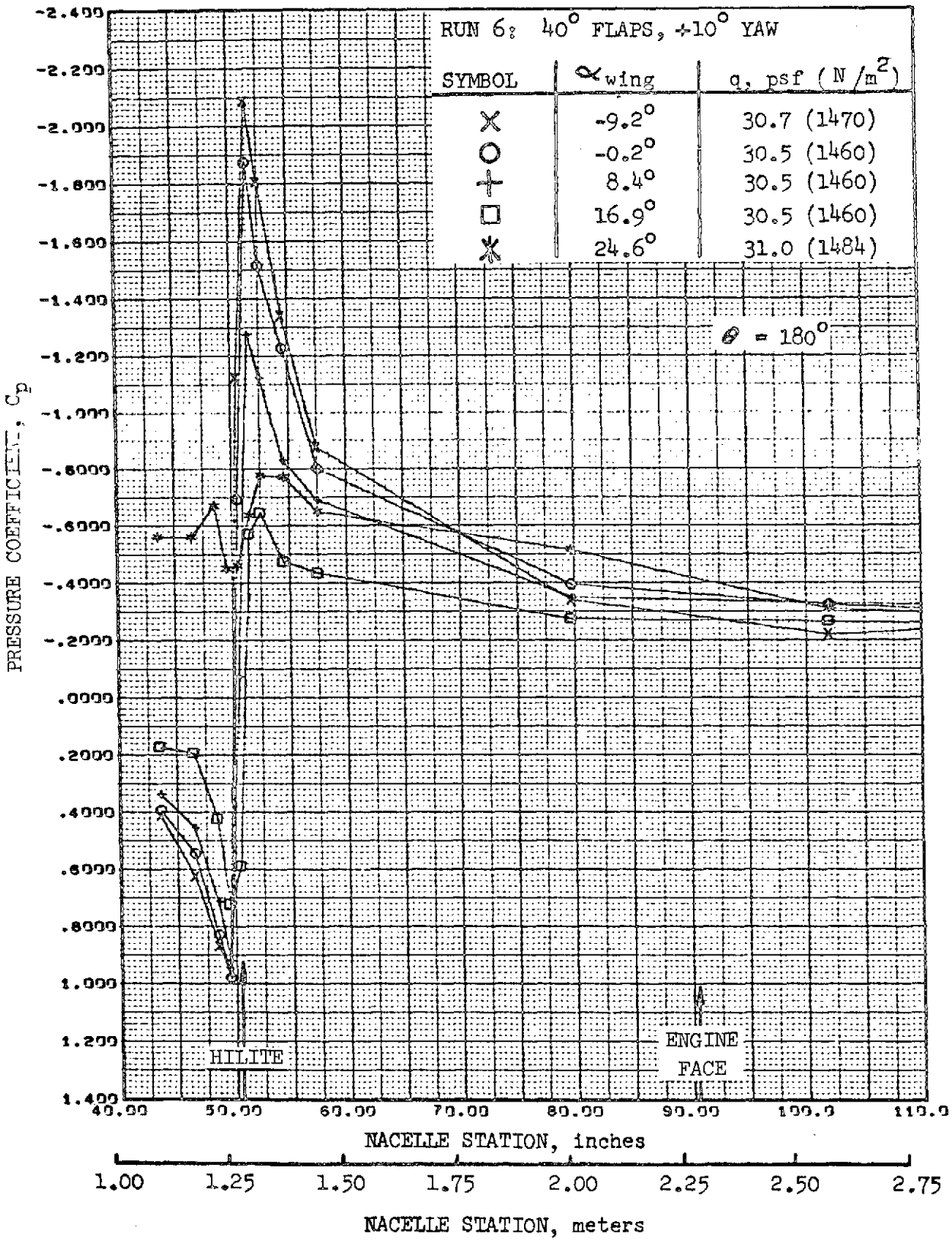

FIGURE 174. -REFAN NACELLE INLET COWL PRESSURE COEFFICIENT DISTRIBUTION, BOTTOM LONGITUDINAL

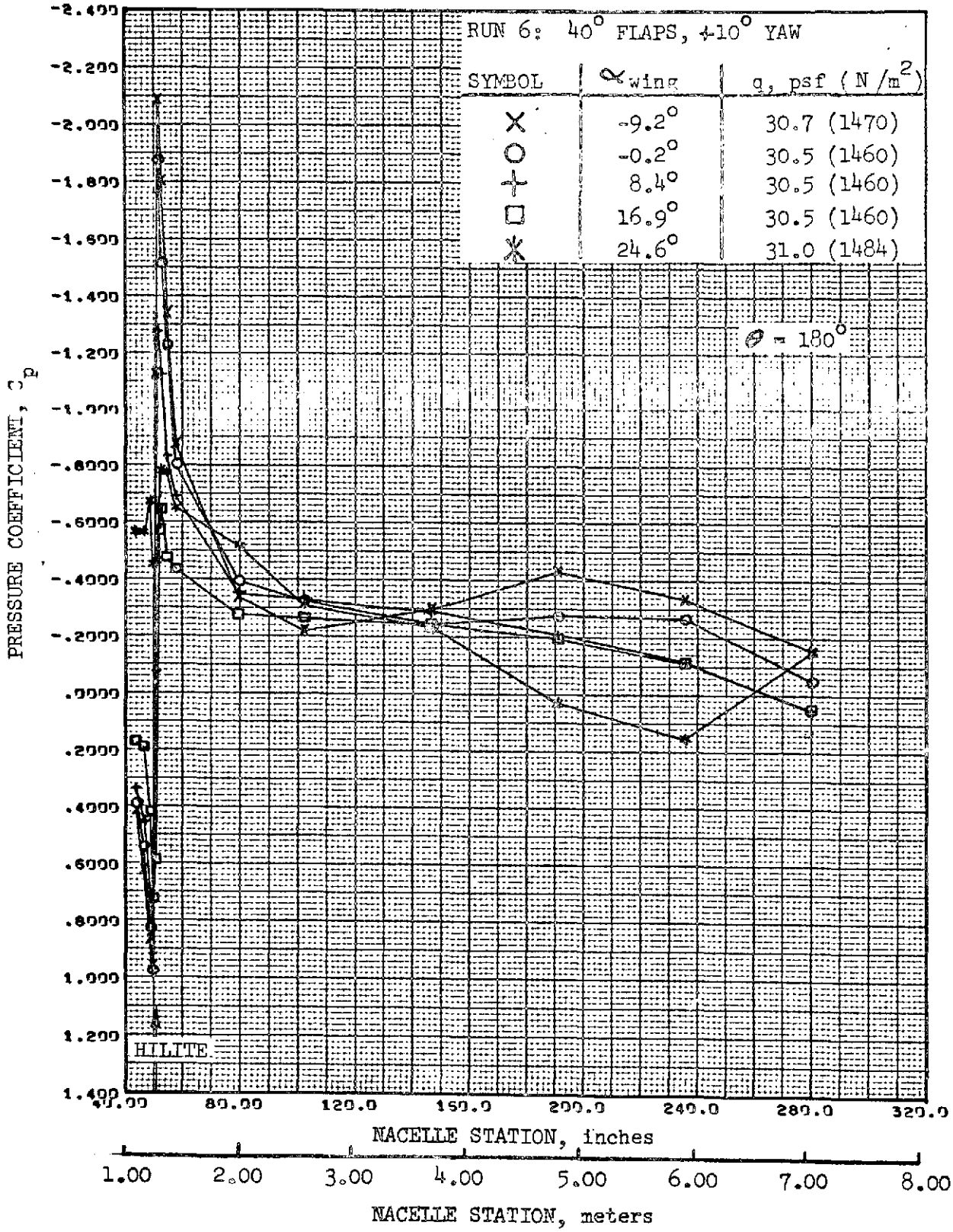

FIGURE 175.-REFAN NACELLE PRESSURE COEFFICIENT DISTRIBUTION, BOTTOM LONGITUDINAL

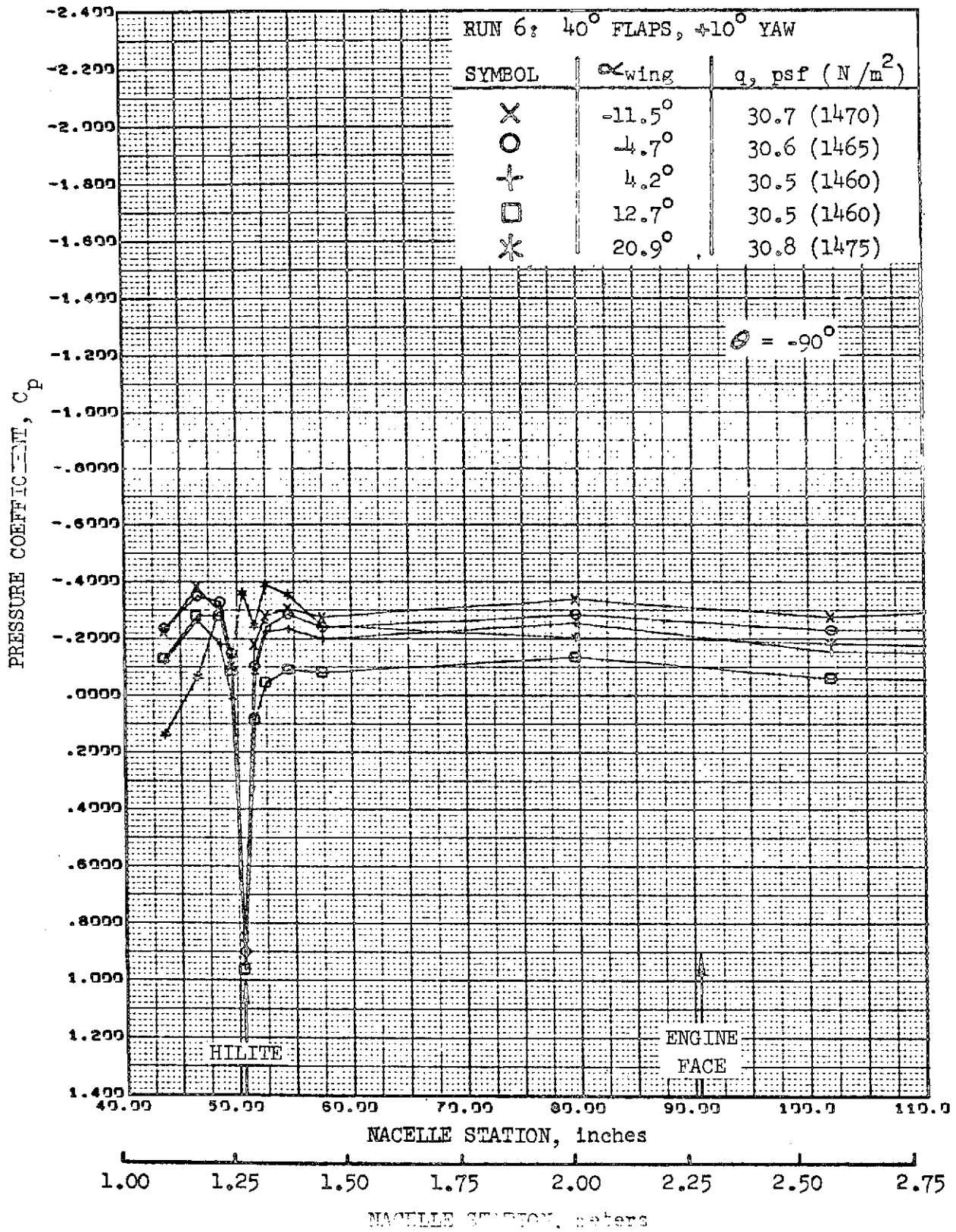

FIGURE 176.-REFAN NACELLE INLET COWL PRESSURE COEFFICIENT DISTRIBUTION, OUTBOARD SIDE

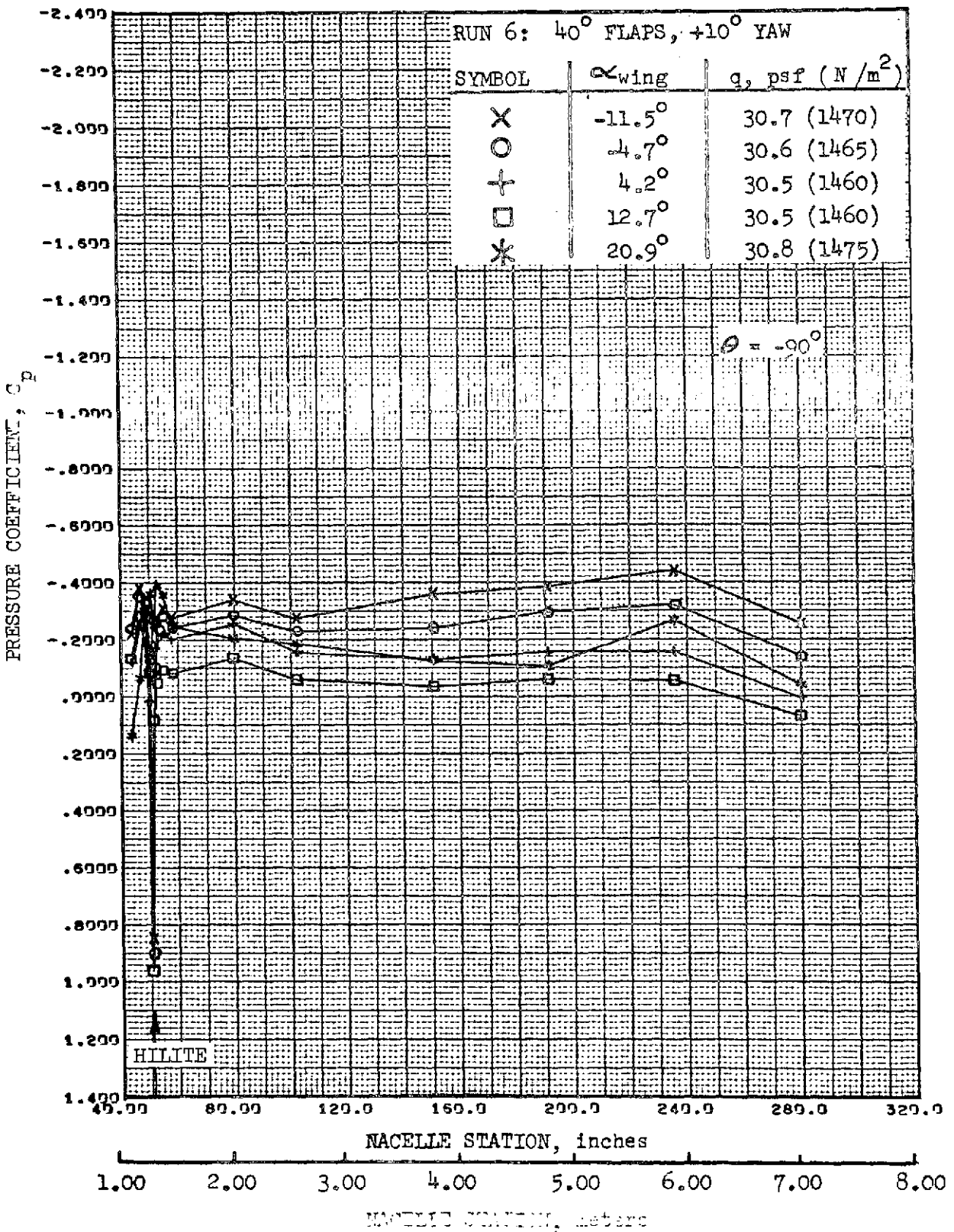

FIGURE 177.-REFAN NACELLE PRESSURE COEFFICIENT DISTRIBUTION, OUTBOARD SIDE

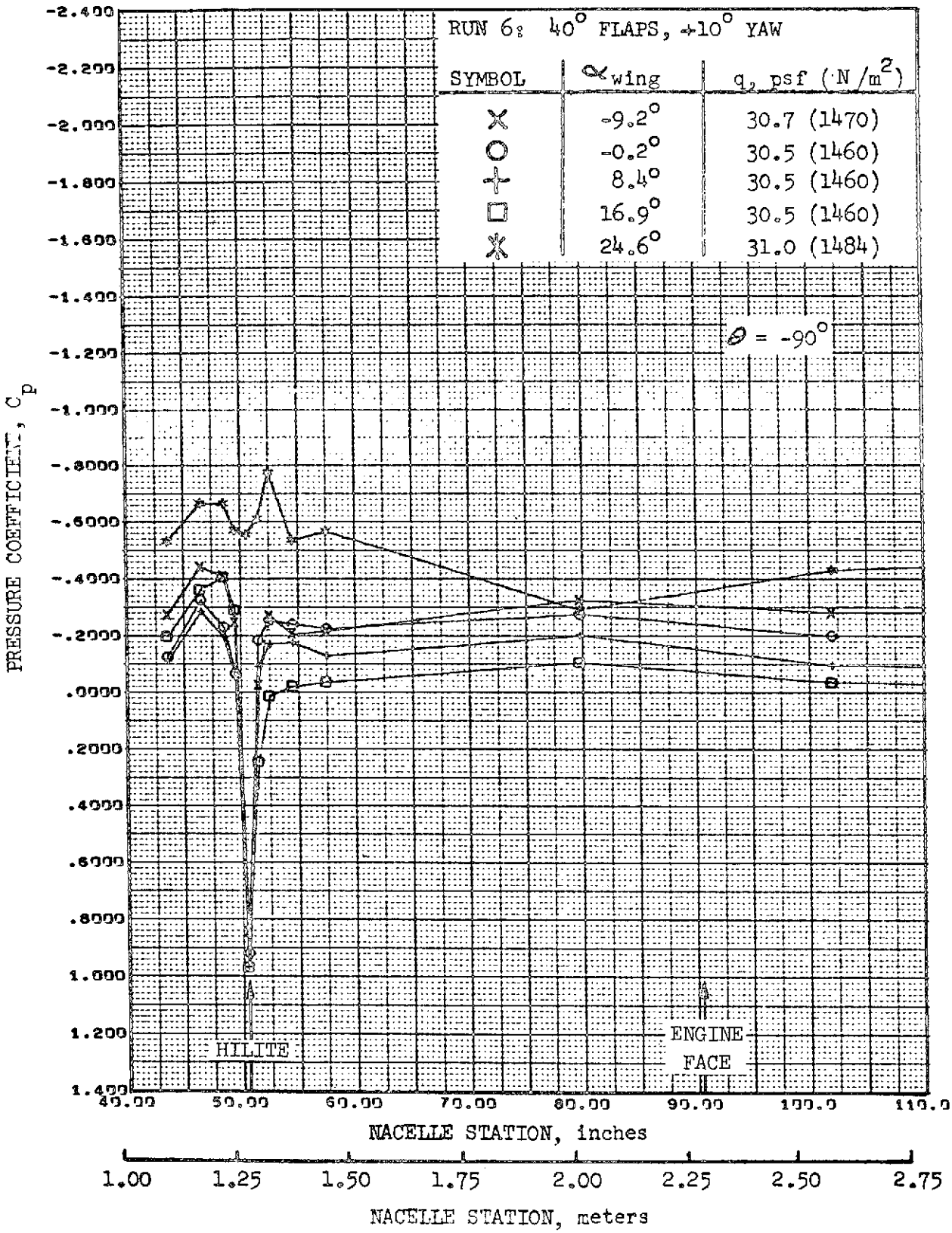

FIGURE 178.-REFAN NACELLE INLET COWL PRESSURE COEFFICIENT DISTRIBUTION, OUTBOARD SIDE

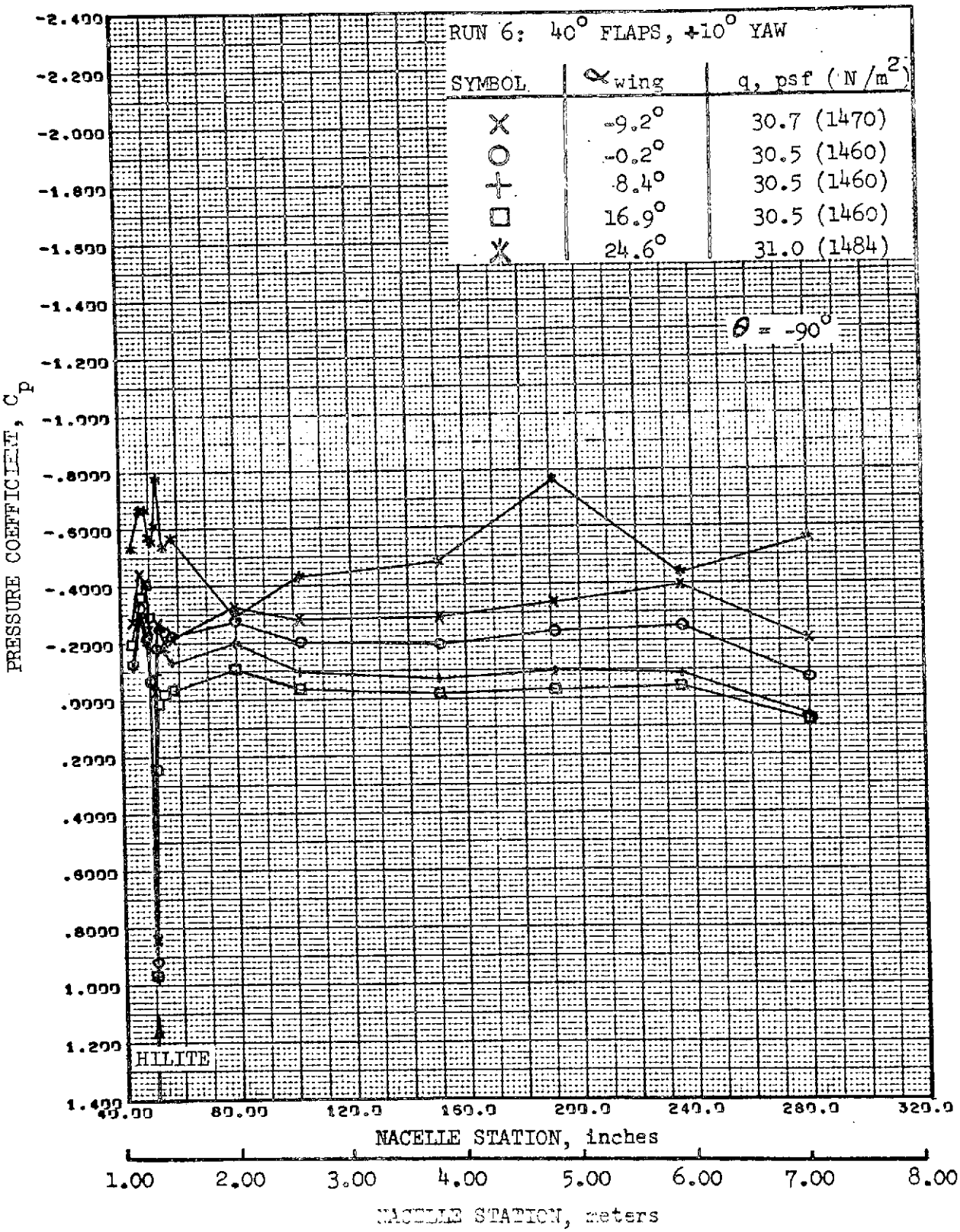

FIGURE 179.-REFAN NACELLE PRESSURE COEFFICIENT DISTRIBUTION, OUTBOARD SIDE

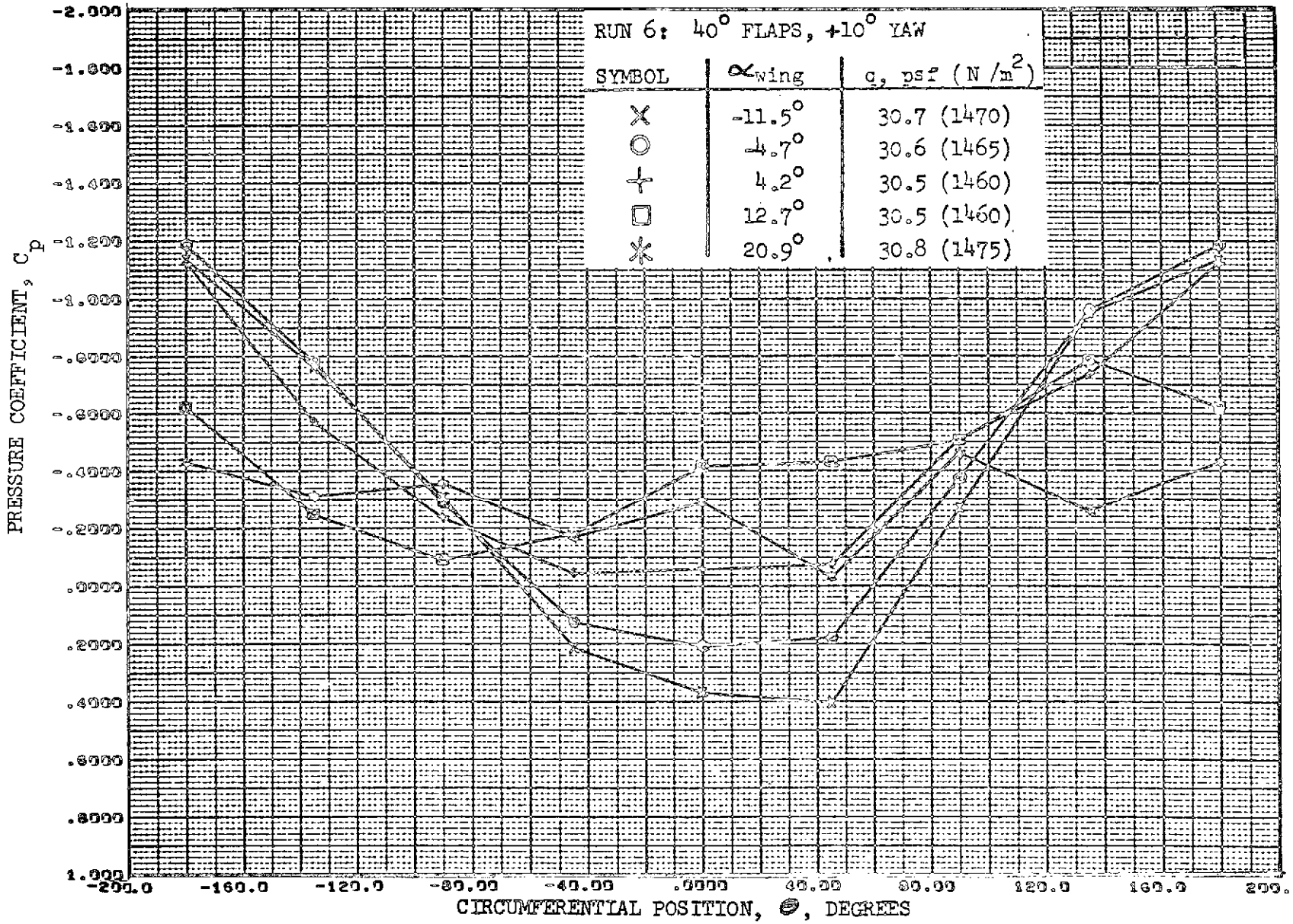

FIGURE 180. - REFAN NACELLE PRESSURE COEFFICIENT DISTRIBUTION, EXTERNAL CIRCUMFERENTIAL AT STATION 54.5 INCHES (1.38 METERS)

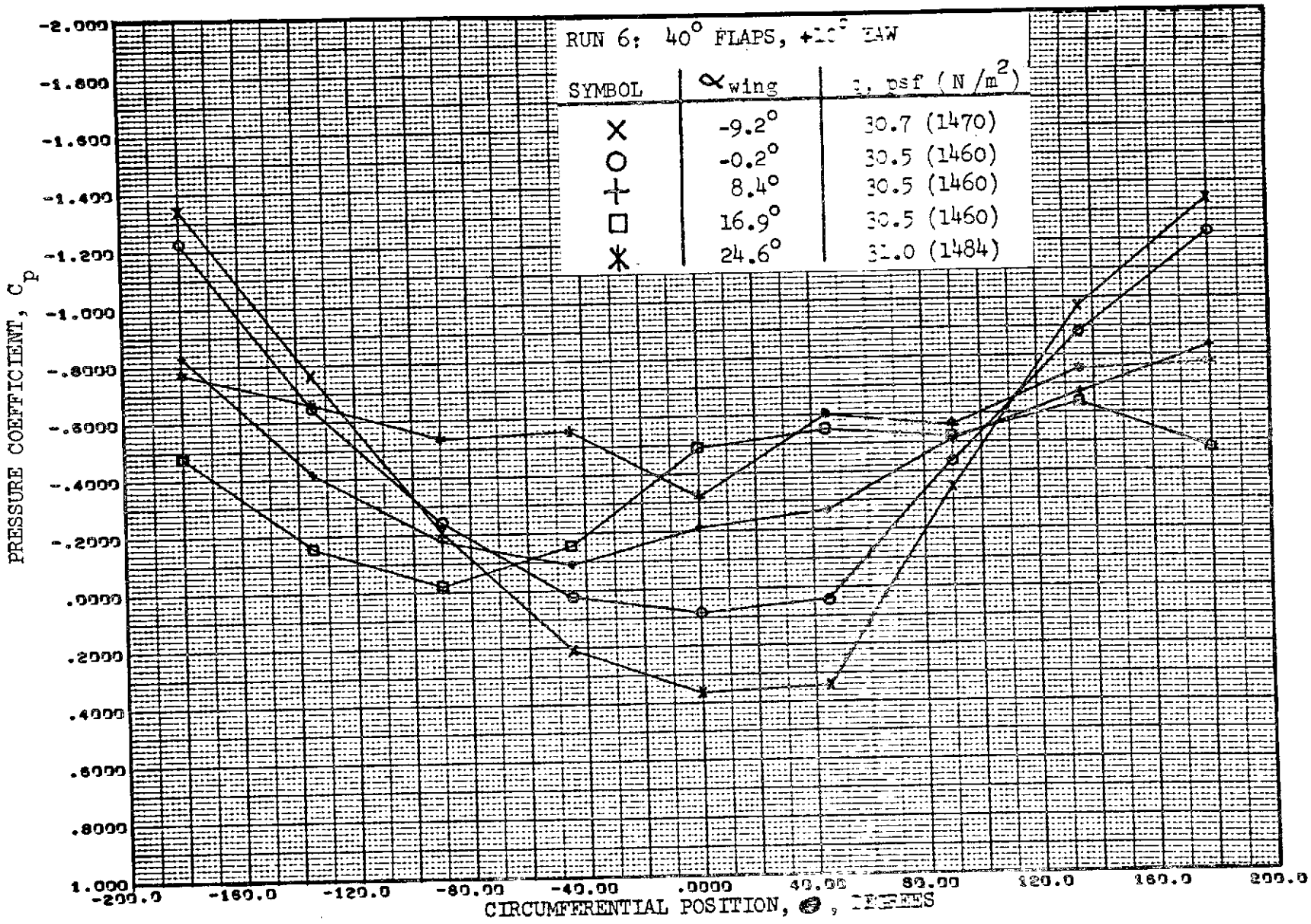

FIGURE 181. - REFAN NACELLE PRESSURE COEFFICIENT DISTRIBUTION, EXTERNAL CIRCUMFERENTIAL AT STATION 54.5 INCHES (1.38 METERS)

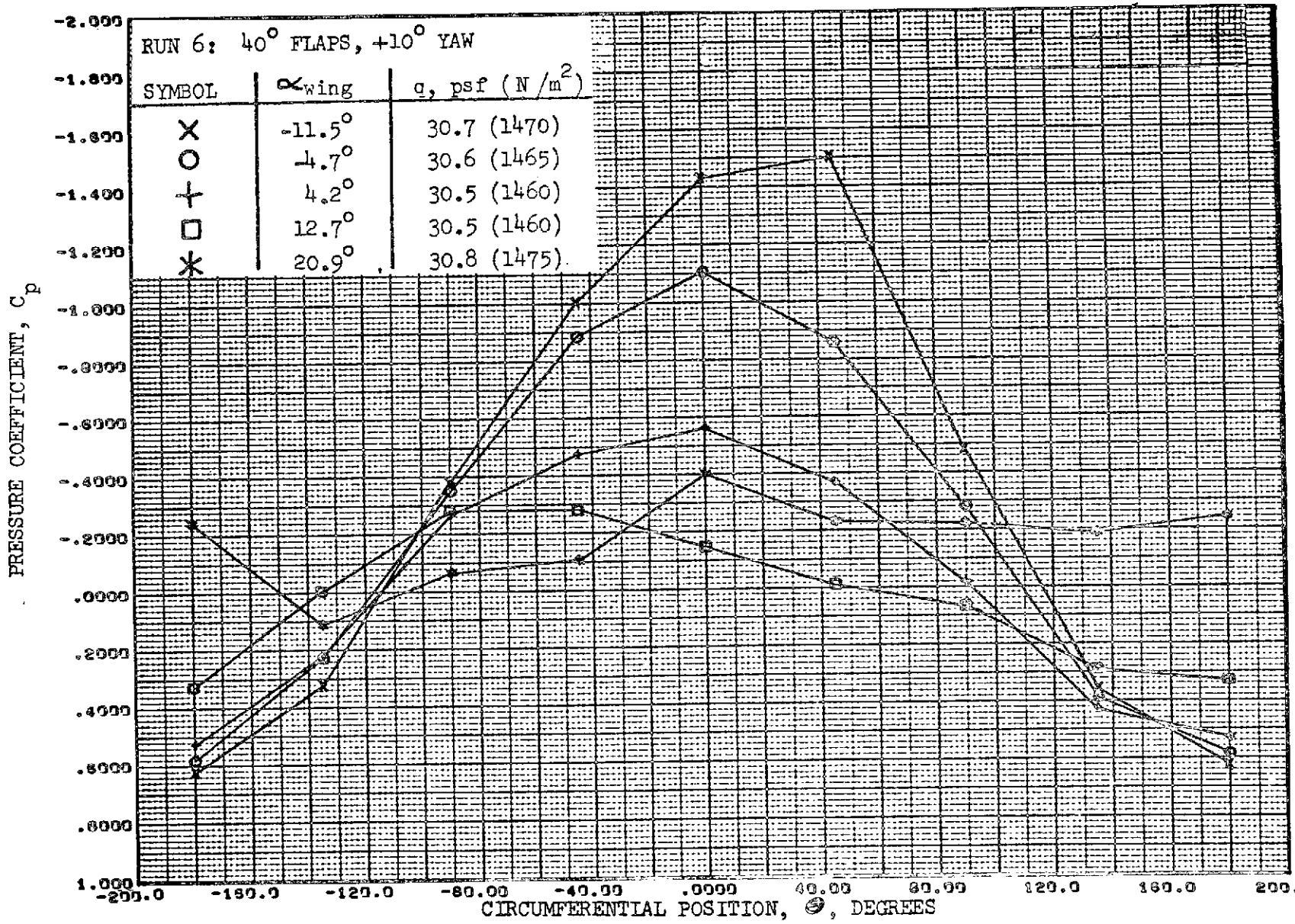

FIGURE 182. - REFAN NACELLE PRESSURE COEFFICIENT DISTRIBUTION, INTERNAL CIRCUMFERENTIAL AT STATION 54.5 INCHES (1.38 METERS)

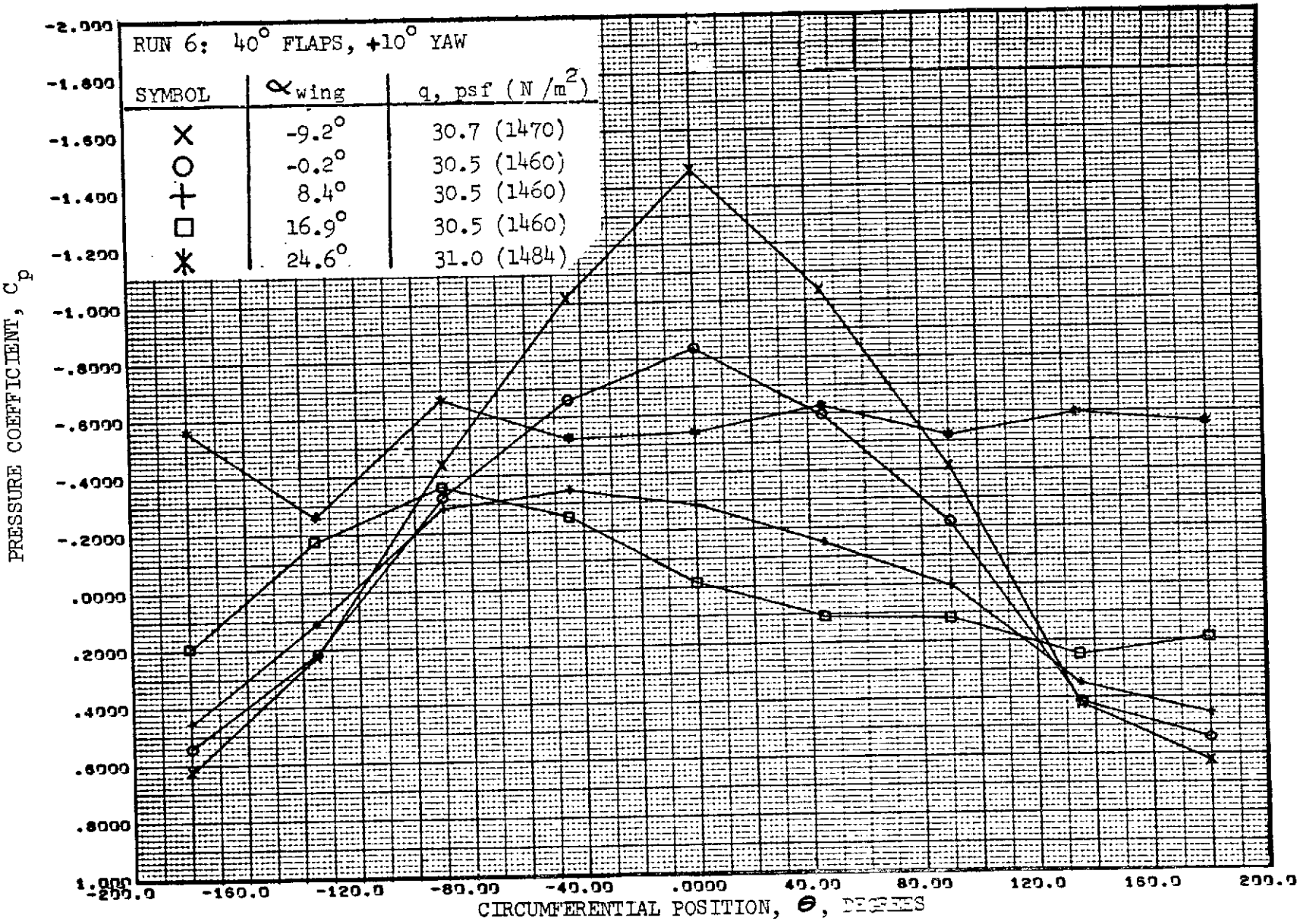

FIGURE 183. - REFAN NACELLE PRESSURE COEFFICIENT DISTRIBUTION, INTERNAL CIRCUMFERENTIAL AT STATION 5-.5 INCHES (1.38 METERS)

7.2.2 NACELLE INFLOW ANGLE TUFT PHOTOGRAPHS

Presented in this section are tuft photographs indicating nacelle inflow angles from the wind tunnel test discussed in Section 4.0. Photographs are presented on pages 206 through 210 as shown in the figure number index below.

FIGURE NUMBER INDEX FOR TUFT PHOTOGRAPHS

TEST CONDITION			RUN	WING ANGLE OF ATTACK, α_w		
FLAPS, δ_f	YAW, ψ	DYNAMIC PRESSURE, q_∞ psf (N/m^2)		-11°	-5°	12°
40°	0°	30 (1440)	4	FIG. 184	FIG. 185	FIG. 186
40°	-10°	30 (1440)	10	—	FIG. 187	—
40°	+10°	30 (1440)	11	—	FIG. 188	—

PRECEDING PAGE BLANK NOT FILMED

TOP VIEW

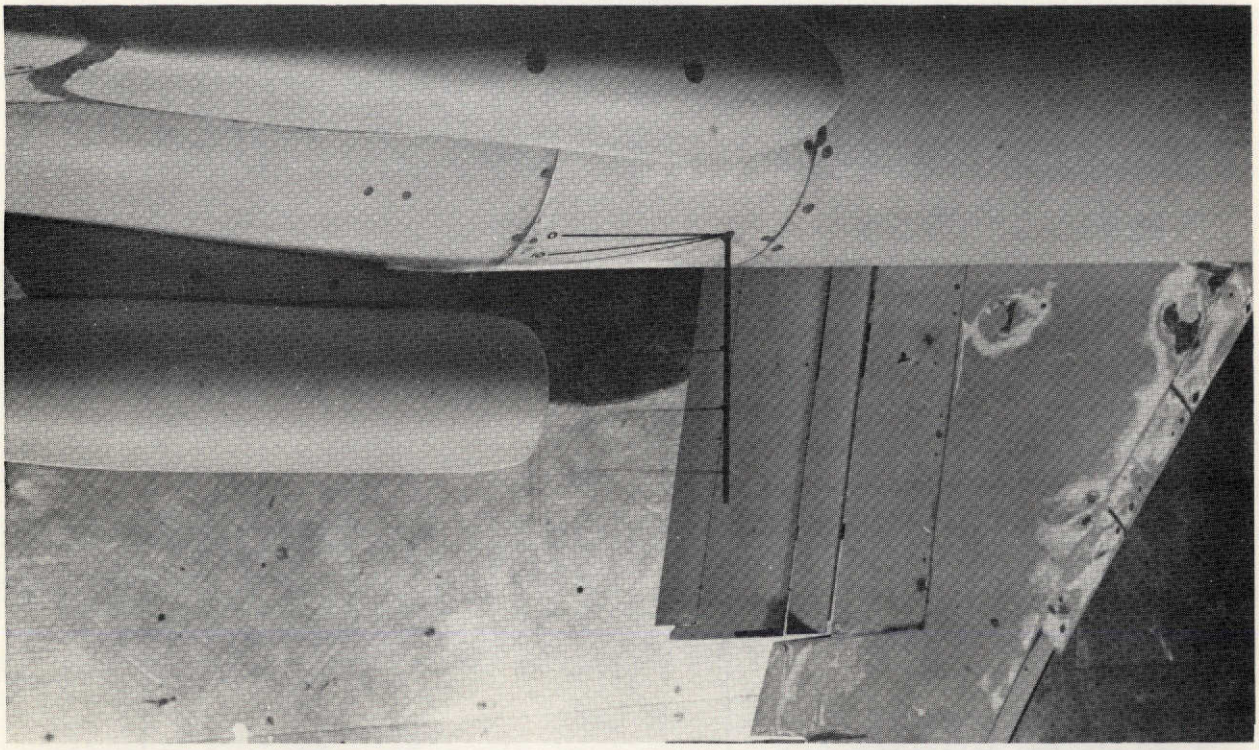

SIDE VIEW

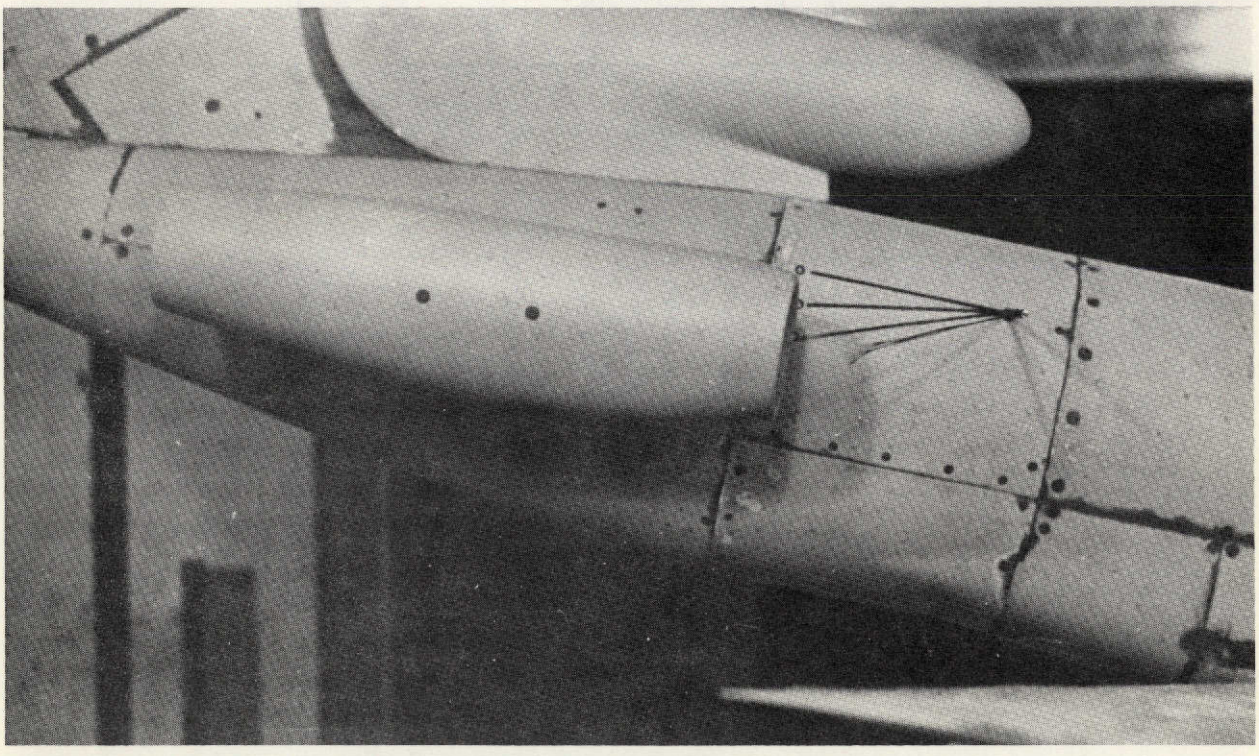

FIGURE 184. - NACELLE INFLOW ANGLES (40° FLAPS, 0° YAW, $-11^{\circ}\alpha_w$)

TOP VIEW

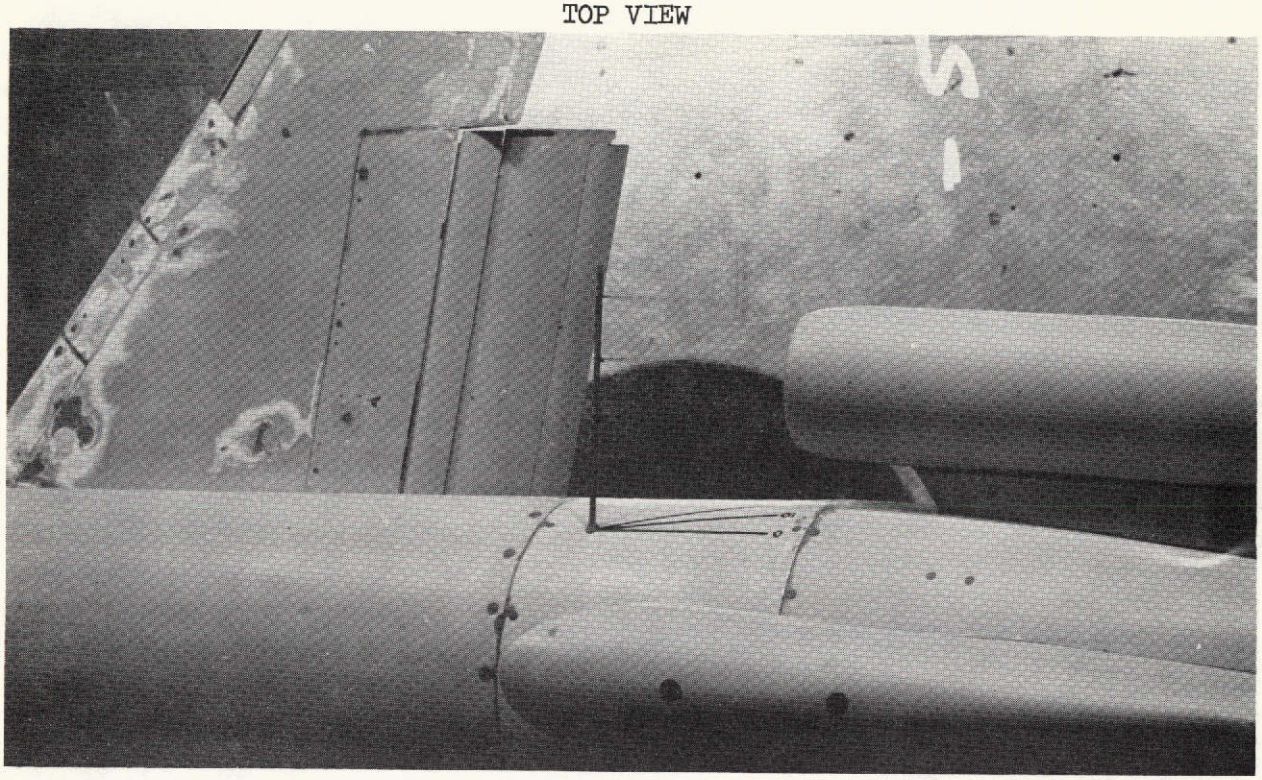

SIDE VIEW

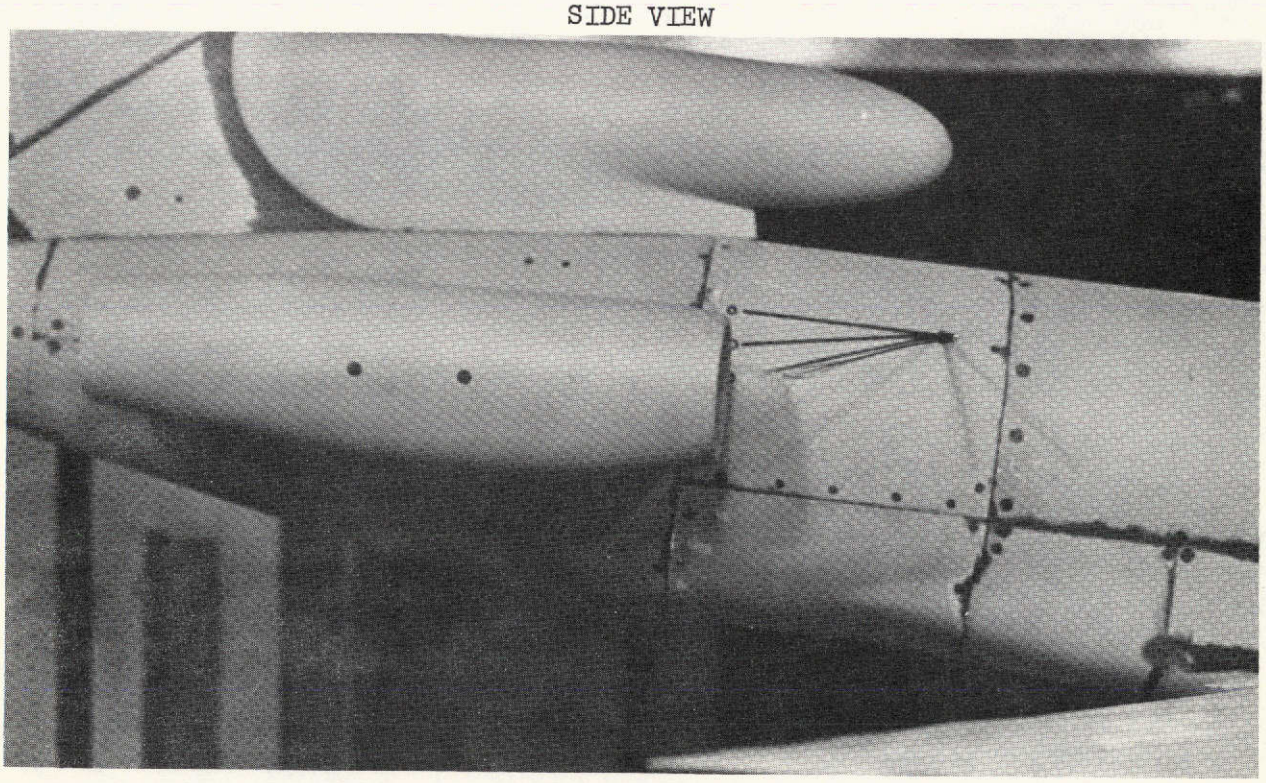

FIGURE 185. - NACELLE INFLOW ANGLES (40° FLAPS, 0° YAW, $-5^{\circ}\alpha_w$)

TOP VIEW

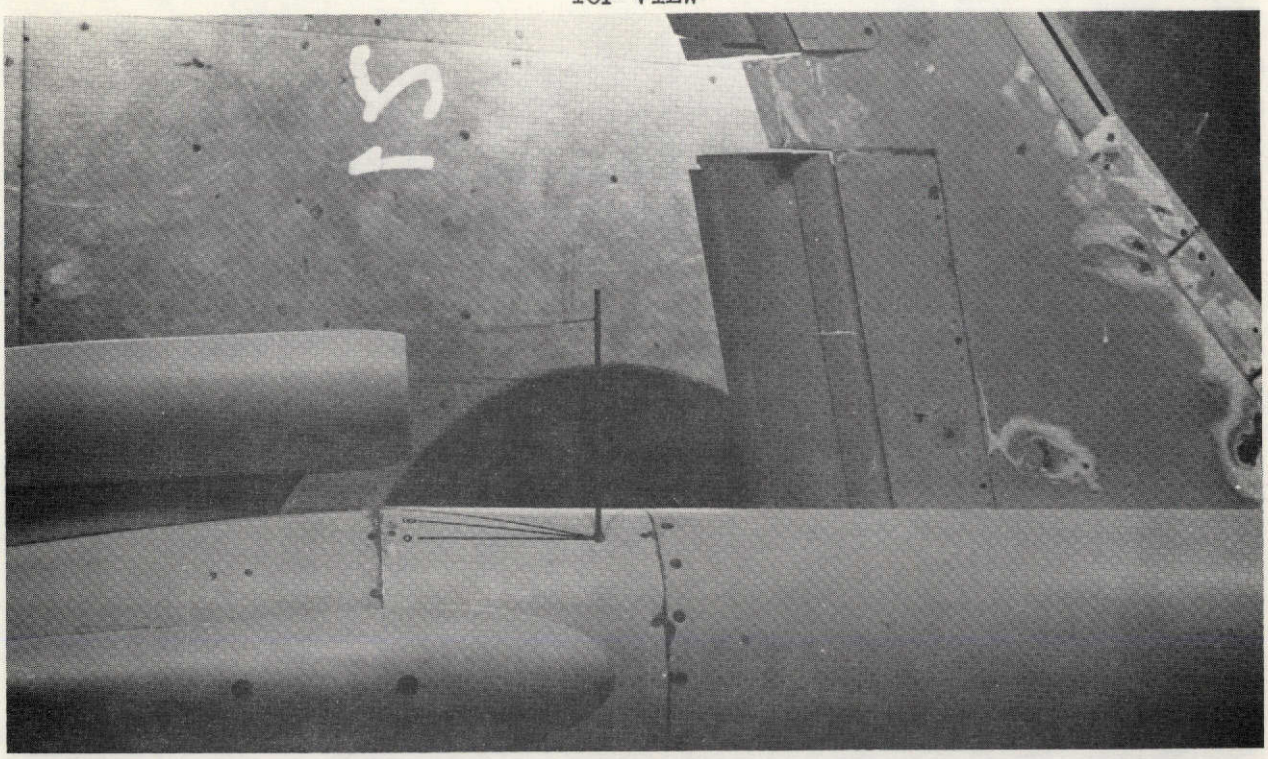

SIDE VIEW

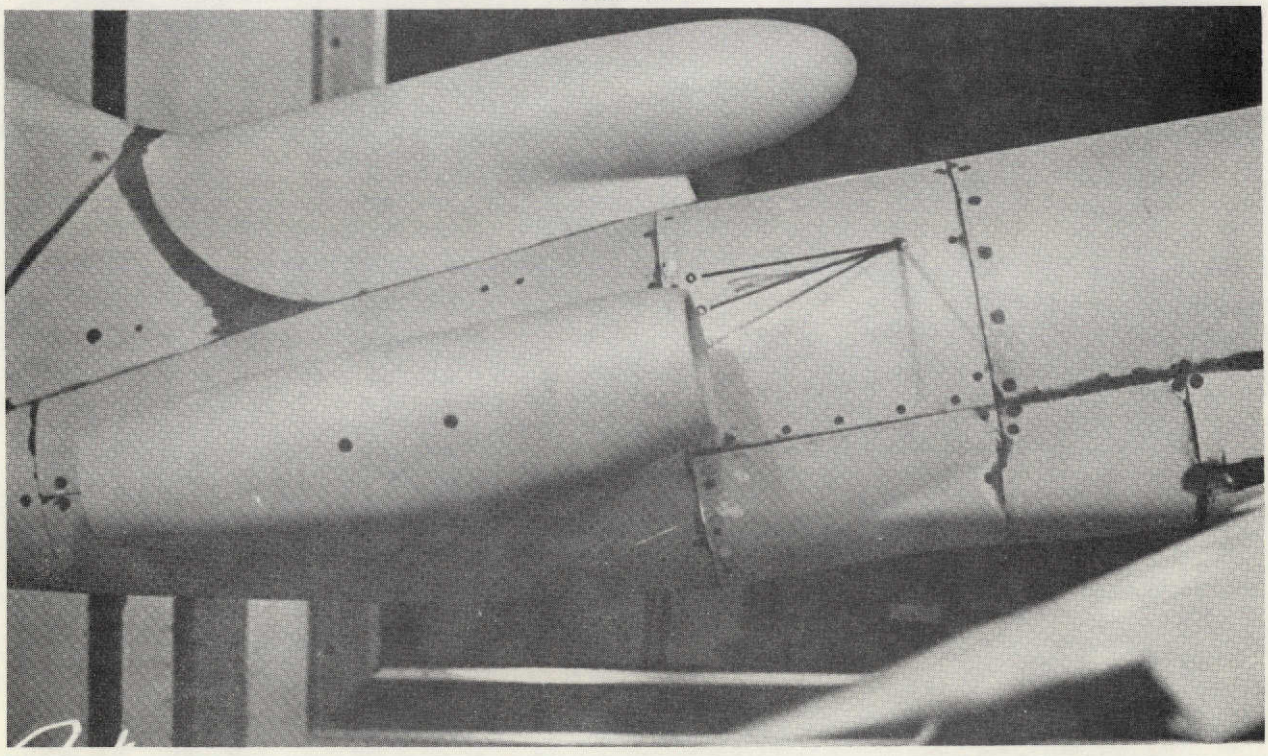

FIGURE 186. - NACELLE INFLOW ANGLES (40° FLAPS, 0° YAW, $12^{\circ}\alpha_w$)

TOP VIEW

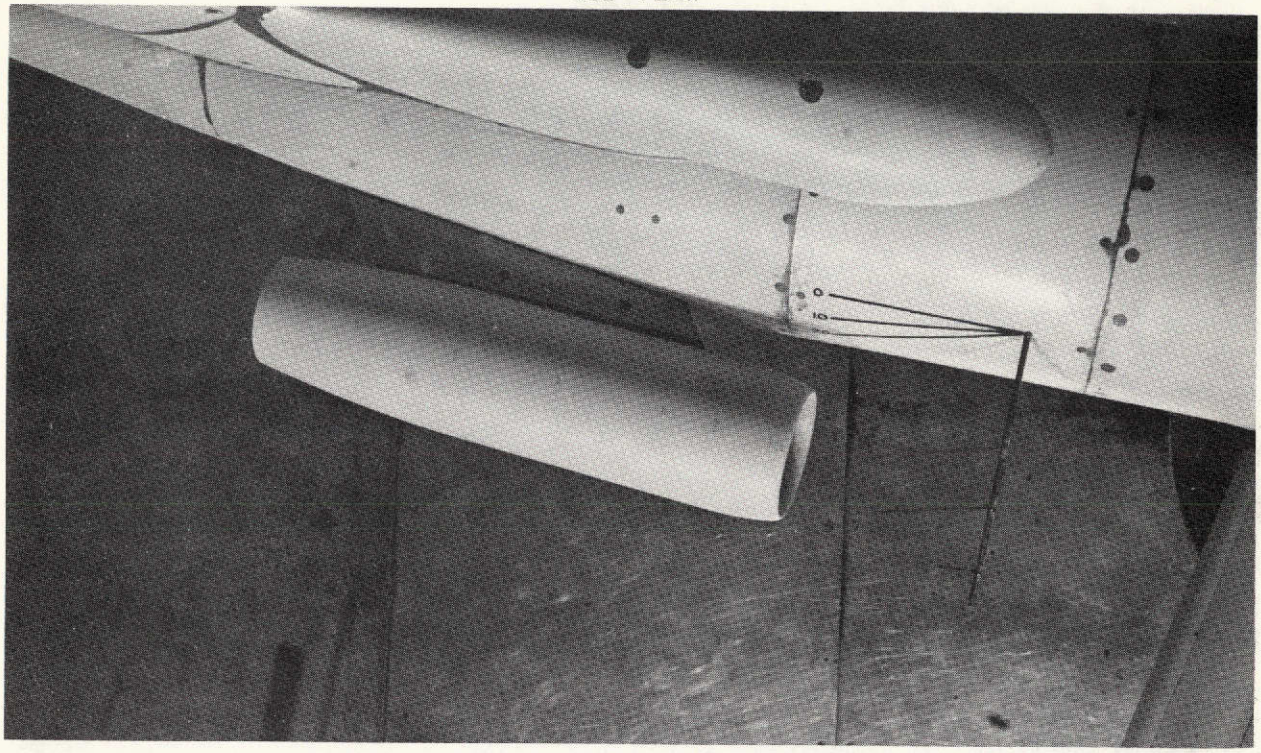

SIDE VIEW

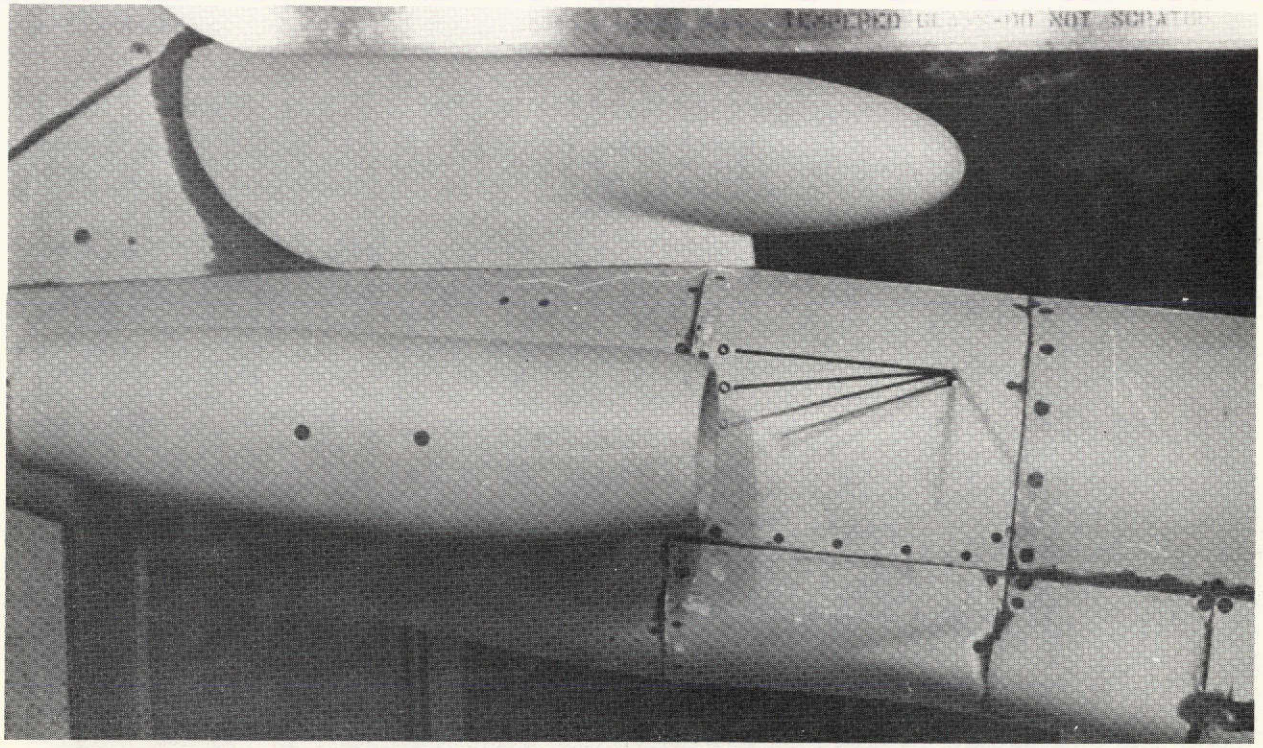

FIGURE 187. - NACELLE INFLOW ANGLES (40° FLAPS, -10° YAW, $-5^{\circ}\alpha_w$)

TOP VIEW

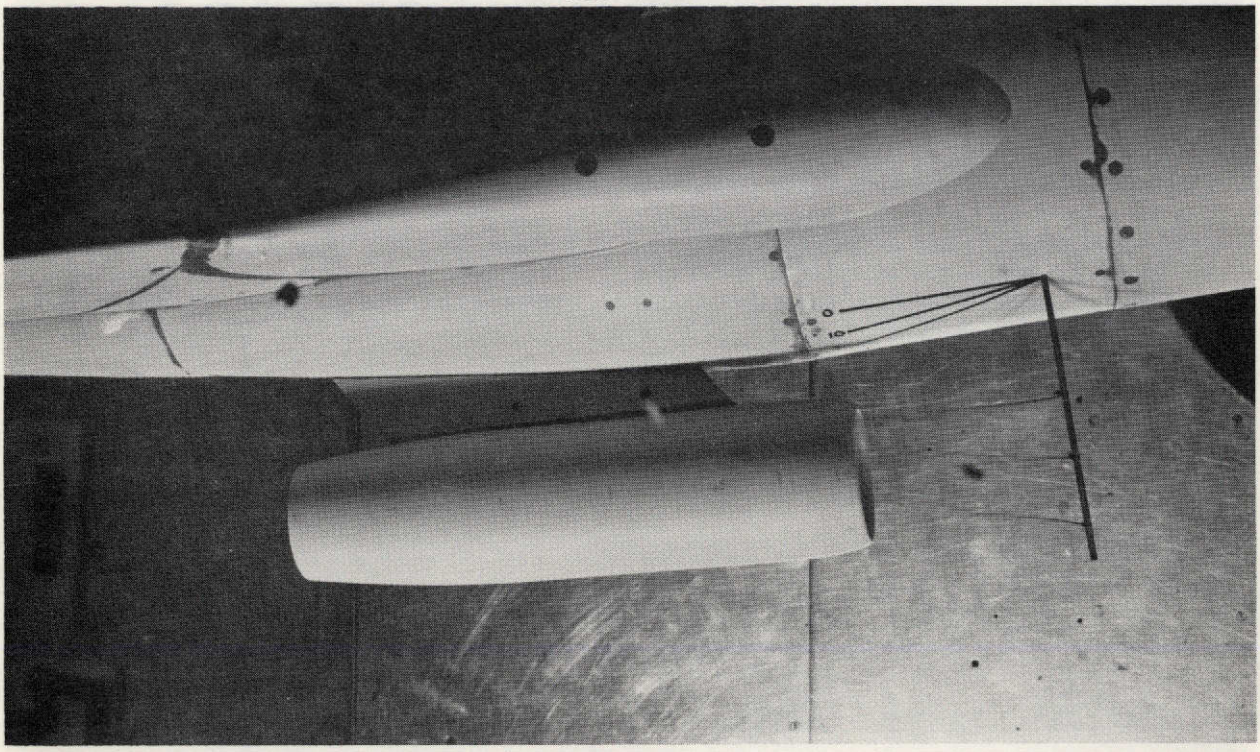

SIDE VIEW

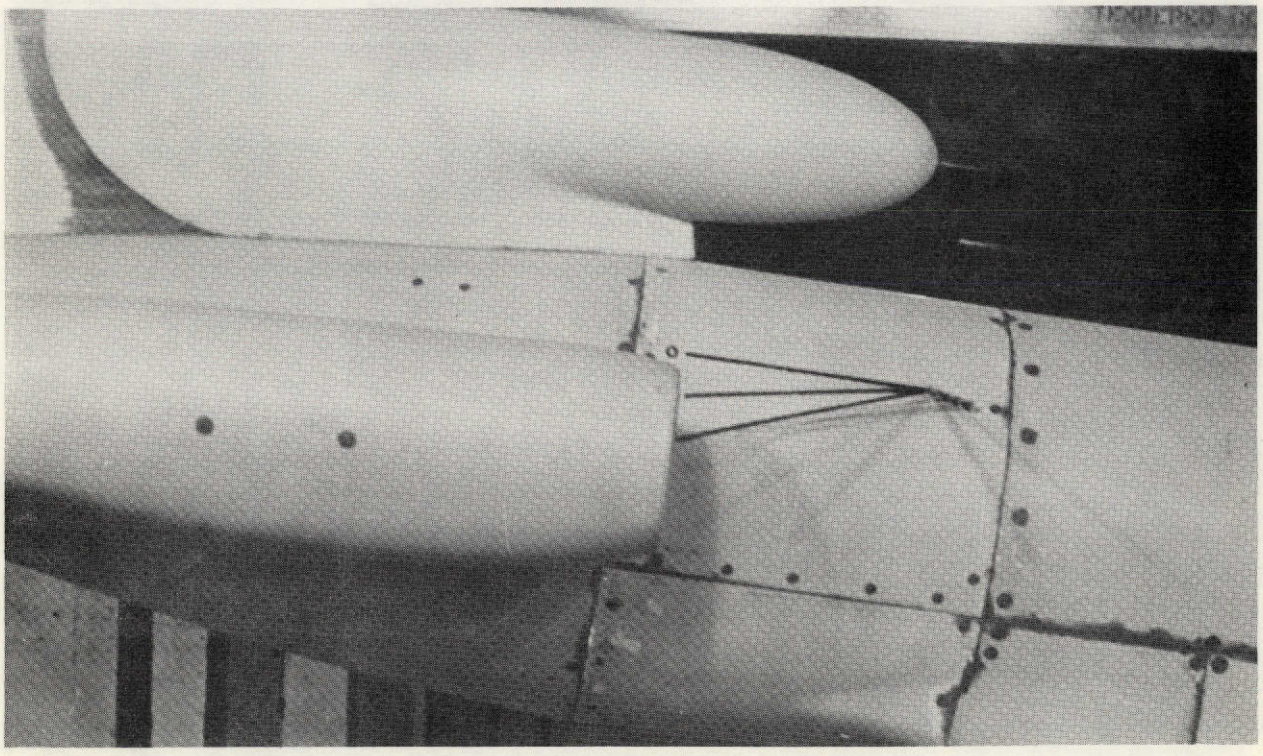

FIGURE 188. - NACELLE INFLOW ANGLES (40° FLAPS, $+10^{\circ}$, $-5\alpha_w$)

7.2.3 INLET SURFACE STATIC PRESSURE RATIO DISTRIBUTIONS

Presented in this section are inlet surface static pressure ratio distributions obtained from the wind tunnel test performed by The Boeing Company, Propulsion Staff, as discussed in Section 4.0. Data are presented on pages 212 through 259 as shown in the figure number index below.

FIGURE NUMBER INDEX FOR INLET SURFACE STATIC PRESSURE RATIO DISTRIBUTIONS

NACELLE INFLOW ANGLE, ζ_N (a)	AIRSPEED, V_∞, kts (m/sec)	CORRECTED MASS FLOW, $\frac{w\sqrt{\theta}}{\delta}$, lbs/sec(kg/sec) 180 (82)	345 (156)	425 (193)	467 (212)	486 (220)	500 (227)
0°	180 (93)	—	189	190	191	192	193
14.8°	100 (51)	194	195	196	197	—	—
	150 (77)	198	199	200	201	—	—
	180 (93)	202	203	204	205	—	—
17.5°	100 (51)	206	207	208	209	210	211
	150 (77)	212	213	214	215	216	217
	180 (93)	218	219	220	221	222	223
22.5°	100 (51)	224	225	226	227	—	—
	120 (62)	228	—	—	—	—	—
	150 (77)	229	230	231	232	—	—
	180 (93)	233	234	235	236	—	—

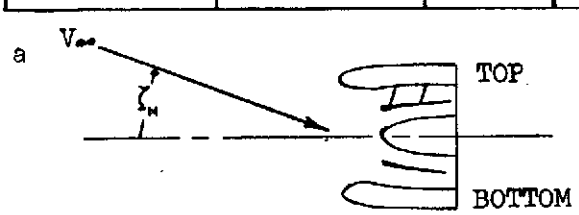

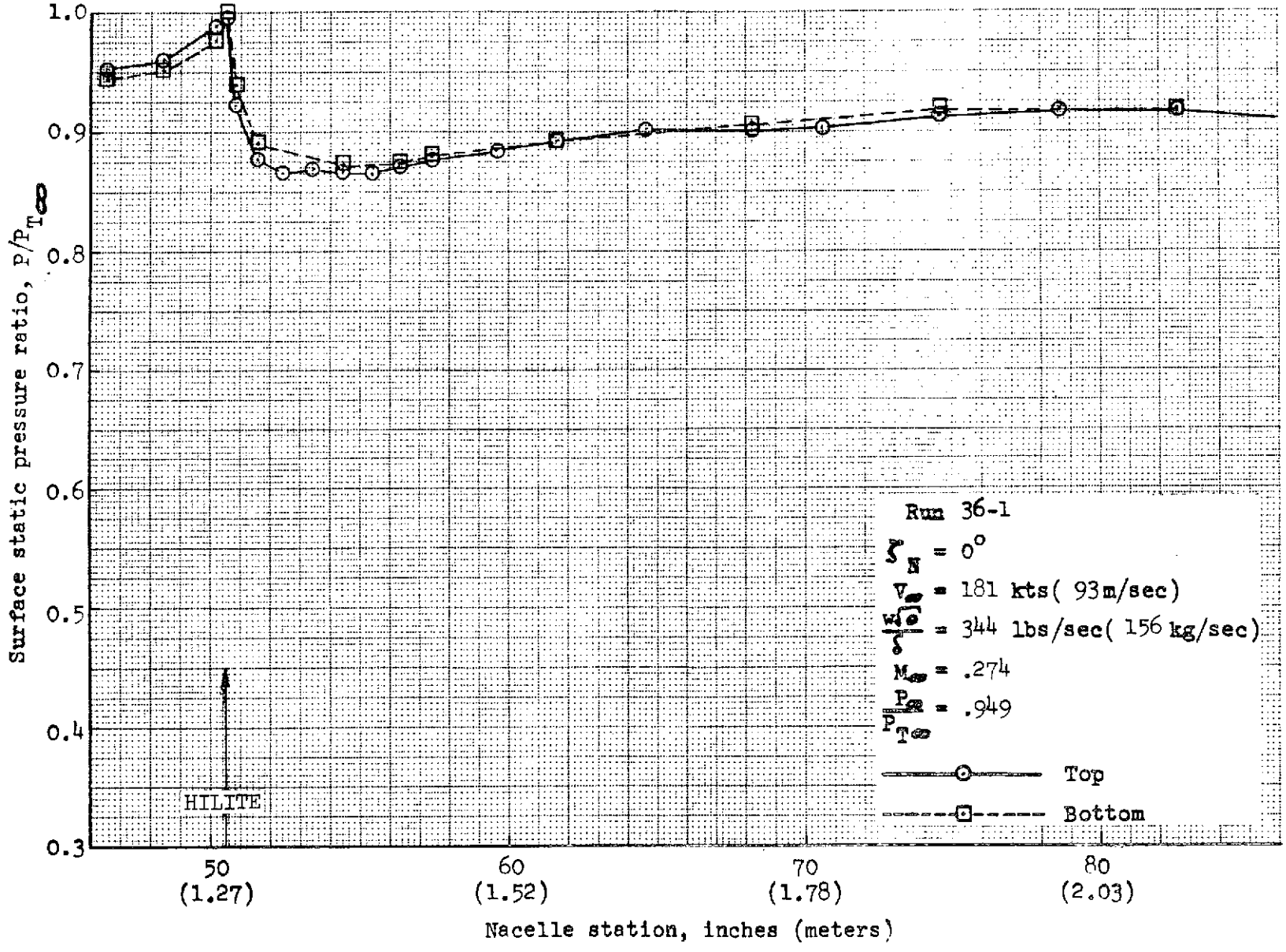

FIGURE 189.- REFAN INLET SURFACE STATIC PRESSURE RATIO DISTRIBUTION

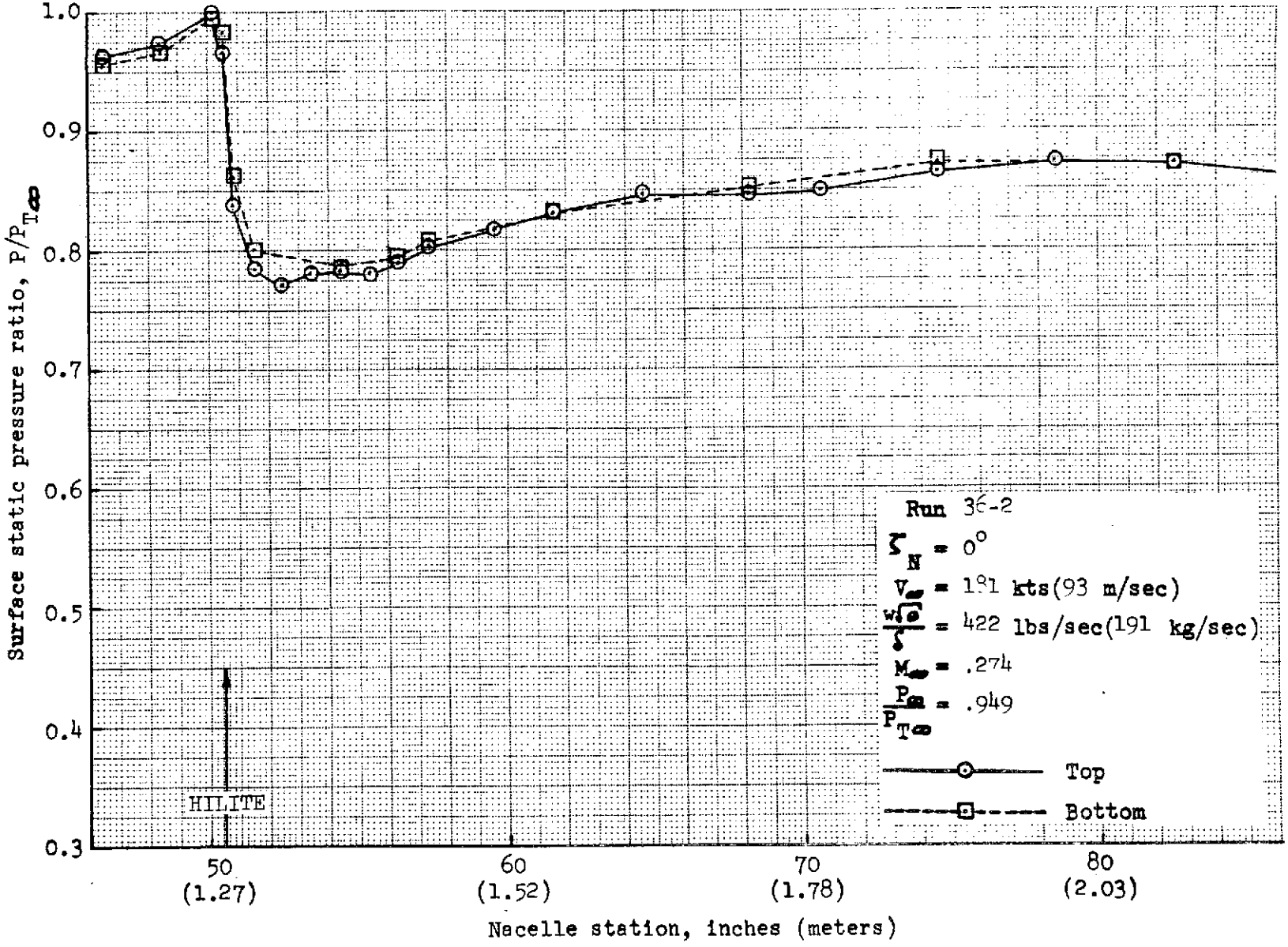

FIGURE 190.- REFAN INLET SURFACE STATIC PRESSURE RATIO DISTRIBUTION

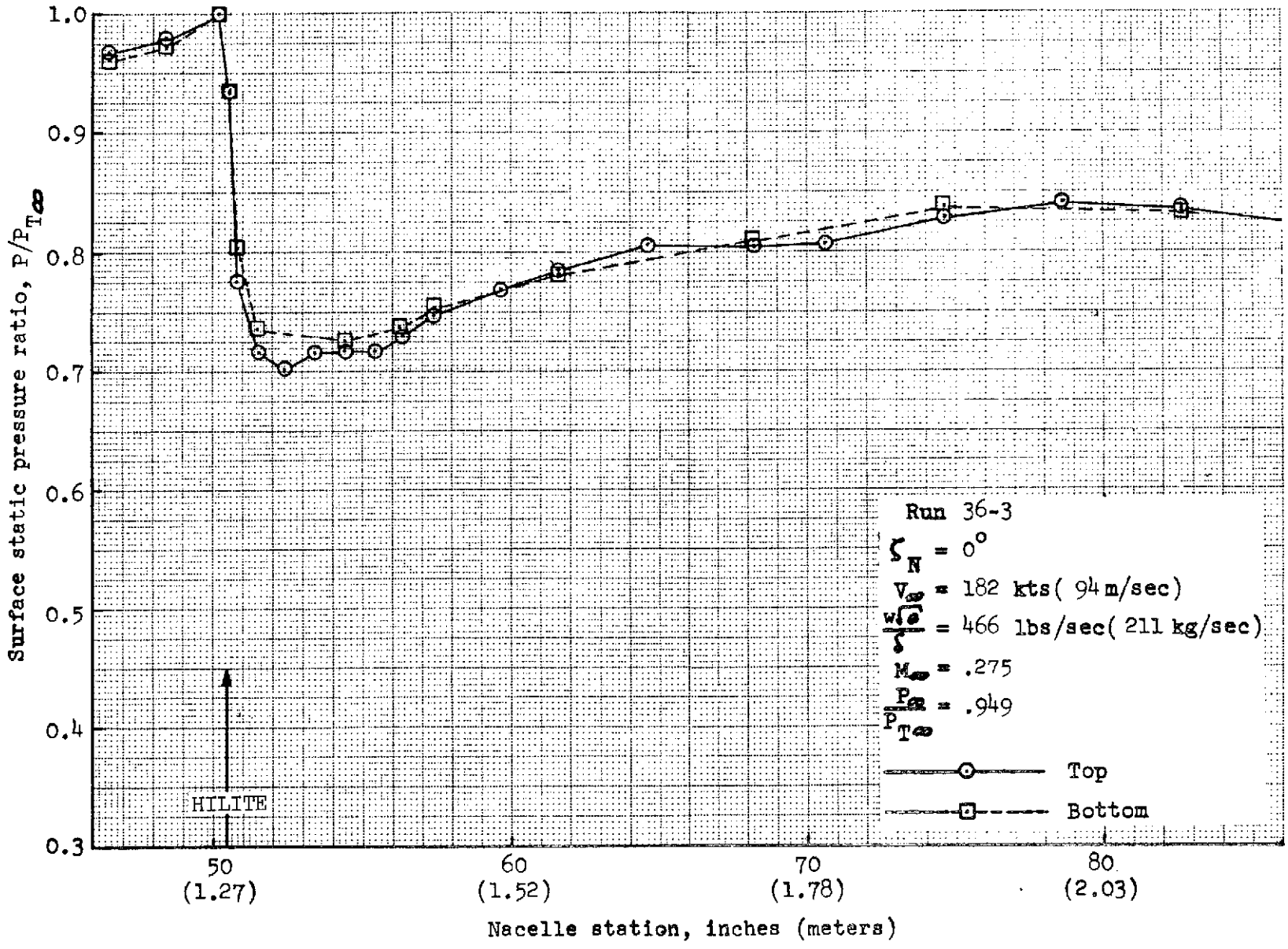

FIGURE 191.- REFAN INLET SURFACE STATIC PRESSURE RATIO DISTRIBUTION

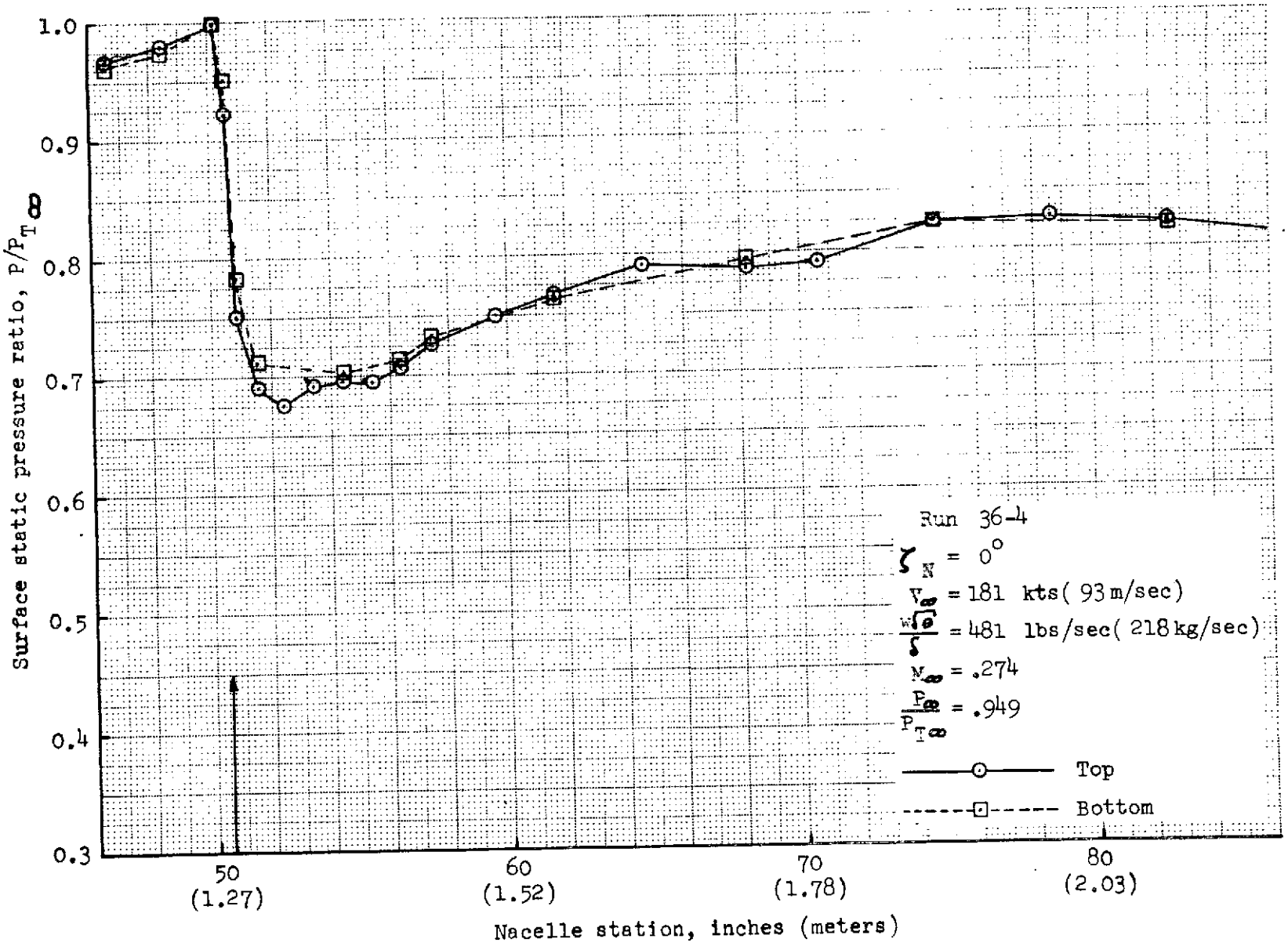

FIGURE 192. - REFAN INLET SURFACE STATIC PRESSURE RATIO DISTRIBUTION

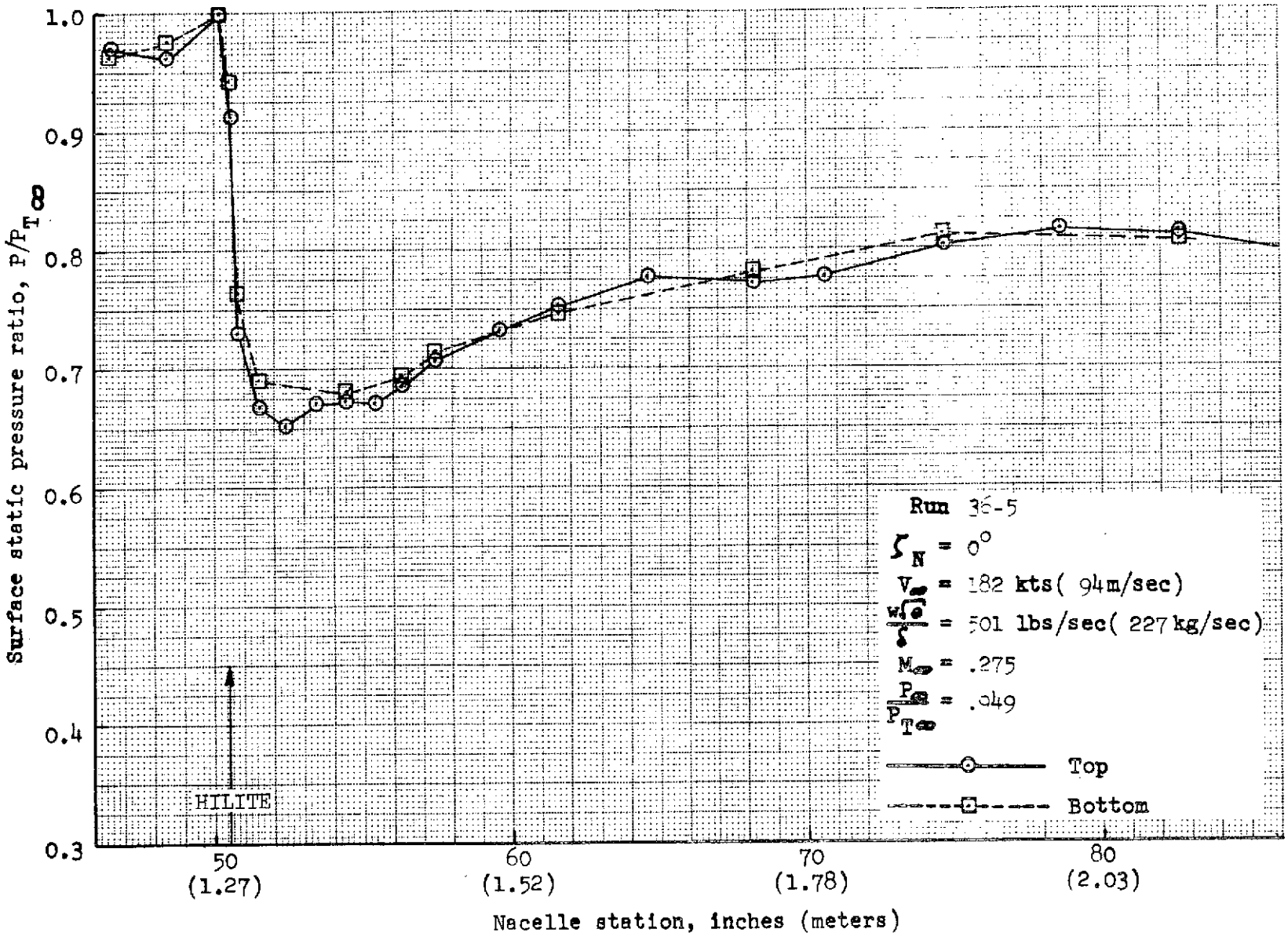

FIGURE 193.- REFAN INLET SURFACE STATIC PRESSURE RATIO DISTRIBUTION

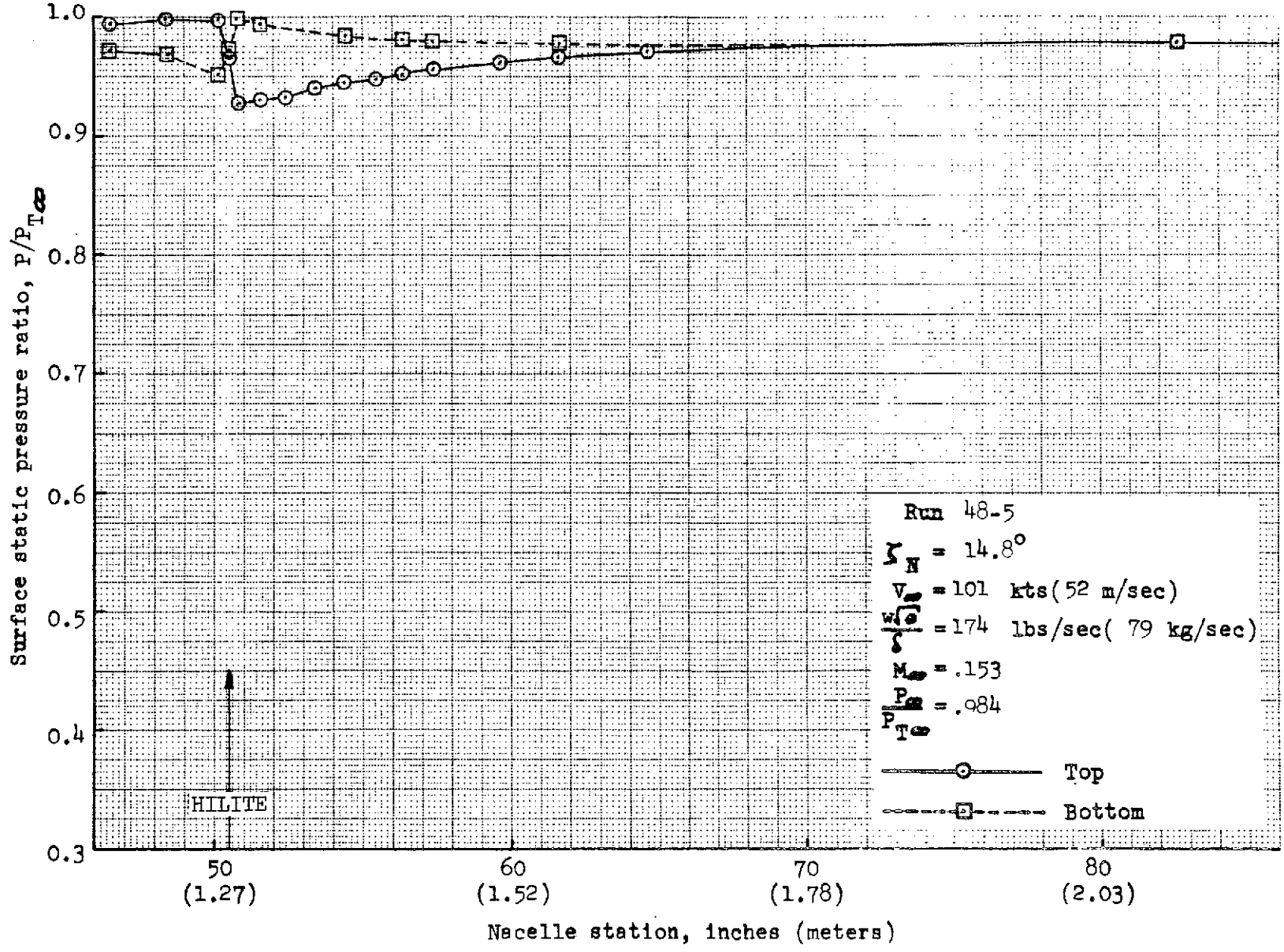

FIGURE 194.- REFAN INLET SURFACE STATIC PRESSURE RATIO DISTRIBUTION

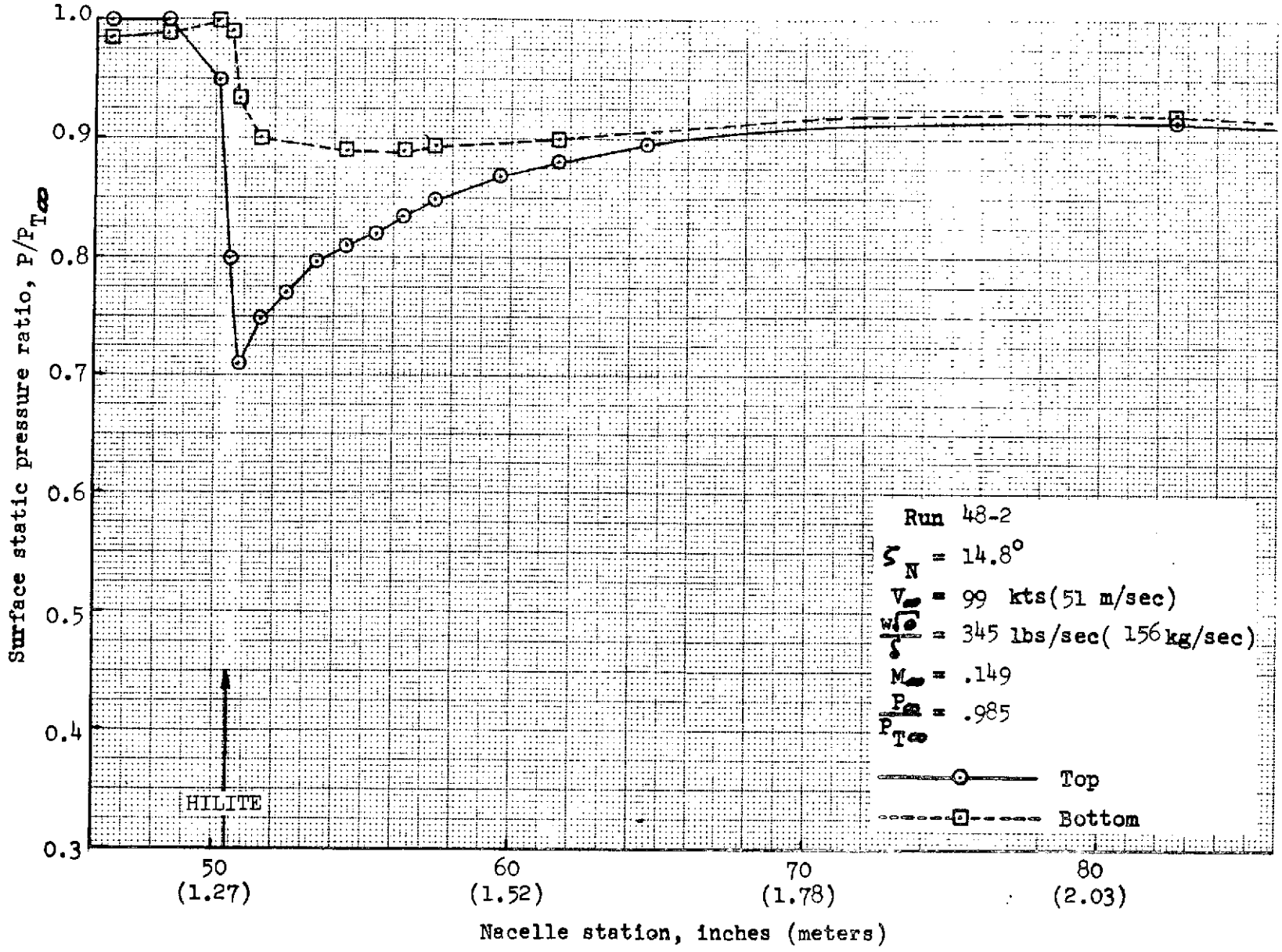

FIGURE 195.- REFAN INLET SURFACE STATIC PRESSURE RATIO DISTRIBUTION

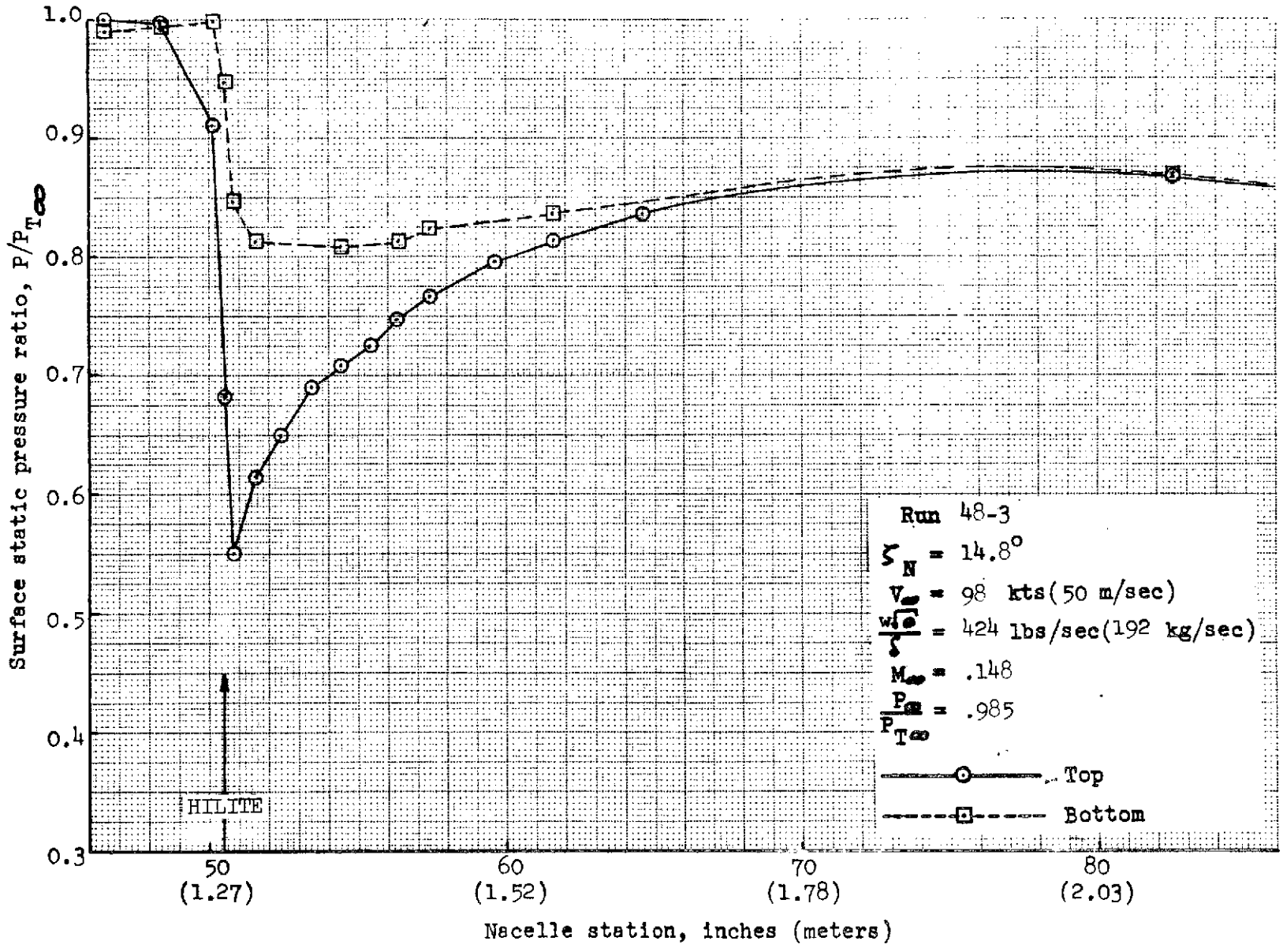

FIGURE 196.- REFAN INLET SURFACE STATIC PRESSURE RATIO DISTRIBUTION

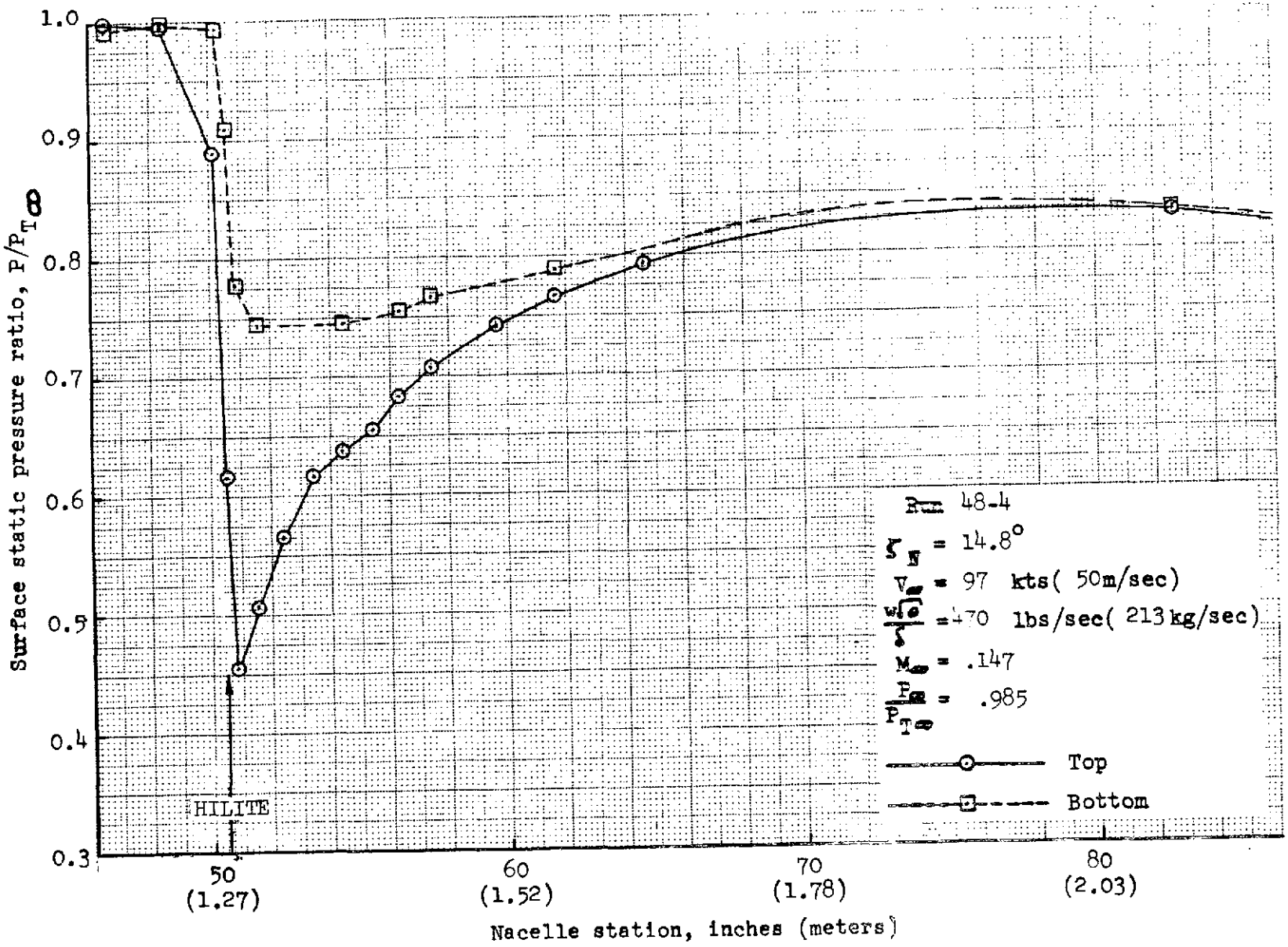

FIGURE 197.- REFAN INLET SURFACE STATIC PRESSURE RATIO DISTRIBUTION

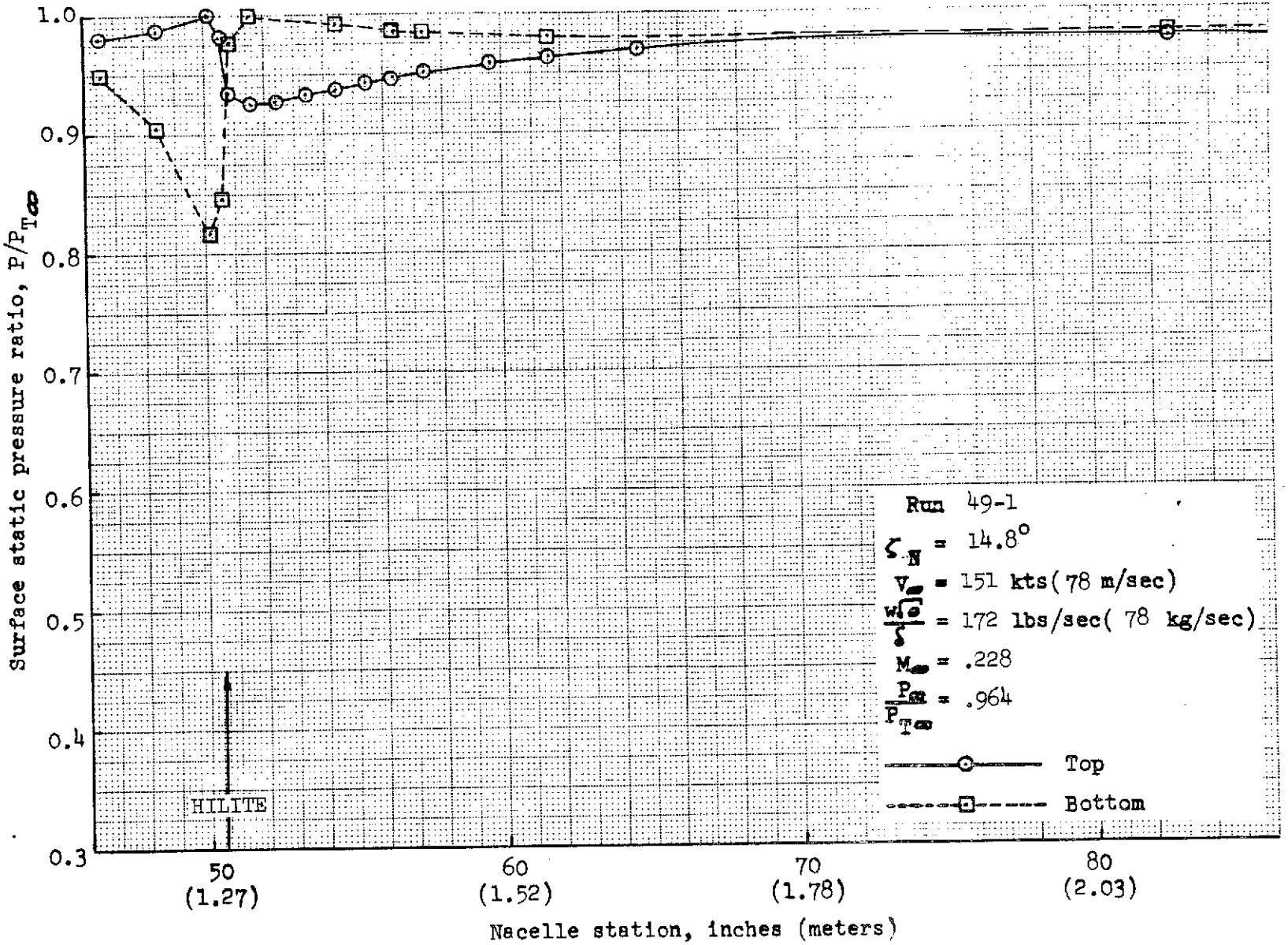

FIGURE 198.- REFAN INLET SURFACE STATIC PRESSURE RATIO DISTRIBUTION

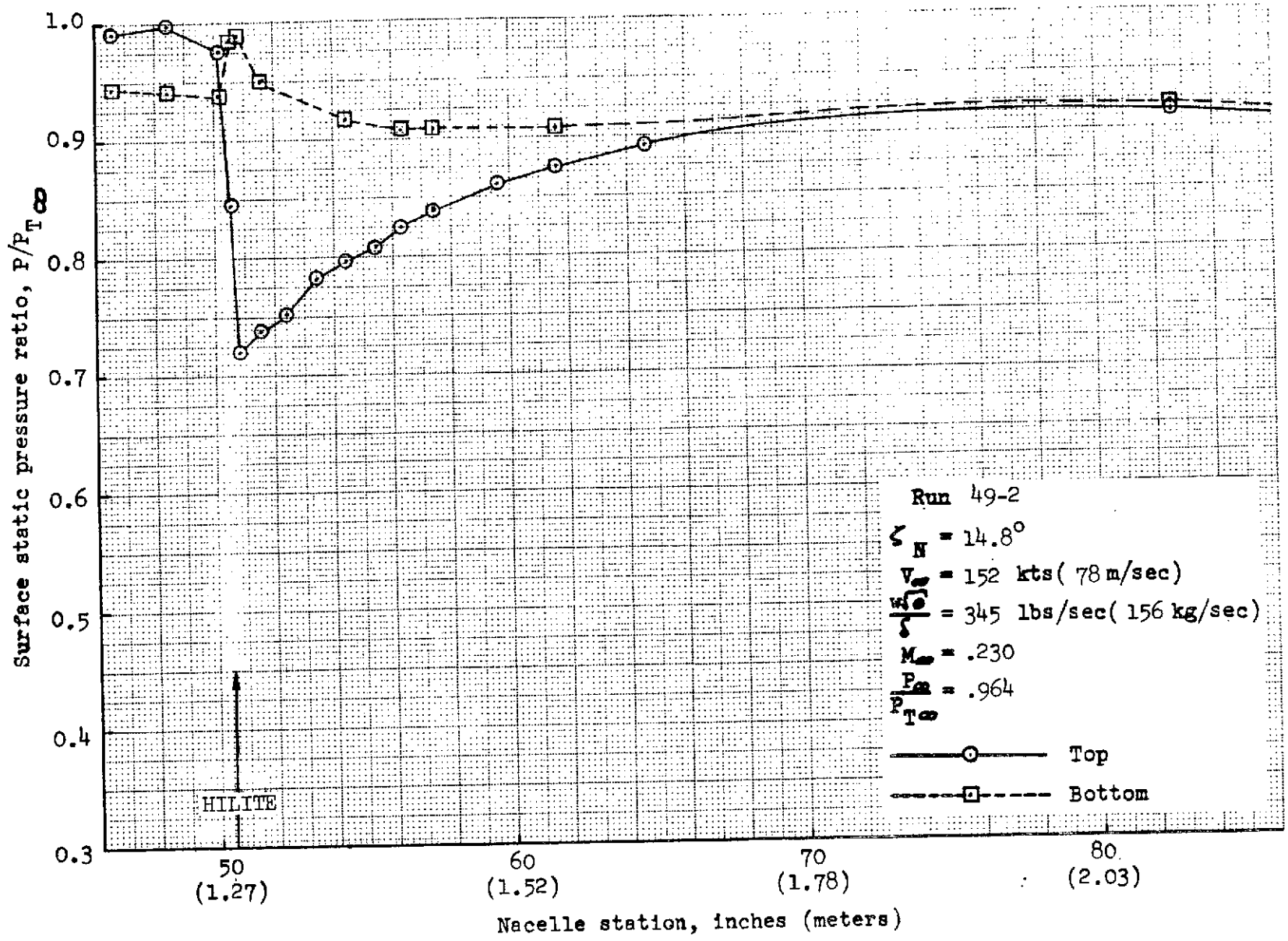

FIGURE 199.- REFAN INLET SURFACE STATIC PRESSURE RATIO DISTRIBUTION

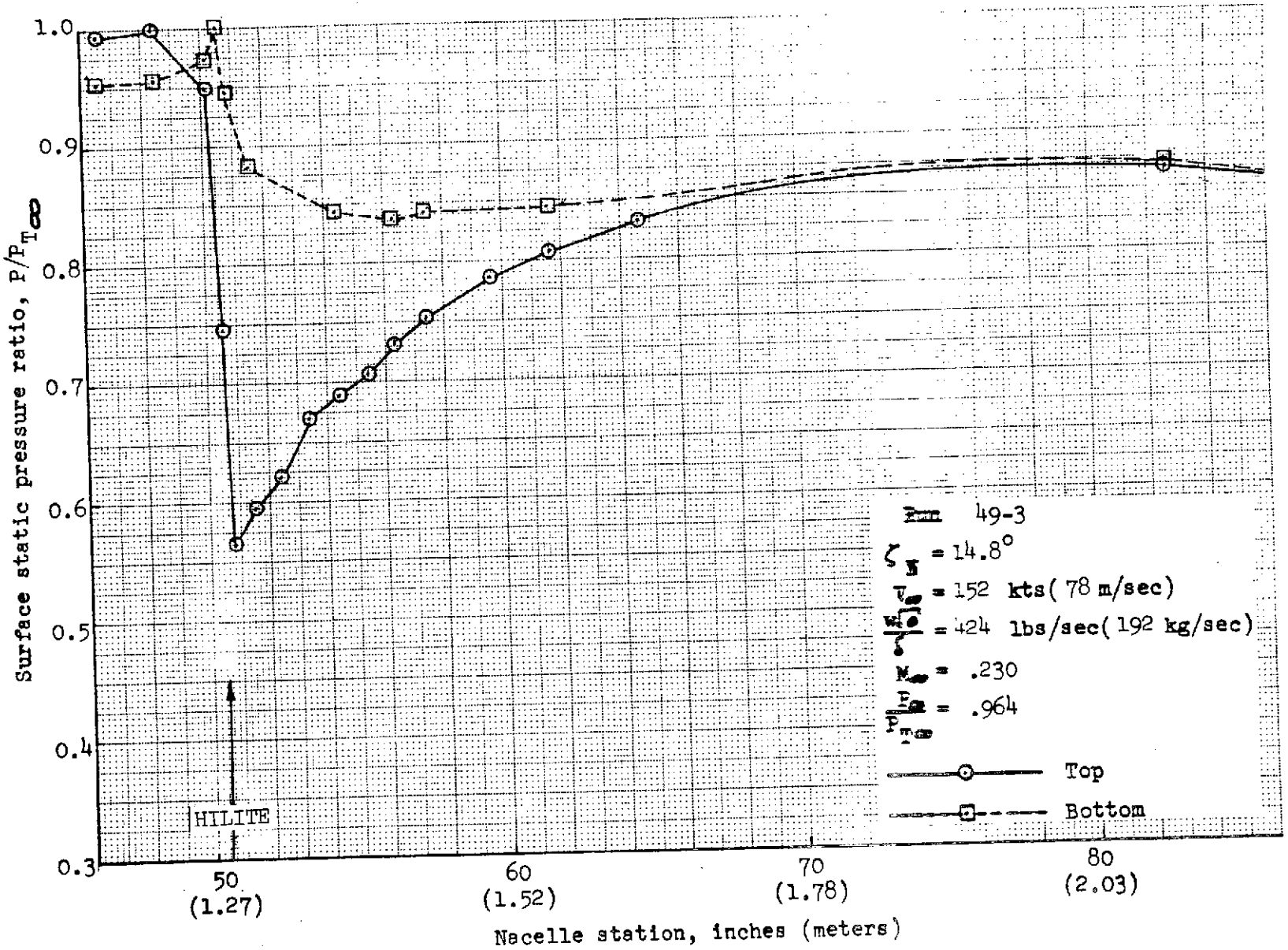

FIGURE 200.- REFAN INLET SURFACE STATIC PRESSURE RATIO DISTRIBUTION

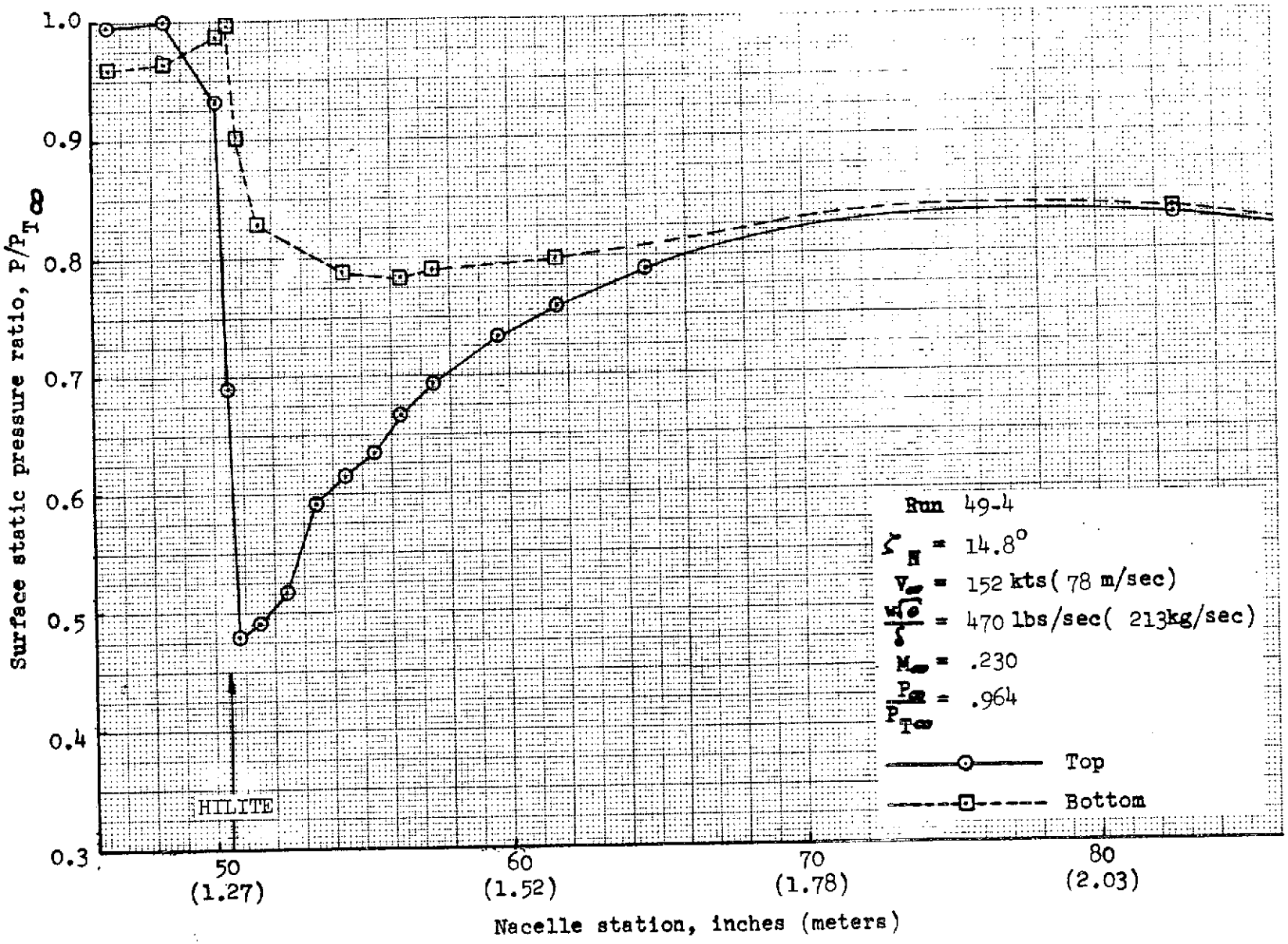

FIGURE 201.- REFAN INLET SURFACE STATIC PRESSURE RATIO DISTRIBUTION

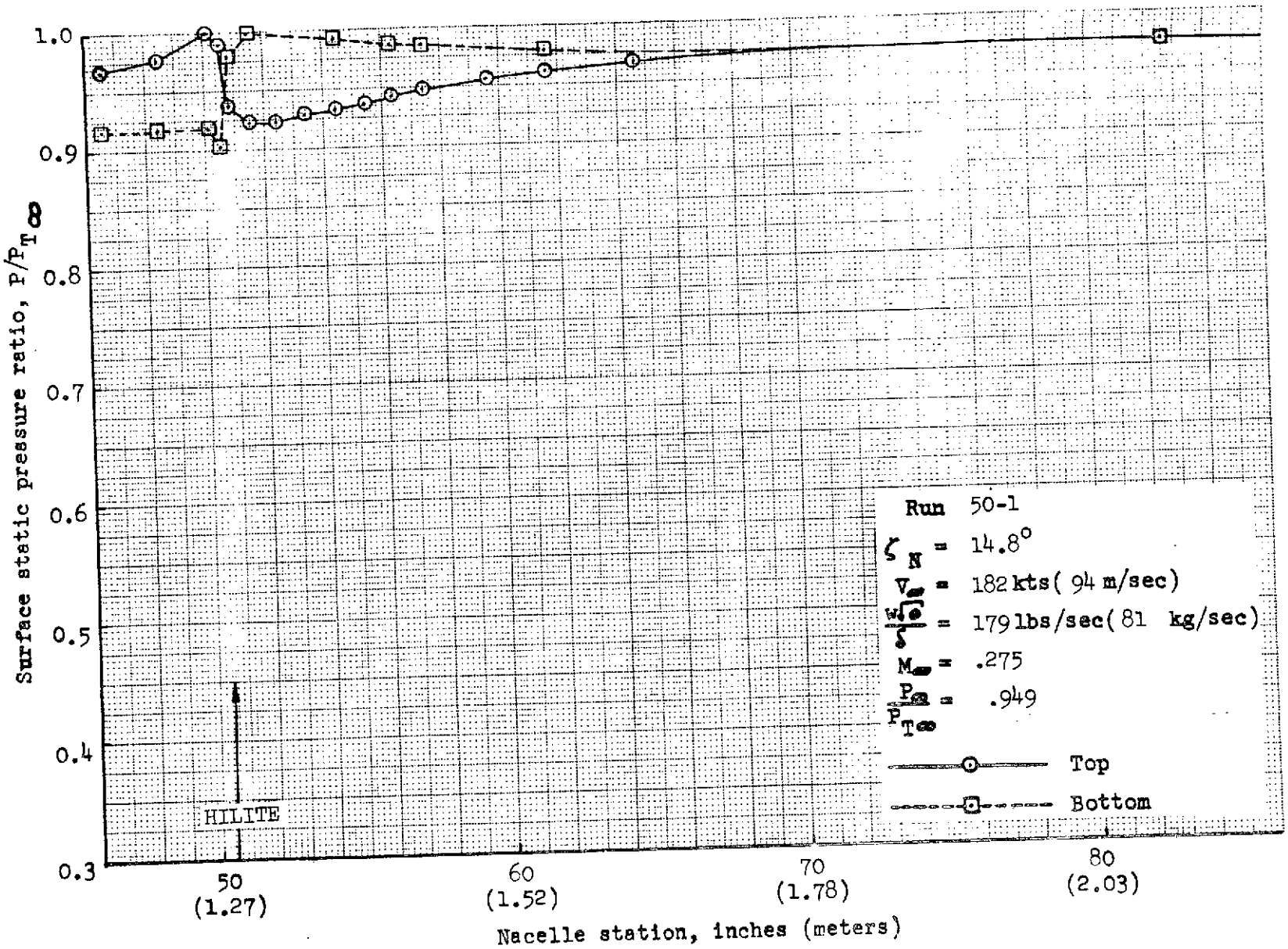

FIGURE 202.- REFAN INLET SURFACE STATIC PRESSURE RATIO DISTRIBUTION

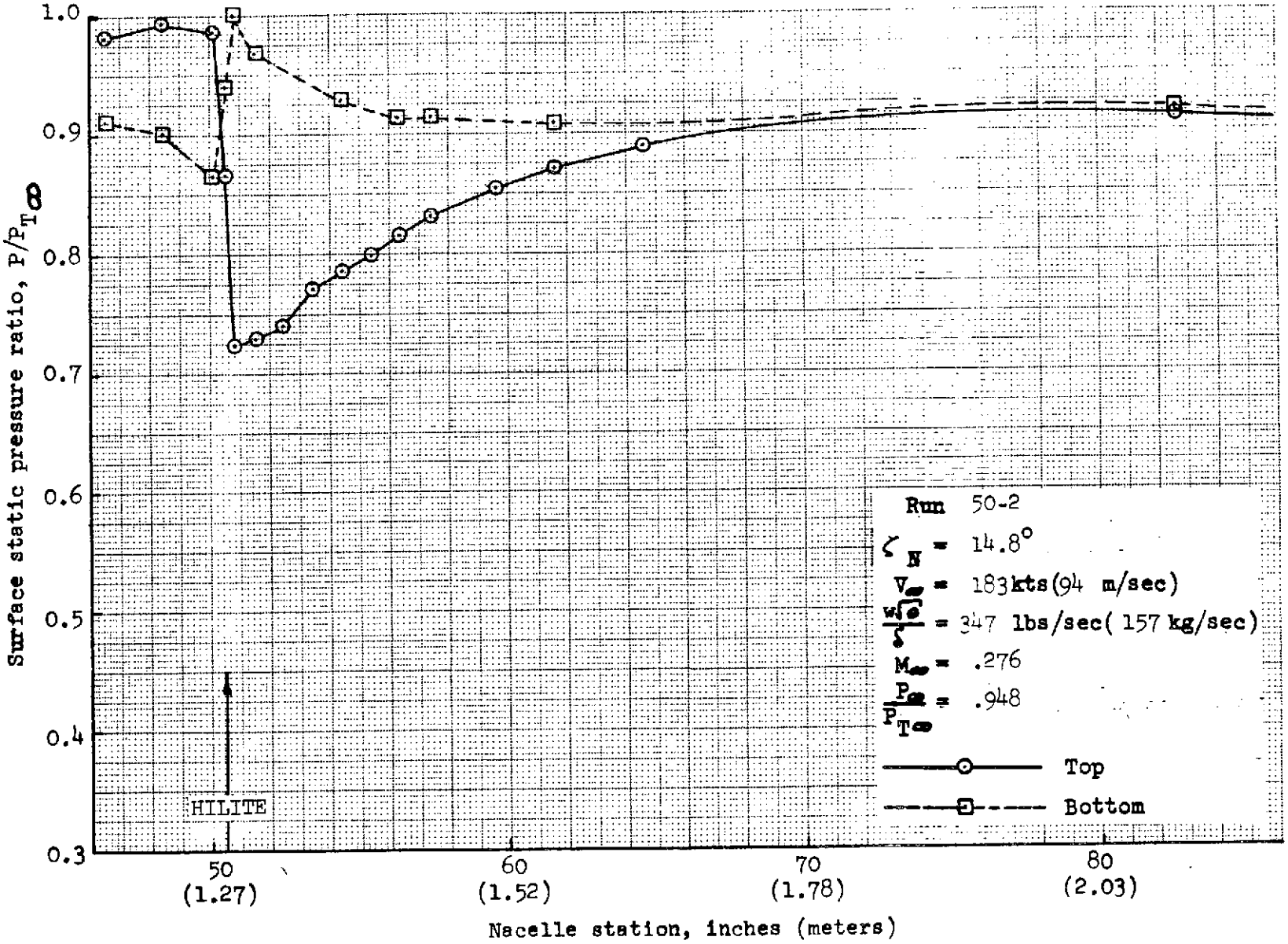

FIGURE 203.- REFAN INLET SURFACE STATIC PRESSURE RATIO DISTRIBUTION

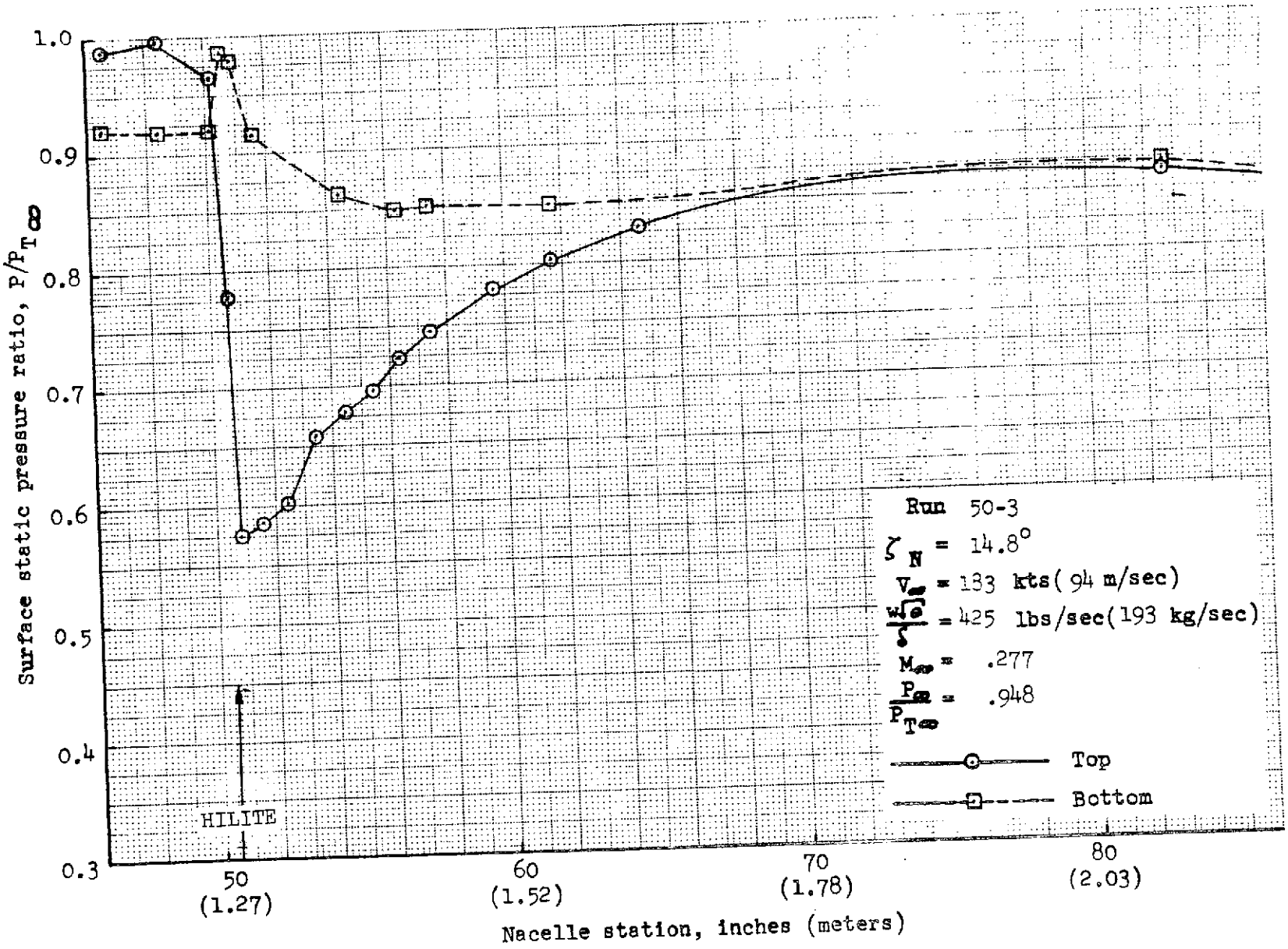

FIGURE 204. - REFAN INLET SURFACE STATIC PRESSURE RATIO DISTRIBUTION

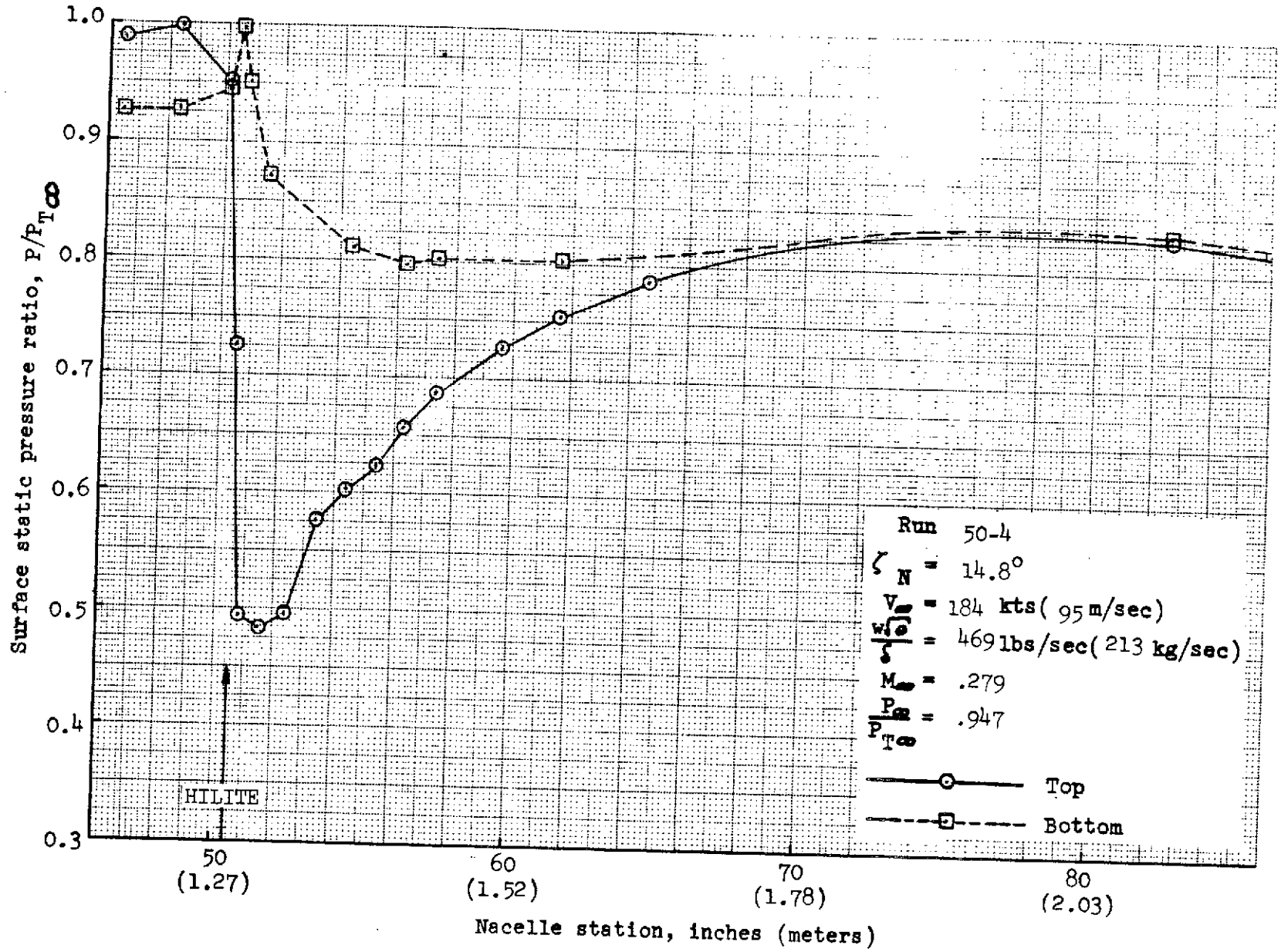

FIGURE 205.- REFAN INLET SURFACE STATIC PRESSURE RATIO DISTRIBUTION

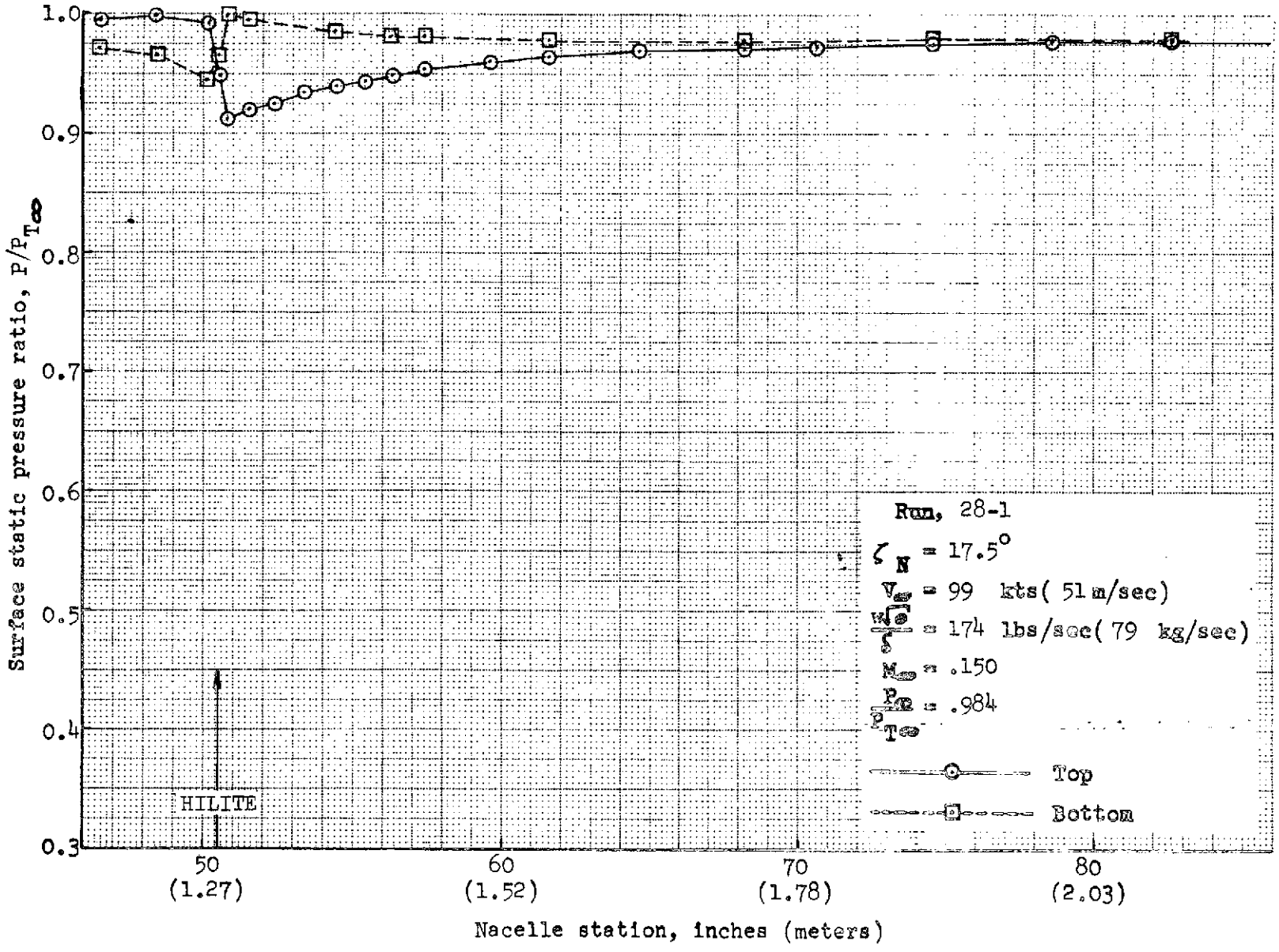

FIGURE 206.- REFAN INLET SURFACE STATIC PRESSURE RATIO DISTRIBUTION

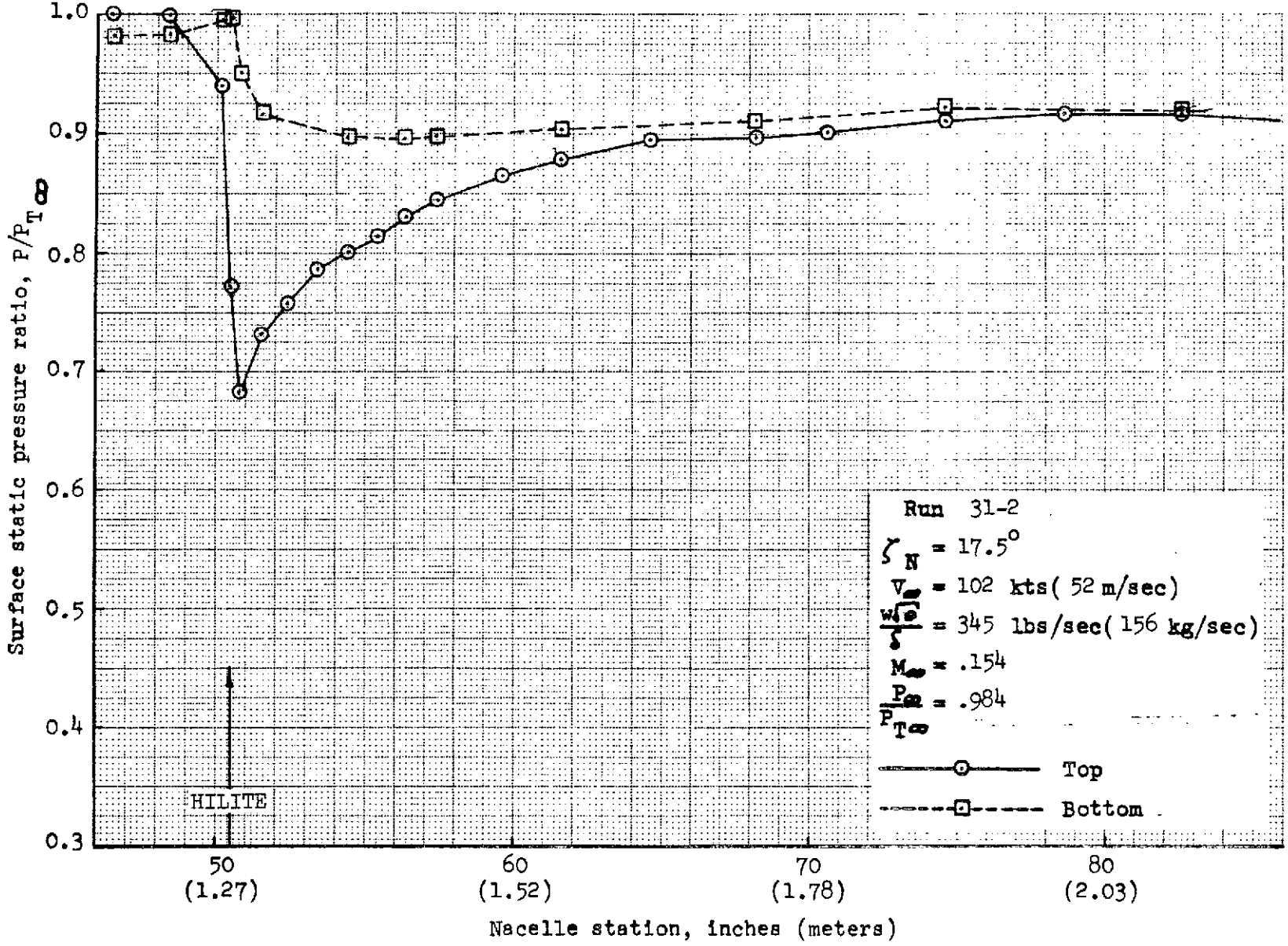

FIGURE 207.- REFAN INLET SURFACE STATIC PRESSURE RATIO DISTRIBUTION

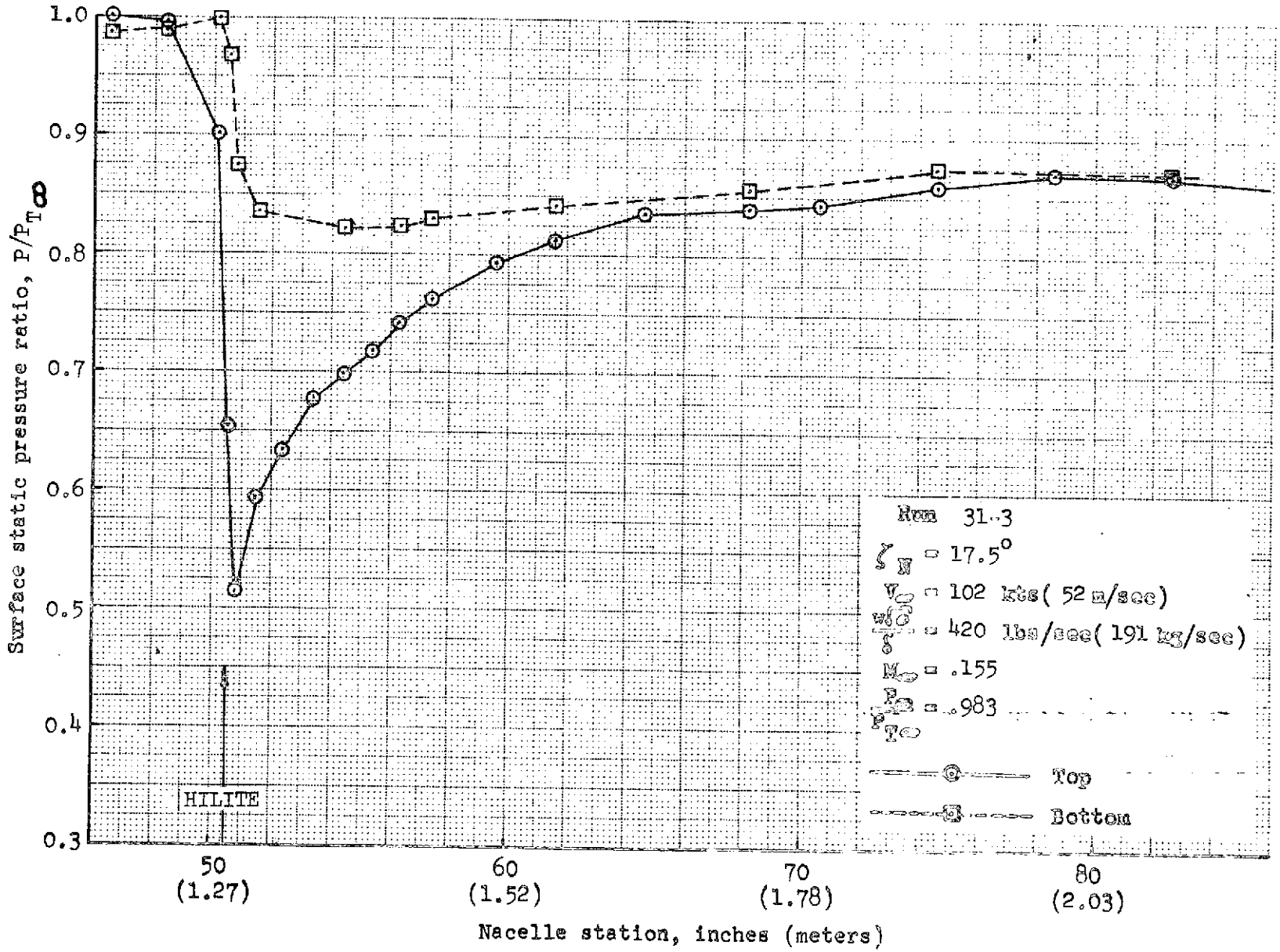

FIGURE 208.- REFAN INLET SURFACE STATIC PRESSURE RATIO DISTRIBUTION

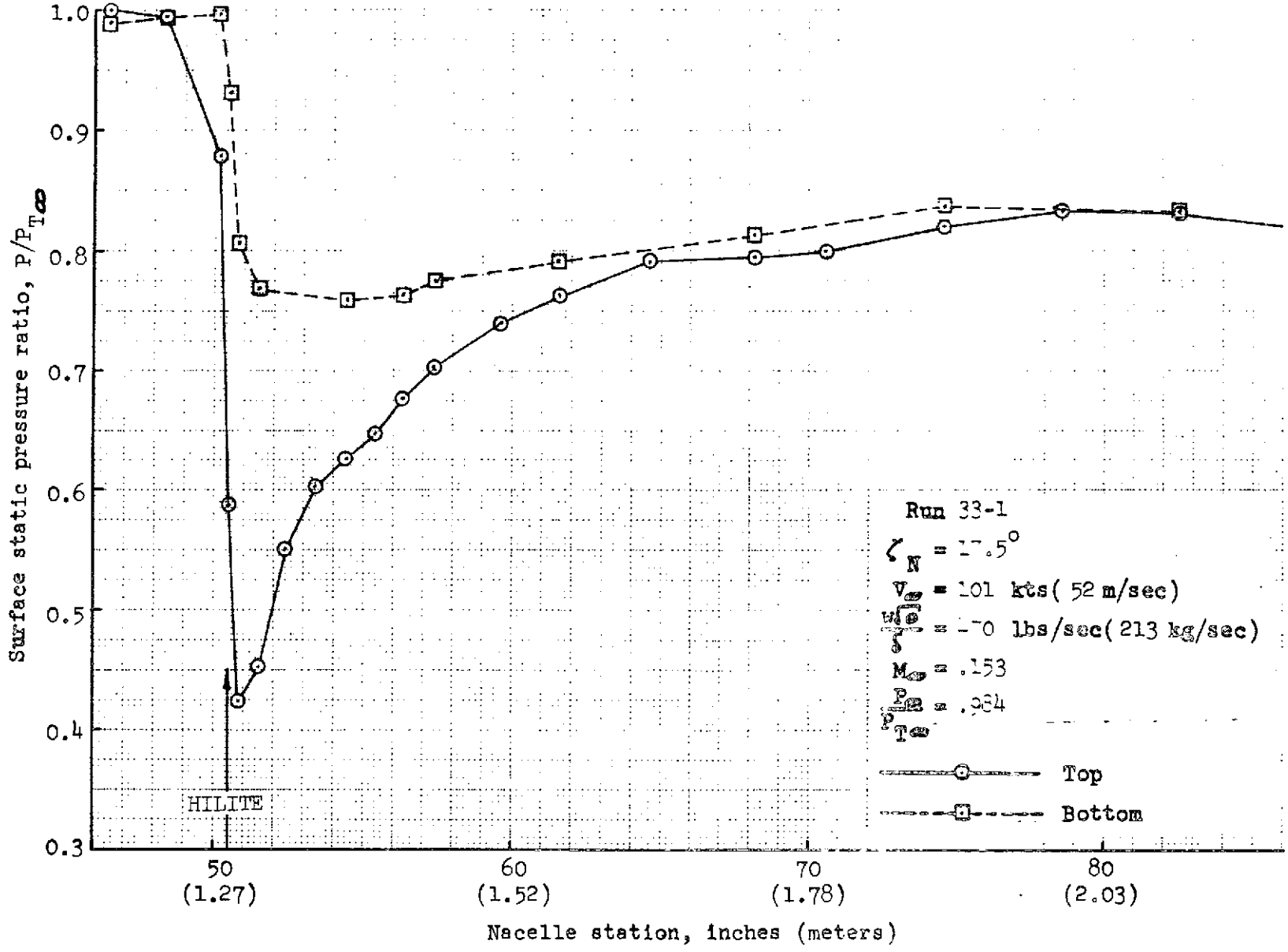

FIGURE 209.- REFAN INLET SURFACE STATIC PRESSURE RATIO DISTRIBUTION

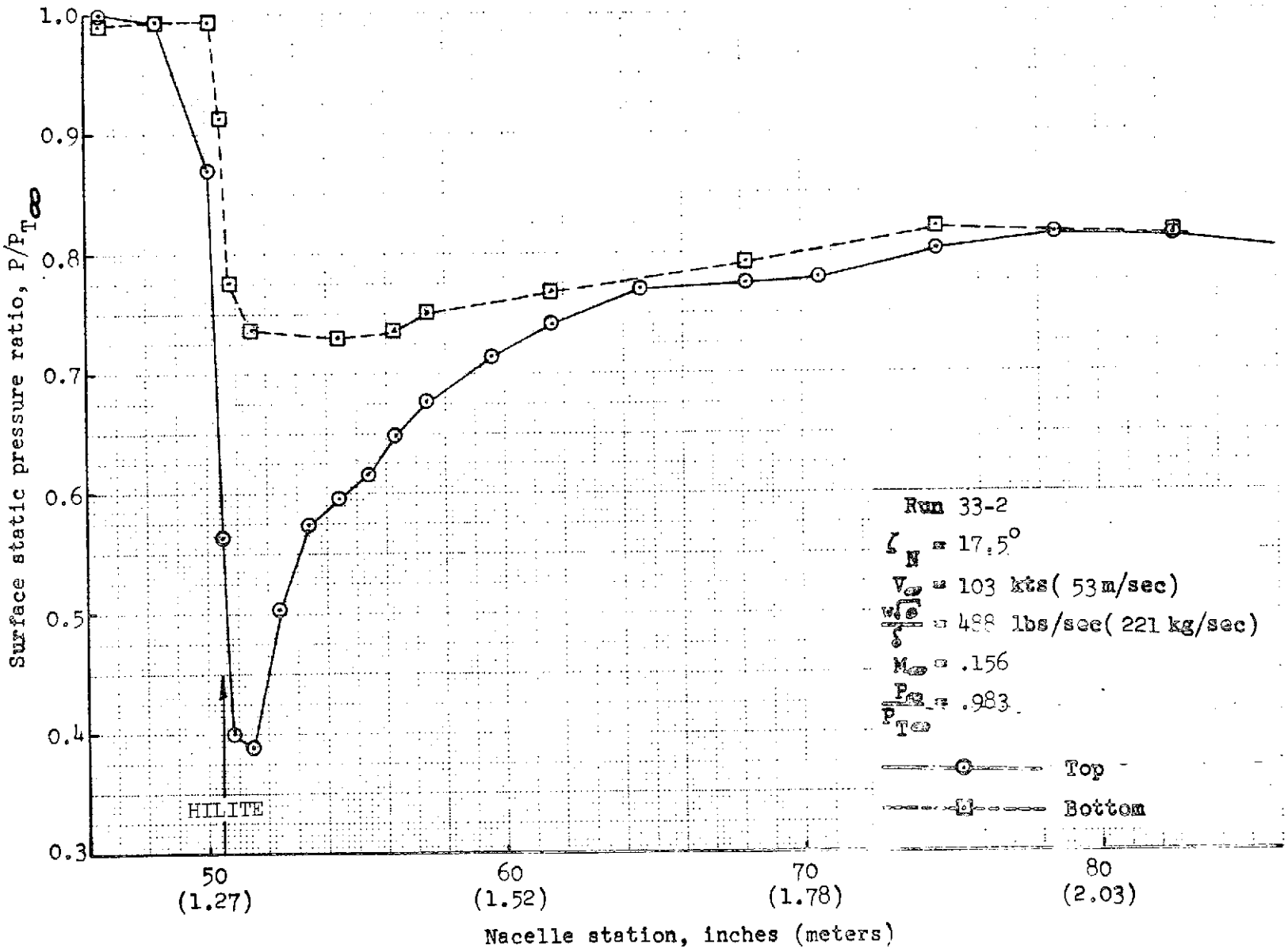

FIGURE 210.- REFAN INLET SURFACE STATIC PRESSURE RATIO DISTRIBUTION

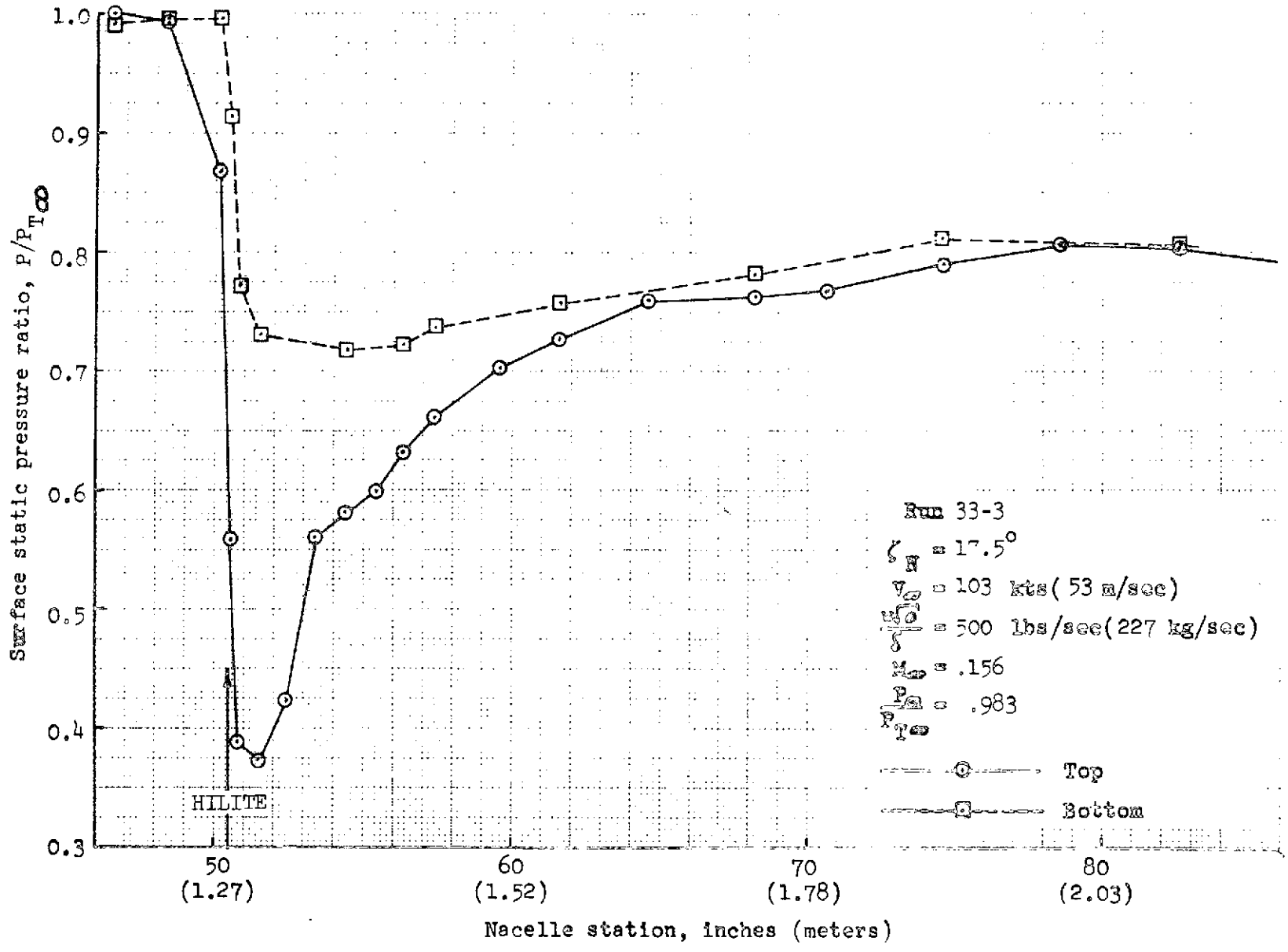

FIGURE 211.- REFAN INLET SURFACE STATIC PRESSURE RATIO DISTRIBUTION

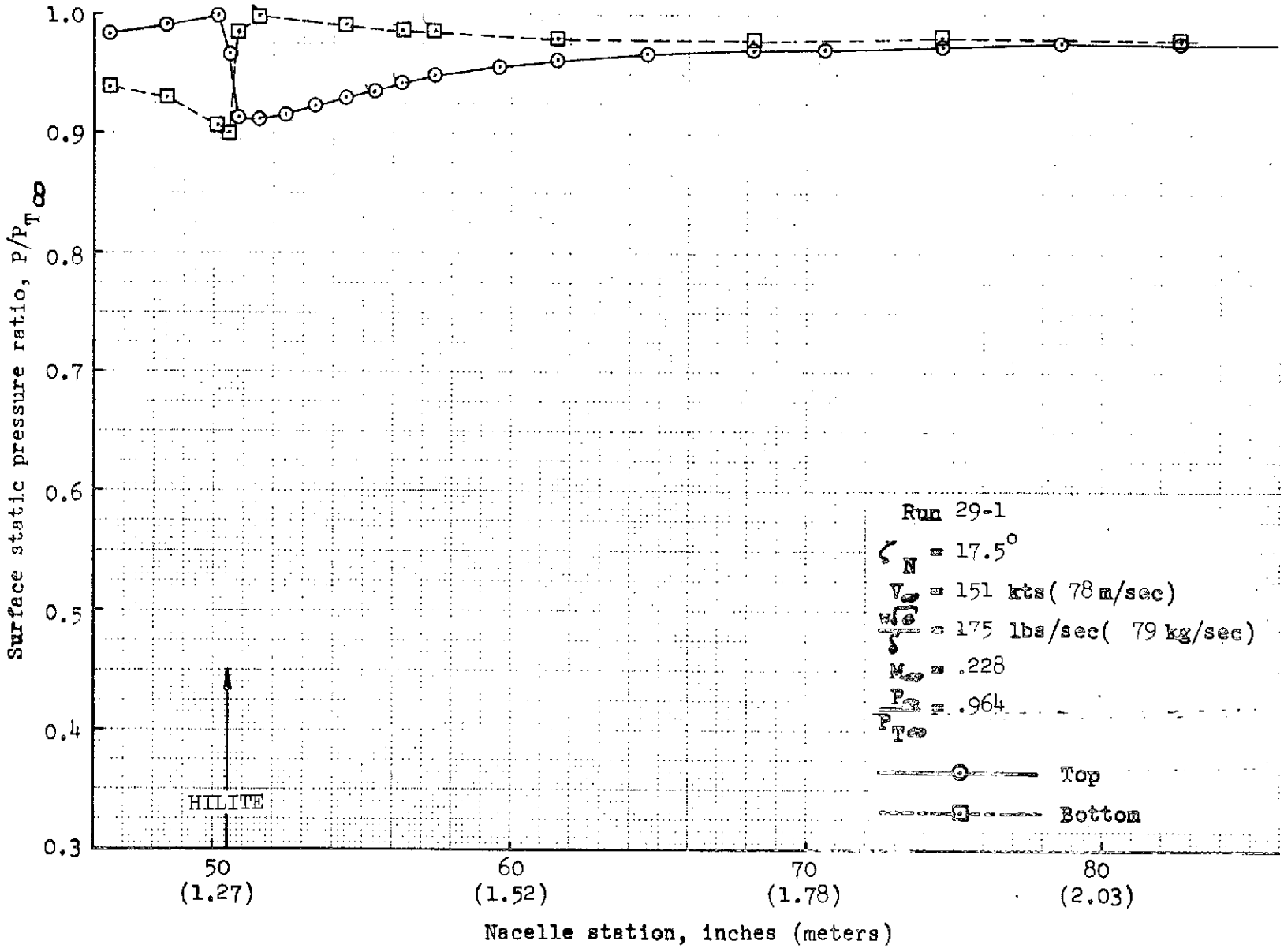

FIGURE 212.- REFAN INLET SURFACE STATIC PRESSURE RATIO DISTRIBUTION

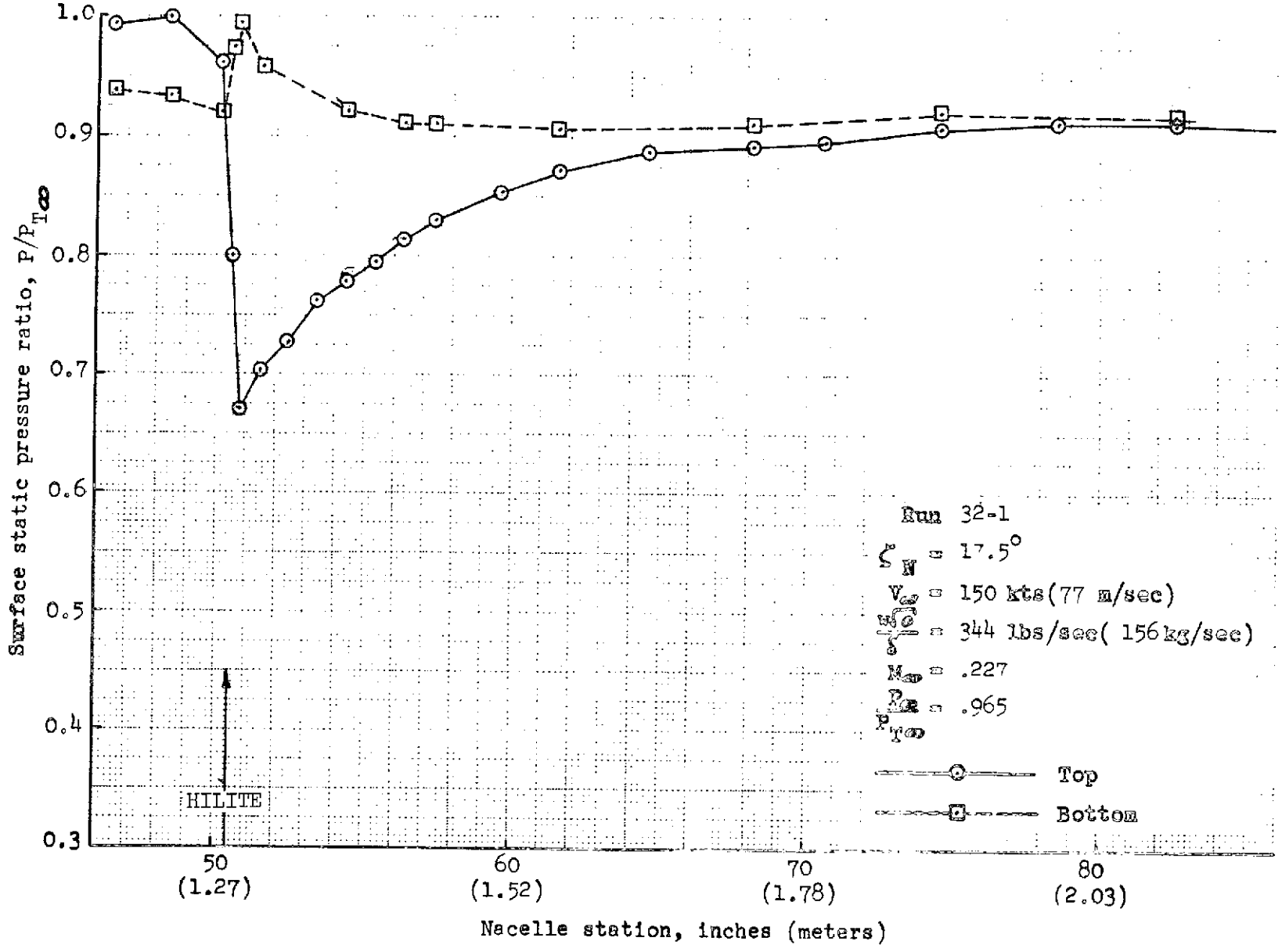

FIGURE 213.- REFAN INLET SURFACE STATIC PRESSURE RATIO DISTRIBUTION

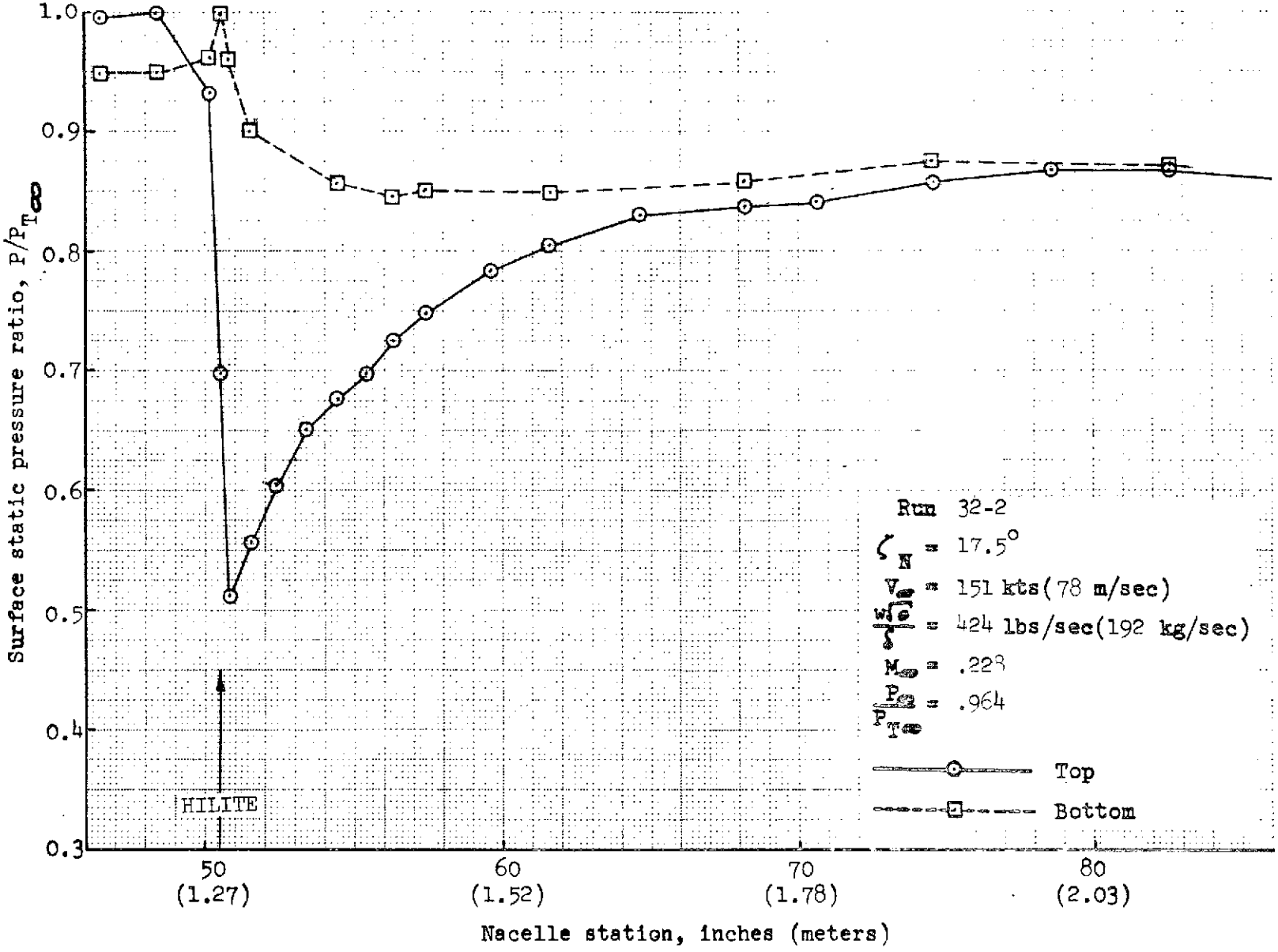

FIGURE 214.- REFAN INLET SURFACE STATIC PRESSURE RATIO DISTRIBUTION

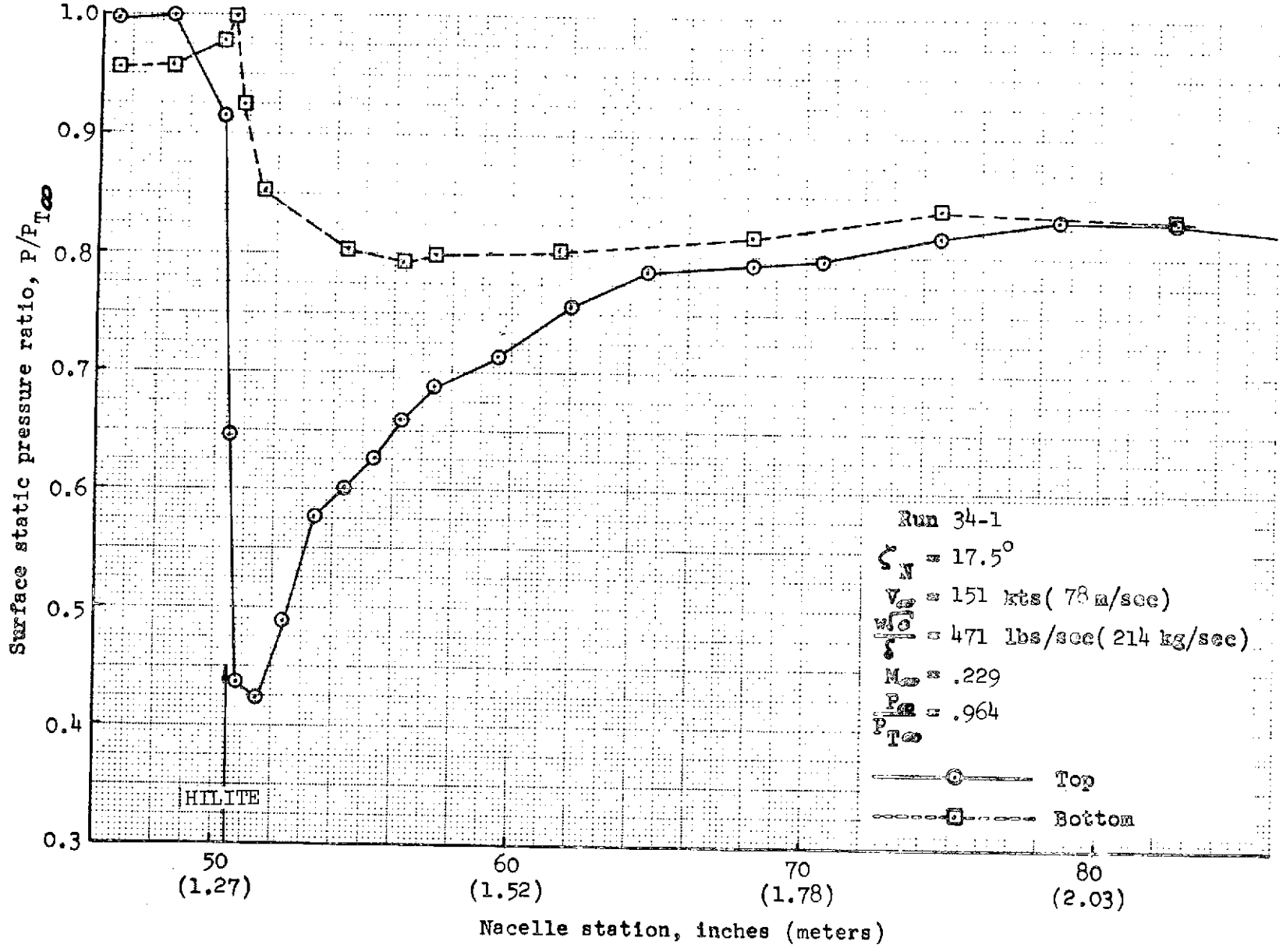

FIGURE 215.- REFAN INLET SURFACE STATIC PRESSURE RATIO DISTRIBUTION

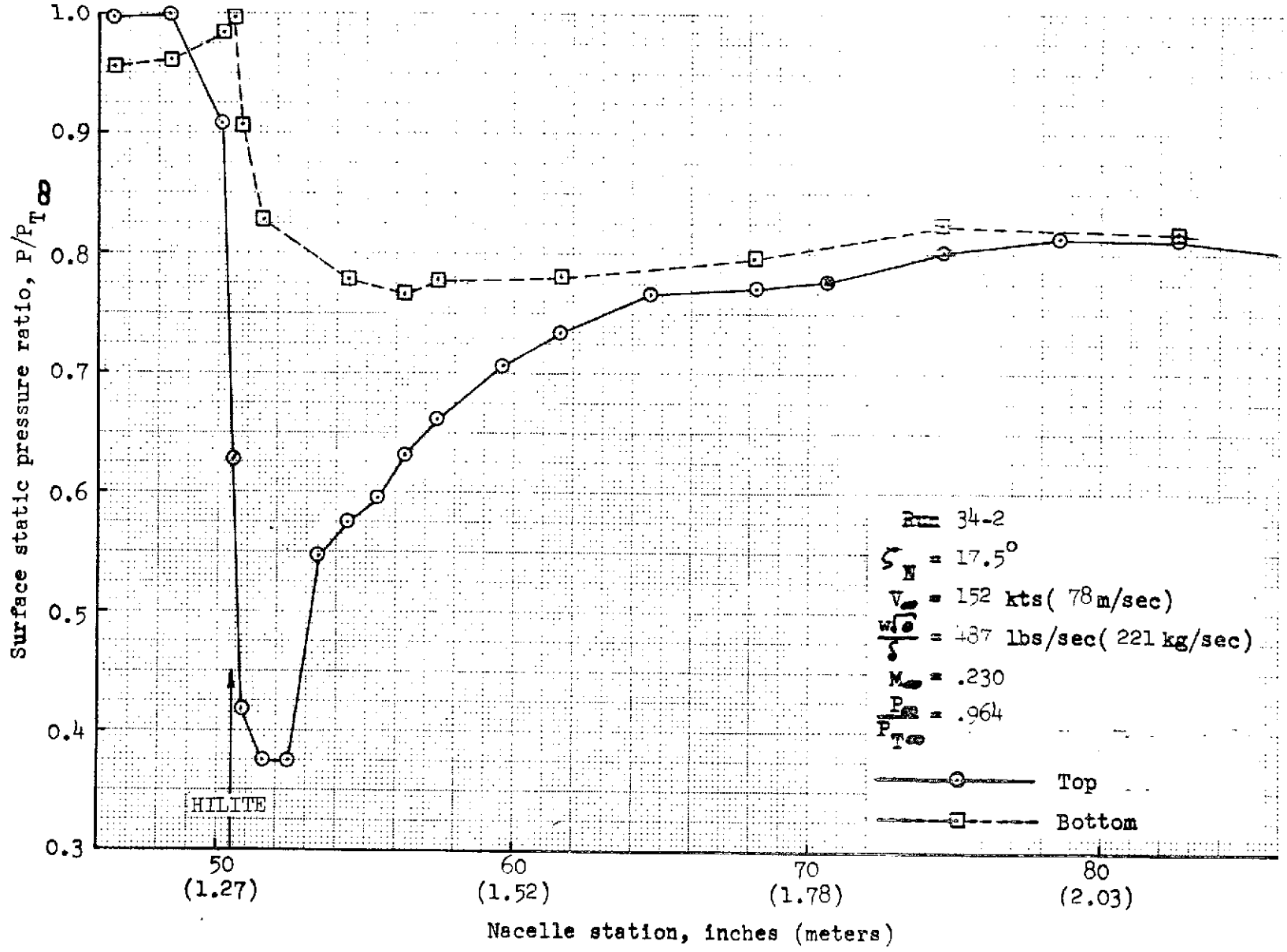

FIGURE 216.- REFAN INLET SURFACE STATIC PRESSURE RATIO DISTRIBUTION

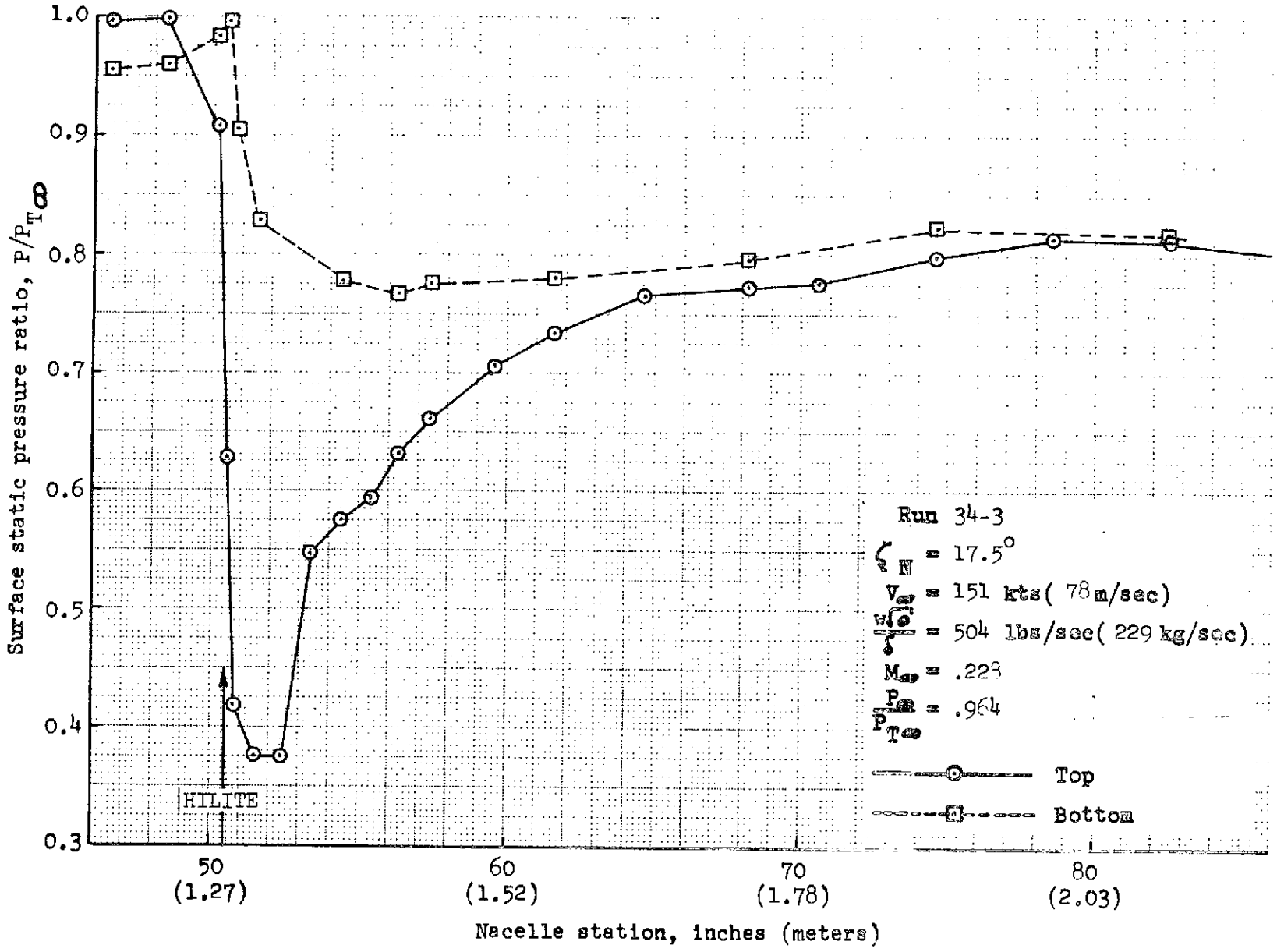

FIGURE 217.- REFAN INLET SURFACE STATIC PRESSURE RATIO DISTRIBUTION

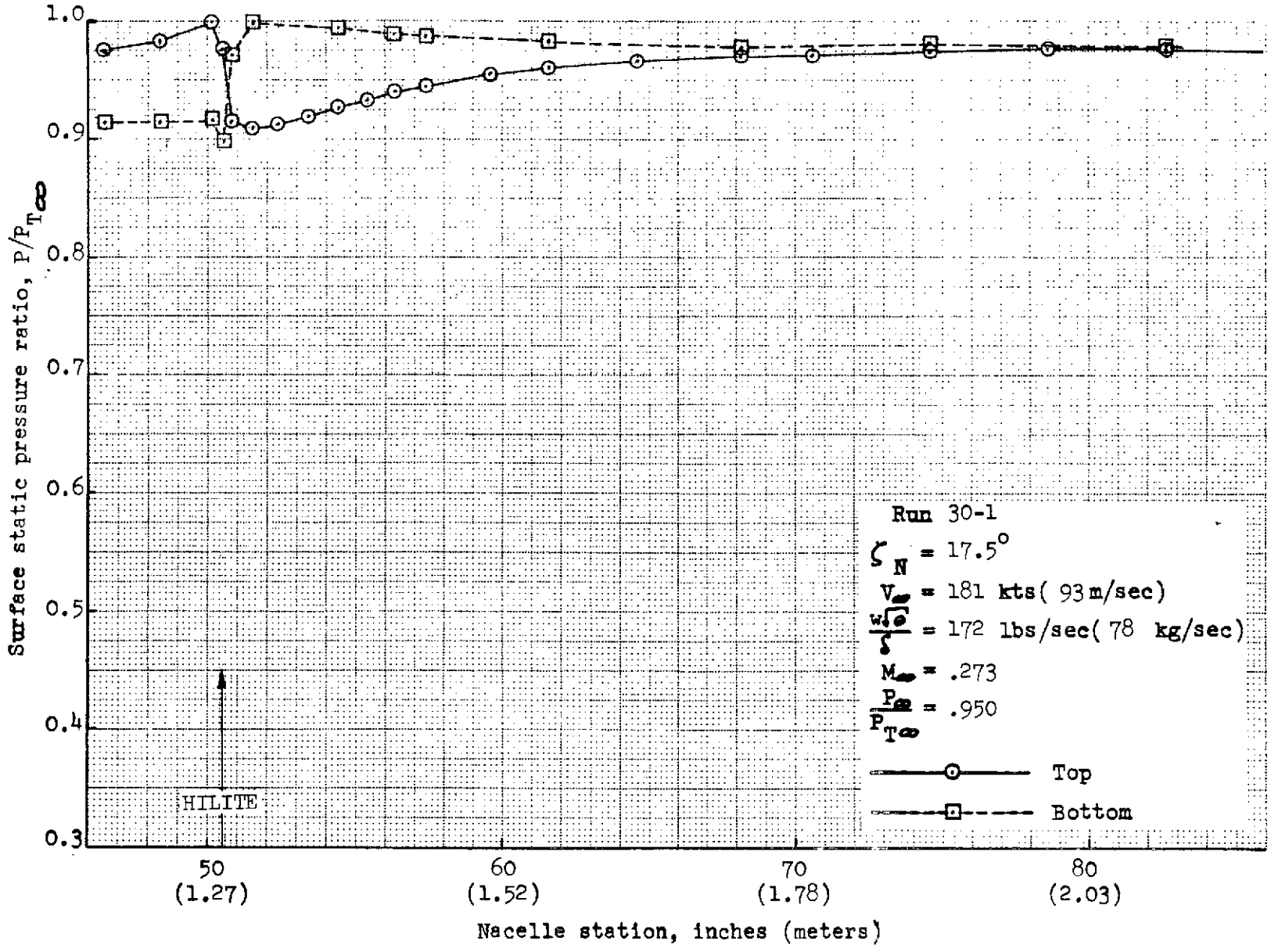

FIGURE 218.- REFAN INLET SURFACE STATIC PRESSURE RATIO DISTRIBUTION

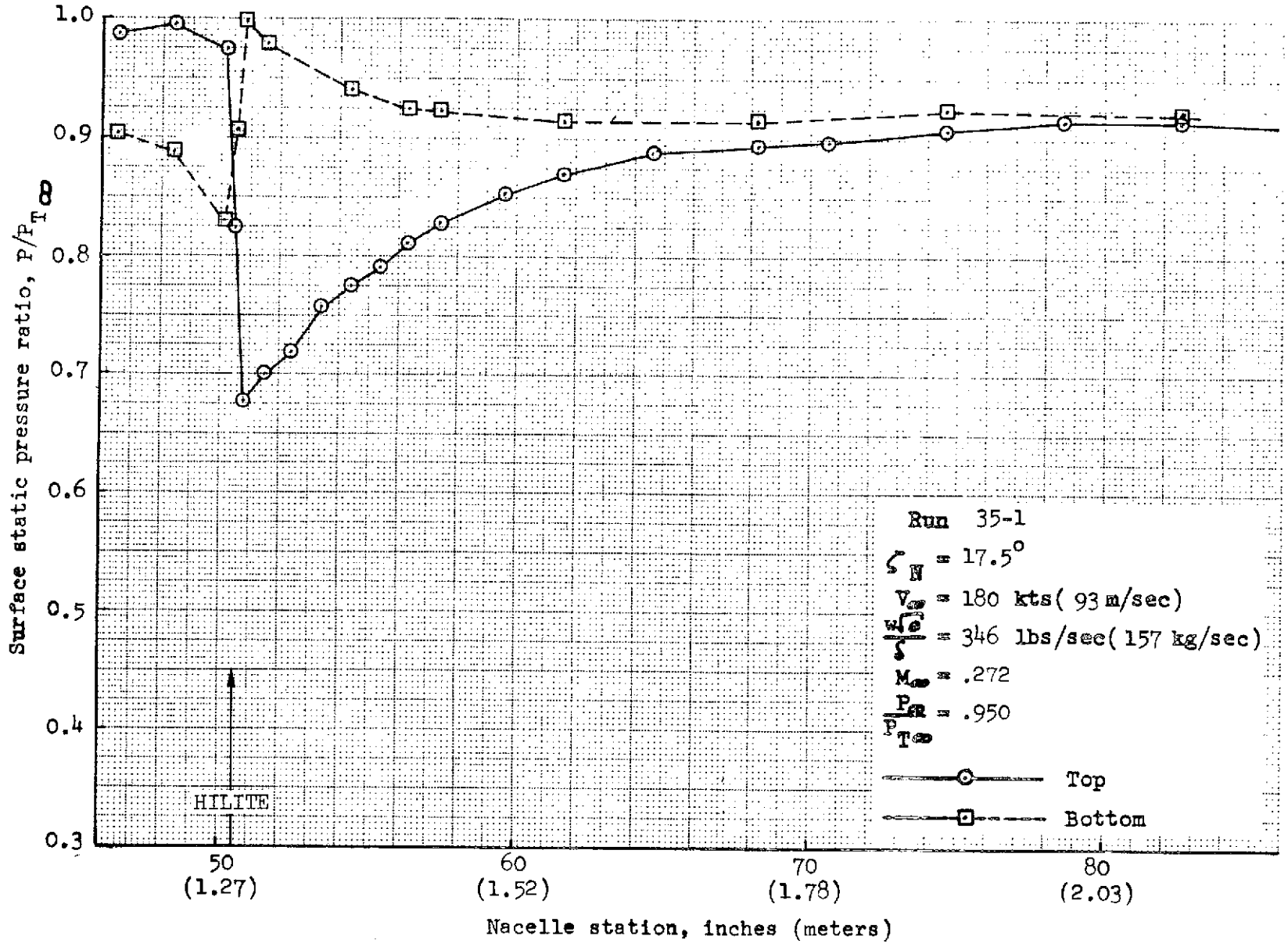

FIGURE 219.- REFAN INLET SURFACE STATIC PRESSURE RATIO DISTRIBUTION

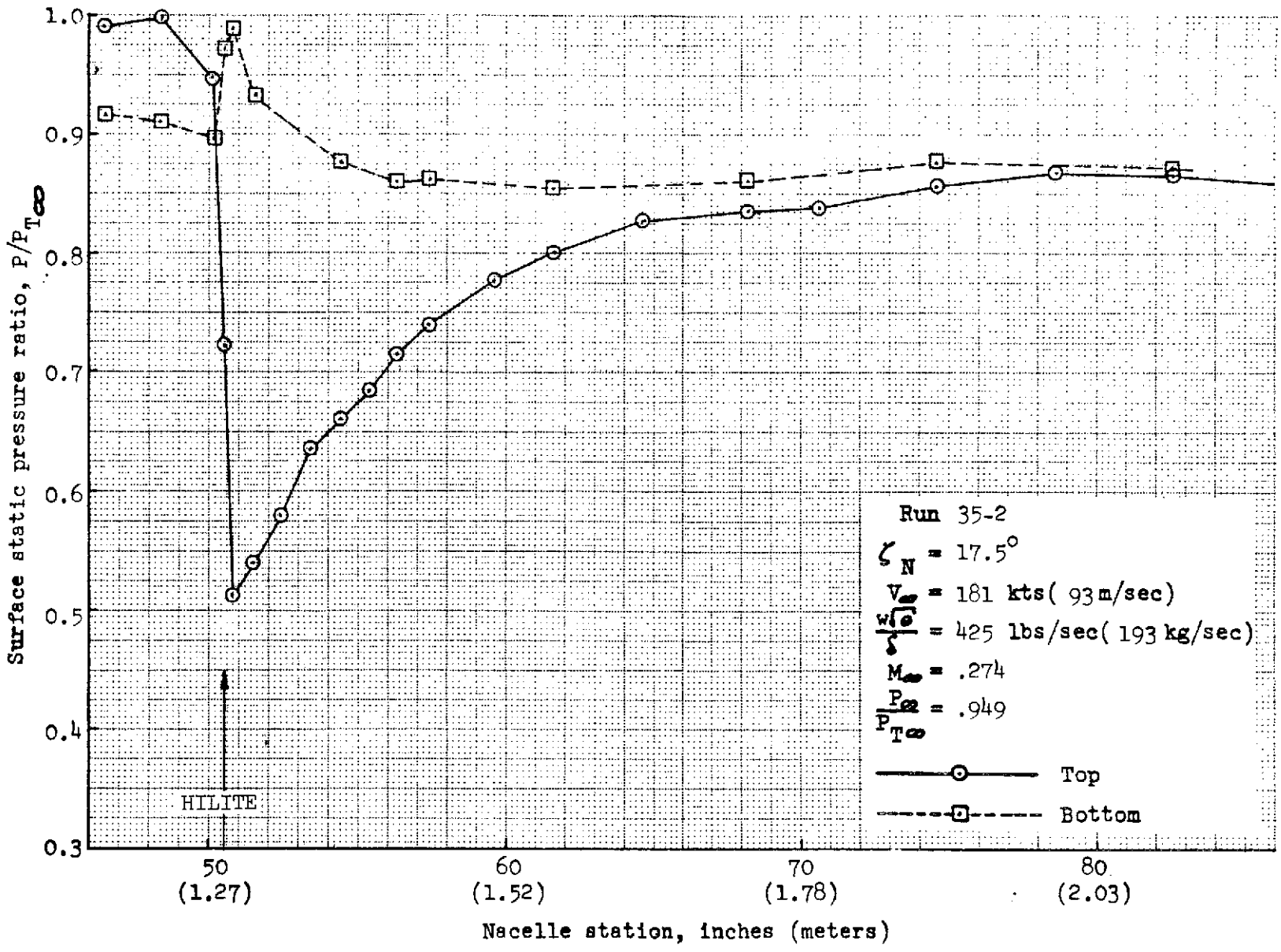

FIGURE 220.- REFAN INLET SURFACE STATIC PRESSURE RATIO DISTRIBUTION

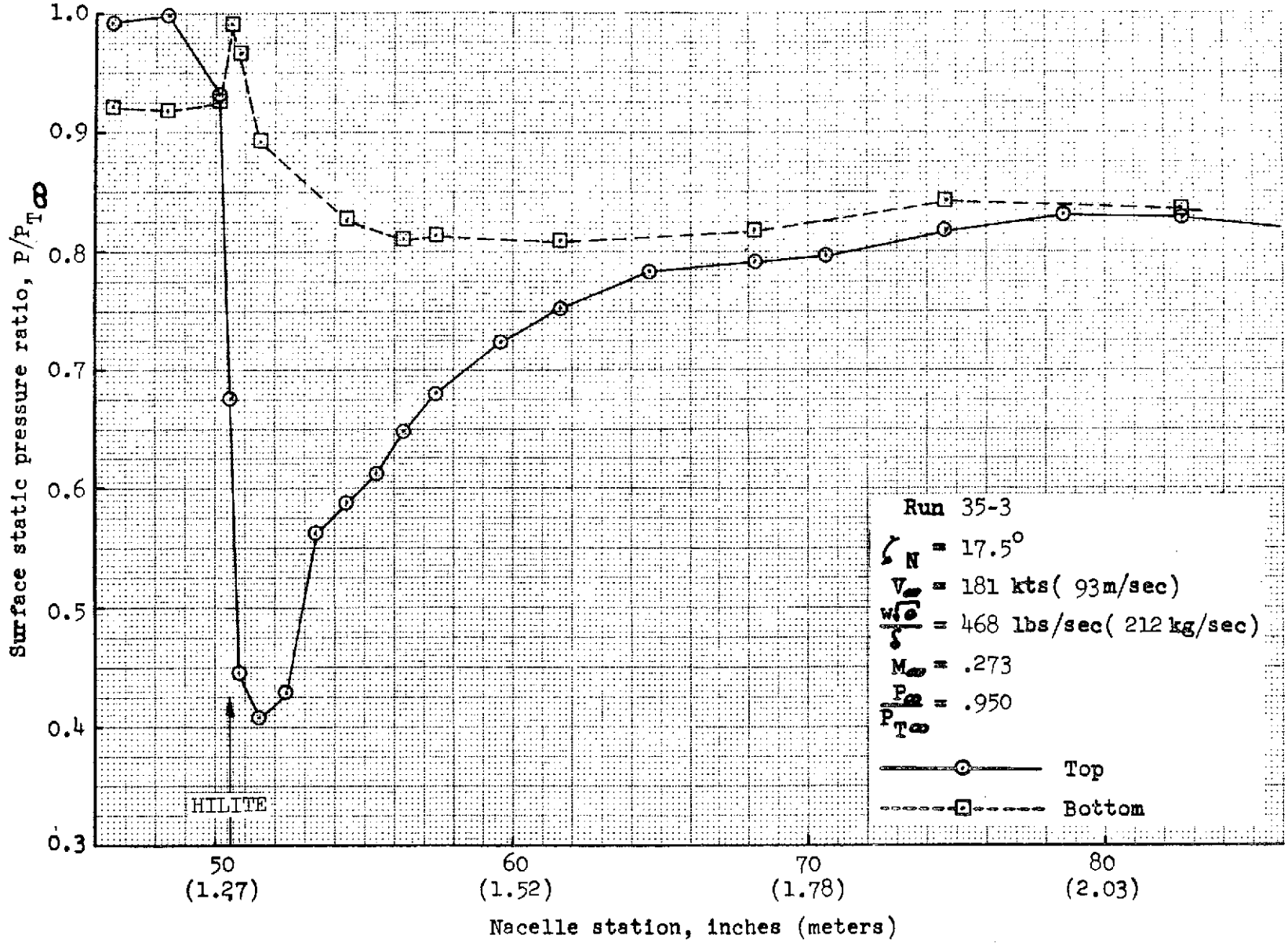

FIGURE 221.- REFAN INLET SURFACE STATIC PRESSURE RATIO DISTRIBUTION

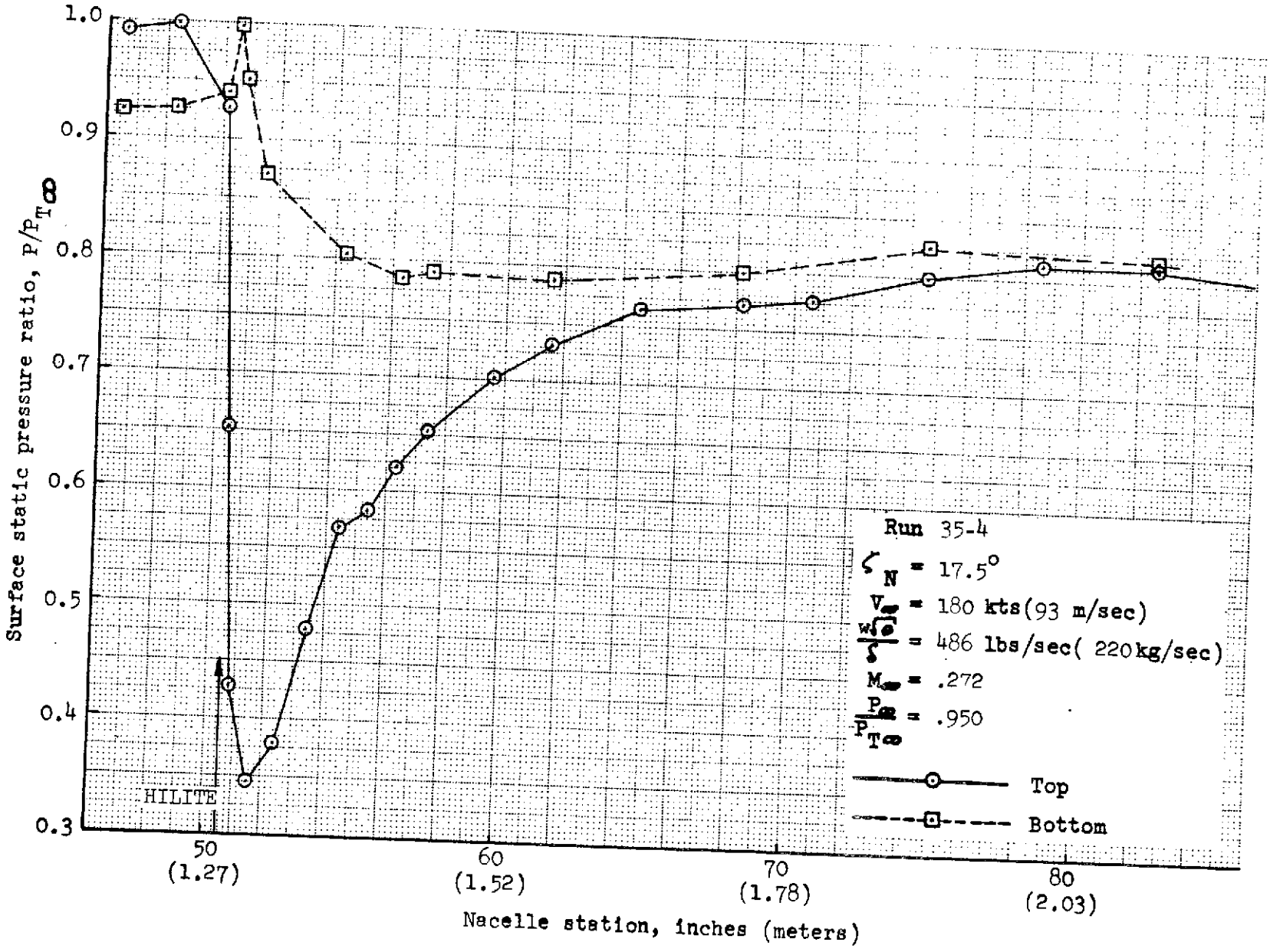

FIGURE 222.- REFAN INLET SURFACE STATIC PRESSURE RATIO DISTRIBUTION

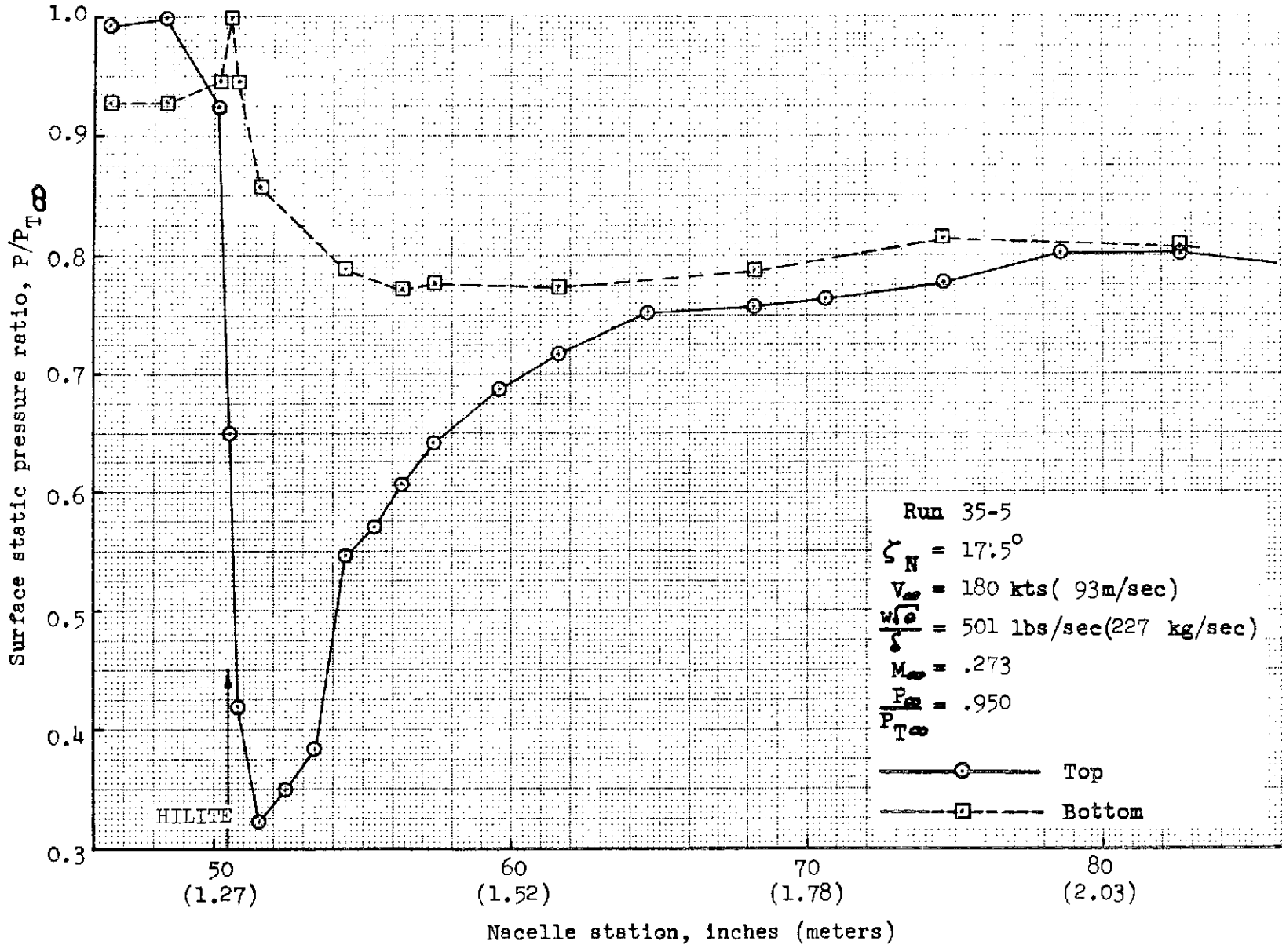

FIGURE 223.- REFAN INLET SURFACE STATIC PRESSURE RATIO DISTRIBUTION

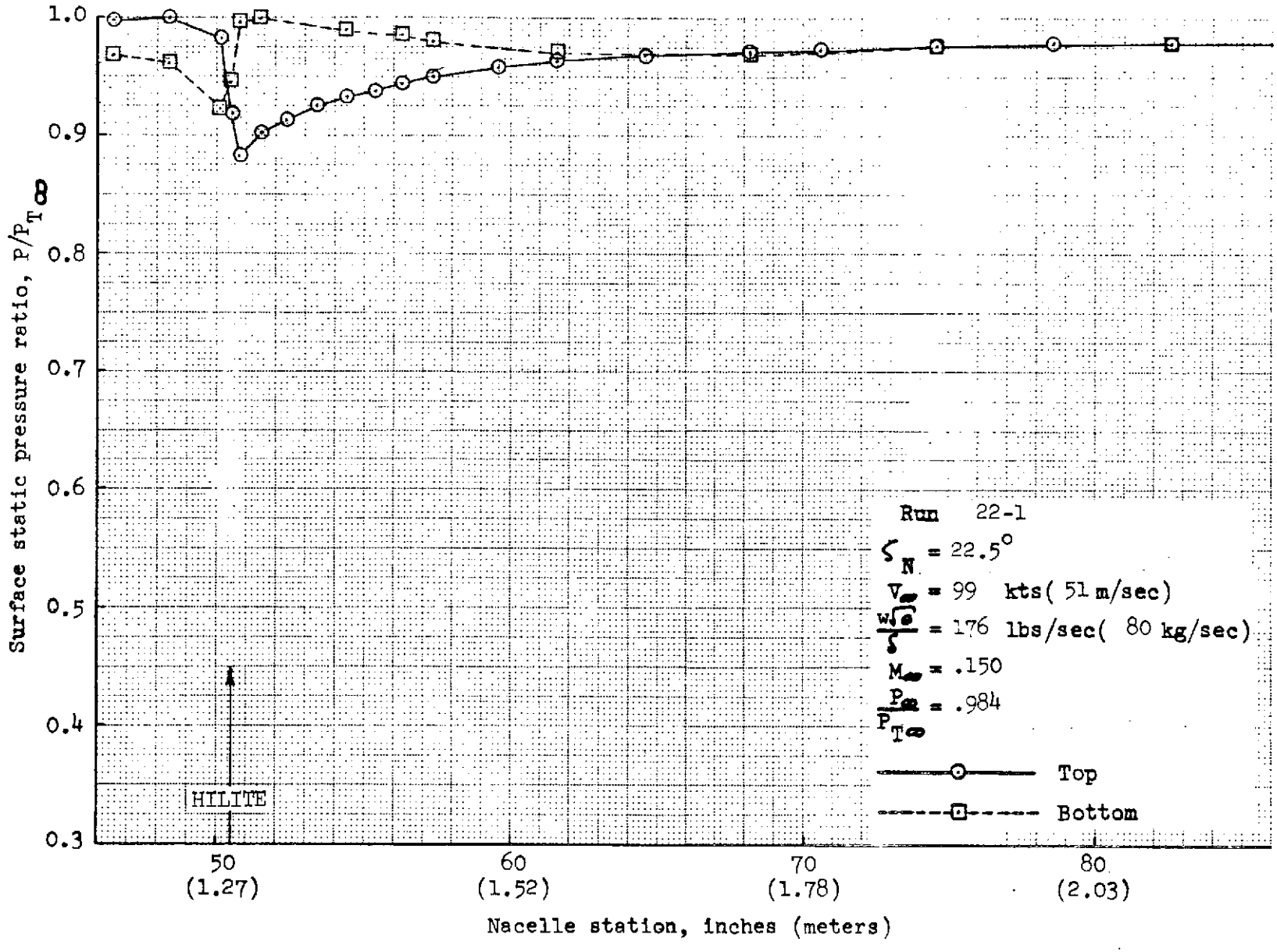

FIGURE 224.- REFAN INLET SURFACE STATIC PRESSURE RATIO DISTRIBUTION

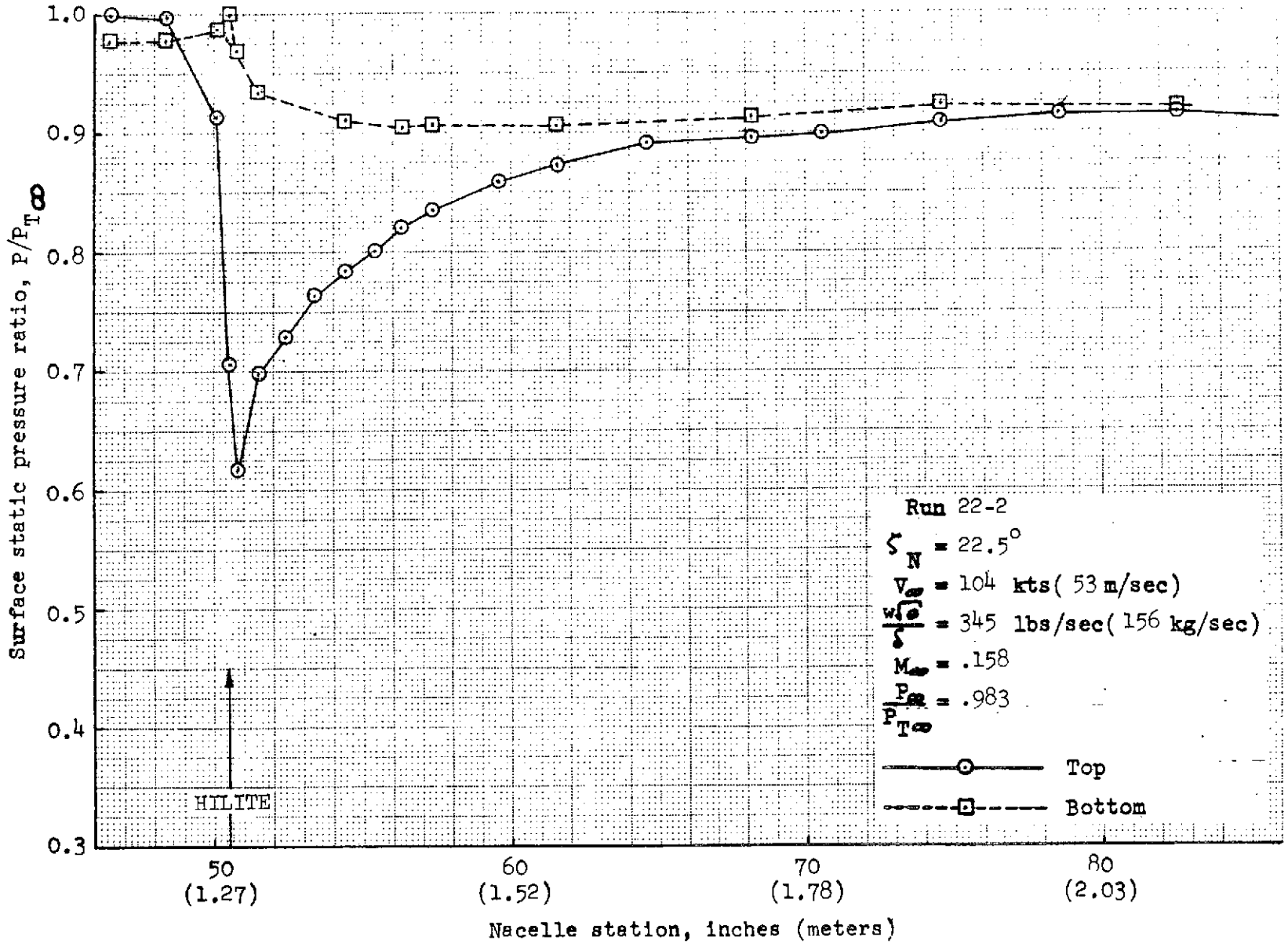

FIGURE 225.- REFAN INLET SURFACE STATIC PRESSURE RATIO DISTRIBUTION

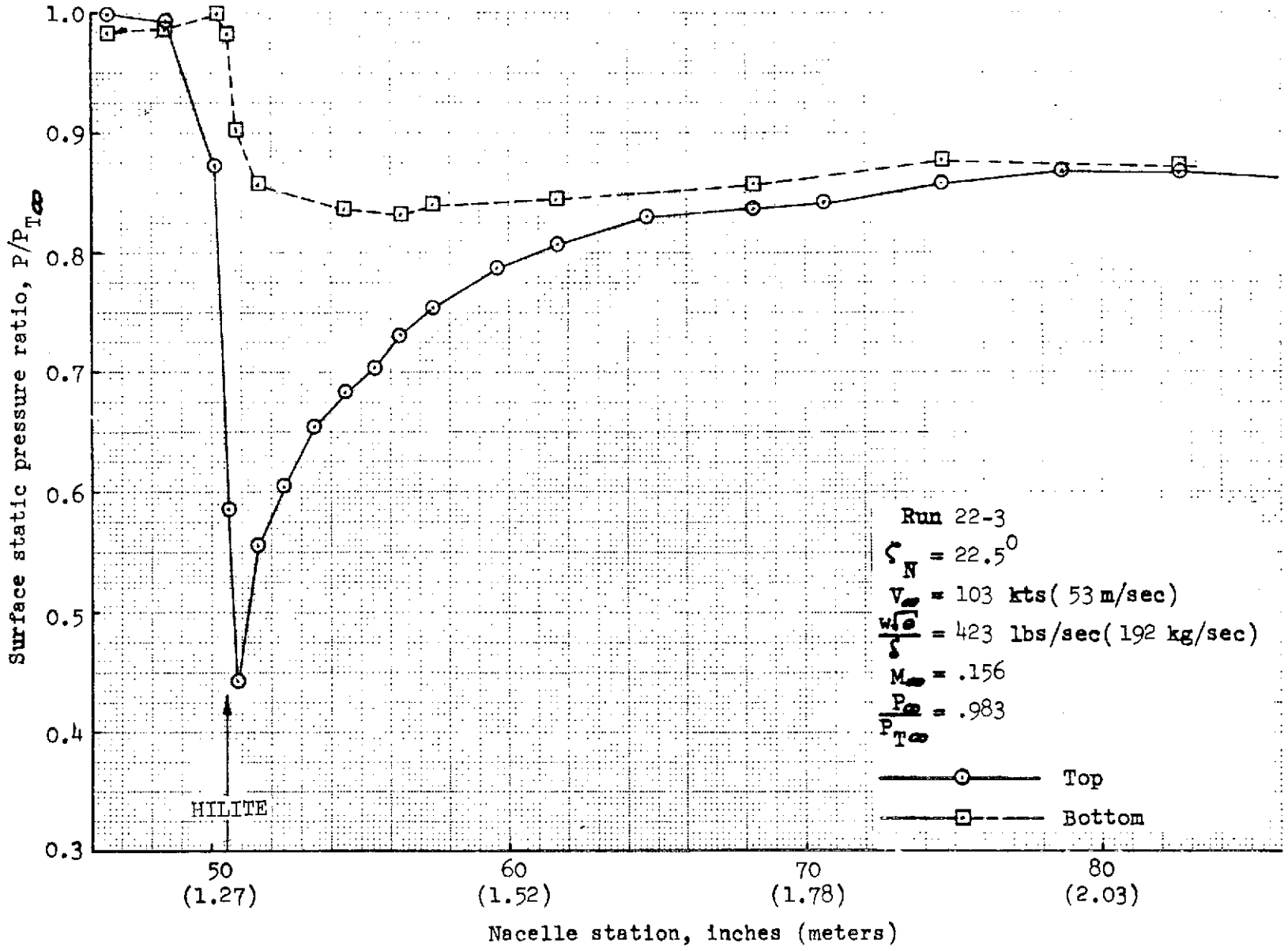

FIGURE 226.- REFAN INLET SURFACE STATIC PRESSURE RATIO DISTRIBUTION

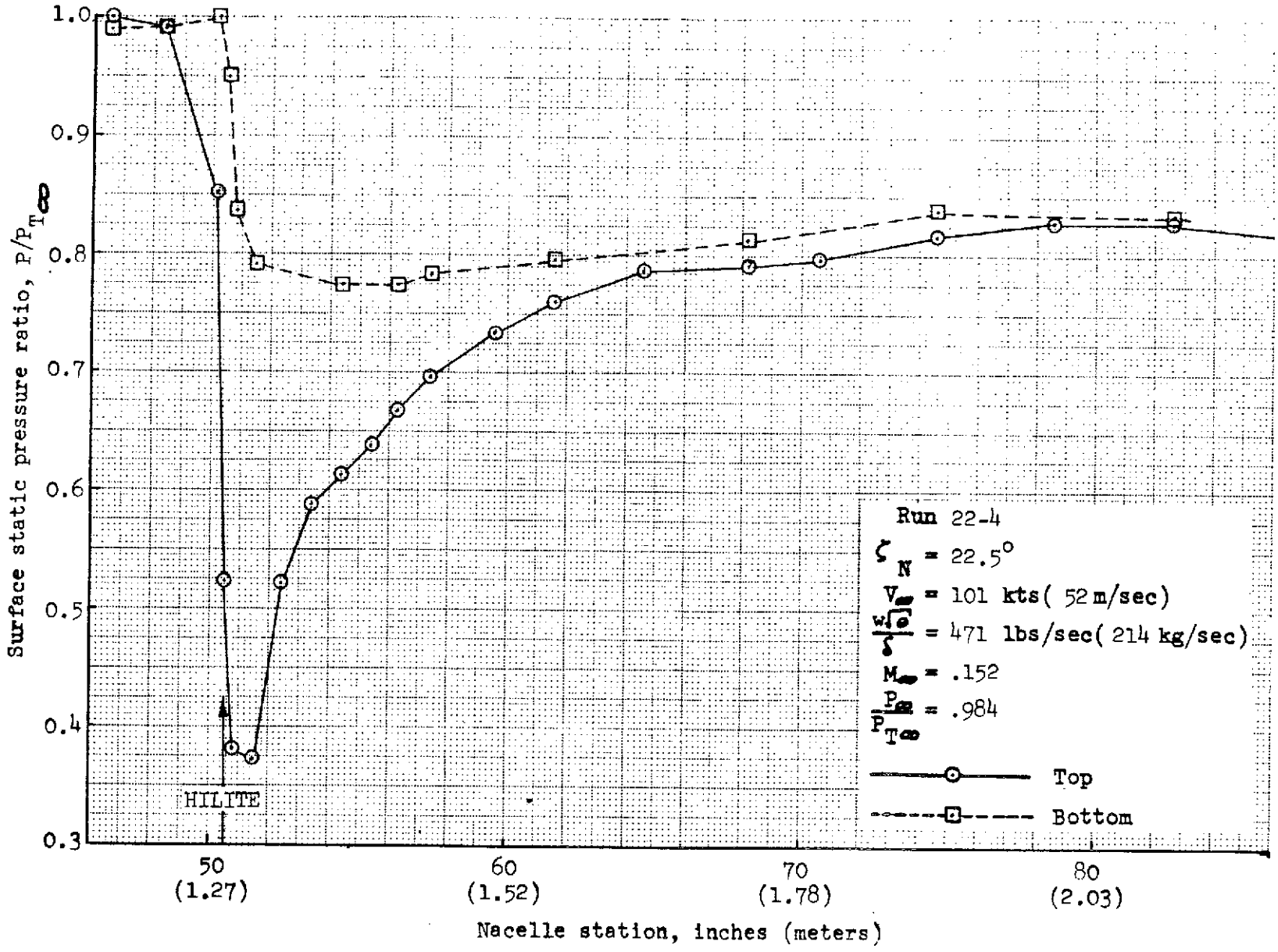

FIGURE 227.- REFAN INLET SURFACE STATIC PRESSURE RATIO DISTRIBUTION

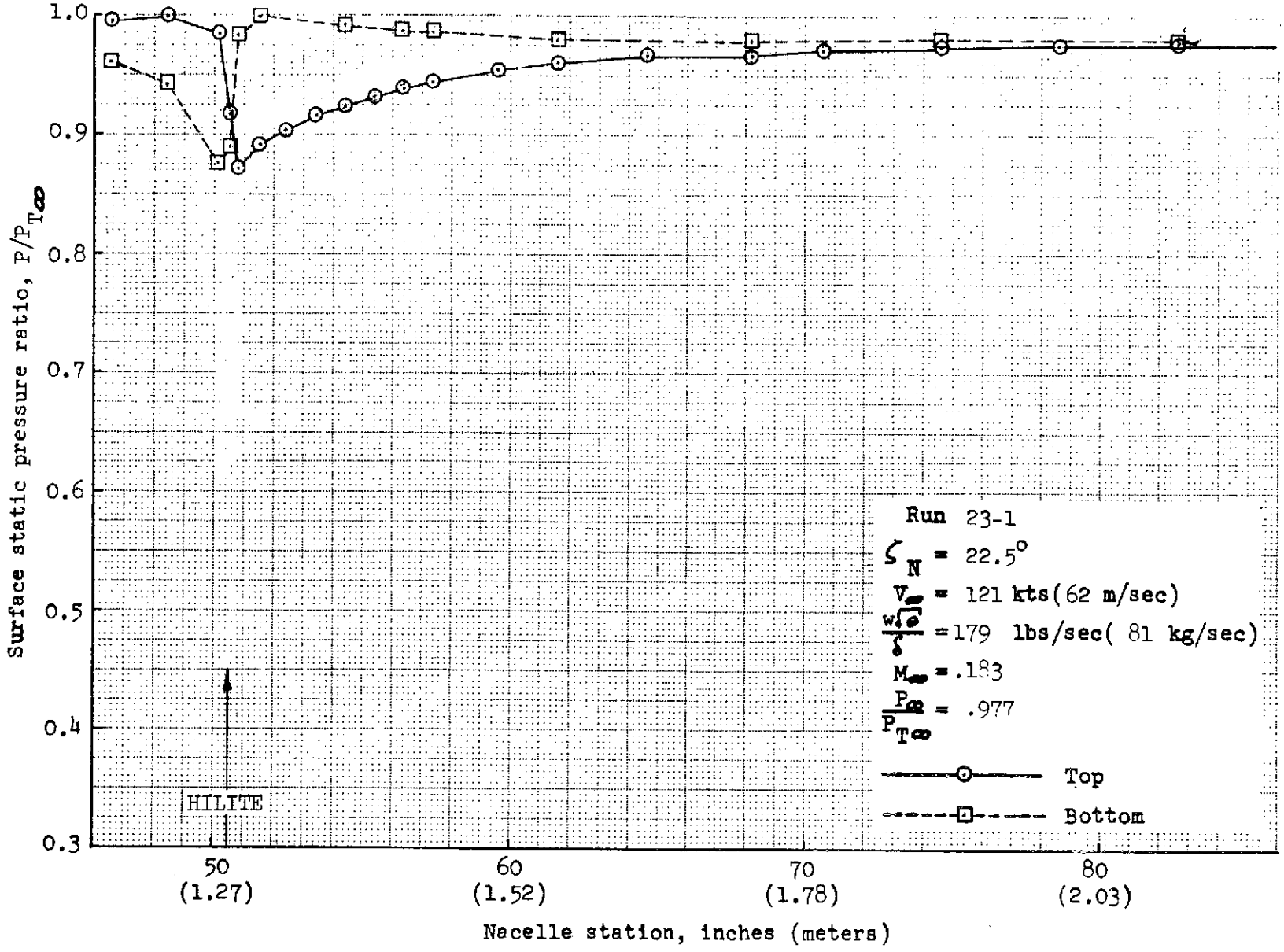

FIGURE 228.- REFAN INLET SURFACE STATIC PRESSURE RATIO DISTRIBUTION

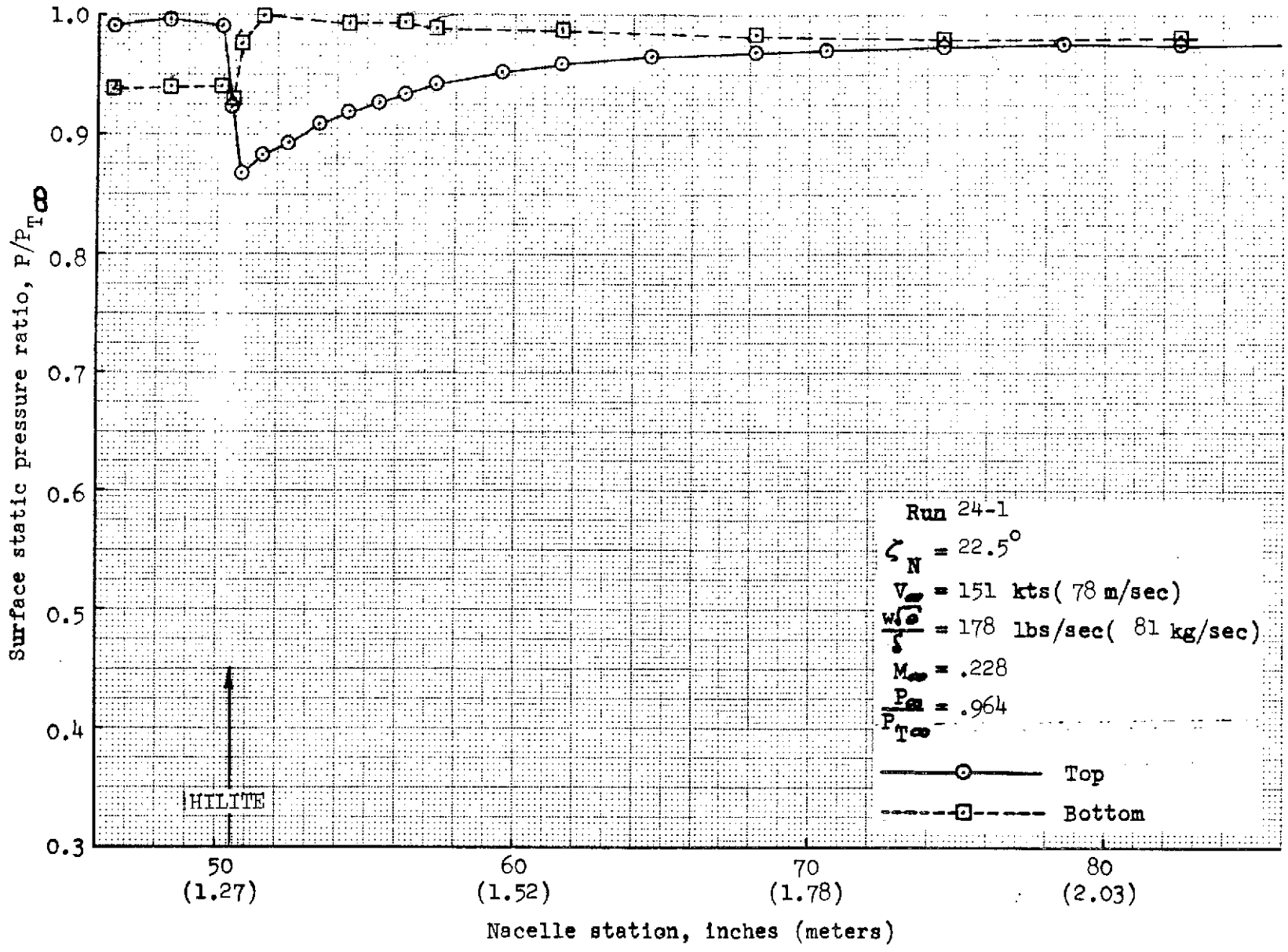

FIGURE 229.- REFAN INLET SURFACE STATIC PRESSURE RATIO DISTRIBUTION

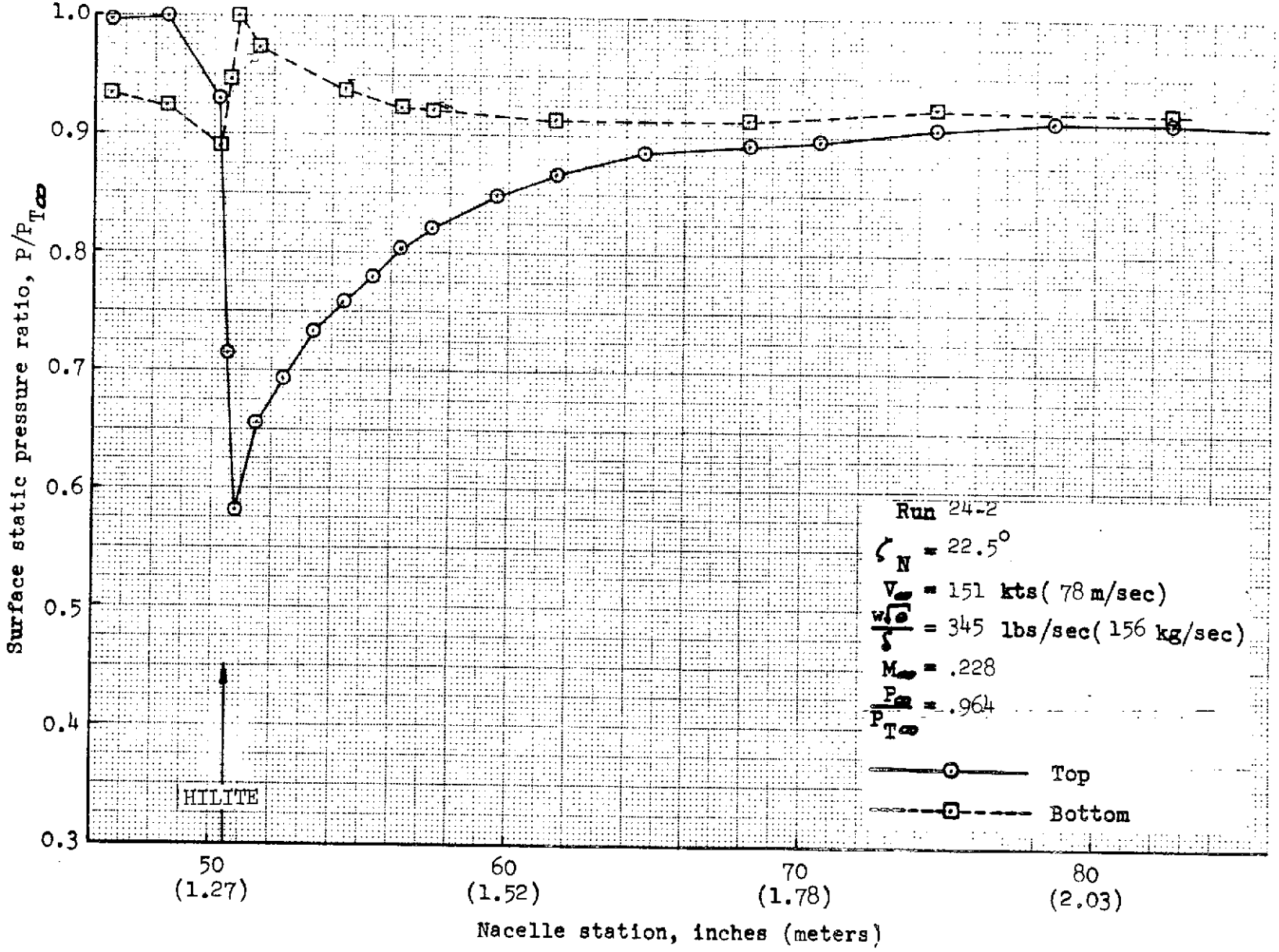

FIGURE 230.- REFAN INLET SURFACE STATIC PRESSURE RATIO DISTRIBUTION

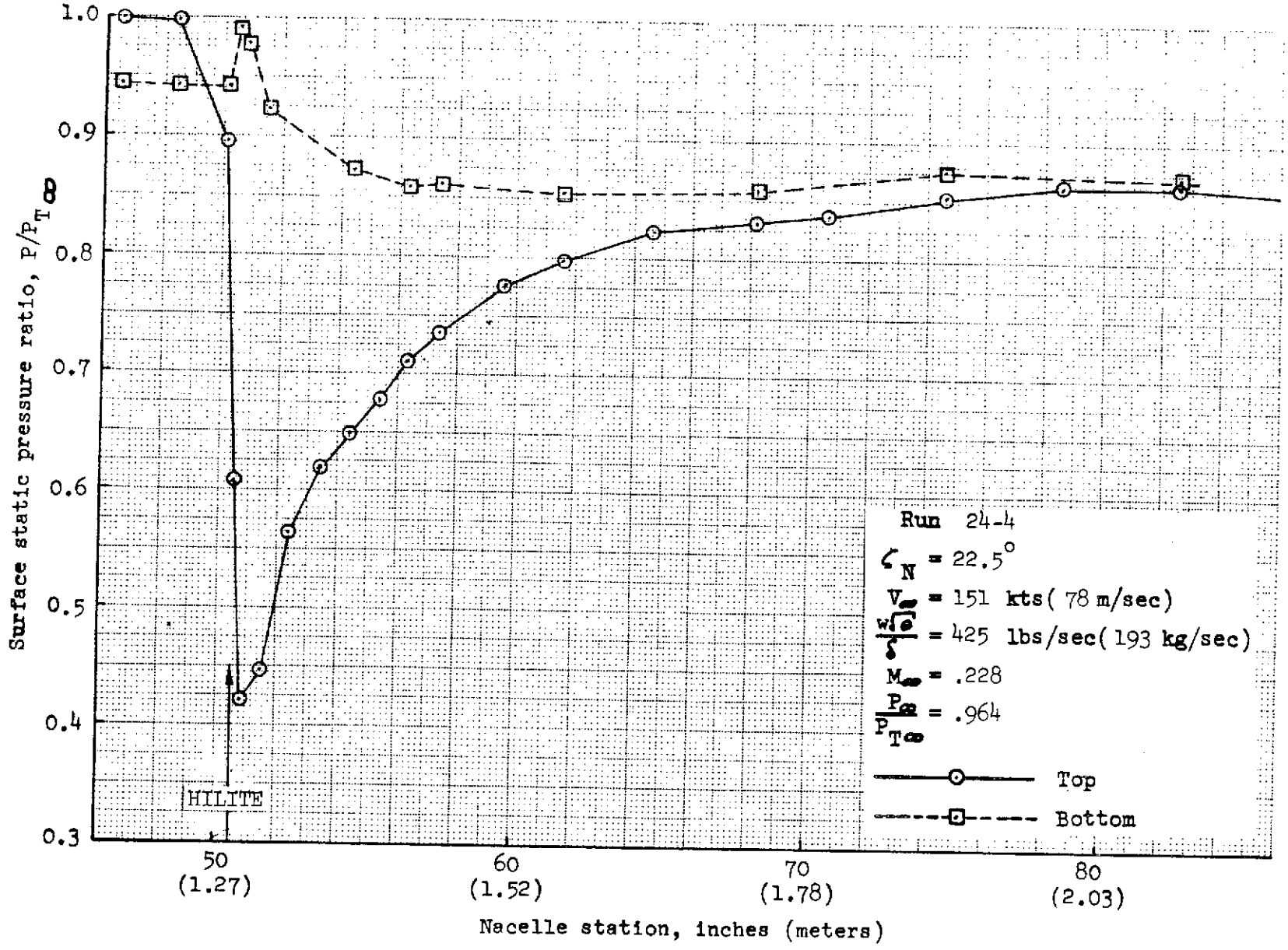

FIGURE 231.- REFAN INLET SURFACE STATIC PRESSURE RATIO DISTRIBUTION

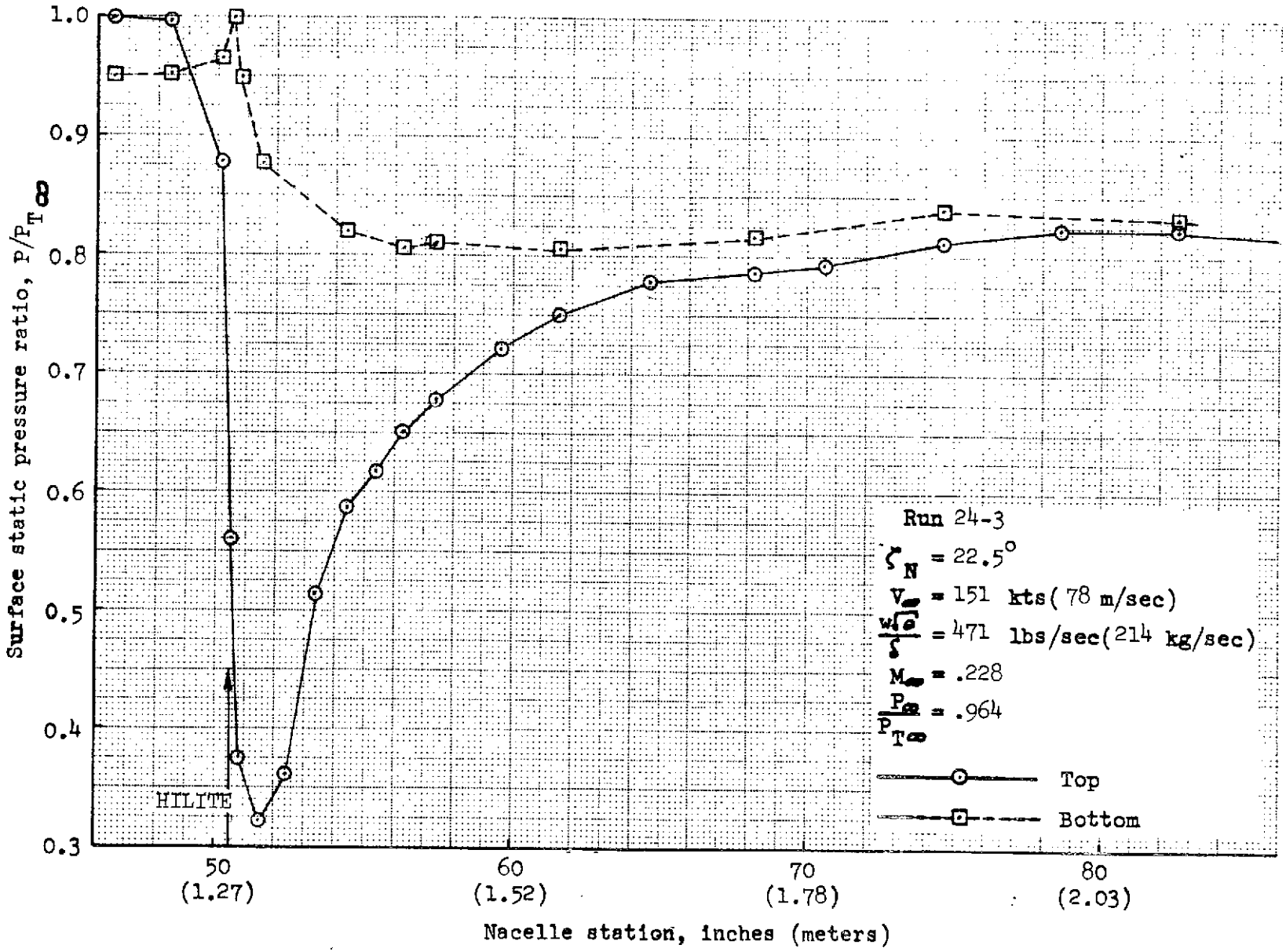

FIGURE 232.- REFAN INLET SURFACE STATIC PRESSURE RATIO DISTRIBUTION

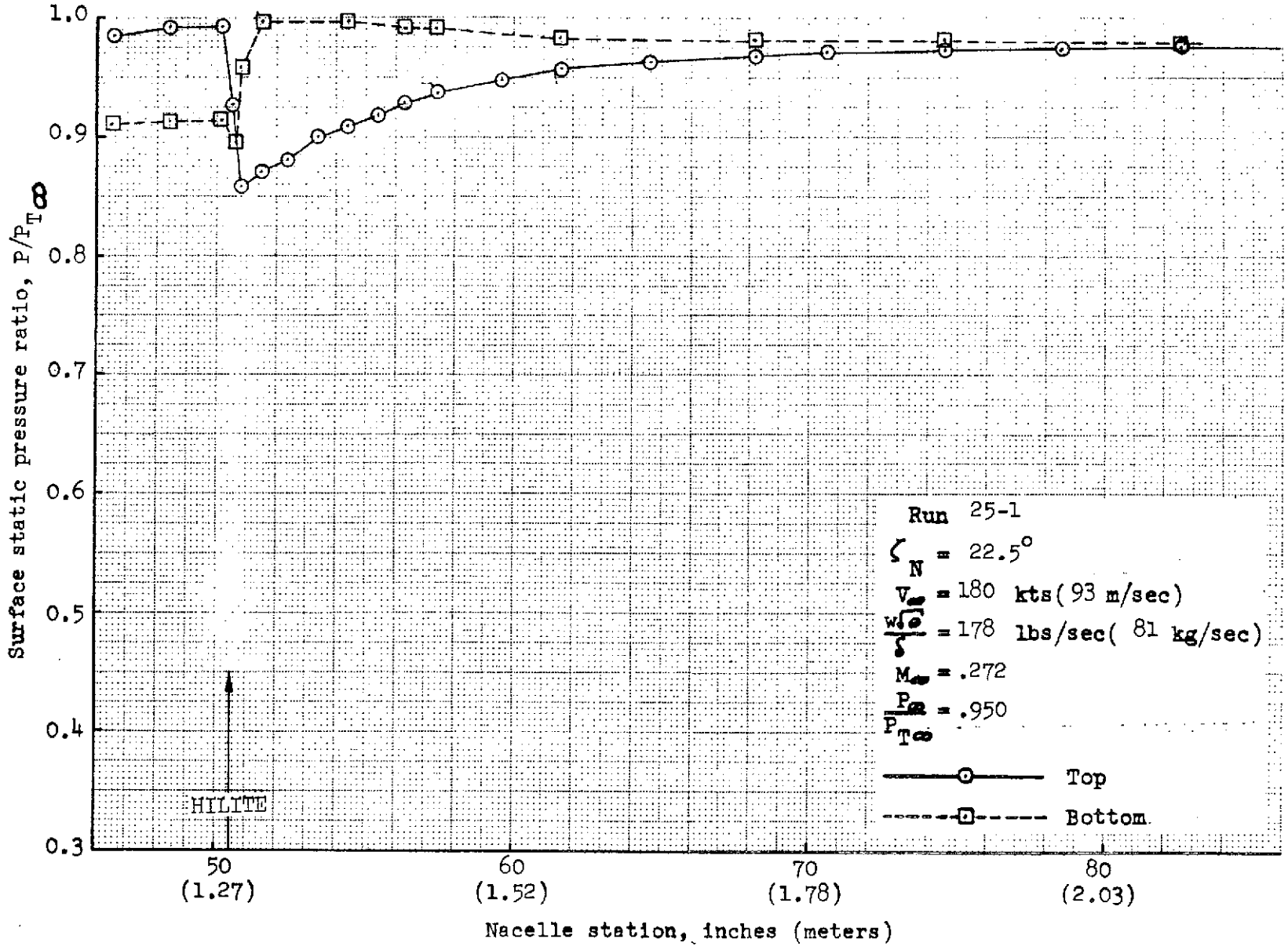

FIGURE 233.- REFAN INLET SURFACE STATIC PRESSURE RATIO DISTRIBUTION

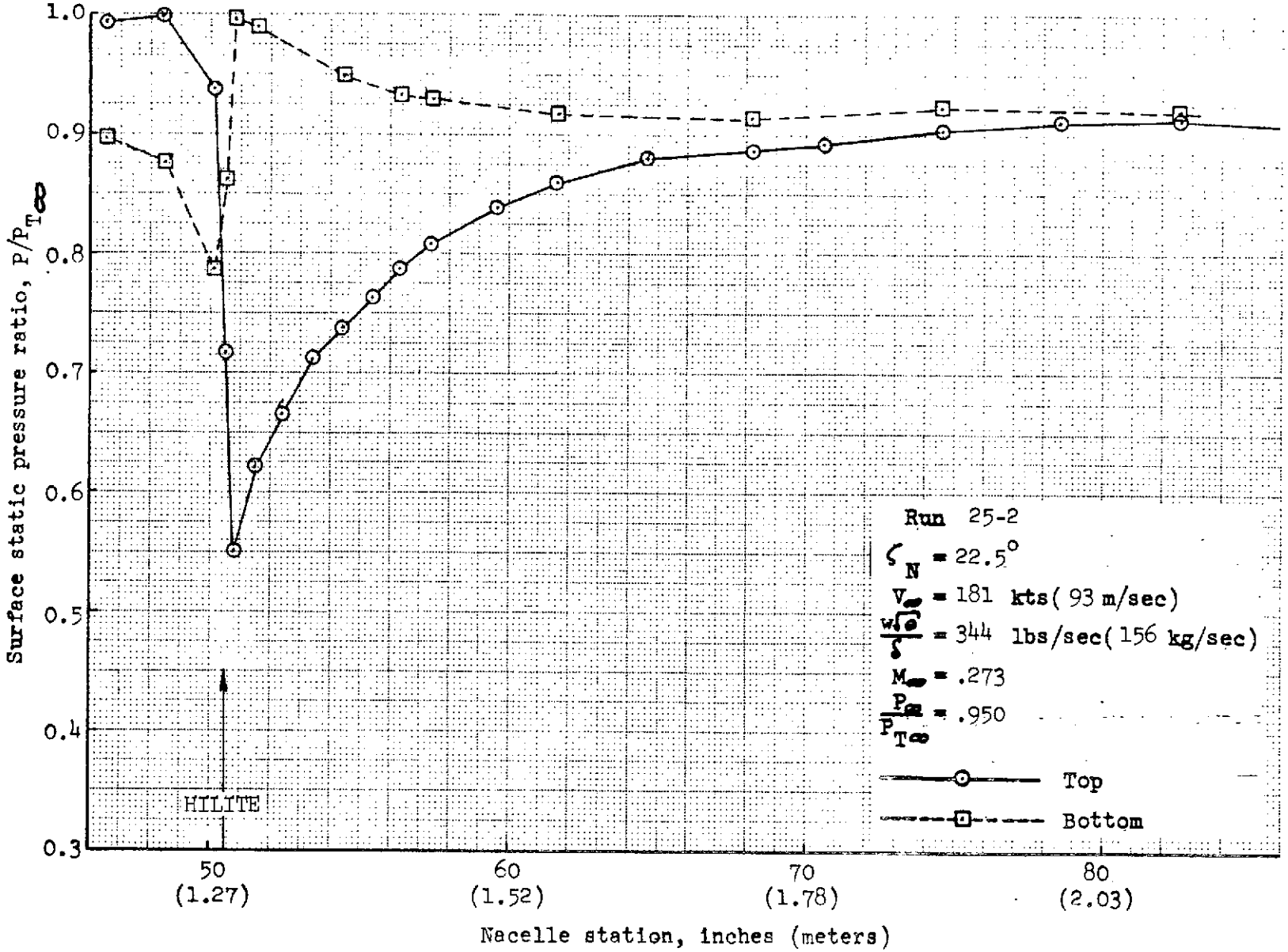

FIGURE 234.- REFAN INLET SURFACE STATIC PRESSURE RATIO DISTRIBUTION

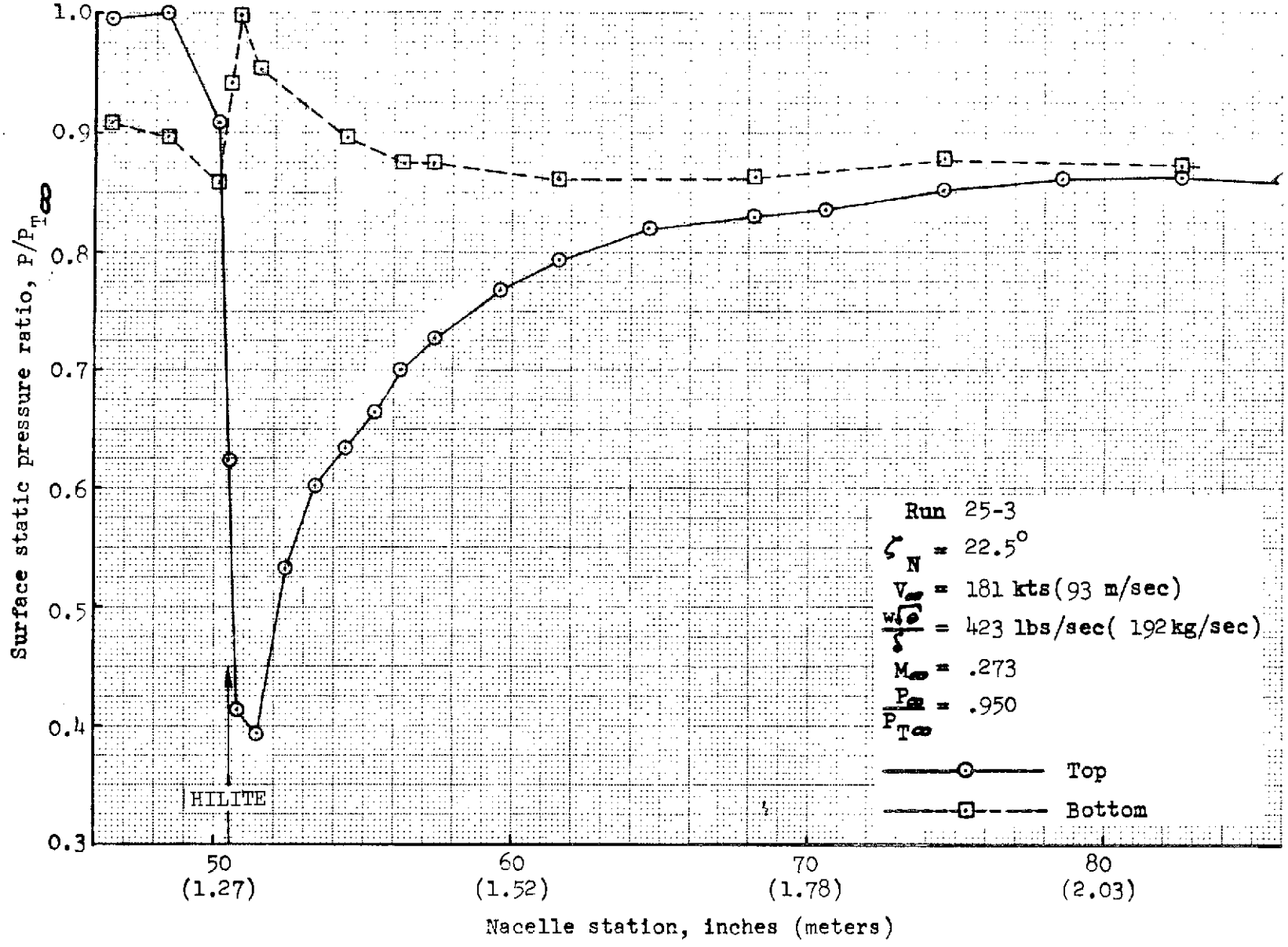

FIGURE 235. - REFAN INLET SURFACE STATIC PRESSURE RATIO DISTRIBUTION

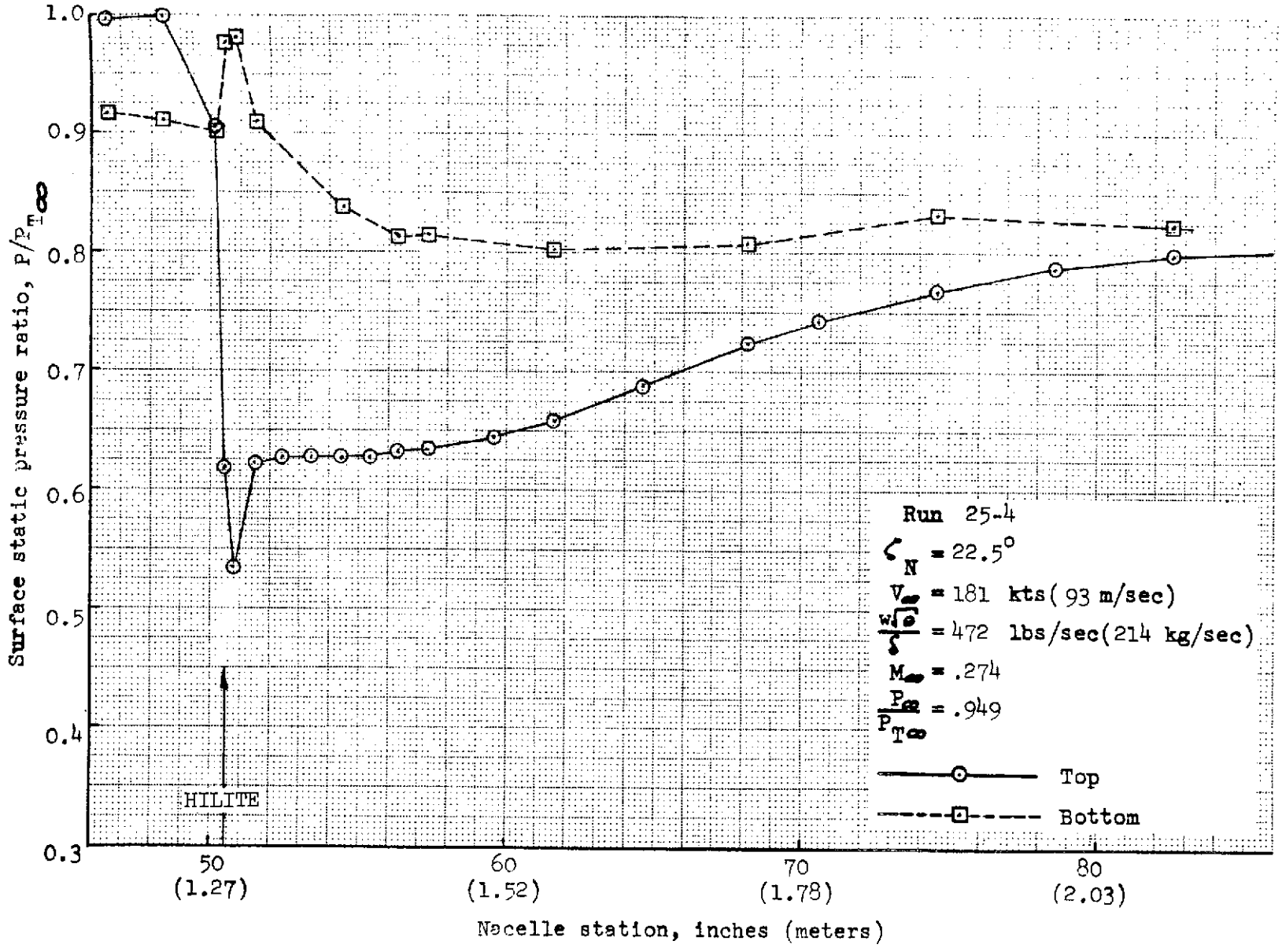

FIGURE 236.- REFAN INLET SURFACE STATIC PRESSURE RATIO DISTRIBUTION

8.0 REFERENCES

1. Schuehle, A. L., 727 Airplane Side Inlet Low-speed Performance Confirmation Model Test for Refanned JT8D JT8D Engines, NASA CR-134609, March 1974.